THE LONG ROAD TO BUILDING A HEAD: SMOOTH TRAVELS AND ACCIDENTS ON THE JOURNEY FROM PATTERNING VIA MORPHOGENESIS TO PHENOTYPE

EDITED BY: Kerstin Feistel, Dalit Sela-Donenfeld and Annette Hammes
PUBLISHED IN: Frontiers in Cell and Developmental Biology

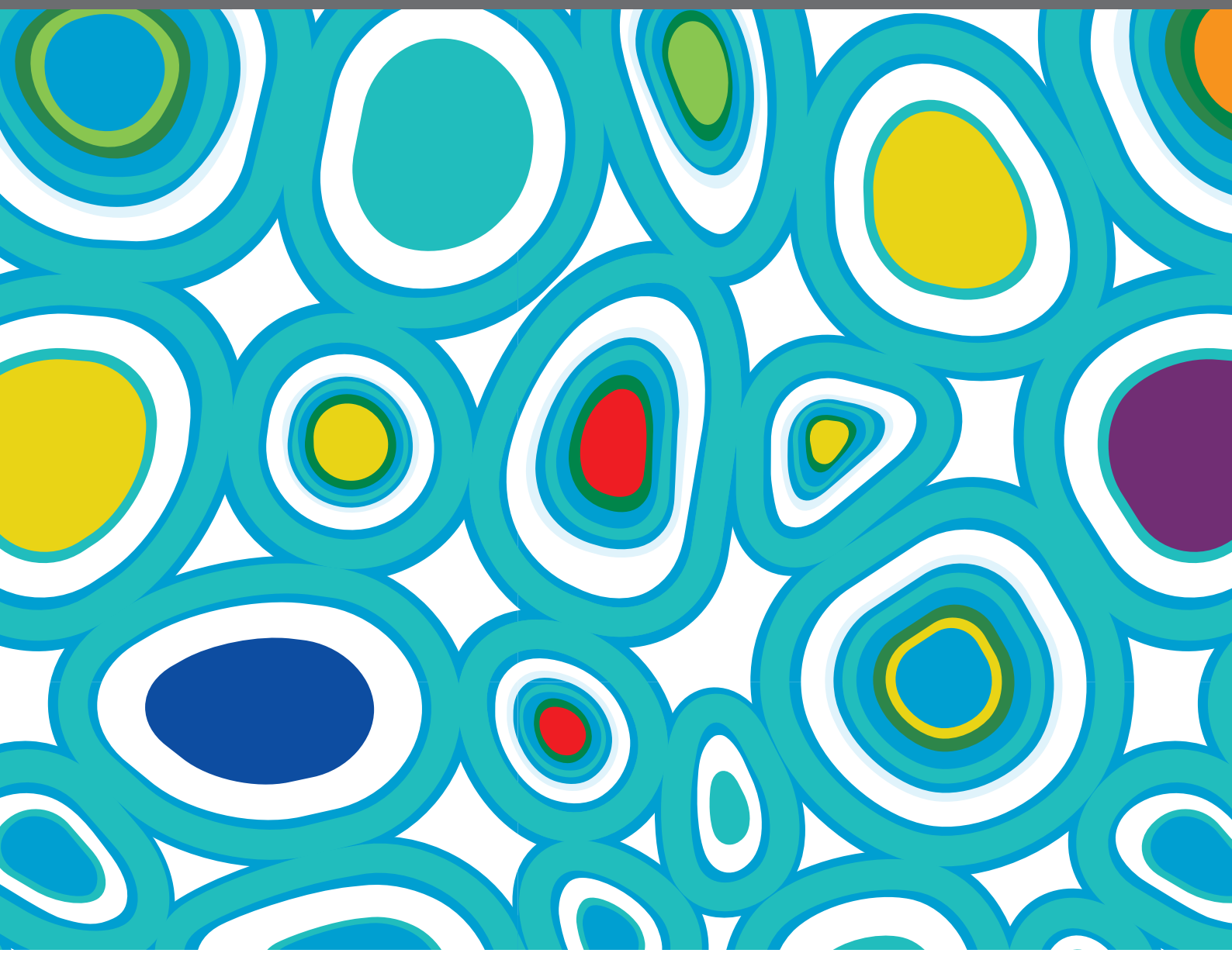

frontiers Research Topics

frontiers

ISSN 1664-8714
ISBN 978-2-88976-157-9
DOI 10.3389/978-2-88976-157-9

About Frontiers

Frontiers is more than just an open-access publisher of scholarly articles: it is a pioneering approach to the world of academia, radically improving the way scholarly research is managed. The grand vision of Frontiers is a world where all people have an equal opportunity to seek, share and generate knowledge. Frontiers provides immediate and permanent online open access to all its publications, but this alone is not enough to realize our grand goals.

Frontiers Journal Series

The Frontiers Journal Series is a multi-tier and interdisciplinary set of open-access, online journals, promising a paradigm shift from the current review, selection and dissemination processes in academic publishing. All Frontiers journals are driven by researchers for researchers; therefore, they constitute a service to the scholarly community. At the same time, the Frontiers Journal Series operates on a revolutionary invention, the tiered publishing system, initially addressing specific communities of scholars, and gradually climbing up to broader public understanding, thus serving the interests of the lay society, too.

Dedication to Quality

Each Frontiers article is a landmark of the highest quality, thanks to genuinely collaborative interactions between authors and review editors, who include some of the world's best academicians. Research must be certified by peers before entering a stream of knowledge that may eventually reach the public - and shape society; therefore, Frontiers only applies the most rigorous and unbiased reviews.
Frontiers revolutionizes research publishing by freely delivering the most outstanding research, evaluated with no bias from both the academic and social point of view. By applying the most advanced information technologies, Frontiers is catapulting scholarly publishing into a new generation.

What are Frontiers Research Topics?

Frontiers Research Topics are very popular trademarks of the Frontiers Journals Series: they are collections of at least ten articles, all centered on a particular subject. With their unique mix of varied contributions from Original Research to Review Articles, Frontiers Research Topics unify the most influential researchers, the latest key findings and historical advances in a hot research area! Find out more on how to host your own Frontiers Research Topic or contribute to one as an author by contacting the Frontiers Editorial Office: frontiersin.org/about/contact

THE LONG ROAD TO BUILDING A HEAD: SMOOTH TRAVELS AND ACCIDENTS ON THE JOURNEY FROM PATTERNING VIA MORPHOGENESIS TO PHENOTYPE

Topic Editors:
Kerstin Feistel, University of Hohenheim, Germany
Dalit Sela-Donenfeld, The Hebrew University of Jerusalem, Israel
Annette Hammes, Max Delbrück Center for Molecular Medicine (MDC), Germany

Citation: Feistel, K., Sela-Donenfeld, D., Hammes, A., eds. (2022). The Long Road to Building a Head: Smooth Travels and Accidents on the Journey From Patterning via Morphogenesis to Phenotype. Lausanne: Frontiers Media SA.
doi: 10.3389/978-2-88976-157-9

Table of Contents

frontiers | Frontiers in Cell and Developmental Biology

EDITORIAL
published: 25 April 2022
doi: 10.3389/fcell.2022.895497

Editorial: The Long Road to Building a Head: Smooth Travels and Accidents on the Journey From Patterning *via* Morphogenesis to Phenotype

Kerstin Feistel[1]*, *Annette Hammes*[2]* and *Dalit Sela-Donenfeld*[3]*

[1]Department of Zoology, Institute of Biology, University of Hohenheim, Stuttgart, Germany, [2]Max Delbrück Center for Molecular Medicine in the Helmholtz Association, Berlin, Germany, [3]Faculty of Agriculture, Food and Environmental Sciences, Koret School of Veterinary Medicine, The Hebrew University of Jerusalem, Rehovot, Israel

Keywords: neural plate, neural crest, cranial placodes, head, vertebrates, brain development, craniofacial malformations, congenital disorders

Editorial on the Research Topic

The Long Road to Building a Head: Smooth Travels and Accidents on the Journey From Patterning *via* Morphogenesis to Phenotype

OPEN ACCESS

Edited and reviewed by:
Rulang Jiang,
Cincinnati Children's Hospital Medical Center, United States

***Correspondence:**
Kerstin Feistel
k.feistel@uni-hohenheim.de
Annette Hammes
hammes@mdc-berlin.de
Dalit Sela-Donenfeld
dalit.seladon@mail.huji.ac.il

Specialty section:
This article was submitted to Morphogenesis and Patterning, a section of the journal Frontiers in Cell and Developmental Biology

Received: *13 March 2022*
Accepted: *07 April 2022*
Published: *25 April 2022*

Citation:
Feistel K, Hammes A and Sela-Donenfeld D (2022) Editorial: The Long Road to Building a Head: Smooth Travels and Accidents on the Journey From Patterning via Morphogenesis to Phenotype. Front. Cell Dev. Biol. 10:895497. doi: 10.3389/fcell.2022.895497

INTRODUCTION

Formation of the vertebrate head is fascinating in its complexity. Originating from ectodermal, mesodermal and endodermal cell lineages, multiple cell types will initially become specified to neural ectoderm, neural crest cells, sensory placode, head mesoderm and the upper-most part of the gastrointestinal tract (Santagati and Rijli, 2003; Thawani and Groves, 2020). These cell types further differentiate to eventually generate the brain, skull bones and cartilage, sensory organs, facial muscles and connective tissues as well as the pharynx. The development of all these structures has to be tightly orchestrated in order to assemble a functional head, which is critical for survival and communication in all vertebrates (Gans and Northcutt, 1983).

Activation of multiple biochemical and mechanical cues in the early embryonic head initiates a crosstalk between different signaling pathways that elicits cell-autonomous and non-autonomous mechanisms to activate complex gene regulatory networks. By regulating the activity of intermediate players, extensive patterning and specification events eventually trigger morphogenetic cell movements such as apical constriction, cell elongation, cell clustering, epithelial-to-mesenchymal transition and cell migration (Gilmour et al., 2017). It is the intricate temporal and spatial orchestration of these morphogenetic dynamics that brings about neural tube closure, creates additional layers from the pseudostratified cranial neuroectoderm to form different brain regions, facilitates neural crest delamination and migration, promotes accumulation of ectodermal cells to form sensory placodes, as well as enables the mesodermal and endodermal cell layer to shape muscles, connective tissues, blood vessels and endodermal lining. Accidents happening anywhere and anytime on that developmental road can impair head morphogenesis, leading to numerous types of craniofacial malformations and neurodevelopmental disorders (LaMantia, 2020).

COMPLEX CONGENITAL MALFORMATIONS OF HEAD DEVELOPMENT

In humans, such accidents during embryonic or fetal development often manifest as complex congenital malformations affecting head and brain development. Autosomal recessive primary microcephaly (MCPH) is a common congenital disorder leading to brain atrophy. Zaqout and Kaindl review the rapidly increasing knowledge on genes associated with MCPH and highlight that the expanding pathomechanism spectrum of this disease goes far beyond the well-established centrosomal component (Zaqout and Kaindl). The authors point out the need for deeper understanding of the MCPH genotype-to-phenotype correlation to elucidate molecular pathways involved in disease etiology. Another common congenital malformation of head and brain is holoprosencephaly (HPE), characterized by failure of proper forebrain hemisphere separation and craniofacial dysmorphologies of varying severity. Lo et al. summarize the interactions between genes and environment that underlie the multifactorial etiology of HPE. Focusing on the SHH pathway, their review emphasizes the need to better understand genetic and environmental factors contributing to HPE to shed light on the mechanisms underlying disease etiology.

ANIMAL MODELS TO STUDY BRAIN AND CRANIOFACIAL MALFORMATIONS

Animal models are especially fruitful in analyzing the pathomechanisms underlying craniofacial malformations. Severe craniofacial malformations such as extreme microphthalmia and midline facial clefting occur in Frontonasal Dysplasia (FND). Iyyanar et al. provide new insights into the genetic mechanisms underlying the etiology of FND using a mouse model. The authors analyze ALX1-related FND in the mouse and demonstrate requirement of the ALX1 transcription factor for correct patterning of neural crest-derived periocular and frontonasal mesenchyme–cell populations that contribute to cartilage and bones in the skull. Schreiner et al. have used the African Clawed Frog *Xenopus laevis* as a vertebrate embryonic model to analyse the craniofacial aspects of Diamond-Blackfan anemia (DBA). Loss of ribosomal protein L5 (RPL5), which is mutated in patients suffering from DBA, caused malformations of the brain, eyes and cranial cartilage, reflecting the craniofacial defects seen in DBA. *Xenopus* has previously been used to analyze the role of the Autism Susceptibility Candidate 2 (AUTS2) gene and its paralog Fibrosin-like protein 1 (FBRSL1) in the etiology of congenital head and brain pathologies. Here, Pauli et al. review recent studies, discuss the transcriptional complexity of both factors and speculate on how FBRSL1 and AUTS2 might interrelate to govern brain and head development.

SIGNALING PATHWAYS IN HEAD DEVELOPMENT

The road to head formation can get bumpy as early as during the first patterning events that specify anterior tissues. Analysis of signaling pathways in head development is thus crucial to understand pathomechanisms all the way from patterning to morphogenetic movements. WNT signaling is one of the essential pathways during all stages of head development–from early anterior-posterior patterning of the neural plate *via* neural plate border specification to neural crest migration. While Sutton et al. summarize the functions of WNT signaling in zebrafish neural crest development from specification through neural crest cell migration, Bou-Rouphael and Durand focus on the role of TCF/LEF as transcriptional repressors associated with canonical WNT signaling activity in various contexts relating to head development, from the Spemann organizer to brain organizers, but also in stem cell homeostasis and cancer. In addition to WNT, the BMP and FGF signaling pathways are essential for all stages of head development. Washausen and Knabe highlight their relevance for morphogenesis and neurogenesis in the three paired epibranchial placodes. Using whole mouse embryo culture, the authors show that the development of each epibranchial placode is individually regulated by differential sensitivity to these morphogen pathways. While paracrine signaling by BMP, FGF and WNT establishes tissue-wide patterning, juxtacrine signaling is used for cell segregation in the formation of tissue boundaries. Wilkinson's review provides an in-depth summary on juxtacrine Eph-Ephrin signaling and its interplay with cadherins for segregation of cells for boundary formation in the developing hindbrain.

GENE REGULATORY NETWORKS IN HEAD DEVELOPMENT

Complex gene regulatory networks are initiated by signaling pathways and govern patterning and cell segregation, e.g. at the neural plate border. Klein et al. study ectoderm segregation into neural plate, neural crest, pre-placodal and *epidermis* lineages using *Xenopus*. The authors show that segregation is initially produced by cell autonomous repressive transcription factor interactions, followed by non-cell autonomous signalling to neighbouring cells/domains. The issue of transcriptional regulation in cranial neural crest cell specification and craniofacial morphogenesis was further elaborated by McMahon et al. The authors knocked out the transcription factor Foxd4 in mouse ESCs and used these cells to generate organoids and chimeric mice. Their analysis suggests that within the regulatory network driving head formation, Foxd1 acts at different times in different tissues. First, Foxd4 in the anterior mesendoderm induces anterior neural tissue and subsequently, it becomes essential in anterior neuroectoderm, regulating cranial neural crest development. This article illustrates that the same transcription factor can function in different lineages at consecutive time points during development and contribute to the formation of distinct tissues.

In summary, the goal of this Research Topic was to gather novel data and discussion about the diverse aspects of vertebrate head development in health and disease. By integrating recent advances on the study of congenital disorders affecting head formation with studies on signaling pathways, gene regulatory networks and mechanisms of cell behavior acting in craniofacial development, this Research Topic provides a wide synopsis on the multiple processes that govern head/brain formation during normal development as well as on molecular pathomechanisms that cause complex developmental defects.

REFERENCES

Gans, C., and Northcutt, R. G. (1983). Neural Crest and the Origin of Vertebrates: A New Head. *Science* 220 (4594), 268–273. doi:10.1126/science.220.4594.268

Gilmour, D., Rembold, M., and Leptin, M. (2017). From Morphogen to Morphogenesis and Back. *Nature* 541 (7637), 311–320. doi:10.1038/nature21348

LaMantia, A.-S. (2020). Why Does the Face Predict the Brain? Neural Crest Induction, Craniofacial Morphogenesis, and Neural Circuit Development. *Front. Physiol.* 11, 610970. doi:10.3389/fphys.2020.610970

Santagati, F., and Rijli, F. M. (2003). Cranial Neural Crest and the Building of the Vertebrate Head. *Nat. Rev. Neurosci.* 4 (10), 806–818. doi:10.1038/nrn1221

Thawani, A., and Groves, A. K. (2020). Building the Border: Development of the Chordate Neural Plate Border Region and its Derivatives. *Front. Physiol.* 11, 608880. doi:10.3389/fphys.2020.608880

AUTHOR CONTRIBUTIONS

All authors listed have made a substantial, direct, and intellectual contribution to the work and approved it for publication.

ACKNOWLEDGMENTS

We sincerely thank all authors of this Research Topic for their contributions and are very grateful to the reviewers for evaluating all manuscripts.

Conflict of Interest: The authors declare that the research was conducted in the absence of any commercial or financial relationships that could be construed as a potential conflict of interest.

Publisher's Note: All claims expressed in this article are solely those of the authors and do not necessarily represent those of their affiliated organizations or those of the publisher, the editors, and the reviewers. Any product that may be evaluated in this article, or claim that may be made by its manufacturer, is not guaranteed or endorsed by the publisher.

frontiers in Cell and Developmental Biology

ORIGINAL RESEARCH
published: 13 September 2021
doi: 10.3389/fcell.2021.712522

Responses of Epibranchial Placodes to Disruptions of the FGF and BMP Signaling Pathways in Embryonic Mice

Stefan Washausen† and Wolfgang Knabe†*

Prosektur Anatomie, Westfälische Wilhelms-Universität Münster, Münster, Germany

OPEN ACCESS

Edited by:
Kerstin Feistel,
University of Hohenheim, Germany

Reviewed by:
Anthony Graham,
King's College London,
United Kingdom
Raj Ladher,
National Centre for Biological Sciences, India

***Correspondence:**
Wolfgang Knabe
w.knabe@uni-muenster.de

†ORCID:
Stefan Washausen
orcid.org/0000-0003-1482-2761
Wolfgang Knabe
orcid.org/0000-0003-1744-0734

Specialty section:
This article was submitted to Morphogenesis and Patterning, a section of the journal Frontiers in Cell and Developmental Biology

Received: *20 May 2021*
Accepted: *17 August 2021*
Published: *13 September 2021*

Citation:
Washausen S and Knabe W (2021) Responses of Epibranchial Placodes to Disruptions of the FGF and BMP Signaling Pathways in Embryonic Mice. Front. Cell Dev. Biol. 9:712522. doi: 10.3389/fcell.2021.712522

Placodes are ectodermal thickenings of the embryonic vertebrate head. Their descendants contribute to sensory organ development, but also give rise to sensory neurons of the cranial nerves. In mammals, the signaling pathways which regulate the morphogenesis and neurogenesis of epibranchial placodes, localized dorsocaudally to the pharyngeal clefts, are poorly understood. Therefore, we performed mouse whole embryo culture experiments to assess the impact of pan-fibroblast growth factor receptor (FGFR) inhibitors, anti-FGFR3 neutralizing antibodies or the pan-bone morphogenetic protein receptor (BMPR) inhibitor LDN193189 on epibranchial development. We demonstrate that each of the three paired epibranchial placodes is regulated by a unique combination of FGF and/or bone morphogenetic protein (BMP) signaling. Thus, neurogenesis depends on fibroblast growth factor (FGF) signals, albeit to different degrees, in all epibranchial placodes (EP), whereas only EP1 and EP3 significantly rely on neurogenic BMP signals. Furthermore, individual epibranchial placodes vary in the extent to which FGF and/or BMP signals (1) have access to certain receptor subtypes, (2) affect the production of Neurogenin (Ngn)2^+ and/or Ngn1^+ neuroblasts, and (3) regulate either neurogenesis alone or together with structural maintenance. In EP2 and EP3, all FGF-dependent production of Ngn2^+ neuroblasts is mediated via FGFR3 whereas, in EP1, it depends on FGFR1 and FGFR3. Differently, production of FGF-dependent Ngn1^+ neuroblasts almost completely depends on FGFR3 in EP1 and EP2, but not in EP3. Finally, FGF signals turned out to be responsible for the maintenance of both placodal thickening and neurogenesis in all epibranchial placodes, whereas administration of the pan-BMPR inhibitor, apart from its negative neurogenic effects in EP1 and EP3, causes only decreases in the thickness of EP3. Experimentally applied inhibitors most probably not only blocked receptors in the epibranchial placodes, but also endodermal receptors in the pharyngeal pouches, which act as epibranchial signaling centers. While high doses of pan-FGFR inhibitors impaired the development of all pharyngeal pouches, high doses of the pan-BMPR

inhibitor negatively affected only the pharyngeal pouches 3 and 4. In combination with partly concordant, partly divergent findings in other vertebrate classes our observations open up new approaches for research into the complex regulation of neurogenic placode development.

Keywords: epibranchial placodes, neurogenesis, induction, pharyngeal pouches, signaling centers, fibroblast growth factors, bone morphogenetic proteins, mouse whole embryo culture

INTRODUCTION

Ectodermal placodes are essential for the formation of sensory organs and parts of the peripheral nervous system of the vertebrate head (Baker and Bronner-Fraser, 2001; Schlosser, 2006; Park and Saint-Jeannet, 2010). They are excellent objects for basic research in developmental biology. This applies first of all to the question to which extent genetic patterning mechanisms, migratory activities and programmed cell death help to transform the "panplacodal primordium" into individual patch-like thickened placodes (Washausen et al., 2005; Schlosser, 2010; Washausen and Knabe, 2013, 2019; Breau and Schneider-Maunoury, 2014; Thiery et al., 2020). Unanswered questions also concern the developmental potential of the panplacodal primordium in different vertebrate classes. For example, in normal developing mice, posterior parts of the primordium ("posterior placodal area"; Schlosser and Ahrens, 2004; Washausen and Knabe, 2017) exclusively produce otic and epibranchial placodes, the latter ones providing gustatory and other viscerosensory neurons for ganglia associated with the facial, glossopharyngeal and vagal nerves. However, experimental suppression of physiologically occurring apoptosis in mouse whole embryo cultures results in the additional generation of lateral line placodes (Washausen and Knabe, 2018). Finally, numerous gaps exist regarding our knowledge about the signaling centers and signaling cascades which are involved in placode formation.

This work focuses on the signaling centers and pathways which support the development of epibranchial placodes in mouse embryos. According to current knowledge, demarcation of the panplacodal primordium from the neural plate, neural crest and surface ectoderm requires fibroblast growth factor (FGF), bone morphogenetic protein (BMP), and Wingless/Int-1 (Wnt) signals. They are provided by the epiblast, by the cephalic mesoderm and by the future neural plate, among others (Streit, 2018). Subsequently, FGF signals from the cephalic mesoderm help to delineate the posterior placodal area. Cell fate decisions that follow pave the way for the assembly of progenitor cells into epibranchial and otic placodes, respectively. They are supported by Wnt signals provided by the hindbrain (Ladher et al., 2010; Chen and Streit, 2013). Regarding the signaling pathways which regulate the morphogenesis and neurogenesis of epibranchial placodes, most extensive findings are available for zebrafish. Specifically, this involves BMP and FGF signals, which are released from the pharyngeal pouches (Holzschuh et al., 2005; Nechiporuk et al., 2005, 2007). Similarly, in chicken embryos, contributions of mesodermal FGF3/FGF19 and pharyngeal BMP signals have been documented (Begbie et al., 1999; Freter et al., 2008; Kriebitz et al., 2009). All that is known about mouse embryos in this context is that neurogenesis of the first epibranchial placode (EP1) critically depends on fibroblast growth factor receptor 1 (FGFR1) activity (Trokovic et al., 2005).

Using mouse embryos, the present study investigates potential contributions of FGF and BMP signals to the morphological establishment and/or to the neurogenesis of mammalian epibranchial placodes. Embryos were exposed to pan-FGFR or pan-bone morphogenetic protein receptor (BMPR) inhibitors in whole embryo culture experiments. Alternatively, anti-FGFR3 neutralizing antibodies were used to obtain more specific information on the relative contributions of distinct FGFRs. Treated embryos were evaluated histologically and statistically for the presence of Neurogenin (Ngn)2- and Ngn1-immunopositive epibranchial neuroblasts. It turned out that each of the three paired epibranchial placodes depends on different patterns of FGF and/or BMP signals, among other factors. At least in some cases, we were additionally able to distinguish (1) between the responses of $Ngn2^+$ or $Ngn1^+$ neuroblasts, (2) between the effects on epibranchial morphogenesis or neurogenesis, and (3) between the responses of epibranchial placodes and pharyngeal pouches, respectively.

MATERIALS AND METHODS

Animals

Mated C57BL/6N mice were obtained from Janvier Labs (Le Genest-Saint-Isle, France). For embryo collection, these animals were killed 8.5–9 days post coitum by cervical dislocation. All handling steps were performed in accordance with animal welfare regulations and were approved by the responsible authority [Landesamt für Natur, Umwelt und Verbraucherschutz (LANUV), North Rhine-Westphalia, Germany; approval number: 84-02.05.50.16.013].

Inhibitors and Antibodies

For blocking of FGF signaling, two different small molecule inhibitors were tested: SU5402 (3-[(3-(2-carboxyethyl)-4-methylpyrrol-2-yl)methylene]-2-indolinone; SML0443, Merck, Darmstadt, Germany) and PD173074 (1-*tert*-Butyl-3-[6-(3,5-dimethoxy-phenyl)-2-(4-diethylamino-butylamino)-pyrido[2,3-d]pyrimidin-7-yl]-urea; P2499, Merck). For use in whole embryo culture experiments, stock solutions of 100 mM SU5402 or 15 mM PD173074 were prepared in dimethyl sulfoxide (DMSO) (5179, Carl Roth, Karlsruhe, Germany). Both compounds were initially found to competitively block the

adenosine triphosphate (ATP)-binding pocket of the tyrosine kinase domain of FGFR1 (Mohammadi et al., 1997, 1998). Later, it turned out that SU5402 and PD173074 additionally inhibit FGFR2, FGFR3, and FGFR4 (Grand et al., 2004; Koziczak et al., 2004; Trudel et al., 2004; St-Germain et al., 2009; Liu et al., 2013; Ranieri et al., 2016). In the context of our scientific questions, comparative testing of both pan-FGFR inhibitors is appropriate for at least two reasons. Firstly, SU5402 is the "classical" pan-FGFR inhibitor which has been applied in many different developmental studies (Raible and Brand, 2001; Corson et al., 2003) including those investigating neurogenesis in the cranial placodes of chick and zebrafish (for a review, see Lassiter et al., 2014). Secondly, PD173074, like SU5402, has already been used successfully in whole embryo cultures of mice. For example, addressing left-right axis formation, Oki et al. (2010) have demonstrated that PD173074 impairs gene expression patterns similar to *Fgf8* and *Fgfr1* knockouts.

For selective inhibition of the FGFR3 pathway, rat anti-FGFR3 neutralizing antibodies were deployed (MAB710, R&D Systems, Minneapolis, MN, United States, lot FTD0216021, RRID: AB_2103386). According to the manufacturer, these antibodies cross-react with the IIIb and IIIc isoforms of recombinant human and mouse FGFR3, and neutralize the bioactivity of mouse FGFR3. That, in fact, the anti-FGFR3 neutralizing antibodies used here actually block FGFR3 was also proven by Arnaud-Dabernat et al. (2007) taking the development and regeneration of mouse pancreatica as an example. Physiologically, activation of FGFR3 inhibits the expansion of immature pancreatic epithelia. Genetic silencing of FGFR3 in a mouse model of pancreas regeneration led to a 1.5-fold increase in the number of proliferating pancreatic ductal cells, as evidenced by BrdU incorporation. Correspondingly, when injected to adult mice for *in vivo* blockage of FGFR3, anti-FGFR3 neutralizing antibodies produced an approximate doubling of $BrdU^+$ pancreatic epithelial cells. Arnaud-Dabernat et al. (2007) conclude that "FGFR3 attenuation by either genetic deletion or immune blockade led to a significant increase in epithelial cell expansion in pancreatic ducts."

Given that only the first of three mouse epibranchial placodes is strongly dependent on FGFR1 activation (Trokovic et al., 2005), it was particularly important for us to apply anti-FGFR3 neutralizing antibodies that do not cross-react with FGFR1. This is exactly the requirement that anti-FGFR3 neutralizing antibodies obtained from R&D Systems fulfill (MAB710). Experimental evidence for this was provided by Shalhoub et al. (2011). These authors have studied FGF23+ membrane co-receptor alpha-Klotho signaling in osteoblastic MC3T3.E1 cells which express FGFR1, FGFR2, and FGFR3. It is demonstrated that the complete blockage of all FGFRs by the pan-FGFR inhibitor SU5402 (see above) causes a massive activation of bone-specific alkaline phosphatase. Comparable effects can be achieved neither by anti-FGFR2 neutralizing antibodies nor by anti-FGFR3 neutralizing antibodies. Consequently, the effect must be due to the activation of FGFR1, which remains undisturbed by the anti-FGFR3 neutralizing antibodies used here.

Inhibition of the BMP signaling pathway was performed with the small molecule inhibitor LDN193189 (4-[6-(4-(piperazin-1-yl)phenyl)pyrazolo[1,5-a]pyrimidin-3-yl] quinoline; SML0559, Merck) which was dissolved in water to produce a stock solution of 50 mM. LDN193189 is structurally derived from dorsomorphin that competitively blocks the ATP-binding pocket of the BMP type I receptor's intracellular kinase domain (Chaikuad et al., 2012). Compared to dorsomorphin, LDN193189 demonstrates increased potency and pharmacokinetic stability (Cuny et al., 2008). In addition to its impact on BMP type I receptors [Activin receptor-like kinases (ALK) 1, 2, 3 and 6; Yu et al., 2008], LDN193189 efficiently binds to the BMP type II receptors Activin receptor IIA and IIB (Horbelt et al., 2015). LDN193189 has previously been applied to block BMP signaling during placode development in zebrafish embryos as well as during the formation and differentiation of human multipotent pre-placodal progenitors (Leung et al., 2013; Nikaido et al., 2017). To ensure that LDN193189 blocks the BMP pathway in cultured embryonic mice, we have tested whether this inhibitor is capable of preventing the expression of the BMP downstream effectors Msx1/2. The antibody used for this purpose (anti-Msx1/2 antibody 4G1, Developmental Studies Hybridoma Bank, Iowa City, IA, United States, lot 2/7/19, RRID: AB_531788) was raised against bacterially expressed chicken Msx2 and recognizes both Msx1 and Msx2 (Liem et al., 1995). Its specificity in chicken and mouse embryos has been further characterized in numerous publications, for example by comparison with *Msx1 in situ* hybridizations or Msx1-nlacZ expression patterns (Hu et al., 2008; Yamagishi et al., 2020). Physiologically, in E9.5 mouse embryos, Msx1/2 are expressed in dorsal parts of the hindbrain as well as in the mesenchyme of the first branchial arch (Coudert et al., 2005). These two expression sites are precisely what we can detect in our cultured control embryos by immunohistochemistry (**Supplementary Figure 1**). Silencing BMP4 by implantation of noggin-filled beads leads to a marked downregulation of *Msx1* in the mesenchyme of the first branchial arch (Tucker et al., 1998). Correspondingly, we demonstrate that the expression levels of Msx1/2 in branchial arch 1 decrease in a dose-dependent manner following exposure to increasing amounts of LDN193189 (**Supplementary Figure 1**). We conclude that LDN193189 indeed inhibits the BMP pathway.

For immunohistochemical detection of Ngn proteins, we applied either the goat anti-Ngn1 antibody (sc-19231, Santa Cruz, Dallas, TX, United States, lot C1215, RRID: AB_2298242) or the mouse anti-neurogenin-2 (Ngn2) antibody (clone 7G4, MAB3314, R&D Systems, lot WWI01, RRID: AB_2149520). The anti-Ngn1 antibody was raised against the peptide ARLQPLASTSGLSVPARRSAK mapping near the N-terminus of mouse Ngn1. It specifically detects a single band of about 19 kDa in Western blots of mouse brain extracts (manufacturer's information). Specific labeling of Ngn1 in mouse tissue sections has already been demonstrated in our previous work on the development of lateral line placodes in mice (Washausen and Knabe, 2018). Additional evidence comes from studies on the regeneration of mouse olfactory epithelium following exposure to methyl bromide (Krolewski et al., 2013, and references therein). Here, findings demonstrated by anti-Ngn1 immunohistochemistry were compared to *Ngn1*

in situ hybridization data and, additionally, validated by studying the distribution patterns of enhanced green fluorescent protein (eGFP) in *Ngn1-eGFP* bacterial artificial chromosome transgenic mice. The anti-Ngn2 antibody was raised against a recombinant protein of the N-terminal basic helix-loop-helix domain of mouse *Ngn2* (Lo et al., 2002). It specifically detects Ngn2 in Western blots of embryonic mouse cortices (Ge et al., 2006), but does not produce immunolabeling in the retinae of postnatal *Ngn2* knock-out mice (Kowalchuk et al., 2018). Correspondingly, this antibody has been successfully used to characterize epibranchial neurogenesis in mice (Washausen and Knabe, 2013, 2018; Zhang et al., 2017). For specific labeling of neural crest cells, we used the mouse anti-Sox10 antibody sc-365692 from Santa Cruz Biotechnology (lot I0516, RRID: AB_10844002). All data required to characterize this antibody as well as the corresponding staining protocol have been provided in Washausen and Knabe (2018). The same applies to the anti-Pax8 antibody (clone BC12, ACI 438, Biocare Medical, Concord, CA, United States, lot 051712, RRID: AB_2864457) used to label epibranchial placode (precursor) cells (Washausen and Knabe, 2017).

Whole Embryo Culture

Whole embryo culture was performed as has been described previously (Washausen and Knabe, 2018). The roller culture apparatus (BTC Engineering, Cambridge, United Kingdom) was connected to a gas mixing device (Gmix31, HiTec Zang, Herzogenrath, Germany) providing continuous gas supply (25 ml/min). Male Sprague Dawley rat serum was purchased from Janvier Labs and used as culture medium. Prior to the onset of embryo culture, heat-inactivated (56°C, 30 min) and centrifuged (2,000 × *g*, 10 min) culture medium was sterilely filtered, mixed with 0.25% antibiotic-antimycotic mix (15240096, Thermo Fisher Scientific, Schwerte, Germany), and equilibrated with 40% O_2, 5% CO_2, and 55% N_2 for at least 1 h. Using a stereomicroscope (M165 FC, Leica, Wetzlar, Germany) in a laminar flow hood, mouse embryos were dissected in Hank's balanced salt solution (L2035, Biochrom, Berlin, Germany) leaving the yolk sac and the ectoplacental cone intact. Embryos were then photographed with a digital camera (DFC450 C, Leica), and head lengths were measured using ImageJ (Rasband, 1997-2018). According to the developmental tables provided by van Maele-Fabry et al. (1993), all embryos were staged. Only those possessing 9–14 pairs of somites were transferred to the culture system (2–4 embryos per bottle, about 1 embryo/ml culture medium). Immediately prior to this transfer, culture bottles had been alternately supplemented either (1) with one of the two tested pan-FGFR inhibitors (SU5402, PD173074), or (2) with anti-FGFR3 neutralizing antibodies, or (3) with the pan-BMPR inhibitor LDN193189, or (4) exclusively with 0.1% DMSO for control. Working solutions (administered with 0.1% DMSO) were used as follows: 20, 40, or 80 μM SU5402; 0.5 or 2.5 μM PD173074; 5, 20, or 40 μg/ml anti-FGFR3 neutralizing antibodies; and 2, 5, or 10 μM LDN193189. Embryos were randomly assigned to each treatment group and incubated at 37.5°C (30 rpm) for 24 h in the dark. After 15 h, the continuous gas supply (40% O_2, 5% CO_2, and 55% N_2) was modified to 70% O_2 and 25% N_2. At the end of the 24 h culture period, development of the embryos was analyzed according to the criteria published by van Maele-Fabry et al. (1990, 1993). Furthermore, stereomicrographs of the embryos were acquired to measure the yolk sac diameter as well as head and crown-rump lengths using ImageJ (**Table 1**). Following fixation in 4% paraformaldehyde in phosphate buffered saline at pH 7.4 for 24 h, the embryos were pre-embedded in 1% Seakem LE agarose (50001, Lonza, Köln, Germany) and, afterward, routinely embedded in Surgipath Formula "R" paraffin (3801450, Leica). Finally, whole specimens were serially sectioned at 5 μm. In order to facilitate staining of adjacent sections with different primary antibodies, consecutive serial sections were alternately placed on two sets of slides (Knabe et al., 2002).

Immunohistochemistry

Neurogenin-2 and Ngn1 immunostainings were carried out according to the protocols published in Washausen and Knabe (2013, 2018). In brief, for epitope retrieval, deparaffinized and rehydrated sections were treated in a high-pressure cooker in 10 mM citrate buffer (pH 6). Activity of endogenous peroxidases was blocked by incubation in 1% H_2O_2 and 0.3% Triton X-100 in Tris-buffered saline (TBS) (pH 7.4) for 30 min. Washing steps were carried out by rinsing slides three times with TBS for 5 min each. For Ngn2 immunohistochemistry, we used the mouse-on-mouse (M.O.M.) immunodetection kit (BMK-2002, Vector Laboratories, Burlingame, CA, United States) and performed protein blocking steps as well as incubations with anti-Ngn2 (dilution of 1:20,000, incubation overnight at 4°C) and secondary antibodies accordingly. The anti-Ngn1 antibody was applied at 1:100 in Dako REAL diluent (S202230-2, Agilent Technologies, Waldbronn, Germany) for 4 h at 37°C and detected with a biotinylated horse anti-goat antibody (1:100; BA-9500, Vector Laboratories, RRID: AB_2336123). Finally, for both Ngn2 and Ngn1 immunohistochemistry, sections were incubated with the avidin-biotin complex peroxidase reagent (PK-7100, Vector Laboratories) for 1 h. Following color reaction with 3,3′-diaminobenzidine (D5637, Merck), sections were counterstained in Mayer's hematoxylin (Romeis, 1948), and embedded with DePeX mounting medium (18243, Serva, Heidelberg, Germany). Negative controls performed without primary antibodies revealed the absence of immunolabeling.

Histological Analysis

In total, 104 completely serially sectioned embryos were examined. These embryos were distributed among the treatment groups as follows: pan-FGFR inhibitor SU5402 (20 μM: $n = 7$, 40 μM: $n = 16$, 80 μM: $n = 7$); pan-FGFR inhibitor PD173074 (0.5 μM: $n = 16$, 2.5 μM: $n = 9$); anti-FGFR3 neutralizing antibodies (5 μg/ml: $n = 6$, 20 μg/ml: $n = 7$, 40 μg/ml: $n = 4$); pan-BMPR inhibitor LDN193189 (2 μM: $n = 5$, 5 μM: $n = 5$, 10 μM: $n = 8$); control with 0.1% DMSO only ($n = 14$). Thickenings of the placodal ectoderm, outgrowth of the pharyngeal pouches and formation of the branchial membranes could be optimally diagnosed in the hematoxylin counterstained serial sections. Epibranchial neurogenic activity was assessed by

TABLE 1 | Developmental characteristics of 9–14 somite mouse embryos cultured for 24 h.

	Control	pan-FGFR inhibition					FGFR3 blocking			BMPR inhibition		
	DMSO	SU5402			PD173074		α-FGFR3			LDN193189		
	0.1% *n* = 14	20 μM *n* = 7	40 μM *n* = 16	80 μM *n* = 7	0.5 μM *n* = 16	2.5 μM *n* = 9	5 μg/ml *n* = 6	20 μg/ml *n* = 7	40 μg/ml *n* = 4	2 μM *n* = 5	5 μM *n* = 5	10 μM *n* = 8
Yolk sac diameter [mm]	3.2 3.0–3.3	3.1 3.0–3.1	3.0* 2.9–3.1	2.9* 2.8–3.0	3.0 2.9–3.3	2.7** 2.7–2.9	3.1 2.8–3.3	3.1 2.9–3.3	3.1 3.0–3.4	3.0 2.9–3.3	3.2 3.1–3.4	3.0 2.8–3.2
Crown-rump length [mm]	3.1 3.1–3.2	2.9* 2.7–3.0	2.7** 2.6–2.7	2.5** 2.3–2.7	3.0* 2.8–3.1	2.1** 2.1–2.2	3.1 2.8–3.6	3.0 2.7–3.4	3.1 3.0–3.3	3.3 2.8–3.5	3.2 2.9–3.4	2.9 2.9–3.3
Head length [mm]	1.9 1.8–1.9	1.6* 1.3–1.6	1.3** 1.2–1.3	1.1** 1.0–1.4	1.8 1.6–1.9	1.4** 1.4–1.4	1.7 1.5–2.0	1.7 1.4–1.9	1.8 1.6–2.0	1.9 1.5–2.0	1.7 1.6–1.9	1.6 1.5–1.8
Number of somites	27.3 26.0–28.0	24.5* 24.0–26.0	24.0** 23.0–26.0	22.0** 21.0–24.5	25.8 25.0–28.5	20.0** 19.5–21.0	26.5 25.5–29.0	26.5 24.5–27.0	28.5 26.5–29.5	26.0* 25.0–26.5	28.0 26.0–29.0	25.5* 24.0–26.3

Medians and interquartile ranges are given.
*Asterisks indicate significant differences between each treatment group and the respective control (Mann–Whitney test: *P < 0.05, **P < 0.001).*
BMPR, bone morphogenetic protein receptor; DMSO, dimethyl sulfoxide; FGFR, fibroblast growth factor receptor.

separately analyzing Ngn2 and Ngn1 expression patterns on both sides of the embryonic body (section intervals: 10 μm). Only immunoreactive nuclei of those neuroblasts were counted that either resided in the epibranchial placode or were still in contact with the placode as emigrating ones. An exception to this is found in 3D reconstructions, where, due to the scientific question to be answered, an even stricter distinction must be made between (1) intraplacodal neuroblasts, (2) delaminating neuroblasts, and (3) neuroblasts that have already reached the mesenchyme adjacent to the placodes. In cases where exposure to the inhibitors suppressed the proper development of placodal thickenings and/or intact branchial membranes, prospective positions of the epibranchial placodes were determined by optically projecting the positions of underdeveloped pharyngeal pouches onto the opposing surface ectoderm. Furthermore, the entire branchial region was screened for $Ngn2^+$ or $Ngn1^+$ neuroblasts. $Ngn2^+$ or $Ngn1^+$ neuroblasts in the spinal cord as well as $Ngn1^+$ neuroblasts in the trigeminal and otic placodes served as internal positive controls (Sommer et al., 1996; Fode et al., 1998; Ma et al., 1998). For each experimental group, 8–20 Ngn2- or Ngn1-immunostained epibranchial placodes were evaluated, respectively. Thus, the number of samples in all treatment groups corresponds to that which has been investigated in similar studies (e.g., Lassiter et al., 2009; Brown and Epstein, 2011).

Statistics

Statistical analyses and creation of box plots were carried out in STATISTICA 13.3 (TIBCO Software, Munich, Germany). Initially, the Kolmogorov-Smirnov and the Levene's test were applied to check normality and homogeneity of variances, respectively. Since not all of the cases examined satisfied both conditions, we selected the non-parametric Mann–Whitney test (two-sided) for comparison of the differences between general developmental characteristics or neuroblast numbers following different treatments. *P* values < 0.05 were regarded as statistically significant.

Photomicrographs and Figures

Whole embryos were photographed using the Leica Application Suite (LAS) 4.6 software with a M165 FC stereomicroscope and a DFC450 C camera (both from Leica). Images of histological sections were acquired with the KS400 3.0 software using an Axioskop 2 MOT microscope and an AxioCam HR digital camera (Carl Zeiss, Göttingen, Germany). Following background and shading corrections in the respective imaging software, digital photographs were cropped and adjusted for brightness, color balance, and sharpness in Photo-Paint 2019 (Corel, Unterschleißheim, Germany). All image adjustments were carried out on the entire images without changing, removing or inserting specific features within the photographs. All figures and lettering were composed using CorelDraw 2019 (Corel). 3D reconstructions were created in the reconstruction and modeling software Free-D 1.15 (Andrey and Maurin, 2005).

RESULTS

Mouse embryos possessing 9–14 pairs of somites were cultured for 24 h in the presence of pan-FGFR inhibitors, anti-FGFR3 neutralizing antibodies, or the pan-BMPR inhibitor LDN193189, respectively (**Figure 1** and **Table 1**). First, we have determined whether the pan-FGFR inhibitors SU5402 and PD173074 interfere with known FGF-dependent developmental steps of the forebrain and limb buds (Paek et al., 2009; Ornitz and Itoh, 2015; **Figure 1A**). Application of high doses of PD173074 (2.5 μM) disturbed the outgrowth of telencephalic hemispheres and limb buds (**Figure 1B**). In contrast, neither low dose exposure to PD173074 (0.5 μM; **Figure 1C**) nor application of SU5402 (20, 40, or 80 μM; **Figure 1D**) triggered such specific defects. Generalized growth retardation, as revealed by decreases in yolk sac diameter, crown-rump length, head length and number of somites (**Table 1**), was caused by SU5402 (**Figure 1D**) or high doses of PD173074 (2.5 μM; **Figure 1B**), but not by low doses of PD173074 (0.5 μM; **Figure 1C**) or by anti-FGFR3 neutralizing antibodies (**Figure 1E**). Embryos treated with the pan-BMPR inhibitor LDN193189 did not reveal statistically significant growth defects except for slight reductions of their somite numbers (**Table 1** and **Figure 1F**).

In a second step, we have investigated whether the formation of pharyngeal pouches is disturbed in the presence

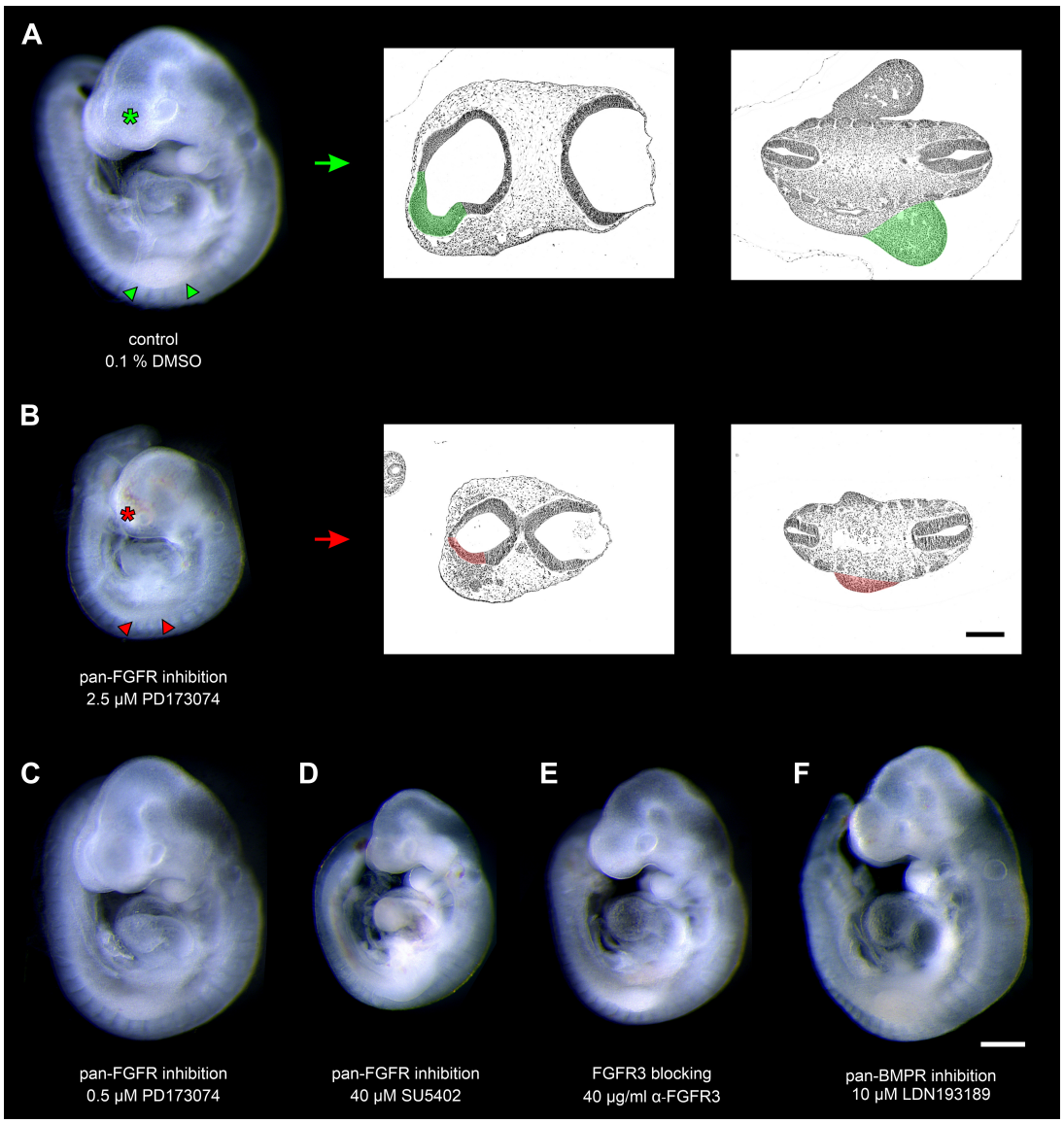

FIGURE 1 | Nine to fourteen somite mouse embryos, cultured for 24 h. **(A)** Control embryo, exposed to the solvent dimethyl sulfoxide (DMSO) only, reveals age-appropriate telencephalic hemispheres (green asterisk) and upper limb buds (green arrowheads); for comparison (green arrow), see corresponding hematoxylin stained histological sections (green colored areas). **(B)** Treatment with 2.5 µM of the pan-FGFR inhibitor PD173074 considerably impairs the development of telencephalic hemispheres (red asterisk) and upper limb buds (red arrowheads); for comparison (red arrow), see corresponding hematoxylin stained histological sections (red colored areas). **(C)** Application of 0.5 µM PD173074 did not cause any obvious abnormalities. **(D)** Embryos incubated with 40 µM of the pan-FGFR inhibitor SU5402 exhibit general growth disturbances (also see **Table 1**). **(E,F)** Treatment with 40 µg/ml of anti-FGFR3 neutralizing antibodies or 10 µM of the pan-BMPR inhibitor LDN193189 were well tolerated. Scale bars: 500 µm for stereomicrographs **(A–F)**, 200 µm for light micrographs **(A,B)**.

of pan-FGFR inhibitors, anti-FGFR3 neutralizing antibodies or the pan-BMPR inhibitor LDN193189. This question is justified for at least three reasons. Firstly, morphogenesis and neurogenesis of epibranchial placodes depend on signals produced by intact pharyngeal pouches (Ladher et al., 2010). Secondly, in zebrafish, FGF and BMP signaling promote pharyngeal pouch formation (Crump et al., 2004; Nechiporuk et al., 2005; Lovely et al., 2016; Li et al., 2019). Thirdly, pharyngeal pouches 3 and 4 are malformed in *Fgf8* hypomorphic mice (Abu-Issa et al., 2002; Frank et al., 2002). Control embryos demonstrated proper formation of all pharyngeal pouches (**Figures 2A–D**). Resembling *in utero* developed embryos, pharyngeal pouch 4 approached, but did not contact the branchial ectoderm (**Figure 2D**). Embryos exposed to low doses of PD173074 (0.5 µM) largely matched the controls according to morphological criteria (**Figures 2E–H**). As an exception, 3D reconstructions and additional serial section analyses revealed that 5 out of 20 body sides (25%) of the embryos treated with low doses of PD173074 presented varying degrees of (mostly discrete) segmentation defects of the pharyngeal pouches 2 and

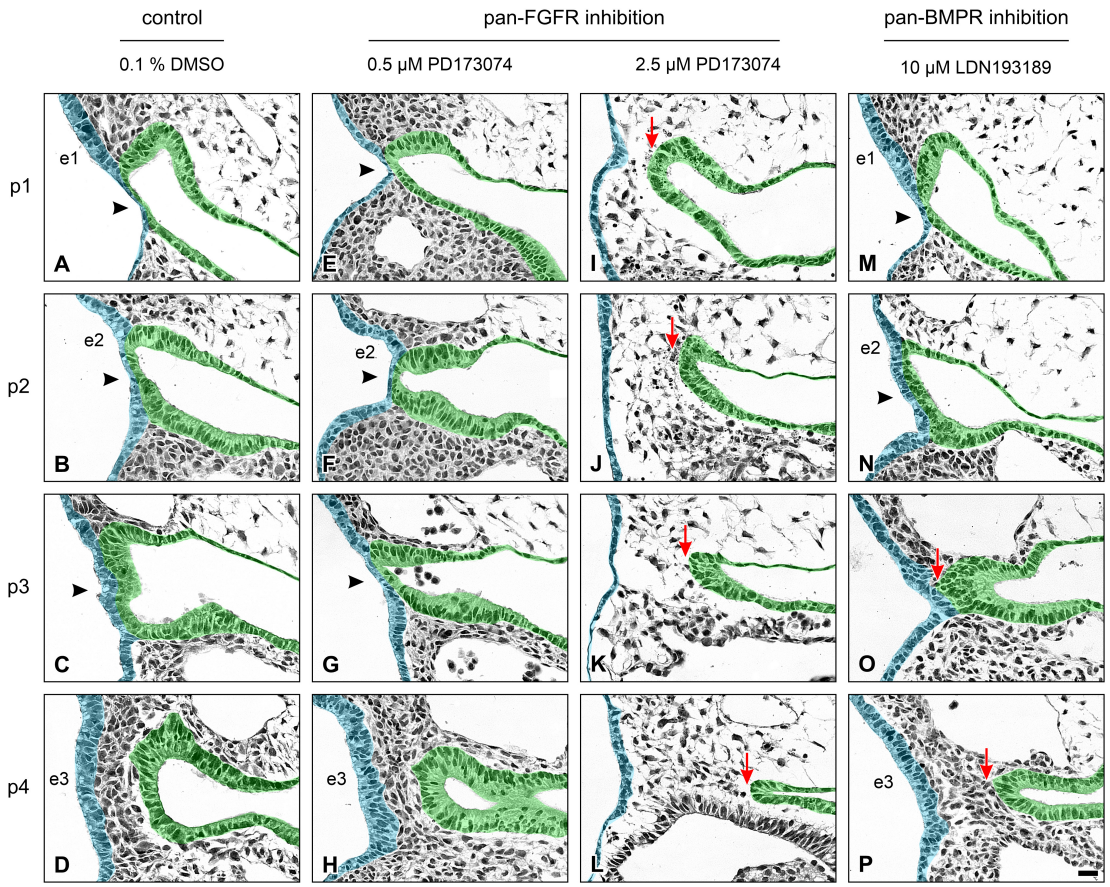

FIGURE 2 | Impact of FGFR or BMPR inhibition on the development of pharyngeal pouches (p1–p4) in 9–14 somite mouse embryos, cultured for 24 h. Hematoxylin stained sections show the pharyngeal pouches (green), the overlying ectoderm (blue), the three epibranchial placodes (e1–e3), and the branchial membranes 1–3 (black arrowheads). **(A–D)** Control embryos: Age-appropriate lateral outgrowth of the pharyngeal pouches 1–4, whereby the latter physiologically does not fuse with the overlying ectoderm to form a "branchial membrane 4". **(E–H)** Embryos incubated with 0.5 µM of the pan-FGFR inhibitor PD173074 develop largely normal pharyngeal pouches. **(I–L)** Treatment with 2.5 µM PD173074 prevents proper outgrowth of all pharyngeal pouches (red arrows). Neither branchial membranes nor epibranchial placodes are discernible. **(M–P)** Following application of the pan-BMPR inhibitor LDN193189, pharyngeal pouches 1 and 2 develop normally, whereas lateral outgrowth of the pharyngeal pouches 3 and 4 is impaired (red arrows) with pharyngeal pouch 3 contacting the ectoderm in one single histological serial section, if at all. Scale bar: 20 µm.

3 (see below). In only 2 other body sides (10%) these defects were severe enough to no longer allow a full distinction between the branchial membranes 2 and 3. In contrast, high doses of PD173074 (2.5 µM) impaired the lateral outgrowth of all four pharyngeal pouches (**Figures 2I–L**). Consequently, branchial membranes were absent. Morphologically normal pharyngeal pouches were again found in all embryos incubated with SU5402 or anti-FGFR3 neutralizing antibodies, respectively (data not shown). Finally, embryos exposed to moderate or high, but not low, doses of the pan-BMPR inhibitor LDN193189 (5 or 10 µM) displayed obvious defects of the pharyngeal pouches 3 and 4, but not 1 and 2 (**Figures 2M–P**).

Next, we have analyzed whether pan-FGFR inhibitors, anti-FGFR3 neutralizing antibodies or the pan-BMPR inhibitor LDN193189 affect epibranchial placode morphogenesis. Resembling *in utero* developed E9.5 to E10 embryos (Washausen and Knabe, 2013, 2017), control embryos cultured for 24 h revealed three pairs of high-grade thickened epibranchial placodes (pseudostratified epithelium with up to four rows of nuclei, **Figures 3A–C**). In contrast, treatment with 40 µM SU5402 already causes slight decreases in the thickness of EP1 and EP2 (**Figures 3D–F**). Correspondingly, embryos treated with low doses of PD173074 (0.5 µM) presented considerably thinned-out EP1 and EP2 (**Figures 3G,H**), whereas EP3 remained high-grade thickened (**Figure 3I**). High doses of PD173074 (2.5 µM) prevented the development of high-grade ectodermal thickenings in the positions of all three epibranchial placodes (**Figures 3J–L**). Embryos incubated with anti-FGFR3 neutralizing antibodies exhibited three regularly formed epibranchial placodes (**Figures 3M–O**). BMPR inhibition with LDN193189 (10 µM) led to an obvious, but moderate thinning only in EP3 (**Figures 3P–R**).

Numbers and distribution patterns of $Ngn2^{+}$ epibranchial neuroblasts in control embryos (**Figures 3A–C**, **4A–C**) matched with those found in *in utero* developed embryos (Washausen and Knabe, 2013). Application of increasing doses of SU5402

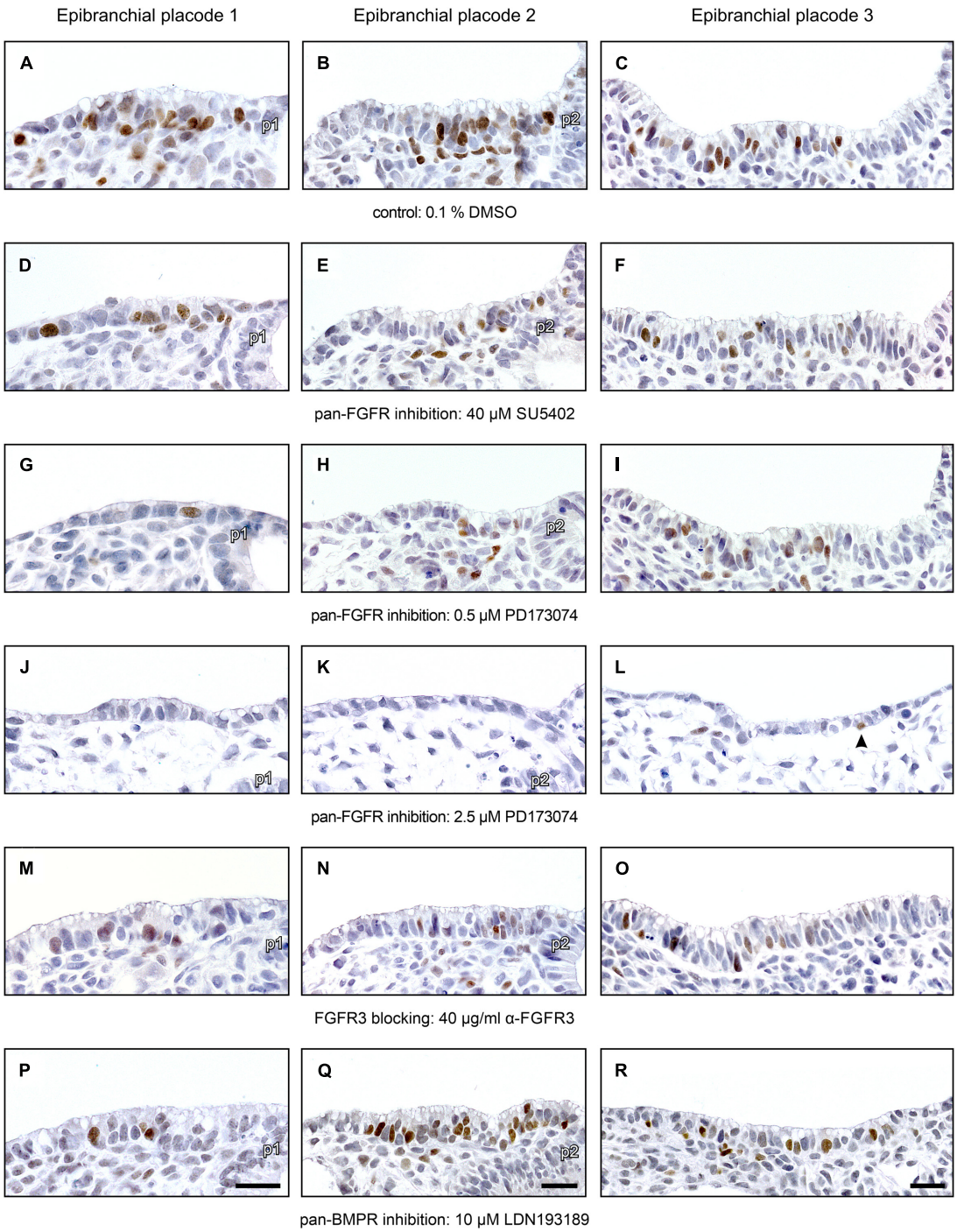

FIGURE 3 | Impact of FGFR and BMPR inhibition on epibranchial placode morphogenesis and neurogenesis in 9–14 somite mouse embryos, cultured for 24 h. Anti-Neurogenin-2 (Ngn2) immunohistochemistry (brown precipitate); shown are maximum numbers of $Ngn2^+$ neuroblasts found per section. **(A–C)** Control placodes reveal high-grade thickened pseudostratified epithelium (2–4 cell nuclei) with 12–16 $Ngn2^+$ neuroblasts. **(D–F)** Pan-FGFR inhibitor SU5402 (40 µM) causes moderate reductions in placode thickness and statistically significant decreases in neuroblast numbers in the epibranchial placodes 1 and 2, but not 3 (also see **Figure 4**). **(G–I)** Pan-FGFR inhibitor PD173074 (0.5 µM) elicits strong decreases in the thickness of the epibranchial placodes 1 and 2 as well as statistically significant decreases in neuroblast numbers in all three epibranchial placodes (also see **Figure 4**). **(J–L)** High doses of PD173074 (2.5 µM) result in the complete absence of high-grade thickened epibranchial placodes. Only single $Ngn2^+$ neuroblasts can be detected, if at all (arrowhead in panel **L**). **(M–O)** Anti-FGFR3 neutralizing antibodies (40 µg/ml) reduce $Ngn2^+$ neuroblast numbers, but do not have negative effects on placode thickness. **(P–R)** Following pan-BMPR inhibition (10 µM LDN193189), epibranchial placode 1 reveals reduced numbers of $Ngn2^+$ neuroblasts, but normal morphology **(P)**; epibranchial placode 2 lacks any obvious impairment **(Q)**; epibranchial placode 3 simultaneously presents slight reductions in $Ngn2^+$ neuroblast numbers and placode thickness **(R)**. p1, p2, pharyngeal pouches 1 and 2. Scale bars: 20 µm.

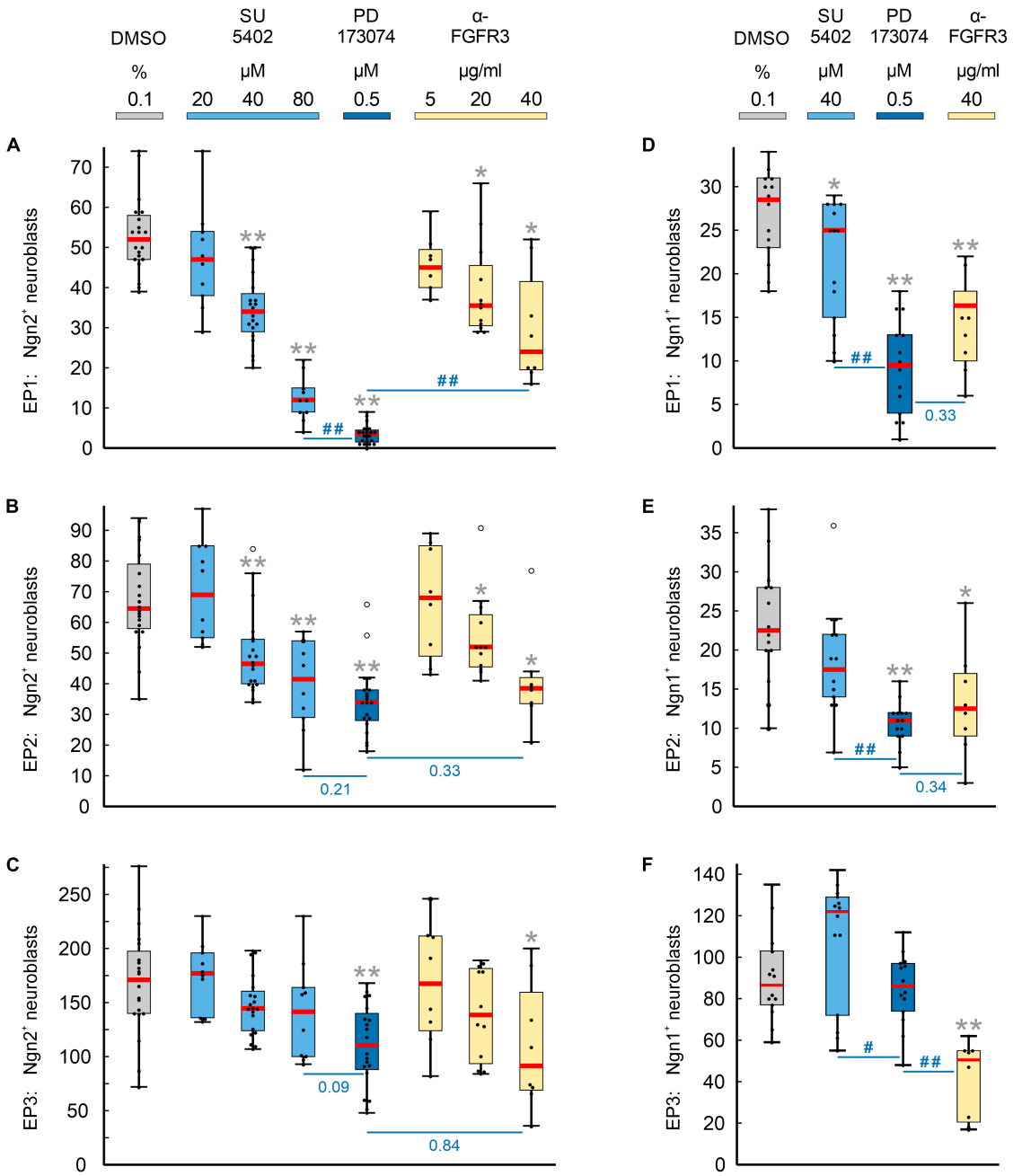

FIGURE 4 | Impact of FGFR inhibition on the neurogenesis of epibranchial placodes (EP) in 9–14 somite mouse embryos, cultured for 24 h. Box plots indicate the numbers of Neurogenin (Ngn)2$^+$ **(A–C)** or Ngn1$^+$ **(D–F)** neuroblasts in EP1 **(A,D)**, EP2 **(B,E)**, or EP3 **(C,F)** following exposure to either dimethyl sulfoxide (DMSO) only (control; gray), or increasing doses of pan-FGFR inhibitor SU5402 (light blue), or 0.5 μM of pan-FGFR inhibitor PD173074 (dark blue), or increasing concentrations of anti-FGFR3 neutralizing antibodies (yellow). Significant differences between each treatment group and the controls are indicated by gray asterisks (*$P < 0.05$, **$P < 0.001$; Mann–Whitney test). Additionally, PD173074-treated embryos were compared to groups exposed to either highest levels of SU5402 or anti-FGFR3 antibodies (significant differences: #$P < 0.05$, ##$P < 0.001$; or specific P values, respectively). Whiskers, lower and upper extremes; box limits, 25th and 75th percentiles; red center lines, medians; black dots, data points; open circles, outliers.

resulted in graded decreases of Ngn2$^+$ neuroblasts in all three epibranchial placodes (**Figures 3D–F**, **4A–C**). Taking the respective medians as reference values (**Table 2**), decreases were strongest in EP1 (−77%), much more moderate in EP2 (−36%), and without statistical significance in EP3 (−18%). That, in fact, EP1 is much more dependent on FGF signaling than EP2 and EP3 came out even clearer when embryos were exposed to low doses of PD173074 (**Figures 3G–I**, **4A–C**). Compared to controls, decreases of Ngn2$^+$ neuroblasts amounted to −93% (EP1), −47% (EP2), and −35% (EP3), respectively. Compared

to the highest dose of SU5402 used here, exposure to low doses of PD173074 led to significantly stronger reduced numbers of Ngn2$^+$ neuroblasts only in EP1.

Whether and to what extent subtypes of FGFRs are expressed in the epibranchial placodes of mice is largely unknown. As an exception, Trokovic et al. (2005) demonstrated that neurogenesis in EP1, but not EP2 and EP3, substantially depends on FGFR1. We have investigated the impact of FGFR3 blockage on epibranchial neurogenesis. Exposure to high doses of anti-FGFR3 neutralizing antibodies (40 μg/ml) significantly decreased the number of Ngn2$^+$ neuroblasts in all three epibranchial placodes (**Figures 3M–O**, **4A–C** and **Table 2**). However, only in EP1 did these decreases lag significantly behind those achieved by low doses of PD173074 (**Figure 4A**). We conclude that FGF-dependent neurogenesis in EP2 and EP3 predominantly occurs via FGFR3 whereas, in EP1, it is controlled by (at least) FGFR1 (Trokovic et al., 2005) and FGFR3 (present results).

In the epibranchial neuroblasts of mice, expression of *Ngn1* is downstream of *Ngn2* in EP1, EP2 and, partly, in EP3. In the latter, a second subpopulation of neuroblasts upregulates *Ngn1* independently of *Ngn2* (Fode et al., 1998). We aimed to find out, whether incubation with pan-FGFR inhibitors, anti-FGFR3 neutralizing antibodies or the pan-BMPR inhibitor LDN193189 provides additional evidence for the existence of differently regulated subpopulations of epibranchial neuroblasts. In line with findings obtained from *in utero* developed embryos (Fode et al., 1998), the number of Ngn1$^+$ neuroblasts in our control embryos reached only about 55% (EP1), 35% (EP2), and 52% (EP3) of the respective numbers of Ngn2$^+$ neuroblasts (**Figure 4** and **Table 2**). SU5402 (40 μM) caused significant decreases of Ngn1$^+$ neuroblasts only in EP1 (**Figures 4D–F**). Exposure to low doses of PD173074 significantly reduced the number of Ngn1$^+$ neuroblasts in EP1 and EP2 (**Figures 4D,E**). It was only EP3 that deviated from this "pattern" in that neither SU5402 (40 μM) nor low doses of PD173074 resulted in significant decreases of Ngn1$^+$ neuroblasts (**Figure 4F** and **Table 2**). Exposure to anti-FGFR3 neutralizing antibodies (40 μg/ml) significantly reduced the number of Ngn1$^+$ (and Ngn2$^+$) neuroblasts in all three epibranchial placodes (**Figures 3M–O**, **4**). However, when comparing the effects resulting from treatments with low doses of PD173074 or anti-FGFR3 neutralizing antibodies, respectively, we found placode-specific responses of Ngn1$^+$ neuroblasts. In EP1 and EP2, statistically significant decreases in Ngn1$^+$ neuroblasts were not observed (**Figures 4D,E**). In contrast, significantly stronger reductions in the number of Ngn1$^+$ neuroblasts occurred in EP3 following incubation with anti-FGFR3 neutralizing antibodies (40 μg/ml; **Figure 4F**).

Next, we have investigated whether the pan-BMPR inhibitor LDN193189 affects epibranchial neurogenesis in mice (**Figure 5**). Significant decreases in Ngn2$^+$ neuroblasts were already observed following treatments with 2 μM (EP1, **Figure 5A**) or 5 μM (EP1, EP3; **Figures 5B,C**). Correspondingly, incubation with 10 μM LDN193189 significantly reduced the numbers of Ngn2$^+$ and Ngn1$^+$ neuroblasts in EP1 (approximately −90%) and EP3 (approximately −40%; **Table 2**). In contrast, LDN193189 was unable to significantly lower the numbers of Ngn1$^+$ and Ngn2$^+$ neuroblasts in EP2 (**Figures 5B,E** and **Table 2**).

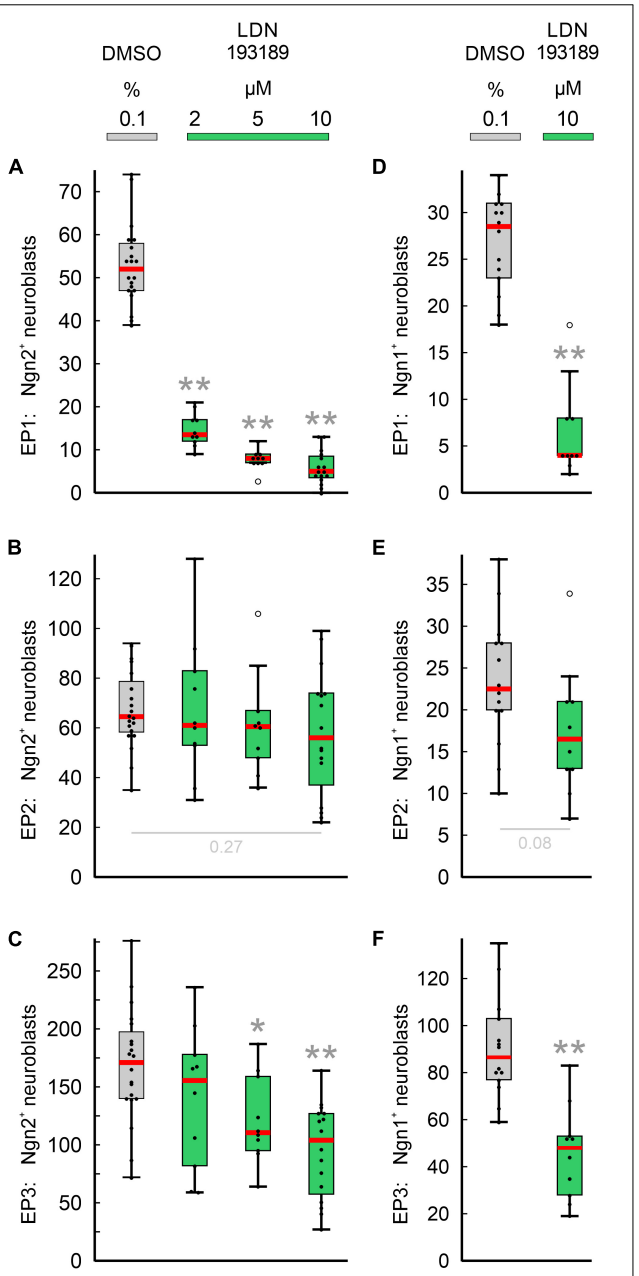

FIGURE 5 | Impact of pan-BMPR inhibition on the neurogenesis of epibranchial placodes (EP) in 9–14 somite mouse embryos, cultured for 24 h. Box plots indicate the numbers of Neurogenin (Ngn)2$^+$ **(A–C)** or Ngn1$^+$ **(D–F)** neuroblasts in EP1 **(A,D)**, EP2 **(B,E)**, or EP3 **(C,F)** following exposure to either dimethyl sulfoxide (DMSO) only (control; gray), or increasing doses of LDN193189 (green). Significant differences between each treatment group and the controls are indicated by gray asterisks (*$P < 0.05$, **$P < 0.001$; Mann–Whitney test). Whiskers, lower and upper extremes; box limits, 25th and 75th percentiles; red center lines, medians; black dots, data points; open circles, outliers.

Finally, we would like to point out that in almost all cases where FGFR inhibitors led to massive disturbances in

TABLE 2 | Relative changes of neuroblast numbers in the epibranchial placodes of 9–14 somite mouse embryos cultured for 24 h.

	Control	pan-FGFR inhibition				FGFR3 blocking		BMPR inhibition	
	DMSO	SU5402		PD173074		α-FGFR3		LDN193189	
Ngn2$^+$	**0.1%** ***n* = 20**	**40 μM** ***n* = 20**	**80 μM** ***n* = 10**	**0.5 μM** ***n* = 20**	**2.5 μM** ***n* = 10**	**20 μg/ml** ***n* = 12**	**40 μg/ml** ***n* = 8**	**5 μg/ml** ***n* = 10**	**10 μg/ml** ***n* = 16**
EP1	**52**	−34.6% **	−76.9% **	−93.2% **	−100% **	−31.7% *	−53.8% *	−84.6% **	−90.4% **
EP2	**64.5**	−27.9% **	−35.7% **	−47.3% **	−100% **	−19.4% *	−40.3% *	−6.2%	−13.2%
EP3	**171**	−15.5%	−17.5%	−35.4% **	−98.8% **	−19.0%	−46.5% *	−35.4% *	−39.2% **
Ngn1$^+$	**0.1%** ***n* = 14**	**40 μM** ***n* = 14**		**0.5 μM** ***n* = 14**	**2.5 μM** ***n* = 8**	**40 μg/ml** ***n* = 8**		**10 μg/ml** ***n* = 10**	
EP1	**28.5**	−14.0% *		−66.7% **	−57.9% **	−50.9% **		−86.0% **	
EP2	**22.5**	−22.2%		−51.1% **	−100% **	−44.4% *		−26.6%	
EP3	**86.5**	+41.0%		−0.6%	−96.5% **	−41.6% **		−44.5% **	

*Medians (bold numbers, provided for controls) served as reference values for calculating the changes (%) in neuroblast numbers for each treatment group. Asterisks indicate significant differences between each treatment group and the respective control (Mann–Whitney test: *P < 0.05, **P < 0.001; also see **Figures 4**, **5**). BMPR, bone morphogenetic protein receptor; DMSO, dimethyl sulfoxide; FGFR, fibroblast growth factor receptor; Ngn1, Neurogenin1; Ngn2, Neurogenin2.*

the outgrowth of the pharyngeal pouches, Ngn2$^+$ or Ngn1$^+$ neuroblasts were virtually absent from the expected positions of the three epibranchial placodes (**Figures 3J–L**, and data not shown). As an exception, approximately 40% of Ngn1$^+$ neuroblasts persisted in EP1 (**Table 2**, also see discussion).

DISCUSSION

The present work shows that, in mice, epibranchial placode development is dependent on both FGF and BMP signaling as revealed by whole embryo culture experiments using pan-FGFR inhibitors (SU5402, PD173074), anti-FGFR3 neutralizing antibodies and the pan-BMPR inhibitor LDN193189 (**Figure 6**). The most parsimonious hypothesis would have been that all three epibranchial placodes would respond in the same way to identical treatments. However, this hypothesis turned out to be unfounded. Furthermore, depending on the respective treatment, impaired epibranchial placodes occurred either in the presence or absence of malformed pharyngeal pouches which act as epibranchial signaling centers (Ladher et al., 2010). We therefore discuss potential implications of FGF and BMP signaling for epibranchial placode development in five consecutive steps.

Methodological Considerations

The pan-FGFR inhibitors SU5402 and PD173074 both block the ATP-binding pocket of the tyrosine kinase domains of the four known FGFR subtypes (Mohammadi et al., 1997, 1998; Raible and Brand, 2001; Kyono et al., 2011). SU5402 has often been used in studies dealing with placode development (Lassiter et al., 2014). In the meantime, it has become clear that substantial limitations must be considered when using SU5402. Firstly, SU5402 not only interferes with FGFRs but also potently blocks several off-target kinases. Secondly, SU5402 is rather toxic in the range of effective doses (Gudernova et al., 2016). Correspondingly, we observed growth impairments of our embryos already at 40 μM SU5402 (**Figure 1D** and **Table 1**), a dose that is commonly applied during the developmental period studied here (Corson et al., 2003; Calmont et al., 2006; Oki et al., 2010; Wang et al., 2015). Thirdly, SU5402 either works or remains without effect in a context-dependent manner (Oki et al., 2010). Fourthly, SU5402 suffers from poor tissue penetration (Ahrens and Schlosser, 2005). Consistent with these limitations, we were unable to reproduce FGF-dependent malformations of the forebrain (Paek et al., 2009), limb buds (Ornitz and Itoh, 2015) and pharyngeal pouches (Abu-Issa et al., 2002; Frank et al., 2002) using SU5402. However, compared to PD173074 which is less toxic and approximately 1000-fold more potent (Pardo et al., 2009; Lamont et al., 2011), SU5402 dose-dependently produced identical, albeit attenuated effects in the epibranchial placodes of mice (present results). Another argument in favor of the alternative use of SU5402 is that only through the separate use of SU5402 and PD173074 we were able to discover that some epibranchial placodes depend completely on FGF signals, while others do so only partially. Thus, low doses of PD173074 completely suppressed the production of Ngn2$^+$ neuroblasts in EP1 but, in EP2 and EP3, did not statistically significantly enhance the moderate decrease of Ngn2$^+$ neuroblasts achieved by the highest doses of SU5402 used here (80 μM).

Another methodological consideration addresses the question whether pharmacological inhibition of the FGF signaling pathway specifically affects branchial mesoderm patterning. The underlying hypothesis is based on the fact that *Fgf10* is upregulated in the branchial mesoderm by *Fgf3* and *Fgf8* (Alvarez et al., 2003; Wright and Mansour, 2003; Wright et al., 2004; Ladher et al., 2005; Aggarwal et al., 2006). FGF signaling in turn causes an upregulation of *Msx1* in the branchial mesoderm during exactly the developmental period we are looking for (Wakamatsu et al., 2019; one embryonic day later: Chen et al., 1996). Exposure of our embryos to 0.5 μM of the pan-FGFR inhibitor PD173074 already leads to a discrete attenuation of the Msx1/2 signal (**Supplementary Figure 2**). Correspondingly, only a few weak Msx$^+$ mesoderm cells remain in the (hypoplastic) branchial arches after treatment with 2.5 μM PD173074 (**Supplementary Figure 2**). These findings suggest that PD173074 indeed specifically interferes with FGF signaling in the branchial arch mesoderm of cultured mouse embryos. Quite similar dose-dependent malformations caused by PD173074 will be discussed in the context of pharyngeal pouch formation.

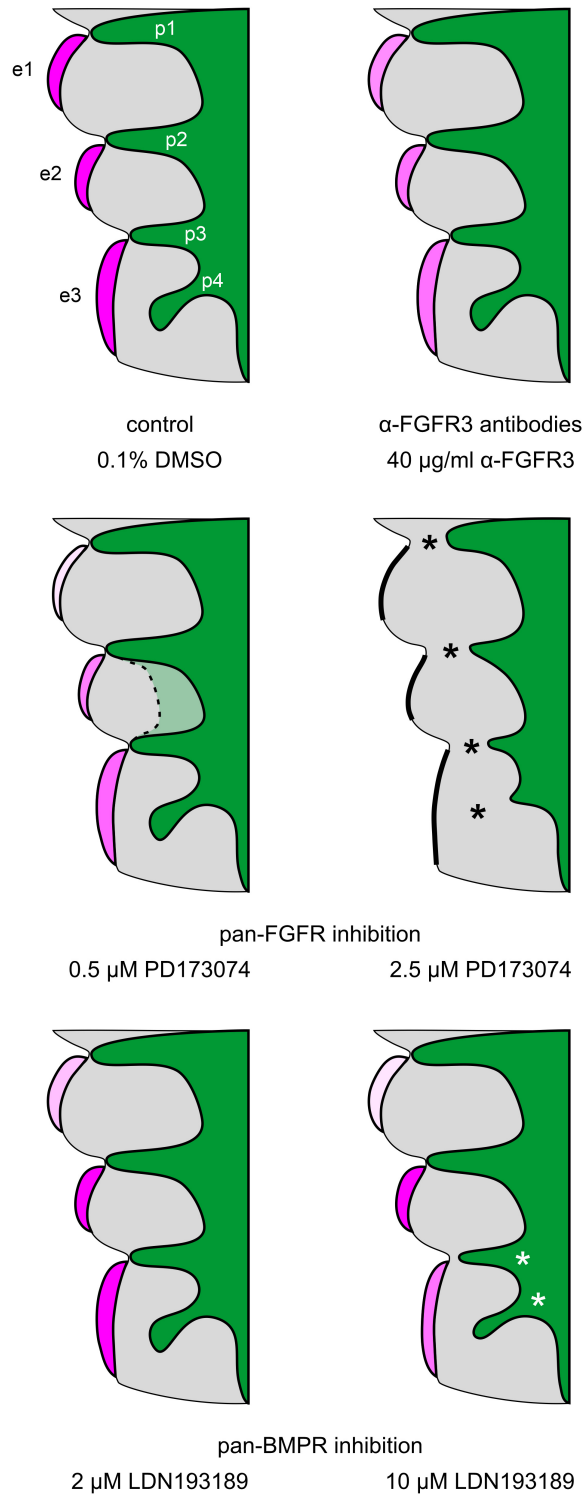

FIGURE 6 | Summary scheme: Impact of FGFR and BMPR inhibition on epibranchial placode morphogenesis and neurogenesis in 9–14 somite mouse embryos, cultured for 24 h. e1, e2, e3, epibranchial placodes 1, 2, and 3; p1, p2, p3, p4, pharyngeal pouches 1, 2, 3, and 4; green, endoderm; gray, branchial arches. Increasing intensities of purple color indicate increasing numbers of Neurogenin2$^+$ epibranchial neuroblasts. Different degrees of *(Continued)*

FIGURE 6 | (Continued)
placode thickness are represented schematically. Thick black lines, complete absence of epibranchial placodes; black or white asterisks, impaired lateral outgrowth of the pharyngeal pouches. The faint green area enclosed by the dashed line indicates that pharyngeal pouches 2 and 3 may show (mostly discrete) segmentation defects in some of the embryos treated with 0.5 µM of the pan-FGFR inhibitor PD173074 (for details, see text).

Impact of FGF Signaling on Epibranchial Placode Development

We first discuss to what extent low doses of PD173074 impair epibranchial placode development in mice. This treatment resulted in a statistically significant decrease of neuroblasts in EP1 (Ngn2$^+$, Ngn1$^+$), EP2 (Ngn2$^+$, Ngn1$^+$), and EP3 (Ngn2$^+$). Overall, the numbers of Ngn2$^+$ neuroblasts declined along a rostrocaudal gradient (EP1: −93%, EP2: −47%, and EP3: −35%; **Table 2**). Individually different responses of the epibranchial placodes to pan-FGFR inhibition were also found in zebrafish when SU5402 was applied in an equivalent time window (onset of treatment: 19–24 hpf). Thus, FGF-dependent neuroblast production is absent in EP2 and EP3$_1$, but decreases only mildly in EP1 as well as in the common anlage of EP3$_2$ to EP3$_4$ (Nechiporuk et al., 2005). Nevertheless, interspecies differences also may exist. For it was only in mice that reductions in neuroblast production were accompanied by significant or even complete reductions in placode thickness (EP1, EP2: **Figures 3G,H**; also see EP1 to EP3 following high doses of PD173074: **Figures 3J–L**; EP1, EP2 following SU5402: **Figures 3D,E**). Instead, structurally unaltered epibranchial placodes were observed in SU5402-treated zebrafish (Nechiporuk et al., 2005). One possible explanation for this latter difference might be that proliferation and neurogenesis follow different time schedules in the epibranchial placodes of zebrafish and mice. Correspondingly, in zebrafish, an earlier onset of SU5402 exposure (10–16.5 hpf) completely suppresses both epibranchial morphogenesis and neurogenesis (Nechiporuk et al., 2007). Conversely, a late onset (26 hpf) does not affect the epibranchial placodes in any way (Nechiporuk et al., 2005).

We further demonstrate that, in mice, FGFR3 is involved to varying degrees in the neurogenesis of distinct epibranchial placodes. Thus, in EP2 and EP3, both treatment with anti-FGFR3 neutralizing antibodies and treatment with low doses of PD173074 reduced the number of Ngn2$^+$ neuroblasts by about the same amount. We conclude that FGFR3 almost completely mediates FGF-dependent effects on Ngn2$^+$ neuroblasts in these two placodes. In contrast, only about one third of the FGF-dependent production of Ngn2$^+$ neuroblasts requires the involvement of FGFR3 in EP1. Our results perfectly complement earlier findings on the roles of FGFR1 in mice. Here, FGFR1 deficiency impairs Ngn2 expression in EP1, but not in EP2 and EP3. Consequently, production of Ngn2$^+$ neuroblasts in EP1 must critically depend on the combined action of at least FGFR1 (Trokovic et al., 2005) and FGFR3 (present results). In this context, interspecies differences once again become apparent. Namely, during epibranchial neurogenesis in zebrafish,

FGF-dependent signals are exclusively transmitted via FGFR1 (Nechiporuk et al., 2005).

In the mice studied here, FGFR3 dependence of $Ngn2^+$ and $Ngn1^+$ epibranchial neuroblasts, respectively, turned out to be different in degree. FGF-dependent effects on $Ngn2^+$ neuroblasts are either fully (EP2, EP3) or only to about one third (EP1) mediated via FGFR3. In FGF-dependent $Ngn1^+$ neuroblasts, however, a practically completely FGFR3-mediated signal transmission occurs in EP1 and EP2. EP3 is somehow out of line as far as the $Ngn1^+$ neuroblasts are concerned. On the one hand, treatment with anti-FGFR3 neutralizing antibodies, as in EP1 and EP2, causes significant declines in the number of $Ngn1^+$ neuroblasts. On the other hand, significant decreases of $Ngn1^+$ neuroblasts observed in EP1 and EP2 under the influence of pan-FGFR inhibitors did not manifest in EP3. This supposedly paradoxical situation might be explained by the hypothesis that, in EP3, FGFRs other than FGFR3 physiologically block the production of $Ngn1^+$ neuroblasts. Consequently, blockage of these other FGFRs by pan-FGFR inhibitors would increase the number of $Ngn1^+$ neuroblasts and, thus, would compensate for any losses caused by the simultaneous blockage of FGFR3. That different FGFRs indeed exert opposing effects on specific cell populations is known from other contexts (Feng et al., 2015). For example, epithelial-mesenchymal transitions in various tumors are promoted by FGFR1 and FGFR4, but are suppressed by FGFR2. Whether, in EP3, "paradoxically" regulated $Ngn1^+$ neuroblasts (present results) belong to the subpopulation of Ngn2-independent $Ngn1^+$ neuroblasts discovered by Fode et al. (1998) remains to be determined. In this context, we will also make a more refined attempt to distinguish between subpopulations of neuroblasts expressing Ngn1, Ngn2, or both.

Wright and Mansour (2003) have examined the roles of *Fgf3* and *Fgf10* in ear development. Unlike our approach, this study worked with knockout mice. This means that potentially disturbing influences on the development of epibranchial placodes which, however, were not explicitly addressed by Wright and Mansour (2003), already affect the induction of epibranchial placodes, but not primarily their neurogenesis. Analysis of the published images shows that $Pax2^+$ epibranchial placodes are neither detectable in $Fgf3^{+/-}$, $Fgf10^{-/-}$ mice nor in $Fgf3^{-/-}$, $Fgf10^{+/-}$ mice. These results are in principle consistent with our current findings. This also applies to the study conducted by Freter et al. (2008). Here, knockdown constructs were used to demonstrate that, in chicken embryos, induction and further development of the epibranchial placodes can be completely disrupted by reducing mesodermal *Ffg3* and *Fgf19* expression. However, given that, again, FGF signaling had been switched off at a much earlier developmental period compared to our approach, neither of the two studies can determine, whether and which components of the FGF signaling pathway are responsible for neurogenesis in individual epibranchial placodes at a later stage.

Finally, we pursue the question whether FGF signaling might be of particular importance for the delamination of epibranchial neuroblasts. Indeed, Lassiter et al. (2009) observed that *Fgfr4* is maximally expressed in the ophthalmic trigeminal placode of chicken embryos during the delamination period. In addition, these authors were able to prove, both by genetic silencing of *Fgfr4* and by pharmacological inhibition of FGFR4 using the pan-FGFR inhibitor SU5402, that FGF signals are responsible for neuroblast delamination as well as for neuroblast differentiation. However, the experimental design did not allow to decide whether or not both processes depend on each other. To address the points raised by Lassiter et al. (2009), we generated 3D reconstructions of mouse control embryos as well as of embryos treated with 0.5 μM of the pan-FGFR inhibitor PD173074. In the control embryos, high numbers of $Ngn2^+$ neuroblasts were found in all three epibranchial placodes as well as in the approximate future positions of the associated geniculate, petrosal, and nodose ganglia, respectively (**Figures 7A,A'**). Exposure to 0.5 μM PD173074 leads to strong (EP1) or only moderate (EP2 > EP3) decreases in the number of $Ngn2^+$ placodal neuroblasts (**Figures 3G–I**, **4A–C**, **6**, **7B**, and **Table 2**). Correspondingly, extremely low (developing geniculate ganglion) or still moderate numbers of $Ngn2^+$ neuroblasts (immature petrosal and nodose ganglia) were observed in the underlying mesenchyme (**Figure 7B'**). The situation is therefore formally similar to the one described by Lassiter et al. (2009). In the ophthalmic trigeminal placode, however, the number of placodal cells, as revealed by the early marker Pax3, remained constant under the influence of FGF inhibition, while it decreased in the underlying mesenchyme. This can be regarded as a clear indication of a delamination disorder. It must be added, however, that an isolated delamination disorder is out of question here, as this should have been accompanied by an increase in the number of $Pax3^+$ premigratory neuroblasts. In mouse epibranchial placodes, the case is certainly different. Here, the number of premigratory placodal cells, as revealed by the early marker Pax8, strongly decreases following FGF inhibition (**Figures 7C–H**, and data not shown). Consequently, FGF inhibition already negatively affects the number of placodal progenitor cells, which ultimately reduces neuroblast delamination, albeit for other reasons.

Contributions of BMP Signaling to Epibranchial Placode Development

In zebrafish and chicken embryos, blockage of BMP signaling completely eliminates neurogenesis in all epibranchial placodes (Holzschuh et al., 2005; Kriebitz et al., 2009). At variance with this pattern, exposure of embryonic mice to the pan-BMPR inhibitor LDN193189 caused different degrees of decrease in the numbers of $Ngn2^+$ neuroblasts in each individual epibranchial placode: EP1 (−90%), EP2 (statistically insignificant), EP3 (−39%). Thus, neurogenesis of $Ngn2^+$ neuroblasts in EP1 and EP3 performed largely as we had observed under the influence of low doses of the pan-FGFR inhibitor PD173074 (EP1: −93%, EP3: −35%). In contrast, neurogenesis of $Ngn2^+$ neuroblasts in EP2 is strongly supported by FGF signals, but practically independent of BMP signals. The latter statement is substantiated by two pieces of evidence. Firstly, the BMPR inhibitor LDN193189 blocks kinase activity of all known BMP type 1 receptors as well as of two out of three known BMP type II receptors (Mohedas et al., 2013; Horbelt et al., 2015). Secondly, the only BMP type II receptor

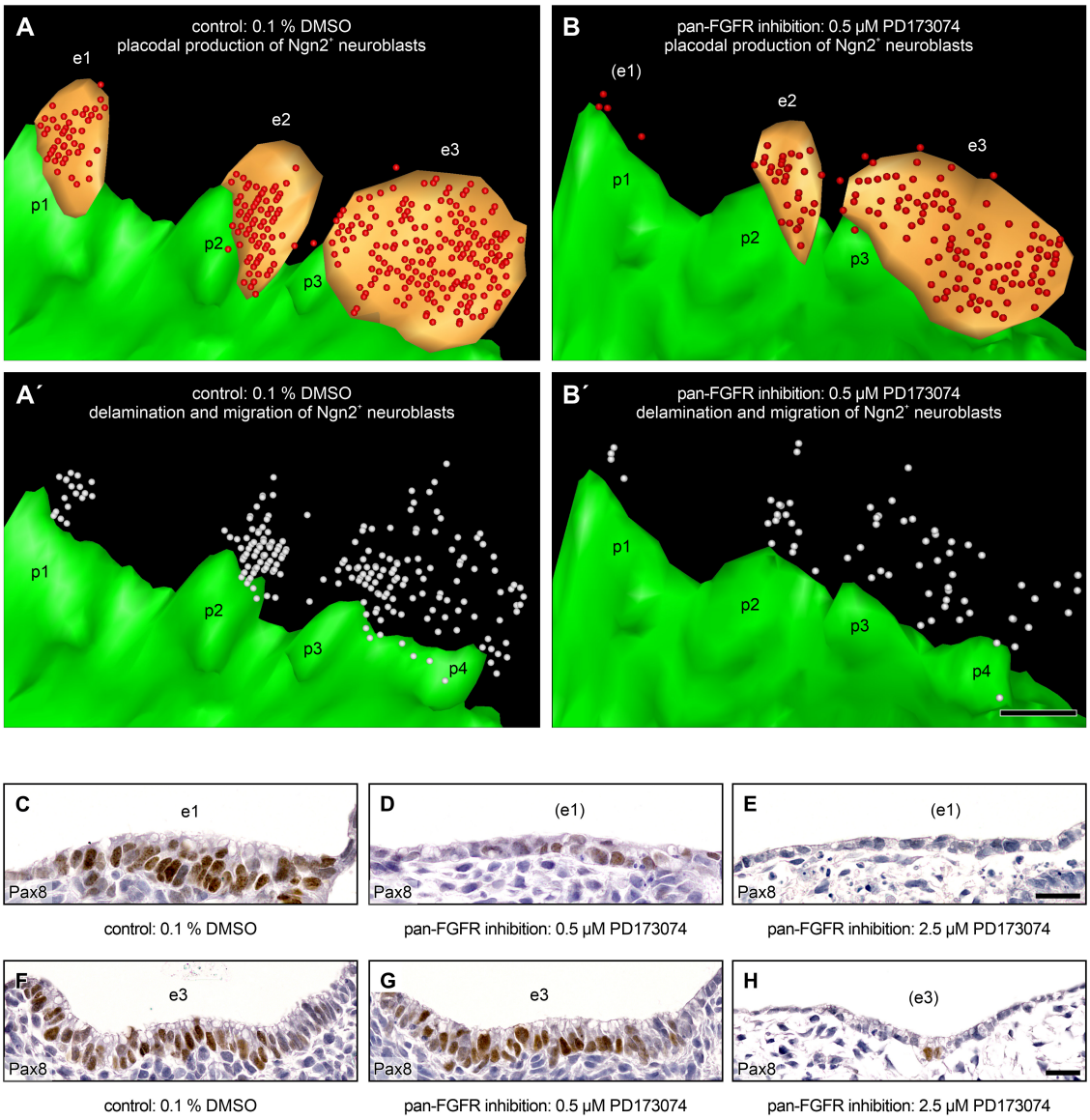

FIGURE 7 | Production and delamination of epibranchial Ngn2$^+$ neuroblasts in 9–14 somite mouse embryos, cultured for 24 h. 3D reconstructions show that, compared to DMSO control embryos **(A)**, the number of Ngn2$^+$ neuroblasts (red spheres) in the epibranchial placodes 1, 2, and 3 (e1, e2, e3; orange) decreases to varying degrees (e1 > > e2 > e3) after exposure to 0.5 µM of the pan-FGFR inhibitor PD173074 (**B**, also note loss of ectodermal thickening in the position of e1; for details, see **Figure 4** and **Table 2**). **(A',B')** Largely proportionally to the number of Ngn2$^+$ intraplacodal neuroblasts, the number of Ngn2$^+$ delaminating neuroblasts respectively of those that have already been deposited within the mesenchyme adjacent to the epibranchial placodes (both populations shown jointly as white spheres) also decreases. **(C–H)** Furthermore, treatment with PD173074 reduces, again roughly proportionally to the number of Ngn2$^+$ intraplacodal neuroblasts, the number of Pax8$^+$ intraplacodal (precursor) cells in a dose-dependent manner. p1, p2, p3, and p4, pharyngeal pouches 1, 2, 3, and 4 (green). Scale bars: 100 µm **(A–B')**, 20 µm **(C–E,F–H)**.

that cannot be blocked by LDN193189 (BMPRII) is not expressed in the developing epibranchial placodes of mice (Figures 4–6 in Danesh et al., 2009).

Compared to Ngn2$^+$ neuroblasts, Ngn1$^+$ neuroblasts responded almost identically to LDN193189 (**Figure 5**); the resulting decreases amounted to −86% (EP1), −45% (EP3), or are statistically insignificant (EP2). Thus, resembling Ngn2$^+$ neuroblasts, Ngn1$^+$ neuroblasts are either dependent on both BMP and FGF signaling (EP1, EP3) or to about 50% on FGF signals, in the absence of effective BMP signals (EP2). We therefore assume that neurogenesis in EP2 is additionally regulated by at least a third signaling pathway.

So far, we have considered possible influences of FGF and/or BMP signaling on epibranchial neurogenesis. FGF signaling, possibly via receptors other than FGFR3, additionally appears to support the development and/or maintenance of the placodal thickenings (**Figures 3**, **6**). In contrast, BMP signals hardly participate in the structural assembly of EP1 and EP2, even

at concentrations that cause a virtually complete extinction of neurogenesis in EP1. As an exception, EP3 is somewhat reduced in thickness under the influence of LDN193189, but this BMP-dependent effect will be discussed in the context of concomitant damages of the pharyngeal pouches. Whether FGF and BMP signals reinforce or override each other during epibranchial placode development, as they do in other contexts (Hayashi et al., 2001; Maier et al., 2010), will be addressed in future studies.

Critical Appraisal of the Developmental Profiles of Individual Epibranchial Placodes

Epibranchial placodes form with a rostral to caudal sequence from EP1 to EP3. Consequently, it needs to be checked whether our postulate that BMP and FGF signaling pathways play at least partially different roles in each of the three epibranchial placodes may unintentionally reflect different developmental profiles, or in other words, rostrocaudal sensitivity differences of EP1, EP2, and EP3. To this end, we referred back to one of our previous papers (Washausen and Knabe, 2013) and graphically documented the developmental profile of each epibranchial placode (**Figures 8A–C**). Our diagrams demonstrate that EP1, EP2, and EP3 start generating $Ngn2^+$ neuroblasts almost simultaneously between E8.5 and E9. The rostrocaudal developmental gradient becomes slightly more evident when neuroblast production reaches maximum numbers at about E9.7 (EP1) or E10.3 (EP2, EP3). Exposure of all three epibranchial placodes to the various inhibitors or neutralizing antibodies occurred uniformly immediately after the onset of neuroblast production. At this time, all three epibranchial placodes were equally well accessible to our reagents, since both overgrowth and/or invagination of the caudal epibranchial placodes begin only after the end of culture. Another consensus between EP1, EP2, and EP3 is that substantial periods of exposure to inhibitors or neutralizing antibodies coincided with the steep increase in neuroblast production. The only relevant difference is that it was solely EP1 that was cultivated beyond its production maximum. However, this difference is put into perspective by the fact that, in the two caudal epibranchial placodes, end of culture occurred at latest when 96.6% (EP2) or 91% (EP3) of the production maximum had been reached. Furthermore, the developmental profiles of EP2 and EP3 overlap almost completely. Critically appraising all these facts, we do not believe that the chosen culture period causes any systematic bias.

This view is supported by several plausibility arguments. Thus, EP2 and EP3, which show virtually identical developmental profiles (**Figures 8B,C**), should behave most similarly to each other in case that all epibranchial placodes would share identical dependencies on the FGF and/or BMP signaling pathways. However, EP2 and EP3 behave significantly differently (1) with respect to the reduction of $Ngn2^+$ neuroblasts following exposure to 10 μM of the pan-BMPR inhibitor LDN193189 and (2) with respect to the reduction of $Ngn1^+$ neuroblasts after treatment with 0.5 μM of the pan-FGFR inhibitor PD173074 (**Figures 8D,E**). A second testable hypothesis is that EP1 generally behaves differently from EP2 and/or EP3 because of its (slightly) different developmental profile. However, completely against this hypothesis stands the fact that the response behavior of EP1 does not differ significantly from EP2 and/or EP3 when placodes are treated (1) with 20 and/or 40 μg/ml neutralizing anti-FGFR3 antibodies (Ngn2, Ngn1; EP2, EP3), (2) with 2.5 μM PD173074 (Ngn2; EP2), or (3) with 0.5 μM PD173074 (Ngn1; EP2) (**Figures 8D,F–I**). In summary, we find no evidence arising from the plausibility checks that our results are picking up a rostrocaudal difference in epibranchial placode development and that our inhibition experiments may reflect a rostrocaudal difference in sensitivity that underlies the differences seen.

Impact of FGF and BMP Signaling on Pharyngeal Pouch Development

Pharyngeal pouches are indispensable signaling centers for the development of epibranchial placodes (Holzschuh et al., 2005; Kriebitz et al., 2009; Ladher et al., 2010). In embryonic mice, incubation with low doses of the pan-FGFR inhibitor PD173074 did not result in generalized malformations of these signaling centers. It must be added, however, that 5 out of 20 body sides (25%) showed mild to moderate and 2 out of 20 body sides (10%) even severe segmentation defects of the pharyngeal pouches 2 and 3 (**Figures 6**, **7B**, **9B**). All in all, we therefore assume that impaired epibranchial placodes primarily arose from FGFR blockage in the placodal ectoderm. However, we cannot exclude that hitherto undetected subtle changes in the contact zone between the pharyngeal endoderm and the branchial ectoderm also contributed to the developmental anomalies. Indeed, using zebrafish *van gogh* (*Tbx1*) mutants, Holzschuh et al. (2005) discovered that even slight increases or decreases of this contact area lead to significant increases or decreases of epibranchial neurogenesis, respectively.

When high doses of PD173074 were applied to cultured mouse embryos, lateral outgrowth of all four pharyngeal pouches was impeded. Furthermore, the degree of placode damage by far exceeded that caused by low doses of PD173074. We hypothesize that, in these severe cases, complete suppression of epibranchial placode development cannot be ascribed to the blocking of ectodermal FGFRs alone. Instead, any pouch-derived signal should become less effective due to the increased distance to its ectodermal targets. Correspondingly, FGF ligands maximally bridge distances of about 16 cell diameters in zebrafish (Scholpp and Brand, 2004) and, in *Xenopus laevis*, BMP signals cannot be transmitted further than approximately 5 to 10 cell diameters (Dosch et al., 1997).

In embryonic mice, pharyngeal pouch formation either was largely undisturbed or strongly impaired depending on the dose of pan-FGFR inhibitor PD173074 administered. Similarly, development of the pharyngeal pouches remained unaffected following exposure to low doses of the pan-BMPR inhibitor LDN193189 (2 μM), but became increasingly disturbed upon incubation with progressively higher doses (5 μM, 10 μM). However, while in the case of high doses of PD173074 all four pharyngeal pouches were affected, high doses of LDN193189 impaired the outgrowth of the pharyngeal pouches 3 and 4, but

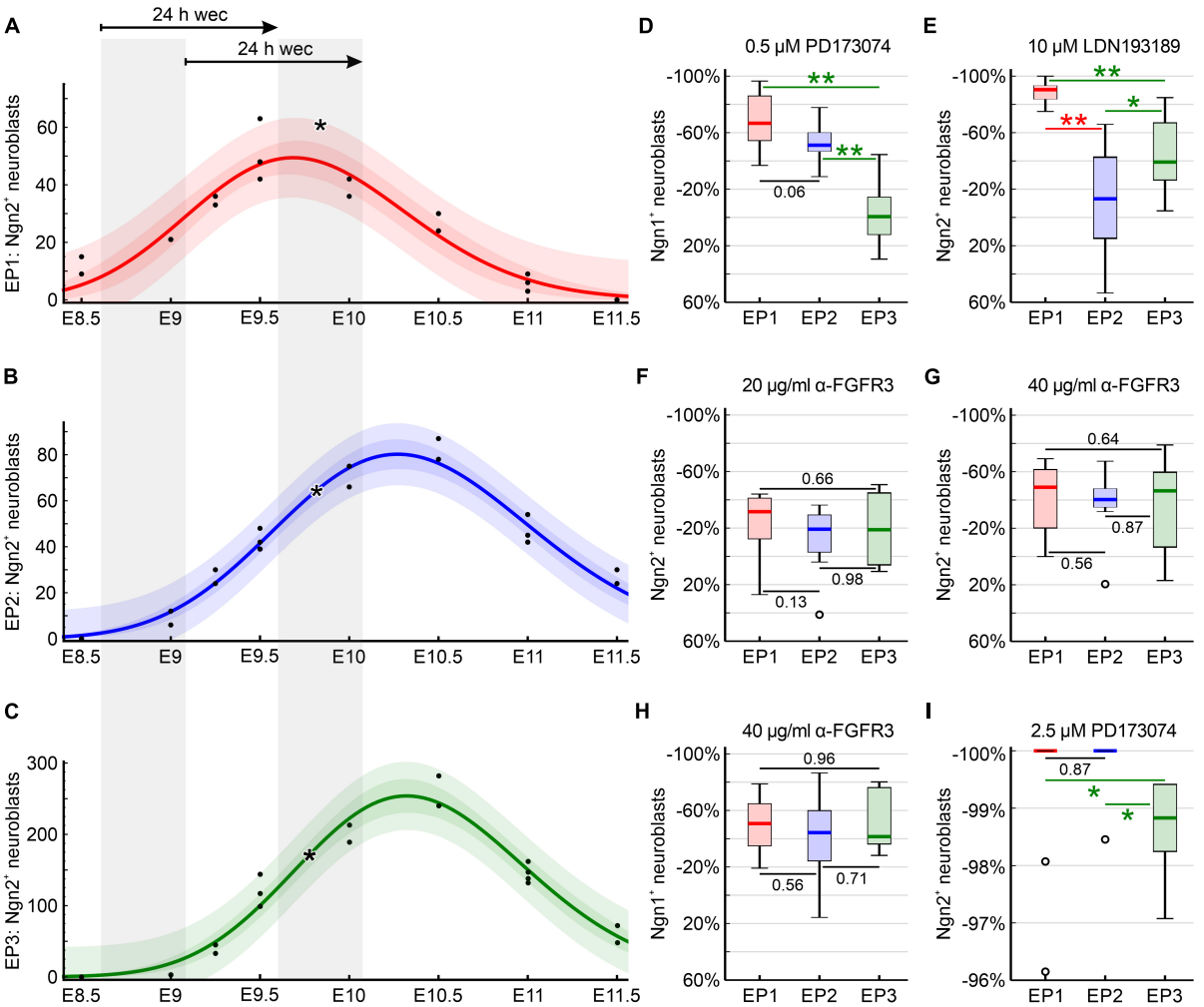

FIGURE 8 | Developmental profiles of the epibranchial placodes of C57BL/6N mice (embryonic days (E) 8.5 to E11.5) as reflected by earlier reconstructions of Ngn2$^+$ intraplacodal neuroblasts (Washausen and Knabe, 2013) recounted for present purposes (n = 11 mouse embryos with 22 body sides). **(A–C)** Using CurveExpert Professional (Hyams Development, Chattanooga, TN, United States), regression curves were generated that represent the developmental profiles of the epibranchial placodes 1, 2, and 3 (EP1, red; EP2, blue; EP3, green). Confidence bands (medium red, blue, or green) most likely contain 95% of all values (black dots). Prediction bands (faint red, blue, or green) indicate the range in which 95% of all future values will fall. Here, embryos possessing 9–14 pairs of somites were included in our whole embryo cultures (WECs). This range is indicated by the left of the two gray columns and is correlated with the embryonic age plotted on the x-axis. The right gray column marks the period within which embryos were removed from the culture after 24 h. Asterisks indicate the respective medians of Ngn2$^+$ neuroblasts for EP1, EP2, and EP3 of DMSO control embryos (**Table 2**). **(D–I)** Box plots display the relative changes in the numbers of Ngn2$^+$ **(E–G,I)** or Ngn1$^+$ **(D,H)** neuroblasts following exposure to either the pan-FGFR inhibitor PD173074 **(D,I)**, to anti-FGFR3 neutralizing antibodies **(F–H)**, or to the pan-BMPR inhibitor LDN193189 **(E)**, respectively (see **Table 2**, also for n values). Significant differences between EP1 (red), EP2 (blue), and/or EP3 (green) are indicated by asterisks ($^*P < 0.05$, $^{**}P < 0.001$; Mann–Whitney test). Whiskers, lower and upper extremes; box limits, 25th and 75th percentiles; red, blue, or green center lines, medians; open circles, outliers. **(D,E)** Plausibility checks demonstrate that EP2 and EP3, which almost synchronously produce neuroblasts, by no means always react in the same way to certain inhibitors. **(D,F–I)** Conversely, EP1, which slightly precedes EP2 and EP3 in terms of neuroblast production, does not always deviate in its behavior toward certain inhibitors from EP2 and/or EP3 (for details, see text).

left the pharyngeal pouches 1 and 2 unaffected. Correspondingly, in zebrafish, application of the BMPR inhibitor dorsomorphin elicits a stronger disturbance of the pharyngeal pouches 3–6 when compared to the pharyngeal pouches 1 and 2 (Lovely et al., 2016). We cannot presently decide whether these differential outcomes are dose-dependent, or whether different sets of molecular signals contribute to the formation of distinct pharyngeal pouches.

Malformations of the pharyngeal pouches may be caused either by the disturbance of direct endodermal effects of BMP and/or FGF signaling, or indirectly by abnormalities that primarily affect the formation of neural crest cells and/or their segment-specific migration into the branchial arches (but see Veitch et al., 1999). To test the latter hypothesis, routinely counterstained serial sections of all control embryos as well as of all mouse embryos treated with either 0.5 µM of the pan-FGFR inhibitor PD173074 or with 2, 5, or 10 µM of the pan-BMPR inhibitor LDN193189 were analyzed. In addition, serial sections of three embryos (control, 0.5 µM PD173074

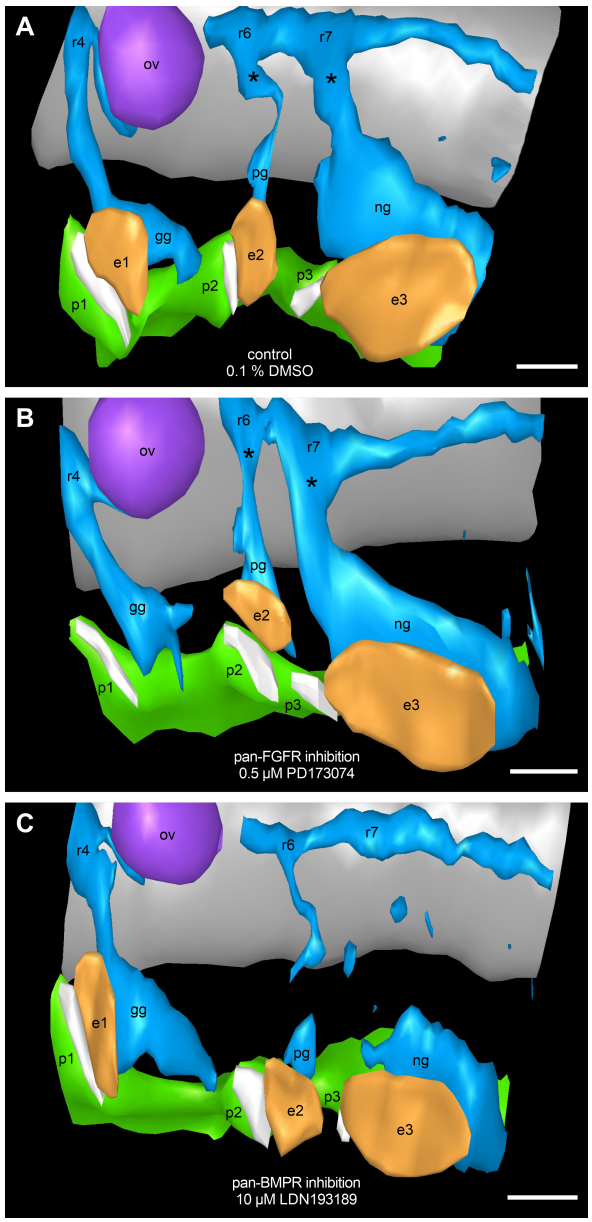

FIGURE 9 | Assessment of potential FGF and/or BMP dependencies of neural crest streams emerging segmentally from the rhombomeres 4, 6, and 7. 9–14 somite mouse embryos, cultured for 24 h. Our 3D reconstructions show that neural crest streams (blue) emerge from rhombomeres 4, 6, and 7 (r4, r6, and r7), and give rise to the proximal ganglia (asterisks) of the cranial nerves IX and X as well as to the geniculate, petrosal, and nodose ganglia (gg, pg, and ng) both in DMSO control embryos **(A)** and after exposure to 0.5 µM of the pan-FGFR inhibitor PD173074 **(B)**. Treatment with 10 µM of the pan-BMPR inhibitor LDN193189, like genetic silencing of the BMP pathway (Kanzler et al., 2000), leads to the partial loss of neural crest streams and proximal ganglia originating from r6 and, to a greater extent, r7 **(C)**. In at least some of the PD173074 treated embryos (for details, see text), pharyngeal pouches 2 and 3 as well as branchial membranes 2 and 3 have approached each other beyond the normal level. Also note loss of ectodermal thickening in the position of epibranchial placode 1. e1, e2, e3, epibranchial placodes 1, 2, and 3 (orange); ov, otic vesicle (purple); p1, p2, p3, pharyngeal pouches 1, 2, and 3 (green); white stripes adjacent to the epibranchial placodes, branchial membranes 1, 2, and 3; gray, hindbrain. Scale bars: 100 µm.

and 10 µM LDN193189) were studied immunohistochemically using antibodies against Sox10 and 3D reconstructed (**Figure 9**). Neither control embryos nor embryos treated with PD173074 showed major deviations from the typical neural crest patterning (**Figures 9A,B**). In contrast, about 90% of the embryos exposed to 10 µM LDN193189 presented massive proximally accentuated defects of the glossopharyngeal and vagal neural crest streams (**Figure 9C**). Furthermore, basically identical defects (data not shown) occurred at 2 µM LDN193189 (50%) and roughly reached the percentage found at 10 µM LDN193189 already at 5 µM LDN193189 (80%).

The first "gain" of these analyses is that they additionally validate the basic experimental approach of this work. In fact, application of LDN193189 in our whole embryo cultures triggers exactly those segment-specific neural crest cell defects that are caused by genetic silencing of the BMP signaling pathway (Kanzler et al., 2000). Secondly, our 3D reconstructions of LDN193189-treated embryos demonstrate that glossopharyngeal and vagal neural crest defects coincide with a discretely reduced approach of the pharyngeal pouches 3 and 4 to the opposing branchial ectoderm. However, we can rule out in all probability that mis-migrated neural crest cells form a cellular barrier that may prevent fusion between pharyngeal endoderm and branchial ectoderm. Consequently, with the current state of knowledge, we favor a scenario in which the observed malformations of the pharyngeal pouches result from the pharmacological blockage of endodermal BMP receptors.

Our findings support the assumption that the pharyngeal pouch signaling center contributes essentially to epibranchial placode neurogenesis (Begbie et al., 1999; for a review, see Ladher et al., 2010). Indeed, massive disruption of pharyngeal pouch formation by exposing mouse embryos to the pan-FGFR inhibitor PD173074 resulted in massive deficiencies of all three epibranchial placodes (**Figure 6**). In line with this observation, less severe damage to the pharyngeal pouches 3 and 4 caused by the pan-BMPR inhibitor LDN193189 led to moderate impairments of EP3 (see above). However, there is also evidence that other signaling centers may be involved in epibranchial neurogenesis in addition to the pharyngeal pouches. Thus, in zebrafish *casanova* (*Sox32*) mutants, disruption of the pharyngeal pouches results on the one hand in complete (EP2, $EP3_1$), on the other hand in only moderate decreases in the numbers of neuroblasts (EP1, $EP3_{2-4}$; Holzschuh et al., 2005; Nechiporuk et al., 2005). Furthermore, McCarroll and Nechiporuk (2013) were able to demonstrate that, in zebrafish, progenitor cells of both the otic and the anterior lateral line placodes serve as epibranchial signaling centers. Whether anlagen of lateral line placodes that we discovered in mice (Washausen and Knabe, 2018) also may execute such signaling functions will be investigated in subsequent studies. However, there is a second possible explanation for the "atypical" findings detected in EP1 and $EP3_{2-4}$ of zebrafish *casanova* mutants. Indeed, different pharyngeal pouches could employ different sets of short- and long-range signals to regulate epibranchial neurogenesis (Schlosser, 2003; Kriebitz et al., 2009), the effectiveness of which would be limited to different degrees in cases of impaired pharyngeal pouch formation.

DATA AVAILABILITY STATEMENT

The raw data supporting the conclusions of this article will be made available by the authors, without undue reservation.

ETHICS STATEMENT

The animal study was reviewed and approved by Landesamt für Natur, Umwelt und Verbraucherschutz (LANUV), North Rhine-Westphalia, Germany; approval number: 84-02.05.50.16.013.

AUTHOR CONTRIBUTIONS

Both authors listed have made a substantial, direct and intellectual contribution to the work, and approved it for publication.

ACKNOWLEDGMENTS

We thank T. Deppe and D. Heinz-Mohr for excellent technical assistance. The monoclonal anti-Msx1/2 antibody 4G1 developed by T. M. Jessell/S. Brenner-Morton was obtained from the Developmental Studies Hybridoma Bank, created by the NICHD of the NIH and maintained at Department of Biology, University of Iowa, Iowa City, IA, United States.

SUPPLEMENTARY MATERIAL

The Supplementary Material for this article can be found online at: https://www.frontiersin.org/articles/10.3389/fcell.2021.712522/full#supplementary-material

REFERENCES

Abu-Issa, R., Smyth, G., Smoak, I., Yamamura, K.-I., and Meyers, E. N. (2002). Fgf8 is required for pharyngeal arch and cardiovascular development in the mouse. *Development* 129, 4613–4625. doi: 10.1242/dev.129.19.4613

Aggarwal, V. S., Liao, J., Bondarev, A., Schimmang, T., Lewandoski, M., Locker, J., et al. (2006). Dissection of Tbx and Fgf interactions in mouse models of 22q11DS suggests functional redundancy. *Hum. Mol. Genet.* 15, 3219–3228. doi: 10.1093/hmg/ddl399

Ahrens, K., and Schlosser, G. (2005). Tissues and signals involved in the induction of placodal Six1 expression in *Xenopus laevis*. *Dev. Biol.* 288, 40–59. doi: 10.1016/j.ydbio.2005.07.022

Alvarez, Y., Alonso, M. T., Vendrell, V., Zelarayan, L. C., Chamero, P., Theil, T., et al. (2003). Requirements for FGF3 and FGF10 during inner ear formation. *Development* 130, 6329–6338. doi: 10.1242/dev.00881

Andrey, P., and Maurin, Y. (2005). Free-D: an integrated environment for three-dimensional reconstruction from serial sections. *J. Neurosci. Methods* 145, 233–244. doi: 10.1016/j.jneumeth.2005.01.006

Arnaud-Dabernat, S., Kritzik, M., Kayali, A. G., Zhang, Y.-Q., Liu, G., Ungles, C., et al. (2007). FGFR3 is a negative regulator of the expansion of pancreatic epithelial cells. *Diabetes Metab. Res. Rev.* 56, 96–106. doi: 10.2337/db05-1073

Baker, C. V. H., and Bronner-Fraser, M. (2001). Vertebrate cranial placodes. I. embryonic induction. *Dev. Biol.* 232, 1–61. doi: 10.1006/dbio.2001.0156

Begbie, J., Brunet, J. F., Rubenstein, J. L., and Graham, A. (1999). Induction of the epibranchial placodes. *Development* 126, 895–902.

Breau, M. A., and Schneider-Maunoury, S. (2014). Mechanisms of cranial placode assembly. *Int. J. Dev. Biol.* 58, 9–19. doi: 10.1387/ijdb.130351mb

Brown, A. S., and Epstein, D. J. (2011). Otic ablation of smoothened reveals direct and indirect requirements for Hedgehog signaling in inner ear development. *Development* 138, 3967–3976. doi: 10.1242/dev.066126

Calmont, A., Wandzioch, E., Tremblay, K. D., Minowada, G., Kaestner, K. H., Martin, G. R., et al. (2006). An FGF response pathway that mediates hepatic gene induction in embryonic endoderm cells. *Dev. Cell* 11, 339–348. doi: 10.1016/j.devcel.2006.06.015

Chaikuad, A., Alfano, I., Kerr, G., Sanvitale, C. E., Boergermann, J. H., Triffitt, J. T., et al. (2012). Structure of the bone morphogenetic protein receptor ALK2 and implications for fibrodysplasia ossificans progressiva. *J. Biol. Chem.* 287, 36990–36998. doi: 10.1074/jbc.M112.365932

Chen, J., and Streit, A. (2013). Induction of the inner ear: stepwise specification of otic fate from multipotent progenitors. *Hear. Res.* 297, 3–12. doi: 10.1016/j.heares.2012.11.018

Chen, Y., Bei, M., Woo, I., Satokata, I., and Maas, R. (1996). Msx1 controls inductive signalling in mammalian tooth morphogenesis. *Development* 122, 3035–3044. doi: 10.1242/dev.122.10.3035

Corson, L. B., Yamanaka, Y., Lai, K.-M. V., and Rossant, J. (2003). Spatial and temporal patterns of ERK signaling during mouse embryogenesis. *Development* 130, 4527–4537. doi: 10.1242/dev.00669

Coudert, A. E., Pibouin, L., Vi-Fane, B., Thomas, B. L., Macdougall, M., Choudhury, A., et al. (2005). Expression and regulation of the Msx1 natural antisense transcript during development. *Nucleic Acids Res.* 33, 5208–5218. doi: 10.1093/nar/gki831

Crump, J. G., Maves, L., Lawson, N. D., Weinstein, B. M., and Kimmel, C. B. (2004). An essential role for Fgfs in endodermal pouch formation influences later craniofacial skeletal patterning. *Development* 131, 5703–5716. doi: 10.1242/dev.01444

Cuny, G. D., Yu, P. B., Laha, J. K., Xing, X., Liu, J.-F., Lai, C. S., et al. (2008). Structure–activity relationship study of bone morphogenetic protein (BMP) signaling inhibitors. *Bioorg. Med. Chem. Lett.* 18, 4388–4392. doi: 10.1016/j.bmcl.2008.06.052

Danesh, S. M., Villasenor, A., Chong, D., Soukup, C., and Cleaver, O. (2009). BMP and BMP receptor expression during murine organogenesis. *Gene Expr. Patterns* 9, 255–265. doi: 10.1016/j.gep.2009.04.002

Dosch, R., Gawantka, V., Delius, H., Blumenstock, C., and Niehrs, C. (1997). Bmp-4 acts as a morphogen in dorsoventral mesoderm patterning in Xenopus. *Development* 124, 2325–2334. doi: 10.1242/dev.124.12.2325

Feng, S., Zhou, L., Nice, E. C., and Huang, C. (2015). Fibroblast growth factor receptors: multifactorial-contributors to tumor initiation and progression. *Histol. Histopathol.* 30, 13–31. doi: 10.14670/HH-30.13

Fode, C., Gradwohl, G., Morin, X., Dierich, A., LeMeur, M., Goridis, C., et al. (1998). The bHLH protein NEUROGENIN 2 is a determination factor for epibranchial placode-derived sensory neurons. *Neuron* 20, 483–494. doi: 10.1016/S0896-6273(00)80989-7

Frank, D. U., Fotheringham, L. K., Brewer, J. A., Muglia, L. J., Tristani-Firouzi, M., Capecchi, M. R., et al. (2002). An Fgf8 mouse mutant phenocopies human 22q11 deletion syndrome. *Development* 129, 4591–4603. doi: 10.1242/dev.129.19.4591

Freter, S., Muta, Y., Mak, S.-S., Rinkwitz, S., and Ladher, R. K. (2008). Progressive restriction of otic fate: the role of FGF and Wnt in resolving inner ear potential. *Development* 135, 3415–3424. doi: 10.1242/dev.026674

Ge, W., He, F., Kim, K. J., Blanchi, B., Coskun, V., Nguyen, L., et al. (2006). Coupling of cell migration with neurogenesis by proneural bHLH factors. *Proc. Natl. Acad. Sci. U S A.* 103, 1319–1324. doi: 10.1073/pnas.0510419103

Grand, E. K., Chase, A. J., Heath, C., Rahemtulla, A., and Cross, N. C. P. (2004). Targeting FGFR3 in multiple myeloma: inhibition of t(4;14)-positive cells by SU5402 and PD173074. *Leukemia* 18, 962–966. doi: 10.1038/sj.leu.2403347

Gudernova, I., Vesela, I., Balek, L., Buchtova, M., Dosedelova, H., Kunova, M., et al. (2016). Multikinase activity of fibroblast growth factor receptor (FGFR) inhibitors SU5402, PD173074, AZD1480, AZD4547 and BGJ398 compromises the use of small chemicals targeting FGFR catalytic activity for therapy

of short-stature syndromes. *Hum. Mol. Genet.* 25, 9–23. doi: 10.1093/hmg/ddv441

Hayashi, H., Ishisaki, A., Suzuki, M., and Imamura, T. (2001). BMP-2 augments FGF-induced differentiation of PC12 cells through upregulation of FGF receptor-1 expression. *J. Cell Sci.* 114, 1387–1395. doi: 10.1242/jcs.114.7.1387

Holzschuh, J., Wada, N., Wada, C., Schaffer, A., Javidan, Y., Tallafuß, A., et al. (2005). Requirements for endoderm and BMP signaling in sensory neurogenesis in zebrafish. *Development* 132, 3731–3742. doi: 10.1242/dev.01936

Horbelt, D., Boergermann, J. H., Chaikuad, A., Alfano, I., Williams, E., Lukonin, I., et al. (2015). Small molecules dorsomorphin and LDN-193189 inhibit myostatin/GDF8 signaling and promote functional myoblast differentiation. *J. Biol. Chem.* 290, 3390–3404. doi: 10.1074/jbc.M114.604397

Hu, J. S., Doan, L. T., Currle, D. S., Paff, M., Rheem, J. Y., Schreyer, R., et al. (2008). Border formation in a Bmp gradient reduced to single dissociated cells. *Proc. Natl. Acad. Sci. U S A.* 105, 3398–3403. doi: 10.1073/pnas.0709100105

Kanzler, B., Foreman, R. K., Labosky, P. A., and Mallo, M. (2000). BMP signalling is essential for development of skeletogenic and neurogenic cranial neural crest. *Development* 127, 1095–1104. doi: 10.1242/dev.127.5.1095

Knabe, W., Washausen, S., Brunnett, G., and Kuhn, H.-J. (2002). Use of "reference series" to realign histological serial sections for three-dimensional reconstructions of the positions of cellular events in the developing brain. *J. Neurosci. Methods* 121, 169–180. doi: 10.1016/S0165-0270(02)00247-9

Kowalchuk, A. M., Maurer, K. A., Shoja-Taheri, F., and Brown, N. L. (2018). Requirements for Neurogenin2 during mouse postnatal retinal neurogenesis. *Dev. Biol.* 442, 220–235. doi: 10.1016/j.ydbio.2018.07.020

Koziczak, M., Holbro, T., and Hynes, N. E. (2004). Blocking of FGFR signaling inhibits breast cancer cell proliferation through downregulation of D-type cyclins. *Oncogene* 23, 3501–3508. doi: 10.1038/sj.onc.1207331

Kriebitz, N. N., Kiecker, C., McCormick, L., Lumsden, A., Graham, A., and Bell, E. (2009). PRDC regulates placode neurogenesis in chick by modulating BMP signaling. *Dev. Biol.* 336, 280–292. doi: 10.1016/j.ydbio.2009.10.013

Krolewski, R. C., Packard, A., and Schwob, J. E. (2013). Global expression profiling of globose basal cells and neurogenic progression within the olfactory epithelium. *J. Comp. Neurol.* 521, 833–859. doi: 10.1002/cne.23204

Kyono, A., Avishai, N., Ouyang, Z., Landreth, G. E., and Murakami, S. (2011). FGF and ERK signaling coordinately regulate mineralization-related genes and play essential roles in osteocyte differentiation. *J. Bone Miner. Metab.* 30, 19–30. doi: 10.1007/s00774-011-0288-2

Ladher, R. K., O'Neill, P., and Begbie, J. (2010). From shared lineage to distinct functions: the development of the inner ear and epibranchial placodes. *Development* 137, 1777–1785. doi: 10.1242/dev.040055

Ladher, R. K., Wright, T. J., Moon, A. M., Mansour, S. L., and Schoenwolf, G. C. (2005). FGF8 initiates inner ear induction in chick and mouse. *Genes Dev.* 19, 603–613. doi: 10.1101/gad.1273605

Lamont, F. R., Tomlinson, D. C., Cooper, P. A., Shnyder, S. D., Chester, J. D., and Knowles, M. A. (2011). Small molecule FGF receptor inhibitors block FGFR-dependent urothelial carcinoma growth in vitro and in vivo. *Br. J. Cancer* 104, 75–82. doi: 10.1038/sj.bjc.6606016

Lassiter, R. N. T., Reynolds, S. B., Marin, K. D., Mayo, T. F., and Stark, M. R. (2009). FGF signaling is essential for ophthalmic trigeminal placode cell delamination and differentiation. *Dev. Dyn.* 238, 1073–1082. doi: 10.1002/dvdy.21949

Lassiter, R. N. T., Stark, M. R., Zhao, T., and Zhou, C. J. (2014). Signaling mechanisms controlling cranial placode neurogenesis and delamination. *Dev. Biol.* 389, 39–49. doi: 10.1016/j.ydbio.2013.11.025

Leung, A. W., Morest, D. K., and Li, J. Y. H. (2013). Differential BMP signaling controls formation and differentiation of multipotent preplacodal ectoderm progenitors from human embryonic stem cells. *Dev. Biol.* 379, 208–220. doi: 10.1016/j.ydbio.2013.04.023

Li, L., Ning, G., Yang, S., Yan, Y., Cao, Y., Cao, Y., et al. (2019). BMP signaling is required for nkx2.3-positive pharyngeal pouch progenitor specification in zebrafish. *PLoS Genet.* 15:e1007996. doi: 10.1371/journal.pgen.1007996

Liem, K. F. Jr., Tremml, G., Roelink, H., and Jessell, T. M. (1995). Dorsal differentiation of neural plate cells induced by BMP-mediated signals from epidermal ectoderm. *Cell* 82, 969–979. doi: 10.1016/0092-8674(95)90276-7

Liu, R., Li, J., Xie, K., Zhang, T., Lei, Y., Chen, Y., et al. (2013). FGFR4 promotes stroma-induced epithelial-to-mesenchymal transition in colorectal cancer. *Cancer Res.* 73, 5926–5935. doi: 10.1158/0008-5472.CAN-12-4718

Lo, L., Dormand, E., Greenwood, A., and Anderson, D. J. (2002). Comparison of the generic neuronal differentiation and neuron subtype specification functions of mammalian achaete-scute and atonal homologs in cultured neural progenitor cells. *Development* 129, 1553–1567. doi: 10.1242/dev.129.7.1553

Lovely, C. B., Swartz, M. E., McCarthy, N., Norrie, J. L., and Eberhart, J. K. (2016). Bmp signaling mediates endoderm pouch morphogenesis by regulating Fgf signaling in zebrafish. *Development* 143, 2000–2011. doi: 10.1242/dev.129379

Ma, Q., Chen, Z., del Barco Barrantes, I., de la Pompa, J. L., and Anderson, D. J. (1998). neurogenin1 is essential for the determination of neuronal precursors for proximal cranial sensory ganglia. *Neuron* 20, 469–482. doi: 10.1016/S0896-6273(00)80988-5

Maier, E., von Hofsten, J., Nord, H., Fernandes, M., Paek, H., Hébert, J. M., et al. (2010). Opposing Fgf and Bmp activities regulate the specification of olfactory sensory and respiratory epithelial cell fates. *Development* 137, 1601–1611. doi: 10.1242/dev.051219

McCarroll, M. N., and Nechiporuk, A. V. (2013). Fgf3 and Fgf10a work in concert to promote maturation of the epibranchial placodes in zebrafish. *PLoS One* 8:e85087. doi: 10.1371/journal.pone.0085087

Mohammadi, M., Froum, S., Hamby, J. M., Schroeder, M. C., Panek, R. L., Lu, G. H., et al. (1998). Crystal structure of an angiogenesis inhibitor bound to the FGF receptor tyrosine kinase domain. *EMBO J.* 17, 5896–5904. doi: 10.1093/emboj/17.20.5896

Mohammadi, M., McMahon, G., Sun, L., Tang, C., Hirth, P., Yeh, B. K., et al. (1997). Structures of the tyrosine kinase domain of fibroblast growth factor receptor in complex with inhibitors. *Science* 276, 955–960. doi: 10.1126/science.276.5314.955

Mohedas, A. H., Xing, X., Armstrong, K. A., Bullock, A. N., Cuny, G. D., and Yu, P. B. (2013). Development of an ALK2-biased BMP type I receptor kinase inhibitor. *ACS Chem. Biol.* 8, 1291–1302. doi: 10.1021/cb300655w

Nechiporuk, A., Linbo, T., Poss, K. D., and Raible, D. W. (2007). Specification of epibranchial placodes in zebrafish. *Development* 134, 611–623. doi: 10.1242/dev.02749

Nechiporuk, A., Linbo, T., and Raible, D. W. (2005). Endoderm-derived Fgf3 is necessary and sufficient for inducing neurogenesis in the epibranchial placodes in zebrafish. *Development* 132, 3717–3730. doi: 10.1242/dev.01876

Nikaido, M., Navajas Acedo, J., Hatta, K., and Piotrowski, T. (2017). Retinoic acid is required and Fgf, Wnt, and Bmp signaling inhibit posterior lateral line placode induction in zebrafish. *Dev. Biol.* 431, 215–225. doi: 10.1016/j.ydbio.2017.09.017

Oki, S., Kitajima, K., and Meno, C. (2010). Dissecting the role of Fgf signaling during gastrulation and left-right axis formation in mouse embryos using chemical inhibitors. *Dev. Dyn.* 239, 1768–1778. doi: 10.1002/dvdy.22282

Ornitz, D. M., and Itoh, N. (2015). The fibroblast growth factor signaling pathway. *Wiley Interdiscip. Rev. Dev. Biol.* 4, 215–266. doi: 10.1002/wdev.176

Paek, H., Gutin, G., and Hébert, J. M. (2009). FGF signaling is strictly required to maintain early telencephalic precursor cell survival. *Development* 136, 2457–2465. doi: 10.1242/dev.032656

Pardo, O. E., Latigo, J., Jeffery, R. E., Nye, E., Poulsom, R., Spencer-Dene, B., et al. (2009). The fibroblast growth factor receptor inhibitor PD173074 blocks small cell lung cancer growth in vitro and in vivo. *Cancer Res.* 69, 8645–8651. doi: 10.1158/0008-5472.CAN-09-1576

Park, B.-Y., and Saint-Jeannet, J.-P. (2010). "Induction and segregation of the vertebrate cranial placodes," in *Colloquium Series on Developmental Biology 1*, eds D. S. Kessler and J.-P. Saint-Jeannet (San Rafael, CA: Morgan & Claypool Publishers), 1–83. doi: 10.4199/C00014ED1V01Y201007DEB003

Raible, F., and Brand, M. (2001). Tight transcriptional control of the ETS domain factors Erm and Pea3 by Fgf signaling during early zebrafish development. *Mech. Dev.* 107, 105–117.

Ranieri, D., Rosato, B., Nanni, M., Magenta, A., Belleudi, F., and Torrisi, M. R. (2016). Expression of the FGFR2 mesenchymal splicing variant in epithelial cells drives epithelial-mesenchymal transition. *Oncotarget* 7, 5440–5460. doi: 10.18632/oncotarget.6706

Rasband, W. S. (1997-2018). *ImageJ*. Bethesda, MD: U. S. National Institutes of Health.

Romeis, B. (1948). *Mikroskopische Technik*. Munich: R. Oldenbourg.

Schlosser, G. (2003). Hypobranchial placodes in Xenopus laevis give rise to hypobranchial ganglia, a novel type of cranial ganglia. *Cell Tissue Res.* 312, 21–29. doi: 10.1007/s00441-003-0710-8

Schlosser, G. (2006). Induction and specification of cranial placodes. *Dev. Biol.* 294, 303–351. doi: 10.1016/j.ydbio.2006.03.009

Schlosser, G. (2010). Making senses: development of vertebrate cranial placodes. *Int. Rev. Cell Mol. Biol.* 283, 129–234. doi: 10.1016/S1937-6448(10)83004-7

Schlosser, G., and Ahrens, K. (2004). Molecular anatomy of placode development in *Xenopus laevis*. *Dev. Biol.* 271, 439–466. doi: 10.1016/j.ydbio.2004.04.013

Scholpp, S., and Brand, M. (2004). Endocytosis controls spreading and effective signaling range of Fgf8 protein. *Curr. Biol.* 14, 1834–1841. doi: 10.1016/j.cub.2004.09.084

Shalhoub, V., Ward, S. C., Sun, B., Stevens, J., Renshaw, L., Hawkins, N., et al. (2011). Fibroblast growth factor 23 (FGF23) and alpha-klotho stimulate osteoblastic MC3T3.E1 cell proliferation and inhibit mineralization. *Calcif. Tissue Int.* 89, 140–150. doi: 10.1007/s00223-011-9501-5

Sommer, L., Ma, Q., and Anderson, D. J. (1996). neurogenins, a novel family of atonal-related bHLH transcription factors, are putative mammalian neuronal determination genes that reveal progenitor cell heterogeneity in the developing CNS and PNS. *Mol. Cell Neurosci.* 8, 221–241. doi: 10.1006/mcne.1996.0060

St-Germain, J. R., Taylor, P., Tong, J., Jin, L. L., Nikolic, A., Stewart, I. I., et al. (2009). Multiple myeloma phosphotyrosine proteomic profile associated with FGFR3 expression, ligand activation, and drug inhibition. *Proc. Natl. Acad. Sci. U S A.* 106, 20127–20132. doi: 10.1073/pnas.0910957106

Streit, A. (2018). Specification of sensory placode progenitors: signals and transcription factor networks. *Int. J. Dev. Biol.* 62, 195–205. doi: 10.1387/ijdb.170298as

Thiery, A., Buzzi, A. L., and Streit, A. (2020). Cell fate decisions during the development of the peripheral nervous system in the vertebrate head. *Curr. Top. Dev. Biol.* 139, 127–167. doi: 10.1016/bs.ctdb.2020.04.002

Trokovic, N., Trokovic, R., and Partanen, J. (2005). Fibroblast growth factor signalling and regional specification of the pharyngeal ectoderm. *Int. J. Dev. Biol.* 49, 797–805. doi: 10.1387/ijdb.051976nt

Trudel, S., Ely, S., Farooqi, Y., Affer, M., Robbiani, D. F., Chesi, M., et al. (2004). Inhibition of fibroblast growth factor receptor 3 induces differentiation and apoptosis in t(4;14) myeloma. *Blood* 103, 3521–3528. doi: 10.1182/blood-2003-10-3650

Tucker, A. S., Khamis, A. A., and Sharpe, P. T. (1998). Interactions between Bmp-4 and Msx-1 act to restrict gene expression to odontogenic mesenchyme. *Dev. Dyn.* 212, 533–539.

van Maele-Fabry, G., Delhaise, F., Gofflot, F., and Picard, J. J. (1993). Developmental table of the early mouse post-implantation embryo. *Toxicol. Vitro* 7, 719–725. doi: 10.1016/0887-2333(93)90073-E

van Maele-Fabry, G., Delhaise, F., and Picard, J. J. (1990). Morphogenesis and quantification of the development of post-implantation mouse embryos. *Toxicol. Vitro* 4, 149–156. doi: 10.1016/0887-2333(90)90037-T

Veitch, E., Begbie, J., Schilling, T. F., Smith, M. M., and Graham, A. (1999). Pharyngeal arch patterning in the absence of neural crest. *Curr. Biol.* 9, 1481–1484. doi: 10.1016/S0960-9822(00)80118-9

Wakamatsu, Y., Egawa, S., Terashita, Y., Kawasaki, H., Tamura, K., and Suzuki, K. (2019). Homeobox code model of heterodont tooth in mammals revised. *Sci. Rep.* 9:12865. doi: 10.1038/s41598-019-49116-x

Wang, J., Rhee, S., Palaria, A., and Tremblay, K. D. (2015). FGF signaling is required for anterior but not posterior specification of the murine liver bud. *Dev. Dyn.* 244, 431–443. doi: 10.1002/dvdy.24215

Washausen, S., and Knabe, W. (2013). Apoptosis contributes to placode morphogenesis in the posterior placodal area of mice. *Brain Struct. Funct.* 218, 789–803. doi: 10.1007/s00429-012-0429-y

Washausen, S., and Knabe, W. (2017). Pax2/Pax8-defined subdomains and the occurrence of apoptosis in the posterior placodal area of mice. *Brain Struct. Funct.* 222, 2671–2695. doi: 10.1007/s00429-016-1364-0

Washausen, S., and Knabe, W. (2018). Lateral line placodes of aquatic vertebrates are evolutionarily conserved in mammals. *Biol. Open* 7:bio031815. doi: 10.1242/bio.031815

Washausen, S., and Knabe, W. (2019). Chicken embryos share mammalian patterns of apoptosis in the posterior placodal area. *J. Anat.* 234, 551–563. doi: 10.1111/joa.12945

Washausen, S., Obermayer, B., Brunnett, G., Kuhn, H.-J., and Knabe, W. (2005). Apoptosis and proliferation in developing, mature, and regressing epibranchial placodes. *Dev. Biol.* 278, 86–102. doi: 10.1016/j.ydbio.2004.10.016

Wright, T. J., Ladher, R., McWhirter, J., Murre, C., Schoenwolf, G. C., and Mansour, S. L. (2004). Mouse FGF15 is the ortholog of human and chick FGF19, but is not uniquely required for otic induction. *Dev. Biol.* 269, 264–275. doi: 10.1016/j.ydbio.2004.02.003

Wright, T. J., and Mansour, S. L. (2003). Fgf3 and Fgf10 are required for mouse otic placode induction. *Development* 130, 3379–3390. doi: 10.1242/dev.00555

Yamagishi, T., Narematsu, M., and Nakajima, Y. (2020). Msx1 upregulates p27 expression to control cellular proliferation during valvuloseptal endocardial cushion formation in the chick embryonic heart. *Anat. Rec.* 304, 1732–1744. doi: 10.1002/ar.24572

Yu, P. B., Deng, D. Y., Lai, C. S., Hong, C. C., Cuny, G. D., Bouxsein, M. L., et al. (2008). BMP type I receptor inhibition reduces heterotopic ossification. *Nat. Med.* 14, 1363–1369. doi: 10.1038/nm.1888

Zhang, H., Wang, L., Yee Man, Wong, E., Lan Tsang, S., Xu, P.-X., et al. (2017). An Eya1-Notch axis specifies bipotential epibranchial differentiation in mammalian craniofacial morphogenesis. *eLife* 6:e30126. doi: 10.7554/eLife.30126

Conflict of Interest: The authors declare that the research was conducted in the absence of any commercial or financial relationships that could be construed as a potential conflict of interest.

Publisher's Note: All claims expressed in this article are solely those of the authors and do not necessarily represent those of their affiliated organizations, or those of the publisher, the editors and the reviewers. Any product that may be evaluated in this article, or claim that may be made by its manufacturer, is not guaranteed or endorsed by the publisher.

frontiers in Cell and Developmental Biology

REVIEW
published: 05 November 2021
doi: 10.3389/fcell.2021.784039

Interplay of Eph-Ephrin Signalling and Cadherin Function in Cell Segregation and Boundary Formation

David G. Wilkinson *

The Francis Crick Institute, London, United Kingdom

The segregation of distinct cell populations to form sharp boundaries is crucial for stabilising tissue organisation, for example during hindbrain segmentation in craniofacial development. Two types of mechanisms have been found to underlie cell segregation: differential adhesion mediated by cadherins, and Eph receptor and ephrin signalling at the heterotypic interface which regulates cell adhesion, cortical tension and repulsion. An interplay occurs between these mechanisms since cadherins have been found to contribute to Eph-ephrin-mediated cell segregation. This may reflect that Eph receptor activation acts through multiple pathways to decrease cadherin-mediated adhesion which can drive cell segregation. However, Eph receptors mainly drive cell segregation through increased heterotypic tension or repulsion. Cadherins contribute to cell segregation by antagonising homotypic tension within each cell population. This suppression of homotypic tension increases the difference with heterotypic tension triggered by Eph receptor activation, and it is this differential tension that drives cell segregation and border sharpening.

Keywords: Eph receptor, ephrin, cadherin, cell segregation, boundary formation, hindbrain segmentation

OPEN ACCESS

Edited by:
Dalit Sela-Donenfeld, The Hebrew University of Jerusalem, Israel

Reviewed by:
Artur Kania, Montreal Clinical Research Institute (IRCM), Canada
Sara L. Banerjee, Centre de recherche du Centre Hospitalier Universitaire (CHU) de Quebec-Université Laval, Canada in collaboration with reviewer AK
Karina S. Cramer, University of California, Irvine, United States

***Correspondence:**
David G. Wilkinson
david.wilkinson@crick.ac.uk

Specialty section:
This article was submitted to Morphogenesis and Patterning, a section of the journal Frontiers in Cell and Developmental Biology

Received: *27 September 2021*
Accepted: *25 October 2021*
Published: *05 November 2021*

Citation:
Wilkinson DG (2021) Interplay of Eph-Ephrin Signalling and Cadherin Function in Cell Segregation and Boundary Formation. Front. Cell Dev. Biol. 9:784039. doi: 10.3389/fcell.2021.784039

INTRODUCTION

The generation and maintenance of precisely patterned embryos requires that following the induction of specific cell or tissue types at the appropriate location, there are mechanisms to prevent intermingling between these distinct cell populations. In craniofacial development, this is exemplified by segmentation of the hindbrain to form a series of seven rhombomeres. The rhombomeres each have a distinct anteroposterior (A-P) identity which underlies the regional specification of neuronal cell types and branchial neural crest cells, and has a central role in coordinating the relationship between the central nervous system and craniofacial structures (Kiecker and Lumsden, 2005; Krumlauf and Wilkinson, 2021). At the molecular level, the segmentation and A-P patterning of the hindbrain involves the spatially-restricted expression of transcription factors, including Hox genes, mafB and Krox20, downstream of graded retinoic acid, Fgf and Wnt signals (Frank and Sela-Donenfeld, 2019; Krumlauf and Wilkinson, 2021). Initially, the borders of segmental gene expression are ragged (Irving et al., 1996; Cooke and Moens, 2002), reflecting imprecision in the formation and interpretation of graded signals (Zhang et al., 2012). Furthermore, the segmental pattern can potentially be scrambled by the intercalation of cells during tissue growth and convergent-extension movements (Fraser et al., 1990; Kimmel et al., 1994). Nevertheless, the initial fuzzy pattern of segmental gene expression is sharpened, at early stages through cell identity regulation (Addison et al., 2018), and later by mechanisms that drive cell segregation and prevent intermingling between segments (Fraser et al., 1990; Xu et al., 1995; Cooke

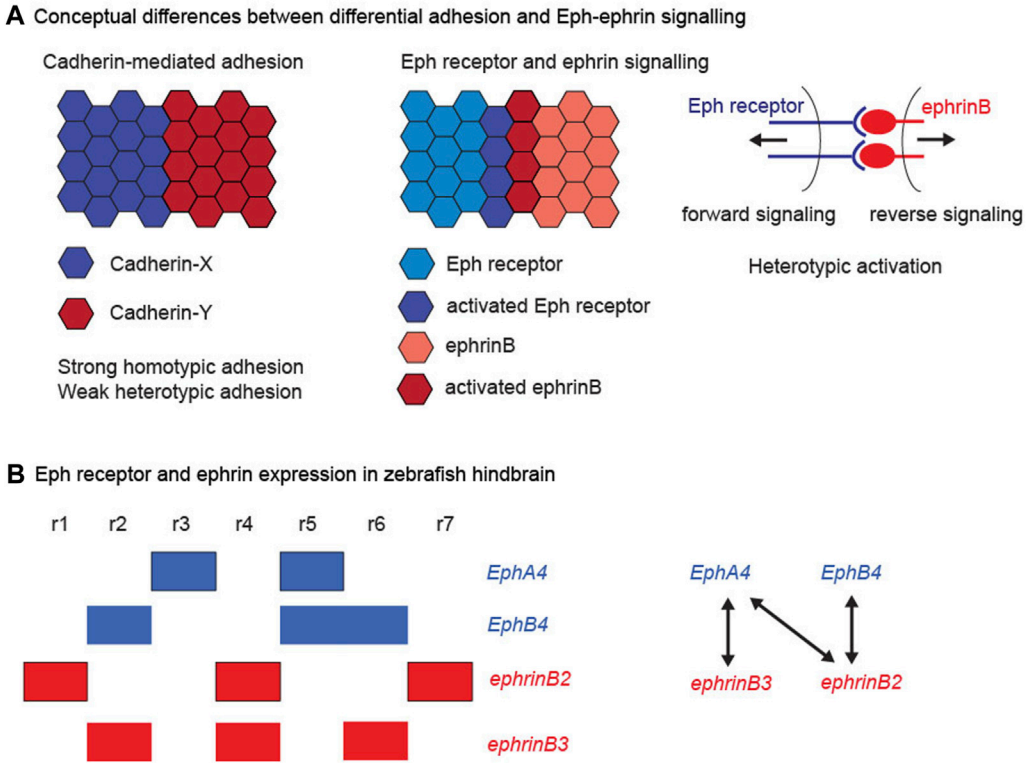

FIGURE 1 | Cadherins, Eph receptors and ephrins. **(A)** Conceptual differences between differential adhesion and Eph-ephrin signalling. The left hand panel illustrates the differential adhesion hypothesis, in which the differential expression of cadherin family members leads to high homotypic adhesion and lower heterotypic adhesion. This global difference in adhesion properties can drive cell segregation. The right hand panels illustrate the complementary expression and bidirectional activation of an interacting Eph receptor and ephrin. This leads to Eph-ephrin activation at the heterotypic interface, which regulates cell responses that can drive cell segregation. **(B)** Eph receptor and ephrin expression in the zebrafish hindbrain. The left hand panel depicts the segmental expression of EphA4, EphB4, ephrinB2, and ephrinB3. The right hand panel depicts the high affinity interactions between the family members, which have complementary expression, thus leading to strong activation at the segment borders.

et al., 2005; Kemp et al., 2009; Calzolari et al., 2014; Cayuso et al., 2019). Likewise, cell segregation mechanisms have critical roles throughout embryogenesis in the formation and maintenance of sharp borders between tissues and between regional domains within tissues (Dahmann et al., 2011).

Two sets of molecular players have been identified that underlie distinct mechanisms of cell segregation. The first to be identified were the classical cadherins, transmembrane proteins that mediate strong homophilic adhesion and are linked to the intracellular cytoskeleton. The cadherins comprise a family of proteins, which are differentially expressed and in some cases associated with specific tissue types, for example E-cadherin in many epithelial tissues and N-cadherin in the neural epithelium and neural crest. Since homophilic adhesion is stronger than heterophilic adhesion, the expression of different cadherin family members in adjacent cell populations leads to differential adhesion, which *in vitro* assays showed can drive cell segregation (Foty and Steinberg, 2005; Steinberg, 2007; Steinberg and Takeichi, 1994). Cadherin-mediated differential adhesion has been found to act in cell segregation *in vivo*, for example for cadherin6 and R-cadherin in subdivisions of the developing forebrain (Inoue et al., 2001) and for MN-cadherin in motor neuron cell types (Price et al., 2002). The second mechanism involves signalling at the interface of cell populations mediated by Eph receptors and ephrins. Eph-ephrin signalling leads to cell responses at the heterotypic interface that can drive cell segregation, and underlies the formation and maintenance of boundaries in many tissues during vertebrate development (Batlle and Wilkinson, 2012; Cayuso et al., 2015; Fagotto, 2020; Fagotto et al., 2014; Klein, 2012). Thus cell segregation can be driven by global differences in cell-cell adhesion or by cell responses to signalling between 2 cell populations (**Figure 1A**). This raises the question of whether cadherin-mediated adhesion and Eph-ephrin signalling act as alternative mechanisms used at distinct sites, and/or work together in some situations. In support of the latter possibility, both Eph-ephrin signalling and cadherins are required for cell segregation in cell culture assays (Cortina et al., 2007; Taylor et al., 2017), in clustering of cells to form discrete sympathetic ganglia (Kasemeier-Kulesa et al., 2006) and in the sharpening of specific borders (Kesavan et al., 2020). This review will first summarise current understanding of the mechanisms by which Eph-ephrin signalling drives cell segregation, and then focus on

the relationships and potential cross-talk between Eph-ephrin signalling and cadherins.

MECHANISMS OF EPH-EPHRIN SIGNALLING IN CELL SEGREGATION

Eph receptors are a family of transmembrane receptor tyrosine kinases with an extracellular domain that interacts with ephrin ligands. Ephrins are also membrane-bound, either through a GPI linkage (ephrinAs) or through a transmembrane domain (ephrinBs), and with a few exceptions interact with the EphA and EphB subfamilies of receptors, respectively (Gale et al., 1996a; Gale et al., 1996b). Binding of Eph receptor to ephrin leads to clustering of the complex, and this triggers intracellular signal transduction downstream of both components, termed forward and reverse signalling, respectively (Pasquale, 2008; Klein, 2012). Both forward and reverse signalling involve tyrosine phosphorylation, either by the receptor tyrosine kinase domain or by cytoplasmic tyrosine kinases that phosphorylate the intracellular domain of ephrinBs. In addition, there are kinase-independent pathways, which include recruitment of PDZ domain proteins to the C-terminus of Eph and ephrinB proteins. Since both Eph receptors and ephrins are membrane-bound this leads to bidirectional cell contact-dependent signalling, but signalling may also occur at a distance through secretion of ligand-bearing exosomes (Gong et al., 2016).

Expression of high affinity Eph receptor and ephrin binding partners often occurs in complementary domains, such that interactions occur at boundaries of distinct tissues or subdivisions within tissues (Gale et al., 1996b). For example, in the zebrafish hindbrain, expression of EphB4 in r2, r5, and r6 is complementary to ephrinB2 in r1, r4, and r7, and expression of EphA4 in r3 and r5 is complementary to ephrinB3 in r2, r4, and r6, as well as to ephrinB2 (**Figure 1B**). There is extensive evidence that signalling through these Eph receptors and ephrins underlies the sharpening of segment borders in the hindbrain (Xu et al., 1995; Xu et al., 1999; Cooke et al., 2001; Cooke et al., 2005; Kemp et al., 2009; Sela-Donenfeld et al., 2009; Calzolari et al., 2014; Cayuso et al., 2019). Studies of cell segregation and border formation *in vivo* have found a dominant role of Eph receptor forward signalling through kinase-dependent pathways (Cayuso et al., 2019; O'Neill et al., 2016; Rohani et al., 2014), although reverse signalling through ephrinBs could also contribute (Wu et al., 2019). Eph receptor activation can lead to three types of cell response that can drive cell segregation and restrict intermingling across borders: (1) A decrease in cadherin-mediated adhesion, which will lead to lower heterotypic compared with homotypic adhesion. (2) An increase in cortical tension by contraction of cortical actomyosin, through Rho kinase activation leading to myosin light chain phosphorylation and myosin II activation. (3) The repulsion and directional migration of cells following cell-cell contact by repolarising the front-rear orientation of migrating cells. Which of these mechanisms is utilised may relate to whether the boundary is within an epithelial tissue, at the interface of tissues, or between mesenchymal cells. For example, the generation of sustained tension requires adhesive contacts between cells (Maitre et al., 2012), as occurs within epithelial tissues, whereas migratory mesenchymal cells can repel and move away from each other after contact.

REQUIREMENT FOR CADHERINS IN EPH-EPHRIN-MEDIATED CELL SEGREGATION

One situation in which Eph-ephrin signalling and cadherins are both required for cell segregation is illustrated by studies of the formation of sympathetic ganglia. Initially the ganglionic cells are spread out along the A-P axis, and then migrate to form a series of discrete clusters (Kasemeier-Kulesa et al., 2006). This segregation is driven by Eph-mediated repulsion that excludes ganglionic cells from interganglionic regions (Krull et al., 1997; Wang and Anderson, 1997), together with N-cadherin-mediated adhesion between ganglionic cells (Kasemeier-Kulesa et al., 2006). Such segregation can be explained by synergy between parallel roles of Eph-ephrin-mediated repulsion and cadherin-mediated adhesion (Kasemeier-Kulesa et al., 2006), in which cells are responding to a pre-pattern of ephrin expression in the adjacent mesenchyme. This is a different scenario from cell segregation between distinct tissues, or subdivisions within a tissue, in which cells are not responding to a prepattern in another tissue. Nevertheless, as discussed below, a similar synergy of repulsion and adhesion mechanisms may contribute to cell segregation.

Studies in cell culture assays and *in vivo* have suggested that cadherins are required for cell segregation that is driven by Eph-ephrin signalling. For example, in cell culture assays, EphB2 and ephrinB1-expressing colorectal cancer cell lines were found to segregate from each other, but this segregation was disrupted by knockdown of E-cadherin (Cortina et al., 2007). Likewise, EphB2 and ephrinB1-expressing HEK293 cells segregate from each other (Poliakov et al., 2008), and this is decreased by knockdown of N-cadherin (Taylor et al., 2017). Assays in which cells from different rhombomeres from chick embryos are mixed *in vitro* suggested a requirement for cadherins in segregation (Wizenmann and Lumsden, 1997), which subsequent work found is driven by Eph receptor and ephrin signalling (Xu et al., 1999; Cooke et al., 2005; Kemp et al., 2009; Sela-Donenfeld et al., 2009; Calzolari et al., 2014; Cayuso et al., 2019). Similarly, recent work has found that both Eph-ephrin signalling and N-cadherin function are required for sharpening of the mid-hindbrain boundary (Kesavan et al., 2020). At the boundaries in the midbrain and hindbrain, and in the cell culture assays, there is no apparent difference in expression of the relevant cadherin between the segregating cell populations. It is therefore unlikely that the segregation involves synergy between differential adhesion and Eph-ephrin-mediated repulsion. There are a number of other potential explanations for the involvement of cadherins: (1) Cadherins are required for the correct expression and/or activation of Eph receptors and ephrins; (2) Eph receptors drive cell segregation through the modulation of cadherin function; (3) Cell segregation involves a balance in cell responses in which Eph receptor signalling and

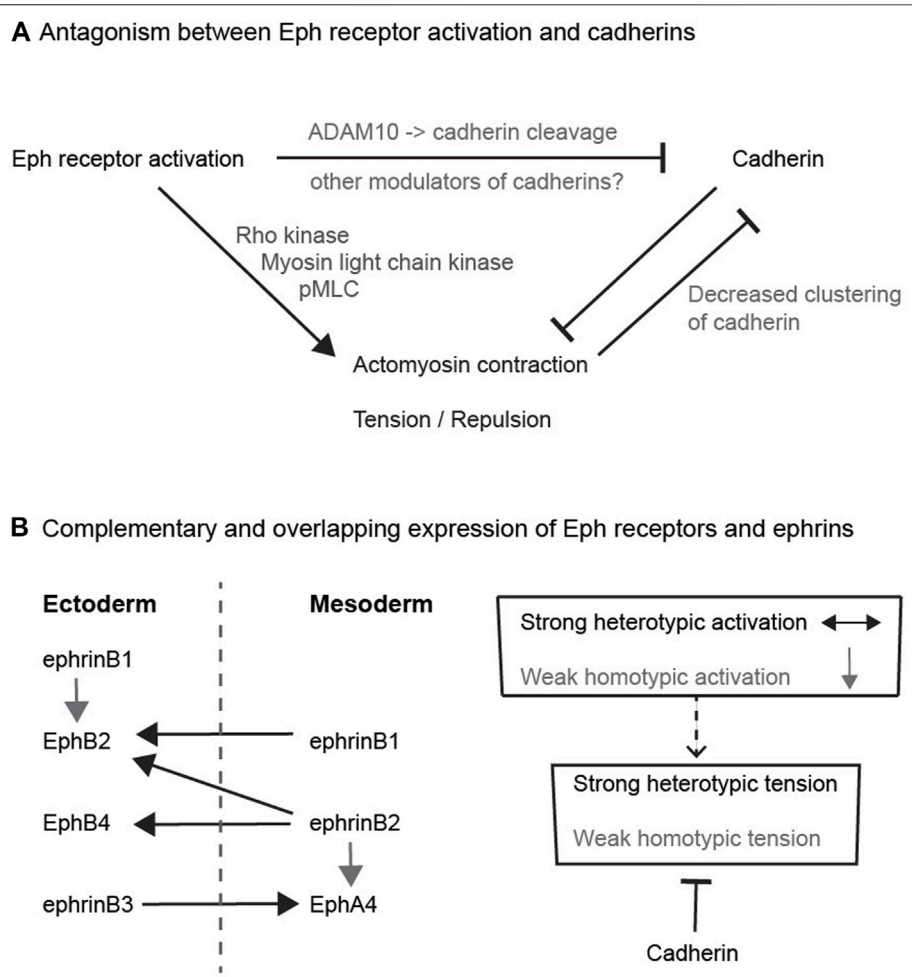

FIGURE 2 | Potential relationships between Eph receptors and cadherins **(A)** Antagonism between Eph receptor activation and cadherins. The diagram depicts the antagonism between adhesion and cortical tension, and pathways that have been found to link Eph receptor activation to decreased cadherin function. **(B)** Complementary and overlapping expression of Eph receptors and ephrins. The left hand diagram depicts the expression pattern and interactions of Eph receptors and ephrins in ectoderm and mesoderm in *Xenopus*. Each tissue expresses a combination of Eph receptors and ephrins that leads to strong heterotypic activation (black arrows) of Eph receptors in both directions that underlies increased cortical tension and cell repulsion. In addition, there is weaker homotypic activation of Eph receptor by low-level or low-affinity ephrin co-expressed within each tissue (grey arrows). The right hand diagram depicts that cadherins may serve to suppress the weaker homotypic tension due to overlapping Eph-ephrin expression, whereas strong heterotypic Eph receptor activation dominates over cadherin-mediated adhesion.

cadherins oppose each other. Evidence in support of these potential relationships are discussed below.

REGULATION OF EPH RECEPTOR EXPRESSION AND LOCALISATION BY CADHERINS

The switching of cadherin expression from E-cadherin to N-cadherin is an important factor in the epithelial to mesenchymal transition and migratory behaviour of neural crest cells (Scarpa et al., 2015). Interestingly, in ES cells mutant for E-cadherin there is a decrease in EphA2 expression and increased expression of EphB4, ephrinA1, ephrinA2, ephrinB1, ephrinB2, and ephrinB3 (Orsulic and Kemler, 2000). The decrease in EphA2 expression was rescued by transfection of E-cadherin but not N-cadherin, and significantly the overexpression of E-cadherin in NIH3T3 cells led to an increase in EphA2 expression (Orsulic and Kemler, 2000). Furthermore, E-cadherin was found to be required for the localisation and phosphorylation of EphA2 at cell-cell contacts (Zantek et al., 1999; Orsulic and Kemler, 2000). It is therefore important to consider the possibility that knockout or knockdown of cadherin genes have led to a change in the developmental expression of Eph receptors and ephrins, and/or a decrease in cell surface localisation and activation of Eph receptors.

Interestingly, there is also evidence for regulatory relationships in the converse direction, in which Eph-ephrin activation can increase the level of cadherins at the cell surface. The segregation and migration of Schwann cells during peripheral nerve regeneration is mediated by EphB2 activation by ephrinB

ligands, which through Sox2 leads to relocalization of N-cadherin to intercellular contacts of Schwann cells (Parrinello et al., 2010). Similarly, Eph-ephrin signalling in the pharyngeal endoderm leads to an increase in junctional E-cadherin, in this case through a pathway that involves targeting of Pak2a to the plasma membrane and Wnt4/Cdc42 activation (Choe and Crump, 2015). Another pathway has been found in neural crest cells, in which ephrinB2 negatively regulates E-cadherin recycling, and upon activation by EphB receptor this inhibition is relieved, leading to increased E-cadherin at the cell surface (Yoon et al., 2018). Intriguingly, recent work has found a direct interaction between E-cadherin and ephrinB1 (Shafraz et al., 2020), suggesting another way in which they could influence the subcellular localisation of each other.

MODULATION OF CADHERIN FUNCTION BY EPH RECEPTORS

Several pathways have been uncovered that link Eph-ephrin interactions to a decrease in cadherin function (**Figure 2A**), such that there is less adhesion across the heterotypic interface than for homotypic contacts. In principle, this quantitative difference between homotypic and heterotypic adhesion could drive cell segregation (Steinberg, 2007). In one mechanism, the extracellular domain of EphB receptors interacts with the metalloproteinase, ADAM10, which is activated upon binding to ephrinB1 (Solanas et al., 2011). Activated ADAM10 cleaves the extracellular domain of E-cadherin, leading to shedding of cadherin and decreased adhesion at the interface (Solanas et al., 2011). Furthermore, blocking of ADAM10 disrupts Eph receptor-mediated cell segregation in cell culture assays and in the intestinal epithelium (Solanas et al., 2011). A related role has been found in the cochlear sensory epithelium, in which EphA4-ephrinB2 interactions lead to E-cadherin cleavage by ADAM10 that enables separation of adjacent cells (Defourny et al., 2019). In addition to cleaving E-cadherin, ADAM10 mediates cleavage of ephrinA ligands from the cell surface following interaction with EphA receptors (Hattori et al., 2000; Janes et al., 2005; Atapattu et al., 2012). Since Eph-ephrin interactions can potentially mediate strong adhesion, such proteolytic cleavage, and/or endocytosis of Eph receptors and ephrins (Marston et al., 2003; Zimmer et al., 2003), are essential for cells to disengage following their interaction.

In a second type of mechanism, EphB4 activation at the notochord-presomitic mesoderm boundary was shown to decrease the clustering of C-cadherin compared with homotypic contacts (Fagotto et al., 2013). The decrease in cadherin clustering was regulated by myosin activation leading to increased cortical tension (Fagotto et al., 2013). Since clustering of cadherins increases adhesion, this pathway leads to a decrease in adhesion at the heterotypic interface. Finally, proteomic studies to identify tyrosine phosphorylation targets downstream of Eph receptor and ephrin activation have found other pathways that potentially modulate cadherin function. For example, analysis of EphB2 and ephrinB1 expressing HEK293 cells found a decrease in tyrosine phosphorylation of several mediators of adhesion, and of regulators of cadherin endocytosis and stability, including Cadm1, Pcdh7, Ctnnd1, Cttn, and Dcs2 (Jorgensen et al., 2009). Furthermore, forward and reverse signalling was found to have distinct effects on the different multiple tyrosine phosphorylation sites of Cttn and Ctnnd1. Ctnnd1 (p120-catenin) is especially interesting as it both stabilises E-cadherin at the cell surface and suppresses RhoA function, and thus a decrease in its activity leads to less adhesion and greater tension (Yu et al., 2016). It will be interesting to determine whether the changes in tyrosine phosphorylation downstream of Eph-ephrin signalling modulate the function of these proteins in the regulation of adhesion.

These findings are consistent with the idea that cadherins are required for Eph-ephrin-mediated cell segregation because decreased heterotypic adhesion is driving segregation. This raises the question of the relative contribution of decreased adhesion compared with increased cortical tension or cell repulsion responses to Eph receptor activation, that can also potentially drive cell segregation. This was addressed in studies in which cell responses were quantitated and the measurements used in computer simulations of cell segregation and border sharpening. The formation of a sharp border between ectoderm and mesoderm in *Xenopus* depends upon activation of Eph receptors that leads to high heterotypic tension and cell repulsion at the interface (Rohani et al., 2011; Canty et al., 2017). In computer simulations it was found that cell segregation and border sharpening is efficiently driven when heterotypic tension is higher than the homotypic tension that occurs within each cell population (Canty et al., 2017). In contrast, global differences in tension or adhesion between the 2 cell populations are less efficient (Canty et al., 2017). This prediction was tested in cell segregation assays and it was found that, unlike Eph-ephrin signalling, differential expression of E-cadherin and N-cadherin does not drive the separation of tissues (Canty et al., 2017).

A similar conclusion came from use of cell culture assays with EphB2 and ephrinB1 expressing HEK293 cells (Taylor et al., 2017). Analysis of cell behaviour at low density revealed strong repulsion and transient adhesion following heterotypic contacts between cells (Taylor et al., 2017). Cell repulsion involves a rapid collapse of cell processes at the site of heterotypic contact, and reorientation of front-rear polarity so that the cells migrate away from each other. This is likely mediated by localised activation of Rho family GTPases that are targets of Eph receptor signalling and regulate the actin cytoskeleton (Pasquale, 2008; Klein, 2012). It may also involve Par proteins that regulate the front-rear polarity of migrating cells since these are among the phosphorylation targets of activated EphB2 (Jorgensen et al., 2009). Since HEK293 cells are intrinsically motile at low density, cell repulsion need not lead to an increase in overall migration, but rather a reorientation after each contact. Agent-based simulations with the measured values of repulsion and cell contact duration found that heterotypic repulsion drives efficient segregation and border sharpening, whereas a heterotypic decrease in adhesion alone does not (Taylor et al., 2017). Taken together, these studies suggest that increased heterotypic repulsion or tension drive efficient segregation and

are the principal mechanisms by which Eph-ephrin signalling leads to border sharpening. Consistent with this, a number of studies have revealed increased tension and cell repulsion at sites of Eph-ephrin interactions at borders of tissues and in cell segregation assays (Fagotto et al., 2013; Kindberg et al., 2021; O'Neill et al., 2016; Rohani et al., 2011). Nevertheless, it remains possible that decreased cadherin-mediated adhesion at heterotypic contacts drives Eph-ephrin-mediated cell segregation in some contexts. Another possibility is that the decrease in cadherin-mediated adhesion can promote cell segregation because there is antagonism between tension and adhesion, as discussed below. A decrease in heterotypic adhesion may thus contribute to the increase in tension and triggering of repulsion following Eph receptor activation.

ANTAGONISM BETWEEN ADHESION AND TENSION

There is an intimate mechanistic relationship in which cadherin-mediated adhesion antagonises the generation of tension and cell repulsion by actomyosin contraction in the cell cortex (Winklbauer, 2015). Conceptually, this is illustrated by the effect of increasing the strength of adhesion between two cells, which increases their area of contact, and is decreased by actomyosin contraction that generates tension (Lecuit and Lenne, 2007). Consideration of the forces that underlie cell segregation suggest that the binding energy of cadherins alone makes a minor contribution, and rather cadherins mainly act by decreasing cortical tension (Winklbauer, 2015). Cadherin-mediated adhesion and actomyosin contraction downstream of Eph-ephrin signalling may thus act in opposition to regulate the strength of cortical tension.

At first sight, it is not intuitive that such antagonism between cadherins and Eph-ephrin signalling would contribute to cell segregation. However, a potential role is suggested by detailed studies of Eph receptor and ephrin expression. Initial studies emphasised that interacting Eph receptors and ephrins have complementary expression, such that interactions only occur at the interface (Gale et al., 1996b). However, more comprehensive analyses have found that there are also some overlaps in expression, which have been best described for ectoderm and mesoderm in *Xenopus*, where Eph receptor activation has a critical role in preventing cell intermingling (Rohani et al., 2011; Rohani et al., 2014). It was found that each cell population expresses a cocktail of Eph receptors and ephrins: EphB4, EphB2, ephrinB3 and ephrinB1 in ectoderm, and EphA4, ephrinB2 and ephrinB1 in mesoderm (Rohani et al., 2014); (**Figure 2B**). The activation of Eph receptors following homotypic or heterotypic cell contacts can be predicted from measurements of Eph-ephrin binding affinity: EphB4 has high affinity only for ephrinB2, EphA4 binds to ephrinB3 and ephrinB2, and EphB2 binds to ephrinB1 and ephrinB2 (Gale et al., 1996a; Gale et al., 1996b). Consequently, there is heterotypic activation of EphB4 by ephrinB2, of EphB2 by ephrinB2 and ephrinB1, and of EphA4 by ephrinB3, such that forward signalling occurs in both directions at the interface of ectoderm and mesoderm (Rohani et al., 2011; Rohani et al., 2014). In addition, there is homotypic activation of EphA4 by ephrinB2, and of EphB2 by ephrinB1, within ectoderm and mesoderm. This predicts that in addition to strong Eph receptor activation at the tissue interface, there is Eph receptor activation within each cell population (**Figure 2B**). Furthermore, depletion of cadherins leads to an increase in homotypic tension and repulsion of cells, consistent with antagonism between adhesion and repulsion (Rohani et al., 2014). The role of such antagonism was tested by analysing the effect of overexpressing cadherin in ephrin-expressing cells juxtaposed with Eph receptor-expressing cells (Canty et al., 2017). It was found that cadherin expression increased cohesion and decreased tension at homotypic contacts, leading to a greater difference between heterotypic and homotypic tension that drives cell segregation (Canty et al., 2017). Importantly, this role of cadherins in suppressing homotypic tension has a much stronger input into cell segregation than differential cadherin-mediated adhesion (Canty et al., 2017).

Similar insights have come from cell culture assays with HEK293 cell lines over-expressing EphB2 or ephrinB1 (Taylor et al., 2017). The segregation and formation of sharp borders between EphB2 and ephrinB1 expressing cells is driven by strong heterotypic activation leading to cell repulsion at low density (Taylor et al., 2017) and increased cortical tension when cells are confluent (Kindberg et al., 2021). There is also a repulsion response, that is less strong. following homotypic interactions between EphB2 expressing cells, which is due to overlapping expression of ephrinB family members intrinsic to HEK293 cells (Taylor et al., 2017). Cell segregation and formation of a sharp border are decreased by knockdown of N-cadherin, the main cadherin expressed by these cells. Measurements of cell behaviour found that N-cadherin knockdown leads to a decrease in adhesive interactions and increase in cell repulsion. The increase in cell repulsion was much greater for homotypic interactions than for heterotypic interactions, leading to a narrowing of the quantitative difference between heterotypic and homotypic repulsion (Taylor et al., 2017). N-cadherin may thus counterbalance the low level cell repulsion response to weak homotypic Eph receptor activation, whereas strong heterotypic Eph receptor activation leads to repulsion that is little affected by N-cadherin. Since the difference between heterotypic versus homotypic cell responses drives segregation, cadherins facilitate segregation by suppressing homotypic tension and repulsion (Canty et al., 2017; Taylor et al., 2017).

A recent study has presented a different perspective on the role of cadherins and EphB2 in cell segregation (Kindberg et al., 2021). Using cell cultures at high density, in which cells are in sustained contact and migration is constrained, the segregation of EphB2 and ephrinB1 cells was shown to be driven by greater heterotypic than homotypic cortical tension. This high heterotypic tension is dependent on actomyosin contraction downstream of Rho kinase (ROCK) and myosin light chain kinase (MLCK). It was found that blocking of cadherin-mediated adhesion by depletion of calcium had no significant effect on EphB2/ephrinB1 cell segregation. This result contrasts with other work with the same cell lines that found a decrease in cell segregation and border sharpening following knockdown of N-cadherin (Taylor et al., 2017). The apparent discrepancy may reflect differences in the sensitivity of the methods used to quantitate segregation, and/or in the effects of calcium depletion compared with N-cadherin

knockdown. Interestingly, both studies found that following mixing with ephrinB1 cells, EphB2 cells aggregate into clusters in which there is increased homotypic contact between cells (Taylor et al., 2017; Kindberg et al., 2021). Kindberg et al. (2021) present evidence that this homotypic EphB2 cell-cell interaction does not involve cadherins, but rather is driven by a high level of cortical tension at the cell-medium interface. In contrast, Taylor et al. (2017) suggest a role of N-cadherin since its knockdown leads to an increase in repulsion and decrease in the duration of contact following homotypic interaction of EphB2 cells. A potential complication to experiments with these cell lines is that heterotypic interactions lead to a major decrease in the steady state level of EphB2 due to endocytosis of receptor-ligand complexes (Wu et al., 2019). Furthermore, HEK293 cells endogenously express low levels of ephrinB ligands that impact on EphB2 cell segregation and likely underlie homotypic repulsion (Taylor et al., 2017). The decrease in homotypic EphB2 cell repulsion and increase in cell contact that occurs following heterotypic activation of EphB2 by ephrinB1-expressing cells (Taylor et al., 2017) may thus be due to the decrease in the steady state level of EphB2. It will be interesting to determine whether this effect of heterotypic Eph receptor activation on homotypic cell interactions in a cell culture model is relevant to cell segregation *in vivo*.

SUMMARY AND PERSPECTIVES ON BORDER SHARPENING IN THE HINDBRAIN

Two main themes have emerged from studies of the relationships between Eph-ephrin signalling and cadherins. The first is that Eph receptors can act through multiple pathways to inhibit cadherin function (**Figure 2A**). However, although this can lead to a heterotypic decrease in adhesion, it is increased cortical tension or repulsion downstream of Eph receptor activation that is the principal driver of cell segregation. Since cadherins antagonise cortical tension, the inhibition of cadherin function may thus contribute to the increase in tension at the heterotypic interface. The second theme is that this antagonism by cadherins may suppress homotypic tension within each cell population. This tension can be due to overlapping expression of Eph receptors and ephrins that leads to weak activation at homotypic contacts, as shown for the ectoderm-mesoderm border (**Figure 2B**). Another possibility is suggested by evidence for ligand-independent responses of cells to Eph receptors and ephrins (Noren et al., 2009; Daar, 2012; Miao and Wang, 2012; Lisabeth et al., 2013). Such ligand-independent pathways can regulate actomyosin contraction and cell morphology (Bochenek et al., 2010; Cayuso et al., 2016), and may thus increase tension at homotypic contacts. Whether through overlapping Eph-ephrin expression, or ligand-independent pathways, an increase in homotypic tension is counteracted by cadherin-mediated adhesion, thus increasing the difference between heterotypic and homotypic tension that drives cell segregation and border sharpening.

A model for how cells segregate to form sharp segment borders in the hindbrain can be proposed based on analyses of Eph-ephrin function in other tissues, summarised above, together with studies in the hindbrain itself. The initial ragged border of hindbrain segments is transformed into a sharp and straight border through a combination of cell identity regulation (Zhang et al., 2012; Addison et al., 2018) and Eph-ephrin-mediated cell segregation (Xu et al., 1995; Xu et al., 1999; Cooke et al., 2001; Cooke et al., 2005; Kemp et al., 2009; Calzolari et al., 2014; Cayuso et al., 2019). Cell segregation is likely driven by increased cortical tension at the heterotypic interface, principally through Eph receptor forward signaling (Cayuso et al., 2019) that acts through ROCK and MLCK to increase actomyosin contraction. An actomyosin cable is detected at the segment borders after they have sharpened, which generates sustained tension required to maintain border sharpness (Calzolari et al., 2014). In addition, through the Yap/Taz pathway the sustained tension induces formation of specialised hindbrain boundary cells (Cayuso et al., 2019) and regulates the balance of cell proliferation and neurogenesis (Voltes et al., 2019).

In this model, the complementary expression of interacting Eph receptors and ephrins (**Figure 1B**) leads to heterotypic activation at the segment borders which drives cell segregation. However, this does not account for the finding that mosaic knockdown of EphA4 (expressed in r3 + r5) leads to segregation of the knockdown cells within r3 + r5 to the segment borders (Cooke et al., 2005). Similarly, mosaic knockdown of ephrinB2 leads to cell segregation within the ephrinB2-expressing segments (Kemp et al., 2009). These findings can be explained if there is weak activation of Eph receptors within segments due to overlapping expression with ligands, analogous to findings for the ectoderm-mesoderm border (Rohani et al., 2014), and/or ligand-independent pathways that increase cortical tension. Such homotypic tension is counter-balanced by N-cadherin-mediated adhesion, thus increasing the difference between homotypic and heterotypic tension. This predicts that hindbrain border sharpening is disrupted in a zebrafish N-cadherin mutant (parachute), similar to findings for the midbrain-hindbrain border (Kesavan et al., 2020). Mosaic knockdown of Eph receptors or ephrins will consequently create a decrease in cortical tension compared with cells lacking the knockdown, thus leading to cell segregation within the segments. A comprehensive understanding of Eph receptor and ephrin expression and function in the hindbrain will be needed to test these ideas.

More broadly, in the context of craniofacial development, it will be interesting to explore potential relationships between Eph-ephrin signalling and cadherins in branchial neural crest migration. Early studies found complementary expression between EphA4 plus EphB1 and ephrinB2 in branchial neural crest streams in *Xenopus*, and that dominant negative blocking and ephrin overexpression led to incorrect migration into branchial arches (Smith et al., 1997). Intriguingly, N-cadherin has an important role in branchial neural crest cell migration in which it promotes homotypic contact repulsion (contact inhibition of locomotion) by polarising Rac activity to be stronger distal to the cell-cell contact (Theveneau et al., 2010;

Scarpa et al., 2015). This suggests a distinct relationship, in which rather than suppressing repulsion responses to Eph receptor activation, N-cadherin itself promotes repulsion. It will therefore be important to understand the mechanistic basis of context-dependent functions of N-cadherin in cell repulsion and adhesion and how these affect the interplay with Eph-ephrin signalling.

AUTHOR CONTRIBUTIONS

The author confirms being the sole contributor of this work and has approved it for publication.

FUNDING

The DW lab is supported by the Francis Crick Institute which receives its core funding from Cancer Research UK (FC001217), the UK Medical Research Council (FC001217), and the Wellcome Trust (FC001217).

ACKNOWLEDGMENTS

I am grateful to Qiling Xu and Monica Tambalo for advice and discussions.

REFERENCES

Addison, M., Xu, Q., Cayuso, J., and Wilkinson, D. G. (2018). Cell Identity Switching Regulated by Retinoic Acid Signaling Maintains Homogeneous Segments in the Hindbrain. *Dev. Cel.* 45, 606–620. doi:10.1016/j.devcel.2018.04.003

Atapattu, L., Saha, N., Llerena, C., Vail, M. E., Scott, A. M., Nikolov, D. B., et al. (2012). Antibodies Binding the ADAM10 Substrate Recognition Domain Inhibit Eph Function. *J. Cel Sci.* 125, 6084–6093. doi:10.1242/jcs.112631

Batlle, E., and Wilkinson, D. G. (2012). Molecular Mechanisms of Cell Segregation and Boundary Formation in Development and Tumorigenesis. *Cold Spring Harbor Perspect. Biol.* 4, a008227. doi:10.1101/cshperspect.a008227

Bochenek, M. L., Dickinson, S., Astin, J. W., Adams, R. H., and Nobes, C. D. (2010). Ephrin-B2 Regulates Endothelial Cell Morphology and Motility Independently of Eph-Receptor Binding. *J. Cel Sci.* 123, 1235–1246. doi:10.1242/jcs.061903

Calzolari, S., Terriente, J., and Pujades, C. (2014). Cell Segregation in the Vertebrate Hindbrain Relies on Actomyosin Cables Located at the Interhombomeric Boundaries. *EMBO J.* 33, 686–701. doi:10.1002/embj.201386003

Canty, L., Zarour, E., Kashkooli, L., François, P., and Fagotto, F. (2017). Sorting at Embryonic Boundaries Requires High Heterotypic Interfacial Tension. *Nat. Commun.* 8, 157. doi:10.1038/s41467-017-00146-x

Cayuso, J., Xu, Q., and Wilkinson, D. G. (2015). Mechanisms of Boundary Formation by Eph Receptor and Ephrin Signaling. *Dev. Biol.* 401, 122–131. doi:10.1016/j.ydbio.2014.11.013

Cayuso, J., Dzementsei, A., Fischer, J. C., Karemore, G., Caviglia, S., Bartholdson, J., et al. (2016). EphrinB1/EphB3b Coordinate Bidirectional Epithelial-Mesenchymal Interactions Controlling Liver Morphogenesis and Laterality. *Dev. Cel.* 39, 316–328. doi:10.1016/j.devcel.2016.10.009

Cayuso, J., Xu, Q., Addison, M., and Wilkinson, D. G. (2019). Actomyosin Regulation by Eph Receptor Signaling Couples Boundary Cell Formation to Border Sharpness. *Elife* 8, e49696. doi:10.7554/eLife.49696

Choe, C. P., and Crump, J. G. (2015). Eph-Pak2a Signaling Regulates Branching of the Pharyngeal Endoderm by Inhibiting Late-Stage Epithelial Dynamics. *Development* 142, 1089–1094. doi:10.1242/dev.115774

Cooke, J. E., and Moens, C. B. (2002). Boundary Formation in the Hindbrain: Eph Only it Were Simple. *Trends Neurosci.* 25, 260–267. doi:10.1016/s0166-2236(02)02134-3

Cooke, J., Moens, C., Roth, L., Durbin, L., Shiomi, K., Brennan, C., et al. (2001). Eph Signalling Functions Downstream of Val to Regulate Cell Sorting and Boundary Formation in the Caudal Hindbrain. *Development* 128, 571–580. doi:10.1242/dev.128.4.571

Cooke, J. E., Kemp, H. A., and Moens, C. B. (2005). EphA4 Is Required for Cell Adhesion and Rhombomere-Boundary Formation in the Zebrafish. *Curr. Biol.* 15, 536–542. doi:10.1016/j.cub.2005.02.019

Cortina, C., Palomo-Ponce, S., Iglesias, M., Fernández-Masip, J. L., Vivancos, A., Whissell, G., et al. (2007). EphB-ephrin-B Interactions Suppress Colorectal Cancer Progression by Compartmentalizing Tumor Cells. *Nat. Genet.* 39, 1376–1383. doi:10.1038/ng.2007.11

Daar, I. O. (2012). Non-SH2/PDZ Reverse Signaling by Ephrins. *Semin. Cel Dev. Biol.* 23, 65–74. doi:10.1016/j.semcdb.2011.10.012

Dahmann, C., Oates, A. C., and Brand, M. (2011). Boundary Formation and Maintenance in Tissue Development. *Nat. Rev. Genet.* 12, 43–55. doi:10.1038/nrg2902

Defourny, J., Peuckert, C., Kullander, K., and Malgrange, B. (2019). EphA4-ADAM10 Interplay Patterns the Cochlear Sensory Epithelium through Local Disruption of Adherens Junctions. *iScience* 11, 246–257. doi:10.1016/j.isci.2018.12.017

Fagotto, F., Rohani, N., Touret, A.-S., and Li, R. (2013). A Molecular Base for Cell Sorting at Embryonic Boundaries: Contact Inhibition of Cadherin Adhesion by Ephrin/Eph-Dependent Contractility. *Dev. Cel.* 27, 72–87. doi:10.1016/j.devcel.2013.09.004

Fagotto, F., Winklbauer, R., and Rohani, N. (2014). Ephrin-Eph Signaling in Embryonic Tissue Separation. *Cell Adhes. Migr.* 8, 308–326. doi:10.4161/19336918.2014.970028

Fagotto, F. (2020). Tissue Segregation in the Early Vertebrate Embryo. *Semin. Cel Dev. Biol.* 107, 130–146. doi:10.1016/j.semcdb.2020.05.020

Foty, R. A., and Steinberg, M. S. (2005). The Differential Adhesion Hypothesis: a Direct Evaluation. *Dev. Biol.* 278, 255–263. doi:10.1016/j.ydbio.2004.11.012

Frank, D., and Sela-Donenfeld, D. (2019). Hindbrain Induction and Patterning during Early Vertebrate Development. *Cell. Mol. Life Sci.* 76, 941–960. doi:10.1007/s00018-018-2974-x

Fraser, S., Keynes, R., and Lumsden, A. (1990). Segmentation in the Chick Embryo Hindbrain Is Defined by Cell Lineage Restrictions. *Nature* 344, 431–435. doi:10.1038/344431a0

Gale, N. W., Flenniken, A., Compton, D. C., Jenkins, N., Copeland, N. G., Gilbert, D. J., et al. (1996a). Elk-L3, a Novel Transmembrane Ligand for the Eph Family of Receptor Tyrosine Kinases, Expressed in Embryonic Floor Plate, Roof Plate and Hindbrain Segments. *Oncogene* 13, 1343–1352.

Gale, N. W., Holland, S. J., Valenzuela, D. M., Flenniken, A., Pan, L., Ryan, T. E., et al. (1996b). Eph Receptors and Ligands Comprise Two Major Specificity Subclasses and Are Reciprocally Compartmentalized during Embryogenesis. *Neuron* 17, 9–19. doi:10.1016/s0896-6273(00)80276-7

Gong, J., Körner, R., Gaitanos, L., and Klein, R. (2016). Exosomes Mediate Cell Contact-independent Ephrin-Eph Signaling during Axon Guidance. *J. Cel Biol.* 214, 35–44. doi:10.1083/jcb.201601085

Hattori, M., Osterfield, M., and Flanagan, J. G. (2000). Regulated Cleavage of a Contact-Mediated Axon Repellent. *Science* 289, 1360–1365. doi:10.1126/science.289.5483.1360

Inoue, T., Tanaka, T., Takeichi, M., Chisaka, O., Nakamura, S., and Osumi, N. (2001). Role of Cadherins in Maintaining the Compartment Boundary between the Cortex and Striatum during Development. *Development* 128, 561–569. doi:10.1242/dev.128.4.561

Irving, C., Nieto, M. A., DasGupta, R., Charnay, P., and Wilkinson, D. G. (1996). Progressive Spatial Restriction ofSek-1andKrox-20Gene Expression during Hindbrain Segmentation. *Dev. Biol.* 173, 26–38. doi:10.1006/dbio.1996.0004

Janes, P. W., Saha, N., Barton, W. A., Kolev, M. V., Wimmer-Kleikamp, S. H., Nievergall, E., et al. (2005). Adam Meets Eph: an ADAM Substrate Recognition Module Acts as a Molecular Switch for Ephrin Cleavage in Trans. *Cell* 123, 291–304. doi:10.1016/j.cell.2005.08.014

Jørgensen, C., Sherman, A., Chen, G. I., Pasculescu, A., Poliakov, A., Hsiung, M., et al. (2009). Cell-specific Information Processing in Segregating Populations of

Eph Receptor Ephrin-Expressing Cells. *Science* 326, 1502–1509. doi:10.1126/science.1176615

Kasemeier-Kulesa, J. C., Bradley, R., Pasquale, E. B., Lefcort, F., and Kulesa, P. M. (2006). Eph/ephrins and N-Cadherin Coordinate to Control the Pattern of Sympathetic Ganglia. *Development* 133, 4839–4847. doi:10.1242/dev.02662

Kemp, H. A., Cooke, J. E., and Moens, C. B. (2009). EphA4 and EfnB2a Maintain Rhombomere Coherence by Independently Regulating Intercalation of Progenitor Cells in the Zebrafish Neural Keel. *Dev. Biol.* 327, 313–326. doi:10.1016/j.ydbio.2008.12.010

Kesavan, G., Machate, A., Hans, S., and Brand, M. (2020). Cell-fate Plasticity, Adhesion and Cell Sorting Complementarily Establish a Sharp Midbrain-Hindbrain Boundary. *Development* 147, dev186882. doi:10.1242/dev.186882

Kiecker, C., and Lumsden, A. (2005). Compartments and Their Boundaries in Vertebrate Brain Development. *Nat. Rev. Neurosci.* 6, 553–564. doi:10.1038/nrn1702

Kimmel, C. B., Warga, R. M., and Kane, D. A. (1994). Cell Cycles and Clonal Strings during Formation of the Zebrafish central Nervous System. *Development* 120, 265–276. doi:10.1242/dev.120.2.265

Kindberg, A. A., Srivastava, V., Muncie, J. M., Weaver, V. M., Gartner, Z. J., and Bush, J. O. (2021). EPH/EPHRIN Regulates Cellular Organization by Actomyosin Contractility Effects on Cell Contacts. *J. Cel Biol.* 220, e202005216. doi:10.1083/jcb.202005216

Klein, R. (2012). Eph/Ephrin Signalling During Development. *Development* 139, 4105–4109. doi:10.1242/dev.074997

Krull, C. E., Lansford, R., Gale, N. W., Collazo, A., Marcelle, C., Yancopoulos, G. D., et al. (1997). Interactions of Eph-Related Receptors and Ligands Confer Rostrocaudal Pattern to Trunk Neural Crest Migration. *Curr. Biol.* 7, 571–580. doi:10.1016/s0960-9822(06)00256-9

Krumlauf, R., and Wilkinson, D. G. (2021). Segmentation and Patterning of the Vertebrate Hindbrain. *Development* 148, dev186460. doi:10.1242/dev.186460

Lecuit, T., and Lenne, P.-F. (2007). Cell Surface Mechanics and the Control of Cell Shape, Tissue Patterns and Morphogenesis. *Nat. Rev. Mol. Cel Biol.* 8, 633–644. doi:10.1038/nrm2222

Lisabeth, E. M., Falivelli, G., and Pasquale, E. B. (2013). Eph Receptor Signaling and Ephrins. *Cold Spring Harb Perspect. Biol.* 5, a009159. doi:10.1101/cshperspect.a009159

Maître, J.-L., Berthoumieux, H., Krens, S. F. G., Salbreux, G., Jülicher, F., Paluch, E., et al. (2012). Adhesion Functions in Cell Sorting by Mechanically Coupling the Cortices of Adhering Cells. *Science* 338, 253–256. doi:10.1126/science.1225399

Marston, D. J., Dickinson, S., and Nobes, C. D. (2003). Rac-dependent Trans-endocytosis of ephrinBs Regulates Eph-Ephrin Contact Repulsion. *Nat. Cel Biol.* 5, 879–888. doi:10.1038/ncb1044

Miao, H., and Wang, B. (2012). EphA Receptor Signaling-Complexity and Emerging Themes. *Semin. Cel Dev. Biol.* 23, 16–25. doi:10.1016/j.semcdb.2011.10.013

Noren, N. K., Yang, N.-Y., Silldorff, M., Mutyala, R., and Pasquale, E. B. (2009). Ephrin-Independent Regulation of Cell Substrate Adhesion by the EphB4 Receptor. *Biochem. J.* 422, 433–442. doi:10.1042/bj20090014

O'Neill, A. K., Kindberg, A. A., Niethamer, T. K., Larson, A. R., Ho, H. H., Greenberg, M. E., et al. (2016). Unidirectional Eph/ephrin Signaling Creates a Cortical Actomyosin Differential to Drive Cell Segregation. *J. Cel Biol.* 215, 217–229. doi:10.1083/jcb.201604097

Orsulic, S., and Kemler, R. (2000). Expression of Eph Receptors and Ephrins Is Differentially Regulated by E-Cadherin. *J. Cel Sci.* 113, 1793–1802. doi:10.1242/jcs.113.10.1793

Parrinello, S., Napoli, I., Ribeiro, S., Digby, P. W., Fedorova, M., Parkinson, D. B., et al. (2010). EphB Signaling Directs Peripheral Nerve Regeneration through Sox2-Dependent Schwann Cell Sorting. *Cell* 143, 145–155. doi:10.1016/j.cell.2010.08.039

Pasquale, E. B. (2008). Eph-Ephrin Bidirectional Signaling in Physiology and Disease. *Cell* 133, 38–52. doi:10.1016/j.cell.2008.03.011

Poliakov, A., Cotrina, M. L., Pasini, A., and Wilkinson, D. G. (2008). Regulation of EphB2 Activation and Cell Repulsion by Feedback Control of the MAPK Pathway. *J. Cel. Biol.* 183, 933–947. doi:10.1083/jcb.200807151

Price, S. R., De Marco Garcia, N. V., Ranscht, B., and Jessell, T. M. (2002). Regulation of Motor Neuron Pool Sorting by Differential Expression of Type II Cadherins. *Cell* 109, 205–216. doi:10.1016/s0092-8674(02)00695-5

Rohani, N., Canty, L., Luu, O., Fagotto, F., and Winklbauer, R. (2011). EphrinB/EphB Signaling Controls Embryonic Germ Layer Separation by Contact-Induced Cell Detachment. *Plos Biol.* 9, e1000597. doi:10.1371/journal.pbio.1000597

Rohani, N., Parmeggiani, A., Winklbauer, R., and Fagotto, F. (2014). Variable Combinations of Specific Ephrin Ligand/eph Receptor Pairs Control Embryonic Tissue Separation. *Plos Biol.* 12, e1001955. doi:10.1371/journal.pbio.1001955

Scarpa, E., Szabó, A., Bibonne, A., Theveneau, E., Parsons, M., and Mayor, R. (2015). Cadherin Switch during EMT in Neural Crest Cells Leads to Contact Inhibition of Locomotion via Repolarization of Forces. *Dev. Cel.* 34, 421–434. doi:10.1016/j.devcel.2015.06.012

Sela-Donenfeld, D., Kayam, G., and Wilkinson, D. G. (2009). Boundary Cells Regulate a Switch in the Expression of FGF3 in Hindbrain Rhombomeres. *BMC Dev. Biol.* 9, 16. doi:10.1186/1471-213x-9-16

Shafraz, O., Xie, B., Yamada, S., and Sivasankar, S. (2020). Mapping Transmembrane Binding Partners for E-Cadherin Ectodomains. *Proc. Natl. Acad. Sci. USA* 117, 31157–31165. doi:10.1073/pnas.2010209117

Smith, A., Robinson, V., Patel, K., and Wilkinson, D. G. (1997). The EphA4 and EphB1 Receptor Tyrosine Kinases and Ephrin-B2 Ligand Regulate Targeted Migration of Branchial Neural Crest Cells. *Curr. Biol.* 7, 561–570. doi:10.1016/s0960-9822(06)00255-7

Solanas, G., Cortina, C., Sevillano, M., and Batlle, E. (2011). Cleavage of E-Cadherin by ADAM10 Mediates Epithelial Cell Sorting Downstream of EphB Signalling. *Nat. Cel Biol.* 13, 1100–1107. doi:10.1038/ncb2298

Steinberg, M. S., and Takeichi, M. (1994). Experimental Specification of Cell Sorting, Tissue Spreading, and Specific Spatial Patterning by Quantitative Differences in Cadherin Expression. *Proc. Natl. Acad. Sci.* 91, 206–209. doi:10.1073/pnas.91.1.206

Steinberg, M. S. (2007). Differential Adhesion in Morphogenesis: a Modern View. *Curr. Opin. Genet. Dev.* 17, 281–286. doi:10.1016/j.gde.2007.05.002

Taylor, H. B., Khuong, A., Wu, Z., Xu, Q., Morley, R., Gregory, L., et al. (2017). Cell Segregation and Border Sharpening by Eph Receptor-Ephrin-Mediated Heterotypic Repulsion. *J. R. Soc. Interf.* 14, 20170338. doi:10.1098/rsif.2017.0338

Theveneau, E., Marchant, L., Kuriyama, S., Gull, M., Moepps, B., Parsons, M., et al. (2010). Collective Chemotaxis Requires Contact-dependent Cell Polarity. *Dev. Cel.* 19, 39–53. doi:10.1016/j.devcel.2010.06.012

Voltes, A., Hevia, C. F., Engel-Pizcueta, C., Dingare, C., Calzolari, S., Terriente, J., et al. (2019). Yap/Taz-TEAD Activity Links Mechanical Cues to Progenitor Cell Behavior during Zebrafish Hindbrain Segmentation. *Development* 146, dev176735. doi:10.1242/dev.176735

Wang, H. U., and Anderson, D. J. (1997). Eph Family Transmembrane Ligands Can Mediate Repulsive Guidance of Trunk Neural Crest Migration and Motor Axon Outgrowth. *Neuron* 18, 383–396. doi:10.1016/s0896-6273(00)81240-4

Winklbauer, R. (2015). Cell Adhesion Strength from Cortical Tension - an Integration of Concepts. *J. Cel Sci.* 128, 3687–3693. doi:10.1242/jcs.174623

Wizenmann, A., and Lumsden, A. (1997). Segregation of Rhombomeres by Differential Chemoaffinity. *Mol. Cell Neurosci.* 9, 448–459. doi:10.1006/mcne.1997.0642

Wu, Z., Ashlin, T. G., Xu, Q., and Wilkinson, D. G. (2019). Role of Forward and Reverse Signaling in Eph Receptor and Ephrin Mediated Cell Segregation. *Exp. Cel Res.* 381, 57–65. doi:10.1016/j.yexcr.2019.04.040

Xu, Q., Alldus, G., Holder, N., and Wilkinson, D. G. (1995). Expression of Truncated Sek-1 Receptor Tyrosine Kinase Disrupts the Segmental Restriction of Gene Expression in the *Xenopus* and Zebrafish Hindbrain. *Development* 121, 4005–4016. doi:10.1242/dev.121.12.4005

Xu, Q., Mellitzer, G., Robinson, V., and Wilkinson, D. G. (1999). *In Vivo* cell Sorting in Complementary Segmental Domains Mediated by Eph Receptors and Ephrins. *Nature* 399, 267–271. doi:10.1038/20452

Yoon, J., Hwang, Y.-S., Lee, M., Sun, J., Cho, H. J., Knapik, L., et al. (2018). TBC1d24-ephrinB2 Interaction Regulates Contact Inhibition of Locomotion in Neural Crest Cell Migration. *Nat. Commun.* 9, 3491. doi:10.1038/s41467-018-05924-9

Yu, H. H., Dohn, M. R., Markham, N. O., Coffey, R. J., and Reynolds, A. B. (2016). p120-catenin Controls Contractility along the Vertical axis of Epithelial Lateral Membranes. *J. Cel Sci* 129, 80–94. doi:10.1242/jcs.177550

Zantek, N. D., Azimi, M., Fedor-Chaiken, M., Wang, B., Brackenbury, R., and Kinch, M. S. (1999). E-Cadherin Regulates the Function of the EphA2 Receptor Tyrosine Kinase. *Cell Growth Differ.* 10, 629–638.

Zhang, L., Radtke, K., Zheng, L., Cai, A. Q., Schilling, T. F., and Nie, Q. (2012). Noise Drives Sharpening of Gene Expression Boundaries in the Zebrafish Hindbrain. *Mol. Syst. Biol.* 8, 613. doi:10.1038/msb.2012.45

Zimmer, M., Palmer, A., Köhler, J., and Klein, R. (2003). EphB-ephrinB Bi-directional Endocytosis Terminates Adhesion Allowing Contact Mediated Repulsion. *Nat. Cel Biol.* 5, 869–878. doi:10.1038/ncb1045

Conflict of Interest: The author declares that the research was conducted in the absence of any commercial or financial relationships that could be construed as a potential conflict of interest.

Publisher's Note: All claims expressed in this article are solely those of the authors and do not necessarily represent those of their affiliated organizations, or those of the publisher, the editors and the reviewers. Any product that may be evaluated in this article, or claim that may be made by its manufacturer, is not guaranteed or endorsed by the publisher.

frontiers in Cell and Developmental Biology

MINI REVIEW
published: 05 November 2021
doi: 10.3389/fcell.2021.779009

Comparing a Novel Malformation Syndrome Caused by Pathogenic Variants in *FBRSL1* to AUTS2 Syndrome

Silke Pauli[1]*, *Hanna Berger*[2], *Roser Ufartes*[1] and *Annette Borchers*[2]*

[1]Institute of Human Genetics, University Medical Center Göttingen, Göttingen, Germany, [2]Faculty of Biology, Molecular Embryology, Philipps-University Marburg, Marburg, Germany

Truncating variants in specific exons of *Fibrosin-like protein 1* (*FBRSL1*) were recently reported to cause a novel malformation and intellectual disability syndrome. The clinical spectrum includes microcephaly, facial dysmorphism, cleft palate, skin creases, skeletal anomalies and contractures, postnatal growth retardation, global developmental delay as well as respiratory problems, hearing impairment and heart defects. The function of FBRSL1 is largely unknown, but pathogenic variants in the *FBRSL1* paralog *Autism Susceptibility Candidate 2* (*AUTS2*) are causative for an intellectual disability syndrome with microcephaly (AUTS2 syndrome). Some patients with AUTS2 syndrome also show additional symptoms like heart defects and contractures overlapping with the phenotype presented by patients with *FBRSL1* mutations. For AUTS2, a dual function, depending on different isoforms, was described and suggested for FBRSL1. Both, nuclear FBRSL1 and AUTS2 are components of the Polycomb subcomplexes PRC1.3 and PRC1.5. These complexes have essential roles in developmental processes, cellular differentiation and proliferation by regulating gene expression via histone modification. In addition, cytoplasmic AUTS2 controls neural development, neuronal migration and neurite extension by regulating the cytoskeleton. Here, we review recent data on FBRSL1 in respect to previously published data on AUTS2 to gain further insights into its molecular function, its role in development as well as its impact on human genetics.

Keywords: FBRSL1, AUTS2, malformation syndrome, embryonic development, polycomb complex

OPEN ACCESS

Edited by:
Kerstin Feistel,
University of Hohenheim, Germany

Reviewed by:
Mareike Albert,
Technical University Dresden, Germany
Tran Tuoc,
Ruhr University Bochum, Germany

***Correspondence:**
Silke Pauli
silke.pauli@med.uni-goettingen.de
Annette Borchers
borchers@uni-marburg.de

Specialty section:
This article was submitted to Morphogenesis and Patterning, a section of the journal Frontiers in Cell and Developmental Biology

Received: *17 September 2021*
Accepted: *22 October 2021*
Published: *05 November 2021*

Citation:
Pauli S, Berger H, Ufartes R and Borchers A (2021) Comparing a Novel Malformation Syndrome Caused by Pathogenic Variants in FBRSL1 *to AUTS2 Syndrome. Front. Cell Dev. Biol. 9:779009. doi: 10.3389/fcell.2021.779009*

FBRSL1 VARIANTS CAUSE A NOVEL DISABILITY SYNDROME WITH AN OVERLAPPING PHENOTYPE TO AUTS2 SYNDROME

Recently, we identified truncating variants in the *FBRSL1* gene in three unrelated children with an unknown malformation syndrome (Ufartes et al., 2020). The patients presented with respiratory insufficiency and feeding difficulties in the neonatal period. During infancy, intellectual disability, no active speech, postnatal microcephaly, growth retardation and contractures became apparent. In addition, two of the three patients showed cleft palate and heart defects (one with atrial septal defect and persistent ductus arteriosus, one with atrial septal defect and ventricular septal defect). In one patient asplenia and in another patient anal atresia were observed. Furthermore, the two more severely affected patients were born with pronounced congenital skin creases at the back, the arms, and legs. During the first year of life the skin creases became less pronounced and disappeared

TABLE 1 | Comparison of clinical features seen in patients with *FBRSL1* mutation and patients with AUTS2 syndrome.

Clinical findings	FBRSL1 syndromic phenotype	AUTS2 syndrome
Growth and feeding		
Low birth weight	2/3	10/54 (18,5%)
Short stature	3/3	26/59 (44,1%)
Microcephaly	3/3	37/57 (64,9%)
Feeding difficulties	3/3	33/55 (60,0%)
Neurodevelopmental disorders		
Intellectual disability	3/3	64/66 (97,0%)
Autism/autistic behaviour	3/3	16/40 (40,0%)
Sound sensitivity	n.a	28/56 (50,0%)
Hyperactivity/ADHD	n.a	17/28 (60,7%)
Neurological disorders		
Generalized hypotonia	n.a	23/60 (38,3%)
Structural brain anomaly	-/1/n.a	11/46 (23,9%)
Cerebral palsy/spasticity	2/3	20/57 (35,1%)
Other: respiratory insufficiency with ventilation therapy	3/3	
Dysmorphic features		
High arched eyebrows	2/3	13/37 (35,1%)
Hypertelorism	0/3	14/37 (37,8%)
Proptosis	0/3	7/37 (18,9%)
Short palpebral fissures	0/3	9/37 (24,3%)
Up slanting palpebral fissures	0/3	5/37 (13,5%)
Ptosis	0/3	11/37 (29,7%)
Epicanthol folds	2/3	8/37 (21,6%)
Strabismus	0/3	9/37 (24,3%)
Prominent nasal tip	1/3	7/37 (18,9%)
Anteverted nares	0/3	7/37 (18,9%)
Deep/broad nasal bridge	2/3	12/37 (32,4%)
Short/upturned philtrum	2/3	11/37 (29,7%)
Micro-/retrognatia	1/3	11/36 (30,6%)
Low set ears	2/3	11/36 (30,6%)
Ear pit	0/3	5/36 (13,9%)
Narrow mouth	1/3	16/37 (43,2%)
Other: widely spaced teeth	2/3	-
Skeletal disorders		
Kyphosis/scoliosis	3/3	10/47 (21,3%)
Arthrogryposis/shallow palmar creases	0/3	6/28 (21,4%)
Tight heel cords	n.a	6/13 (46,2%)
Other (camptodactyly/contractures)	3/3	-
Congenital malformation		
Hernia umbilicalis/inguinalis	0/3	6/59 (10,2%)
Patent foramen ovale/atrial septum defect	2/3	4/26 (15,4%)
Other		
•Cleft palate	2/3	-
•Asplenia	1/3	-
•Anal atresia	1/3	-
•Abnormality of the skin	2/3	-
•Hearing impairment	2/3	-

The clinical feature terminology is based on the list of features used for the AUTS2 syndrome severity scoring system (Beunders et al., 2013). The data for AUTS2 syndrome were adapted from Sanchez-Jimeno et al. which is based on nine different studies (Sultana et al., 2002; Kalscheuer et al., 2007; Bakkaloglu et al., 2008; Huang et al., 2010; Girirajan et al., 2011; Jolley et al., 2013; Nagamani et al., 2013; Liu et al., 2015; Beunders et al., 2016). In addition, the data include a cohort of five patients published by Sanchez-Jimeno et al. (Sanchez-Jimeno et al., 2021). The data for the FBRSL1 syndromic phenotype is based on the three patients published in Ufartes et al. (Ufartes et al., 2020). Abbreviations: n.a. = not assessed, ADHD = attention deficit/hyperactivity disorder. A remarkable overlap between the two syndromes was observed with a wider spectrum and higher rate of congenital malformations in children with a pathogenic variant in FBRSL1.

(Ufartes et al., 2020). Interestingly, the clinical phenotype of the newly described malformation syndrome caused by *FBRSL1* variants partially overlaps with the severe form of AUTS2 syndrome (**Table 1**).

AUTS2 syndrome (MIM 615834) was first described in 2013 (Beunders et al., 2013), as a neurodevelopmental disorder caused by pathogenic variants and deletions of the *AUTS2* gene (MIM 607270, activator of transcription and developmental regulator). Depending on the location of *AUTS2* point mutations/deletions the phenotype ranges from an isolated neurodevelopmental disorder (e.g., autism spectrum disorder, attention deficit hyperactivity disorder, learning disabilities and/or intellectual disability) to a syndromic disorder with microcephaly, short stature, feeding difficulties, heart defects, skeletal anomalies, contractures and dysmorphic features (Beunders et al., 2013; Beunders et al., 2016; Saeki et al., 2019; Sanchez-Jimeno et al.,

2021). To date, more than 60 patients with AUTS2 syndrome have been described in the literature and most of them carry an intragenic *de novo* deletion of *AUTS2*, whereas point mutations leading to the disease are rarely described (Sanchez-Jimeno et al., 2021). Due to a high inter- and intrafamilial variability an AUTS2 syndrome severity scoring system (ASSS) was established by Beunders and colleagues 2013. The scoring system is based on 32 features seen with a frequency of over 10% in AUTS2 syndrome patients of the first described cohort (Beunders et al., 2013). The ASSS revealed that patients with small deletions at the N-terminus of *AUTS2* typically present a mild phenotype; in some cases, these deletions were inherited from a mildly or unaffected parent (Beunders et al., 2013). In contrast, deletions of the C-terminus of AUTS2 are mostly associated with a severe AUTS2 syndrome phenotype combining neurodevelopmental features with malformations and dysmorphic features (Beunders et al., 2013). Therefore, it was suggested that the AUTS2 C-terminus plays a critical role in AUTS2 syndrome (Beunders et al., 2013; Beunders et al., 2016; Saeki et al., 2019; Sanchez-Jimeno et al., 2021). Interestingly, the situation seems to be different for the truncating *FBRSL1* variants characterized in Ufartes et al. (2020), which all localized to the N-terminus of the *FBRLS1* gene. As the patients carrying *FBRSL1* variants showed features associated with AUTS2 syndrome, we also used the ASSS to compare the phenotype of the three patients with a variant in *FBRSL1* (Ufartes et al., 2020) to patients with AUTS2 syndrome (**Table 1**). A remarkable clinical overlap between the FBRSL1 syndromic phenotype and the severe form of AUTS2 syndrome was observed. Although, so far only three patients with the FBRSL1 syndromic phenotype have been described (Ufartes et al., 2020), it seems that they show a wider range of congenital malformations compared to the symptoms observed in AUTS2 patients. To gain insight into common and distinct functions of FBRSL1 and AUTS2, we take a closer look at their evolutionary conservation and potential functions.

FBRSL1 AND AUTS2 ARE PARALOGS THAT LIKELY SHARE CONSERVED FUNCTIONS

FBRSL1 and AUTS2 belong to a tripartite gene family, the AUTS2 family, which also includes Fibrosin (FBRS) (Singh et al., 2015). The AUTS2 family is predicted to be an ohnolog gene family (Singh et al., 2015), representing a group of paralog genes generated by two rounds of whole genome duplication during vertebrate evolution and frequently implicated in human disease (Dickerson and Robertson, 2012; Singh et al., 2012; Malaguti et al., 2014; Mclysaght et al., 2014). The AUTS2 family ohnologs show a large overlap of conserved regions, but also unique elements which likely contribute to the functional diversity of the proteins (Sellers et al., 2020). Detailed information about the conserved regions shared by AUTS2-related proteins as well as an evolutionary analysis of the AUTS2 family can be found in Sellers et al., 2020 (Sellers et al., 2020). Based on their extended phylogenetic analysis, Sellers et al. recommended to rename FBRSL1 to AUTS2-like Protein 1, because AUTS2 and FBRSL1 share a most recent common ancestor, suggesting that these proteins are evolutionary closer related to each other than to FBRS (Sellers et al., 2020). Thus, it is intriguing to speculate that both proteins may share common functions, which may also explain their overlapping phenotypes observed in the respective syndromes.

Research using animal model systems indicate that FBRSL1 and AUTS2 share common functions in vertebrate development. As Auts2 function in neurodevelopmental disorders has been addressed in a number of comprehensive reviews (Oksenberg and Ahituv, 2013; Hori and Hoshino, 2017; Pang et al., 2021), we will here only briefly discuss its role in mouse and zebrafish development. In the mouse, *Auts2* is broadly expressed in the developing brain, with high expression in key areas of higher cognitive brain function (Bedogni et al., 2010). Heterozygous disruption of *Auts2* results in similar symptoms as seen in AUTS2 syndrome patients including growth reduction, defects in communication, exploratory behavior as well as learning and memory, while social behavior and sensor motor gating functions were normal (Gao et al., 2014; Hori et al., 2015). In zebrafish, *auts2* is highly expressed in the developing brain and Morpholino-mediated knockdown resulted in microcephaly, reduced lower jaws, swimming defects and a reduced response to tactile stimuli (Beunders et al., 2013; Oksenberg et al., 2013).

Currently, data analyzing the function of Fbrsl1 in animal model systems are limited. The expression of *fbrsl1* has been analyzed in zebrafish and these data show that it is mainly expressed in the developing brain, but also in the spinal cord, the cranial ganglia and the somites (Kondrychyn et al., 2017). In *Xenopus*, *fbrsl1* is expressed throughout early developmental stages (Ufartes et al., 2020). At tailbud stages, it is expressed in the brain and craniofacial structures including the branchial arches and the cranial nerves (Ufartes et al., 2020). Morpholino-mediated Fbrsl1 knockdown resulted in craniofacial defects and the embryos showed cartilage hypoplasia as well as a reduction in brain size on the injected side (**Figures 1A–C**). Furthermore, the cranial nerves (**Figure 1D**) and motor neurons displayed impaired neuronal migration (Ufartes et al., 2020). Thus, the first functional data on Fbrsl1 in *Xenopus* development indicate that FBRSL1 may share similar functions with AUTS2 in neural development, but may also have a unique role in craniofacial development, which is also consistent with the findings in patients affected by the respective disorders.

AUTS2 HAS NUCLEAR AND CYTOPLASMIC FUNCTIONS WHICH MAY BE SHARED BY FBRSL1

For AUTS2 a dual function, acting either in the cytoplasm or in the nucleus of developing neurons has been described (Hori et al., 2014). In the nucleus, AUTS2 was identified as a component of the Polycomb repressive complex PRC1 (Gao et al., 2012; Gao et al., 2014). Polycomb repressive complexes are multiprotein complexes acting as epigenetic regulators during development (Aranda et al., 2015; Chittock et al., 2017). Traditionally, they exert their function as transcriptional repressors (Simon and Kingston, 2013; Chittock et al., 2017; Kassis et al., 2017). The

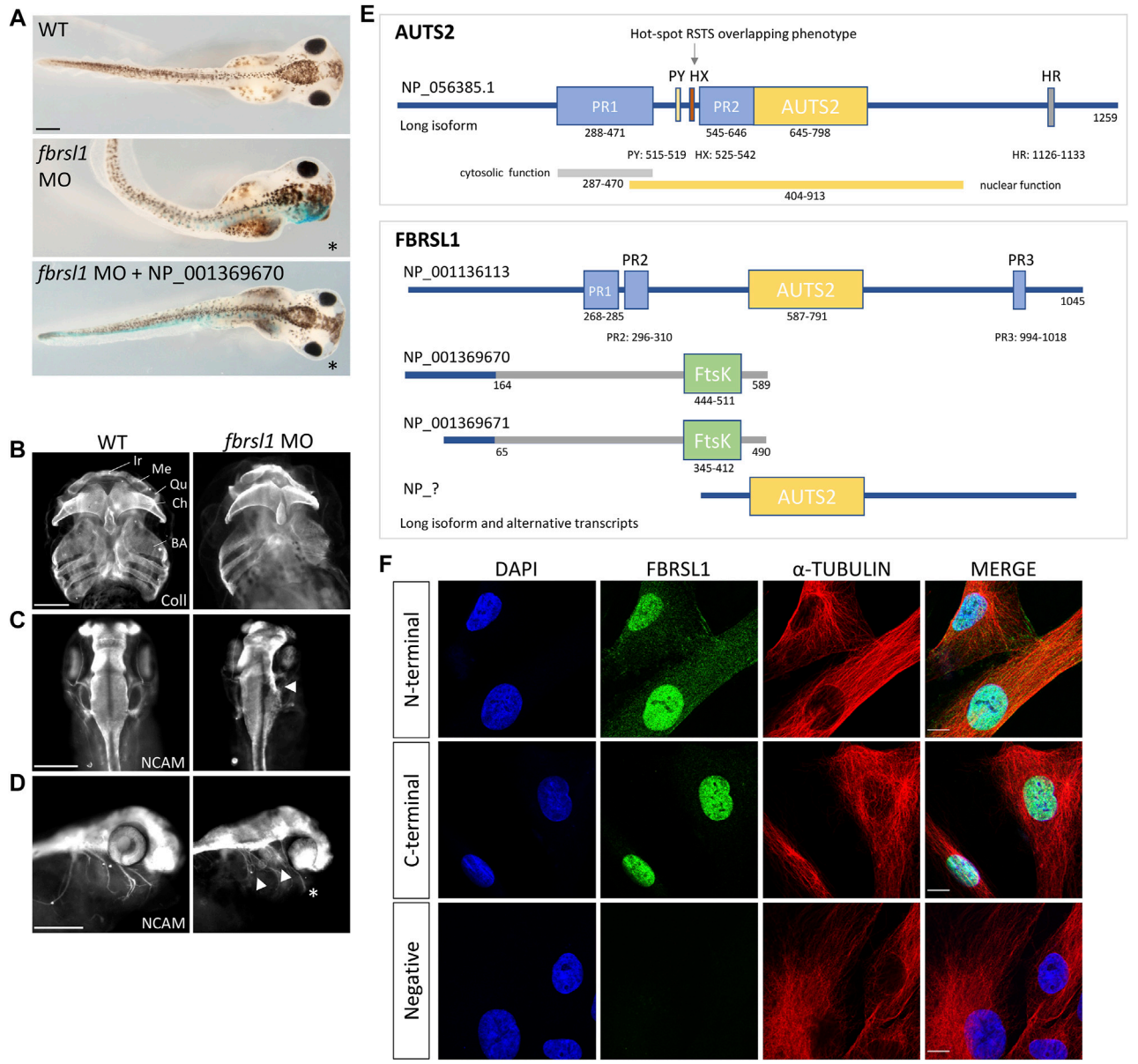

FIGURE 1 | Fbrsl1 knockdown phenotypes in *Xenopus laevis* and cellular localization of distinct human *FBRSL1* transcripts. **(A)** Knockdown of Fbrsl1 by injection of a *fbrsl1* Morpholino oligonucleotide (MO) leads to craniofacial defects that can be rescued by co-injection of RNA coding for the human short N-terminal *FBRSL1 isoform NP_001369670* (Ufartes et al., 2020). *LacZ RNA* was co-injected as a lineage tracer, the injected side is marked by blue staining. **(B)** Anti-Collagen Type II immunofluorescence visualizes the cartilage and indicates cartilage hypoplasia on the *fbrsl1* MO-injected side. BA, branchial arches; Ch, ceratohyal; Ir, infrarostral; Me, Meckel's cartilage; Qu, quadrate. **(C)** Neural cell adhesion molecule (NCAM) staining shows reduced brain size and **(D)** impaired outgrowth of cranial nerves on the *fbrsl1* MO-injected side; * marks the injected side. Scale bar in A-D: 500 µm. **(E)** Human *FBRSL1* transcripts/isoforms compared to the human AUTS2 long isoform as previously published (Sultana et al., 2002; Oksenberg and Ahituv, 2013; Sellers et al., 2020). Like its AUTS2 ohnolog, the long isoform has a AUTS2 domain and proline rich (PR) regions (predicted with MobiDB (Piovesan et al., 2020)). Both short N-terminal isoforms differ in their C-terminal sequence from the long isoform (presented in grey) due to an alternative exon 3, which contains an Ftsk-domain. In addition, a predicted C-terminal isoform (marked with "?") including the AUTS2 domain is shown as this isoform was validated for mouse Fbrsl1. PR, proline-rich domain; PY, PPPY motif; HX, hexanucleotide repeat; HR, trinucleotide (H) repeat; AUTS2, AUTS2/FBRSL1/FBRSL homology region. **(F)** Immunofluorescence analysis performed on human fibroblasts. Antibodies directed against the N-terminal as well as the C-terminal part of FBRSL1 detected FBRSL1 isoforms (green) in the nucleus. However, only the N-terminal FBRSL1 antibody also detected FBRSL1 in the cytoplasm, suggesting that the short N-terminal FBRSL1 isoforms show cytoplasmic and nuclear localization. The negative control showed no signal. Cytoskeletal staining was detected using an α-Tubulin antibody and nuclei were stained using DAPI. Images were obtained using a confocal laser microscope with ×600 magnification. Scale Bar: 10 µm. All experimental data have been previously published (Ufartes et al., 2020).

two main Polycomb complexes are PRC1 and PRC2 (reviewed in Barbour et al., 2020; Cohen et al., 2020; Geng and Gao, 2020). The PRC1 complex acts as an E3 ubiquitin ligase that monoubiquitinates lysine 119 of histone H2A (H2AK119ub1) (De Napoles et al., 2004; Wang et al., 2004). The consequences of Polycomb dependent histone H2A ubiquitination were recently reviewed by Tamburri et al. (2021). In addition, the PRC1 complex is involved in ubiquitination-independent chromatin compaction (Eskeland et al., 2010). At least six PRC1 subcomplexes (PRC1.1-PRC1.6) were identified consisting of the E3 ubiquitin ligase RING1A or RING1B and one of the six Polycomb Group Ring Fingers (PCGF1-6) (Chittock et al., 2017; Varlet et al., 2020). AUTS2 has been described as a component of the subcomplexes PRC1.3 and PRC1.5 (Gao et al., 2012; Gao et al., 2014). The PRC1.5 complex contains the components AUTS2, PCGF5, RING1B, CK2B, and RYBP (Gao et al., 2012; Gao et al., 2014). The binding of AUTS2 to the PRC1.5 complex switches its function to a transcriptional activator by recruiting the histone acetyltransferase EP300 and casein kinase 2 (CK2) (Gao et al., 2014; Liu et al., 2021). Co-immunoprecipitation experiments revealed that RING1B interacts with AUTS2 only in the presence of PCGF5 (Gao et al., 2014), suggesting a bridging function of PCGF5. The recruitment of CK2 to the complex is likely mediated by direct AUTS2 binding and this interaction suppresses monoubiquitination of H2AK119 by RING1B (Gao et al., 2014). The C-terminal part of AUTS2 (404–913) is sufficient to mediate the transcriptional activation via EP300 binding (Gao et al., 2014). Therefore, the recruitment of CK2 to the PRC1.5 complex and the AUTS2-EP300 interaction seem to be responsible for converting the repressive PRC1 function into an activator function (Gao et al., 2014; Monderer-Rothkoff et al., 2021). Recently, *de novo* pathogenic variants in the HX repeat region *of AUTS2* were described in patients with a phenotype overlapping with Rubinstein-Taybi syndrome (Liu et al., 2021). Rubinstein-Taybi syndrome (RSTS, OMIM 180849 and OMIM 613684) is a neurodevelopmental disorder characterized by intellectual disability, autism spectrum disorders, microcephaly, facial dysmorphism, growth retardation, large thumbs and hallux and a variable degree of additional malformations and symptoms (reviewed in Van Gils et al., 2021). The underlying cause of RSTS are pathogenic variants in *EP300* and *CREBBP* (Petrij et al., 1995; Roelfsema et al., 2005). Interestingly, the *AUTS2* variants leading to an RSTS-overlapping phenotype disrupt the binding of AUTS2 to EP300, suggesting that the HX repeat domain is responsible for this interaction (Liu et al., 2021). The binding of AUTS2 to PRC1.3 and the recruitment to chromatin was shown to be directed by the transcription factor nuclear respiratory factor 1 (NRF1). In motor neurons, AUTS2 and NRF1 colocalize at actively transcribed loci, whereby AUTS2 binding requires NRF1, but NRF1 binding is independent of AUTS2 (Liu et al., 2021). Thus, it was suggested that NRF1 recruits AUTS2 in the context of the PRC1.3 complex to genes involved in neuronal differentiation. The transcription of these genes will then be activated by binding of EP300 to the AUTS2 HX repeat domain (Liu et al., 2021).

Like AUTS2, FBRSL1 was also identified by tandem affinity purification and mass spectrometry as an interaction partner of PRC1.3 and PRC1.5 (Gao et al., 2012). Further, it was shown that FBRSL1 competes with AUTS2 for binding to the PRC1.5 complex (Gao et al., 2014). Thus, it will be interesting to see if a PRC1.3 or PRC1.5 complex containing FBRSL1 in place of AUTS2 has again a repressive function instead of an active role. While interaction of FBRSL1 and AUTS2 with Polycomb complexes indicates a role of these proteins in transcriptional gene regulation, they likely also control additional processes in the cytoplasm.

For AUTS2 it has been shown that—in addition to its function in the nucleus—it also functions in the cytoplasm by controlling cytoskeletal dynamics. Cytoplasmic AUTS2 functions by regulating small GTPases of the Rho family thereby affecting actin dynamics in the developing brain (Hori et al., 2014). By stimulating small guanine exchange factors (GEFs) AUTS2 activates Rac1 and induces lamellipodia formation and neurite extension. Conversely, AUTS2 inhibits Cdc42 thereby suppressing filopodia formation (Hori et al., 2014). For Rac1 activation, the N-terminal PR1 region of the AUTS2 protein seems to be important, as overexpression of mutant AUTS2, lacking the N-terminal PR1 domain, did not lead to lamellipodia formation (Hori et al., 2014). Currently, it is unknown if FBRSL1 may play a similar role. However, we recently demonstrated that FBRSL1 is localized in the cytoplasm as well as in the nucleus of HEK293 cells and human fibroblasts (**Figures 1E,F**) (Ufartes et al., 2020). Consistent with the AUTS2 data (Hori et al., 2014), mainly a nuclear FBRSL1 pattern was detected with an antibody directed against the C-terminal part of FBRSL1, while nuclear and cytoplasmic FBRSL1 was observed with an antibody targeted against the N-terminal part of the protein (**Figure 1F**) (Ufartes et al., 2020). Thus, it is likely that FBRSL1—like AUTS2—has nuclear versus cytoplasmic functions which may require distinct domains of the protein.

FBRSL1 AND *AUTS2* SHOW TRANSCRIPTIONAL COMPLEXITY

Consistent with the concept of distinct subcellular functions, different transcripts have been identified for *AUTS2* and *FBRSL1*. The longest *AUTS2* and *FBRSL1* transcripts are encoded by 19 exons, in addition shorter N-terminal or C-terminal transcripts of the respective proteins have been described. For AUTS2, two isoforms have been extensively studied: the long transcript containing 19 exons (NM_015570.4) and a short C-terminal isoform containing the last 11 exons, starting at exon 9, first characterized by Beunders et al., 2013 (Beunders et al., 2013). The C-terminal isoform contains a region of homology to the paralogs FBRSL1 and FBRS, which was called AUTS2 family domain (Kondrychyn et al., 2017), and is critical for the nuclear function of AUTS2 (Beunders et al., 2013). Beunders et al. showed that the characteristic dysmorphic features were more pronounced in patients with 3' AUTS2 deletions (Beunders et al., 2013). Furthermore, they showed that Morpholino-mediated knockdown of zebrafish Auts2 resulted in microcephaly and

reduced lower jaw size, comparable to defects seen in patients with an *AUTS2* disruption. The morphant phenotypes could be rescued with wild-type human full-length *Auts2* RNA, but also with a short C-terminal *Auts2* isoform encoded by exons 9–19 (Beunders et al., 2013) demonstrating the important role for the AUTS2 C-terminus during development.

Like for *AUTS2*, a long *FBRSL1* transcript containing 19 exons (NM_001142641.2) was identified (**Figure 1E**) (Ufartes et al., 2020). In addition, two N-terminal isoforms were validated (**Figure 1E**) and studied in more detail. The two short isoforms contain an alternative exon three leading to a stop codon. These two short N-terminal forms lack the homologous AUTS2 family domain, but include a predicted DNA translocase domain (Ftsk) (NCBI conserved database, CDD) (Ufartes et al., 2020). Interestingly, while the severe AUTS2 syndrome phenotype was caused by variants of the C-terminus (Beunders et al., 2013), the situation was different for the three patients with the FBRSL1-associated syndromic phenotype: all three patients harbor a truncating variant (stop mutation in two patients and a frameshift variant with premature stop codon in the other patient) in the N-terminus of FBRSL1 affecting the short N-terminal isoforms (Ufartes et al., 2020). Consistently, using the *Xenopus* systems, we could show that a human N-terminal isoform of FBRSL1 was able to rescue the *Xenopus* morphant craniofacial defects. However, neither a patient variant of this isoform nor the long FBRSL1 isoform, which both lack the Ftsk domain, were able to rescue the morphant phenotype (Ufartes et al., 2020). These data suggest that mutations of the short N-terminal FBRSL1 isoforms are causative for the developmental phenotype in the animal model system and possibly also in human patients.

It is tempting to speculate that this transcriptional complexity is also responsible for the distinct functions of FBRSL1 and AUTS2. For example, in zebrafish it has been shown that the transcriptional complexity of distinct Auts2 family ohnologs is mediated by alternative splicing and alternative promotor use (Kondrychyn et al., 2017). Interestingly, the expression of the distinct Auts2 paralogs is temporally and spatially tightly controlled during development (Kondrychyn et al., 2017). Thus, there are multiple levels, by which distinct functions can be regulated by this gene family.

CONCLUSION

According to currently available data on FBRSL1, we would speculate that the N-terminal region of FBRSL1, has an important function in mammalian development. This hypothesis is also supported by the finding that all three patients, affected by a novel severe malformation syndrome, carry *FBRSL1* variants localizing to the N-terminal region of *FBRSL1*. Although these patients show overlapping features to patients with AUTS2 syndrome, which is caused by variants in the *FBRSL1*-paralog *AUTS2*, they have a higher rate and wider spectrum of congenital malformations. As the number of described patients with *FBRSL1* variants are currently small, larger patient cohorts with clinical description of the disease are required to confirm these first observations. FBRSL1 and AUTS2 are closely related paralogs, but the presently published data indicate that they have distinct functions and cannot replace each other. Thus, future research will need to address the molecular and cellular mechanism of FBRSL1 to reveal its unique role in development and disease.

AUTHOR CONTRIBUTIONS

AB and SP conceptualized the article and wrote the original draft. HB and RU conceptualized and designed **Figure 1** and critical revised the original draft.

FUNDING

This work was supported by the Deutsche Forschungsgemeinschaft (DFG, German Research Foundation) grant PA 2030/5-1 to SP.

ACKNOWLEDGMENTS

The authors thank Katharina Till for critical reading of the manuscript.

REFERENCES

Aranda, S., Mas, G., and Di Croce, L. (2015). Regulation of Gene Transcription by Polycomb Proteins. *Sci. Adv.* 1, e1500737. doi:10.1126/sciadv.1500737

Bakkaloglu, B., O'roak, B. J., Louvi, A., Gupta, A. R., Abelson, J. F., Morgan, T. M., et al. (2008). Molecular Cytogenetic Analysis and Resequencing of Contactin Associated Protein-like 2 in Autism Spectrum Disorders. *Am. J. Hum. Genet.* 82, 165–173. doi:10.1016/j.ajhg.2007.09.017

Barbour, H., Daou, S., Hendzel, M., and Affar, E. B. (2020). Polycomb Group-Mediated Histone H2A Monoubiquitination in Epigenome Regulation and Nuclear Processes. *Nat. Commun.* 11, 5947. doi:10.1038/s41467-020-19722-9

Bedogni, F., Hodge, R. D., Nelson, B. R., Frederick, E. A., Shiba, N., Daza, R. A., et al. (2010). Autism Susceptibility Candidate 2 (Auts2) Encodes a Nuclear Protein Expressed in Developing Brain Regions Implicated in Autism Neuropathology. *Gene Expr. Patterns* 10, 9–15. doi:10.1016/j.gep.2009.11.005

Beunders, G., Van De Kamp, J., Vasudevan, P., Morton, J., Smets, K., Kleefstra, T., et al. (2016). A Detailed Clinical Analysis of 13 Patients with AUTS2 Syndrome Further Delineates the Phenotypic Spectrum and Underscores the Behavioural Phenotype. *J. Med. Genet.* 53, 523–532. doi:10.1136/jmedgenet-2015-103601

Beunders, G., Voorhoeve, E., Golzio, C., Pardo, L. M., Rosenfeld, J. A., Talkowski, M. E., et al. (2013). Exonic Deletions in AUTS2 Cause a Syndromic Form of Intellectual Disability and Suggest a Critical Role for the C Terminus. *Am. J. Hum. Genet.* 92, 210–220. doi:10.1016/j.ajhg.2012.12.011

Chittock, E. C., Latwiel, S., Miller, T. C. R., and Müller, C. W. (2017). Molecular Architecture of Polycomb Repressive Complexes. *Biochem. Soc. Trans.* 45, 193–205. doi:10.1042/bst20160173

Cohen, I., Bar, C., and Ezhkova, E. (2020). Activity of PRC1 and Histone H2AK119 Monoubiquitination: Revising Popular Misconceptions. *Bioessays* 42, e1900192. doi:10.1002/bies.201900192

De Napoles, M., Mermoud, J. E., Wakao, R., Tang, Y. A., Endoh, M., Appanah, R., et al. (2004). Polycomb Group Proteins Ring1A/B Link

Ubiquitylation of Histone H2A to Heritable Gene Silencing and X Inactivation. *Developmental Cel* 7, 663–676. doi:10.1016/j.devcel.2004.10.005

Dickerson, J. E., and Robertson, D. L. (2012). On the Origins of Mendelian Disease Genes in Man: the Impact of Gene Duplication. *Mol. Biol. Evol.* 29, 61–69. doi:10.1093/molbev/msr111

Eskeland, R., Leeb, M., Grimes, G. R., Kress, C., Boyle, S., Sproul, D., et al. (2010). Ring1B Compacts Chromatin Structure and Represses Gene Expression Independent of Histone Ubiquitination. *Mol. Cel* 38, 452–464. doi:10.1016/j.molcel.2010.02.032

Gao, Z., Lee, P., Stafford, J. M., Von Schimmelmann, M., Schaefer, A., and Reinberg, D. (2014). An AUTS2-Polycomb Complex Activates Gene Expression in the CNS. *Nature* 516, 349–354. doi:10.1038/nature13921

Gao, Z., Zhang, J., Bonasio, R., Strino, F., Sawai, A., Parisi, F., et al. (2012). PCGF Homologs, CBX Proteins, and RYBP Define Functionally Distinct PRC1 Family Complexes. *Mol. Cel* 45, 344–356. doi:10.1016/j.molcel.2012.01.002

Geng, Z., and Gao, Z. (2020). Mammalian PRC1 Complexes: Compositional Complexity and Diverse Molecular Mechanisms. *Int. J. Mol. Sci.* 21. doi:10.3390/ijms21228594

Girirajan, S., Brkanac, Z., Coe, B. P., Baker, C., Vives, L., Vu, T. H., et al. (2011). Relative burden of Large CNVs on a Range of Neurodevelopmental Phenotypes. *Plos Genet.* 7, e1002334. doi:10.1371/journal.pgen.1002334

Hori, K., and Hoshino, M. (2017). Neuronal Migration and AUTS2 Syndrome. *Brain Sci.* 7. doi:10.3390/brainsci7050054

Hori, K., Nagai, T., Shan, W., Sakamoto, A., Abe, M., Yamazaki, M., et al. (2015). Heterozygous Disruption of Autism Susceptibility Candidate 2 Causes Impaired Emotional Control and Cognitive Memory. *PLoS One* 10, e0145979. doi:10.1371/journal.pone.0145979

Hori, K., Nagai, T., Shan, W., Sakamoto, A., Taya, S., Hashimoto, R., et al. (2014). Cytoskeletal Regulation by AUTS2 in Neuronal Migration and Neuritogenesis. *Cel Rep.* 9, 2166–2179. doi:10.1016/j.celrep.2014.11.045

Huang, X.-L., Zou, Y. S., Maher, T. A., Newton, S., and Milunsky, J. M. (2010). A De Novo Balanced Translocation Breakpoint Truncating the Autism Susceptibility Candidate 2 (AUTS2) Gene in a Patient with Autism. *Am. J. Med. Genet.* 152A, 2112–2114. doi:10.1002/ajmg.a.33497

Jolley, A., Corbett, M., Mcgregor, L., Waters, W., Brown, S., Nicholl, J., et al. (2013). De Novo intragenic Deletion of Theautism Susceptibility Candidate 2(AUTS2) Gene in a Patient with Developmental Delay: A Case Report and Literature Review. *Am. J. Med. Genet.* 161, 1508–1512. doi:10.1002/ajmg.a.35922

Kalscheuer, V. M., Fitzpatrick, D., Tommerup, N., Bugge, M., Niebuhr, E., Neumann, L. M., et al. (2007). Mutations in Autism Susceptibility Candidate 2 (AUTS2) in Patients with Mental Retardation. *Hum. Genet.* 121, 501–509. doi:10.1007/s00439-006-0284-0

Kassis, J. A., Kennison, J. A., and Tamkun, J. W. (2017). Polycomb and Trithorax Group Genes in Drosophila. *Genetics* 206, 1699–1725. doi:10.1534/genetics.115.185116

Kondrychyn, I., Robra, L., and Thirumalai, V. (2017). Transcriptional Complexity and Distinct Expression Patterns of Auts2 Paralogs in *Danio rerio*. *G3 (Bethesda)* 7, 2577–2593. doi:10.1534/g3.117.042622

Liu, S., Aldinger, K. A., Cheng, C. V., Kiyama, T., Dave, M., Mcnamara, H. K., et al. (2021). NRF1 Association with AUTS2-Polycomb Mediates Specific Gene Activation in the Brain. *Mol. Cel* S1097-2765, 00754–761. doi:10.1016/j.molcel.2021.09.020

Liu, Y., Zhao, D., Dong, R., Yang, X., Zhang, Y., Tammimies, K., et al. (2015). De Novo exon 1 Deletion ofAUTS2gene in a Patient with Autism Spectrum Disorder and Developmental Delay: A Case Report and a Brief Literature Review. *Am. J. Med. Genet.* 167, 1381–1385. doi:10.1002/ajmg.a.37050

Malaguti, G., Singh, P. P., and Isambert, H. (2014). On the Retention of Gene Duplicates Prone to Dominant Deleterious Mutations. *Theor. Popul. Biol.* 93, 38–51. doi:10.1016/j.tpb.2014.01.004

Mclysaght, A., Makino, T., Grayton, H. M., Tropeano, M., Mitchell, K. J., Vassos, E., et al. (2014). Ohnologs Are Overrepresented in Pathogenic Copy Number Mutations. *Proc. Natl. Acad. Sci. USA* 111, 361–366. doi:10.1073/pnas.1309324111

Monderer-Rothkoff, G., Tal, N., Risman, M., Shani, O., Nissim-Rafinia, M., Malki-Feldman, L., et al. (2021). AUTS2 Isoforms Control Neuronal Differentiation. *Mol. Psychiatry* 26, 666–681. doi:10.1038/s41380-019-0409-1

Nagamani, S. C. S., Erez, A., Ben-Zeev, B., Frydman, M., Winter, S., Zeller, R., et al. (2013). Detection of Copy-Number Variation in AUTS2 Gene by Targeted Exonic Array CGH in Patients with Developmental Delay and Autistic Spectrum Disorders. *Eur. J. Hum. Genet.* 21, 343–346. doi:10.1038/ejhg.2012.157

Oksenberg, N., and Ahituv, N. (2013). The Role of AUTS2 in Neurodevelopment and Human Evolution. *Trends Genet.* 29, 600–608. doi:10.1016/j.tig.2013.08.001

Oksenberg, N., Stevison, L., Wall, J. D., and Ahituv, N. (2013). Function and Regulation of AUTS2, a Gene Implicated in Autism and Human Evolution. *Plos Genet.* 9, e1003221. doi:10.1371/journal.pgen.1003221

Pang, W., Yi, X., Li, L., Liu, L., Xiang, W., and Xiao, L. (2021). Untangle the Multi-Facet Functions of Auts2 as an Entry Point to Understand Neurodevelopmental Disorders. *Front. Psychiatry* 12, 580433. doi:10.3389/fpsyt.2021.580433

Petrij, F., Giles, R. H., Dauwerse, H. G., Saris, J. J., Hennekam, R. C., Masuno, M., et al. (1995). Rubinstein-Taybi Syndrome Caused by Mutations in the Transcriptional Co-activator CBP. *Nature* 376, 348–351. doi:10.1038/376348a0

Piovesan, D., Hatos, A., Minervini, G., Quaglia, F., Monzon, A. M., and Tosatto, S. C. E. (2020). Assessing Predictors for New post Translational Modification Sites: A Case Study on Hydroxylation. *Plos Comput. Biol.* 16, e1007967. doi:10.1371/journal.pcbi.1007967

Roelfsema, J. H., White, S. J., Ariyürek, Y., Bartholdi, D., Niedrist, D., Papadia, F., et al. (2005). Genetic Heterogeneity in Rubinstein-Taybi Syndrome: Mutations in Both the CBP and EP300 Genes Cause Disease. *Am. J. Hum. Genet.* 76, 572–580. doi:10.1086/429130

Saeki, S., Enokizono, T., Imagawa, K., Fukushima, H., Kajikawa, D., Sakai, A., et al. (2019). A Case of Autism Spectrum Disorder with Cleft Lip and Palate Carrying a Mutation in Exon 8 of AUTS2. *Clin. Case Rep.* 7, 2059–2063. doi:10.1002/ccr3.2377

Sanchez-Jimeno, C., Blanco-Kelly, F., López-Grondona, F., Losada-Del Pozo, R., Moreno, B., Rodrigo-Moreno, M., et al. (2021). Attention Deficit Hyperactivity and Autism Spectrum Disorders as the Core Symptoms of AUTS2 Syndrome: Description of Five New Patients and Update of the Frequency of Manifestations and Genotype-Phenotype Correlation. *Genes* 12, 1360. doi:10.3390/genes12091360

Sellers, R. A., Robertson, D. L., and Tassabehji, M. (2020). Ancestry of the AUTS2 Family-A Novel Group of Polycomb-Complex Proteins Involved in Human Neurological Disease. *PLoS One* 15, e0232101. doi:10.1371/journal.pone.0232101

Simon, J. A., and Kingston, R. E. (2013). Occupying Chromatin: Polycomb Mechanisms for Getting to Genomic Targets, Stopping Transcriptional Traffic, and Staying Put. *Mol. Cel* 49, 808–824. doi:10.1016/j.molcel.2013.02.013

Singh, P. P., Affeldt, S., Cascone, I., Selimoglu, R., Camonis, J., and Isambert, H. (2012). On the Expansion of "dangerous" Gene Repertoires by Whole-Genome Duplications in Early Vertebrates. *Cel Rep.* 2, 1387–1398. doi:10.1016/j.celrep.2012.09.034

Singh, P. P., Arora, J., and Isambert, H. (2015). Identification of Ohnolog Genes Originating from Whole Genome Duplication in Early Vertebrates, Based on Synteny Comparison across Multiple Genomes. *Plos Comput. Biol.* 11, e1004394. doi:10.1371/journal.pcbi.1004394

Sultana, R., Yu, C.-E., Yu, J., Munson, J., Chen, D., Hua, W., et al. (2002). Identification of a Novel Gene on Chromosome 7q11.2 Interrupted by a Translocation Breakpoint in a Pair of Autistic Twins. *Genomics* 80, 129–134. doi:10.1006/geno.2002.6810

Tamburri, S., Conway, E., and Pasini, D. (2021). Polycomb-dependent Histone H2A Ubiquitination Links Developmental Disorders with Cancer. *Trends Genet.* 11. doi:10.1016/j.tig.2021.07.011

Ufartes, R., Berger, H., Till, K., Salinas, G., Sturm, M., Altmuller, J., et al. (2020). De Novo mutations in FBRSL1 Cause a Novel Recognizable Malformation and Intellectual Disability Syndrome. *Hum. Genet.* 139, 1363–1379. doi:10.1007/s00439-020-02175-x

Van Gils, J., Magdinier, F., Fergelot, P., and Lacombe, D. (2021). Rubinstein-Taybi Syndrome: A Model of Epigenetic Disorder. *Genes (Basel)* 12. doi:10.3390/genes12070968

Varlet, E., Ovejero, S., Martinez, A. M., Cavalli, G., and Moreaux, J. (2020). Role of Polycomb Complexes in Normal and Malignant Plasma Cells. *Int. J. Mol. Sci.* 21. doi:10.3390/ijms21218047

Wang, H., Wang, L., Erdjument-Bromage, H., Vidal, M., Tempst, P., Jones, R. S., et al. (2004). Role of Histone H2A Ubiquitination in Polycomb Silencing. *Nature* 431, 873–878. doi:10.1038/nature02985

Conflict of Interest: The authors declare that the research was conducted in the absence of any commercial or financial relationships that could be construed as a potential conflict of interest.

Publisher's Note: All claims expressed in this article are solely those of the authors and do not necessarily represent those of their affiliated organizations, or those of the publisher, the editors and the reviewers. Any product that may be evaluated in this article, or claim that may be made by its manufacturer, is not guaranteed or endorsed by the publisher.

frontiers in Cell and Developmental Biology

REVIEW
published: 24 November 2021
doi: 10.3389/fcell.2021.784998

T-Cell Factors as Transcriptional Inhibitors: Activities and Regulations in Vertebrate Head Development

*Johnny Bou-Rouphael and Béatrice C. Durand**

Sorbonne Université, CNRS UMR7622, IBPS Developmental Biology Laboratory, Campus Pierre et Marie Curie, Paris, France

Since its first discovery in the late 90s, Wnt canonical signaling has been demonstrated to affect a large variety of neural developmental processes, including, but not limited to, embryonic axis formation, neural proliferation, fate determination, and maintenance of neural stem cells. For decades, studies have focused on the mechanisms controlling the activity of β-catenin, the sole mediator of Wnt transcriptional response. More recently, the spotlight of research is directed towards the last cascade component, the T-cell factor (TCF)/Lymphoid-Enhancer binding Factor (LEF), and more specifically, the TCF/LEF-mediated switch from transcriptional activation to repression, which in both embryonic blastomeres and mouse embryonic stem cells pushes the balance from pluri/multipotency towards differentiation. It has been long known that Groucho/Transducin-Like Enhancer of split (Gro/TLE) is the main co-repressor partner of TCF/LEF. More recently, other TCF/LEF-interacting partners have been identified, including the pro-neural BarH-Like 2 (BARHL2), which belongs to the evolutionary highly conserved family of homeodomain-containing transcription factors. This review describes the activities and regulatory modes of TCF/LEF as transcriptional repressors, with a specific focus on the functions of *Barhl2* in vertebrate brain development. Specific attention is given to the transcriptional events leading to formation of the Organizer, as well as the roles and regulations of Wnt/β-catenin pathway in growth of the caudal forebrain. We present TCF/LEF activities in both embryonic and neural stem cells and discuss how alterations of this pathway could lead to tumors.

Keywords: Tcf/Lef, transcription, signalization, stem cells, Barhl, forebrain, Wnt

OPEN ACCESS

Edited by:
Kerstin Feistel,
University of Hohenheim, Germany

Reviewed by:
Kris Vleminckx,
Ghent University, Belgium
Sally Ann Moody,
George Washington University, United States

****Correspondence:***
Béatrice C. Durand
beatrice.durand@sorbonne-universite.fr

Specialty section:
This article was submitted to Morphogenesis and Patterning, a section of the journal Frontiers in Cell and Developmental Biology

Received: *28 September 2021*
Accepted: *28 October 2021*
Published: *24 November 2021*

Citation:
Bou-Rouphael J and Durand BC (2021) T-Cell Factors as Transcriptional Inhibitors: Activities and Regulations in Vertebrate Head Development. Front. Cell Dev. Biol. 9:784998. doi: 10.3389/fcell.2021.784998

INTRODUCTION

Understanding how the vertebrate nervous system emerges from a homogeneous layer of neuroepithelial cells, the neural plate, has long been a subject of intense fascination. Fate-mapping experiments performed at the end of the 20th century demonstrated that the primordia of the forebrain, midbrain, hindbrain, and spinal cord are all already established along the antero-posterior (AP) axis when the neural plate emerges. These studies revealed that a construction blueprint of the neural organization, and specifically that of the forebrain, is set up during gastrulation (reviewed in Wilson and Houart, 2004; Hoch et al., 2009; Andoniadou and Martinez-Barbera, 2013). In 1924, Hans Spemann and Hilde Mangold discovered that the dorsal lip of a newt blastopore, when grafted into the ventral part of a host embryo, is able to induce a secondary axis containing a complete nervous system (Spemann and Mangold, 1924). This small group of specialized cells, referred to as the "Organizer," emerges during embryonic development at gastrulation, acts as a local source of secreted signaling factors and drives both neural induction and

TABLE 1 | TCF/LEF, Gro/TLE and BARHL homologues across species.

	Drosophila melanogaster	*Caenorhabditis elegans*	*Xenopus laevis*	*Mus musculus*	*Homo sapiens*
TCF/LEF	Pan	POP1	Tcf7 (Tcf1) Tcf7l1 (Tcf3) Tcf7l2 (Tcf4) Lef1 (Lef1)	TCF7 (TCF1) TCF7l1 (TCF3) TCF7l2 (TCF4) LEF1 (LEF1)	TCF7 (TCF1) TCF7l1 (TCF3) TCF7l2 (TCF4) LEF1 (LEF1)
Gro/TLE	Gro	UNC-37	Gro1-4	GRG1-4, GRG5	TLE1-4
BARHL1	BarH2	CEH30	Barhl1	BARHL1 (MBH2)	BARHL1
BARHL2	BarH1		Barhl2	BARHL2 (MBH1)	BARHL2

Invertebrate have a single T-cell factor/Lymphoid enhancer-binding factor (TCF/LEF): Pangolin (Pan) in flies and POP1 in worm. Vertebrate have four TCF/LEF known as TCF7, TCF7l1, TCF7l2 and LEF1, previously termed TCF1, TCF3, TCF4 and LEF1 respectively. *Drosophila* Groucho (Gro) and *C. elegans* UNC-37 corepressors have four vertebrate orthologs: Gro1-4 in frogs, Groucho-related gene (GRG1-4) in mice, and Transducin-like enhancer of split (TLE1-4) in human. In mice, GRG5 acts as a dominant negative. The homeobox-containing proteins BarH1 and BarH2 have been first identified in *Drosophila.* Homologues have been described in vertebrate, named BarH-like or BARHL. In mice, BARHL have been previously referred to as mammalian BarH (MBH1 and MBH2). *C. elegans* Bar homeodomain gene (CEH30) represents the homologue of *Drosophila* BarH1 and BarH2 and their vertebrate counterparts.

patterning of the prospective neuroepithelium and thereby of the developing head (reviewed in De Robertis et al., 2000; Niehrs, 2004; Kiecker and Lumsden, 2012; Anderson and Stern, 2016). Since this discovery, an organizing center has been found in other model organisms: Hensen's node in the chick, the node in the mouse and the shield in zebrafish, and the capacity of the blastopore-associated tissue to induce naïve cells to form a fully developed twin embryo was found conserved in non-bilaterian metazoan species (Kraus et al., 2016).

Initial regionalization of the neural plate relies on the synergistic action of at least five major signaling pathways that convey spatial and temporal information to naïve cells, consequently inducing developmental programs that drive their behavior (reviewed in Stern, 2002; Wessely and De Robertis, 2002; Ozair et al., 2013). Amongst the cell-to-cell signaling pathways coordinating development, one of the most conserved in the animal kingdom is the Wnt/β-catenin, or canonical pathway. During emergence of the central nervous system, Wnt/β-catenin acts in a coordinated manner with Sonic HedgeHog (Shh), Notch, Transforming Growth Factor (TGF-β), and Fibroblast Growth Factor (FGF) pathways and contributes to neural patterning, proliferation, and fate determination. Notably, the Wnt/β-catenin machinery drives the transcriptional events leading to the induction of the Organizer, and thereby formation of the embryonic axes. Its participation is also crucial in Neural Stem Cell (NSC) maintenance and self-renewal. Not surprisingly, dysregulation of Wnt/β-catenin signaling is linked to serious brain developmental defects, including cancer (reviewed in Hoppler and Moon, 2014; Brafman and Willert, 2017; Nusse and Clevers, 2017).

After four decades of intense research following the initial discovery of Wnt signals (Nusse and Varmus, 1982, reviewed in Nusse and Varmus, 2012), 19 ligands have been characterized in mammals, together with two families of receptors comprising 10 Frizzled receptors, and two Low-Density Lipoprotein (LDL) receptor-related proteins (LRP5/6) (reviewed in MacDonald et al., 2009; Niehrs, 2012). Despite this complexity, the large majority of Wnt/β-catenin transcriptional targets are regulated by T-Cell Factor/Lymphoid Enhancer-binding Factor (TCF/LEF) transcription factors (TF). Loss of function analysis performed in invertebrate such as the nematode *Caenorhabditis elegans (C. elegans)* and in flies, where a single TCF/LEF has been characterized, provided evidence that TCF/LEF act through a transcriptional switch, which either activates or represses Wnt/β-catenin target genes' expression. This feature has been further validated in vertebrate, whose genome contains four TCF/LEF members: TCF1, TCF3, TCF4, and LEF1. In this review, the vertebrate TCF/LEF members will be referred to as TCF7 (previously TCF1), TCF7L1 (TCF3), TCF7L2 (TCF4) and LEF1 following the Human Genome Organization (HUGO) nomenclature (**Table 1**). As will be discussed below, some of the vertebrate TCF/LEF have a more specialized function compared to their invertebrate counterparts.

In most of the species investigated so far, TCF/LEF activate transcription in Wnt-stimulated cells by interacting with the sole transcriptional activator β-catenin (Schuijers et al., 2014), but TCF/LEF can recruit other partners to the transcriptional activating machinery. A massive effort has been deployed to understand TCF/β-catenin transcriptional modes of activation. Very elegant and detailed accounts of the current models supporting Wnt-dependent transcriptional activation events have been published recently (reviewed in van Amerongen and Nusse, 2009; Wiese et al., 2018; Söderholm and Cantù, 2021).

In the absence of Wnt ligands, TCF/LEF interact with repressor partners to inhibit Wnt target genes' expression. The best-characterized co-repressor partner is Groucho/Transducin-Like Enhancer of split (Gro/TLE) (Brantjes, 2001). Under certain conditions, Gro/TLE can recruit Histone Deacetylases (Hdac) to the complex, a chromatin remodeling enzyme which removes acetyl groups from the N-terminal lysine residues of the core histones, inducing gene expression silencing through chromatin condensation (Sekiya and Zaret, 2007). Recent evidence reveals a role for the homeodomain (HD)-containing TF BarH-Like Homeobox-2 (BARHL2) in enhancing TCF/Gro repressive activity *in vitro* and *in vivo* and preventing the β-catenin-mediated transactivation of TCF/LEF target genes (Sena et al., 2019). These data highlight a novel mechanism regulating Wnt/β-catenin transcriptional response, probably involving the chromatin modifier Hdac1. Studies from hemichordates to vertebrate, which are evolutionarily more than 500 million years apart, have revealed that, despite the differences between species, they all carry two *Barhl* genes: *Barhl1* and *Barhl2*, each

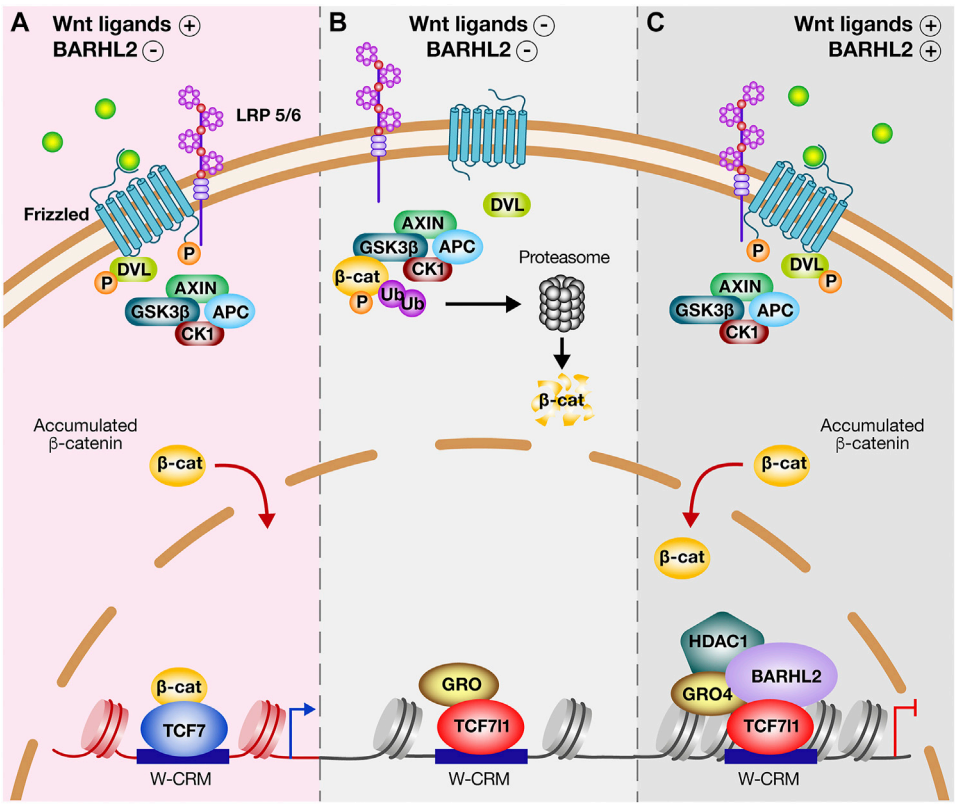

FIGURE 1 | BARHL2 regulatory mode of Wnt canonical pathway. **(A)** Upon Wnt binding to Frizzled (Frz) and Low-Density Lipoprotein Receptor-related Protein (LRP) family of receptors 5 and 6, the multiprotein destruction complex components (Scaffold protein AXIN, Adenomatous Polyposis Coli (APC) tumour suppressor protein, Casein Kinase 1 (CK1), and Glycogen Synthase kinase 3β (Gsk3β)) are recruited to the receptor complex, where they are internalized. Frz binds to Disheveled (DVL) keeping AXIN and Gsk3β inactive. β-catenin (β-cat) escapes degradation, accumulates and translocates into the nucleus, where it binds to activating T-Cell Factors such as TCF7. TCF7 bound on Wnt-Cis regulatory motif (W-CRM) acts as transcriptional activator. **(B)** In the absence of Wnt ligands, the destruction complex is activated. Gsk3β and CK1 phosphorylate β-cat, allowing for its recognition by the E3 ubiquitin ligase (Ub) and targeting it for ubiquitination and proteasomal degradation. In the nucleus, the co-repressive factor Groucho (Gro) binds through its Glutamine (Q)-rich domain to TCF7l1 inducing a transcriptional repression. **(C)** In Wnt-stimulated cells, the presence of BARHL2 inhibits the cell response to β-cat. BARHL2 interacts with the Tryptophan/Aspartic acid (WD)-rich domains of Gro4 *via* its Engrailed Homology 1 (EH1) motifs and interacts with TCF7l1. The domain mediating BARHL2-TCF7l1 interaction is unknown. BARHL2 stabilizes the TCF7l1/Gro4 complex, reinforcing transcriptional repression of Wnt target genes. The complex containing TCF7l1, Gro, and BARHL2 could recruit histone deacetylases (HDAC), which induces inherited epigenetic modifications.

having a remarkably evolutionarily conserved structure, distribution, and function. The spectrum of TCF/Gro transcriptional targets is large. Both TCF/LEF and Gro/TLE proteins interact with other TFs, and are targets for developmental signals, which influence their activities. The extent and importance of TCF repressive roles, and their regulatory modes during embryogenesis are neither fully grasped, nor fully understood.

In this review, we present the activities and regulatory modes of TCF as transcriptional repressors with a focus on the developmental roles of *Barhl2*. Specific attention is given to the transcriptional events leading to the formation of the Organizer, as well as the roles and regulations of the Wnt/β-catenin pathway in the growth of the caudal forebrain. We present core activities of TCF/LEF in Embryonic Stem Cells (ESCs) self-renewal and pluripotency, and maintenance of NSCs, as well as their identified deregulations and the emergence of cancer.

Transcriptional Regulation of Wnt Target Genes by the TCF/LEF Factors – A Focus on the TCF-Mediated Transcriptional Repression

TCF/LEF proteins are the major mediators of Wnt-responsive gene transcription in the nucleus. In the absence of Wnt ligands, β-catenin is phosphorylated by the destruction complex containing Glycogen Synthase Kinase 3β (GSK3β), Casein Kinase 1 (CK1), Adenomatous Polyposis Coli (APC) tumour suppressor protein, and Axin. Phosphorylated β-catenin is targeted towards ubiquitination and further proteasome-mediated degradation. In the nucleus, inhibitory TCF/LEF members are bound on Wnt Cis-Regulary-Motifs (W-CRM), interact with co-repressors such as Gro/TLE proteins, and act as transcriptional repressors. Conversely, in Wnt-stimulated cells, the destruction complex is inhibited leading to the cytoplasmic accumulation of β-catenin and further nuclear translocation.

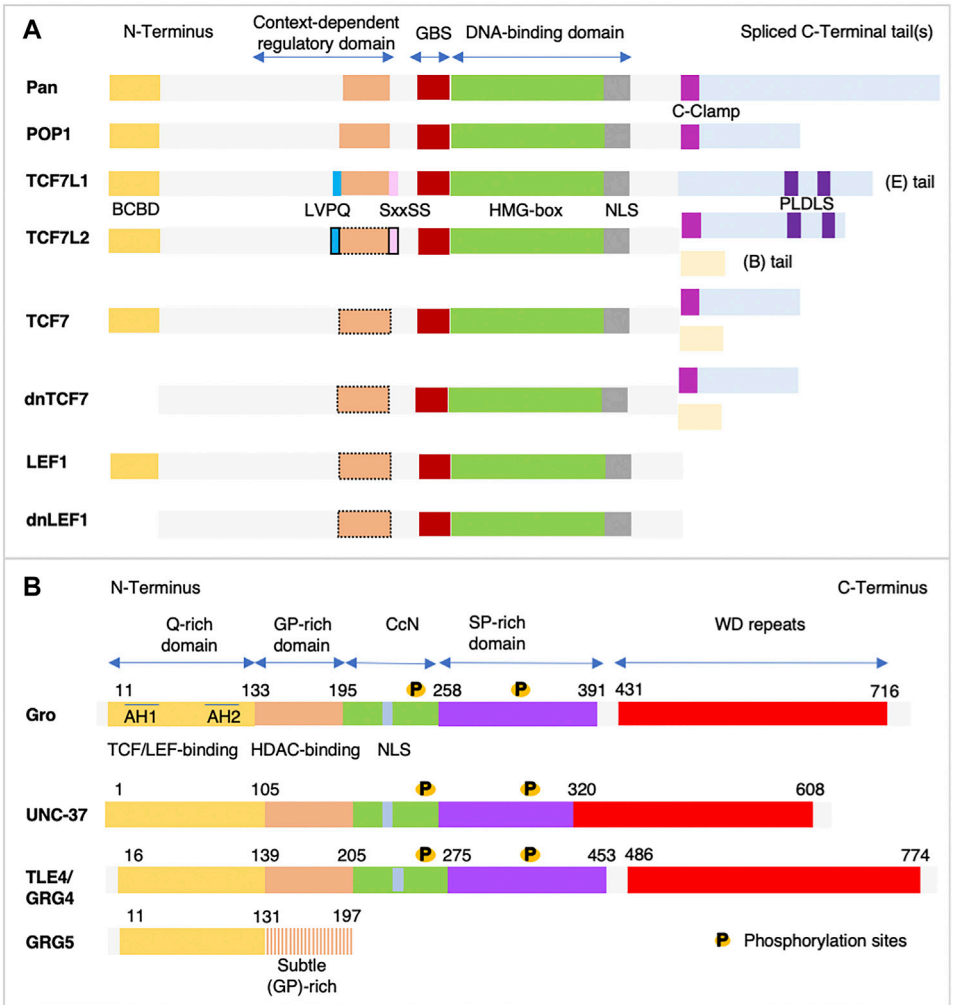

FIGURE 2 | (A) Structural organization of the TCF/LEF proteins. Invertebrate (Pangolin (Pan) in *Drosophila*, POP1 in *C. elegans*), and vertebrate T-Cell Factor/ Lymphoid Enhancer Factor (TCF/LEF) proteins share several highly conserved domains: the N-terminal β-catenin-binding domain (BCBD) shown in dark yellow, the DNA-binding domain which contains a High-Mobility Group box (HMG-box) shown in green and a Nuclear Localization Signal (NLS) shown in grey. The DNA-binding domain is preceded by a less well-defined binding sequence for the Groucho/Transducin-like enhancer of split (Gro/TLE) (Gro-binding sequence, GBS) shown in dark red. Several protein isoforms are encoded by the genome of vertebrate, except for TCF7l1. The Context-dependent Regulatory Domain (CRD) is less conserved and is encoded by three exons. One of them, indicated in orange, can be alternatively spliced in all vertebrate isoforms except *TCF7L1*. Black dotted lines indicate possible alternative splicing. In TCF7l1 and in TCF7l2, this CRD domain is flanked by two small motifs LVPQ shown in blue at its N-terminal end, and SxxSS shown in pink at its C terminal end, which contribute to TCF7L1/2 repressive activity. Whereas these two motifs are always present in TCF7l1, in TCF7l2 they can be alternatively spliced. Less conservation is found in the C-terminal tail, as it is highly variable in length. The long (E) tails shown in light blue contain additional regulatory domains: the C-clamp DNA-binding motif shown in violet, present in most invertebrate and in the vertebrate TCF7l2 and TCF7, and two C-terminal-binding protein (CtBP) motifs (PLDLS) shown in dark blue, found in TCF7l1 and TCF7l2. Isoforms of TCF7 and LEF1 expressed from alternative promoters and encoding proteins lacking BCBD behave as dominant-negative. Alternative splicing also generates proteins with short (B) tails shown in light yellow. LEF1 isoform lacks the C-terminal tail. This scheme is inspired by (Hoppler and Waterman, 2014). **(B)** Schematic representations of Gro/TLE proteins functional domains. Sequence comparison of the *Drosophila* Groucho (Gro) (NP_001247309.1), human TLE4 (NP_001269677.1), mouse Groucho-related gene 4 (GRG4) (NP_001289876.1), and *C. elegans* UNC-37 (NP_491932.1) reveals the presence of five domains. The two most highly conserved domains are: 1- the amino-terminal glutamine-rich (Q) domain shown in dark yellow that contains two amphipathic α-helices (AH1 and AH2) and is required for Gro/TLE oligomerization, and interactions with other proteins including the TCF/LEF proteins; and 2- the Tryptophane/Aspartic acid (WD)-repeats shown in red that mediates protein-protein interactions, such as those with the Engrailed Homology (EH1)-containing proteins. The central portion of Gro/TLE is less well conserved and contains a Glycine/Proline-rich (GP) domain implicated in the recruitment of the *Drosophila* Rpd3/mammalian Histone Deacetylase (HDAC) shown in orange, a central portion (CcN) domain shown in green containing a Nuclear Localization Signal (NLS) shown in grey, and a Serine/ Proline-rich (SP) domain shown in violet. Phosphorylation sites are found in both the CcN and SP domains. Numbers indicate the positions of the boundary amino acids (aa). GRG-5 only contains the Q-rich domain and a GP-rich domain with aa differences compared to the long forms of Gro/TLE, which impede its ability to interact with HDAC. GRG-5 acts as a dominant negative.

Increase in the nuclear β-catenin levels transiently converts TCF/LEF into transcriptional activators (**Figures 1A,B**) (reviewed in MacDonald et al., 2009).

Observations from mammalian cells (Schuijers et al., 2014), flies (Franz et al., 2017), and amphibian (Nakamura et al., 2016) among others, reported the requirement of TCF/LEF for the transcriptional regulation of most β-catenin target genes, supporting the classical model of Wnt transcriptional regulation. Mammalian cells lacking all four genes encoding TCF/LEF proteins display perturbations in the association of β-catenin with DNA. In such cells, β-catenin was found to regulate different transcriptional targets (Doumpas et al., 2019), revealing that only when TCF/LEF is absent, β-catenin autonomously regulates a subgroup of genes whose transcription does not initially require TCF/LEF. Genome-wide analysis methods identified Wnt/TCF target genes that are available at http://www.stanford.edu/group/nusselab/cgi-bin/wnt/.

TCF/LEF Members and Structure

TCF/LEF sequence alignment and phylogenetic trees in species such as the hemichordate *Saccoglossus kowalevskii (S. kowalevskii)*, *Caenorhabditis elegans (C. elegans)*, *Drosophila melanogaster*, *Hydra magnipapillata*, and *Ciona intestinalis* reveal the presence, in the TCF/LEF structure, of the four major binding domains found in vertebrate (Atcha et al., 2007; Žídek et al., 2018), indicating that the TCF/LEF in invertebrate is probably the ancestral precursor of that described in vertebrate. Further complexity has been added through evolution following the emergence of the different TCF/LEF isoforms in mammals which are generated through alternative transcription, translation start sites, and alternative splicing (reviewed in Hoppler and Waterman, 2014).

Structural and functional analysis of TCF/LEF provided important cues on the domains mediating their transcriptional activities (**Figure 2A**). On their N-terminal region, all TCF/LEF isoforms have a β-catenin-binding domain (BCBD), which contains 50 amino acids (aa). Three sets of aa are involved in the TCF/LEF-β-catenin interactions: residues 2–15 (known as the β-hairpin module) fit into the groove of the central Armadillo (Arm) repeat domain (the homologue of the vertebrate β-catenin and signal transducer of wingless (Wg) signaling in flies). Residues 16–29 form an extended strand, and residues 40–51 form an α-helix (Graham et al., 2000). TCF/LEF interaction with β-catenin is necessary for their activity (Kratochwil, 2002). Isoforms of TCF7 and LEF1 expressed from alternative promoters, and encoding proteins lacking BCBD, behave as dominant-negative (van de Wetering et al., 1997; Hovanes et al., 2001). Recognition of the specific DNA sequence motif (CCTTTGAT(G/C)) by TCF/LEF is mediated by a highly conserved High Mobility Group (HMG)-box, whose DNA-binding domain structure and general mechanisms of DNA binding and bending, have been extensively studied (van Beest et al., 2000; reviewed in; Malarkey and Churchill, 2012). This HMG-box is followed by a Nuclear Localization Signal (NLS). The BCBD and the DNA-binding domain are separated by a less conserved context-dependent regulatory domain (CRD), partly encoded by an exon (exon VI), which can be alternatively spliced in all TCF/LEF except TCF7L1. Two conserved aa motifs, LVPQ and SxxSS, flank exon VI in *Xenopus* Tcf7l1 and Tcf7l2, but not in Tcf7 or Lef1, and can be alternatively spliced in Tcf7l2. Mutations in these two motifs validate their strict requirement for Tcf7l1 repressive activity. Furthermore, their insertion into the *lef1* sequence abolishes Lef1 activator capacity, as detected through its inability to induce an ectopic secondary axis when injected ventrally in *Xenopus* embryos (Pukrop et al., 2001; Gradl et al., 2002; Liu et al., 2005). Other studies suggest that the Gro/TLE-binding domain encompasses the entire CRD and part of exon VII. Indeed, alternative splicing within the CRD (exon V to exon VII) modifies the interactions of TCF/LEF with Gro/TLE (Young et al., 2019) (reviewed in Hoppler and Waterman, 2014). The C-terminal tail is the most variable region among the TCF/LEF, where much of the aa sequence exhibit a low level of conservation. The C-terminal tail exists either as a long C-terminal extension, referred to as E tail, that contains additional domains, or as a short C-terminal extension, referred to as B tail, lacking the additional transcriptional regulators' binding domains. Whereas TCF7L1 only carries an E tail, the *LEF1* gene lacks the E-tail-encoding exon (Atcha et al., 2003). The E-tails encode two copies of a specific short motif (PLDLS) that binds the evolutionarily conserved co-repressor phosphoprotein C-terminal-Binding Protein (CtBP). Indeed, CtBP binds to both Tcf7l1, and the Tcf7l2 isoforms carrying an E tail (Brannon et al., 1999; Valenta et al., 2003; Fang et al., 2006). An additional small, highly conserved 30 aa motif (CRARF) is present in invertebrate TCF/LEF and in vertebrate splice variants Tcf7-E and Tcf7l2-E, but not in Tcf7l1. CRARF is required for the β-catenin-mediated transcriptional activation of the *lef1* promoter, and forms a C-Clamp (Cysteine-rich domain) that allows TCF/LEF to bind an additional DNA motif known as the Helper site (5′-RCCGCCR-3′) (Atcha et al., 2007; Ravindranath and Cadigan, 2014).

A Brief Picture of the Evolution of the TCF/LEF Family

TCF/LEF are metazoan inventions (Adamska et al., 2010). In choanoflagellates, which are unicellular eukaryotes considered the closest known relatives to metazoans, there is no evidence supporting the existence of any TCF/LEF protein and the only found component of the Wnt pathway is GSK3 (King et al., 2008). In invertebrate genome, only one *Tcf/Lef* gene is detected (reviewed in Hoppler and Waterman, 2014). One exception is found in the phylum of Platyhelminthes, in which five *Tcf/Lef* have been found in the genome of the flatworm *Schmidtea mediterranea*. Only two of these Tcf/Lef have a putative BCBD, which suggests a function in mediating Wnt transcription (Brown et al., 2018).

Most of our knowledge about TCF/LEF activity in invertebrate derives from studies performed in *Drosophila* and *C. elegans*. As in vertebrate, their Tcf/Lef is converted from a transcriptional repressor to activator by increasing nuclear levels of β-catenin. *Drosophila* Arm/β-catenin promotes transcriptional activation by binding Pangolin (Pan), the Tcf/Lef in fly (referred to as Tcf) (van de Wetering et al., 1997). Consequently, co-repressors such as

Gro are displaced, allowing Arm binding to transcriptional co-activators such as Pygopus (Pygo) (Parker et al., 2002). As in vertebrate, in the absence of Arm, Tcf acts as a transcriptional repressor (Cavallo et al., 1998). Transcriptional repression appears to be directly mediated by the Tcf/Arm interactions with a specific DNA sequence motif (AGAWAW). The exchange of the AGAWAW motif into a standard Tcf-binding site (CCTTTGAT(G/C)) reversed the mode of regulation, resulting in Wnt-mediated activation instead of repression. Whereas both transcriptional activation and repression require binding of Arm to the N-terminal part of Tcf, allosteric regulation has been proposed to explain differences in Tcf/Lef transcriptional capacity. Indeed, Tcf binding to different DNA motifs may allow its interaction with distinct co-regulators, which subsequently controls its transcriptional activity (Blauwkamp et al., 2008).

In *C. elegans*, loss-of-function phenotypes indicate a dual regulatory mode for the Tcf/Lef termed POsterior Pharynx defect (POP1). An interesting mechanism has been reported for mesoderm and endoderm fate specification during embryogenesis (Rocheleau et al., 1997; Thorpe et al., 1997). At the four-cells stage, two sister cells, the anterior (MS) and the posterior (E) are fated to respectively generate the mesoderm and the endoderm. Higher levels of *pop1* are detected in the MS blastomere (Lin et al., 1995), where it represses the transcription of Wnt-responsive endoderm-determining gene *end1* through the recruitment of the histone deacetylase HDA-1 and UNCoordinated (UNC)-37 (the homologue of the Gro/TLE) (Calvo et al., 2001). In a POP1 mutant, both blastomeres adopt an endoderm-like fate. However, in the E blastomere receiving Wnt signals, WRM1/β-catenin binds to the N-terminal domain of POP1 protein and decreases its nuclear levels, alleviating POP1 repressive activity, which will then activate the expression of *end1* and induce the specification of the endodermal fate (Rocheleau et al., 1997; Shetty et al., 2005). Another model proposes that the switch of POP1 from a transcriptional repressor to an activator depends on its DNA-binding site. The C-terminal tail of POP1 contains a C-clamp, which enables POP1 to recognize another DNA motif (the Helper site). When Wnt signaling is activated, β-catenin stabilizes the interaction between the C-Clamp of POP1 and the Helper sites found in the *end1* sequence, which enables *end1* transcription (Bhambhani et al., 2014).

The vertebrate TCF/LEF are somewhat specialized in transcriptional activation or repression

In vertebrate, the founder members of the TCF/LEF family are TCF7 (van de Wetering et al., 1991) and LEF1 (Travis et al., 1991), initially identified as lymphocyte-regulators in mice. The two other members, TCF7l1 and TCF7l2 have been characterized few years later (Castrop et al., 1992).

TCF/LEF are largely expressed during vertebrate embryogenesis in some overlapping but also distinct regions including the central nervous system, suggesting a functional redundancy of the TCF/LEF members. For instance, in mice, *Tcf7l2* and *Lef1* transcripts are detected in the mesencephalon and the diencephalon (Korinek et al., 1998). In zebrafish, *tcf1* and *lef1* expression overlaps in the tail bud, fin buds and paraxial mesoderm (Veien et al., 2005). Observations made in lung epithelial progenitors also supports redundant and additive functions between the different TCF/LEF members (Gerner-Mauro et al., 2020). However, genetic mutants lacking a single *Tcf/Lef* gene, as well as double knockout (KO) mutants, exhibit severe developmental alterations (van Genderen et al., 1994; Galceran et al., 2000), indicating expanded and diversified roles for each TCF/LEF. Based on these findings among others, a specific activity as Wnt transcriptional activator and/or repressor has been attributed to each TCF/LEF.

Lef1 and *Tcf7l2* KO mice show reduced Wnt transcriptional activity and are considered to mostly act as activators of the pathway (Korinek et al., 1998; Kratochwil, 2002). Similarly, analysis in zebrafish reveals activating functions for Tcf7, Lef1, and Tcf7l2. Loss of Lef1, expressed in several embryonic tissues, specifically the neural crest, decreases β-catenin activity (Dorsky et al., 1999, 2003). Additional observations from Tcf7l2 mutants show that it maintains proliferation of the intestinal epithelium through activating Wnt target genes' transcription (Muncan et al., 2007).

In contrast, numerous studies strongly argue that Tcf7l1 mediates Wnt repressive activity. Mice depleted of *Tcf7l1* gene phenocopy those with ectopic activation of Wnt signaling, suffering severe forebrain abnormalities in addition to perturbations in the midbrain and hindbrain (Merrill et al., 2004). Similarly, the zebrafish genome contains two *tcf7l1* genes, *headless hdl/tcf7l1a* (Kim et al., 2000) and *tcf7l1b* (Dorsky et al., 2003), giving a total of five *tcf/lef* genes. The two Tcf7l1 appear to normally act as transcriptional repressors. *hdl/tcf7l1a* mutants exhibit truncated Tcf7l1 protein, which cannot undergo nuclear translocation. Such mutants show severe head defects including a lack of eyes, forebrain, and a part of the midbrain, a hallmark of Wnt overactivation. This phenotype could be rescued by overexpressing *tcf7l1b*, which in this context also act as a negative regulator of the Wnt pathway (Dorsky et al., 2003). Compared to zebrafish, the medaka genome contains a single *tcf7l1* gene. Medaka lacking *tcf7l1* have the same phenotype as the double-mutant zebrafish *hdl/tcf7l1b* (Doenz et al., 2018).

Some of the most informative studies regarding transcriptional activities of the four TCF/LEF members came from investigating the development of Spemann organizer (SO) in the amphibian *Xenopus* (also *see* next section). The early *Xenopus* embryo expresses three maternally inherited *tcf/lef* mRNAs: *tcf7*, *tcf7l1* and *tcf7l2* (Molenaar et al., 1998; Houston et al., 2002; Roël et al., 2002). Tcf/Lef activities are not redundant during mesoderm induction in amphibian. At late blastula/early gastrula stages, maternally encoded *tcf7l1* represses the dorsal organizer genes' expression (Houston et al., 2002), whereas both *tcf7* and *tcf7l2* act as transcriptional activators of SO genes (Standley et al., 2006). In this developmental context, whereas an activating form of *tcf7l1* can rescue the Tcf7-morphant phenotype, only a constitutive repressor form of *tcf7l1* rescues the Tcf7l1-morphant phenotype (Liu et al., 2005). Taken together, these observations indicate that during early *Xenopus* mesoderm induction, Tcf7l1 is mostly required for transcriptional repression, whereas Tcf7 and Tcf7l2 mostly

mediate transcriptional activation. Interestingly, *lef1* transcripts are first detected after the mid-blastula transition (MBT) (Molenaar et al., 1998), and during mesoderm induction, Lef1 transcriptional activity appears to be redundant with that of Tcf7 (Liu et al., 2005).

The Interaction Between TCF/LEF and Gro/TLE: A Partnership at the Core of TCF Inhibitory Activity

All the TCF/LEF members need to bind with nuclear co-factors to regulate target genes' transcription. A key insight into the mechanism of Wnt transcriptional inhibition mediated by the TCF was the finding that they can directly bind to members of the Gro/TLE family of transcriptional co-repressors.

Structure and Interactions of Gro/TLE Co-repressors

Gro/TLE are evolutionary conserved nuclear proteins. The invertebrate genome encodes a single member: Gro, initially identified in *Drosophila*, and UNC-37 in *C. elegans*, both of which antagonize signaling by Wnt (Cavallo et al., 1998; Calvo et al., 2001). Four members have been identified in human, known as TLE1-4, and in mice, named the Groucho-Related Genes (GRG1-4) (reviewed in Jennings and Ish-Horowicz, 2008; Turki-Judeh and Courey, 2012). In mice, a fifth family member (GRG-5) has also been identified as a gene encoding a shorter variant. GRG-5 is thought to act as a naturally occurring dominant negative (**Table 1**) (Brantjes, 2001; Wang et al., 2004).

A conserved structural organization comprising five domains characterizes Gro/TLE proteins (**Figure 2B**). Lacking a DNA-binding domain, Gro/TLE rely on their interaction with transcription factors for their specific recognition of promoter and/or enhancer DNA sequences. The highly conserved N-terminal glutamine-rich (Q) domain contains two motifs termed the amphipathic α-helices (AH1 and AH2), which mediate both Gro/TLE homo-oligomerization and their interactions with various transcription factors, including TCF/LEF (reviewed in Jennings and Ish-Horowicz, 2008). The central portion of Gro/TLE contains three less well-conserved domains. Gro/TLE was found to bind to the *Drosophila* Hdac known as Rpd3 (Chen et al., 1999), and with the mammalian HDAC1 an interaction mediated by the glycine (G) and proline (P)-rich domain (GP) (Chen et al., 1999; Arce et al., 2009). Second, the central (CcN) domain which includes a NLS, and third, a Serine (S) Proline (P)-rich domain (SP) generally involved in repression. The CcN and SP domains contain phosphorylation sites, which can modulate Gro/TLE-mediated repression (reviewed in Jennings and Ish-Horowicz, 2008). Of note, GRG5 contains the TCF/LEF binding domain and a GP domain that carries mutations impeding its ability to interact with HDAC (Brantjes, 2001). At their C-terminal end, Gro/TLE have a four tryptophan-aspartic acid repeat domain (WD), which is highly conserved across evolution. The WD motif is involved in nucleosome binding and condensation (Sekiya and Zaret, 2007), and mediates Gro/TLE interactions with repressor proteins. The WD motif of Gro/TLE interacts with two distinct peptidic motifs, the Engrailed Homology-1 (EH1) motif, and the WRPW (Trp-Arg-Pro-Trp) motif.

The EH1 motif is a Phenylalanine/Isoleucine/Leucine (FIL)-rich domain (FxIxxIL), required for transcriptional repression *in vitro* and *in vivo* (Smith and Jaynes, 1996; Muhr et al., 2001; Jennings et al., 2006). The EH1 motif is found in a large number of HD-containing TFs involved in neuronal specification such as Gastrulation Brain homeobox 2 (GBX2), Orthodenticle homeobox 2 (OTX2) (Heimbucher et al., 2007), Forkhead box (FOX) family of TFs (Yaklichkin et al., 2007), Engrailed (EN) (Jimenez et al., 1997) and BARHL that are notably the only Gro/TLE partners containing two EH1 domains (Offner et al., 2005). The TF Dorsal is involved in DV axis patterning in *Drosophila*. Dorsal was found to physically interact with Gro. Interestingly, in embryos lacking Gro, Dorsal functions as a transcriptional activator rather than as a repressor (Dubnicoff et al., 1997). It has been demonstrated that Gro interacts with a motif with partial homology to the EH1, located in the C-terminal part of Dorsal (Flores-Saaib et al., 2001). This interaction is weak and is stabilized by the presence of additional Gro-binding repressors (Valentine et al., 1998).

The second Gro/TLE-interacting motif is the WRPW present in basic-helix-loop-helix (bHLH) proteins including the Hairy/Enhancer of Split (E(spl))/HES proteins, transcriptional repressors that function as downstream targets of activated Notch receptors (Grbavec et al., 1998) (reviewed in Cinnamon and Paroush, 2008; Turki-Judeh and Courey, 2012). In the absence of Notch signaling, Gro/TLE is recruited *via* Hairless to a complex containing Suppressor of Hairless (Su(H)) and CtBP, which represses Notch target genes, including E(spl). Upon activation of Notch signaling, the Notch intracellular domain (NICD) enters the nucleus, displaces the Gro-containing complex, recruits Mastermind (Mam) on Su(H) an interaction which further results in the transcriptional activation of E(spl). E(spl) encoded factors interact with Gro/TLE to repress proneural genes (reviewed in Cinnamon and Paroush, 2008; Turki-Judeh and Courey, 2012). In *Drosophila*, and mammals association of Gro/TLE to bHLH proteins is required in cell fate decisions during tissue development including neurogenesis, segmentation, sex determination and myogenesis (Paroush, 1994; Jimenez et al., 1997). The WRPW motif has been demonstrated to be a functional transcriptional repression domain. It is sufficient to confer active repression to Hairy-related proteins or a heterologous DNA-binding protein through its ability to recruit Gro/TLE to target gene promoters (Fisher et al., 1996). Similar to Dorsal, in *Drosophila*, the Runx family member Lozenge that contains a WRPW motif exhibit low affinity for Gro/TLE and requires the Cut HD protein to form a stable repressive complex (Canon, 2003).

Gro/TLE Acts as Co-repressor in the Presence and Absence of β-catenin

The Gro/TLE-binding site in the central portion of TCF/LEF extends and overlaps the β-catenin binding site (Daniels and Weis, 2005). Therefore, association of Gro/TLE with TCF/LEF counteracts the TCF/β-catenin transactivation activity (Cavallo et al., 1998; Roose et al., 1998; Brantjes, 2001). Together with other observations, these data lead to the generally accepted

model where β-catenin activates Wnt-responsive genes by simply displacing Gro/TLE. Whereas recent studies provide arguments for a more complex regulation of Wnt-driven transcriptional switch (reviewed in Ramakrishnan et al., 2018), a large spectrum of genes are regulated by both β-catenin and Gro/TLE through their respective interactions with TCF/LEF. Chromatin immunoprecipitation sequencing (ChIP-seq) data from *Xenopus* embryos provide over 80% correlation between β-catenin and Gro/TLE-binding sites (Nakamura et al., 2016). In mouse hair follicle stem cells, more than half the genes occupied by TCF/LEF are also occupied by Gro/TLE (Lien et al., 2014).

The way Gro/TLE mediate transcriptional repression is still a matter of debate. Recent observations indicate that Gro/TLE could act either short distance *via* modulating RNA-polymerase II (RNA-Pol II) activity, and/or long distance *via* chromatin remodeling. ChIP-seq analysis combined to RNA-seq data performed in *Drosophila* identified the Gro/TLE direct targets. Such analysis suggested that Gro/TLE doesn't affect the recruitment of RNA-Pol II to the transcription start sites but further increases RNA-Pol II pausing time (Kaul et al., 2014). Other studies indicate that in some context, Tcf/Gro complex promotes compaction of the chromatin when the canonical Wnt pathway is switched off. As previously mentioned, Gro/TLE interact with Hdac. In the presence of an Hdac-inhibitor, Wnt target genes are de-repressed (Billin et al., 2000). It is therefore possible that Gro/TLE interaction with Hdac drives long distance, transmittable changes in the chromatin state. Other studies argue that Hdac recruitment does not account for full co-repressor activity, suggesting that another Gro/TLE-dependent silencing could occur *via* tetramerization of Gro on a Tcf7l1/Gro complex, thereby promoting structural transitions of chromatin leading to transcriptional repression (Sekiya and Zaret, 2007; Chodaparambil et al., 2014).

The Gro/TLE and TCF/LEF interaction(s) in Early Axis Specification

In *Xenopus* embryos, injection of *gro* represses transcription of Wnt target genes (Roose et al., 1998), and mutations in Gro/TLE-binding sites of *tcf7l1* reduces Tcf7l1 repressive activity (Liu et al., 2005; Tsuji and Hashimoto, 2005). Analysis performed on the *Xenopus siamois (sia)* promoter demonstrated that Tcf/Lef-binding sites mediate both basal repression and β-catenin-dependent activation at the W-CRM (Brannon et al., 1997; Fan et al., 1998). More recently, large-scale analysis demonstrates that in the dorsal blastomeres, Gro/TLE binds to the same W-CRM as β-catenin (Yasuoka et al., 2014; Nakamura and Hoppler, 2017; Afouda et al., 2020). In this context a few lines of evidence indicate that β-catenin activates Wnt-responsive genes by displacing the whole Tcf7l1/Gro repressor complex and replacing it with an activator complex, containing β-catenin in association with Tcf7 (Chambers et al., 2017) (reviewed in Cinnamon et al., 2008; Sokol, 2011; Ramakrishnan et al., 2018)

In conclusion, the mechanisms by which Gro/TLE mediate transcriptional repression in the presence and/or absence of TCF/LEF are still not fully understood. To add complexity, both TCF/LEF and Gro/TLE proteins are targets for developmental signals, which influence the affinity of Gro/TLE to TCF/LEF and/or W-CRM. Thereby, the developmental and cellular contexts in which Gro/TLE repression causes epigenetic regulations *via* the binding of HDAC by Gro/TLE as well as the exact role(s) of such transcriptomic regulations during development are still poorly understood.

TCF/LEF AND BARHL2 IN THE DEVELOPMENTAL DYNAMICS OF SPEMANN ORGANIZER (SO)

Both Tcf/Lef Repressor and Activator Functions Are Required for Normal SO Development

One of the earliest, well-documented, and evolutionarily conserved functions of Wnt/β-catenin signaling is the induction of the blastopore lip organizer. The discovery made by Spemann and Mangold in 1924 has revolutionized our understanding of embryonic axis formation. In their classic transplantation experiment in newt, the authors showed that a mesodermal region - the dorsal lip of the blastopore - of a gastrula embryo induces a secondary axis including a complete nervous system when grafted ventrally (reviewed in De Robertis et al., 2000). This primary embryonic organizing center known as SO determines the dorso-ventral (DV) body axis. Requirement of canonical Wnt signaling for axis formation has been demonstrated following overexpression of Wnt signaling components. For instance, in *Xenopus, wnt1* (McMahon and Moon, 1989), *wnt8* (Sokol et al., 1991), and *β-catenin* (McCrea et al., 1993) can induce a complete dorsal axis when overexpressed ventrally. A similar phenotype has been observed when two Wnt inhibitors are depleted: Tcf7l1 (Merrill et al., 2004) and Axin2 (Zeng et al., 1997). More recently, it was shown in non-bilaterian metazoan species that the same molecular mechanism was used for inducing secondary axes as in chordates: the Wnt/β-catenin signaling, indeed demonstrating that the emergence of the Wnt/β-catenin driven blastopore-associated axial organizer predates the cnidarian-bilaterian split, which occurred over 600 million years ago (Kraus et al., 2016).

Investigations from the past decades lead to the current model of SO development. Before initiation of zygotic transcription, Tcf7l1 represses gene transcription throughout the embryo (**Figure 3**) (Molenaar et al., 1996; Houston et al., 2002). Accumulation and stabilization of β-catenin by maternal determinants in the nucleus of the dorsal cells, inhibit Tcf7l1 repressors' activity (Schneider et al., 1996; Larabell et al., 1997), and activate the transcription of *sia* and *siamois homologue 2 (twin)* (Lemaire et al., 1995; Carnac et al., 1996), which in turn activate the transcription of 123 genes, including *goosecoid (gsc)* and *chordin (chd)*, leading to the formation of the SO territory. All genes de-repressed by β-catenin in this region have been identified (Ding et al., 2017b). *sia* and *twin* are directly regulated by binding Tcf/Lef to their promoters, and poised

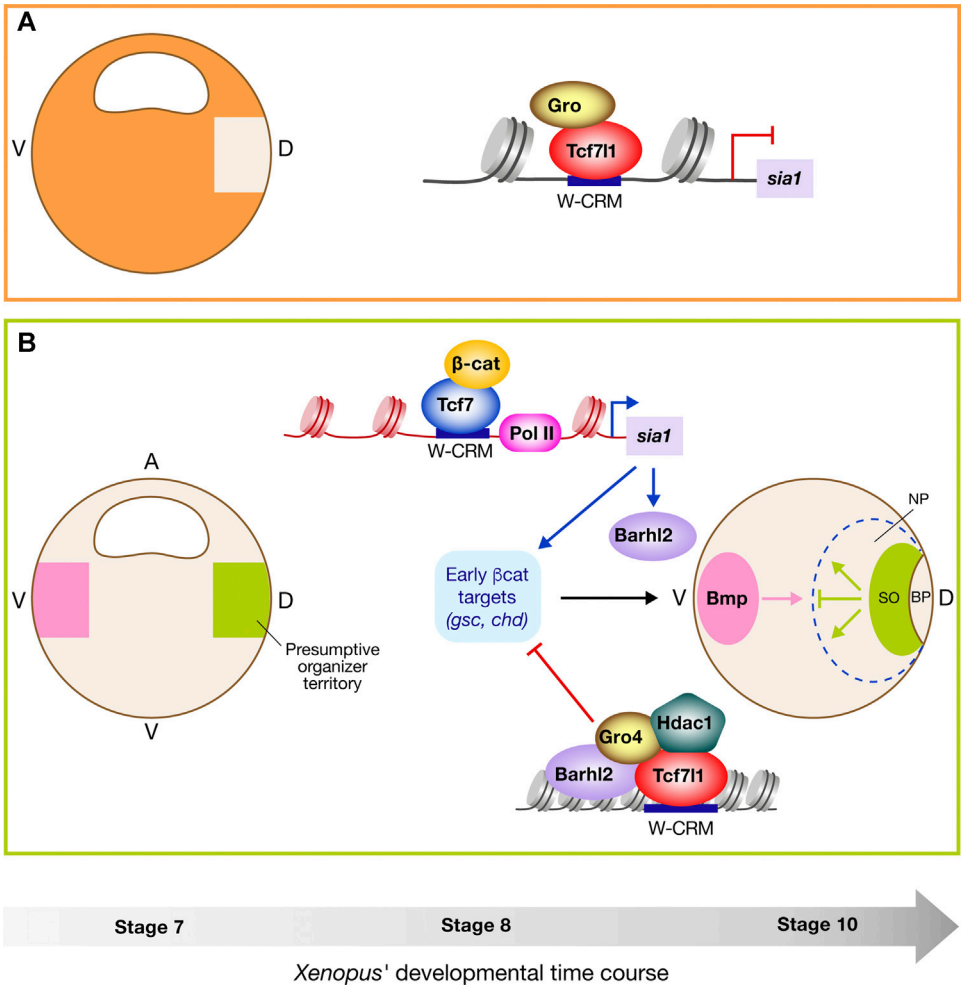

FIGURE 3 | Barhl2 switches off early β-catenin response during establishment of Spemann organizer in Xenopus. **(A)** Maternally encoded Tcf7l1 represses Wnt target genes' transcription (e.g., *siamois-1 (sia1)*) throughout the entire embryo except dorsally in the presumptive organizer territory starting at stage 7. **(B)** Dorsally (green area), nuclear β-catenin (β-cat) level locally increases allowing its interaction with T-Cell Factor (probably mostly Tcf7 and Tcf7l2), and the initiation of *sia1* transcription. Between stage 8 and 9, Sia1, together with β-cat, induce expression of the dorsal early β-cat target signature including *goosecoid* (*gsc*) and *chordin* (*chd*) leading to the formation of Spemann organizer (SO). Evidence argues that around the same time, *sia1* induces *barhl2* transcription. Barhl2 being a part of a repressive complex together with Groucho-4 (Gro4), Tcf7l1, and Histone deacetylase-1 (Hdac1), switches off the early β-cat dorsal signature *via* an inherited epigenetic regulatory mode thereby limiting SO establishment in time and/or space. SO gives rise to the prechordal plate and the notochord, two tissues that send planar and vertical signals to the overlying prospective neuroepithelium. At stage 10, signals secreted by the SO, including Bone Morphogenetic Protein (Bmp) inhibitors and Wnt signals, enable initiation of the dorsal developmental program: The first blastopore lip cells invaginating into the embryo will give rise to the prechordal plate, followed by the cells that will generate the notochord. Together, the prechordal plate, and the notochord, will send planar and vertical signals that both induce and pattern the overlying neuroepithelium and thereby constitute a secondary organizer (the axial organizer). The prechordal plate plays a major role in inducing and patterning of the anterior neural plate, generating the forebrain and midbrain. The notochord participates in formation of the Sonic hedgehog (Shh)-secreting floor plate and induces and patterns the posterior neural plate (reviewed in Stern, 2002; Wessely and De Robertis, 2002; Niehrs, 2004; Wilson and Houart, 2004; Hoch et al., 2009; Ozair et al., 2013; Brafman and Willert, 2017). V, ventral; D, dorsal; BP, blastopore; NP, neuroepithelium; A, Animal pole; V, Vegetal pole.

for transcriptional activation by β-catenin before the Mid blastula transition (MBT) (Brannon et al., 1997; Laurent et al., 1997; Fan et al., 1998; Blythe et al., 2010). In the absence of β-catenin, Tcf7l1, together with Gro/Tle, inhibit *sia* and *twin* transcription (Roose et al., 1998). More recently, a thorough transcriptomic analysis, combined with genome-wide β-catenin association using ChIP-seq, identified stage-specific direct Wnt target genes. The direct comparison of genome-wide occupancy of β-catenin with a stage-matched Wnt-regulated transcriptome reveals that only a subset of β-catenin-bound genomic loci are transcriptionally regulated by Wnt signaling. The differences in classes of direct Wnt target genes appear to be context specific, and dependent on the presence of co-factors such as FoxH1, Nodal/TGFβ signaling (Afouda et al., 2020), Bone Morphogenetic Protein (BMP), and FGF signaling (Nakamura et al., 2016). These studies reveal that the cellular transcriptional responses to Wnt signal are highly dependent on the context, and thereby on the tissue, the developmental steps, the presence of co-factors and/or activation of co-signaling pathways (reviewed in Nakamura and Hoppler, 2017).

The Evolutionary Conserved BARHL Proteins Interact Independently With Both Gro/TLE and TCF/LEF

The Bar-class HD, BarH1 and BarH2, are HD-containing transcription factors initially discovered in *Drosophila* (Kojima et al., 1991; Higashijima et al., 1992). *Barhl* genes have subsequently been identified in fish (zebrafish, medaka), amphibian (*Xenopus*), birds (chicken), mammals (mouse, human), nematode (*C. elegans*) and *S. kowalevskii* among others (Lowe et al., 2003; Pani et al., 2012; Yao et al., 2016). Phylogenetic analysis shows that BARHL1 and BARHL2 proteins are extremely well conserved in the chordate phylum and are predominantly expressed in the central nervous system (CNS), where their expression patterns are distinct but partially overlapping (**Figure 4**) (Bulfone, 2000; Patterson et al., 2000; Offner et al., 2005; Colombo et al., 2006) (reviewed in Schuhmacher et al., 2011). BARHL1 and BARHL2 are involved in diverse processes such as the acquisition of a neural identity in the retina, specification of commissural neurons in the spinal cord and cell migration in the cerebellum and the hindbrain (Chellappa et al., 2008; Ding et al., 2009; Jusuf et al., 2012) (reviewed in Reig et al., 2007).

BARHL proteins are characterized by a conserved HD sequence of about 60 amino acids, which forms a three-dimensional helix-loop-helix structure required for their fixation to DNA (**Figures 4A,B**) (Gehring et al., 1994). Unlike other homeoproteins, BARHLs contain a tyrosine (Y) at site 49 as opposed to phenylalanine (F) at this site of the HD. Whilst the biological significance behind this substitution is unknown; it is thought that there could be a difference in the specificity of the DNA recognition motif. BARHL sequence also contains an NLS, and at their amino-terminal region, two EH1 domains. Sequence comparison reveals a conserved domain with an unknown function at the C-terminal part of BARHL proteins.

Biochemical experiments performed in both mammalian cells and *Xenopus* embryo validate the physical interaction between BARHL2 and Gro/TLE. Surprisingly, BARHL2 was found to interact with TCF/LEF, more specifically TCF7l1, and dramatically enhance the ability of TCF7l1 to co-immunoprecipitate Gro4/TLE4, at least in mammalian cells. This interaction is independent of TCF7L1 binding to Gro/TLE. Functional observations confirm that Barhl2 enhances the capacity of to repress transcription, and abolishes the β-catenin-driven activation of TCF/LEF target genes (**Figure 1C**) (Sena et al., 2019).

Barhl2 Normally Limits SO Formation Through Enhancing the Ability of Tcf to Repress Transcription

In *Xenopus, barhl2* is not expressed maternally. Whereas W-CRM have been identified in the *barhl2* loci (Nakamura et al., 2016), *barhl2* is neither part of the early dorsal β-catenin signature, nor induced by overexpression of RNA coding for *wnt8b*. It is however expressed following the initiation of early β-catenin induction, and its expression increases following *sia1* mRNA overexpression (Owens et al., 2016; Session et al., 2016; Ding et al., 2017b; Sena et al., 2019), suggesting that at these developmental stages, *barhl2* transcription is under the control of both *sia1* and β-catenin (**Figure 3**).

In *Xenopus*, overexpression of *barhl2* generates massive developmental defects including loss of the SO territory and all anterior structures, including the cement gland and the head. In contrast, Barhl2 depletion expands both the organizer territory and its signaling activity, as detected through a massive increase in neuroepithelium size, and patterning alterations (Offner et al., 2005; Sena et al., 2019). Experimental evidence demonstrates that these developmental defects are direct consequences of Barhl2 normally enhancing Tcf7l1-mediated transcriptional repression. These observations lead to a model in which stabilization of β-catenin first de-represses Tcf7l1, and then initiates the dorsal developmental program through activating Tcf7 and/or Tcf7l1. The presence of Barhl2 locks Tcf7l1 and/or Tcf7 in an inhibitory state, and consequently limits induction of the dorsal development program. In this way Barhl2 participates in progression of the blastula development, and normally limits SO formation in time and/or in space.

Analysis of Barhl2 proteins that are mutated either in their ability to interact with DNA, or to bind Gro/TLE, indicate that its normal role requires both. As previously stated, Gro/TLE can silence target genes by tetramerizing on a Tcf7l1-Gro complex (Chen et al., 1999; Chodaparambil et al., 2014). It is therefore possible that Barhl2 enhances the binding of the complex to histones, associated with the long-term silencing of Tcf/Lef target genes through increasing Gro/TLE stoichiometry in a protein complex containing Tcf7l1. Moreover, the presence of Hdac1 is detected in a protein complex containing Barhl2, Tcf7l1 and Gro4. Hdac1 depletion promotes SO development. In parallel, Barhl2 depletion promotes key organizer genes' acetylation. Thereby, Hdac1 activity could contribute to the Barhl2-mediated repression of Wnt target genes. ChIP-qPCR observations on the promoter of *gsc* indicate that both Barhl2 and Tcf7l1 can interact with the same Tcf-W-CRM in the absence of an adjacent Barhl2-W-CRM.

Overall, these observations are consistent with Barhl2 acting over long distance *via* its specific binding on DNA, perhaps on super-enhancers as previously suggested (Lin et al., 2016), and inducing long-term silencing of SO target genes maybe *via* Hdac1 activity and/or direct interaction with chromatin. In this way Barhl2 irreversibly locks cells in a SO identity.

IN THE DIENCEPHALIC PRIMORDIUM, BARHL2 LIMITS WNT/TCF ACTIVITY

Patterning and Growth of the Diencephalic Territory Requires High Levels of Wnt Signals and the Presence of the Morphogen Sonic HedgeHog (Shh)

The forebrain (telencephalon and diencephalon) is derived from the most anterior part of the neuroepithelium: the

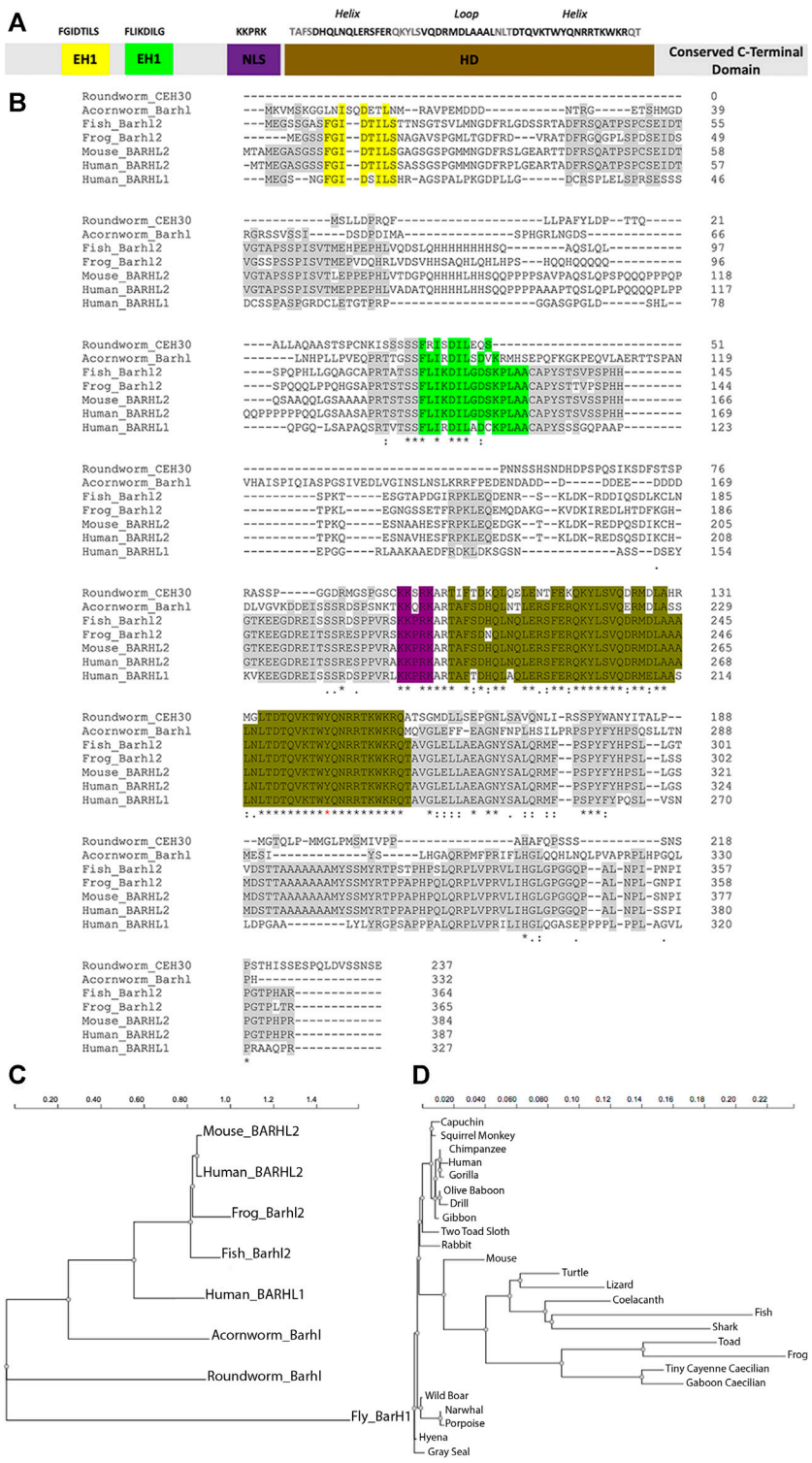

FIGURE 4 | BARHL proteins are highly conserved through evolution. **(A)** Scheme of BARHL1 and BARHL2 proteins. Both proteins share high similarities in their aa sequences. The most conserved regions are the two Engrailed Homology (EH1) domains shown in yellow and green, the homeodomain (HD) shown in brown, the Nuclear Localisation Signal (NLS) shown in violet, and a functionally uncharacterized C-terminal region. **(B)** Multiple sequence alignment of BARHL proteins. Shown is a representative selection of some BARHL2 protein sequences in vertebrate including frog *Xenopus laevis* (NP_001082021.1), fish *Danio rerio* (NP_991303.1), mouse *Mus musculus* (NP_001005477.1) and human *Homo sapiens* (NP_064447.1) among several other vertebrate sharing the same amino acid (aa) sequences, together with the human BARHL1 protein sequence (NP_064448.1), in addition to the invertebrate roundworm *Caenorhabditis elegans* Bar homeodomain CEH-30 (NP_508524.2) and hemichordate acornworm *Saccoglossus Kowalevskii* Barhl (NP_001158386.1). Mouse MBH1 (mammalian BarH1) is referred to as BARHL2.

(*Continued*)

FIGURE 4 | Alignments are generated by ClustalW. Identical aa within the conserved regions are highlighted. EH1 domains (yellow and green) are highly conserved in vertebrate. However, only the second EH1 domain (green) is found in roundworm and acornworm. The most conserved region between vertebrate and invertebrate is the HD (brown), preceded by a NLS (purple). Other conserved aa, specifically those located on the C terminus, haven't been functionally characterized and are depicted in grey. The HD of BARHL proteins contains a tyrosine (Y) at site 49 (red asterisk), as opposed to phenylalanine (F49) in other homeoproteins. Below the protein sequences is a key denoting conserved sequence (*), conservative mutations (:), and semi-conservative mutations (.). Phylogenetic trees showing evolutionary distance between **(C)** the BARHL protein sequences in invertebrate and vertebrate, and **(D)** a larger selection of vertebrate BARHL2 protein sequences. The Trees were constructed by NGPhylogeny.fr (Lemoine et al., 2019) using FastME2.0 program which provides distance algorithms to infer phylogenies based on the balanced minimum evolution approach. The trees are drawn to scale, which represents the number of differences between sequences through evolution. *Drosophila melanogaster* (NP_001259642.1) shows several divergent regions: fly BarH1 (mammalian BARHL2) protein carries the first EH1 domain and HD but has several additional aa found on the N-terminal and C-terminal parts. BARHL2 protein sequence is similar in all higher vertebrate (less than 2% difference).

prosencephalic neural plate. Fate mapping analysis revealed that the telencephalon emerges from the most anterior part of the neural plate, whereas the diencephalon is formed within the caudal forebrain.Whereas inhibition of Wnt pathway is strictly necessary for telencephalic development (Glinka et al., 1998) (reviewed in Wilson and Houart, 2004), growth and patterning of the diencephalic territories (thalamus and epithalamus) require high levels of Wnt. While the *Wnt1* or *Wnt3A* KO mice lose both the midbrain and hippocampal areas, double *Wnt3A/Wnt1* mutant embryos exhibit an additional reduction in the diencephalon, caudal hindbrain, and rostral spinal cord (Thomas and Capecchi, 1990; Lee et al., 2000). Conversely, ectopic expression of *Wnt1* or *Wnt3A* induces the enlargement of the neural tube along the DV axis, without altering the cellular identities of diencephalic neurons (Megason and McMahon, 2002; Panhuysen et al., 2004). Zebrafish *masterblind (mbl)*-mutant embryos carrying a mutation in the GSK3-binding domain of Axin1, which constitutively activates Wnt signaling, show a net reduction in the telencephalic and retinal territories in favor of the diencephalic territory (Heisenberg, 2001). Indeed, the diencephalic primordium, more specifically the diencephalic alar and roof plates, express Wnt ligands such as *Wnt3*, *Wnt3A*, *Wnt8B*, *Wnt4* and *Wnt2B* (Colombo et al., 2006; Juraver-Geslin et al., 2011, 2014; Schuhmacher et al., 2011). Wnt target genes' expression as well as the Wnt signaling machinery are enriched in the thalamus of all vertebrate analyzed so far (Jones and Rubenstein, 2004; Shimogori et al., 2004; Quinlan et al., 2009; Mattes et al., 2012).

Besides its role in fate determination, Wnt promotes cell-cycle progression, and cell growth. Its ability to modulate the activity of GSK3β promotes a general increase in protein stability, specifically that of β-catenin (Taelman et al., 2010), and through activation of Target of Rapamycin (TOR) pathway, it stimulates growth and protein synthesis. β-catenin nuclear accumulation induces TCF/LEF-mediated expression of the proto-oncogene *c-Myc* (He et al., 1998), which encodes a bHLH leucine zipper (bHLHZip) TF that has two distinct roles in the G1 progression. On one hand, it increases the expression of *CyclinD1* and *CyclinD2* that promotes progression from the G1 to the S phase; on the other, it represses the cell cycle inhibitors *p27Kip1* and *p21Cip1*, thereby promoting cell cycle progression, and enhancing cell proliferation (reviewed in Juraver-Geslin and Durand, 2015).

The Sonic hedgehog (Shh)-secreting Mid-Diencephalic Organizer (MDO), also known as the *Zona Limitans Intrathalamica* (*zli*), develops within the diencephalic primordium (Larsen et al., 2001). Within the thalamic complex, Shh secreted by *zli* cells participates in the survival, growth, and patterning of neuronal progenitor subpopulations (Hashimoto-Torii et al., 2003; Scholpp et al., 2006, 2007; Vieira and Martinez, 2006). Mice lacking *Shh* show severe defects in most of the diencephalic territory (Chiang et al., 1996; Ishibashi and McMahon, 2002). Investigation of the chick neural tube growth revealed an epistatic relationship between Shh and Wnt in progression of the G1 cell cycle phase: Shh permits transcriptional activation of *Tcf7l1* and *Tcf7l2*, which then induces β-catenin dependent expression of *Cyclin-D1* (Alvarez-Medina et al., 2008). Phenotypic observations of *Shh* mutated mice suggest a conservation of these interactions in the diencephalon. Such mice develop a reduced diencephalon with decreased *Tcf7l2* expression (Ishibashi and McMahon, 2002).

In the Diencephalon, Barhl2 Acts as a Brake on Progenitors' Proliferation by Limiting Wnt Activity

Shh and Wnt synergistically promote proliferation in the alar diencephalon, whereas cell-cycle analysis in chicken and mice reported slow proliferation kinetics in the diencephalon compared to its neighboring territories (reviewed in Martínez and Puelles, 2000). Moreover, diencephalic changing patterns observed upon manipulation of Wnt activity appear to be primarily due to altered fate specification rather than changes in proliferation (reviewed in Wilson and Houart, 2004). *barhl2* transcripts are detected in the diencephalic histogenic field at late gastrula/early neurula stages in *Xenopus* (Offner et al., 2005; Juraver-Geslin et al., 2011), zebrafish (Staudt and Houart, 2007), and mice (Mo et al., 2004). In the diencephalic anlage, Barhl2 acts upstream of Shh in establishment of the *zli* and its absence generates massive defects specifically in the patterning of the alar diencephalon (Juraver-Geslin et al., 2014; Yao et al., 2016; Ding et al., 2017a) (reviewed in Sena et al., 2016). Besides its role in *zli* formation, Barhl2 normally limits diencephalic progenitors' proliferation: Barhl2-depleted *Xenopus* embryos exhibit both a dramatic hyperplasia, and a neuroepithelial architectural disorganization in the caudal forebrain (Juraver-Geslin et al., 2011, 2014). In depth analysis of Barhl2-depleted embryos revealed an excessive Wnt

transcriptional activation that stimulates neuroepithelial cell proliferation and induces defects in β-catenin intracellular localization together with an upregulation of *axin2* and *cyclinD1*. Measurement of the relative velocity of the cell cycle in Barhl2-depleted embryos reveals a shortening of the cell cycle length (6 versus 8 h). As the length of the S-phase in these cells remains unchanged (1.5 h), and CyclinD1 is part of the G1-S cell cycle checkpoint, Barhl2 probably acts on the length of G1 phase (Juraver-Geslin et al., 2011).

Interestingly, in the developing diencephalon, a non-apoptotic function of the effector caspase, Caspase-3, limits neuroepithelial cell proliferation by inhibiting the activation of Tcf/Lef by the β-catenin (Juraver-Geslin et al., 2011). In this context, Caspase-3 acts either in parallel, or downstream of Barhl2, and its activity does not depend on its apoptosis-effector function. In addition, in the neuroepithelium, Caspase-7 acts as the executioner Caspase leading to cell death (Sena et al., 2020). Indeed, how Barhl2 regulates Caspase-3 non-apoptotic activity in *Xenopus* and limits β-catenin levels and stability in the developing diencephalon is unknown.

In conclusion, in the caudal forebrain, Barhl2 acts as a brake on Wnt transcriptional activation, probably through the stabilization of the inhibitory Tcf/Gro complex. Barhl2 could increase the length of diencephalic progenitors' G1 phase, thereby modulating neuronal progenitors' response to extracellular signals, including those of Wnt and Shh.

Wnt Signals Influence Diencephalic *Barhl2* Expression

What are the extracellular signals influencing *Barhl2* expression and activity in the caudal forebrain? *Wnt3a* is expressed in E9.5 mice (Louvi et al., 2007) at the onset of *Barhl2* expression in the same territories. Pioneer studies performed in *Drosophila* presented the wg pathway as a positive regulator of *barhl2* expression in the notum. *barhl2* expression was lost in clones mutated for Arm (reviewed in Reig et al., 2007). Conversely, the expression of a constitutively active form of *arm* induces an ectopic expression of *barhl2* in the pre-scrutum, associated with a decrease of wg (Sato et al., 1999). In *Xenopus,* RNA-sequencing analysis revealed that both morpholino-mediated depletion of Tcf7l1, and pharmacological activation of Wnt canonical signaling, induce an increase in *barhl2* transcripts (Wills and Baker, 2015; Stevens et al., 2017).

Taken together, these observations suggest a model where Barhl2 could be a direct, or an indirect, target of the canonical Wnt signaling pathway. In return, Barhl2 would establish a negative feedback loop that limits Wnt' activity.

OTHER REGULATORS OF TCF/LEF-Gro/TLE TRANSCRIPTIONAL ACTIVITY

Transcription Factors Binding to Tcf7l1 Influence Its Repressor Activity in a Positive And/Or Negative Way

Beside Barhl2, other co-repressors influence Tcf7l1 inhibitory activity. Indeed, cDNA expression screens performed in mammalian cells, combined with functional analysis in *Xenopus*, identified 45 inducers and 96 inhibitors of Tcf/Lef activity (Freeman et al., 2015). Co-repressors' modes of action are diverse, sometimes divergent between vertebrate and invertebrate, and involve protein–protein interactions, changes in Tcf7l1 affinity for Wnt-target gene promoters, recruitment of co-repressors or co-activators, modulation of protein stability, and nuclear translocation.

CtBP, first described in *Xenopus* and later in rodents and human, binds to the C-terminal part of Tcf7l1-E and Tcf7l2-E isoforms. In fly, CtBP appears to be required for both activation of some Wnt targets and the repression of others, in parallel to, and independently of Tcf/Lef (Fang et al., 2006). However, the vertebrate CtBP acts as a co-factor for Tcf7l1, enhancing its repressor activity (Brannon et al., 1999; Xia et al., 2011). Lack of both Gro/TLE-binding domain and of the C-terminal region of Tcf7l1 leads to target genes' transcriptional activation (Gradl et al., 2002). Notably, during *Xenopus* SO formation, the C-terminal part of Tcf7l1, which recruits the CtBP, is not required (Liu et al., 2005). In colorectal cancer cells, TCF7l1 recruits both CtBP and HDAC1 to repress expression of the Wnt antagonist DICKKOPF4 (DKK4) (Valenta et al., 2003; Eshelman et al., 2017). Besides CtBP, Tcf7l1 directly interacts with the methyl-CpG-dependent transcriptional repressor Kaiso in *Xenopus*. This interaction results in their mutual disengagement from the respective DNA-binding sites in such a way that Tcf7l1 can be inhibited following Kaiso overexpression both in cell lines, and *Xenopus* embryos (Daniel and Reynolds, 1999). Kaiso cooperates with Tcf7l1 to repress β-catenin target genes such as *sia*, through epigenetic regulation (Park et al., 2005). The interaction of Kaiso with Tcf7l1 depends on Kaiso zinc-finger domains, and on the HMG-box DNA-binding domain of Tcf/Lef factors (Ruzov et al., 2009). The LIM (Lin-11, Islet-1, and Mec-3; the three original members of the family) protein HIC-5 [Hydrogen Peroxide-Induced Clone 5, also termed ARA-55 (Androgen Receptor Activator of 55 kDa)] has been also identified as a binding partner to Tcf7l1 and Tcf7l2. Overexpression of HIC-5 acts as a negative regulator of a subset of Tcf/Lef family members, and can suppress secondary axis formation in *Xenopus* (Ghogomu et al., 2006). Important modulators of TCF/LEF activity are also found in the family of SOX (SRY-related HMG box) factors containing over 20 members (reviewed in Kormish et al., 2009; Bernard and Harley, 2010). In both mammalian cells and *Xenopus*, SOX17 and SOX4 directly bind to the HMG-box of TCF7l1, TCF7l2 and LEF1, an interaction that modulates the stability of the TCF/β-catenin complex (Sinner et al., 2007). More recently, SOX17 was shown to functionally cooperate with Wnt/β-catenin to specify an endodermal fate while repressing the meso-ectodermal fate. In this context, SOX17 and β-catenin co-occupy hundreds of key enhancers. In some cases, SOX17 and β-catenin synergistically activate transcription, apparently independently of TCF/LEF, whereas on other enhancers, SOX17 represses β-catenin/TCF-mediated transcription to

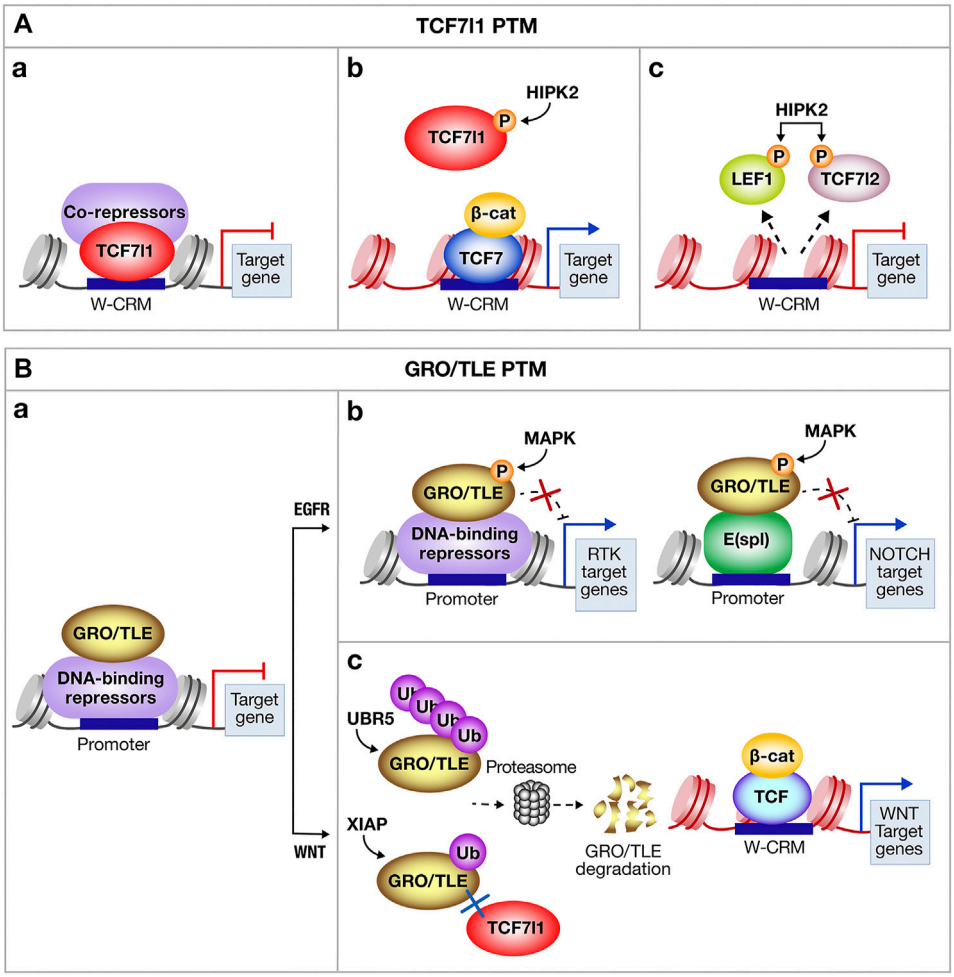

FIGURE 5 | Some Post-Translational Modifications modulating the transcriptional activities of TCF7l1 and Gro/TLE. Post-translational modifications (PTM) including phosphorylation and/or ubiquitination of **(A)** T-cell factor-like-1 (TCF7l1) and **(B)** Groucho/Transducin-like enhancer of split (Gro/TLE) influence positively, or negatively, the transcriptional output of TCF7l1/Gro complex. **(A) (a)** TCF7l1 bound on W-CRM with co-repressors normally limits transcription. **(b)** The Homeodomain-Interacting Protein Kinase-2 (HIPK2) acts as a positive or negative regulator of Wnt target genes' expression. Phosphorylation of TCF7l1 by HIPK2 decreases TCF7l1 affinity to target genes' promoter and enables transcription through the β-catenin/T-Cell Factor-7 (β-cat/TCF7) complex. **(c)** Conversely, phosphorylation of the transcriptional activators Lymphoid Enhancer Factor-1 (LEF1) and TCF7l2 abolishes their binding to the promoter and blocks gene transcription. **(B) (a)** Gro/TLE together with DNA binding Co-repressor normally limits RNA Pol II mediated transcription. **(b)** The Receptor Tyrosine Kinase (RTK) phosphorylates Gro/TLE through the Mitogen-Activated Protein Kinase (MAPK) pathway, resulting in a decrease of Gro/TLE repressive activity. Gro/TLE mediates crosstalk between Notch and MAPK signaling pathways. Notch signaling activation leads to the expression of the Enhancer of split E(spl), which is a major transcriptional repressor of Notch target genes. E(spl) complexes with Gro/TLE to block target genes' expression, including proneural genes. Phosphorylation of Gro/TLE by the MAPK pathway inhibits its function as a repressor. **(c)** When Wnt signaling is activated, the E3 ubiquitin ligase (UBR5) polyubiquitinates Gro/TLE in flies. Similarly, in vertebrate, the X-linked Inhibitor of Apoptosis (XIAP) is recruited to the transcriptional complex containing TCF7l1 and Gro/TLE, and monoubiquitinates Gro/TLE. Mono/polyubiquitination of Gro/TLE enables its degradation by the proteasome and blocks its re-association to TCF7l1, allowing the recruitment of the transcriptional co-activator β-cat to the activating TCF/LEF, and further expression of Wnt target genes. W-CRM, Wnt-Cis regulatory motif; EGFR, Epidermal Growth Factor Receptor.

spatially restrict gene expression domains. In this context, SOX17 acts as a tissue-specific modifier of the TCF/LEF responses (Mukherjee et al., 2021). Another modulator of the canonical Wnt signaling is SOX9, which was found to associate with β-catenin and further inhibit its activity (Topol et al., 2009). Further observations show that SOX9 proteins, together with Krüppel-like factor 4 (KLF4), suppress the Wnt-induced transcription through competing with TCF/LEF for the same β-catenin promoter sites, inhibiting the β-catenin-TCF/LEF (more specifically TCF7l2) binding and transcriptional activity (Sellak et al., 2012).

Post-Translational Modifications Influence Both TCF/LEF and Gro/TLE Interactions

Besides the spatial and temporal distribution of repressor partners, PTM, including ubiquitination and/or phosphorylation of TCF/LEF and Gro/TLE, influence

positively or negatively, Gro/TLE-TCF/LEF interactions (reviewed in Cinnamon et al., 2008; Turki-Judeh and Courey, 2012; Ramakrishnan et al., 2018). In gastrulating *Xenopus* embryos and in mammalian cells, phosphorylation of TCF7l1 by the Homeodomain Interacting Protein Kinase 2 (HIPK2) inhibits its capacity to bind its target genes (**Figure 5A**). β-catenin was found to serve as a scaffold that promotes HIPK2 interaction with TCF7l1 and the subsequent dissociation of TCF7l1 from the target gene promoter, thereby opening the way for β-catenin interaction with the non-phosphorylated TCF7, and activation of Wnt target genes' transcription (**Figure 5Ab**). Mutated TCF7l1 proteins resistant to Wnt-dependent phosphorylation function as constitutive inhibitors. HIPK2-dependent phosphorylation also causes the dissociation of LEF1 and TCF7l2 from their targets' promoter (**Figure 5Ac**) and its effect is thereby highly context specific: HIPK2 up-regulates transcription by phosphorylating TCF7l1, a transcriptional repressor, but inhibits transcription by phosphorylating LEF1, a transcriptional activator (Hikasa et al., 2010; Hikasa and Sokol, 2011). Alternatively, in mouse embryonic stem cells (mESCs), β-catenin inactivates TCF7l1 by removing it from DNA, which is followed by TCF7l1 protein degradation. Interestingly, in this context, genetic cues indicate that TCF7l1 inactivation appears to be the only required effect of the TCF7l1/β-catenin interaction (Shy et al., 2013).

Gro/TLE co-repressors are targets of PTM, which modulate their affinity not only for Wnt effectors, but also Notch, and Epidermal Growth Factor Receptor (EGFR) signaling cascades (**Figure 5B**). One example comes from studies in *Drosophila* demonstrating that EGFR signaling, mediated *via* the Mitogen-Activated Protein Kinase (MAPK), phosphorylates Gro/TLE, and leads to the weakening of its repressor function, and attenuation of Gro/TLE-dependent transcriptional silencing by the E(spl) proteins, which are the effectors of the Notch cascade (**Figure 5Bb**). Reversibly, when RAS/MAPK signaling is impeded, Gro/TLE-mediated repression is enhanced both *in vitro* and *in vivo*. Thus, downregulation of Gro/TLE-dependent repression by MAPK modulates the transcriptional output of the Notch pathway, and possibly of other pathways (reviewed in Cinnamon et al., 2008). In both *Drosophila* and human cell lines, the E3 ubiquitin ligase UBR5 is required for Wnt cellular response. In this context, Wnt signaling induces the ubiquitination of Gro/TLE by UBR5, which happens downstream of β-catenin stabilization (**Figure 5Bc**). *In vivo* observations argue that ubiquitination inactivates Gro/TLE, thereby enabling Arm/β-catenin to activate transcription (Flack et al., 2017). Interestingly, inactivation of Gro3/TLE3 occurs *via* the activity of AAA ATPase Valosin-containing protein (VCP, also known as p97). VCP unfolds ubiquitinated proteins *via* its ATPase activity and disrupts ubiquitinated Gro3/TLE3 tetramerization, a process required for Gro/TLE to repress Wnt targets (Chodaparambil et al., 2014). Moreover mono-ubiquitination of Gro3/TLE3 by the E3 ubiquitin ligase XIAP (X-linked Inhibitor of Apoptosis) at its N-terminal Q-rich domain disrupts the ability of Gro3/TLE3 to bind TCF7l1, and consequently inhibits TCF7l1 repressor activity. XIAP is recruited to the Gro/TCF complex upon Wnt pathway activation, which enhances β-catenin/TCF complex assembly and the initiation of a Wnt-specific transcriptional activation program (Hanson et al., 2012). Because UBR5 and XIAP ubiquitinate Gro3/TLE3 in distinct ways (poly vs. mono) and at different locations on the Gro3/TLE3 protein, it is possible that the two E3 ligases modulate the Wnt transcriptional switch either in parallel, or simultaneously, depending on the cellular context. In addition to its ubiquitination activity, XIAP has been shown to play a role in inhibiting Caspases. In vertebrate, XIAP directly binds to and functionally blocks Caspase-3, Caspase-7 and Caspase-9 proteolytic activity (reviewed in Liston et al., 2003). However, there is no evidence for the XIAP-mediated degradation of vertebrate Caspases *in vivo*, which appears to depend on the type of ubiquitination and on the cell type.

Evolutionary Conservation of BARHL Protein's Structure and Functions

As previously described, BARHL1 and BARHL2 proteins have a strong degree of homology between one another. BARHL2 is highly conserved amongst distant species in the evolutionary scale, as observed through the high aa sequence conservation throughout its entire sequence (**Figure 4**). Besides, they are amongst the TFs essential for patterning the body axis of the developing embryo that are conserved in simpler organisms beyond the phylum of chordates. For example, genetic programs ancestral to the ones required for vertebrate development were found conserved in hemichordates. In *S. kowalevskii*, which is thought to be the closest species to the common ancestor at the base of the phylogenetic tree of chordates, *Barhl2* ortholog gene shares close similarities in its distribution and expression patterns compared to chordates (reviewed in Röttinger and Lowe, 2012; Sena et al., 2016). A conserved Shh Brain Enhancer (SBE1) has been discovered in mice with an equivalent function to that described in the *S. kowalevskii*. SBE1 directly regulates *Shh* expression in the *zli* through binding the second intron of the *Shh* gene. Diverse transcription factors, including Otx2 and Barhl2, directly regulate SBE1 within the *zli*. Functional analysis in both species demonstrated sufficient conservation between *Barhl2* and one of the *S. kowalevskii barH* HD for both binding, and activating CRM, thereby controlling *Shh* expression (Yao et al., 2016) (reviewed in Sena et al., 2016).

In *C. elegans*, the cephalic chemosensory neurons (CEM) undergo PCD during hermaphrodite embryogenesis but not in males (Sulston et al., 1983), a process relying on CEH30, a Bar-HD transcription factor (Schwartz and Horvitz, 2007). CEH30 protein interacts with UNC-37, which is the *C. elegans* homologue of Gro/TLE, through its N-terminal EH1 motif. It thereby prevents cell death (Peden et al., 2007) and inhibits transcription of *egl-1* gene, which encodes the executioner cell death protein CED-3, one of the major components of the PCD in worm (Nehme et al., 2010). Sequence comparison between human BARHL2 and CEH-30 proteins reveals 64% identical amino acids in the region including the HD and the motif immediately next to the HD on the C-terminal side called the BARC motif (Bar homeodomain C-terminal motif) (**Figure 4**). Interestingly, murine *Barhl1* or *Barhl2* genes compensate for the loss of function of CEH-30 in *C. elegans* (Schwartz and Horvitz, 2007), which is consistent with a conservation of *Barhl* genes' function through evolution.

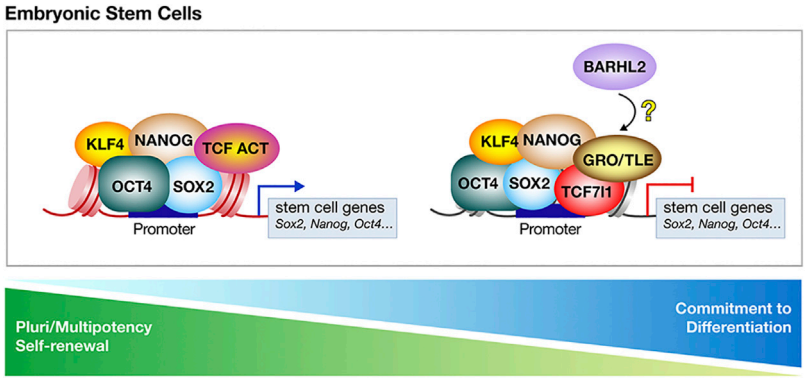

FIGURE 6 | TCF7l1-mediated repression is at play in committed mouse embryonic stem cells (mESCs). In mESCs, the T-Cell Factor/Lymphoid Enhancer Factor (TCF/LEF) switch from a transcriptional activator to inhibitor, controls the balance between pluripotency and differentiation. Key pluripotency genes Octamer-binding transcription factor-4 (OCT4), SRY-box 2 (SOX2), NANOG and Krüppler-like factor-4 (KLF4) mark the pluripotent state of mESCs and are associated with the co-activators TCF7. In mESCs, TCF7l1 is the most expressed member of the Tcf/Lef family. TCF7l1 associates with regulatory regions that are bound by OCT4, SOX2, NANOG, and KLF4. Through interacting with Groucho/Transducin-like enhancer of split (Gro/TLE), TCF7l1 inhibits the expression of "stem cells" genes and allows mESCs to differentiate. Eliminating TCF7l1 repressive activity on mESCs pluripotency network allows the reacquisition of pluripotency and self-renewal. BARHL2 is expressed in mESCs during their commitment phase and could participate in driving mESCs towards irreversible commitment and differentiation by blocking TCF7l1 in a transcriptional inhibitory state.

THE CORE ROLE OF TCF7L1 AS A TRANSCRIPTIONAL INHIBITOR IN DRIVING EMBRYONIC AND NEURAL STEM CELLS TOWARDS DIFFERENTIATION

In Mouse Embryonic Stem Cells, Inhibition of TCF7l1-Mediated Repression Promotes Self-Renewal and Pluripotency

mESC isolated from the inner cell mass of the blastocyst, the pre-implementation stage mammalian embryo, are characterized by their ability to self-renew and to differentiate into all types of somatic cells, a process referred to as pluripotency (reviewed in Chen et al., 2017). A specific core set of transcription factors including OCT4 (Octamer-binding transcription factor 4), NANOG, SOX2 and KLF4 form regulatory circuitry consisting of autoregulatory and feedforward loops thereby supporting pluripotency and self-renewal of these cells (Boyer et al., 2005). Extracellular signaling including LIF/JAK/STAT3 (Leukemia Inhibitory Factor/Janus Kinase/Signal Transducer and Activator of Transcription) (Williams et al., 1988; Ying et al., 2008), Wnt (Hao et al., 2006; ten Berge et al., 2011), BMP (Ying et al., 2003), and the MAPK/ERK (Yang et al., 2012) cascades, influence mESCs fate decision. Indeed, in mESC, Wnt signaling has been demonstrated to have important, somewhat difficult to interpret, activities (reviewed in Niwa, 2011; Merrill, 2012). From all these studies, a consensus emerges that inhibition of TCF7l1-mediated repression is at the core of mESC self-renewal and pluripotency (**Figure 6**) (Atlasi et al., 2013) (reviewed in Sokol, 2011; Wray and Hartmann, 2012). Reversibly, enhancement of TCF7l1 repressive activity blocks mESC self-renewal, and allows mESCs to differentiate, even in the presence of Wnt signaling (Wray et al., 2011).

In mESCs, TCF7l1 is the most expressed member among the TCF/LEF protein family (Pereira et al., 2006; Salomonis et al., 2010). Whole-genome approaches including RNA-seq and ChIP-seq show that TCF7l1 transcriptionally represses many genes important for maintaining pluripotency, and self-renewal, as well as those involved in lineage commitment, and stem cell differentiation. TCF7l1 associates with the regulatory regions of 1369 genes (Tam et al., 2008). Among those regions, 1173 bind TCF7l1 and OCT4 (Cole et al., 2008) with more than 940 binding TCF7l1, OCT4, SOX2, and NANOG (Boyer et al., 2005; Pereira et al., 2006; Marson et al., 2008). Depletion of TCF7l1 generates mESC' refractory to differentiation (Cole et al., 2008). Moreover, both the Gro/TLE and CtBP interacting domains of TCF7l1 are required for *OCT4* repression (Tam et al., 2008). Finally, *KLF4* gene contains conserved TCF/LEF binding sites, and its expression is downregulated by TCF7l1 (Park et al., 2015). Interestingly, two TCF7l1 isoforms have been discovered, and are expressed equally in mESCs, where they regulate both an overlapping, as well as different sets of target genes. Removal of one of both TCF7l1 isoforms was found sufficient to stimulate self-renewal and delay the differentiation through repression of *NODAL* and *KLF4* (Salomonis et al., 2010). Further analysis revealed that binding of β-catenin to both TCF7l1 and TCF7 contributes to the maintenance of self-renewal and gene expression, at least partly through their recruitment to OCT4-binding sites on ESC chromatin (Yi et al., 2011).

The crucial role of TCF7l1 is reinforced by analysis of mESCs lacking all full-length TCF/LEF. In such cells, re-expression of TCF7l1 makes mESCs capable of differentiating into the three lineages, including neuronal cells (Moreira et al., 2017). In this context, TCF7l1 has been shown to directly interact with OCT4, and compete with SOX2 at some SOX-CRM, a process under the influence of MEK/MAPK (Zhang et al., 2013). Indeed, besides limiting TCF7l1-mediated repression of the pluripotency network, inhibition of the MAPK/ERK pathway participates in

maintenance of pluripotency and self-renewal (reviewed in de Jaime-Soguero et al., 2018). In mESCs, inhibition of MEK suppresses *LEF1* expression, and depletion of LEF1 partially mimics the self-renewal-promoting effect of MEK inhibitors. In the absence of the exogenous factors, cytokines or inhibitors, depletion of both TCF7l1 and LEF1 enables maintenance of undifferentiated mESCs (Ye et al., 2017).

In agreement with all these data, Gro/TLE, more specifically Gro4, is not required for sustaining pluripotency, and suppressing differentiation genes in mESC. Rather, Gro/TLE activity appears necessary for early differentiation where it acts to suppress the pluripotency network, allowing for the initiation of lineage specific gene expression programs. In mESCs, most of the genes occupied by TCF7l1 were found co-occupied by Gro/TLE (Laing et al., 2015). Through interacting with Gro/TLE, TCF7l1 represses *NANOG* (Pereira et al., 2006), and repression of *OCT4* was found to rely on TCF7l1/Gro2 interactions (Tam et al., 2008). Interestingly, the dominant-negative GRG5 is highly expressed in mESC, and its expression drops once mESCs exit the pluripotent state, to increase again during neuroectodermal cell specification. Whereas overexpression of *GRG5* promotes self-renewal, its siRNA-mediated KD deregulates the mESC pluripotent state. Transcriptomic analysis reveals that, in this context, GRG5 represses mesendodermal-related genes, and promotes neuronal specification *via* inhibition of Wnt and BMP signaling. Moreover, GRG5 maintains the self-renewal of NSCs by sustaining the activity of Notch/HES and STAT3 signaling pathways (Chanoumidou et al., 2018).

In contrast to what is reported in mESC, in human ESC (hESCs), Wnt/β-catenin signaling appears to be actively repressed in an OCT4-dependent manner during self-renewal. In these cells, activation of Wnt signaling appears to induce loss of self-renewal, and differentiation into mesodermal lineages (Davidson et al., 2012). Although such discrepancy is a little puzzling, it has been shown that generation of neural lineages from hESCs requires inhibition of Wnt signaling (Tabar and Studer, 2014) and that activation of Wnt signaling in hESCs-derived neural precursor cells promotes transcription of midbrain-like genes through TCF7l2 directly binding the *Engrailed-1 (EN1)* promoter (Kim et al., 2018).

The Case of Neural Stem Cells During Development

Besides its role in development of the CNS, Wnt/β-catenin signaling is crucial for NSCs maintenance. NSCs emerge from territories that have kept their neuroepithelium properties and respond to Wnt signals from embryogenesis through adulthood (Selvadurai and Mason, 2011; Garbe and Ring, 2012; Borday et al., 2018). In the subventricular zone of the developing mouse brain, Wnt signaling is a hallmark of self-renewing, specifically of NSCs' (Kalani et al., 2008). Investigation of the developmental fate of Wnt/β-catenin–responsive cells in embryonic and postnatal mouse brain using a reporter for *Axin2*, demonstrates the continued importance of persistent Wnt/β-catenin signaling for NSCs and progenitor cells emergence (Bowman et al., 2013). In mouse adult hippocampus, where new neurons are continuously generated from NSCs, expression of the pro-neural TF Neurogenic Differentiation 1 (*NEUROD1*) is a landmark of cells dropping out of self-renewal and entering neuronal commitment. Overlapping binding sites for the TCF/LEF factors and SOX2, a marker of most uncommitted cells of the CNS, are present in the promoter region of *Neurod1*. In this context, Wnt signaling together with removal of SOX2 triggers the expression of *NEUROD1*, demonstrating that the SOX2-TCF/LEF regulatory elements are critical for *NEUROD1* expression, and consequently for the switch from the SOX2-mediated repression to the TCF/LEF-mediated activation, towards a neuronal fate ((Kuwabara et al., 2009). In neural precursor cells of the mouse' neocortex, expression of TCF7l1 was found to repress Wnt activity (Ohtsuka et al., 2011; Kuwahara et al., 2014), and active Wnt signaling in the rodents' neocortex apical progenitors sustain their fate plasticity (Oberst et al., 2019). In cultured rat adult hippocampal NSCs, fate decision is influenced by the temporal variations of β-catenin. Optogenetic approaches reveal that continuous activation of β-catenin in cultured NSCs specifies neuronal differentiation, whereas short β-catenin signals activate proliferation but remain insufficient to induce neuronal differentiation. Loss of β-catenin signals promotes apoptosis in differentiating cells, which could be due to inappropriate cell-cycle re-entry (Rosenbloom et al., 2020).

BARHL2 Promotes mESCs Differentiation

Does BARHL2 play a part in mESC biology *via* its ability to enhance TCF7l1 repressive activity? Although such a question has not been directly asked, it is known that *BARHL2* is expressed in mESCs during their commitment phase (Lee et al., 2006). Global expression profile analysis of mESC lines in which BARHL2 overexpression was induced in a doxycycline-controllable manner, reveals that BARHL2 induces a significant fold-change in more than three thousand genes with more than two thousand genes being upregulated, and more than one thousand genes downregulated. In this context, BARHL2 was one of the most influential TF analyzed. Two days following BARHL2 induction, mESCs start to express mesodermal lineage markers (Yamamizu et al., 2016). In a study using another BARHL2 overexpression design in mESCs, a significant increase in the population of neural cells was observed 14 days post-induction (Teratani-Ota et al., 2016). In this context, Notch signaling pathway played a significant influence in driving neural differentiation, and the majority of neuron-like cells generated by induction of BARHL2 expressed markers of GABAergic neurons.

Work is still needed to understand the context-specific regulation of TCF/LEF activities in the biology of ESC, specifically in hESCs. However, studies from the last 15 years strongly support inhibition of TCF7l1-repression as the necessary downstream effect of Wnt signaling in the promotion of mESCs' self-renewal and pluripotency. Reversibly, the formation and stabilization of the TCF7l1/Gro complex, and its inhibitory influence on specific chromatin loci, is one of the crucial switches driving ESCs towards cellular commitment (reviewed in Sokol, 2011). Genetic and functional studies demonstrated that the Gene Regulatory Networks (GRN) underlying acquisition/loss of the pluripotent state are similar in the rodent, fish, and amphibian's blastomeres, and in mESCs, with slight differences observed in hESCs. In early blastomeres, BARHL2-mediated lock of TCF7l1 in an inhibitory state pushes early SO cells towards

irreversible commitment and differentiation, arguing for a similar function in mESCs.

Wnt Signaling Deregulation and Stem Cells: The Emergence of Cancer

In the past years, an increasing number of studies have demonstrated that mutations, loss, or aberrant regulation of Wnt signaling are at the origin of a wide variety of diseases (reviewed in Noelanders and Vleminckx, 2017; Ng et al., 2019). In one of its severest forms, Wnt constitutive activation is associated with diverse cancer types including melanoma, leukemia, breast cancer, gastro-intestinal cancers, and others (reviewed in Zhan et al., 2017). Cancer Stem Cells (CSCs), also known as Tumor Initiating Cells (TICs), are characterized by their "stemness" characteristics that contribute to tumor progression and drug resistance and play deterministic roles in cancer recurrence. Cancer cells exhibit many of the same features as stem cells including self-renewal and their low level of differentiation. Whereas the exact connection between cancer and stem cells is not completely understood, it is well established that both cells use similar signaling pathway machineries, specifically those of the Wnt/β-catenin, Shh, MAPK/ERK and Notch pathways (reviewed in Friedmann-Morvinski and Verma, 2014). In this section, we focus on the impact of Wnt signaling on CSCs, and on medulloblastoma (MB), a pediatric tumor of cerebellar origins in which contributions of both TCF/LEF and the BARHLs are relevant.

Wnt and Cancer Stem Cells

As observed through activity of a TCF/LEF reporter gene, Wnt/β-catenin signaling is highly active in various types of CSCs including colon, lung, breast, and gastric cells (Vermeulen et al., 2010; Horst et al., 2012). A pharmacological antagonist of β-catenin/TCF7l2 interaction blocks CSCs' self-renewal and suppresses tumorigenesis. Treatment of human colon cancer cells, and mouse salivary gland cells with such compound did not only reduce the β-catenin/TCF7l2-mediated proliferation rate and self-renewal, but also induced the differentiation of tumor cells (Fang et al., 2016), making it a potential therapeutic target of the β-catenin-TCF/LEF-dependent tumors, among other tested drugs (reviewed in Jung and Park, 2020; Walcher et al., 2020; Zhang and Wang, 2020). Non-coding RNAs have also been identified as modulators of Wnt-TCF/LEF activity in CSCs. For example, miR-142, which is absent in normal mammary cells but highly expressed in mammary CSCs, increases Wnt activity by inducing degradation of APC, a negative regulator of canonical Wnt signaling (Isobe et al., 2014). Additionally, the long non-coding RNA lncTCF7 has been characterized in hepatocellular carcinoma cells. lncTCF7 maintains CSCs' properties *via* TCF7-dependent activation of Wnt signaling (Wang et al., 2015). Notably, the ability of both normal and CSCs to maintain long telomeres – an important feature to prevent their cellular aging – appears to be under direct transcriptional control of β-catenin-TCF/LEF (Park et al., 2009; Noureen et al., 2021). Whereas the promoter of the telomerase enzymatic subunit, *TERT*, neither bind TCF7l2 nor TCF7l1, it is enriched with TCF7-binding sites located close to the transcription start site that binds β-catenin specifically (Hoffmeyer et al., 2012).

Medulloblastoma

Medulloblastoma (MB), the most common childhood malignant brain tumor, emerges from the cerebellum and accounts for 30% of pediatric brain tumors. Integrated genomic studies allowed the identification of four types of human MB, corresponding to specific genetic alterations (reviewed in Hatten and Roussel, 2011; Wang et al., 2018). One group is associated with alterations in the Wnt/β-catenin signaling pathway (15% of the cases) and originates from brain stem cells. A second group (25% of the cases) is characterized by the constitutive activation of the Shh pathway and derives from Granule Neuron (GN) progenitors. Group 3 (30% of the cases) is specifically found in infants and is thought to originate from overexpression of the MYC oncogene in cerebellar NSCs. Whereas group 4 is the most common MB subgroup (30% of the cases), its underlying biology is not well understood.

In the rodent brain, the cerebellar upper Rhombic Lip (uRhL) produces the GNs that constitute the largest neuronal population in the brain. The GN population exhibits a unique developmental trait: committed GN progenitors (GNPs) are characterized by a very long period of "quiescence" occurring before birth, followed by a long proliferative phase – i.e., 2 weeks in mouse, 2 years in human - occurring after birth, before their final differentiation step (reviewed in Leto et al., 2016). Due to this developmental specificity, this cell population is at risk when it comes to the appearance of developmental defects, including oncogenic events (reviewed in Hatten and Roussel, 2011). At birth, the RhL stem/progenitor cells become responsive to secreted SHH that stimulates their proliferation and self-renewal. The uRhL exhibits stem cell niche properties and exhibit positive TCF/LEF transcriptional activity (Selvadurai and Mason, 2011; Bowman et al., 2013; Yeung et al., 2014; Borday et al., 2018). Atonal Homologue 1 (ATOH1/MATH1) is the master gene of GNPs' development (reviewed in Leto et al., 2016). ATOH1 directly induces the expression of *Barhl1* and *Barhl2* (Kawauchi and Saito, 2008). A thorough single-cell RNA-seq performed on mouse cerebellar cells reveals that *Tcf7l1* is expressed strongly early in the GNPs' differentiation pathway (Wizeman et al., 2019), and that *Barhl2* expression is uniquely associated with early fate commitment in the GNPs (Carter et al., 2018). Taken together, these observations argue that BARHL2 could participate in driving GN stem/progenitor cells towards irreversible commitment.

Rodent cerebellar uRhL cells are known to be at the origin of group 2 MB that are associated with deregulation of the Shh pathway (reviewed in Hovestadt et al., 2020; Garcia-Lopez et al., 2021). Some tumor-propagating cells from this subgroup are not only resistant to Shh inhibitors but are also TCF/LEF-dependent for their self-renewal (Rodriguez-Blanco et al., 2017). *in silico* analysis associates *BARHL2* expression with the emergence of group 2 MB, and *BARHL1* expression with emergence of group 3 and group 4 MB (Pöschl et al., 2011; Lin et al., 2016). Taken together, these observations are a good starting point for future

research that should evaluate whether BARHLs act as roadblocks for de-differentiation that are corrupted in MB.

CONCLUSION AND PERSPECTIVES

In this review, we provide an overview of the TCF/LEF activities as transcriptional repressors focusing on the highly evolutionarily conserved roles of Wnt signaling in axis establishment, neural proliferation, and stem cell biology. We also described the importance of the pro-neural TF BARHL2 as an enhancer of TCF7L1 repressor activities in both SO formation, and forebrain progenitor proliferation.

Currently, numerous conundrums regarding the developmental regulation(s) of TCF/LEF activities, including their interactions with the Barhls, are unresolved. An important point is to clarify the interactions between Barhl2, and generally the Barhls, with the different TCF/LEF members: which Barhl interacts with each of the TCF/LEF family? Are these interactions specific to the different TCF/LEF isoforms and their splice variants? What characterizes the TCF/LEF-BARHL binding interface? Is the interface evolutionarily conserved? Numerous signaling pathways interplay to orchestrate the multipotency/commitment/proliferation states of neural stem/progenitor during embryogenesis. Besides Wnt signaling, the activation and/or inhibition of TCF/LEF activity is under the influence of Notch, Shh, and MAPK/ERK pathways. The context, the repression partners, and the PTM involved in controlling these subtle levels of regulation in NSCs are still poorly understood. Exploration of *Barhl2* developmental expression indicates that it is either a direct, or an indirect, target of the canonical Wnt signaling pathway, thereby contributing to the establishment of a negative feedback loop, that limits the TCF/LEF transcriptional activity in neural progenitors. Analysis of TCF/LEF activity in pluripotent versus committed ESCs indicate that TCF/LEF mostly act by changing the chromatin state in such a way that the expression of the pluripotency-related genes is switched off (reviewed in Sokol, 2011). As BARHL2 blocks TCF7L1 in a transcriptional inhibitory state, it is tempting to speculate that BARHL2 participates to driving stem/progenitor cells towards irreversible commitment, thereby establishing a roadblock on the cell trajectory towards differentiation.

Another important unresolved question relates to how BARHL2, TCF/LEF and Gro/TLE act long distance to transcriptionally inhibit key "commitment" genes. Understanding the specificity of BARHL2 DNA-binding alone, or together with TCF/LEF, should be a first step in identifying the set of genes whose expression is silenced *via* BARHL2/TCF7L1 activity. Moreover, understanding how the BARHL2/TCF7L1 modulates the open/close state of the chromatin, together with probable roles of PTM on the complex stability and its transcriptional activity, shall prove quite beneficial beyond understanding early embryogenesis. Finally, in both amphibian, and rodent, Barhl2 participates in the formation of the caudal forebrain organizer, partly through its direct activation of *Shh* transcription together with *Otx2* (Yao et al., 2016) (reviewed in Sena et al., 2016). Thereby, BARHL2's function is not strictly restricted to its activity as a Wnt transcriptional repressor, but probably depends on the cellular context, adding another level of complexity that should be taken into consideration.

AUTHOR CONTRIBUTIONS

JB-R and BD wrote the manuscript and drafted the figures.

FUNDING

BD is funded by the Centre National de la Recherche Scientifique (CNRS UMR 7622). JB-R is supported by a fellowship from the "Ministère de la Recherche." The work was supported by the Centre National de la Recherche Scientifique (CNRS – UMR7622), Sorbonne Université, Fondation Pierre Gilles de Gennes (FPGG0039), Ligue Nationale contre le Cancer Comité Ile de France (RS19/75-52) and private donors to BD project. Money from private donors was used to pay for the open access publication fees.

ACKNOWLEDGMENTS

The authors greatly acknowledge Sophie Gournet (IBPS, CNRS –UMR7622) for the illustrations, Paul Johnson and Pamela Waked for editing the manuscript content.

REFERENCES

Adamska, M., Larroux, C., Adamski, M., Green, K., Lovas, E., Koop, D., et al. (2010). Structure and Expression of Conserved Wnt Pathway Components in the Demosponge Amphimedon Queenslandica. *Evol. Develop.* 12, 494–518. doi:10.1111/j.1525-142X.2010.00435.x

Afouda, B. A., Nakamura, Y., Shaw, S., Charney, R. M., Paraiso, K. D., Blitz, I. L., et al. (2020). Foxh1/Nodal Defines Context-specific Direct Maternal Wnt/β-Catenin Target Gene Regulation in Early Development. *iScience* 23, 101314. doi:10.1016/j.isci.2020.101314

Alvarez-Medina, R., Cayuso, J., Okubo, T., Takada, S., and Marti´, E. (2008). Wnt Canonical Pathway Restricts Graded Shh/Gli Patterning Activity Through the Regulation of Gli3 Expression. *Development* 135, 237–247. doi:10.1242/dev.012054

Anderson, C., and Stern, C. D. (2016). Organizers in Development. *Curr. Top. Dev. Biol.* 117, 435–454. doi:10.1016/bs.ctdb.2015.11.023

Andoniadou, C. L., and Martinez-Barbera, J. P. (2013). Developmental Mechanisms Directing Early Anterior Forebrain Specification in Vertebrates. *Cell. Mol. Life Sci.* 70, 3739–3752. doi:10.1007/s00018-013-1269-5

Arce, L., Pate, K. T., and Waterman, M. L. (2009). Groucho Binds Two Conserved Regions of LEF-1 for HDAC-dependent Repression. *BMC Cancer* 9, 159. doi:10.1186/1471-2407-9-159

Atcha, F. A., Munguia, J. E., Li, T. W. H., Hovanes, K., and Waterman, M. L. (2003). A New β-Catenin-dependent Activation Domain in T Cell Factor. *J. Biol. Chem.* 278, 16169–16175. doi:10.1074/jbc.M213218200

Atcha, F. A., Syed, A., Wu, B., Hoverter, N. P., Yokoyama, N. N., Ting, J.-H. T., et al. (2007). A Unique DNA Binding Domain Converts T-Cell Factors into Strong Wnt Effectors. *Mol. Cel Biol* 27, 8352–8363. doi:10.1128/MCB.02132-06

Atlasi, Y., Noori, R., Gaspar, C., Franken, P., Sacchetti, A., Rafati, H., et al. (2013). Wnt Signaling Regulates the Lineage Differentiation Potential of Mouse Embryonic Stem Cells Through Tcf3 Down-Regulation. *Plos Genet.* 9, e1003424. doi:10.1371/journal.pgen.1003424

Bernard, P., and Harley, V. R. (2010). Acquisition of SOX Transcription Factor Specificity through Protein-Protein Interaction, Modulation of Wnt Signalling and Post-translational Modification. *Int. J. Biochem. Cel Biol.* 42, 400–410. doi:10.1016/j.biocel.2009.10.017

Bhambhani, C., Ravindranath, A. J., Mentink, R. A., Chang, M. V., Betist, M. C., Yang, Y. X., et al. (2014). Distinct DNA Binding Sites Contribute to the TCF Transcriptional Switch in C. elegans and Drosophila. *Plos Genet.* 10, e1004133. doi:10.1371/journal.pgen.1004133

Billin, A. N., Thirlwell, H., and Ayer, D. E. (2000). β-Catenin-Histone Deacetylase Interactions Regulate the Transition of LEF1 from a Transcriptional Repressor to an Activator. *Mol. Cel Biol* 20, 6882–6890. doi:10.1128/MCB.20.18.6882-6890.2000

Blauwkamp, T. A., Chang, M. V., and Cadigan, K. M. (2008). Novel TCF-Binding Sites Specify Transcriptional Repression by Wnt Signalling. *EMBO J.* 27, 1436–1446. doi:10.1038/emboj.2008.80

Blythe, S. A., Cha, S.-W., Tadjuidje, E., Heasman, J., and Klein, P. S. (2010). β-Catenin Primes Organizer Gene Expression by Recruiting a Histone H3 Arginine 8 Methyltransferase, Prmt2. *Develop. Cel* 19, 220–231. doi:10.1016/j.devcel.2010.07.007

Borday, C., Parain, K., Thi Tran, H., Vleminckx, K., Perron, M., and Monsoro-Burq, A. H. (2018). An Atlas of Wnt Activity During Embryogenesis in Xenopus Tropicalis. *PLoS ONE* 13, e0193606. doi:10.1371/journal.pone.0193606

Bowman, A. N., van Amerongen, R., Palmer, T. D., and Nusse, R. (2013). Lineage Tracing with Axin2 Reveals Distinct Developmental and Adult Populations of Wnt/-Catenin-Responsive Neural Stem Cells. *Proc. Natl. Acad. Sci.* 110, 7324–7329. doi:10.1073/pnas.1305411110

Boyer, L. A., Lee, T. I., Cole, M. F., Johnstone, S. E., Levine, S. S., Zucker, J. P., et al. (2005). Core Transcriptional Regulatory Circuitry in Human Embryonic Stem Cells. *Cell* 122, 947–956. doi:10.1016/j.cell.2005.08.020

Brafman, D., and Willert, K. (2017). Wnt/β-catenin Signaling during Early Vertebrate Neural Development. *Devel Neurobio* 77, 1239–1259. doi:10.1002/dneu.22517

Brannon, M., Brown, J. D., Bates, R., Kimelman, D., and Moon, R. T. (1999). XCtBP Is a XTcf-3 Co-repressor with Roles Throughout Xenopus Development. *Development* 126, 3159–3170. doi:10.1242/dev.126.14.3159

Brannon, M., Gomperts, M., Sumoy, L., Moon, R. T., and Kimelman, D. (1997). A Beta -catenin/XTcf-3 Complex Binds to the Siamois Promoter to Regulate Dorsal Axis Specification in Xenopus. *Genes Develop.* 11, 2359–2370. doi:10.1101/gad.11.18.2359

Brantjes, H. (2001). All Tcf HMG Box Transcription Factors Interact with Groucho-Related Co-repressors. *Nucleic Acids Res.* 29, 1410–1419. doi:10.1093/nar/29.7.1410

Brown, D. D. R., Molinaro, A. M., and Pearson, B. J. (2018). The Planarian TCF/LEF Factor Smed-Tcf1 Is Required for the Regeneration of Dorsal-Lateral Neuronal Subtypes. *Develop. Biol.* 433, 374–383. doi:10.1016/j.ydbio.2017.08.024

Bulfone, A. (2000). Barhl1, A Gene Belonging to a New Subfamily of Mammalian Homeobox Genes, Is Expressed in Migrating Neurons of the CNS. *Hum. Mol. Genet.* 9, 1443–1452. doi:10.1093/hmg/9.9.1443

Calvo, D., Victor, M., Gay, F., Sui, G., Po-Shan Luke, M., Dufourcq, P., et al. (2001). A POP-1 Repressor Complex Restricts Inappropriate Cell Type-specific Gene Transcription During Caenorhabditis elegans Embryogenesis. *EMBO J.* 20, 7197–7208. doi:10.1093/emboj/20.24.7197

Canon, J. (2003). In Vivo Analysis of a Developmental Circuit for Direct Transcriptional Activation and Repression in the Same Cell by a Runx Protein. *Genes Develop.* 17, 838–843. doi:10.1101/gad.1064803

Carnac, G., Kodjabachian, L., Gurdon, J. B., and Lemaire, P. (1996). The Homeobox Gene Siamois Is a Target of the Wnt Dorsalisation Pathway and Triggers Organiser Activity in the Absence of Mesoderm. *Development* 122, 3055–3065. doi:10.1242/dev.122.10.3055

Carter, R. A., Bihannic, L., Rosencrance, C., Hadley, J. L., Tong, Y., Phoenix, T. N., et al. (2018). A Single-Cell Transcriptional Atlas of the Developing Murine Cerebellum. *Curr. Biol.* 28, 2910–2920. doi:10.1016/j.cub.2018.07.062

Castrop, J., van Norren, K., and Clevers, H. (1992). A Gene Family of HMG-Box Transcription Factors with Homology to TCF-1. *Nucl. Acids Res.* 20, 611. doi:10.1093/nar/20.3.611

Cavallo, R. A., Cox, R. T., Moline, M. M., Roose, J., Polevoy, G. A., Clevers, H., et al. (1998). Drosophila Tcf and Groucho Interact to Repress Wingless Signalling Activity. *Nature* 395, 604–608. doi:10.1038/26982

Chambers, M., Turki-Judeh, W., Kim, M. W., Chen, K., Gallaher, S. D., and Courey, A. J. (2017). Mechanisms of Groucho-Mediated Repression Revealed by Genome-wide Analysis of Groucho Binding and Activity. *BMC Genomics* 18, 215. doi:10.1186/s12864-017-3589-6

Chanoumidou, K., Hadjimichael, C., Athanasouli, P., Ahlenius, H., Klonizakis, A., Nikolaou, C., et al. (2018). Groucho Related Gene 5 (GRG5) Is Involved in Embryonic and Neural Stem Cell State Decisions. *Sci. Rep.* 8, 13790. doi:10.1038/s41598-018-31696-9

Chellappa, R., Li, S., Pauley, S., Jahan, I., Jin, K., and Xiang, M. (2008). Barhl1 Regulatory Sequences Required for Cell-specific Gene Expression and Autoregulation in the Inner Ear and Central Nervous System. *Mol. Cel Biol* 28, 1905–1914. doi:10.1128/MCB.01454-07

Chen, C.-Y., Cheng, Y.-Y., Yen, C. Y. T., and Hsieh, P. C. H. (2017). Mechanisms of Pluripotency Maintenance in Mouse Embryonic Stem Cells. *Cel. Mol. Life Sci.* 74, 1805–1817. doi:10.1007/s00018-016-2438-0

Chen, G., Fernandez, J., Mische, S., and Courey, A. J. (1999). A Functional Interaction Between the Histone Deacetylase Rpd3 and the Corepressor Groucho in Drosophila Development. *Genes Develop.* 13, 2218–2230. doi:10.1101/gad.13.17.2218

Chiang, C., Litingtung, Y., Lee, E., Young, K. E., Corden, J. L., Westphal, H., et al. (1996). Cyclopia and Defective Axial Patterning in Mice Lacking Sonic Hedgehog Gene Function. *Nature* 383, 407–413. doi:10.1038/383407a0

Chodaparambil, J. V., Pate, K. T., Hepler, M. R. D., Tsai, B. P., Muthurajan, U. M., Luger, K., et al. (2014). Molecular Functions of the TLE Tetramerization Domain in Wnt Target Gene Repression. *EMBO J.* 33, 719–731. doi:10.1002/embj.201387188

Cinnamon, E., Helman, A., Ben-Haroush Schyr, R., Orian, A., Jime´nez, G., and Paroush, Z. e. (2008). Multiple RTK Pathways Downregulate Groucho-Mediated Repression inDrosophilaembryogenesis. *Development* 135, 829–837. doi:10.1242/dev.015206

Cinnamon, E., and Paroush, Z. e. (2008). Context-dependent Regulation of Groucho/TLE-Mediated Repression. *Curr. Opin. Genet. Develop.* 18, 435–440. doi:10.1016/j.gde.2008.07.010

Cole, M. F., Johnstone, S. E., Newman, J. J., Kagey, M. H., and Young, R. A. (2008). Tcf3 Is an Integral Component of the Core Regulatory Circuitry of Embryonic Stem Cells. *Genes Develop.* 22, 746–755. doi:10.1101/gad.1642408

Colombo, A., Reig, G., Mione, M., and Concha, M. L. (2006). Zebrafish BarH-like Genes Define Discrete Neural Domains in the Early Embryo. *Gene Expr. Patterns* 6, 347–352. doi:10.1016/j.modgep.2005.09.011

Daniel, J. M., and Reynolds, A. B. (1999). The Catenin P120(ctn) Interacts with Kaiso, a Novel BTB/POZ Domain Zinc finger Transcription Factor. *Mol. Cel Biol* 19, 3614–3623. doi:10.1128/MCB.19.5.3614

Daniels, D. L., and Weis, W. I. (2005). Beta-catenin Directly Displaces Groucho/TLE Repressors from Tcf/Lef in Wnt-Mediated Transcription Activation. *Nat. Struct. Mol. Biol.* 12, 364–371. doi:10.1038/nsmb912

Davidson, K. C., Adams, A. M., Goodson, J. M., McDonald, C. E., Potter, J. C., Berndt, J. D., et al. (2012). Wnt/β-catenin Signaling Promotes Differentiation, Not Self-Renewal, of Human Embryonic Stem Cells and Is Repressed by Oct4. *Proc. Natl. Acad. Sci. U S A.* 109, 4485–4490. doi:10.1073/pnas.1118777109

de Jaime-Soguero, A., Abreu de Oliveira, W., and Lluis, F. (2018). The Pleiotropic Effects of the Canonical Wnt Pathway in Early Development and Pluripotency. *Genes* 9, 93. doi:10.3390/genes9020093

De Robertis, E. M., Larraín, J., Oelgeschläger, M., and Wessely, O. (2000). The Establishment of Spemann's Organizer and Patterning of the Vertebrate Embryo. *Nat. Rev. Genet.* 1, 171–181. doi:10.1038/35042039

Ding, Q., Balasubramanian, R., Zheng, D., Liang, G., and Gan, L. (2017). Barhl2 Determines the Early Patterning of the Diencephalon by Regulating Shh. *Mol. Neurobiol.* 54, 4414–4420. doi:10.1007/s12035-016-0001-5

Ding, Q., Chen, H., Xie, X., Libby, R. T., Tian, N., and Gan, L. (2009). BARHL2 Differentially Regulates the Development of Retinal Amacrine and Ganglion Neurons. *J. Neurosci.* 29, 3992–4003. doi:10.1523/JNEUROSCI.5237-08.2009

Ding, Y., Colozza, G., Zhang, K., Moriyama, Y., Ploper, D., Sosa, E. A., et al. (2017). Genome-wide Analysis of Dorsal and Ventral Transcriptomes of the Xenopus laevis Gastrula. *Dev. Biol.* 426, 176–187. doi:10.1016/j.ydbio.2016.02.032

Doenz, G., Dorn, S., Aghaallaei, N., Bajoghli, B., Riegel, E., Aigner, M., et al. (2018). The Function of Tcf3 in Medaka Embryos: Efficient Knockdown with pePNAs. *BMC Biotechnol.* 18, 1. doi:10.1186/s12896-017-0411-0

Dorsky, R. I., Itoh, M., Moon, R. T., and Chitnis, A. (2003). Two Tcf3 Genes Cooperate to Pattern the Zebrafish Brain. *Development* 130, 1937–1947. doi:10.1242/dev.00402

Dorsky, R. I., Snyder, A., Cretekos, C. J., Grunwald, D. J., Geisler, R., Haffter, P., et al. (1999). Maternal and Embryonic Expression of Zebrafish Lef1. *Mech. Dev.* 86, 147–150. doi:10.1016/S0925-4773(99)00101-X

Doumpas, N., Lampart, F., Robinson, M. D., Lentini, A., Nestor, C. E., Cantù, C., et al. (2019). TCF/LEF Dependent and Independent Transcriptional Regulation of Wnt/β-Catenin Target Genes. *EMBO J.* 38, e98873. doi:10.15252/embj.201798873

Dubnicoff, T., Valentine, S. A., Chen, G., Shi, T., Lengyel, J. A., Paroush, Z., et al. (1997). Conversion of Dorsal from an Activator to a Repressor by the Global Corepressor Groucho. *Genes Dev.* 11, 2952–2957. doi:10.1101/gad.11.22.2952

Eshelman, M. A., Shah, M., Raup-Konsavage, W. M., Rennoll, S. A., and Yochum, G. S. (2017). TCF7L1 Recruits CtBP and HDAC1 to Repress DICKKOPF4 Gene Expression in Human Colorectal Cancer Cells. *Biochem. Biophys. Res. Commun.* 487, 716–722. doi:10.1016/j.bbrc.2017.04.123

Fan, M. J., Grüning, W., Walz, G., and Sokol, S. Y. (1998). Wnt Signaling and Transcriptional Control of Siamois in Xenopus Embryos. *Proc. Natl. Acad. Sci. U S A.* 95, 5626–5631. doi:10.1073/pnas.95.10.5626

Fang, L., Zhu, Q., Neuenschwander, M., Specker, E., Wulf-Goldenberg, A., Weis, W. I., et al. (2016). A Small-Molecule Antagonist of the β-Catenin/TCF4 Interaction Blocks the Self-Renewal of Cancer Stem Cells and Suppresses Tumorigenesis. *Cancer Res.* 76, 891–901. doi:10.1158/0008-5472.CAN-15-1519

Fang, M., Li, J., Blauwkamp, T., Bhambhani, C., Campbell, N., and Cadigan, K. M. (2006). C-terminal-binding Protein Directly Activates and Represses Wnt Transcriptional Targets in Drosophila. *EMBO J.* 25, 2735–2745. doi:10.1038/sj.emboj.7601153

Fisher, A. L., Ohsako, S., and Caudy, M. (1996). The WRPW Motif of the Hairy-Related Basic Helix-loop-helix Repressor Proteins Acts as a 4-Amino-Acid Transcription Repression and Protein-Protein Interaction Domain. *Mol. Cel Biol* 16, 2670–2677. doi:10.1128/MCB.16.6.2670

Flack, J. E., Mieszczanek, J., Novcic, N., and Bienz, M. (2017). Wnt-Dependent Inactivation of the Groucho/TLE Co-repressor by the HECT E3 Ubiquitin Ligase Hyd/UBR5. *Mol. Cel* 67, 181–193.e5. doi:10.1016/j.molcel.2017.06.009

Flores-Saaib, R. D., Jia, S., and Courey, A. J. (2001). Activation and Repression by the C-Terminal Domain of Dorsal. *Development* 128, 1869–1879. doi:10.1242/dev.128.10.1869

Franz, A., Shlyueva, D., Brunner, E., Stark, A., and Basler, K. (2017). Probing the Canonicity of the Wnt/Wingless Signaling Pathway. *Plos Genet.* 13, e1006700. doi:10.1371/journal.pgen.1006700

Freeman, J., Smith, D., Latinkic, B., Ewan, K., Samuel, L., Zollo, M., et al. (2015). A Functional Connectome: Regulation of Wnt/TCF-dependent Transcription by Pairs of Pathway Activators. *Mol. Cancer* 14, 206. doi:10.1186/s12943-015-0475-1

Friedmann-Morvinski, D., and Verma, I. M. (2014). Dedifferentiation and Reprogramming: Origins of Cancer Stem Cells. *EMBO Rep.* 15, 244–253. doi:10.1002/embr.201338254

Galceran, J., Miyashita-Lin, E. M., Devaney, E., Rubenstein, J. L., and Grosschedl, R. (2000). Hippocampus Development and Generation of Dentate Gyrus Granule Cells Is Regulated by LEF1. *Development* 127, 469–482. doi:10.1242/dev.127.3.469

Garbe, D. S., and Ring, R. H. (2012). Investigating Tonic Wnt Signaling Throughout the Adult CNS and in the Hippocampal Neurogenic Niche of BatGal and Ins-TopGal Mice. *Cell Mol Neurobiol* 32, 1159–1174. doi:10.1007/s10571-012-9841-3

Garcia-Lopez, J., Kumar, R., Smith, K. S., and Northcott, P. A. (2021). Deconstructing Sonic Hedgehog Medulloblastoma: Molecular Subtypes, Drivers, and beyond. *Trends Genet.* 37, 235–250. doi:10.1016/j.tig.2020.11.001

Gehring, W. J., Qian, Y. Q., Billeter, M., Furukubo-Tokunaga, K., Schier, A. F., Resendez-Perez, D., et al. (1994). Homeodomain-DNA Recognition. *Cell* 78, 211–223. doi:10.1016/0092-8674(94)90292-5

Gerner-Mauro, K. N., Akiyama, H., and Chen, J. (2020). Redundant and Additive Functions of the Four Lef/Tcf Transcription Factors in Lung Epithelial Progenitors. *Proc. Natl. Acad. Sci. U S A.* 117, 12182–12191. doi:10.1073/pnas.2002082117

Ghogomu, S. M., van Venrooy, S., Ritthaler, M., Wedlich, D., and Gradl, D. (2006). HIC-5 Is a Novel Repressor of Lymphoid Enhancer factor/T-Cell Factor-Driven Transcription. *J. Biol. Chem.* 281, 1755–1764. doi:10.1074/jbc.M505869200

Glinka, A., Wu, W., Delius, H., Monaghan, A. P., Blumenstock, C., and Niehrs, C. (1998). Dickkopf-1 Is a Member of a New Family of Secreted Proteins and Functions in Head Induction. *Nature* 391, 357–362. doi:10.1038/34848

Gradl, D., König, A., and Wedlich, D. (2002). Functional Diversity of Xenopus Lymphoid Enhancer Factor/T-Cell Factor Transcription Factors Relies on Combinations of Activating and Repressing Elements. *J. Biol. Chem.* 277, 14159–14171. doi:10.1074/jbc.M107055200

Graham, T. A., Weaver, C., Mao, F., Kimelman, D., and Xu, W. (2000). Crystal Structure of a Beta-catenin/Tcf Complex. *Cell* 103, 885–896. doi:10.1016/s0092-8674(00)00192-6

Grbavec, D., Lo, R., Liu, Y., and Stifani, S. (1998). Transducin-like Enhancer of Split 2, a Mammalian Homologue of Drosophila Groucho, Acts as a Transcriptional Repressor, Interacts with Hairy/Enhancer of Split Proteins, and Is Expressed During Neuronal Development. *Eur. J. Biochem.* 258, 339–349. doi:10.1046/j.1432-1327.1998.2580339.x

Hanson, A. J., Wallace, H. A., Freeman, T. J., Beauchamp, R. D., Lee, L. A., and Lee, E. (2012). XIAP Monoubiquitylates Groucho/TLE to Promote Canonical Wnt Signaling. *Mol. Cel* 45, 619–628. doi:10.1016/j.molcel.2011.12.032

Hao, J., Li, T. G., Qi, X., Zhao, D. F., and Zhao, G. Q. (2006). WNT/beta-catenin Pathway Up-Regulates Stat3 and Converges on LIF to Prevent Differentiation of Mouse Embryonic Stem Cells. *Dev. Biol.* 290, 81–91. doi:10.1016/j.ydbio.2005.11.011

Hashimoto-Torii, K., Motoyama, J., Hui, C. C., Kuroiwa, A., Nakafuku, M., and Shimamura, K. (2003). Differential Activities of Sonic Hedgehog Mediated by Gli Transcription Factors Define Distinct Neuronal Subtypes in the Dorsal Thalamus. *Mech. Dev.* 120, 1097–1111. doi:10.1016/j.mod.2003.09.001

Hatten, M. E., and Roussel, M. F. (2011). Development and Cancer of the Cerebellum. *Trends Neurosci.* 34, 134–142. doi:10.1016/j.tins.2011.01.002

He, T. C., Sparks, A. B., Rago, C., Hermeking, H., Zawel, L., da Costa, L. T., et al. (1998). Identification of C-MYC as a Target of the APC Pathway. *Science* 281, 1509–1512. doi:10.1126/science.281.5382.1509

Heimbucher, T., Murko, C., Bajoghli, B., Aghaallaei, N., Huber, A., Stebegg, R., et al. (2007). Gbx2 and Otx2 Interact with the WD40 Domain of Groucho/Tle Corepressors. *Mol. Cel Biol* 27, 340–351. doi:10.1128/MCB.00811-06

Heisenberg, C. P., Houart, C., Take-Uchi, M., Rauch, G. J., Young, N., Coutinho, P., et al. (2001). A Mutation in the Gsk3-Binding Domain of Zebrafish Masterblind/Axin1 Leads to a Fate Transformation of Telencephalon and Eyes to Diencephalon. *Genes Dev.* 15, 1427–1434. doi:10.1101/gad.194301

Higashijima, S., Kojima, T., Michiue, T., Ishimaru, S., Emori, Y., and Saigo, K. (1992). Dual Bar Homeo Box Genes of Drosophila Required in Two Photoreceptor Cells, R1 and R6, and Primary Pigment Cells for Normal Eye Development. *Genes Dev.* 6, 50–60. doi:10.1101/gad.6.1.50

Hikasa, H., Ezan, J., Itoh, K., Li, X., Klymkowsky, M. W., and Sokol, S. Y. (2010). Regulation of TCF3 by Wnt-dependent Phosphorylation During Vertebrate Axis Specification. *Dev. Cel* 19, 521–532. doi:10.1016/j.devcel.2010.09.005

Hikasa, H., and Sokol, S. Y. (2011). Phosphorylation of TCF Proteins by Homeodomain-Interacting Protein Kinase 2. *J. Biol. Chem.* 286, 12093–12100. doi:10.1074/jbc.M110.185280

Hoch, R. V., Rubenstein, J. L., and Pleasure, S. (2009). Genes and Signaling Events that Establish Regional Patterning of the Mammalian Forebrain. *Semin. Cel Dev Biol* 20, 378–386. doi:10.1016/j.semcdb.2009.02.005

Hoffmeyer, K., Raggioli, A., Rudloff, S., Anton, R., Hierholzer, A., Del Valle, I., et al. (2012). Wnt/β-catenin Signaling Regulates Telomerase in Stem Cells and Cancer Cells. *Science* 336, 1549–1554. doi:10.1126/science.1218370

Hoppler, S., and Waterman, M. L. (2014). "Evolutionary Diversification of Vertebrate TCF/LEF Structure, Function, and Regulation," in *Wnt Signaling*

In Development And Disease. Editors S. Hoppler and R. T. Moon (Hoboken, NJ: John Wiley & Sons), 225–237. doi:10.1002/9781118444122.ch17

Horst, D., Chen, J., Morikawa, T., Ogino, S., Kirchner, T., and Shivdasani, R. A. (2012). Differential WNT Activity in Colorectal Cancer Confers Limited Tumorigenic Potential and Is Regulated by MAPK Signaling. *Cancer Res.* 72, 1547–1556. doi:10.1158/0008-5472.CAN-11-3222

Houston, D. W., Kofron, M., Resnik, E., Langland, R., Destree, O., Wylie, C., et al. (2002). Repression of Organizer Genes in Dorsal and Ventral Xenopus Cells Mediated by Maternal XTcf3. *Development* 129, 4015–4025. doi:10.1242/dev.129.17.4015

Hovanes, K., Li, T. W. H., Munguia, J. E., Truong, T., Milovanovic, T., Lawrence Marsh, J., et al. (2001). β-catenin–sensitive Isoforms of Lymphoid Enhancer Factor-1 Are Selectively Expressed in colon Cancer. *Nat. Genet.* 28, 53–57. doi:10.1038/ng0501-53

Hovestadt, V., Ayrault, O., Swartling, F. J., Robinson, G. W., Pfister, S. M., and Northcott, P. A. (2020). Medulloblastomics Revisited: Biological and Clinical Insights from Thousands of Patients. *Nat. Rev. Cancer* 20, 42–56. doi:10.1038/s41568-019-0223-8

Ishibashi, M., and McMahon, A. P. (2002). A Sonic Hedgehog-dependent Signaling Relay Regulates Growth of Diencephalic and Mesencephalic Primordia in the Early Mouse Embryo. *Development* 129, 4807–4819.

Isobe, T., Hisamori, S., Hogan, D. J., Zabala, M., Hendrickson, D. G., Dalerba, P., et al. (2014). miR-142 Regulates the Tumorigenicity of Human Breast Cancer Stem Cells Through the Canonical WNT Signaling Pathway. *Elife* 3, e01977. doi:10.7554/eLife.01977

Jennings, B. H., and Ish-Horowicz, D. (2008). The Groucho/TLE/Grg Family of Transcriptional Co-repressors. *Genome Biol.* 9, 205. doi:10.1186/gb-2008-9-1-205

Jennings, B. H., Pickles, L. M., Wainwright, S. M., Roe, S. M., Pearl, L. H., and Ish-Horowicz, D. (2006). Molecular Recognition of Transcriptional Repressor Motifs by the WD Domain of the Groucho/TLE Corepressor. *Mol. Cel* 22, 645–655. doi:10.1016/j.molcel.2006.04.024

Jiménez, G., Paroush, Z., and Ish-Horowicz, D. (1997). Groucho Acts as a Corepressor for a Subset of Negative Regulators, Including Hairy and Engrailed. *Genes Dev.* 11, 3072–3082. doi:10.1101/gad.11.22.3072

Jones, E. G., and Rubenstein, J. L. (2004). Expression of Regulatory Genes During Differentiation of Thalamic Nuclei in Mouse and Monkey. *J. Comp. Neurol.* 477, 55–80. doi:10.1002/cne.20234

Jung, Y. S., and Park, J. I. (2020). Wnt Signaling in Cancer: Therapeutic Targeting of Wnt Signaling beyond β-catenin and the Destruction Complex. *Exp. Mol. Med.* 52, 183–191. doi:10.1038/s12276-020-0380-6

Juraver-Geslin, H. A., Ausseil, J. J., Wassef, M., and Durand, B. C. (2011). Barhl2 Limits Growth of the Diencephalic Primordium Through Caspase3 Inhibition of Beta-Catenin Activation. *Proc. Natl. Acad. Sci. U S A.* 108, 2288–2293. doi:10.1073/pnas.1014017108

Juraver-Geslin, H. A., and Durand, B. C. (2015). Early Development of the Neural Plate: New Roles for Apoptosis and for One of its Main Effectors Caspase-3. *Genesis* 53, 203–224. doi:10.1002/dvg.22844

Juraver-Geslin, H. A., Gómez-Skarmeta, J. L., and Durand, B. C. (2014). The Conserved barH-like Homeobox-2 Gene Barhl2 Acts Downstream of Orthodentricle-2 and Together with iroquois-3 in Establishment of the Caudal Forebrain Signaling center Induced by Sonic Hedgehog. *Dev. Biol.* 396, 107–120. doi:10.1016/j.ydbio.2014.09.027

Jusuf, P. R., Albadri, S., Paolini, A., Currie, P. D., Argenton, F., Higashijima, S., et al. (2012). Biasing Amacrine Subtypes in the Atoh7 Lineage Through Expression of Barhl2. *J. Neurosci.* 32, 13929–13944. doi:10.1523/JNEUROSCI.2073-12.2012

Kalani, M. Y., Cheshier, S. H., Cord, B. J., Bababeygy, S. R., Vogel, H., Weissman, I. L., et al. (2008). Wnt-mediated Self-Renewal of Neural Stem/progenitor Cells. *Proc. Natl. Acad. Sci. U S A.* 105, 16970–16975. doi:10.1073/pnas.0808616105

Kaul, A., Schuster, E., and Jennings, B. H. (2014). The Groucho Co-repressor Is Primarily Recruited to Local Target Sites in Active Chromatin to Attenuate Transcription. *Plos Genet.* 10, e1004595. doi:10.1371/journal.pgen.1004595

Kawauchi, D., and Saito, T. (2008). Transcriptional Cascade from Math1 to Mbh1 and Mbh2 Is Required for Cerebellar Granule Cell Differentiation. *Dev. Biol.* 322, 345–354. doi:10.1016/j.ydbio.2008.08.005

Kiecker, C., and Lumsden, A. (2012). The Role of Organizers in Patterning the Nervous System. *Annu. Rev. Neurosci.* 35, 347–367. doi:10.1146/annurev-neuro-062111-150543

Kim, C. H., Oda, T., Itoh, M., Jiang, D., Artinger, K. B., Chandrasekharappa, S. C., et al. (2000). Repressor Activity of Headless/Tcf3 Is Essential for Vertebrate Head Formation. *Nature* 407, 913–916. doi:10.1038/35038097

Kim, J. Y., Lee, J. S., Hwang, H. S., Lee, D. R., Park, C. Y., Jung, S. J., et al. (2018). Wnt Signal Activation Induces Midbrain Specification Through Direct Binding of the Beta-catenin/TCF4 Complex to the EN1 Promoter in Human Pluripotent Stem Cells. *Exp. Mol. Med.* 50, 24–13. doi:10.1038/s12276-018-0044-y

King, N., Westbrook, M. J., Young, S. L., Kuo, A., Abedin, M., Chapman, J., et al. (2008). The Genome of the Choanoflagellate Monosiga Brevicollis and the Origin of Metazoans. *Nature* 451, 783–788. doi:10.1038/nature06617

Kojima, T., Ishimaru, S., Higashijima, S., Takayama, E., Akimaru, H., Sone, M., et al. (1991). Identification of a Different-type Homeobox Gene, BarH1, Possibly Causing Bar (B) and Om(1D) Mutations in Drosophila. *Proc. Natl. Acad. Sci. U S A.* 88, 4343–4347. doi:10.1073/pnas.88.10.4343

Korinek, V., Barker, N., Willert, K., Molenaar, M., Roose, J., Wagenaar, G., et al. (1998). Two Members of the Tcf Family Implicated in Wnt/beta-Catenin Signaling During Embryogenesis in the Mouse. *Mol. Cel Biol* 18, 1248–1256. doi:10.1128/MCB.18.3.1248

Kormish, J. D., Sinner, D., and Zorn, A. M. (2009). Interactions Between SOX Factors and Wnt/β-Catenin Signaling in Development and Disease. *Dev. Dyn.* 239, 56–68. doi:10.1002/dvdy.22046

Kratochwil, K., Galceran, J., Tontsch, S., Roth, W., and Grosschedl, R. (2002). FGF4, a Direct Target of LEF1 and Wnt Signaling, Can Rescue the Arrest of Tooth Organogenesis in Lef1(-/-) Mice. *Genes Dev.* 16, 3173–3185. doi:10.1101/gad.1035602

Kraus, Y., Aman, A., Technau, U., and Genikhovich, G. (2016). Pre-bilaterian Origin of the Blastoporal Axial Organizer. *Nat. Commun.* 7, 11694. doi:10.1038/ncomms11694

Kuwabara, T., Hsieh, J., Muotri, A., Yeo, G., Warashina, M., Lie, D. C., et al. (2009). Wnt-mediated Activation of NeuroD1 and Retro-Elements During Adult Neurogenesis. *Nat. Neurosci.* 12, 1097–1105. doi:10.1038/nn.2360

Kuwahara, A., Sakai, H., Xu, Y., Itoh, Y., Hirabayashi, Y., and Gotoh, Y. (2014). Tcf3 Represses Wnt-β-Catenin Signaling and Maintains Neural Stem Cell Population During Neocortical Development. *PLoS One* 9, e94408. doi:10.1371/journal.pone.0094408

Laing, A. F., Lowell, S., and Brickman, J. M. (2015). Gro/TLE Enables Embryonic Stem Cell Differentiation by Repressing Pluripotent Gene Expression. *Dev. Biol.* 397, 56–66. doi:10.1016/j.ydbio.2014.10.007

Larabell, C. A., Torres, M., Rowning, B. A., Yost, C., Miller, J. R., Wu, M., et al. (1997). Establishment of the Dorso-Ventral axis in Xenopus Embryos Is Presaged by Early Asymmetries in Beta-Catenin that Are Modulated by the Wnt Signaling Pathway. *J. Cel Biol* 136, 1123–1136. doi:10.1083/jcb.136.5.1123

Larsen, C. W., Zeltser, L. M., and Lumsden, A. (2001). Boundary Formation and Compartition in the Avian Diencephalon. *J. Neurosci.* 21, 4699–4711. doi:10.1523/JNEUROSCI.21-13-04699.2001

Laurent, M. N., Blitz, I. L., Hashimoto, C., Rothbächer, U., and Cho, K. W. (1997). The Xenopus Homeobox Gene Twin Mediates Wnt Induction of Goosecoid in Establishment of Spemann's Organizer. *Development* 124, 4905–4916. doi:10.1242/dev.124.23.4905

Lee, S. M., Tole, S., Grove, E., and McMahon, A. P. (2000). A Local Wnt-3a Signal Is Required for Development of the Mammalian hippocampus. *Development* 127, 457–467. doi:10.1242/dev.127.3.457

Lee, T. I., Jenner, R. G., Boyer, L. A., Guenther, M. G., Levine, S. S., Kumar, R. M., et al. (2006). Control of Developmental Regulators by Polycomb in Human Embryonic Stem Cells. *Cell* 125, 301–313. doi:10.1016/j.cell.2006.02.043

Lemaire, P., Garrett, N., and Gurdon, J. B. (1995). Expression Cloning of Siamois, a Xenopus Homeobox Gene Expressed in Dorsal-Vegetal Cells of Blastulae and Able to Induce a Complete Secondary Axis. *Cell* 81, 85–94. doi:10.1016/0092-8674(95)90373-9

Lemoine, F., Correia, D., Lefort, V., Doppelt-Azeroual, O., Mareuil, F., Cohen-Boulakia, S., et al. (2019). NGPhylogeny.fr: New Generation Phylogenetic Services for Non-specialists. *Nucleic Acids Res.* 47, W260–W265. doi:10.1093/nar/gkz303

Leto, K., Arancillo, M., Becker, E. B., Buffo, A., Chiang, C., Ding, B., et al. (2016). Consensus Paper: Cerebellar Development. *Cerebellum* 15, 789–828. doi:10.1007/s12311-015-0724-2

Lien, W. H., Polak, L., Lin, M., Lay, K., Zheng, D., and Fuchs, E. (2014). In vivo Transcriptional Governance of Hair Follicle Stem Cells by Canonical Wnt Regulators. *Nat. Cel Biol* 16, 179–190. doi:10.1038/ncb2903

Lin, C. Y., Erkek, S., Tong, Y., Yin, L., Federation, A. J., Zapatka, M., et al. (2016). Active Medulloblastoma Enhancers Reveal Subgroup-specific Cellular Origins. *Nature* 530, 57–62. doi:10.1038/nature16546

Lin, R., Thompson, S., and Priess, J. R. (1995). pop-1 Encodes an HMG Box Protein Required for the Specification of a Mesoderm Precursor in Early C. elegans Embryos. *Cell* 83, 599–609. doi:10.1016/0092-8674(95)90100-0

Liston, P., Fong, W. G., and Korneluk, R. G. (2003). The Inhibitors of Apoptosis: There Is More to Life Than Bcl2. *Oncogene* 22, 8568–8580. doi:10.1038/sj.onc.1207101

Liu, F., van den Broek, O., Destrée, O., and Hoppler, S. (2005). Distinct Roles for Xenopus Tcf/Lef Genes in Mediating Specific Responses to Wnt/beta-Catenin Signalling in Mesoderm Development. *Development* 132, 5375–5385. doi:10.1242/dev.02152

Louvi, A., Yoshida, M., and Grove, E. A. (2007). The Derivatives of the Wnt3a Lineage in the Central Nervous System. *J. Comp. Neurol.* 504, 550–569. doi:10.1002/cne.21461

Lowe, C. J., Wu, M., Salic, A., Evans, L., Lander, E., Stange-Thomann, N., et al. (2003). Anteroposterior Patterning in Hemichordates and the Origins of the Chordate Nervous System. *Cell* 113, 853–865. doi:10.1016/S0092-8674(03)00469-0

MacDonald, B. T., Tamai, K., and He, X. (2009). Wnt/beta-catenin Signaling: Components, Mechanisms, and Diseases. *Dev. Cel* 17, 9–26. doi:10.1016/j.devcel.2009.06.016

Malarkey, C. S., and Churchill, M. E. (2012). The High Mobility Group Box: The Ultimate Utility Player of a Cell. *Trends Biochem. Sci.* 37, 553–562. doi:10.1016/j.tibs.2012.09.003

Marson, A., Levine, S. S., Cole, M. F., Frampton, G. M., Brambrink, T., Johnstone, S., et al. (2008). Connecting microRNA Genes to the Core Transcriptional Regulatory Circuitry of Embryonic Stem Cells. *Cell* 134, 521–533. doi:10.1016/j.cell.2008.07.020

Martínez, S., and Puelles, L. (2000). "Neurogenetic Compartments of the Mouse Diencephalon and Some Characteristic Gene Expression Patterns," in *Mouse Brain Development Results and Problems in Cell Differentiation*. Editors A. M. Goffinet and P. Rakic (Berlin, Heidelberg: Springer Berlin Heidelberg), 91–106. doi:10.1007/978-3-540-48002-0_4

Mattes, B., Weber, S., Peres, J., Chen, Q., Davidson, G., Houart, C., et al. (2012). Wnt3 and Wnt3a Are Required for Induction of the Mid-diencephalic Organizer in the Caudal Forebrain. *Neural Dev.* 7, 12. doi:10.1186/1749-8104-7-12

McCrea, P. D., Brieher, W. M., and Gumbiner, B. M. (1993). Induction of a Secondary Body axis in Xenopus by Antibodies to Beta-Catenin. *J. Cel Biol* 123, 477–484. doi:10.1083/jcb.123.2.477

McMahon, A. P., and Moon, R. T. (1989). Ectopic Expression of the Proto-Oncogene Int-1 in Xenopus Embryos Leads to Duplication of the Embryonic axis. *Cell* 58, 1075–1084. doi:10.1016/0092-8674(89)90506-0

Megason, S. G., and McMahon, A. P. (2002). A Mitogen Gradient of Dorsal Midline Wnts Organizes Growth in the CNS. *Development* 129, 2087–2098. doi:10.1242/dev.129.9.2087

Merrill, B. J., Pasolli, H. A., Polak, L., Rendl, M., García-García, M. J., Anderson, K. V., et al. (2004). Tcf3: A Transcriptional Regulator of axis Induction in the Early Embryo. *Development* 131, 263–274. doi:10.1242/dev.00935

Merrill, B. J. (2012). Wnt Pathway Regulation of Embryonic Stem Cell Self-Renewal. *Cold Spring Harbor Perspect. Biol.* 4, a007971. doi:10.1101/cshperspect.a007971

Mo, Z., Li, S., Yang, X., and Xiang, M. (2004). Role of the Barhl2 Homeobox Gene in the Specification of Glycinergic Amacrine Cells. *Development* 131, 1607–1618. doi:10.1242/dev.01071

Molenaar, M., Roose, J., Peterson, J., Venanzi, S., Clevers, H., and Destrée, O. (1998). Differential Expression of the HMG Box Transcription Factors XTcf-3 and XLef-1 During Early Xenopus Development. *Mech. Dev.* 75, 151–154. doi:10.1016/S0925-4773(98)00085-9

Molenaar, M., van de Wetering, M., Oosterwegel, M., Peterson-Maduro, J., Godsave, S., Korinek, V., et al. (1996). XTcf-3 Transcription Factor Mediates Beta-Catenin-Induced Axis Formation in Xenopus Embryos. *Cell* 86, 391–399. doi:10.1016/S0092-8674(00)80112-9

Moreira, S., Polena, E., Gordon, V., Abdulla, S., Mahendram, S., Cao, J., et al. (2017). A Single TCF Transcription Factor, Regardless of its Activation Capacity, Is Sufficient for Effective Trilineage Differentiation of ESCs. *Cell Rep* 20, 2424–2438. doi:10.1016/j.celrep.2017.08.043

Muhr, J., Andersson, E., Persson, M., Jessell, T. M., and Ericson, J. (2001). Groucho-mediated Transcriptional Repression Establishes Progenitor Cell Pattern and Neuronal Fate in the Ventral Neural Tube. *Cell* 104, 861–873. doi:10.1016/S0092-8674(01)00283-5

Mukherjee, S., Luedeke, D. M., Brown, L., and Zorn, A. M. (2021). SOX Transcription Factors Direct TCF-independent WNT/beta-catenin Transcription. *bioRxiv* doi:10.1101/2021.08.25.457694

Muncan, V., Faro, A., Haramis, A. P., Hurlstone, A. F., Wienholds, E., van Es, J., et al. (2007). T-cell Factor 4 (Tcf7l2) Maintains Proliferative Compartments in Zebrafish Intestine. *EMBO Rep.* 8, 966–973. doi:10.1038/sj.embor.7401071

Nakamura, Y., and Hoppler, S. (2017). Genome-wide Analysis of Canonical Wnt Target Gene Regulation in Xenopus Tropicalis Challenges β-catenin Paradigm. *Genesis* 55, e22991. doi:10.1002/dvg.22991

Nakamura, Y., de Paiva Alves, E., Veenstra, G. J., and Hoppler, S. (2016). Tissue- and Stage-specific Wnt Target Gene Expression Is Controlled Subsequent to β-catenin Recruitment. *Development* 143, 1914–1925. doi:10.1242/dev.131664

Nehme, R., Grote, P., Tomasi, T., Löser, S., Holzkamp, H., Schnabel, R., et al. (2010). Transcriptional Upregulation of Both Egl-1 BH3-Only and Ced-3 Caspase Is Required for the Death of the Male-specific CEM Neurons. *Cell Death Differ* 17, 1266–1276. doi:10.1038/cdd.2010.3

Ng, L. F., Kaur, P., Bunnag, N., Suresh, J., Sung, I. C. H., Tan, Q. H., et al. (2019). WNT Signaling in Disease. *Cells* 8, 826. doi:10.3390/cells8080826

Niehrs, C. (2004). Regionally Specific Induction by the Spemann-Mangold Organizer. *Nat. Rev. Genet.* 5, 425–434. doi:10.1038/nrg1347

Niehrs, C. (2012). The Complex World of WNT Receptor Signalling. *Nat. Rev. Mol. Cel Biol* 13, 767–779. doi:10.1038/nrm3470

Niwa, H. (2011). Wnt: What's Needed to Maintain Pluripotency? *Nat. Cel Biol* 13, 1024–1026. doi:10.1038/ncb2333

Noelanders, R., and Vleminckx, K. (2017). How Wnt Signaling Builds the Brain: Bridging Development and Disease. *Neuroscientist* 23, 314–329. doi:10.1177/1073858416667270

Noureen, N., Wu, S., Lv, Y., Yang, J., Alfred Yung, W. K., Gelfond, J., et al. (2021). Integrated Analysis of Telomerase Enzymatic Activity Unravels an Association with Cancer Stemness and Proliferation. *Nat. Commun.* 12, 139. doi:10.1038/s41467-020-20474-9

Nusse, R., and Clevers, H. (2017). Wnt/β-Catenin Signaling, Disease, and Emerging Therapeutic Modalities. *Cell* 169, 985–999. doi:10.1016/j.cell.2017.05.016

Nusse, R., and Varmus, H. (2012). Three Decades of Wnts: A Personal Perspective on How a Scientific Field Developed. *EMBO J.* 31, 2670–2684. doi:10.1038/emboj.2012.146

Nusse, R., and Varmus, H. E. (1982). Many Tumors Induced by the Mouse Mammary Tumor Virus Contain a Provirus Integrated in the Same Region of the Host Genome. *Cell* 31, 99–109. doi:10.1016/0092-8674(82)90409-3

Oberst, P., Fièvre, S., Baumann, N., Concetti, C., Bartolini, G., and Jabaudon, D. (2019). Temporal Plasticity of Apical Progenitors in the Developing Mouse Neocortex. *Nature* 573, 370–374. doi:10.1038/s41586-019-1515-6

Offner, N., Duval, N., Jamrich, M., and Durand, B. (2005). The Pro-apoptotic Activity of a Vertebrate Bar-like Homeobox Gene Plays a Key Role in Patterning the Xenopus Neural Plate by Limiting the Number of Chordin- and Shh-Expressing Cells. *Development* 132, 1807–1818. doi:10.1242/dev.01712

Ohtsuka, T., Shimojo, H., Matsunaga, M., Watanabe, N., Kometani, K., Minato, N., et al. (2011). Gene Expression Profiling of Neural Stem Cells and Identification of Regulators of Neural Differentiation During Cortical Development. *Stem Cells* 29, 1817–1828. doi:10.1002/stem.731

Owens, N. D. L., Blitz, I. L., Lane, M. A., Patrushev, I., Overton, J. D., Gilchrist, M. J., et al. (2016). Measuring Absolute RNA Copy Numbers at High Temporal Resolution Reveals Transcriptome Kinetics in Development. *Cel Rep* 14, 632–647. doi:10.1016/j.celrep.2015.12.050

Ozair, M. Z., Kintner, C., and Brivanlou, A. H. (2013). Neural Induction and Early Patterning in Vertebrates. *Wiley Interdiscip. Rev. Dev. Biol.* 2, 479–498. doi:10.1002/wdev.90

Panhuysen, M., Vogt Weisenhorn, D. M., Blanquet, V., Brodski, C., Heinzmann, U., Beisker, W., et al. (2004). Effects of Wnt1 Signaling on Proliferation in the Developing Mid-/hindbrain Region. *Mol. Cel Neurosci.* 26, 101–111. doi:10.1016/j.mcn.2004.01.011

Pani, A. M., Mullarkey, E. E., Aronowicz, J., Assimacopoulos, S., Grove, E. A., and Lowe, C. J. (2012). Ancient Deuterostome Origins of Vertebrate Brain Signalling Centres. *Nature* 483, 289–294. doi:10.1038/nature10838

Park, J. I., Kim, S. W., Lyons, J. P., Ji, H., Nguyen, T. T., Cho, K., et al. (2005). Kaiso/p120-catenin and TCF/beta-catenin Complexes Coordinately Regulate Canonical Wnt Gene Targets. *Dev. Cel* 8, 843–854. doi:10.1016/j.devcel.2005.04.010

Park, J. I., Venteicher, A. S., Hong, J. Y., Choi, J., Jun, S., Shkreli, M., et al. (2009). Telomerase Modulates Wnt Signalling by Association with Target Gene Chromatin. *Nature* 460, 66–72. doi:10.1038/nature08137

Park, M. S., Kausar, R., Kim, M. W., Cho, S. Y., Lee, Y. S., and Lee, M. A. (2015). Tcf7l1-mediated Transcriptional Regulation of Krüppel-like Factor 4 Gene. *Anim. Cell Syst.* 19, 16–29. doi:10.1080/19768354.2014.991351

Parker, D. S., Jemison, J., and Cadigan, K. M. (2002). Pygopus, A Nuclear PHD-finger Protein Required for Wingless Signaling in Drosophila. *Development* 129, 2565–2576. doi:10.1242/dev.129.11.2565

Paroush, Z., Finley, R. L., Kidd, T., Wainwright, S. M., Ingham, P. W., Brent, R., et al. (1994). Groucho Is Required for Drosophila Neurogenesis, Segmentation, and Sex Determination and Interacts Directly with Hairy-Related bHLH Proteins. *Cell* 79, 805–815. doi:10.1016/0092-8674(94)90070-1

Patterson, K. D., Cleaver, O., Gerber, W. V., White, F. G., and Krieg, P. A. (2000). Distinct Expression Patterns for Two Xenopus Bar Homeobox Genes. *Dev. Genes Evol.* 210, 140–144. doi:10.1007/s004270050020

Peden, E., Kimberly, E., Gengyo-Ando, K., Mitani, S., and Xue, D. (2007). Control of Sex-specific Apoptosis in C. elegans by the BarH Homeodomain Protein CEH-30 and the Transcriptional Repressor UNC-37/Groucho. *Genes Dev.* 21, 3195–3207. doi:10.1101/gad.1607807

Pereira, L., Yi, F., and Merrill, B. J. (2006). Repression of Nanog Gene Transcription by Tcf3 Limits Embryonic Stem Cell Self-Renewal. *Mol. Cel Biol* 26, 7479–7491. doi:10.1128/MCB.00368-06

Pöschl, J., Lorenz, A., Hartmann, W., von Bueren, A. O., Kool, M., Li, S., et al. (2011). Expression of BARHL1 in Medulloblastoma Is Associated with Prolonged Survival in Mice and Humans. *Oncogene* 30, 4721–4730. doi:10.1038/onc.2011.173

Pukrop, T., Gradl, D., Henningfeld, K. A., Knochel, W., Wedlich, D., and Kuhl, M. (2001). Identification of Two Regulatory Elements Within the High Mobility Group Box Transcription Factor XTCF-4. *J. Biol. Chem.* 276, 8968–8978. doi:10.1074/jbc.M007533200

Quinlan, R., Graf, M., Mason, I., Lumsden, A., and Kiecker, C. (2009). Complex and Dynamic Patterns of Wnt Pathway Gene Expression in the Developing Chick Forebrain. *Neural Dev.* 4, 35. doi:10.1186/1749-8104-4-35

Ramakrishnan, A. B., Sinha, A., Fan, V. B., and Cadigan, K. M. (2018). The Wnt Transcriptional Switch: TLE Removal or Inactivation? *Bioessays* 40, 1700162. doi:10.1002/bies.201700162

Ravindranath, A., and Cadigan, K. M. (2014). Structure-Function Analysis of the C-Clamp of TCF/Pangolin in Wnt/ß-Catenin Signaling. *PLoS ONE* 9, e86180. doi:10.1371/journal.pone.0086180

Reig, G., Cabrejos, M. E., and Concha, M. L. (2007). Functions of BarH Transcription Factors During Embryonic Development. *Dev. Biol.* 302, 367–375. doi:10.1016/j.ydbio.2006.10.008

Rocheleau, C. E., Downs, W. D., Lin, R., Wittmann, C., Bei, Y., Cha, Y. H., et al. (1997). Wnt Signaling and an APC-Related Gene Specify Endoderm in Early C. elegans Embryos. *Cell* 90, 707–716. doi:10.1016/S0092-8674(00)80531-0

Rodriguez-Blanco, J., Pednekar, L., Penas, C., Li, B., Martin, V., Long, J., et al. (2017). Inhibition of WNT Signaling Attenuates Self-Renewal of SHH-Subgroup Medulloblastoma. *Oncogene* 36, 6306–6314. doi:10.1038/onc.2017.232

Roël, G., Hamilton, F. S., Gent, Y., Bain, A. A., Destrée, O., and Hoppler, S. (2002). Lef-1 and Tcf-3 Transcription Factors Mediate Tissue-specific Wnt Signaling During Xenopus Development. *Curr. Biol.* 12, 1941–1945. doi:10.1016/S0960-9822(02)01280-0

Roose, J., Molenaar, M., Peterson, J., Hurenkamp, J., Brantjes, H., Moerer, P., et al. (1998). The Xenopus Wnt Effector XTcf-3 Interacts with Groucho-Related Transcriptional Repressors. *Nature* 395, 608–612. doi:10.1038/26989

Rosenbloom, A. B., Tarczyński, M., Lam, N., Kane, R. S., Bugaj, L. J., and Schaffer, D. V. (2020). β-Catenin Signaling Dynamics Regulate Cell Fate in Differentiating Neural Stem Cells. *Proc. Natl. Acad. Sci. U S A.* 117, 28828–28837. doi:10.1073/pnas.2008509117

Röttinger, E., and Lowe, C. J. (2012). Evolutionary Crossroads in Developmental Biology: Hemichordates. *Development* 139, 2463–2475. doi:10.1242/dev.066712

Ruzov, A., Hackett, J. A., Prokhortchouk, A., Reddington, J. P., Madej, M. J., Dunican, D. S., et al. (2009). The Interaction of xKaiso with xTcf3: A Revised Model for Integration of Epigenetic and Wnt Signalling Pathways. *Development* 136, 723–727. doi:10.1242/dev.025577

Salomonis, N., Schlieve, C. R., Pereira, L., Wahlquist, C., Colas, A., Zambon, A. C., et al. (2010). Alternative Splicing Regulates Mouse Embryonic Stem Cell Pluripotency and Differentiation. *Proc. Natl. Acad. Sci. U S A.* 107, 10514–10519. doi:10.1073/pnas.0912260107

Sato, M., Kojima, T., Michiue, T., and Saigo, K. (1999). Bar Homeobox Genes Are Latitudinal Prepattern Genes in the Developing Drosophila Notum Whose Expression Is Regulated by the Concerted Functions of Decapentaplegic and Wingless. *Development* 126, 1457–1466. doi:10.1242/dev.126.7.1457

Schneider, S., Steinbeisser, H., Warga, R. M., and Hausen, P. (1996). Beta-catenin Translocation into Nuclei Demarcates the Dorsalizing Centers in Frog and Fish Embryos. *Mech. Dev.* 57, 191–198. doi:10.1016/0925-4773(96)00546-1

Scholpp, S., Foucher, I., Staudt, N., Peukert, D., Lumsden, A., and Houart, C. (2007). Otx1l, Otx2 and Irx1b Establish and Position the ZLI in the Diencephalon. *Development* 134, 3167–3176. doi:10.1242/dev.001461

Scholpp, S., Wolf, O., Brand, M., and Lumsden, A. (2006). Hedgehog Signalling from the Zona Limitans Intrathalamica Orchestrates Patterning of the Zebrafish Diencephalon. *Development* 133, 855–864. doi:10.1242/dev.02248

Schuhmacher, L. N., Albadri, S., Ramialison, M., and Poggi, L. (2011). Evolutionary Relationships and Diversification of Barhl Genes within Retinal Cell Lineages. *BMC Evol. Biol.* 11, 340. doi:10.1186/1471-2148-11-340

Schuijers, J., Mokry, M., Hatzis, P., Cuppen, E., and Clevers, H. (2014). Wnt-induced Transcriptional Activation Is Exclusively Mediated by TCF/LEF. *EMBO J.* 33, 146–156. doi:10.1002/embj.201385358

Schwartz, H. T., and Horvitz, H. R. (2007). The C. elegans Protein CEH-30 Protects Male-specific Neurons from Apoptosis Independently of the Bcl-2 Homolog CED-9. *Genes Dev.* 21, 3181–3194. doi:10.1101/gad.1607007

Sekiya, T., and Zaret, K. S. (2007). Repression by Groucho/TLE/Grg Proteins: Genomic Site Recruitment Generates Compacted Chromatin In Vitro and Impairs Activator Binding In Vivo. *Mol. Cel* 28, 291–303. doi:10.1016/j.molcel.2007.10.002

Sellak, H., Wu, S., and Lincoln, T. M. (2012). KLF4 and SOX9 Transcription Factors Antagonize β-catenin and Inhibit TCF-Activity in Cancer Cells. *Biochim. Biophys. Acta* 1823, 1666–1675. doi:10.1016/j.bbamcr.2012.06.027

Selvadurai, H. J., and Mason, J. O. (2011). Wnt/β-catenin Signalling Is Active in a Highly Dynamic Pattern During Development of the Mouse Cerebellum. *PLoS One* 6, e23012. doi:10.1371/journal.pone.0023012

Sena, E., Bou-Rouphael, J., Rocques, N., Carron-Homo, C., and Durand, B. C. (2020). Mcl1 Protein Levels and Caspase-7 Executioner Protease Control Axial Organizer Cells Survival. *Dev. Dyn.* 249, 847–866. doi:10.1002/dvdy.169

Sena, E., Feistel, K., and Durand, B. C. (2016). An Evolutionarily Conserved Network Mediates Development of the Zona Limitans Intrathalamica, A Sonic Hedgehog-Secreting Caudal Forebrain Signaling Center. *J. Dev. Biol.* 4, 31. doi:10.3390/jdb4040031

Sena, E., Rocques, N., Borday, C., Amin, H. S. M., Parain, K., Sitbon, D., et al. (2019). Barhl2 Maintains T-Cell Factors as Repressors, and Thereby Switches off the Wnt/β-Catenin Response Driving Spemann Organizer Formation. *Development* 146, dev 173112. doi:10.1242/dev.173112

Session, A. M., Uno, Y., Kwon, T., Chapman, J. A., Toyoda, A., Takahashi, S., et al. (2016). Genome Evolution in the Allotetraploid Frog Xenopus laevis. *Nature* 538, 336–343. doi:10.1038/nature19840

Shetty, P., Lo, M. C., Robertson, S. M., and Lin, R. (2005). C. elegans TCF Protein, POP-1, Converts from Repressor to Activator as a Result of Wnt-Induced

Lowering of Nuclear Levels. *Dev. Biol.* 285, 584–592. doi:10.1016/j.ydbio.2005.07.008

Shimogori, T., VanSant, J., Paik, E., and Grove, E. A. (2004). Members of the Wnt, Fz, and Frp Gene Families Expressed in Postnatal Mouse Cerebral Cortex. *J. Comp. Neurol.* 473, 496–510. doi:10.1002/cne.20135

S. Hoppler and R. T. Moon (Editors) (2014). *Wnt Signaling in Development and Disease: Molecular Mechanisms and Biological Functions* (Hoboken, NJ: Wiley Blackwell).

Shy, B. R., Wu, C. I., Khramtsova, G. F., Zhang, J. Y., Olopade, O. I., Goss, K. H., et al. (2013). Regulation of Tcf7l1 DNA Binding and Protein Stability as Principal Mechanisms of Wnt/β-Catenin Signaling. *Cel Rep* 4, 1–9. doi:10.1016/j.celrep.2013.06.001

Sinner, D., Kordich, J. J., Spence, J. R., Opoka, R., Rankin, S., Lin, S.-C. J., et al. (2007). Sox17 and Sox4 Differentially Regulate β-Catenin/T-Cell Factor Activity and Proliferation of Colon Carcinoma Cells. *Mol. Cel Biol* 27, 7802–7815. doi:10.1128/MCB.02179-06

Smith, S. T., and Jaynes, J. B. (1996). A Conserved Region of Engrailed, Shared Among All En-, Gsc-, Nk1-, Nk2- and Msh-Class Homeoproteins, Mediates Active Transcriptional Repression In Vivo. *Development* 122, 3141–3150. doi:10.1242/dev.122.10.3141

Söderholm, S., and Cantù, C. (2021). The WNT/β-catenin Dependent Transcription: A Tissue-specific Business. *WIREs Mech. Dis.* 13, e1511. doi:10.1002/wsbm.1511

Sokol, S., Christian, J. L., Moon, R. T., and Melton, D. A. (1991). Injected Wnt RNA Induces a Complete Body Axis in Xenopus Embryos. *Cell* 67, 741–752. doi:10.1016/0092-8674(91)90069-B

Sokol, S. Y. (2011). Maintaining Embryonic Stem Cell Pluripotency with Wnt Signaling. *Development* 138, 4341–4350. doi:10.1242/dev.066209

Spemann, H., and Mangold, H. (1924). über Induktion von Embryonalanlagen durch Implantation artfremder Organisatoren. *Archiv für mikroskopische Anatomie und Entwicklungsmechanik* 100, 599–638. doi:10.1007/BF02108133

Standley, H. J., Destrée, O., Kofron, M., Wylie, C., and Heasman, J. (2006). Maternal XTcf1 and XTcf4 Have Distinct Roles in Regulating Wnt Target Genes. *Dev. Biol.* 289, 318–328. doi:10.1016/j.ydbio.2005.10.012

Staudt, N., and Houart, C. (2007). The Prethalamus Is Established during Gastrulation and Influences Diencephalic Regionalization. *Plos Biol.* 5, e69. doi:10.1371/journal.pbio.0050069

Stern, C. D. (2002). Induction and Initial Patterning of the Nervous System - the Chick Embryo Enters the Scene. *Curr. Opin. Genet. Dev.* 12, 447–451. doi:10.1016/S0959-437X(02)00324-6

Stevens, M. L., Chaturvedi, P., Rankin, S. A., Macdonald, M., Jagannathan, S., Yukawa, M., et al. (2017). Genomic Integration of Wnt/β-Catenin and BMP/Smad1 Signaling Coordinates Foregut and Hindgut Transcriptional Programs. *Development* 144, 1283–1295. doi:10.1242/dev.145789

Sulston, J. E., Schierenberg, E., White, J. G., and Thomson, J. N. (1983). The Embryonic Cell Lineage of the Nematode Caenorhabditis elegans. *Dev. Biol.* 100, 64–119. doi:10.1016/0012-1606(83)90201-4

Tabar, V., and Studer, L. (2014). Pluripotent Stem Cells in Regenerative Medicine: Challenges and Recent Progress. *Nat. Rev. Genet.* 15, 82–92. doi:10.1038/nrg3563

Taelman, V. F., Dobrowolski, R., Plouhinec, J. L., Fuentealba, L. C., Vorwald, P. P., Gumper, I., et al. (2010). Wnt Signaling Requires Sequestration of Glycogen Synthase Kinase 3 inside Multivesicular Endosomes. *Cell.* 143, 1136–1148. doi:10.1016/j.cell.2010.11.034

Tam, W.-L., Lim, C. Y., Han, J., Zhang, J., Ang, Y.-S., Ng, H.-H., et al. (2008). T-cell Factor 3 Regulates Embryonic Stem Cell Pluripotency and Self-Renewal by the Transcriptional Control of Multiple Lineage Pathways. *Stem Cells* 26, 2019–2031. doi:10.1634/stemcells.2007-1115

ten Berge, D., Kurek, D., Blauwkamp, T., Koole, W., Maas, A., Eroglu, E., et al. (2011). Embryonic Stem Cells Require Wnt Proteins to Prevent Differentiation to Epiblast Stem Cells. *Nat. Cel Biol.* 13, 1070–1075. doi:10.1038/ncb2314

Teratani-Ota, Y., Yamamizu, K., Piao, Y., Sharova, L., Amano, M., Yu, H., et al. (2016). Induction of Specific Neuron Types by Overexpression of Single Transcription Factors. *In Vitro Cel Dev Biol Anim.* 52, 961–973. doi:10.1007/s11626-016-0056-7

Thomas, K. R., and Capecchi, M. R. (1990). Targeted Disruption of the Murine Int-1 Proto-Oncogene Resulting in Severe Abnormalities in Midbrain and Cerebellar Development. *Nature* 346, 847–850. doi:10.1038/346847a0

Thorpe, C. J., Schlesinger, A., Carter, J. C., and Bowerman, B. (1997). Wnt Signaling Polarizes an Early C. elegans Blastomere to Distinguish Endoderm from Mesoderm. *Cell* 90, 695–705. doi:10.1016/S0092-8674(00)80530-9

Topol, L., Chen, W., Song, H., Day, T. F., and Yang, Y. (2009). Sox9 Inhibits Wnt Signaling by Promoting β-Catenin Phosphorylation in the Nucleus. *J. Biol. Chem.* 284, 3323–3333. doi:10.1074/jbc.M808048200

Travis, A., Amsterdam, A., Belanger, C., and Grosschedl, R. (1991). LEF-1, a Gene Encoding a Lymphoid-specific Protein with an HMG Domain, Regulates T-Cell Receptor Alpha Enhancer Function [corrected]. *Genes Dev.* 5, 880–894. doi:10.1101/gad.5.5.880

Tsuji, S., and Hashimoto, C. (2005). Choice of Either Beta-Catenin or Groucho/TLE as a Co-factor for Xtcf-3 Determines Dorsal-Ventral Cell Fate of Diencephalon during Xenopus Development. *Dev. Genes Evol.* 215, 275–284. doi:10.1007/s00427-005-0474-0

Turki-Judeh, W., and Courey, A. J. (2012). Groucho: A Corepressor with Instructive Roles in Development. *Curr. Top. Dev. Biol.* 98, 65–96. doi:10.1016/B978-0-12-386499-4.00003-3

Valenta, T., Lukas, J., and Korinek, V. (2003). HMG Box Transcription Factor TCF-4's Interaction with CtBP1 Controls the Expression of the Wnt Target Axin2/Conductin in Human Embryonic Kidney Cells. *Nucleic Acids Res.* 31, 2369–2380. doi:10.1093/nar/gkg346

Valentine, S. A., Chen, G., Shandala, T., Fernandez, J., Mische, S., Saint, R., et al. (1998). Dorsal-mediated Repression Requires the Formation of a Multiprotein Repression Complex at the Ventral Silencer. *Mol. Cel Biol.* 18, 6584–6594. doi:10.1128/MCB.18.11.6584

van Amerongen, R., and Nusse, R. (2009). Towards an Integrated View of Wnt Signaling in Development. *Development* 136, 3205–3214. doi:10.1242/dev.033910

van Beest, M., Dooijes, D., van de Wetering, M., Kjaerulff, S., Bonvin, A., Nielsen, O., et al. (2000). Sequence-specific High Mobility Group Box Factors Recognize 10–12-Base Pair Minor Groove Motifs. *J. Biol. Chem.* 275, 27266–27273. doi:10.1016/S0021-9258(19)61506-1

van de Wetering, M., Cavallo, R., Dooijes, D., van Beest, M., van Es, J., Loureiro, J., et al. (1997). Armadillo Coactivates Transcription Driven by the Product of the Drosophila Segment Polarity Gene dTCF. *Cell* 88, 789–799. doi:10.1016/S0092-8674(00)81925-X

van de Wetering, M., Oosterwegel, M., Dooijes, D., and Clevers, H. (1991). Identification and Cloning of TCF-1, a T Lymphocyte-specific Transcription Factor Containing a Sequence-specific HMG Box. *EMBO J.* 10, 123–132. doi:10.1002/j.1460-2075.1991.tb07928.x

van Genderen, C., Okamura, R. M., Farinas, I., Quo, R.-G., Parslow, T. G., Bruhn, L., et al. (1994). Development of Several Organs That Require Inductive Epithelial-Mesenchymal Interactions Is Impaired in LEF-1-Deficient Mice. *Genes Dev.* 8, 2691–2703.

Veien, E. S., Grierson, M. J., Saund, R. S., and Dorsky, R. I. (2005). Expression Pattern of Zebrafish Tcf7 Suggests Unexplored Domains of Wnt/beta-Catenin Activity. *Dev. Dyn.* 233, 233–239. doi:10.1002/dvdy.20330

Vermeulen, L., De Sousa E Melo, F., van der Heijden, M., Cameron, K., de Jong, J. H., Borovski, T., et al. (2010). Wnt Activity Defines Colon Cancer Stem Cells and Is Regulated by the Microenvironment. *Nat. Cel Biol.* 12, 468–476. doi:10.1038/ncb2048

Vieira, C., and Martinez, S. (2006). Sonic Hedgehog from the Basal Plate and the Zona Limitans Intrathalamica Exhibits Differential Activity on Diencephalic Molecular Regionalization and Nuclear Structure. *Neuroscience* 143, 129–140. doi:10.1016/j.neuroscience.2006.08.032

Walcher, L., Kistenmacher, A. K., Suo, H., Kitte, R., Dluczek, S., Strauß, A., et al. (2020). Cancer Stem Cells-Origins and Biomarkers: Perspectives for Targeted Personalized Therapies. *Front. Immunol.* 11, 1280. doi:10.3389/fimmu.2020.01280

Wang, J., Garancher, A., Ramaswamy, V., and Wechsler-Reya, R. J. (2018). Medulloblastoma: From Molecular Subgroups to Molecular Targeted Therapies. *Annu. Rev. Neurosci.* 41, 207–232. doi:10.1146/annurev-neuro-070815-013838

Wang, W., Wang, Y. G., Reginato, A. M., Glotzer, D. J., Fukai, N., Plotkina, S., et al. (2004). Groucho Homologue Grg5 Interacts with the Transcription Factor Runx2-Cbfa1 and Modulates its Activity during Postnatal Growth in Mice. *Dev. Biol.* 270, 364–381. doi:10.1016/j.ydbio.2004.03.003

Wang, Y., He, L., Du, Y., Zhu, P., Huang, G., Luo, J., et al. (2015). The Long Noncoding RNA lncTCF7 Promotes Self-Renewal of Human Liver Cancer Stem Cells Through Activation of Wnt Signaling. *Cell Stem Cell.* 16, 413–425. doi:10.1016/j.stem.2015.03.003

Wessely, O., and De Robertis, E. M. (2002). Neural Plate Patterning by Secreted Signals. *Neuron.* 33, 489–491. doi:10.1016/s0896-6273(02)00596-2

Wiese, K. E., Nusse, R., and van Amerongen, R. (2018). Wnt Signalling: Conquering Complexity. *Development.* 145, dev165902. doi:10.1242/dev.165902

Williams, R. L., Hilton, D. J., Pease, S., Willson, T. A., Stewart, C. L., Gearing, D. P., et al. (1988). Myeloid Leukaemia Inhibitory Factor Maintains the Developmental Potential of Embryonic Stem Cells. *Nature.* 336, 684–687. doi:10.1038/336684a0

Wills, A. E., and Baker, J. C. (2015). E2a Is Necessary for Smad2/3-dependent Transcription and the Direct Repression of Lefty During Gastrulation. *Dev. Cel.* 32, 345–357. doi:10.1016/j.devcel.2014.11.034

Wilson, S. W., and Houart, C. (2004). Early Steps in the Development of the Forebrain. *Develop. Cel.* 6, 167–181. doi:10.1016/S1534-5807(04)00027-9

Wizeman, J. W., Guo, Q., Wilion, E. M., and Li, J. Y. (2019). Specification of Diverse Cell Types during Early Neurogenesis of the Mouse Cerebellum. *Elife.* 8, e42388. doi:10.7554/eLife.42388

Wray, J., and Hartmann, C. (2012). WNTing Embryonic Stem Cells. *Trends Cel Biol.* 22, 159–168. doi:10.1016/j.tcb.2011.11.004

Wray, J., Kalkan, T., Gomez-Lopez, S., Eckardt, D., Cook, A., Kemler, R., et al. (2011). Inhibition of Glycogen Synthase Kinase-3 Alleviates Tcf3 Repression of the Pluripotency Network and Increases Embryonic Stem Cell Resistance to Differentiation. *Nat. Cel Biol.* 13, 838–845. doi:10.1038/ncb2267

Xia, Z., Guo, M., and Ma, H. (2011). Functional Analysis of Novel Phosphorylation Sites of CREB-Binding Protein Using Mass Spectrometry and Mammalian Two-Hybrid Assays. *Proteomics* 11, 3444–3451. doi:10.1002/pmic.201100121

Yaklichkin, S., Vekker, A., Stayrook, S., Lewis, M., and Kessler, D. S. (2007). Prevalence of the EH1 Groucho Interaction Motif in the Metazoan Fox Family of Transcriptional Regulators. *BMC Genomics.* 8, 201. doi:10.1186/1471-2164-8-201

Yamamizu, K., Sharov, A. A., Piao, Y., Amano, M., Yu, H., Nishiyama, A., et al. (2016). Generation and Gene Expression Profiling of 48 Transcription-Factor-Inducible Mouse Embryonic Stem Cell Lines. *Sci. Rep.* 6, 25667. doi:10.1038/srep25667

Yang, S. H., Kalkan, T., Morrisroe, C., Smith, A., and Sharrocks, A. D. (2012). A Genome-wide RNAi Screen Reveals MAP Kinase Phosphatases as Key ERK Pathway Regulators During Embryonic Stem Cell Differentiation. *Plos Genet.* 8, e1003112. doi:10.1371/journal.pgen.1003112

Yao, Y., Minor, P. J., Zhao, Y. T., Jeong, Y., Pani, A. M., King, A. N., et al. (2016). Cis-regulatory Architecture of a Brain Signaling Center Predates the Origin of Chordates. *Nat. Genet.* 48, 575–580. doi:10.1038/ng.3542

Yasuoka, Y., Suzuki, Y., Takahashi, S., Someya, H., Sudou, N., Haramoto, Y., et al. (2014). Occupancy of Tissue-specific Cis-Regulatory Modules by Otx2 and TLE/Groucho for Embryonic Head Specification. *Nat. Commun.* 5, 4322. doi:10.1038/ncomms5322

Ye, S., Zhang, T., Tong, C., Zhou, X., He, K., Ban, Q., et al. (2017). Depletion of *Tcf3* and *Lef1* Maintains Mouse Embryonic Stem Cell Self-Renewal. *Biol. Open, bio.* 6, 511–517. doi:10.1242/bio.022426

Yeung, J., Ha, T. J., Swanson, D. J., Choi, K., Tong, Y., and Goldowitz, D. (2014). Wls Provides a New Compartmental View of the Rhombic Lip in Mouse Cerebellar Development. *J. Neurosci.* 34, 12527–12537. doi:10.1523/JNEUROSCI.1330-14.2014

Yi, F., Pereira, L., Hoffman, J. A., Shy, B. R., Yuen, C. M., Liu, D. R., et al. (2011). Opposing Effects of Tcf3 and Tcf1 Control Wnt Stimulation of Embryonic Stem Cell Self-Renewal. *Nat. Cel Biol.* 13, 762–770. doi:10.1038/ncb2283

Ying, Q. L., Nichols, J., Chambers, I., and Smith, A. (2003). BMP Induction of Id Proteins Suppresses Differentiation and Sustains Embryonic Stem Cell Self-Renewal in Collaboration with STAT3. *Cell.* 115, 281–292. doi:10.1016/S0092-8674(03)00847-X

Ying, Q. L., Wray, J., Nichols, J., Batlle-Morera, L., Doble, B., Woodgett, J., et al. (2008). The Ground State of Embryonic Stem Cell Self-Renewal. *Nature.* 453, 519–523. doi:10.1038/nature06968

Young, R. M., Ewan, K. B., Ferrer, V. P., Allende, M. L., Godovac-Zimmermann, J., Dale, T. C., et al. (2019). Developmentally Regulated Tcf7l2 Splice Variants Mediate Transcriptional Repressor Functions During Eye Formation. *Elife.* 8, e51447. doi:10.7554/eLife.51447

Zeng, L., Fagotto, F., Zhang, T., Hsu, W., Vasicek, T. J., Perry, W. L., et al. (1997). The Mouse Fused Locus Encodes Axin, an Inhibitor of the Wnt Signaling Pathway that Regulates Embryonic Axis Formation. *Cell.* 90, 181–192. doi:10.1016/S0092-8674(00)80324-4

Zhan, T., Rindtorff, N., and Boutros, M. (2017). Wnt Signaling in Cancer. *Oncogene.* 36, 1461–1473. doi:10.1038/onc.2016.304

Zhang, X., Peterson, K. A., Liu, X. S., McMahon, A. P., and Ohba, S. (2013). Gene Regulatory Networks Mediating Canonical Wnt Signal-Directed Control of Pluripotency and Differentiation in Embryo Stem Cells. *Stem Cells.* 31, 2667–2679. doi:10.1002/stem.1371

Zhang, Y., and Wang, X. (2020). Targeting the Wnt/β-Catenin Signaling Pathway in Cancer. *J. Hematol. Oncol.* 13, 165. doi:10.1186/s13045-020-00990-3

Žídek, R., Machoň, O., and Kozmik, Z. (2018). Wnt/β-catenin Signalling Is Necessary for Gut Differentiation in a Marine Annelid, Platynereis Dumerilii. *EvoDevo.* 9, 14. doi:10.1186/s13227-018-0100-7

Conflict of Interest: The authors declare that the research was conducted in the absence of any commercial or financial relationships that could be construed as a potential conflict of interest.

Publisher's Note: All claims expressed in this article are solely those of the authors and do not necessarily represent those of their affiliated organizations, or those of the publisher, the editors and the reviewers. Any product that may be evaluated in this article, or claim that may be made by its manufacturer, is not guaranteed or endorsed by the publisher.

frontiers in Cell and Developmental Biology

REVIEW
published: 29 November 2021
doi: 10.3389/fcell.2021.782445

Review: The Role of Wnt/β-Catenin Signalling in Neural Crest Development in Zebrafish

Gemma Sutton[1], *Robert N. Kelsh*[2] *and Steffen Scholpp*[1]*

[1]Living Systems Institute, School of Biosciences, College of Life and Environmental Sciences, University of Exeter, Exeter, United Kingdom, [2]Department of Biology and Biochemistry, University of Bath, Bath, United Kingdom

The neural crest (NC) is a multipotent cell population in vertebrate embryos with extraordinary migratory capacity. The NC is crucial for vertebrate development and forms a myriad of cell derivatives throughout the body, including pigment cells, neuronal cells of the peripheral nervous system, cardiomyocytes and skeletogenic cells in craniofacial tissue. NC induction occurs at the end of gastrulation when the multipotent population of NC progenitors emerges in the ectodermal germ layer in the neural plate border region. In the process of NC fate specification, fate-specific markers are expressed in multipotent progenitors, which subsequently adopt a specific fate. Thus, NC cells delaminate from the neural plate border and migrate extensively throughout the embryo until they differentiate into various cell derivatives. Multiple signalling pathways regulate the processes of NC induction and specification. This review explores the ongoing role of the Wnt/β-catenin signalling pathway during NC development, focusing on research undertaken in the Teleost model organism, zebrafish (*Danio rerio*). We discuss the function of the Wnt/β-catenin signalling pathway in inducing the NC within the neural plate border and the specification of melanocytes from the NC. The current understanding of NC development suggests a continual role of Wnt/β-catenin signalling in activating and maintaining the gene regulatory network during NC induction and pigment cell specification. We relate this to emerging models and hypotheses on NC fate restriction. Finally, we highlight the ongoing challenges facing NC research, current gaps in knowledge, and this field's potential future directions.

Keywords: Wnt/β-catenin signalling, neural crest, gene regulatory network, NC induction, NC specification, pigment cells, melanocyte, Zebrafish

OPEN ACCESS

Edited by:
Kerstin Feistel,
University of Hohenheim, Germany

Reviewed by:
Kristin Artinger,
University of Colorado Anschutz Medical Campus, United States
Jan Kaslin,
Australian Regenerative Medicine Institute (ARMI), Australia

***Correspondence:**
Steffen Scholpp
s.scholpp@exeter.ac.uk

Specialty section:
This article was submitted to Morphogenesis and Patterning, a section of the journal Frontiers in Cell and Developmental Biology

Received: *24 September 2021*
Accepted: *16 November 2021*
Published: *29 November 2021*

Citation:
Sutton G, Kelsh RN and Scholpp S (2021) Review: The Role of Wnt/β-Catenin Signalling in Neural Crest Development in Zebrafish. Front. Cell Dev. Biol. 9:782445. doi: 10.3389/fcell.2021.782445

INTRODUCTION

The neural crest (NC) is a transient and multipotent embryonic cell population with extraordinary migratory capacity. The NC is crucial for vertebrate development and is an entire model system in its own right in developmental biology. NC cells (NCCs) give rise to many cell derivatives, including body pigment cells, neuronal cells of the peripheral nervous system, cardiomyocytes, and skeletogenic cells in craniofacial tissue (Le Douarin, 1999). Although recently an NC rudiment was identified in tunicates (Abitua et al., 2012), the NC is considered as an evolutionary novelty of vertebrates that facilitated the emergence of the specialised vertebrate cranium, including the hinged jaw, specialised neural structures and sensory organs (Gans and Northcutt, 1983). This emergence of the NC population and the

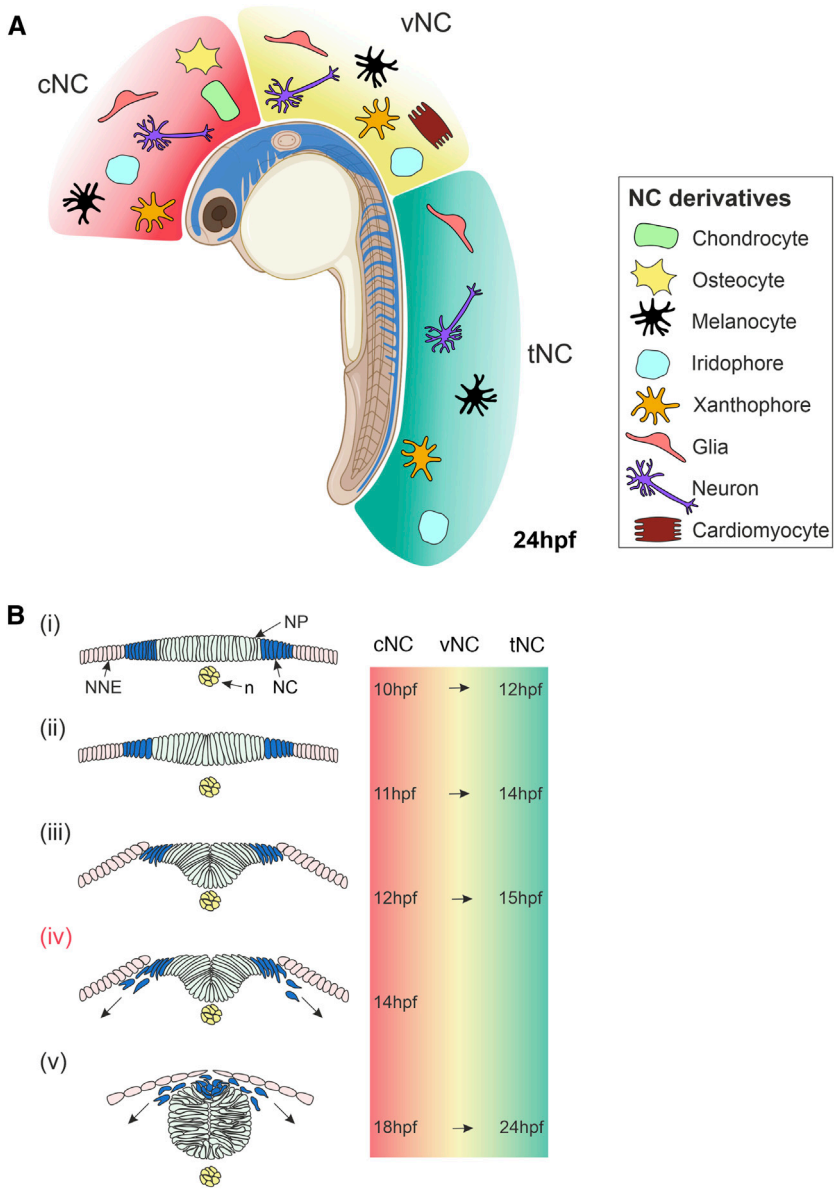

FIGURE 1 | Overview of Neural Crest Development in Zebrafish. **(A)** Lateral view of a zebrafish embryo at 24 hpf showing NC cells (blue). The NC is subdivided along the anteroposterior axis into cNC, vNC and tNC, indicated in red, yellow and green, respectively. These NC populations give rise to different NC derivatives. **(B)** Cross-sections of zebrafish embryo showing NC cells emerge, delaminate and start migrating. **(i)** NC cells originate in the neural plate border at the interface of the NNE and NP. **(ii,iii)** NC cells begin to delaminate during the formation of the neural keel. **(iv)** Cranial NC cells begin migrating as the neural keel folds up (Schilling and Kimmel, 1994). **(v)** When the neural rod has formed., NC cells emerge from the neural plate border and the dorsal neural tube, delaminate and begin migrating around the embryo. The times at which these stages of NC development occur in zebrafish are indicated on the right for cNC at the level of the midbrain and for tNC at the level of the somites. The time of onset of vNC migration is yet to be defined. Schematics of transverse sections of zebrafish embryos indicate dorsal to the top **(Bi–v)**. cNC, cranial neural crest; vNC, vagal neural crest; tNC, trunk neural crest; NC, neural crest; NP, neural plate; NNE, non-neural ectoderm; n, notochord; hpf, hours post-fertilisation. Created with BioRender.com.

"new head" enabled vertebrates to acquire active feeding behaviours and contributed to the remarkable radiation of the vertebrate lineage (Hall, 2000).

NC development begins during early embryogenesis, specifically during gastrulation, in the ectodermal germ layer and proceeds concurrently with neurulation (**Figure 1**). The NC is induced within a region of ectoderm located at the non-neural and neural ectoderm interface, known as the neural plate border (NPB). NCCs undergo epithelial-to-mesenchymal transition (EMT) in an anterior-posterior (AP) progression and migrate large distances across the embryo, during which they integrate a wide array of signals and execute a complex choreography of gene regulatory changes until their final cell fates at their final destinations in the body are determined. The timing of the

specification of multipotent NCC progenitors towards their final cellular fate is only partially defined; for the better-studied melanocytes, it is thought to initiate prior to migration.

Developmental biologists have used various vertebrate model organisms to gain insight into the fundamental biology of the NC, including zebrafish, amphibians, chicks and mice. In the mid-20th century, the quail-chick chimaera system advanced NC research, uncovering specific migratory pathways and cell fates (Le Douarin, 1973). In these fundamental fate-mapping studies, homotopic and heterotopic transplantation of quail NCCs to chick embryos enabled the regional fate mapping of NCCs *in vivo* and established NC plasticity (Le Douarin, 1999). At the end of the 20th century, similar fate-mapping experiments were carried out in zebrafish by microinjecting fluorescent dyes and imaging by light and electron microscopy (Raible et al., 1992; Schilling and Kimmel, 1994). These studies demonstrated the extraordinary potency of the NC and revealed the conservation of NCC derivatives and migratory pathways in zebrafish and other vertebrates. Subsequently, one study extended these iontophoretic labelling investigations, confirming both the apparent fate-restriction of many NCCs and the small size of wild-type zebrafish NCC clones. It also characterised a partial failure of NC migration and fate specification in the zebrafish mutants of Sox10 transcription factor (Dutton et al., 2001).

The NC fate map demonstrated discrete populations of NCCs along the AP axis, which are conserved across the vertebrate models investigated. Cranial NC is the anterior-most NC population that emerges from the NPB, adjacent to the midbrain and hindbrain position of the developing embryo (Kague et al., 2012). Cranial NC derivatives contribute to the craniofacial skeleton and gills, as well as neurons of the sensory and parasympathetic ganglia and pigment cells (**Figure 1A**) (Kague et al., 2012; Lee et al., 2013; Mongera et al., 2013; Schilling and Kimmel, 1994). Trunk NC cells are located more posteriorly, originating along the spinal cord, adjacent to the somites. Trunk NC forms neuronal and glial derivatives in the dorsal root ganglia (DRG), sympathetic and parasympathetic ganglia, and pigment cells (**Figure 1A**) (An et al., 2002; Raible and Eisen, 1994; Raible et al., 1992). The cardiac/vagal NC domain is located between the trunk and cranial NC. This neural crest population spans from immediately rostral to the otic vesicle to caudal to somite 6 (Sato and Yost, 2003). The precise AP boundaries of the zebrafish cardiac/vagal NC domain remain to be fully defined. However, cells from this NC group are essential for zebrafish heart looping and contribute neurons and glia to the enteric nervous system (**Figure 1A**) (Shepherd et al., 2004; Elworthy et al., 2005; Olden et al., 2008). A recent study suggests that two distinct populations of cardiac/vagal NC migrate to the heart, with one population forming cardiomyocytes in the heart tube and the other migrating to the bulbus arteriosus (Cavanaugh et al., 2015). Pigment cells are a ubiquitous feature of the NC and are not regionally localised. Paracrine signalling from surrounding cells is essential for the specification of these various NC derivatives; however, many aspects of this communication process and its implication in fate restriction is not well understood.

During vertebrate development, the Wnt/β-catenin signalling pathway acts as a long-range morphogen system providing concentration-dependent positional information in many tissues and organs. Moreover, many experimental observations from multiple model systems suggested that the Wnt/β-catenin signalling pathway is essential for the emergence of the NC. For example, in *Xenopus* animal cap explants, over-expression of Wnt ligands induces expression of NC markers, whereas expression of dominant-negative Wnts represses the expression of these markers (SaintJeannet et al., 1997; Chang and Hemmati-Brivanlou, 1998; LaBonne and Bronner-Fraser, 1998; Bang et al., 1999; Tan et al., 2001; Villanueva et al., 2002). Similarly, in avian embryos, inhibition of Wnt/β-catenin signalling blocks NC marker expression and the addition of Wnt to neural tube explants is sufficient to induce NC (Garcia-Castro et al., 2002). Furthermore, exogenous Wnt/β-catenin signalling can induce NC in human inducible pluripotent stem cells (Gomez et al., 2019).

There is also extensive evidence supporting the requirement of Wnt/β-catenin signalling after forming the NC during the selection of differentiation pathways, reversible fate specification followed by final, irreversible fate determination. For example, in mice, Wnt/β-catenin signalling promotes the specification of sensory neurons and melanocytes over alternative NC fates (Hari et al., 2002; Lee et al., 2004). Furthermore, in zebrafish, activation of Wnt/β-catenin signalling in the pre-migratory NC promotes pigment cell types at the expense of neuronal cell fates (Dorsky et al., 1998). These findings have led to the perception that the Wnt/β-catenin signalling pathway is required in two stages of NC development, firstly in NC induction and secondly in the specification of NC derivatives.

This review will primarily discuss NC induction and specification processes, with a focus on pigment cell determination. We will provide an extensive analysis of the role of the Wnt/β-catenin signalling pathway during these stages of NC development. We will highlight contributions from studies undertaken in the Teleost model organism, zebrafish, and compare and contrast these to findings from other vertebrate model systems. Although zebrafish was a relatively late arrival to NC research compared to other model organisms, we believe this model excels in studies of NC development, particularly in fate specification. Zebrafish is now established at the forefront of NC research due to the powerful genetic and transgenic tools available and transparent embryos that make ideal samples for high- and super-resolution imaging. Finally, we will discuss the potential future directions of Wnt/β-catenin signalling research in the context of the NC and anticipate the upcoming challenges of this field.

The Wnt/β-Catenin Signalling Pathway

Wnt proteins are secreted ligands that activate signalling pathways that regulate many developmental processes (Angers and Moon, 2009; Nusse and Clevers, 2017). Wnt signalling controls pattern formation and cell behaviour through changes in gene expression and cell morphology. Wnt signal transduction pathways are classified as β-catenin dependent (also known as the canonical pathway) or β-catenin

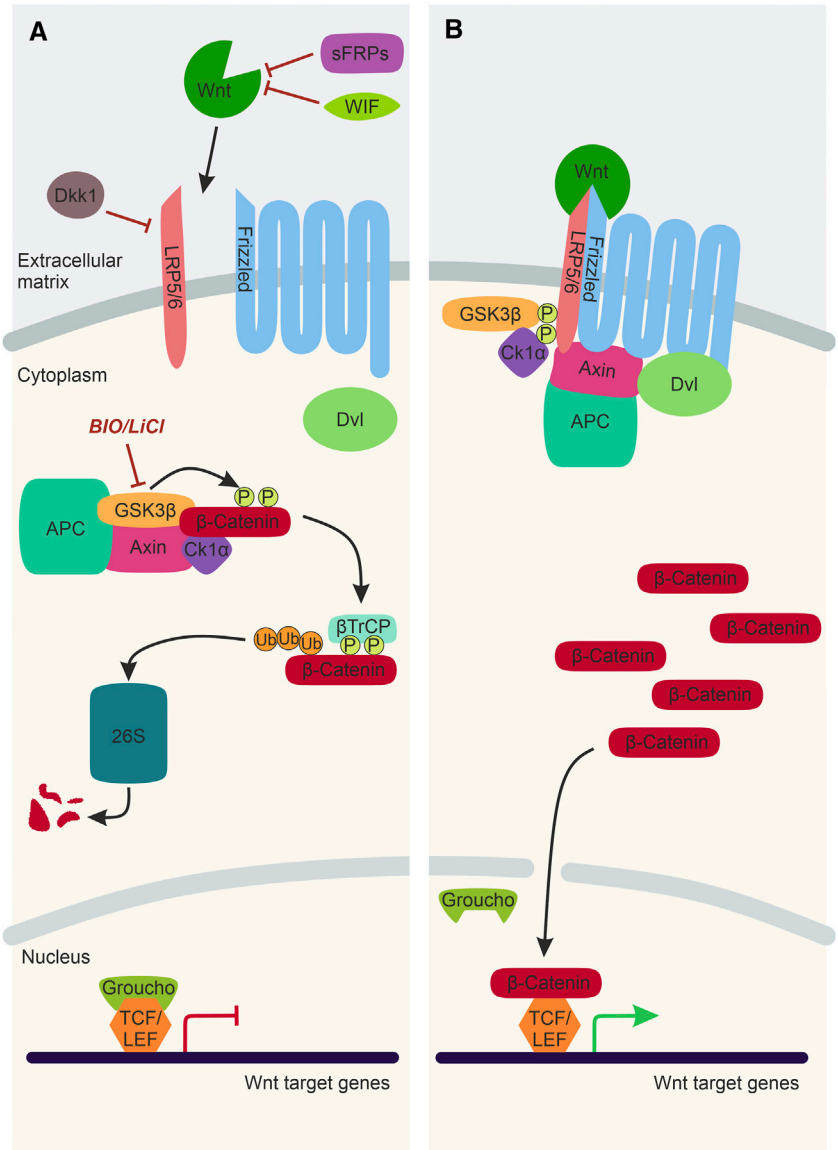

FIGURE 2 | The Wnt/β-catenin Signalling Pathway. **(A)** In the absence of a Wnt ligand, transcription co-activator β-catenin is phosphorylated by the destruction complex, composed of Gsk3β, Axin, CK1α and APC. Following phosphorylation, β-catenin is ubiquitinated by βTrCP and sent to the 26S proteasome for degradation. Thus, Wnt target genes, which are repressed by TCF/LEF factors and Groucho, cannot be expressed. Activation of the Wnt/β-catenin signalling pathway can be inhibited by WIF and sFRPs and Dkk1. LiCl and BIO are chemical inhibitors of Gsk3β, which can be used experimentally to stimulate Wnt/β-catenin signalling. **(B)** In the presence of a Wnt ligand, the Wnt binds to Frizzled and Lrp5/6 co-receptors. This sequesters Dvl, Axin and the destruction complex to the plasma membrane. As a result, the destruction complex is inactivated, and β-catenin is no longer degraded and can translocate to the nucleus, bind to TCF/Lef factors and activate Wnt target gene expression. Lrp5/6, lipoprotein receptor-related protein-5/6; WIF, Wnt-inhibitory factor; sFRP, secreted Frizzled-related protein; Dkk1, Dickkopf1; Dvl, Dishevelled; Gsk3β, Glycogen synthase kinase 3β; APC, Adenomatous polyposis coli; CK1α, Casein kinase 1α; βTrCP, ubiquitin ligase; 26S, 26S proteasome; TCF/LEF, T cell factor/ lymphoid enhancer factor.

independent (the non-canonical pathways). The type of Wnt signalling pathway activated depends on the combination of Wnt ligands, receptors and co-receptors, and the cellular context (Niehrs, 2012). There is significant variation in the number of Wnt genes between different species. For example, 19 Wnt genes have been identified in humans and mice, whereas zebrafish can have up to 25 Wnt genes due to the teleost-specific whole-genome duplication (Miller, 2002; Duncan et al., 2015; Ruzicka et al., 2019). There are also a variety of Wnt receptors and co-receptors. The seven-pass-membrane protein Frizzled is the predominant receptor of Wnt signalling pathways. Mammals have 10 Frizzled genes, and zebrafish are predicted to have at least 17 Frizzled genes (Nikaido et al., 2013; Ruzicka et al., 2019).

Wnt/β-catenin signalling is the best characterised Wnt signalling pathway implicated in NC development (**Figure 2**).

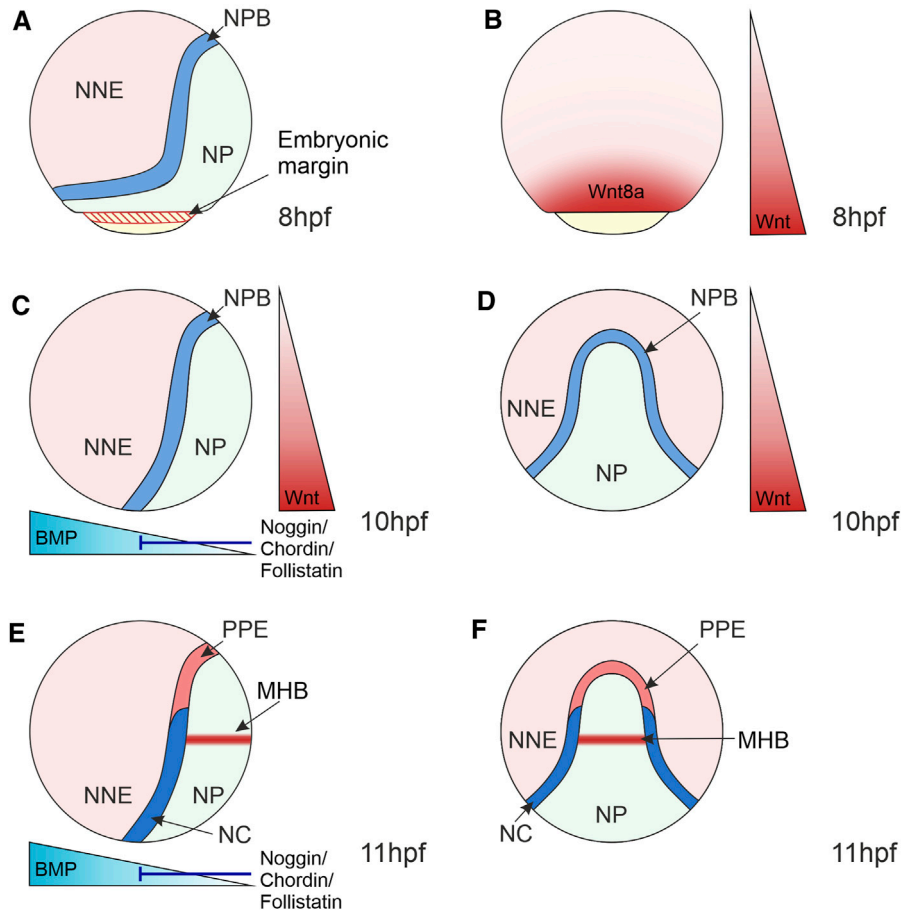

FIGURE 3 | Morphogen Gradients during Neural Crest Induction in Zebrafish 8–11 hpf. **(A)** At the end of gastrulation, the ectoderm is regionalised into the NP located medially, NNE located laterally and the NPB at the interface of NNE and NP. NP and NNE will form the central nervous system and epidermis, respectively. **(B)** At 8 hpf, the Wnt ligand, Wnt8a, is expressed in a broad domain at the embryonic margin overlapping with the NPB, implicating this ligand in NC induction. **(C–F)** At the bud stage (10 hpf) and 3-somite stage (11 hpf), the dorsoventral BMP gradient is established that patterns the ectoderm, with BMPs expressed ventrally and BMP antagonists (Noggin, Chordin and Follistatin) expressed dorsally. Intermediate levels of BMP signalling induce the NPB and NC. **(C,D)** Wnt/β-catenin signalling ligands are expressed posteriorly and act to posteriorize the NP and induce NC. **(E,F)** By 11hpf a separate Wnt source is established in the MHB within the NP that is required for NC fate specification. Lateral views show anterior to the top and dorsal to the right **(A,–C,E)**. Dorsal views indicate anterior to the top **(D,F)**. NNE, non-neural ectoderm; NP, neural plate; NPB, neural plate border; NC, neural crest; PPE, pre-placodal ectoderm; MHB, midbrain-hindbrain boundary; hpf, hours post-fertilisation.

Canonical Wnt ligands act as morphogens by establishing a gradient and influencing receiving-cell behaviour in a concentration-dependent manner. Wnt1, Wnt3a, and Wnt8a ligands predominantly activate Wnt/β-catenin signalling, ultimately stabilising the transcription factor β-catenin that translocates to the nucleus and activates target gene expression. In the absence of a Wnt/β-catenin ligand, Axin, APC, CK1, and Gsk3β form a destruction complex in the cytoplasm that phosphorylates β-catenin resulting in proteasomal degradation of this transcriptional co-factor (**Figure 2A**). The Wnt/β-catenin signalling pathway is activated upon the Wnt ligand interacting with a Frizzled receptor and Lrp5/6 co-receptor. The intracellular scaffolding proteins Dishevelled (Dvl) and Axin are recruited to this membrane-tethered complex, where they interact with Frizzled and Lrp5/6, respectively. The subsequent recruitment of the destruction complex to the plasma membrane leads to its inactivation, and thus β-catenin can no longer be degraded. The stabilised β-catenin thus translocates to the nucleus, where it interacts with TCF/LEF co-transcription factors to activate Wnt target gene expression (**Figure 2B**).

Furthermore, there are negative regulators of the Wnt/β-catenin signalling pathway that inhibit transcription activation by β-catenin. There are secreted Wnt antagonists, including secreted Frizzled-related proteins (sFRPs) and Wnt inhibitory factors (WIF), which directly bind and sequester Wnt ligands (Hsieh et al., 1999; Leyns et al., 1997) (**Figure 2A**). Dickkopf1 (Dkk1) is another secreted Wnt inhibitor that interacts with the Lrp5/6 co-receptors, inhibiting the formation of the ligand/receptor/co-receptor complex required for pathway activation (Bafico et al., 2001) (**Figure 2A**). Wnt/β-catenin signalling can also be manipulated experimentally using chemical inhibitors such as LiCl and Bromoindirubin-3′-oxime (BIO) (Meijer et al., 2003; Alexander et al., 2014; Vibert

et al., 2017). These chemical inhibitors target Gsk3β and prevent the phosphorylation and subsequent degradation of β-catenin, resulting in over-activation of the Wnt/β-catenin pathway (**Figure 2A**).

Wnt-mediated regulation of target gene expression is crucial during cell fate determination in development. During gastrulation, Wnt/β-catenin signalling is essential for the specification of posterior and ventral fates resulting from the expression of Wnt8a at the ventrolateral margin (Dorsky et al., 2002; Erter et al., 2001) (**Figures 3A,B**). In the ectoderm, expression of Wnt8a is crucial for the specification of posterior neural fates, but also in the induction of the NC (Lekven et al., 2001; Lewis et al., 2004). In NC development, TCF/LEF-regulated transcription plays a pivotal role in activating a gene regulatory network in the NC and subsequent NC fate restriction.

NEURAL CREST INDUCTION

NC induction takes place during gastrulation in the NPB. The NPB is exposed to signals from surrounding tissues, including the neural and non-neural ectoderm, as well as the underlying mesoderm, which induce and maintain the expression of NC markers (**Figure 3**). The role of signals originating from the mesoderm in NC induction was previously discounted as disruption of mesoderm involution in zebrafish embryos did not affect NC induction (Ragland and Raible, 2004). However, *Xenopus* explant experiments that conjugated animal caps with mesoderm regions found that mesoderm from the dorsolateral marginal zone specifically induced NC marker expression (Steventon et al., 2009). This suggests that mesoderm acts as a signalling source to the NC, even when involution is disrupted during gastrulation. It is essential to recognise that the NC emerges alongside other cell lineages within the NPB. For example, in the anterior NPB, the cranial NC is adjacent to the pre-placodal ectoderm that forms sensory structures in the vertebrate head and the lateral line system in aquatic vertebrates (Theveneau et al., 2013) (**Figures 3E,F**). In anamniote vertebrates, such as fish and amphibians, the posterior NPB gives rise to trunk NC and a population of transient embryonic sensory neurons known as Rohon-Beard cells (Lamborghini, 1980; Cornell and Eisen, 2000).

NEURAL CREST GENE REGULATORY NETWORK

The induction of the NPB and NC involves the interplay of the Wnt/β-catenin signalling, Bone Morphogenetic Protein (BMP), and Fibroblast Growth Factor (FGF) pathways, which activate a complex network of transcription factors within the NC, known as the NC gene regulatory network (GRN) (Sauka-Spengler and Bronner-Fraser, 2008). The NC GRN in zebrafish has been structured as a hierarchy of transcription factors. Here we provide a brief overview of the zebrafish NC GRN; a more detailed analysis can be found in a recent review (Rocha et al., 2020).

A combination of extracellular signals activates the NC GRN. During gastrulation, the first group of transcription factors activated are coined "NPB specifiers". At the end of gastrulation, the NC is specified within the NPB, a process characterised by the expression of further transcription factors, collectively referred to as "NC specifiers". These NC specifiers are activated by the upstream NPB specifiers and from extracellular signalling inputs. The action of the NC specifiers, combined with extracellular signals, subsequently activates lineage-specific GRNs in the process of NC specification and subsequent fate commitment (see section on NC specification).

WNT SIGNALLING AND THE NEURAL CREST GENE REGULATORY NETWORK

Wnt/β-catenin signalling, as well as BMP and FGF signalling pathways, coordinate the activation of the NC GRN. A BMP morphogen gradient is established through the expression of BMPs in the ventral side of the embryo and BMP antagonists, Noggin, Chordin and Follistatin, from the dorsal side (Hammerschmidt et al., 1996) (**Figures 3C,E**). This gradient patterns the ectoderm along the dorsoventral axis, with those cells that receive intermediate BMP levels forming the NC (Nguyen et al., 1998; Tucker et al., 2008; Schumacher et al., 2011).

Wnt/β-catenin signalling plays a fundamental role during zebrafish NC induction. In zebrafish, this was elucidated using a conditional heatshock promotor that activates expression of a mutant version of the TCF co-transcription factor that cannot bind β-catenin and thus blocks target gene expression (**Figure 2**). Expression of this mutant TCF during gastrulation resulted in a loss of expression of the NC specifier gene *foxd3* (Lewis et al., 2004). Interestingly, this approach did not affect the expression of markers of the neighbouring Rohon-Beard cells, suggesting a specific requirement of Wnt/β-catenin signalling in NC induction. In this study, Wnt8a was implicated in NC induction due to localised expression in the presumptive NC domain that overlapped with the expression of *pax3* NPB specifier during gastrulation (**Figures 3A,B**). Furthermore, the Morpholino (MO)-based knockdown of Wnt8a resulted in the loss of expression of the NPB specifier *pax3* and the NC specifiers *sox10* and *foxd3*. MO oligomers were microinjected at the 1-cell stage of zebrafish development. Therefore, it is not clear whether changes in NC specifier expression domains in the MO knockdowns reflects a role of Wnt8a specifically during NC induction or a downstream effect resulting from defects in Wnt8a signalling in early embryo development (Lewis et al., 2004). However, TCF/LEF binding sites have been identified in the *sox10* promoter, suggesting that this NC specifier is directly regulated by Wnt/β-catenin signalling (Dutton et al., 2008).

A further study on NC induction used a heat-shock promoter to overexpress the Wnt antagonist Dickkopf1 (Dkk1) that inhibits the Wnt/β-catenin signalling pathway by removing Lrp5/6 co-receptors from the plasma membrane (He et al., 2004) (**Figure 2A**). This study indicated that activation of Dkk1 expression at the end of gastrulation leads to a marked decrease in the expression of NPB markers *pax3a* and *zic3*

(Garnett et al., 2012). Through a series of elegant experiments, *cis*-regulatory elements of *pax3a* and *zic3* were identified containing putative TCF/LEF binding sites. One enhancer of *pax3a* (IR1) contained six putative TCF/LEF binding sites, and mutating this enhancer reduced the expression of *pax3a* in the NPB. In addition, they identified two enhancers of *zic3* (E1 and E2) that contain putative TCF/LEF binding sites and mutating E2 decreased expression of *zic3* in the NPB (Garnett et al., 2012).

Overall, findings from these studies indicate a crucial role for Wnt/β-catenin signalling in establishing the NPB during gastrulation (by activating expression of *pax3a* and *zic3*) and NC induction (by activating expression of *foxd3* and *sox10*). These studies used heat-shock inducible constructs to inhibit different components of the Wnt/β-catenin signalling pathway at discrete developmental stages. Notably, both studies identified changes in gene expression of NPB specifiers and NC specifiers upon inhibition of Wnt/β-catenin signalling. This is likely to reflect an ongoing role of Wnt/β-catenin signalling during gastrulation to specify the NPB and subsequently induce the NC within the NPB.

Although only a few genes were identified in the zebrafish NPB and NC directly regulated by Wnt/β-catenin signalling, there are likely to be many other NPB and NC specifiers regulated by Wnt/β-catenin signalling. A recent study in chick embryos examined the nuclear architecture of the cells expressing the pan-NC marker Pax7 using chromatin conformation capture. Strikingly, a map of active enhancers in NCCs during induction stages shows that the most highly enriched motif in their enhancer map were TCF/LEF-binding sites (Azambuja and Simoes-Costa, 2021a). This analysis led the authors to rethink the NC GRN and proposed that the GRN has a hub-and-spoke architecture whereby Wnt/β-catenin signalling is connected to multiple components through these signal-responsive regulatory elements (Azambuja and Simoes-Costa, 2021a). Further in-depth analysis of *cis*-regulatory elements of a direct Wnt target gene in the NC revealed an intricate regulatory system with inputs from multiple upstream signalling pathways and positive and repressive elements that, as a combination, finely tune the expression of NC specifier genes (Azambuja and Simoes-Costa, 2021a, b). Therefore, it is probable that Wnt/β-catenin signalling has a role both in the initial activation of the GRN and subsequently in maintaining and fine-tuning expression of intrinsic factors through regulation of both positive and negative gene regulatory elements.

DICKKOPF PROTEINS IN NEURAL CREST INDUCTION

The activation of the NC GRN by the Wnt/β-catenin signalling pathway is also regulated by the activity of its antagonists. One member of the Dkk family of secreted Wnt antagonists, Dkk1, was characterised as a potent inhibitor of Wnt/β-catenin signalling from studies in *Xenopus* and mouse embryos (**Figure 2**). Overexpression of Dkk1 resulted in anteriorized embryos due to increased inhibition of Wnt/β-catenin signalling that induces posterior neural fates (Glinka et al., 1998; Mukhopadhyay et al., 2001). Dkk1 is expressed in the anterior prechordal mesoderm, where it functions to promote anterior neural fates in the neural ectoderm as well as modulating Wnt/β-catenin signalling in the NPB during NC induction (Glinka et al., 1998; Caneparo et al., 2007; Carmona-Fontaine et al., 2007). Consistent with its function as an inhibitor of the Wnt/β-catenin signalling pathway, loss-of-function of Dkk1 in *Xenopus* and mouse embryos resulted in ectopic expression of NPB specifiers and NC specifiers in the anterior neural fold. Therefore, expression of this Wnt/β-catenin signalling antagonist inhibits NC induction and specification in the anterior ectoderm (Carmona-Fontaine et al., 2007).

Despite the well-documented activity of Dkk1 as a negative regulator of Wnt/β-catenin signalling, studies on the role of Dkk2 suggest that this secreted factor can positively and negatively regulate Wnt/β-catenin signalling in a context-dependent manner. In *Xenopus* embryos, Dkk2 overexpression phenotypes are characterised by microcephaly, similar to phenotypes of embryos with ectopic expression of Wnt8 (Wu et al., 2000). In a study of the role of Dkk2 in NC development, MO-knockdown in *Xenopus* embryos resulted in reduced expression of NC specifiers, but not NPB specifiers or mesodermal genes. This suggests that Dkk2 functions during NC induction to exclusively promote the expression of NC specifiers (Devotta et al., 2018). Furthermore, in animal caps exposed to Wnt8 and BMP antagonist (Noggin) to induce NC, knockdown of Dkk2 resulted in depletion of NC specifiers. This is indicative of a requirement for Dkk2 in Wnt/β-catenin signal transduction during NC induction. Consistent with these findings, Dkk2 is expressed in the posterior of the embryo, unlike Dkk1. Furthermore, rescue of NC specifier expression in Dkk2 knockdown embryos was tested using the Gsk3β chemical inhibitor, BIO, to stimulate Wnt/β-catenin signalling (**Figure 2A**). Intriguingly, they found that this stimulation of Wnt/β-catenin signalling did not restore normal expression levels of the NC specifier *sox10*. The authors, therefore, speculate that Dkk2 functions to positively regulate Wnt/β-catenin signalling independently of Gsk3β (Devotta et al., 2018). An alternative mechanism by which Dkk2 promotes β-catenin-dependent gene transcription in the NC has not yet been identified.

FURTHER LEVELS OF WNT/β-CATENIN SIGNALLING AND NC INDUCTION

It is essential to recognise that the NC is exposed to many extracellular signalling inputs during induction stages. However, it seems that many are involved in regulating directly or indirectly the Wnt/β-catenin signalling pathway. Studies on a DEAD/H-box RNA helicase, DDX3, in *Xenopus* provided insight into the interplay of signalling pathways in the NC. In the first study on DDX3 function, this RNA helicase was shown to activate Wnt/β-catenin signalling by stimulating CK1 phosphorylation of Dvl, resulting in

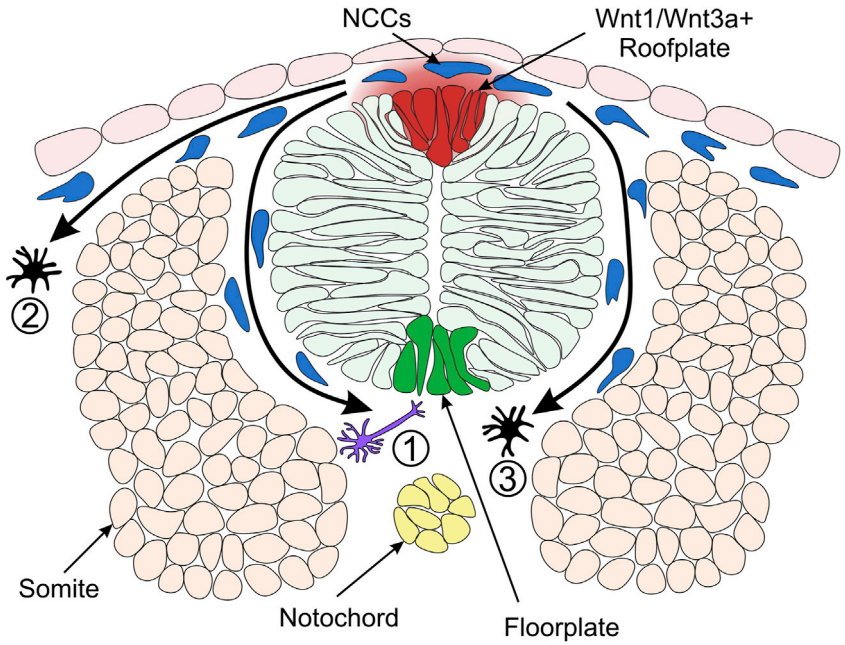

FIGURE 4 | Model of Neural Crest Fate Specification in Zebrafish. Wnt/β-catenin signalling ligands such as Wnt1 and Wnt3a are expressed in the zebrafish dorsal neural tube and bias the fate of NCCs (neural crest cells). The trunk NCCs begin to migrate through the ventrolateral pathway between the neural tube and somites (1). These cells receive a low level of Wnt/β-catenin signalling and are biased towards a neuronal cell fate. For example, the early migrating NCCs taking the ventrolateral pathway give rise to dorsal root ganglia of the peripheral nervous system (Artinger and Bronner-Fraser, 1992). NCCs originating from the dorsal-medial region of the neural plate border are exposed to a high level of Wnt ligands and form pigment cells. These cells of the melanocytic lineage migrate through the dorsolateral pathway between the ectoderm and somite (2) (Henion and Weston, 1997). In a second migratory wave, pigment cells can also take the ventrolateral route (3). Cross-section of zebrafish neural tube **(dorsal to the top)** illustrating overlying epidermis, neural plate border region, neural tube, somites (simplified as the dorsal muscle block) and notochord on the dorsoventral axis.

increased formation of Wnt signalosomes and increased expression of downstream genes (Cruciat et al., 2013). More recently, an in-depth study of DDX3 in *Xenopus* NC development demonstrated that activation of this RNA helicase stabilises β-catenin, activating the expression of NPB and NC specifiers. Rather than directly modulating elements of the Wnt/β-catenin pathway, the authors found that DDX3 regulates the serine/threonine kinase, AKT, in an RNA helicase-dependent manner. In the NC, DDX3 RNA helicase activity stimulates AKT, which phosphorylates and inhibits Gsk3β, resulting in the accumulation of β-catenin (Perfetto et al., 2021). AKT is also regulated upstream by phosphatidylinositol 3-kinase (PI3K) implicated in NC induction (Ciarlo et al., 2017). Therefore, there is evidence of an interplay between the PI3K-AKT and Wnt/β-catenin signalling pathways, which has downstream effects on the NC GRN. Furthermore, there is evidence of an interplay between BMP and Wnt/β-catenin signalling pathways reported in *Xenopus*. Mesodermal expression of *wnt8* is dependent on BMP signalling (Hoppler and Moon, 1998). More recently, BMP responsive elements were identified upstream of the transcriptional start site of *wnt8*. The transcriptional activator of the BMP signalling pathway, Smad1, was able to bind these *cis*-regulatory elements in the presence of a scaffold protein, Fhl3 (Alkobtawi et al., 2021). A further interaction has been reported on the level of the secreted BMP antagonist Gremlin (Pegge et al., 2020), which interacts with heparan sulfate proteoglycans (HSPGs), a family of cell surface macromolecules that regulate Wnt distribution and signalling (reviewed in Routledge and Scholpp, 2019). This coordination of multiple signalling pathways is often overlooked in NC studies which focus on the function of signalling pathways separately. These studies provide evidence of other signalling pathways that modulate Wnt/β-catenin signalling during NC induction.

Given the precise requirement of Wnt/β-catenin signalling during NC induction, it is not surprising that several studies have implicated specific Wnt/β-catenin ligands in the process. Wnt8a was implicated in NPB specification and NC induction through Morpholino-based knockdown studies (Garnett et al., 2012; Lewis et al., 2004). However, further Wnt/β-catenin ligands originating from the neural ectoderm have been implicated in NC induction. In mice, Wnt1, Wnt3 and Wnt3a are expressed in the dorsal roof plate of the neural tube during the stages of NC induction (Parr et al., 1993). Furthermore, mouse Wnt1 and Wnt3a double mutants displayed defects in NC formation, consistent with the role of Wnt/β-catenin signalling in NC induction (Ikeya et al., 1997). Similarly, zebrafish Wnt1 and Wnt3a are expressed in the dorsal neural keel adjacent to the NPB (Dorsky et al., 1998) (**Figure 4**). Wnt3 is also expressed in the zebrafish dorsal roof plate; however, whether Wnt3 has a

functional role in NC development has not yet been explored (Teh et al., 2015). Strikingly, it was demonstrated that the murine mutants of Wnt1 and Wnt3a not only displayed a reduction in the size of NC clones, which would be indicative of a function in NC induction, but they also altered the balance of NCC derivatives. This led to the perception that Wnt/β-catenin signalling has a continued role in NC development following NC induction (Ikeya et al., 1997).

NC Fate Specification

Analysis of the role of Wnt1 and Wnt3a signalling in mouse and zebrafish NC shows that fates of NCCs are biased by Wnt/β-catenin signalling (Dorsky et al., 1998; Ikeya et al., 1997). In a study of cranial NC, fluorescein-dextran cell labelling suggested that NCCs located ventrolaterally furthest away from the origin of Wnt/β-catenin signals in the neural keel are destined to become neuronal cells (Dorsky et al., 1998) (**Figure 4**). On the other hand, NCCs that form pigment cell derivatives are located in the medial domain of the NC, adjacent to the source of Wnt1 and Wnt3a ligands in the neural keel (Schilling and Kimmel, 1994) (**Figure 4**). Furthermore, overexpression of β-catenin in NCCs in the lateral domain resulted in pigment cell generation instead of neuronal cells. Conversely, injection of a dominant-negative Wnt1 or a mutated form of TCF3 into medial NCCs generated neuronal cell types instead of pigment cells (Dorsky et al., 1998). These early experiments established the long-standing model whereby NCCs receiving a high level of Wnt/β-catenin signalling are biased towards pigment cell fates.

In contrast, NCCs that receive low levels of Wnt form neuronal cell derivatives. These findings demonstrate a requirement for Wnt/β-catenin signalling in the specification of NC pigment cell derivatives over neuronal derivatives. How can NCCs acquire different fates if all of them originate from one cell population adjacent to the same signalling source, the Wnt1/Wnt3a$^+$ roof plate? There are two hypotheses explaining this paradox. The NCCs specified to neuronal lineages could delaminate and migrate away from the dorsal neural tube earlier than NCCs specified as melanocytes. Such a temporal difference in migration of NC derivatives could result in different periods of exposure to Wnt ligands, with melanophores exposed to Wnt for a longer duration than neuronal cells (**Figure 4**) (Dorsky et al., 1998; Nitzan et al., 2013). Indeed, the transition from pre-migratory to migratory NCCs is facilitated by Cadherin2 (Ahsan et al., 2019; Scarpa et al., 2015). By blocking Cadherin2 function, pre-migratory NCCs accumulate at the dorsal midline, adjacent to the Wnt1/Wnt3a$^+$ roof plate (**Figure 4**) and start to express the pigment cell marker *microphthalmia-associated transcription factor a* (*mitfa*) (Piloto and Schilling, 2010; Tuttle et al., 2014). However, employing a high-resolution method of detecting RNA transcripts in whole-mount embryos suggested that these NCCs may not be fate-restricted to the pigment cell lineage at this stage (Tatarakis et al., 2020). Therefore, despite the long-standing model of NC fate specification whereby Wnt1/Wnt3a ligands originating in the dorsal neural tube promote pigment cell fates over neuronal cell fates, the underlying mechanisms of the Wnt morphogen gradient and the timing of specification is not fully understood.

WNT/β-CATENIN SIGNALLING AND PIGMENT CELL (CHROMATOPHORE) SPECIFICATION

The specification of the pigment cell lineages of the NC has been extensively studied due to their distinctive colour and morphology that enables easy identification of mutants in genetic screens (Kelsh et al., 1996; Lamoreux, 2010). Mammals only have one type of pigment cell, melanocytes, whereas zebrafish have three types; melanocytes, xanthophores and iridophores (Fujii, 1993; Rawls et al., 2001; Schartl et al., 2016). Of these three cell derivatives, the GRN that specifies the melanocyte cell lineage has been best characterised. The NC transcription factor *sox10* is required to specify all three pigment cell derivatives (Kelsh and Eisen, 2000; Dutton et al., 2001). *Sox10* transcription factor is an NC specifier, which is first expressed in pre-migratory NCCs. *sox10* (also known as *colourless*) mutants have defects in all NC derivatives except for ectomesenchymal lineages (Kelsh and Eisen, 2000; Dutton et al., 2001). A similar phenotype was also shown in *sox10* mutant mice (Kapur, 1999). *sox10* expression is transiently maintained in NCCs during migration before being switched off in all lineages apart from iridophores and glia (Dutton et al., 2001). It has been suggested that *sox10* functions in the fate specification of NC derivatives from multipotent progenitors, e.g., sensory neurons (Carney et al., 2006).

In melanocyte specification, Sox10 works in conjunction with Wnt/β-catenin signalling to activate and maintain the expression of the melanocyte master regulator, *mitfa* (Hodgkinson et al., 1993; Opdecamp et al., 1997; Lister et al., 1999; Elworthy et al., 2003; Vibert et al., 2017). Interactions between SOX family transcription factors and Wnt/β-catenin signalling have been widely reported in many systems (Kormish et al., 2010). Recently a study using human pluripotent stem cells showed that two SOX factors, SOX2 and SOX17, directly bind β-catenin and this protein-protein interaction results in the recruitment of β-catenin to lineage-specific regulatory elements in both the presence and absence of TCF/LEF (Mukherjee et al., 2021). These findings lead us to speculate on potential interactions between Sox10 and β-catenin in NCCs, which could mediate a lineage-specific Wnt-responsive transcriptional program.

Similarly to *pax3a* and *zic3*, *mitfa* has *cis*-regulatory elements that contain LEF-binding sites enabling regulation of *mitfa* expression by Wnt/β-catenin signalling, and a different regulatory element containing Sox10-binding sites (Dorsky et al., 1998; Dorsky et al., 2000; Takeda et al., 2000; Jin et al., 2001; Elworthy et al., 2003; Hou et al., 2006). *mitfa* expression is required for the process of melanogenesis and melanocyte cell survival and proliferation (Lister et al., 1999). However, it has been shown that *mitfa* is transiently expressed in all NCCs even though only a subpopulation of NCCs form melanocytes (Curran et al., 2010). Therefore, maintaining *mitfa* expression is crucial for establishing the melanocyte cell lineage (Nikaido et al., 2021).

Experiments with BIO, the chemical inhibitor of Gsk3β, helped further unravel the link between Wnt/β-catenin signalling and melanocyte specification (Vibert et al., 2017). Incubation with this compound stabilises β-catenin to activate

Wnt/β-catenin dependent gene expression (**Figure 2A**). Indeed, zebrafish embryos incubated in BIO at 15–30 hours post-fertilisation (hpf) increased melanocyte specification due to enhanced Wnt/β-catenin signalling. On the other hand, BIO treatment at 24–72 hpf, when *sox10* expression is no longer detected in melanocytes, showed no changes in melanocyte number. However, the melanocyte morphology was affected (Vibert et al., 2017). Therefore, a two-stage model was proposed: At 15–30 hpf, Sox10-mediated melanocyte specification needs Wnt/β-catenin signalling, and at 24–72 hpf, the maintenance of melanocytes requires Wnt/β-catenin signalling together with *mitfa* expression.

One evident bottleneck in our understanding of the specification of these pigment cell lineages is the lack of identification of the Frizzled receptors involved in melanocyte specification. Characterising expression patterns and performing Morpholino-mediated knockdowns of numerous Frizzled genes was used to assess Frizzled receptors as candidates for NC development and pigment cell specification in zebrafish (Nikaido et al., 2013). This analysis, however, proved ineffective; none of the assessed Frizzled receptors was expressed in NCCs or melanocytes, and no pigment cell defects were detected in the knockdowns explored (Nikaido et al., 2013). Thus, the possibility remains that other Frizzled members, not included in the study, may be required in the NC. In addition, other higher-resolution methods to detect expression localisation, such as Nanostring, could provide insight into this elusive receptor repertoire of NCCs (Petratou et al., 2018). Alternatively, it has been suggested that Wnt co-receptors can signal without the need for Frizzled receptors (Brinkmann et al., 2016).

MODELS OF NC SPECIFICATION

The mechanisms regulating NC specification, whereby NCCs are fate-restricted to individual cell types, remain controversial. NC fate decisions are imposed by environmental signalling cues, and it was assumed that this results in fully multipotent NCCs becoming determined as unipotent cells of specific fates. Two explanatory models were proposed in the late 20th century. The direct fate restriction (DFR) model was proposed based on single-cell labelling studies in the chick dorsal neural tube and envisaged fully multipotent NCCs as directly adopting single fates; this model was supported by work using rat NC stem cells that identified key extracellular signals that instruct NCCs to adopt an individual fate from multiple options (Bronner-Fraser and Fraser, 1988; Bronner-Fraser and Fraser, 1989; Fraser and Bronner-Fraser, 1991; Stemple and Anderson, 1992).

The second model, and nowadays the prevailing one, has been the progressive fate restriction (PFR) hypothesis. The PFR hypothesis proposes that multipotent NC progenitor fates adopt specific fates through a series of partially restricted intermediate progenitors, each with limited but distinct potencies (Sieber-Blum and Cohen, 1980; Weston, 1991; Calloni et al., 2009). Single-cell profiling of mouse NC has supported this model by tracking pre-migratory NCCs through successive fate restrictions towards neural and ectomesenchymal fates (Soldatov et al., 2019). Similarly, single-cell RNA analysis of NC-derived cells taken from various stages of embryonic, larval, juvenile and adult fish have each identified putative pigment cell progenitors (Lencer et al., 2021; Howard IV et al., 2021; Saunders et al., 2021), although in each case the markers used to identify these progenitors does not include all the genetically best-characterised genes with known functional roles in pigment cell fate choice so that the exact identities of these cells and the relationship between the cells described in each study merits further detailed investigation. Thus, the PFR hypothesis has become dominant over the alternative DFR model.

However, a direct test of the PFR model for zebrafish pigment cell development, using sensitive NanoString single-cell profiling of NCCs throughout embryonic development, unexpectedly failed to identify the predicted tripotent (chromatoblasts) and bipotent (melanoiridoblast) progenitors (Nikaido et al., 2021). Furthermore, the same study revealed broad potency, for pigment *and* neural fates, for early NCCs expressing *leukocyte tyrosine kinase*, *ltk*, previously hypothesised to be a chromatoblast marker. The authors proposed an alternative model of NC fate restriction, known as the cyclical fate restriction (CFR) hypothesis, which proposes a more dynamic view of NC specification than either the PFR or DFR models. In the PFR model, the transition from one progenitor state to another of more restricted potency (e.g., from chromatoblast to melanoiridoblast) is associated with loss of potential for one or more fates. In contrast, the CFR hypothesis proposes that NC-derived Highly Multipotent Progenitors cycle through different sub-states, each primed towards a particular cell fate; however, because these cells cycle through sub-states primed for all fates, in turn, they retain multipotency, even although in a "snap-shot" view they appear fate-specified. It is proposed that the priming is reflected in fluctuating expression levels of fate-specification receptors and key fate-specific transcription factors such as Mitfa. The CFR hypothesis suggests that adopting a specific fate occurs when the primed sub-state is exposed to sufficient levels and duration of the fate-specification ligand, driving the differentiation of a specific fate (Kelsh et al., 2021). Although the CFR hypothesis is, at this point, somewhat speculative, it is supported by several observations and by theoretical modelling studies (Farjami et al., 2021). For example, the *ltk*, encoding a receptor tyrosine kinase, is crucial for iridophore specification but shows heterogeneous expression in premigratory NCCs (Lopes et al., 2008). The CFR model also helps to explain recent observations of a group of NC progenitors that simultaneously express factors involved in the specification of all pigment cell lineages – *ltk* and *tfec* (iridophores (Lopes et al., 2008; Petratou et al., 2021), *mitfa* (melanocytes (Lister et al., 1999)) and *pax7* (xanthophores (Minchin and Hughes, 2008)), but also factors crucial for neural fate specification (Nikaido et al., 2021). One important, but underappreciated, implication of all of these observations is that fate restriction to a specific fate depends as much on the repression of fate-specific transcription factors and receptors specifying other fates, as well as the upregulation and maintenance of those for the selected fate (Petratou et al.,

2018). Thus, the upregulation of Ltk and Tfec, as well as downregulation of, for example, a Frizzled receptor and Mitfa, all in response to exposure to ALKALs (ligands of Ltk) would result in an iridophore fate. In contrast, upregulation of Frizzled and Mitfa, following exposure to Wnt/β-catenin ligands and downregulation of Ltk and Tfec (and others) would drive the cell towards a melanocyte fate (Kelsh et al., 2021). It is conceivable that Wnt signalling plays a key role in the entry and exit from the NC-HMP cycling progenitor state and may act alongside other signals to initiate entry into the cycling state and to allow differentiation of each derivative fate from the cells in the cycling state (Farjami et al., 2021). The CFR model shares similarities with the so-called "phase-stage model", which has been proposed for embryonic stem (ES) cell fate restrictions following the observation that an ES cell can occupy a state, known as the phase stage when it can "explore" several potential states (distinguished by oscillating levels of Nanog; Miyanari and Torres-Padilla, 2012) over time (Garcia-Ojalvo and Martinez Arias, 2012). In conclusion, the CFR offers a novel and dynamic framework explaining the previous data supporting either the DFR or the PFR model. Distinguishing these models will require sensitive assessment of the broadest range of markers of each cell-fate, especially those known to drive fate decisions, and development of tools for highly sensitive detection of the dynamic expression of transcription factors and fate-specification receptors in living embryos.

CONCLUDING REMARKS AND FUTURE PERSPECTIVES

The vertebrate novelty of the NC continues to fascinate the scientific community. NC research has benefitted from applying multidisciplinary techniques, from the cell lineage tracing experiments pioneered by Nicole Le Douarin to the single-cell sequencing technologies that continue to uncover the NC GRN. In this review, we have discussed the current knowledge of the role of Wnt/β-catenin signalling in NC induction and specification. It is well-established that β-catenin-dependent Wnt signalling is required for NC induction and specification, particularly during pigment cell specification. Although some canonical Wnt ligand candidates have been implicated in NC development, there remains a significant lack of understanding of the mechanism of Wnt ligand transport during NC development. Localising these ligands and clarifying their mechanisms of transport would allow refinement of our knowledge of when and how Wnt/β-catenin signalling influences NC development at each of the stages outlined above.

Wnt morphogens are hydrophobic due to post-translational modification with lipid moieties during intracellular trafficking (Willert et al., 2003; Takada et al., 2006). It is, therefore, improbable that Wnt ligands are secreted by cells and diffuse freely through extracellular space (reviewed in Routledge and Scholpp, 2019). As a result, several alternative mechanisms of long-range Wnt transport have been explored, including specialised signalling filopodia, known as cytonemes (Stanganello et al., 2015; Brunt et al., 2021). Although there is strong evidence for canonical Wnt expression in the dorsal roof plate of the zebrafish neural tube during NC induction and specification stages, there is no published research on the ligand transport mechanisms regulating this process. Therefore, high-resolution imaging could be utilised to visualise the mechanism of Wnt transport during NC development. Zebrafish is the ideal model organism for this research, given the powerful transgenic tools and superb *in vivo* imaging due to the embryos' transparency.

Furthermore, studying the function of the Wnt/β-catenin signalling pathway during NC development has proven challenging due to its necessity during early embryonic development, in gastrulation for AP patterning, and neural plate patterning. In this review, we have highlighted studies in which authors have provided temporal control to the modulation of the Wnt/β-catenin signalling pathway, for example, using the heat-shock promoter or incubation of chemical inhibitors at different developmental stages (Lewis et al., 2004; Garnett et al., 2012; Vibert et al., 2017). However, studies have also relied on whole organism knockouts and MO-based knockdowns to study the impact of specific Wnt ligand candidates on NC development. Such a strategy is not ideal as Wnt/β-catenin signalling is vital in the early embryo and successive stages of NC development. Therefore, it is unclear whether the phenotypes observed in the NC result from inhibition of Wnt/β-catenin signalling during NC stages of development or whether researchers observe downstream effects from inhibition of Wnt/β-catenin signalling earlier in development. As an alternative, we propose using conditional gene knockouts that can be spatially and temporally controlled in the developing embryo. Such a strategy could enable the knockout of essential components of the Wnt/β-catenin signalling pathway only in NCCs during NC induction or specification stages. Indeed, conditional knockout lines using CRISPR/Cas9 technology are appearing in the literature. For example, the Cre/LoxP system has been introduced to control the expression of Cas9 and gRNAs in zebrafish (Hans et al., 2021). Further research will be required to compare the relative efficiency and specificity of this novel conditional knockout system. However, it is undeniable that these new knockout strategies will be invaluable to the future of NC research.

AUTHOR CONTRIBUTIONS

GS drafted the manuscript and designed the figures. SS and RK contributed to drafting the manuscript, revised and polished the manuscript. All authors approved the final version.

FUNDING

Research in the SS lab is supported by the BBSRC (Research Grant, BB/S016295/1 and an Equipment grant, BB/R013764/1) and the Living Systems Institute, University of Exeter. In addition, GS is funded by a BBSRC DTP SWBio studentship.

REFERENCES

Abitua, P. B., Wagner, E., Navarrete, I. A., and Levine, M. (2012). Identification of a Rudimentary Neural Crest in a Non-vertebrate Chordate. *Nature* 492, 104–107. doi:10.1038/nature11589

Ahsan, K., Singh, N., Rocha, M., Huang, C., and Prince, V. E. (2019). Prickle1 Is Required for EMT and Migration of Zebrafish Cranial Neural Crest. *Develop. Biol.* 448, 16–35. doi:10.1016/j.ydbio.2019.01.018

Alexander, C., Piloto, S., Le Pabic, P., and Schilling, T. F. (2014). Wnt Signaling Interacts with Bmp and Edn1 to Regulate Dorsal-Ventral Patterning and Growth of the Craniofacial Skeleton. *Plos Genet.* 10, e1004479. doi:10.1371/journal.pgen.1004479

Alkobtawi, M., Pla, P., and Monsoro-Burq, A. H. (2021). BMP Signaling Is Enhanced Intracellularly by FHL3 Controlling WNT-dependent Spatiotemporal Emergence of the Neural Crest. *Cel Rep.* 35, 109289. doi:10.1016/j.celrep.2021.109289

An, M., Luo, R., and Henion, P. D. (2002). Differentiation and Maturation of Zebrafish Dorsal Root and Sympathetic Ganglion Neurons. *J. Comp. Neurol.* 446, 267–275. doi:10.1002/cne.10214

Angers, S., and Moon, R. T. (2009). Proximal Events in Wnt Signal Transduction. *Nat. Rev. Mol. Cel Biol* 10, 468–477. doi:10.1038/nrm2717

Artinger, K. B., and Bronner-Fraser, M. (1992). Partial Restriction in the Developmental Potential of Late Emigrating Avian Neural Crest Cells. *Develop. Biol.* 149, 149–157. doi:10.1016/0012-1606(92)90271-h

Azambuja, A. P., and Simoes-Costa, M. (2021b). A Regulatory Sub-circuit Downstream of Wnt Signaling Controls Developmental Transitions in Neural Crest Formation. *Plos Genet.* 17, e1009296. doi:10.1371/journal.pgen.1009296

Azambuja, A. P., and Simoes-Costa, M. (2021a). The Connectome of Neural Crest Enhancers Reveals Regulatory Features of Signaling Systems. *Develop. Cel* 56, 1268e1266–1282. doi:10.1016/j.devcel.2021.03.024

Bafico, A., Liu, G., Yaniv, A., Gazit, A., and Aaronson, S. A. (2001). Novel Mechanism of Wnt Signalling Inhibition Mediated by Dickkopf-1 Interaction with LRP6/Arrow. *Nat. Cel Biol* 3, 683–686. doi:10.1038/35083081

Bang, A. G., Papalopulu, N., Goulding, M. D., and Kintner, C. (1999). Expression of Pax-3 in the Lateral Neural Plate Is Dependent on a Wnt-Mediated Signal from Posterior Nonaxial Mesoderm. *Develop. Biol.* 212, 366–380. doi:10.1006/dbio.1999.9319

Brinkmann, E.-M., Mattes, B., Kumar, R., Hagemann, A. I. H., Gradl, D., Scholpp, S., et al. (2016). Secreted Frizzled-Related Protein 2 (sFRP2) Redirects Non-canonical Wnt Signaling from Fz7 to Ror2 during Vertebrate Gastrulation. *J. Biol. Chem.* 291, 13730–13742. doi:10.1074/jbc.m116.733766

Bronner-Fraser, M., and Fraser, S. (1989). Developmental Potential of Avian Trunk Neural Crest Cells *In Situ*. *Neuron* 3, 755–766. doi:10.1016/0896-6273(89)90244-4

Bronner-Fraser, M., and Fraser, S. E. (1988). Cell Lineage Analysis Reveals Multipotency of Some Avian Neural Crest Cells. *Nature* 335, 161–164. doi:10.1038/335161a0

Brunt, L., Greicius, G., Rogers, S., Evans, B. D., Virshup, D. M., Wedgwood, K. C. A., et al. (2021). Vangl2 Promotes the Formation of Long Cytonemes to Enable Distant Wnt/β-Catenin Signaling. *Nat. Commun.* 12, 2058. doi:10.1038/s41467-021-22393-9

Calloni, G. W., Le Douarin, N. M., and Dupin, E. (2009). High Frequency of Cephalic Neural Crest Cells Shows Coexistence of Neurogenic, Melanogenic, and Osteogenic Differentiation Capacities. *Proc. Natl. Acad. Sci.* 106, 8947–8952. doi:10.1073/pnas.0903780106

Caneparo, L., Huang, Y.-L., Staudt, N., Tada, M., Ahrendt, R., Kazanskaya, O., et al. (2007). Dickkopf-1 Regulates Gastrulation Movements by Coordinated Modulation of Wnt/βcatenin and Wnt/PCP Activities, through Interaction with the Dally-like Homolog Knypek. *Genes Dev.* 21, 465–480. doi:10.1101/gad.406007

Carmona-Fontaine, C., Acuña, G., Ellwanger, K., Niehrs, C., and Mayor, R. (2007). Neural Crests Are Actively Precluded from the Anterior Neural Fold by a Novel Inhibitory Mechanism Dependent on Dickkopf1 Secreted by the Prechordal Mesoderm. *Develop. Biol.* 309, 208–221. doi:10.1016/j.ydbio.2007.07.006

Carney, T. J., Dutton, K. A., Greenhill, E., Delfino-Machín, M., Dufourcq, P., Blader, P., et al. (2006). A Direct Role for Sox10 in Specification of Neural Crest-Derived Sensory Neurons. *Development* 133, 4619–4630. doi:10.1242/dev.02668

Cavanaugh, A. M., Huang, J., and Chen, J.-N. (2015). Two Developmentally Distinct Populations of Neural Crest Cells Contribute to the Zebrafish Heart. *Develop. Biol.* 404, 103–112. doi:10.1016/j.ydbio.2015.06.002

Chang, C., and Hemmati-Brivanlou, A. (1998). Neural Crest Induction by Xwnt7B in Xenopus. *Develop. Biol.* 194, 129–134. doi:10.1006/dbio.1997.8820

Ciarlo, C., Kaufman, C. K., Kinikoglu, B., Michael, J., Yang, S., D Amato, C., et al. (2017). A Chemical Screen in Zebrafish Embryonic Cells Establishes that Akt Activation Is Required for Neural Crest Development. *Elife* 6. doi:10.7554/eLife.29145

Cornell, R. A., and Eisen, J. S. (2000). Delta Signaling Mediates Segregation of Neural Crest and Spinal Sensory Neurons from Zebrafish Lateral Neural Plate. *Development* 127, 2873–2882. doi:10.1242/dev.127.13.2873

Cruciat, C.-M., Dolde, C., de Groot, R. E. A., Ohkawara, B., Reinhard, C., Korswagen, H. C., et al. (2013). RNA Helicase DDX3 Is a Regulatory Subunit of Casein Kinase 1 in Wnt-β-Catenin Signaling. *Science* 339, 1436–1441. doi:10.1126/science.1231499

Curran, K., Lister, J. A., Kunkel, G. R., Prendergast, A., Parichy, D. M., and Raible, D. W. (2010). Interplay between Foxd3 and Mitf Regulates Cell Fate Plasticity in the Zebrafish Neural Crest. *Develop. Biol.* 344, 107–118. doi:10.1016/j.ydbio.2010.04.023

Devotta, A., Hong, C. S., and Saint-Jeannet, J. P. (2018). Dkk2 Promotes Neural Crest Specification by Activating Wnt/β-Catenin Signaling in a GSK3β Independent Manner. *eLife* 7, e34404. doi:10.7554/eLife.34404

Dorsky, R. I., Moon, R. T., and Raible, D. W. (1998). Control of Neural Crest Cell Fate by the Wnt Signalling Pathway. *Nature* 396, 370–373. doi:10.1038/24620

Dorsky, R. I., Raible, D. W., and Moon, R. T. (2000). Direct Regulation of Nacre, a Zebrafish MITF Homolog Required for Pigment Cell Formation, by the Wnt Pathway. *Genes Dev.* 14, 158–162. doi:10.1101/gad.14.2.158

Dorsky, R. I., Sheldahl, L. C., and Moon, R. T. (2002). A Transgenic Lef1/β-catenin-dependent Reporter Is Expressed in Spatially Restricted Domains throughout Zebrafish Development. *Develop. Biol.* 241, 229–237. doi:10.1006/dbio.2001.0515

Duncan, R. N., Panahi, S., Piotrowski, T., and Dorsky, R. I. (2015). Identification of Wnt Genes Expressed in Neural Progenitor Zones during Zebrafish Brain Development. *PLoS One* 10, e0145810. doi:10.1371/journal.pone.0145810

Dutton, J. R., Antonellis, A., Carney, T. J., Rodrigues, F. S., Pavan, W. J., Ward, A., et al. (2008). An Evolutionarily Conserved Intronic Region Controls the Spatiotemporal Expression of the Transcription Factor Sox10. *BMC Dev. Biol.* 8, 105. doi:10.1186/1471-213x-8-105

Dutton, K. A., Pauliny, A., Lopes, S. S., Elworthy, S., Carney, T. J., Rauch, J., et al. (2001). Zebrafishcolourlessencodessox10and Specifies Non-ectomesenchymal Neural Crest Fates. *Development* 128, 4113–4125. doi:10.1242/dev.128.21.4113

Elworthy, S., Lister, J. A., Carney, T. J., Raible, D. W., and Kelsh, R. N. (2003). Transcriptional Regulation of Mitfa Accounts for the Sox10 Requirement in Zebrafish Melanophore Development. *Development* 130, 2809–2818. doi:10.1242/dev.00461

Elworthy, S., Pinto, J. P., Pettifer, A., Cancela, M. L., and Kelsh, R. N. (2005). Phox2b Function in the Enteric Nervous System Is Conserved in Zebrafish and Is Sox10-dependent. *Mech. Develop.* 122, 659–669. doi:10.1016/j.mod.2004.12.008

Erter, C. E., Wilm, T. P., Basler, N., Wright, C. V. E., and Solnica-Krezel, L. (2001). Wnt8 Is Required in Lateral Mesendodermal Precursors for Neural Posteriorization *In Vivo*. *Development* 128, 3571–3583. doi:10.1242/dev.128.18.3571

Fraser, S. E., and Bronner-Fraser, M. (1991). Migrating Neural Crest Cells in the Trunk of the Avian Embryo Are Multipotent. *Development* 112, 913–920. doi:10.1242/dev.112.4.913

Fujii, R. (1993). Cytophysiology of Fish Chromatophores. *Int. Rev. Cytol.* 143, 191–255. doi:10.1016/s0074-7696(08)61876-8

Gans, C., and Northcutt, R. G. (1983). Neural Crest and the Origin of Vertebrates: a New Head. *Science* 220, 268–273. doi:10.1126/science.220.4594.268

García-Castro, M. I., Marcelle, C., and Bronner-Fraser, M. (2002). Ectodermal Wnt Function as a Neural Crest Inducer. *Science* 297, 848–851. doi:10.1126/science.1070824

Garcia-Ojalvo, J., and Martinez Arias, A. (2012). Towards a Statistical Mechanics of Cell Fate Decisions. *Curr. Opin. Genet. Develop.* 22, 619–626. doi:10.1016/j.gde.2012.10.004

Garnett, A. T., Square, T. A., and Medeiros, D. M. (2012). BMP, Wnt and FGF Signals Are Integrated through Evolutionarily Conserved Enhancers to Achieve Robust Expression of Pax3 and Zic Genes at the Zebrafish Neural Plate Border. *Development* 139, 4220–4231. doi:10.1242/dev.081497

Glinka, A., Wu, W., Delius, H., Monaghan, A. P., Blumenstock, C., and Niehrs, C. (1998). Dickkopf-1 Is a Member of a New Family of Secreted Proteins and Functions in Head Induction. *Nature* 391, 357–362. doi:10.1038/34848

Gomez, G. A., Prasad, M. S., Sandhu, N., Shelar, P. B., Leung, A. W., and García-Castro, M. I. (2019). Human Neural Crest Induction by Temporal Modulation of WNT Activation. *Develop. Biol.* 449, 99–106. doi:10.1016/j.ydbio.2019.02.015

Hall, B. K. (2000). The Neural Crest as a Fourth Germ Layer and Vertebrates as Quadroblastic Not Triploblastic. *Evol. Dev.* 2, 3–5. doi:10.1046/j.1525-142x.2000.00032.x

Hammerschmidt, M., Serbedzija, G. N., and McMahon, A. P. (1996). Genetic Analysis of Dorsoventral Pattern Formation in the Zebrafish: Requirement of a BMP-like Ventralizing Activity and its Dorsal Repressor. *Genes Dev.* 10, 2452–2461. doi:10.1101/gad.10.19.2452

Hans, S., Zöller, D., Hammer, J., Stucke, J., Spiess, S., Kesavan, G., et al. (2021). Cre-Controlled CRISPR Mutagenesis Provides Fast and Easy Conditional Gene Inactivation in Zebrafish. *Nat. Commun.* 12, 1125. doi:10.1038/s41467-021-21427-6

Hari, L., Brault, V., Kle´ber, M., Lee, H.-Y., Ille, F., Leimeroth, R., et al. (2002). Lineage-specific Requirements of β-catenin in Neural Crest Development. *J. Cel Biol.* 159, 867–880. doi:10.1083/jcb.200209039

He, X., Semenov, M., Tamai, K., and Zeng, X. (2004). LDL Receptor-Related Proteins 5 and 6 in Wnt/β-Catenin signaling:Arrows point the Way. *Development* 131, 1663–1677. doi:10.1242/dev.01117

Henion, P. D., and Weston, J. A. (1997). Timing and Pattern of Cell Fate Restrictions in the Neural Crest Lineage. *Development* 124, 4351–4359. doi:10.1242/dev.124.21.4351

Hodgkinson, C. A., Moore, K. J., Nakayama, A., Steingrímsson, E., Copeland, N. G., Jenkins, N. A., et al. (1993). Mutations at the Mouse Microphthalmia Locus Are Associated with Defects in a Gene Encoding a Novel basic-helix-loop-helix-zipper Protein. *Cell* 74, 395–404. doi:10.1016/0092-8674(93)90429-t

Hoppler, S., and Moon, R. T. (1998). BMP-2/-4 and Wnt-8 Cooperatively Pattern the Xenopus Mesoderm. *Mech. Develop.* 71, 119–129. doi:10.1016/s0925-4773(98)00004-5

Hou, L., Arnheiter, H., and Pavan, W. J. (2006). Interspecies Difference in the Regulation of Melanocyte Development by SOX10 and MITF. *Proc. Natl. Acad. Sci.* 103, 9081–9085. doi:10.1073/pnas.0603114103

Howard, A. G., Baker, P. A., Ibarra-García-Padilla, R., Moore, J. A., Rivas, L. J., Tallman, J. J., et al. (2021). An Atlas of Neural Crest Lineages along the Posterior Developing Zebrafish at Single-Cell Resolution. *Elife* 10, e60005. doi:10.7554/eLife.60005

Hsieh, J.-C., Kodjabachian, L., Rebbert, M. L., Rattner, A., Smallwood, P. M., Samos, C. H., et al. (1999). A New Secreted Protein that Binds to Wnt Proteins and Inhibits Their Activites. *Nature* 398, 431–436. doi:10.1038/18899

Ikeya, M., Lee, S. M. K., Johnson, J. E., McMahon, A. P., and Takada, S. (1997). Wnt Signalling Required for Expansion of Neural Crest and CNS Progenitors. *Nature* 389, 966–970. doi:10.1038/40146

Jin, E.-J., Erickson, C. A., Takada, S., and Burrus, L. W. (2001). Wnt and BMP Signaling Govern Lineage Segregation of Melanocytes in the Avian Embryo. *Develop. Biol.* 233, 22–37. doi:10.1006/dbio.2001.0222

Kague, E., Gallagher, M., Burke, S., Parsons, M., Franz-Odendaal, T., and Fisher, S. (2012). Skeletogenic Fate of Zebrafish Cranial and Trunk Neural Crest. *PLoS One* 7, e47394. doi:10.1371/journal.pone.0047394

Kapur, R. P. (1999). Early Death of Neural Crest Cells Is Responsible for Total Enteric Aganglionosis in Sox10Dom/Sox10Dom Mouse Embryos. *Pediatr. Dev. Pathol.* 2, 559–569. doi:10.1007/s100249900162

Kelsh, R. N., Brand, M., Jiang, Y. J., Heisenberg, C. P., Lin, S., Haffter, P., et al. (1996). Zebrafish Pigmentation Mutations and the Processes of Neural Crest Development. *Development* 123, 369–389. doi:10.1242/dev.123.1.369

Kelsh, R. N., Camargo Sosa, K., Farjami, S., Makeev, V., Dawes, J. H. P., and Rocco, A. (2021). Cyclical Fate Restriction: a New View of Neural Crest Cell Fate Specification. *Development* 148, dev176057. doi:10.1242/dev.176057

Kelsh, R. N., and Eisen, J. S. (2000). The Zebrafish Colourless Gene Regulates Development of Non-ectomesenchymal Neural Crest Derivatives. *Development* 127, 515–525. doi:10.1242/dev.127.3.515

Kormish, J. D., Sinner, D., and Zorn, A. M. (2010). Interactions between SOX Factors and Wnt/beta-Catenin Signaling in Development and Disease. *Develop. Dyn.* 239, 56–68. doi:10.1002/dvdy.22046

LaBonne, C., and Bronner-Fraser, M. (1998). Neural Crest Induction in Xenopus: Evidence for a Two-Signal Model. *Development* 125, 2403–2414. doi:10.1242/dev.125.13.2403

Lamborghini, J. E. (1980). Rohon-beard Cells and Other Large Neurons inXenopus Embryos Originate during Gastrulation. *J. Comp. Neurol.* 189, 323–333. doi:10.1002/cne.901890208

Lamoreux, M. L. (2010). *The Colors of Mice : A Model Genetic Network*. Chichester, West Sussex ; Hoboken, NJ: Wiley-Blackwell.

Le Douarin, N. (1973). A Biological Cell Labeling Technique and its Use in Experimental Embryology. *Develop. Biol.* 30, 217–222. doi:10.1016/0012-1606(73)90061-4

Le Douarin, N. M., and Kalcheim, C. (1999). *The Neural Crest*. 2nd ed. Cambridge: Cambridge University Press.

Lee, H.-Y., Kle´ber, M., Hari, L., Brault, V., Suter, U., Taketo, M. M., et al. (2004). Instructive Role of Wnt/ß-Catenin in Sensory Fate Specification in Neural Crest Stem Cells. *Science* 303, 1020–1023. doi:10.1126/science.1091611

Lee, R. T. H., Knapik, E. W., Thiery, J. P., and Carney, T. J. (2013). An Exclusively Mesodermal Origin of Fin Mesenchyme Demonstrates that Zebrafish Trunk Neural Crest Does Not Generate Ectomesenchyme. *Development* 140, 2923–2932. doi:10.1242/dev.093534

Lekven, A. C., Thorpe, C. J., Waxman, J. S., and Moon, R. T. (2001). Zebrafish Wnt8 Encodes Two Wnt8 Proteins on a Bicistronic Transcript and Is Required for Mesoderm and Neurectoderm Patterning. *Develop. Cel* 1, 103–114. doi:10.1016/s1534-5807(01)00007-7

Lencer, E., Prekeris, R., and Artinger, K. B. (2021). Single-cell RNA Analysis Identifies Pre-migratory Neural Crest Cells Expressing Markers of Differentiated Derivatives. *Elife* 10, e66078. doi:10.7554/eLife.66078

Lewis, J. L., Bonner, J., Modrell, M., Ragland, J. W., Moon, R. T., Dorsky, R. I., et al. (2004). Reiterated Wnt Signaling during Zebrafish Neural Crest Development. *Development* 131, 1299–1308. doi:10.1242/dev.01007

Leyns, L., Bouwmeester, T., Kim, S.-H., Piccolo, S., and De Robertis, E. M. (1997). Frzb-1 Is a Secreted Antagonist of Wnt Signaling Expressed in the Spemann Organizer. *Cell* 88, 747–756. doi:10.1016/s0092-8674(00)81921-2

Lister, J. A., Robertson, C. P., Lepage, T., Johnson, S. L., and Raible, D. W. (1999). Nacre Encodes a Zebrafish Microphthalmia-Related Protein that Regulates Neural-Crest-Derived Pigment Cell Fate. *Development* 126, 3757–3767. doi:10.1242/dev.126.17.3757

Lopes, S. S., Yang, X., Müller, J., Carney, T. J., McAdow, A. R., Rauch, G.-J., et al. (2008). Leukocyte Tyrosine Kinase Functions in Pigment Cell Development. *Plos Genet.* 4, e1000026. doi:10.1371/journal.pgen.1000026

Meijer, L., Skaltsounis, A.-L., Magiatis, P., Polychronopoulos, P., Knockaert, M., Leost, M., et al. (2003). GSK-3-Selective Inhibitors Derived from Tyrian Purple Indirubins. *Chem. Biol.* 10, 1255–1266. doi:10.1016/j.chembiol.2003.11.010

Miller, J. R. (2002). The Wnts. *Genome Biol.* 3, REVIEWS3001. doi:10.1186/gb-2001-3-1-reviews3001

Minchin, J. E. N., and Hughes, S. M. (2008). Sequential Actions of Pax3 and Pax7 Drive Xanthophore Development in Zebrafish Neural Crest. *Develop. Biol.* 317, 508–522. doi:10.1016/j.ydbio.2008.02.058

Miyanari, Y., and Torres-Padilla, M.-E. (2012). Control of Ground-State Pluripotency by Allelic Regulation of Nanog. *Nature* 483, 470–473. doi:10.1038/nature10807

Mongera, A., Singh, A. P., Levesque, M. P., Chen, Y.-Y., Konstantinidis, P., and Nüsslein-Volhard, C. (2013). Genetic Lineage Labeling in Zebrafish Uncovers Novel Neural Crest Contributions to the Head, Including Gill Pillar Cells. *Development* 140, 916–925. doi:10.1242/dev.091066

Mukherjee, S., Luedeke, D. M., Brown, L., and Zorn, A. M. (2021). SOX Transcription Factors Direct TCF-independent WNT/beta-catenin Transcription. *bioRxiv* 2000, 457694.

Mukhopadhyay, M., Shtrom, S., Rodriguez-Esteban, C., Chen, L., Tsukui, T., Gomer, L., et al. (2001). Dickkopf1 Is Required for Embryonic Head Induction and Limb Morphogenesis in the Mouse. *Develop. Cel* 1, 423–434. doi:10.1016/s1534-5807(01)00041-7

Nguyen, V. H., Schmid, B., Trout, J., Connors, S. A., Ekker, M., and Mullins, M. C. (1998). Ventral and Lateral Regions of the Zebrafish Gastrula, Including the Neural Crest Progenitors, Are Established by abmp2b/swirlPathway of Genes. *Develop. Bio.* 199, 93–110. doi:10.1006/dbio.1998.8927

Niehrs, C. (2012). The Complex World of WNT Receptor Signalling. *Nat. Rev. Mol. Cel Biol* 13, 767–779. doi:10.1038/nrm3470

Nikaido, M., Law, E. W. P., and Kelsh, R. N. (2013). A Systematic Survey of Expression and Function of Zebrafish Frizzled Genes. *PLoS One* 8, e54833. doi:10.1371/journal.pone.0054833

Nikaido, M., Subkhankulova, T., Uroshlev, L. A., Kasianov, A. J., Sosa, K. C., Bavister, G., et al. (2021). Zebrafish Pigment Cells Develop Directly from Persistent Highly Multipotent Progenitors. *bioRxiv* 2006, 448805.

Nitzan, E., Krispin, S., Pfaltzgraff, E. R., Klar, A., Labosky, P. A., and Kalcheim, C. (2013). A Dynamic Code of Dorsal Neural Tube Genes Regulates the Segregation between Neurogenic and Melanogenic Neural Crest Cells. *Development* 140, 2269–2279. doi:10.1242/dev.093294

Nusse, R., and Clevers, H. (2017). Wnt/β-Catenin Signaling, Disease, and Emerging Therapeutic Modalities. *Cell* 169, 985–999. doi:10.1016/j.cell.2017.05.016

Olden, T., Akhtar, T., Beckman, S. A., and Wallace, K. N. (2008). Differentiation of the Zebrafish Enteric Nervous System and Intestinal Smooth Muscle. *Genesis* 46, 484–498. doi:10.1002/dvg.20429

Opdecamp, K., Nakayama, A., Nguyen, M. T., Hodgkinson, C. A., Pavan, W. J., and Arnheiter, H. (1997). Melanocyte Development *In Vivo* and in Neural Crest Cell Cultures: Crucial Dependence on the Mitf basic-helix-loop-helix-zipper Transcription Factor. *Development* 124, 2377–2386. doi:10.1242/dev.124.12.2377

Parr, B. A., Shea, M. J., Vassileva, G., and McMahon, A. P. (1993). Mouse Wnt Genes Exhibit Discrete Domains of Expression in the Early Embryonic CNS and Limb Buds. *Development* 119, 247–261. doi:10.1242/dev.119.1.247

Pegge, J., Tatsinkam, A. J., Rider, C. C., and Bell, E. (2020). Heparan Sulfate Proteoglycans Regulate BMP Signalling during Neural Crest Induction. *Develop. Biol.* 460 (2), 108–114. doi:10.1016/j.ydbio.2019.12.015

Perfetto, M., Xu, X., Lu, C., Shi, Y., Yousaf, N., Li, J., et al. (2021). The RNA Helicase DDX3 Induces Neural Crest by Promoting AKT Activity. *Develop.* 148, dev18434. doi:10.1242/dev.184341

Petratou, K., Spencer, S. A., Kelsh, R. N., and Lister, J. A. (2021). The MITF Paralog Tfec Is Required in Neural Crest Development for Fate Specification of the Iridophore Lineage from a Multipotent Pigment Cell Progenitor. *PLOS ONE* 16, e0244794. doi:10.1371/journal.pone.0244794

Petratou, K., Subkhankulova, T., Lister, J. A., Rocco, A., Schwetlick, H., and Kelsh, R. N. (2018). A Systems Biology Approach Uncovers the Core Gene Regulatory Network Governing Iridophore Fate Choice from the Neural Crest. *Plos Genet.* 14, e1007402. doi:10.1371/journal.pgen.1007402

Piloto, S., and Schilling, T. F. (2010). Ovo1 Links Wnt Signaling with N-Cadherin Localization during Neural Crest Migration. *Development* 137, 1981–1990. doi:10.1242/dev.048439

Ragland, J. W., and Raible, D. W. (2004). Signals Derived from the Underlying Mesoderm Are Dispensable for Zebrafish Neural Crest Induction. *Develop. Biol.* 276, 16–30. doi:10.1016/j.ydbio.2004.08.017

Raible, D. W., and Eisen, J. S. (1994). Restriction of Neural Crest Cell Fate in the Trunk of the Embryonic Zebrafish. *Development* 120, 495–503. doi:10.1242/dev.120.3.495

Raible, D. W., Wood, A., Hodsdon, W., Henion, P. D., Weston, J. A., and Eisen, J. S. (1992). Segregation and Early Dispersal of Neural Crest Cells in the Embryonic Zebrafish. *Dev. Dyn.* 195, 29–42. doi:10.1002/aja.1001950104

Rawls, J. F., Mellgren, E. M., and Johnson, S. L. (2001). How the Zebrafish Gets its Stripes. *Develop. Biol.* 240, 301–314. doi:10.1006/dbio.2001.0418

Rocha, M., Singh, N., Ahsan, K., Beiriger, A., and Prince, V. E. (2020). Neural Crest Development: Insights from the Zebrafish. *Develop. Dyn.* 249, 88–111. doi:10.1002/dvdy.122

Routledge, D., and Scholpp, S. (2019). Mechanisms of Intercellular Wnt Transport. *Development* 146 (10), 146. doi:10.1242/dev.176073

Ruzicka, L., Howe, D. G., Ramachandran, S., Toro, S., Van Slyke, C. E., Bradford, Y. M., et al. (2019). The Zebrafish Information Network: New Support for Non-coding Genes, Richer Gene Ontology Annotations and the Alliance of Genome Resources. *Nucleic Acids Res.* 47, D867–D873. doi:10.1093/nar/gky1090

Saint-Jeannet, J.-P., He, X., Varmus, H. E., and Dawid, I. B. (1997). Regulation of Dorsal Fate in the Neuraxis by Wnt-1 and Wnt-3a. *Proc. Natl. Acad. Sci.* 94, 13713–13718. doi:10.1073/pnas.94.25.13713

Sato, M., and Yost, H. J. (2003). Cardiac Neural Crest Contributes to Cardiomyogenesis in Zebrafish. *Develop. Biol.* 257, 127–139. doi:10.1016/s0012-1606(03)00037-x

Sauka-Spengler, T., and Bronner-Fraser, M. (2008). A Gene Regulatory Network Orchestrates Neural Crest Formation. *Nat. Rev. Mol. Cel Biol* 9, 557–568. doi:10.1038/nrm2428

Scarpa, E., Szabó, A., Bibonne, A., Theveneau, E., Parsons, M., and Mayor, R. (2015). Cadherin Switch during EMT in Neural Crest Cells Leads to Contact Inhibition of Locomotion via Repolarization of Forces. *Develop. Cel* 34, 421–434. doi:10.1016/j.devcel.2015.06.012

Schartl, M., Larue, L., Goda, M., Bosenberg, M. W., Hashimoto, H., and Kelsh, R. N. (2016). What Is a Vertebrate Pigment Cell. *Pigment Cel Melanoma Res.* 29, 8–14. doi:10.1111/pcmr.12409

Schilling, T. F., and Kimmel, C. B. (1994). Segment and Cell Type Lineage Restrictions during Pharyngeal Arch Development in the Zebrafish Embryo. *Development* 120, 483–494. doi:10.1242/dev.120.3.483

Schumacher, J. A., Hashiguchi, M., Nguyen, V. H., and Mullins, M. C. (2011). An Intermediate Level of BMP Signaling Directly Specifies Cranial Neural Crest Progenitor Cells in Zebrafish. *PLoS One* 6, e27403. doi:10.1371/journal.pone.0027403

Shepherd, I. T., Pietsch, J., Elworthy, S., Kelsh, R. N., and Raible, D. W. (2004). Roles for GFRα1 Receptors in Zebrafish Enteric Nervous System Development. *Development* 131, 241–249. doi:10.1242/dev.00912

Sieber-Blum, M., and Cohen, A. M. (1980). Clonal Analysis of Quail Neural Crest Cells. *Develop. Biol.* 80, 96–106. doi:10.1016/0012-1606(80)90501-1

Soldatov, R., Kaucka, M., Kastriti, M. E., Petersen, J., Chontorotzea, T., Englmaier, L., et al. (2019). Spatiotemporal Structure of Cell Fate Decisions in Murine Neural Crest. *Science* 364. doi:10.1126/science.aas9536

Stanganello, E., Hagemann, A. I. H., Mattes, B., Sinner, C., Meyen, D., Weber, S., et al. (2015). Filopodia-based Wnt Transport during Vertebrate Tissue Patterning. *Nat. Commun.* 6, 5846. doi:10.1038/ncomms6846

Stemple, D. L., and Anderson, D. J. (1992). Isolation of a Stem Cell for Neurons and Glia from the Mammalian Neural Crest. *Cell* 71, 973–985. doi:10.1016/0092-8674(92)90393-q

Steventon, B., Araya, C., Linker, C., Kuriyama, S., and Mayor, R. (2009). Differential Requirements of BMP and Wnt Signalling during Gastrulation and Neurulation Define Two Steps in Neural Crest Induction. *Development* 136, 771–779. doi:10.1242/dev.029017

Takada, R., Satomi, Y., Kurata, T., Ueno, N., Norioka, S., Kondoh, H., et al. (2006). Monounsaturated Fatty Acid Modification of Wnt Protein: its Role in Wnt Secretion. *Develop. Cel* 11, 791–801. doi:10.1016/j.devcel.2006.10.003

Takeda, K., Yasumoto, K.-i., Takada, R., Takada, S., Watanabe, K.-i., Udono, T., et al. (2000). Induction of Melanocyte-specific Microphthalmia-Associated Transcription Factor by Wnt-3a. *J. Biol. Chem.* 275, 14013–14016. doi:10.1074/jbc.c000113200

Tan, C., Deardorff, M. A., Saint-Jeannet, J.-P., Yang, J., Arzoumanian, A., and Klein, P. S. (2001). Kermit, a Frizzled Interacting Protein, Regulates Frizzled 3 Signaling in Neural Crest Development. *Development* 128, 3665–3674. doi:10.1242/dev.128.19.3665

Tatarakis, D., Tuttle, A., and Schilling, T. F. (2020). *Lmo7a Coordinates Neural Crest Migration and Lineage Specification by Regulating Cell Adhesion Dynamics*. BioRxiv; May 2020.

Teh, C., Sun, G., Shen, H., Korzh, V., and Wohland, T. (2015). Modulating the Expression Level of Secreted Wnt3 Influences Cerebellum Development in Zebrafish Transgenics. *Development* 142, 3721–3733. doi:10.1242/dev.127589

Theveneau, E., Steventon, B., Scarpa, E., Garcia, S., Trepat, X., Streit, A., et al. (2013). Chase-and-run between Adjacent Cell Populations Promotes Directional Collective Migration. *Nat. Cel Biol* 15, 763–772. doi:10.1038/ncb2772

Tucker, J. A., Mintzer, K. A., and Mullins, M. C. (2008). The BMP Signaling Gradient Patterns Dorsoventral Tissues in a Temporally Progressive Manner along the Anteroposterior axis. *Develop. Cel* 14, 108–119. doi:10.1016/j.devcel.2007.11.004

Tuttle, A. M., Hoffman, T. L., and Schilling, T. F. (2014). Rabconnectin-3a Regulates Vesicle Endocytosis and Canonical Wnt Signaling in Zebrafish Neural Crest Migration. *Plos Biol.* 12, e1001852. doi:10.1371/journal.pbio.1001852

Vibert, L., Aquino, G., Gehring, I., Subkankulova, T., Schilling, T. F., Rocco, A., et al. (2017). An Ongoing Role forWntsignaling in Differentiating Melanocytes *In Vivo*. *Pigment Cel Melanoma Res.* 30, 219–232. doi:10.1111/pcmr.12568

Villanueva, S., Glavic, A., Ruiz, P., and Mayor, R. (2002). Posteriorization by FGF, Wnt, and Retinoic Acid Is Required for Neural Crest Induction. *Develop. Biol.* 241, 289–301. doi:10.1006/dbio.2001.0485

Weston, J. A. (1991). 6 Sequential Segregation and Fate of Developmentally Restricted Intermediate Cell Populations in the Neural Crest Lineage. *Curr. Top. Dev. Biol.* 25, 133–153. doi:10.1016/s0070-2153(08)60414-7

Willert, K., Brown, J. D., Danenberg, E., Duncan, A. W., Weissman, I. L., Reya, T., et al. (2003). Wnt Proteins Are Lipid-Modified and Can Act as Stem Cell Growth Factors. *Nature* 423, 448–452. doi:10.1038/nature01611

Wu, W., Glinka, A., Delius, H., and Niehrs, C. (2000). Mutual Antagonism between Dickkopf1 and Dickkopf2 Regulates Wnt/β-Catenin Signalling. *Curr. Biol.* 10, 1611–1614. doi:10.1016/s0960-9822(00)00868-x

Conflict of Interest: The authors declare that the research was conducted in the absence of any commercial or financial relationships that could be construed as a potential conflict of interest.

Publisher's Note: All claims expressed in this article are solely those of the authors and do not necessarily represent those of their affiliated organizations, or those of the publisher, the editors and the reviewers. Any product that may be evaluated in this article, or claim that may be made by its manufacturer, is not guaranteed or endorsed by the publisher.

frontiers in Cell and Developmental Biology

REVIEW
published: 22 December 2021
doi: 10.3389/fcell.2021.795194

Concepts in Multifactorial Etiology of Developmental Disorders: Gene-Gene and Gene-Environment Interactions in Holoprosencephaly

Hsiao-Fan Lo[†], *Mingi Hong*[†] *and Robert S. Krauss* *

Department of Cell, Developmental, and Regenerative Biology, Icahn School of Medicine at Mount Sinai, New York, NY, United States

Many common developmental disorders are thought to arise from a complex set of genetic and environmental risk factors. These factors interact with each other to affect the strength and duration of key developmental signaling pathways, thereby increasing the possibility that they fail to achieve the thresholds required for normal embryonic patterning. One such disorder, holoprosencephaly (HPE), serves as a useful model system in understanding various forms of multifactorial etiology. Genomic analysis of HPE cases, epidemiology, and mechanistic studies of animal models have illuminated multiple potential ways that risk factors interact to produce adverse developmental outcomes. Among these are: 1) interactions between driver and modifier genes; 2) oligogenic inheritance, wherein each parent provides predisposing variants in one or multiple distinct loci; 3) interactions between genetic susceptibilities and environmental risk factors that may be insufficient on their own; and 4) interactions of multiple genetic variants with multiple non-genetic risk factors. These studies combine to provide concepts that illuminate HPE and are also applicable to additional disorders with complex etiology, including neural tube defects, congenital heart defects, and oro-facial clefting.

Keywords: birth defect, holoprosencephaly, hedgehog signaling, teratogen, fetal alcohol, genetics, epidemiology

OPEN ACCESS

Edited by:
Annette Hammes, Max Delbrück Center for Molecular Medicine (MDC), Germany

Reviewed by:
Thomas Willnow, Helmholtz Association of German Research Centers (HZ), Germany
Philippa Francis-West, King's College London, United Kingdom

***Correspondence:**
Robert S. Krauss
Robert.Krauss@mssm.edu

[†]*These authors have contributed equally to this work*

Specialty section:
This article was submitted to Morphogenesis and Patterning, a section of the journal Frontiers in Cell and Developmental Biology

Received: *14 October 2021*
Accepted: *29 November 2021*
Published: *22 December 2021*

Citation:
Lo H-F Hong M and Krauss RS (2021) Concepts in Multifactorial Etiology of Developmental Disorders: Gene-Gene and Gene-Environment Interactions in Holoprosencephaly. Front. Cell Dev. Biol. 9:795194. doi: 10.3389/fcell.2021.795194

INTRODUCTION

Holoprosencephaly (HPE) is a very common developmental disorder defined as a failure in midline patterning of the forebrain and/or midface (Muenke and Beachy, 2001; Tekendo-Ngongang et al., 2020). It is usually stated that HPE arises approximately once per 250 conceptuses, but a recent study suggested that this figure may be as high as once per 32 conceptuses (Shiota and Yamada, 2010; Shiota, 2021). Due to *in utero* lethality, live birth frequency is only ~1 in 10,000 (Leoncini et al., 2008). An unbroken continuum of HPE phenotypes (sometimes called the HPE spectrum) is broadly classified into three categories based on the degree of midline cleavage of the forebrain (Muenke and Beachy, 2001; Tekendo-Ngongang et al., 2020). Alobar HPE, the most severe form, is characterized by complete failure to partition the forebrain into left and right hemispheres, resulting in a single, centrally-located ventricle. Semilobar and lobar HPE are progressively less severe forms and display partial, or mostly complete, forebrain cleavage, respectively. HPE-associated midline anomalies of the face include cyclopia, single nostril, midfacial midline clefting, hypotelorism (i.e., very close set eyes), and solitary median maxillary central incisor (**Figure 1**). Mild facial midline abnormalities may occur without clinically obvious brain malformations and are called HPE microforms (Tekendo-

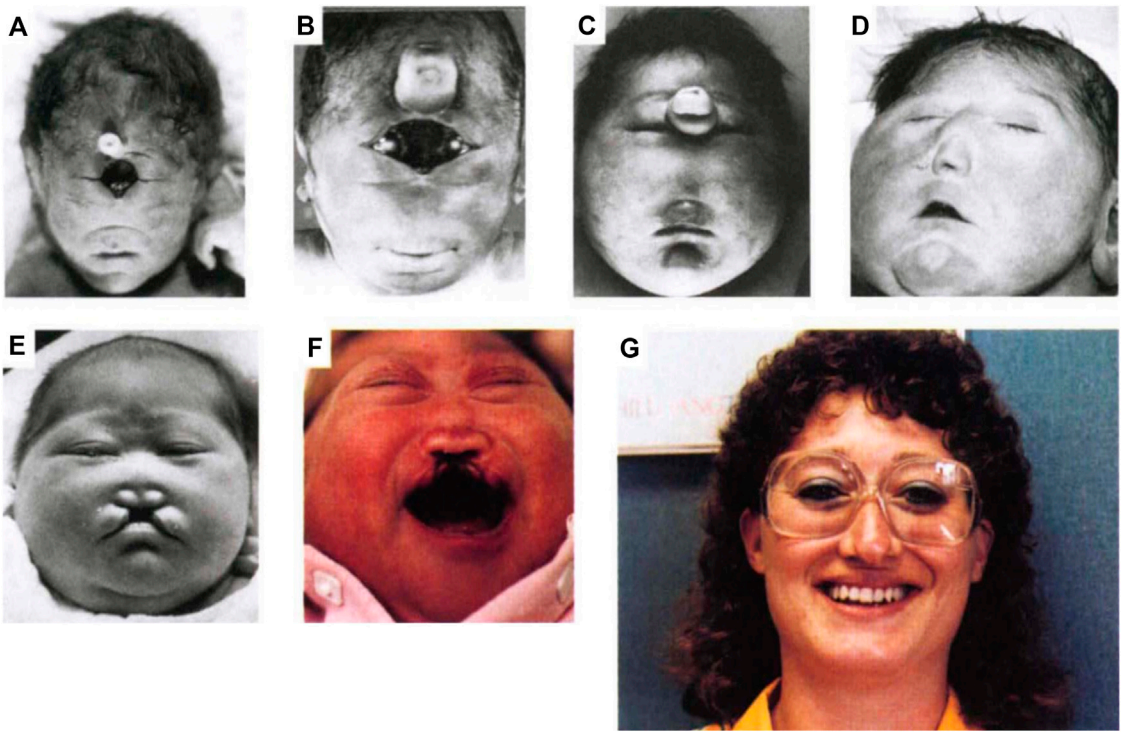

FIGURE 1 | Spectrum of HPE phenotypes. A spectrum of facial phenotypes in patients with HPE, including cyclopia with a proboscis **(A)**, undivided eye field with proboscis **(B)**, proboscis between separated eyes **(C)**, closely spaced eyes (hypotelorism) and single-nostril nose **(D)**, hypotelorism with midfacial hypoplasia and midline cleft lip **(E)**, hypotelorism, absence of nasal bones, and midline cleft lip **(F)**, and solitary median maxillary central incisor **(G)**. Reprinted with permission of Springer Nature (Roessler et al., 1996).

Ngongang et al., 2020). A variant HPE subtype, middle interhemispheric (MIH) HPE, is relatively rare and differs in its developmental origins from the classical forms (Monuki, 2007; Tekendo-Ngongang et al., 2020), which are all thought to share a similar etiology but vary in expressivity.

Development of the forebrain is a complex, multistep process [for detailed reviews, see (Wilson and Houart, 2004; Grinblat and Lipinski, 2019)]. Briefly, neuroectodermal cells at the rostral end of the neuraxis develop into the anterior neural plate, followed by dorsoventral patterning. The forebrain in turn provides signals that pattern the face. It has long been said for HPE that, "the face predicts the brain", an aphorism that holds true in about 80% of cases (DeMyer, 1964; Krauss, 2007). HPE is generally associated with defects in ventral patterning, a process regulated by morphogenetic signals that begin with Nodal pathway signaling during gastrulation, followed by Hedgehog (HH) and FGF pathway signaling in the ventral midline of the developing forebrain and, ultimately, facial primordia (Wilson and Houart, 2004; Marcucio et al., 2015; Grinblat and Lipinski, 2019). Mutations in genes encoding components and regulators of these pathways are found in HPE. Partitioning of the forebrain into hemispheres initiates dorsally, and it is not clear how defects in ventral patterning perturb this process in classical HPE. In contrast, MIH HPE appears to arise as a consequence of defects in dorsal patterning, and the characteristic craniofacial abnormalities associated with classical HPE are observed infrequently in this form of HPE (Monuki, 2007; Fernandes and Hébert, 2008).

The wide spectrum of defects that characterize classical forms of HPE likely arise from alterations in both signaling pathway levels and timing. Sonic HH (SHH) can function as a morphogen, specifying distinct outcomes for cells within a target field in a concentration-dependent manner; failures to reach signaling output thresholds required for specific development patterning events may help dictate a spectrum of HPE phenotypes (Young et al., 2010; Sagner and Briscoe, 2019). The developmental stage at which suboptimal signaling by these pathways occurs also plays a significant role in the expressivity of HPE outcomes, with earlier deficits resulting in more severe phenotypes, and progressively later deficits yielding progressively less severe phenotypes (Cordero et al., 2004; Krauss, 2007; Marcucio et al., 2015).

HPE occurs most often as part of a syndrome; some of these syndromes are associated with specific chromosomal aberrations, including various trisomies, structural chromosomal abnormalities, and pathogenic copy number variations (CNVs) (Kruszka and Muenke, 2018). Isolated HPE (i.e., HPE not associated with gross chromosomal aberrations or as a feature of a syndrome) accounts for approximately ~25% of cases but ~75% of patients, and occurs both in pedigrees and sporadically (Roessler et al., 2018a; Tekendo-Ngongang et al., 2020). Mutations at known gene loci have been identified in <30% of individuals with isolated HPE (Kim et al., 2018; Tekendo-

Ngongang et al., 2020). Clinical presentation of HPE is highly variable, even in pedigrees, and many mutation carriers in these families have no obvious clinical manifestation (Lacbawan et al., 2009; Solomon et al., 2012; Stokes et al., 2018). It appears that a complex interplay of multiple genetic and/or environmental influences underlies a substantial fraction of isolated HPE cases (Hong and Krauss, 2018; Beames and Lipinski, 2020).

One may ask, why study HPE? The developmental events that go awry happen in the third and fourth weeks of human gestation, before many women know they are pregnant (Hong and Krauss, 2018; Tekendo-Ngongang et al., 2020). Reversing the causative developmental patterning defects after they have occurred is not possible, so successful therapeutic intervention is unlikely. Moreover, the vast majority of holoprosencephalic fetuses succumb *in utero*, often in the first trimester (Shiota and Yamada, 2010; Shiota, 2021). A superficial focus on the relatively low live birth frequency, however, ignores the difficulties facing surviving patients and their families, as well as the pain to families experiencing pregnancy loss. There are many additional important reasons to study HPE. First, understanding the etiology of HPE may aid in its prevention. The prime example of such a success is maternal dietary supplementation of folic acid, which reduces the risk of neural tube defects, another developmental disorder associated with errors in early patterning and high rates of prenatal mortality (Finnell et al., 2021). Second, HPE serves as an ideal model of a developmental disorder with complex, multifactorial etiology. Recent genomic analyses and epidemiological studies promise insight into this phenomenon. Animal models accurately mimic this situation and allow both experimental validation of observations made in human populations and testing of ideas that may provide new leads in human studies. Importantly, multifactorial etiology is likely to apply to many developmental disorders. HPE is well positioned to serve as a model system in which broadly applicable concepts are established. Here we review the evidence for multifactorial etiology in HPE in humans and how animal models contribute to our understanding of this phenomenon.

GENE-GENE INTERACTIONS IN HPE

The three most frequently mutated genes in isolated HPE are *SHH*, *ZIC2*, and *SIX3*, but across many studies none of them accounts for more than 10% of total cases (Tekendo-Ngongang et al., 2020). Mutations in *FGF8* and *FGFR1* are also relatively frequently observed in isolated HPE (>2% of cases), but they are also implicated in syndromes that include HPE (e.g., Kallman and Hartsfield syndromes) (Dubourg et al., 2016; Roessler et al., 2018a). Interestingly, most of these factors interact during rostroventral midline patterning; SHH and SIX3 regulate each other's expression, and the FGF and HH signaling pathways cross-regulate each other' activities (Wilson and Houart, 2004; Geng et al., 2008; Grinblat and Lipinski, 2019). Mutations in many other genes (mainly encoding components and regulators of HH signaling) have been identified, but these are considered "minor" or rare HPE loci (≤1% of cases for individual genes) (Bae et al., 2011; Dubourg et al., 2016; Roessler et al., 2018a; Roessler et al., 2018b; Kruszka et al., 2019a; Kruszka et al., 2019b; Tekendo-Ngongang et al., 2019). Virtually all these mutations are heterozygous and, where tested, are generally loss-of-function variants. Autosomal recessive mutations in HPE have been documented, but are very rare. Examples include mutations in *HHAT* (encoding Hedgehog acyltransferase), *PLCH1* (encoding phospholipase C eta-1), and *STIL* [encoding a factor required for maintenance of primary cilia, a subcellular structure critical for HH signaling (Kakar et al., 2015; Mouden et al., 2015; Drissi et al., 2021; Pande et al., 2021)].

Driver and Modifier Genes in HPE

Heterozygous mutations in the most frequently involved loci are viewed as "drivers" of HPE, in that the alleles are of low frequency in the population, their functions fit the known developmental biology of HPE, and they are generally accepted to be essential to the phenotype. But are they actually sufficient to induce the full range of phenotypes seen in HPE patients? For *SHH* and *SIX3*, the answer to this question is likely, "no". Only 10 and 14% of *SHH* and *SIX3* mutations occur *de novo*, respectively (Lacbawan et al., 2009; Solomon et al., 2012). Additionally, large HPE pedigrees exist wherein many individuals across generations have mutations in either *SHH* or *SIX3*, with up to ~30% of carriers lacking obvious clinical manifestation and the rest displaying a full spectrum of phenotypes (Lacbawan et al., 2009; Solomon et al., 2012). Furthermore, even in sporadic HPE cases, the majority of *SHH* and *SIX3* mutations are inherited from unaffected, or very mildly affected, parents (Lacbawan et al., 2009; Solomon et al., 2012). In contrast, *ZIC2* heterozygosity may be sufficient. More than 70% of *ZIC2* mutations arise *de novo*, and large pedigrees have not been observed (Solomon et al., 2010). Interestingly, *ZIC2*-associated HPE is phenotypically distinct from that associated with *SHH* and *SIX3*, in that it lacks the classical facial midline features of the latter (Solomon et al., 2010).

A statistical evaluation of these results led to an "autosomal dominant mutation plus modifier" model, in which the penetrance and expressivity of heterozygous mutations in *SHH* or *SIX3* (or other, rarer HPE genes) is determined by additional risk factors—genetic, environmental, or both—acting as modifiers (Roessler et al., 2012). Initial evidence for the existence of HPE modifier genes came from studies with mice. Germline mutation of HPE driver genes in mice also produces HPE, but for reasons that are still not fully clear, mice require homozygous mutations for phenotypic manifestation (i.e., HPE is autosomal recessive in mice) (Hong and Krauss, 2018). Even in the homozygous mutant state, the penetrance and expressivity of HPE for some of these genes is highly dependent on the genetic background of the mice. C57BL/6 mice are a more sensitive strain than are various 129 substrains for HPE associated with null mutation of *Six3*, as well as of the rare HPE genes, *Cdon*, and *Gli2* (Zhang et al., 2006; Geng et al., 2008; Heyne et al., 2016). Therefore, the genetic background differences in these strains function to modify the phenotypic outcome of the same mutation. The gene loci responsible for HPE sensitivity *vs.* resistance in these various inbred lines have not been identified. In fact, differential strain sensitivity to many

mutations has long been recognized, but few such modifiers have been found. Alternative approaches have therefore been pursued. Mecklenburg et al. recently reported that mutation of *Lrp2* (which encodes an auxiliary HH receptor) produces HPE in C57BL/6N mice but not in FVB/N mice (Mecklenburg et al., 2021). The authors generated transcriptomes from embryonic forebrains of wild type and *Lrp2* mutant mice of both backgrounds and of F1 mice (which, like FVB/N mice, are resistant to *Lrp2* mutation). Comparative analysis of these datasets uncovered differentially expressed genes encoding previously unidentified regulators of HH signaling (Mecklenburg et al., 2021). These genes may in turn be candidate modifiers in human HPE.

Identification of HPE modifier genes has been challenging, and few are known. A classical modifier gene with high explanatory power for the variability of HPE phenotypes would be anticipated to have alleles with a frequency higher than the live birth rate and be enriched in HPE cases, relative to the general population. Furthermore, at least some HPE patients who carry the putative modifier allele should also have heterozygous mutations in known HPE driver genes, providing a genetic substrate on which the modifier acts. Finally, such modifier genes should have a biological function consistent with a role in rostroventral midline patterning (though such functions may be unknown at the time of the modifier's discovery). Only one such modifier has been identified: *BOC*, which encodes a HH coreceptor (Petrov et al., 2017). In studying *BOC* missense variants present in HPE patients, two alleles were identified in cases that also had mutations in either *ZIC2* or *TGIF1* (a *bone fide* HPE gene) (Hong et al., 2017). One *BOC* variation had a minor allele frequency of 0.0017, higher than the HPE live birth frequency of 1:10,000. These alleles were then demonstrated to have a loss of function in *in vitro* HH signaling assays (Hong et al., 2017). *BOC* missense alleles are not commonly found in HPE, however, suggesting they are relatively low frequency participants in this disorder. Nevertheless, there are hundreds of *BOC* missense mutations listed in gnomAD, and their potential roles are as yet unclear.

Strengthening the conclusion that *BOC* is a human HPE modifier gene is that its murine counterpart acts as a true silent HPE modifier gene in mice. *Boc*-null mice do not have HPE, but removal of *Boc* from *Cdon* mutant mice enhances HPE associated with the latter, on both C57BL/6 and 129 backgrounds (Zhang et al., 2011). However, BOC regulates HH-dependent craniofacial patterning in complex ways. Although *Boc*-null mice do not display defects in craniofacial development on any studied genetic background, *Boc* mutations interact differentially with mutations of another HH coreceptor, GAS1, dependent on the genetic background. *Boc* mutation enhances craniofacial midline defects of *Gas1* mutants on a mixed genetic background, whereas it partially rescues such defects in *Gas1* mutants on a C57BL/6 background (Seppala et al., 2014; Echevarría-Andino and Allen, 2020). BOC, as well as its paralog CDON, can therefore function as both a positive and negative regulator of HH-dependent patterning in various model organisms (Gallardo and Bovolenta, 2018). Significantly, a *BOC* variant identified in an HPE patient displayed a HH ligand-dependent, *gain*-of-function phenotype in in vitro assays, opposite what would be predicted for an allele that promoted HPE (Hong et al., 2017). This variant is unique to the genome databases and may represent a rare HPE suppressor allele that dampened clinical phenotypes, allowing patient survival and the ability to be analyzed. These results suggest that HPE modifiers may be very complex in function.

Oligogenic Inheritance

A view of gene-gene interactions in HPE etiology that is complementary to an "autosomal dominant driver mutation-plus-modifier" model is a more generalized oligogenic inheritance model; i.e., HPE can arise from a combination of multiple inherited mutations, without necessarily involving a strict hierarchy of driver and modifier genes (Dubourg et al., 2018). Until relatively recently, targeted sequencing for mutations in four known HPE genes (*SHH*, *ZIC2*, *SIX3*, and *TGIF1*) was the standard applied to new cases, and very few cases presented with variants in more than one gene. As the list of potential HPE genes grew, and whole exome sequencing (WES) became more affordable, it became possible to screen many individuals in families for variants in many genes at once. Kim et al. applied this approach to 26 families in which asymptomatic or mildly affected parents had children with HPE, ranging from alobar to microform HPE (Kim et al., 2018). A prioritization strategy that included bioinformatic analyses, expression analyses, and mouse knockout phenotypes led to a focus on 180 genes and, in turn, identification of oligogenic inheritance in 10 of the 26 families. HPE cases had between two and five variants from the list of 180 genes and always inherited at least one variant from each parent. Mutations in *SHH*, a classic driver gene, and in *BOC*, the sole known gene that can be viewed as a pure modifier, were identified in multiple cases, including one that had variants in both genes (Kim et al., 2018). This study also identified genes not previously implicated in human HPE, but for which mouse studies suggested a potential role, including *COL2A1*, and *NDST1*. *COL2A1* encodes a collagen isoform and *NDST1* encodes a heparan sulfate-modifying enzyme; these factors act extracellularly to regulate HH signaling in forebrain and craniofacial development (Grobe et al., 2005; Leung et al., 2010). Additionally, variants in several genes encoding components of primary cilia were identified (Kim et al., 2018). Primary cilia are the cellular site of HH signaling to GLI transcription factors (Gigante and Caspary, 2020). Finally, some recurrent oligogenic events were observed, including two families with variants in *BOC* and *SCUBE2*. *SCUBE2* encodes a secreted chaperone for HH ligands, which interacts directly with the HH coreceptor BOC (Petrov et al., 2017).

Statistical analyses demonstrated that oligogenic inheritance in the selected candidate genes occurred much more frequently in HPE cases than controls; nevertheless, it will be valuable to follow up these observations with experimental approaches. First, functional analyses on these alleles can be performed to assess whether they are indeed loss-of-function variants. Second, it will be interesting to generate mouse models to further test the specificity of these genetic interactions. For example, CNVs and a single example of a nucleotide variant in the Notch ligand *DLL1* were identified in HPE patients, suggested a previously unknown role for the Notch pathway in

rostroventral midline patterning (Dupé et al., 2010). Subsequent studies with mice demonstrated a genetic interaction between Notch and HH signaling in development of the pituitary gland, a structure commonly affected in HPE and midline disorders (Hamdi-Rozé et al., 2020).

There is much overlap between the autosomal dominant mutation-plus-modifier model and oligogenic inheritance model. In the latter, genes considered drivers (e.g., *SHH*) were sometimes found, suggesting that some of the additional variant genes present in specific cases may have provided a modifier function to heterozygous loss of a more powerful driver mutation. Additionally, the presence of as many as five variants in some cases of oligogenic inheritance logically suggests that not all variants contribute equally strongly towards the ultimate phenotype. In both models, a combination of genetic variants interact to elevate the likelihood of a defect in rostroventral midline patterning. Furthermore, both models offer potential explanatory power for the incomplete penetrance and variable expressivity that is characteristic of HPE.

GENE-ENVIRONMENT INTERACTIONS IN HPE

Multigenic interactions provide an appealing explanation for many of the complexities associated with HPE, and such analyses should continue to bear fruit. However, mutations have been identified in only a minority of isolated HPE cases, even in WES studies that led to discovery of new HPE genes (Kruszka et al., 2019a; Kruszka et al., 2019b; Tekendo-Ngongang et al., 2019). The fraction of cases with an identifiable genetic component is sure to rise as whole genome sequencing and yet more sophisticated bioinformatic analyses are applied to HPE. However, HPE has long been associated with teratogenic causes also, and it is possible that in some individual cases, mutations and/or genetic predispositions are irrelevant or only minor etiological factors.

The archetypal HH pathway inhibitor cyclopamine was discovered as the major teratogen in corn lilies, which when eaten by pregnant ewes caused cyclopia in their offspring (Chen, 2016). This tour de force of agricultural and scientific discovery demonstrated that *in utero* exposure to a chemical inhibitor of HH signaling at a sensitive period of development is sufficient to induce the most severe form of HPE. Although people do not consume corn lilies, exposure to specific teratogens, or to combinations of non-genetic risk factors, may therefore contribute to human HPE, potentially working with the types of genetic predisposition described in the previous section.

Several epidemiological studies of HPE have been performed, but conclusions were limited by both the number of cases available (generally live births) and the likelihood of incomplete reporting on exposures that occurred during the very early sensitive period for HPE (the third to fourth weeks after conception) (Linn et al., 1983). Maternal pregestational diabetes, which is implicated in several structural birth defects, has reproducibly been associated with elevated HPE risk in these studies (Miller et al., 2010; Summers et al., 2018; Addissie et al., 2021). Prenatal alcohol exposure (PAE) has also been implicated as a risk factor for HPE, in some but not all studies (Croen et al., 2000; Miller et al., 2010; Abe et al., 2018; Summers et al., 2018; Addissie et al., 2021). This may be partly related to how much detail is obtained from questionnaires; one recent case-control study did not find an association between HPE and alcohol consumption *vs.* non-consumption, but increasing amounts of alcohol consumed correlated with higher HPE risk, suggesting a possible threshold effect and dose-responsive outcomes (Addissie et al., 2021).

Prenatal Alcohol Exposure

PAE is an acknowledged human teratogen and the cause of fetal alcohol spectrum disorders (FASD), including fetal alcohol syndrome (FAS) (Hoyme et al., 2005; Hoyme et al., 2016). An overlap between FASD and mild forms of HPE has been noted by clinicians and laboratory scientists since the 1980s (Sulik and Johnston, 1982; Webster et al., 1983; Neri et al., 1988). Defects of the midfacial midline are commonly seen in FAS, including smooth philtrum, and hypoplastic midface (Hoyme et al., 2005; Hoyme et al., 2016). Midline CNS structures affected in HPE, such as the corpus collosum, are also disproportionately affected in FAS (Coulter et al., 1993; Johnson et al., 1996; Bookstein et al., 2002; Suttie et al., 2018). Two recent papers from leading FASD clinicians reported that reduced interpupillary distance and its severe form, hypotelorism (which are midline patterning defects common in HPE) are useful diagnostic criteria in FASD (Bandoli et al., 2020; Gomez et al., 2020). HPE phenotypes are restricted to the midline, while FASD phenotypes are not; however, the midline defects that define milder HPE are a common feature of FASD, leading numerous investigators to conclude that related mechanisms account for these similarities. As mild HPE phenotypes are a common feature of FASD, this scenario can be viewed as analogous to HPE being a feature of specific genetic syndromes.

Studies with mice offer strong support for this point of view. In 1981, Sulik and colleagues developed a mouse model of FASD with C57BL/6 mice, and it was quickly noted that HPE-like phenotypes were among those observed (Sulik et al., 1981; Sulik and Johnston, 1982). As noted above, C57BL/6 mice are sensitive to mutation-induced HPE, and HPE is observed in ~20% of the mice subjected to this PAE protocol (Aoto et al., 2008). Furthermore, PAE-induced HPE is enhanced in C57BL/6 mice heterozygous for *Shh* or *Gli2*, thereby demonstrating a gene-environment interaction (Kietzman et al., 2014). 129S6 mice, which are much more resistant to mutation-induced HPE than C57BL/6 mice, are also resistant to PAE-induced HPE, and other craniofacial phenotypes (Downing et al., 2009; Hong and Krauss, 2012). 129S6 mice with a mutation in the HH coreceptor CDON have a subthreshold deficit in HH signaling and are sensitive to HPE induced by "second hits", genetic or environmental (Hong and Krauss, 2018). PAE in these mice produced a complete spectrum of HPE phenotypes with high penetrance and high fidelity to human HPE (Hong and Krauss, 2012). PAE therefore induces HPE in mice that are genetically sensitive due to: 1) strain

background modifiers; 2) the presence of true predisposing mutations; or 3) both. These results suggest that, in humans, PAE may function as an environmental modifier of HPE.

Δ9-Tetrahydrocannabinol

In 2015, Khaliullina et al. demonstrated that endocannabinoids, a class of endogenous fatty acids/alcohols, inhibited HH signaling in developing fruit flies, and cultured mouse cells (Khaliullina et al., 2015). Additionally, phytocannabinoids, the active ingredients in cannabis [e.g., Δ9-tetrahydrocannabinol (THC) and cannabidiol], also inhibited HH signaling in cultured cells. This raised the possibility that *in utero* exposure to phytocannabinoids might be teratogenic, perhaps in concert with genetic predisposition. This hypothesis was tested with *Cdon* mutant mice, already proven to be valuable for testing the effects of HPE modifiers. THC inhibited HH signaling during development of 129S6 *Cdon* mutant embryos, resulting in two hallmark HH loss of function phenotypes: mild HPE and ventral neural tube patterning defects (Lo et al., 2021). THC produced these effects in *Cdon* mutants but not wild type mice, indicating it acted as a conditional teratogen, dependent on a complementary but insufficient genetic defect. THC acts as a direct, albeit relatively weak, inhibitor of the essential HH signal transducer Smoothened (SMO), the same target as the more potent teratogen cyclopamine (Chen et al., 2002; Lo et al., 2021). Interestingly, THC also exacerbated developmental defects induced by PAE in C57BL/6 mice (Fish et al., 2019). THC is therefore a potential environmental risk factor for HPE and other developmental disorders linked to HH signaling deficiency. Recent epidemiological studies have correlated increased cannabis usage with specific structural birth defects (Reece and Hulse, 2019; Reece and Hulse, 2020). Additional work is needed to address the possibility that cannabis usage during early pregnancy is teratogenic to humans, and whether individuals with genetic predisposition may be at elevated risk.

Piperonyl Butoxide

Studies with agricultural and experimental animals demonstrate that SMO inhibitors are HPE-inducing teratogens. SMO is a seven-pass transmembrane protein of the G protein-coupled receptor superfamily. It has multiple binding modalities for small molecules, and many SMO agonists and antagonists have been identified (Sharpe et al., 2015). There are thousands of synthetic compounds present in the environment and it is possible that among them exist some which inhibit SMO and could be HPE risk factors. Wang et al. used a high-content cell culture assay to test a library of more than 1,400 environmental toxicants for SMO antagonist activity (Wang et al., 2012). One SMO inhibitor was identified: piperonyl butoxide (PBO), a pesticide synergist in wide use and among the top 10 chemicals detected in indoor dust (Rivera-González et al., 2021). In utero exposure of C57BL/6 mice to PBO dose-dependently produced forebrain and facial phenotypes characteristic of HPE (Everson et al., 2019). Furthermore, C57BL/6 $Shh^{+/-}$ mice were sensitized to lower doses of PBO (Everson et al., 2019). Importantly, a recent case-control study provided evidence that maternal exposure to pesticides during pregnancy elevated the risk of HPE (Addissie et al., 2020). Follow-up studies with larger cohorts are clearly warranted.

Future Directions in Studying Gene-Environment Interactions in HPE

The structures of small molecule SMO antagonists are diverse, and they vary in potency. High-resolution structures of SMO alone or bound by natural or synthetic inhibitors have been derived (Sharpe et al., 2015; Kowatsch et al., 2019; Qi and Li, 2020), and it may be possible to combine this information with modeling studies to identify potential SMO inhibitors among the enormous number of unregulated chemicals present in the environment. Although SMO inhibitors are clearly a concern as potential HPE risk factors, SMO inhibition is not the sole mechanism whereby chemical compounds may raise the risk of HPE. First, HH signaling is subject to small molecule inhibition at multiple steps, and other components of the pathway could also be targets of potential teratogens (McMillan and Matsui, 2012). Second, other pathways are also relevant to HPE. For example, the Nodal pathway lies developmentally upstream of the HH pathway in rostroventral midline patterning. Ethanol's major HPE-inducing teratogenic effect in mice is likely *via* inhibition of Nodal signaling, with effects on HH signaling occurring as an indirect consequence (Hong et al., 2020). Although the direct target of ethanol's inhibitory effects on Nodal signaling are as yet unknown, it rapidly induces an inhibitory pattern of phosphorylation in SMAD2, the pathway-responsive transcription factor (Hong et al., 2020). In zebrafish, ethanol also inhibits anterior migration of the prechordal plate, a key structure induced by Nodal signaling and which secretes SHH (Blader and Strahle, 1998).

Recent epidemiological studies have revealed additional potential environmental risk factors for HPE. Polycyclic aromatic hydrocarbons (PAHs) are produced by incomplete combustion of naturally occurring organic compounds and are present at high levels in specific work environments, as well as in cigarette smoke and charred meats. A 2020 study indicated that maternal occupational exposure to PAHs elevated the risk for HPE and selected other defects of the face and CNS (Santiago-Colón et al., 2020). A second recent study by Addissie et al. identified pregnancy-associated risk with exposure to consumer products such as bleach, air fresheners, and aerosols or sprays, including hair sprays (Addissie et al., 2021). Importantly, this study also showed a protective effect of folic acid intake during the first month of pregnancy (Addissie et al., 2021). Addissie et al. added several important features to their analysis that should lead the way for future epidemiological studies on HPE. First, controls included children with Williams-Beuren syndrome, a congenital anomaly with etiology and pathology distinct from HPE. This may help control for differences in recollection of exposures between parents of unaffected and affected children. Second, most probands underwent genetic testing for variants of *SHH*, *ZIC2*, *SIX3*, and *TGIF1*, allowing assessment of gene-environment interactions. Interestingly, the severity of HPE phenotypes in offspring of mothers with pathogenic variants was significantly *reduced* with higher amounts of maternal

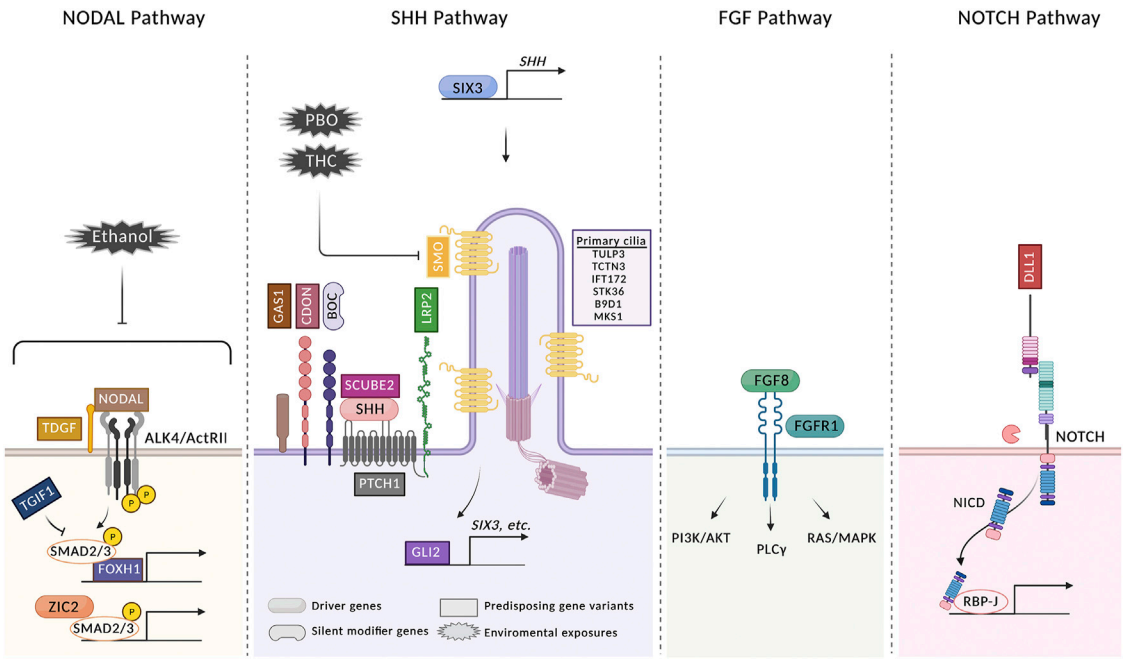

FIGURE 2 | HPE arises from a confluence of multiple genetic and environmental risk factors. Four signaling pathways in which gene variants have been identified in HPE patients are shown. Variants in genes identified in HPE patients are classified as driver genes, silent modifier genes, and predisposing gene variants. Driver genes are defined as those accepted to be essential to the phenotype of the patient carrying a variant and include *SHH*, *ZIC2*, *SIX3*, *FGF8*, *and FGFR1*. A single silent modifier gene (*BOC*) is listed; see text for further discussion. All other genes are categorized as predisposing gene variants. Variants of these genes may function as drivers in individual HPE cases, but the relative infrequency of their involvement currently makes this difficult to assess, as it is also possible that they can function as modifiers of a more critical insult, genetic or environmental. Variants in some additional genes identified in HPE cases are not shown because their roles in these pathways are not known [see (Roessler et al., 2018b; Tekendo-Ngongang et al., 2020) for complete lists]. Three environmental risk factors are shown. PBO and THC both directly inhibit SMO. Ethanol inhibits Nodal signaling, but the direct target is not known. For simplicity, not every regulator of each pathway is pictured. See text for further details. The figure was created with BioRender.com.

cheese consumption (Addissie et al., 2021). This could conceivably be related to the high cholesterol levels in cheese, as cholesterol is required for HH signaling (Radhakrishnan et al., 2020).

CONCLUSION

HPE is almost certainly caused by a complex set of genetic and environmental risk factors (**Figure 2**). These factors interact with each other to affect the strength and duration of key developmental signaling pathways, thereby increasing the possibility that they fail to achieve the thresholds required for normal patterning. The same is likely true of many common birth defects, including congenital heart defects, neural tube defects, and oro-facial clefting (Krauss and Hong, 2016; Beames and Lipinski, 2020; Martinelli et al., 2020; Finnell et al., 2021; Kodo et al., 2021). Genome sequencing analyses and epidemiology, plus mechanistic studies with animal models, have provided conceptual insights into HPE etiology which should prove applicable to these other developmental disorders.

To fully understand HPE etiology, it is necessary to continue these efforts. Eventually, whole genome sequencing of trios will need to be performed to get a complete picture of the genetic contribution in individual cases. Variants in genes not previously associated with HPE were identified in the first rounds of WES, and more are likely to come. Furthermore, reproducible co-occurrence of variants in specific combinations of genes is hinted at by Kim et al. (2018). As these become clearer, it should shed light on mechanisms whereby incomplete deficiency of multiple pathways synergize to result in clinical phenotypes. Finally, it is known that mutations in transcriptional regulatory elements can occur in HPE (e.g., in a brain-specific enhancer for SHH expression) (Jeong et al., 2008), but the frequency of such events is unknown.

Assessment of gene-environment interactions in human studies will be very important as investigation of HPE and other developmental disorders with complex etiology progresses. Potential mechanisms of gene-environment interactions are myriad (Krauss and Hong, 2016); molecular insight into such mechanisms will be best addressed with animal models and *in vitro* systems. Interactions between non-genetic risk factors must also eventually be included. Animal models will be helpful here. A recent study showed that PAE and PBO synergized in a zebrafish model of craniofacial defects, some of which resemble HPE; moreover, this combination of

environmental risk factors further interacted with heterozygous mutation of *shh* (Everson et al., 2020). It should be emphasized that many potential environmental risk factors may *require* complementary insults for their effects to manifest [e.g., THC in 129S6 mice (Lo et al., 2021)]. Additionally, the doses of potential teratogens that are, on their own, sufficient to produce phenotypes in animal models may not be achieved in average human populations (although they may occur in occupational settings or through excessive self-exposure, e.g., binge drinking). Subthreshold doses of such factors may be additive or synergistic in human populations and they may also interact with predisposing genetic sensitivities. Animal model studies are well positioned to illuminate such interactions, and may spur investigation of specific interactions in human populations. In summary, the study of HPE has produced important insights not only into how this complex and very common developmental disorder occurs but also concepts expected to shed light on causation in other similarly complex and frequently occurring birth defects.

AUTHOR CONTRIBUTIONS

All authors discussed the scope of the article, the first draft was written by RK, all authors edited the article, the figure was made by MH and H-FL.

ACKNOWLEDGMENTS

We thank Allison Kann for assistance with **Figure 2**. Work in the authors' laboratory on this topic has been funded by NIDCR, NIAAA, March of Dimes, and the Mindich Child Health and Development Institute at Mount Sinai.

REFERENCES

Abe, Y., Kruszka, P., Martinez, A. F., Roessler, E., Shiota, K., Yamada, S., et al. (2018). Clinical and Demographic Evaluation of a Holoprosencephaly Cohort from the Kyoto Collection of Human Embryos. *Anat. Rec.* 301, 973–986. doi:10.1002/ar.23791

Addissie, Y. A., Kruszka, P., Troia, A., Wong, Z. C., Everson, J. L., Kozel, B. A., et al. (2020). Prenatal Exposure to Pesticides and Risk for Holoprosencephaly: a Case-Control Study. *Environ. Health* 19, 65. doi:10.1186/s12940-020-00611-z

Addissie, Y. A., Troia, A., Wong, Z. C., Everson, J. L., Kozel, B. A., Muenke, M., et al. (2021). Identifying Environmental Risk Factors and Gene-Environment Interactions in Holoprosencephaly. *Birth Defects Res.* 113, 63–76. doi:10.1002/bdr2.1834

Aoto, K., Shikata, Y., Higashiyama, D., Shiota, K., and Motoyama, J. (2008). Fetal Ethanol Exposure Activates Protein Kinase a and impairsShh Expression in Prechordal Mesendoderm Cells in the Pathogenesis of Holoprosencephaly. *Birth Defect Res. A.* 82, 224–231. doi:10.1002/bdra.20447

Bae, G.-U., Domené, S., Roessler, E., Schachter, K., Kang, J.-S., Muenke, M., et al. (2011). Mutations in CDON, Encoding a Hedgehog Receptor, Result in Holoprosencephaly and Defective Interactions with Other Hedgehog Receptors. *Am. J. Hum. Genet.* 89, 231–240. doi:10.1016/j.ajhg.2011.07.001

Bandoli, G., Jones, K., Wertelecki, W., Yevtushok, L., Zymak-Zakutnya, N., Granovska, I., et al. (2020). Patterns of Prenatal Alcohol Exposure and Alcohol-Related Dysmorphic Features. *Alcohol. Clin. Exp. Res.* 44, 2045–2052. doi:10.1111/acer.14430

Beames, T. G., and Lipinski, R. J. (2020). Gene-environment Interactions: Aligning Birth Defects Research with Complex Etiology. *Development* 147, dev191064. doi:10.1242/dev.191064

Blader, P., and Strähle, U. (1998). Ethanol Impairs Migration of the Prechordal Plate in the Zebrafish Embryo. *Develop. Biol.* 201, 185–201. doi:10.1006/dbio.1998.8995

Bookstein, F. L., Sampson, P. D., Connor, P. D., and Streissguth, A. P. (2002). Midline Corpus Callosum Is a Neuroanatomical Focus of Fetal Alcohol Damage. *Anat. Rec.* 269, 162–174. doi:10.1002/ar.10110

Chen, J. K. (2016). I Only Have Eye for Ewe: the Discovery of Cyclopamine and Development of Hedgehog Pathway-Targeting Drugs. *Nat. Prod. Rep.* 33, 595–601. doi:10.1039/c5np00153f

Chen, J. K., Taipale, J., Cooper, M. K., and Beachy, P. A. (2002). Inhibition of Hedgehog Signaling by Direct Binding of Cyclopamine to Smoothened. *Genes Dev.* 16, 2743–2748. doi:10.1101/gad.1025302

Cordero, D., Marcucio, R., Hu, D., Gaffield, W., Tapadia, M., and Helms, J. A. (2004). Temporal Perturbations in Sonic Hedgehog Signaling Elicit the Spectrum of Holoprosencephaly Phenotypes. *J. Clin. Invest.* 114, 485–494. doi:10.1172/jci200419596

Coulter, C. L., Leech, R. W., Schaefer, G. B., Scheithauer, B. W., and Brumback, R. A. (1993). Midline Cerebral Dysgenesis, Dysfunction of the Hypothalamic-Pituitary Axis, and Fetal Alcohol Effects. *Arch. Neurol.* 50, 771–775. doi:10.1001/archneur.1993.00540070083022

Croen, L. A., Shaw, G. M., and Lammer, E. J. (2000). Risk Factors for Cytogenetically normal Holoprosencephaly in California: a Population-Based Case-Control Study. *Am. J. Med. Genet.* 90, 320–325. doi:10.1002/(sici)1096-8628(20000214)90::4<320:aid-ajmg11>3.0.co;2-8

DeMyer, W., Zeman, W., and Palmer, C. G. (1964). The Face Predicts the Brain: Diagnostic Significance of Median Facial Anomalies for Holoprosencephaly (Arhinencephaly). *Pediatrics* 34, 256–263.

Downing, C., Balderrama-Durbin, C., Broncucia, H., Gilliam, D., and Johnson, T. E. (2009). Ethanol Teratogenesis in Five Inbred Strains of Mice. *Alcohol. Clin. Exp. Res.* 33, 1238–1245. doi:10.1111/j.1530-0277.2009.00949.x

Drissi, I., Fletcher, E., Shaheen, R., Nahorski, M., Alhashem, A. M., Lisgo, S., et al. (2021). Mutations in Phospholipase C Eta-1 (PLCH1) Are Associated with Holoprosencephaly. *J. Med. Genet.* Online ahead of print, 1–8. doi:10.1136/jmedgenet-2020-107237

Dubourg, C., Carré, W., Hamdi-Rozé, H., Mouden, C., Roume, J., Abdelmajid, B., et al. (2016). Mutational Spectrum in Holoprosencephaly Shows that FGF Is a New Major Signaling Pathway. *Hum. Mutat.* 37, 1329–1339. doi:10.1002/humu.23038

Dubourg, C., Kim, A., Watrin, E., de Tayrac, M., Odent, S., David, V., et al. (2018). Recent Advances in Understanding Inheritance of Holoprosencephaly. *Am. J. Med. Genet.* 178, 258–269. doi:10.1002/ajmg.c.31619

Dupé, V., Rochard, L., Mercier, S., Le Pétillon, Y., Gicquel, I., Bendavid, C., et al. (2010). NOTCH, a New Signaling Pathway Implicated in Holoprosencephaly. *Hum. Mol. Genet.* 20, 1122–1131. doi:10.1093/hmg/ddq556

Echevarría-Andino, M. L., and Allen, B. L. (2020). The Hedgehog Co-receptor BOC Differentially Regulates SHH Signaling during Craniofacial Development. *Development* 147, dev189076. doi:10.1242/dev.189076

Everson, J. L., Batchu, R., and Eberhart, J. K. (2020). Multifactorial Genetic and Environmental Hedgehog Pathway Disruption Sensitizes Embryos to Alcohol-Induced Craniofacial Defects. *Alcohol. Clin. Exp. Res.* 44, 1988–1996. doi:10.1111/acer.14427

Everson, J. L., Sun, M. R., Fink, D. M., Heyne, G. W., Melberg, C. G., Nelson, K. F., et al. (2019). Developmental Toxicity Assessment of Piperonyl Butoxide Exposure Targeting Sonic Hedgehog Signaling and Forebrain and Face Morphogenesis in the Mouse: An *In Vitro* and *In Vivo* Study. *Environ. Health Perspect.* 127, 107006. doi:10.1289/ehp5260

Fernandes, M., and Hébert, J. (2008). The Ups and downs of Holoprosencephaly: Dorsal versus Ventral Patterning Forces. *Clin. Genet.* 73, 413–423. doi:10.1111/j.1399-0004.2008.00994.x

Finnell, R. H., Caiaffa, C. D., Kim, S.-E., Lei, Y., Steele, J., Cao, X., et al. (2021). Gene Environment Interactions in the Etiology of Neural Tube Defects. *Front. Genet.* 12, 659612. doi:10.3389/fgene.2021.659612

Fish, E. W., Murdaugh, L. B., Zhang, C., Boschen, K. E., Boa-Amponsem, O., Mendoza-Romero, H. N., et al. (2019). Cannabinoids Exacerbate Alcohol Teratogenesis by a CB1-Hedgehog Interaction. *Sci. Rep.* 9, 16057. doi:10.1038/s41598-019-52336-w

Gallardo, V., and Bovolenta, P. (2018). Positive and Negative Regulation of Shh Signalling in Vertebrate Retinal Development. *F1000Research* 7 (F1000 Faculty Rev), 1934. doi:10.12688/f1000research.16190.1

Geng, X., Speirs, C., Lagutin, O., Inbal, A., Liu, W., Solnica-Krezel, L., et al. (2008). Haploinsufficiency of Six3 Fails to Activate Sonic Hedgehog Expression in the Ventral Forebrain and Causes Holoprosencephaly. *Develop. Cel* 15, 236–247. doi:10.1016/j.devcel.2008.07.003

Gigante, E. D., and Caspary, T. (2020). Signaling in the Primary Cilium through the Lens of the Hedgehog Pathway. *WIREs Dev. Biol.* 9, e377. doi:10.1002/wdev.377

Gomez, D. A., May, P. A., Tabachnick, B. G., Hasken, J. M., Lyden, E. R., Kalberg, W. O., et al. (2020). Ocular Measurements in Fetal Alcohol Spectrum Disorders. *Am. J. Med. Genet.* 182, 2243–2252. doi:10.1002/ajmg.a.61759

Grinblat, Y., and Lipinski, R. J. (2019). A Forebrain Undivided: Unleashing Model Organisms to Solve the Mysteries of Holoprosencephaly. *Dev. Dyn.* 248, 626–633. doi:10.1002/dvdy.41

Grobe, K., Inatani, M., Pallerla, S. R., Castagnola, J., Yamaguchi, Y., and Esko, J. D. (2005). Cerebral Hypoplasia and Craniofacial Defects in Mice Lacking Heparan Sulfate Ndst1 Gene Function. *Development* 132, 3777–3786. doi:10.1242/dev.01935

Hamdi-Rozé, H., Ware, M., Guyodo, H., Rizzo, A., Ratié, L., Rupin, M., et al. (2020). Disrupted Hypothalamo-Pituitary Axis in Association with Reduced SHH Underlies the Pathogenesis of NOTCH-Deficiency. *J. Clin. Endocrinol. Metab.* 105, e3183–e3196. doi:10.1210/clinem/dgaa249

Heyne, G. W., Everson, J. L., Ansen-Wilson, L. J., Melberg, C. G., Fink, D. M., Parins, K. F., et al. (2016). Gli2 Gene-Environment Interactions Contribute to the Etiological Complexity of Holoprosencephaly: Evidence from a Mouse Model. *Dis. Model. Mech.* 9, 1307–1315. doi:10.1242/dmm.026328

Hong, M., Christ, A., Christa, A., Willnow, T. E., and Krauss, R. S. (2020). *Cdon* Mutation and Fetal Alcohol Converge on Nodal Signaling in a Mouse Model of Holoprosencephaly. *eLife* 9, e60351. doi:10.7554/eLife.60351

Hong, M., and Krauss, R. S. (2012). *Cdon* Mutation and Fetal Ethanol Exposure Synergize to Produce Midline Signaling Defects and Holoprosencephaly Spectrum Disorders in Mice. *PLOS Genet.* 8, e1002999. doi:10.1371/journal.pgen.1002999

Hong, M., and Krauss, R. S. (2018). Modeling the Complex Etiology of Holoprosencephaly in Mice. *Am. J. Med. Genet.* 178, 140–150. doi:10.1002/ajmg.c.31611

Hong, M., Srivastava, K., Kim, S., Allen, B. L., Leahy, D. J., Hu, P., et al. (2017). BOC Is a Modifier Gene in Holoprosencephaly. *Hum. Mutat.* 38, 1464–1470. doi:10.1002/humu.23286

Hoyme, H. E., Kalberg, W. O., Elliott, A. J., Blankenship, J., Buckley, D., Marais, A.-S., et al. (2016). Updated Clinical Guidelines for Diagnosing Fetal Alcohol Spectrum Disorders. *Pediatrics* 138, e20154256. doi:10.1542/peds.2015-4256

Hoyme, H. E., May, P. A., Kalberg, W. O., Kodituwakku, P., Gossage, J. P., Trujillo, P. M., et al. (2005). A Practical Clinical Approach to Diagnosis of Fetal Alcohol Spectrum Disorders: Clarification of the 1996 Institute of Medicine Criteria. *Pediatrics* 115, 39–47. doi:10.1542/peds.2004-0259

Jeong, Y., Leskow, F. C., El-Jaick, K., Roessler, E., Muenke, M., Yocum, A., et al. (2008). Regulation of a Remote Shh Forebrain Enhancer by the Six3 Homeoprotein. *Nat. Genet.* 40, 1348–1353. doi:10.1038/ng.230

Johnson, V. P., Swayze, V. W., Sato, Y., and Andreasen, N. C. (1996). Fetal Alcohol Syndrome: Craniofacial and central Nervous System Manifestations. *Am. J. Med. Genet.* 61, 329–339. doi:10.1002/(sici)1096-8628(19960202)61:4<329::aid-ajmg6>3.0.co;2-p

Kakar, N., Ahmad, J., Morris-Rosendahl, D. J., Altmüller, J., Friedrich, K., Barbi, G., et al. (2015). STIL Mutation Causes Autosomal Recessive Microcephalic Lobar Holoprosencephaly. *Hum. Genet.* 134, 45–51. doi:10.1007/s00439-014-1487-4

Khaliullina, H., Bilgin, M., Sampaio, J. L., Shevchenko, A., and Eaton, S. (2015). Endocannabinoids Are Conserved Inhibitors of the Hedgehog Pathway. *Proc. Natl. Acad. Sci. USA* 112, 3415–3420. doi:10.1073/pnas.1416463112

Kietzman, H. W., Everson, J. L., Sulik, K. K., and Lipinski, R. J. (2014). The Teratogenic Effects of Prenatal Ethanol Exposure Are Exacerbated by Sonic Hedgehog or GLI2 Haploinsufficiency in the Mouse. *PLOS ONE* 9 (2), e89448. doi:10.1371/journal.pone.0089448

Kim, A., Savary, C., Dubourg, C., Carré, W., Mouden, C., Hamdi-Rozé, H., et al. (2018). Integrated Clinical and Omics Approach to Rare Diseases: Novel Genes and Oligogenic Inheritance in Holoprosencephaly. *Brain* 142, 35–49. doi:10.1093/brain/awy290

Kodo, K., Uchida, K., and Yamagishi, H. (2021). Genetic and Cellular Interaction during Cardiovascular Development Implicated in Congenital Heart Diseases. *Front. Cardiovasc. Med.* 8, 10–3389. doi:10.3389/fcvm.2021.653244

Kowatsch, C., Woolley, R. E., Kinnebrew, M., Rohatgi, R., and Siebold, C. (2019). Structures of Vertebrate Patched and Smoothened Reveal Intimate Links between Cholesterol and Hedgehog Signalling. *Curr. Opin. Struct. Biol.* 57, 204–214. doi:10.1016/j.sbi.2019.05.015

Krauss, R. S. (2007). Holoprosencephaly: New Models, New Insights. *Expert Rev. Mol. Med.* 9, 1–17. doi:10.1017/s1462399407000440

Krauss, R. S., and Hong, M. (2016). Gene-Environment Interactions and the Etiology of Birth Defects. *Curr. Top. Dev. Biol.* 116, 569–580. doi:10.1016/bs.ctdb.2015.12.010

Kruszka, P., Berger, S. I., Casa, V., Dekker, M. R., Gaesser, J., Weiss, K., et al. (2019a). Cohesin Complex-Associated Holoprosencephaly. *Brain* 142, 2631–2643. doi:10.1093/brain/awz210

Kruszka, P., Berger, S. I., Weiss, K., Everson, J. L., Martinez, A. F., Hong, S., et al. (2019b). A CCR4-NOT Transcription Complex, Subunit 1, CNOT1, Variant Associated with Holoprosencephaly. *Am. J. Hum. Genet.* 104, 990–993. doi:10.1016/j.ajhg.2019.03.017

Kruszka, P., and Muenke, M. (2018). Syndromes Associated with Holoprosencephaly. *Am. J. Med. Genet.* 178, 229–237. doi:10.1002/ajmg.c.31620

Lacbawan, F., Solomon, B. D., Roessler, E., El-Jaick, K., Domene, S., Velez, J. I., et al. (2009). Clinical Spectrum of SIX3-Associated Mutations in Holoprosencephaly: Correlation between Genotype, Phenotype and Function. *J. Med. Genet.* 46, 389–398. doi:10.1136/jmg.2008.063818

Leoncini, E., Baranello, G., Orioli, I. M., Annerén, G., Bakker, M., Bianchi, F., et al. (2008). Frequency of Holoprosencephaly in the International Clearinghouse Birth Defects Surveillance Systems: Searching for Population Variations. *Birth Defect Res. A.* 82, 585–591. doi:10.1002/bdra.20479

Leung, A. W. L., Wong, S. Y. Y., Chan, D., Tam, P. P. L., and Cheah, K. S. E. (2010). Loss of Procollagen IIA from the Anterior Mesendoderm Disrupts the Development of Mouse Embryonic Forebrain. *Dev. Dyn.* 239, 2319–2329. doi:10.1002/dvdy.22366

Linn, S., Schoenbaum, S. C., Monson, R. R., Rosner, R., Stubblefield, P. C., and Ryan, K. J. (1983). The Association of Marijuana Use with Outcome of Pregnancy. *Am. J. Public Health* 73, 1161–1164. doi:10.2105/ajph.73.10.1161

Lo, H. F., Hong, M., Szutorisz, H., Hurd, Y. L., and Krauss, R. S. (2021). Δ9-Tetrahydrocannabinol Inhibits Hedgehog-dependent Patterning during Development. *Development* 148, dev199585. doi:10.1242/dev.199585

Marcucio, R., Hallgrimsson, B., and Young, N. M. (2015). Facial Morphogenesis. *Curr. Top. Dev. Biol.* 115, 299–320. doi:10.1016/bs.ctdb.2015.09.001

Martinelli, M., Palmieri, A., Carinci, F., and Scapoli, L. (2020). Non-syndromic Cleft Palate: An Overview on Human Genetic and Environmental Risk Factors. *Front. Cel Dev. Biol.* 8, 592271. doi:10.3389/fcell.2020.592271

McMillan, R., and Matsui, W. (2012). Molecular Pathways: The Hedgehog Signaling Pathway in Cancer: Figure 1. *Clin. Cancer Res.* 18, 4883–4888. doi:10.1158/1078-0432.ccr-11-2509

Mecklenburg, N., Kowalczyk, I., Witte, F., Görne, J., Laier, A., Mamo, T. M., et al. (2021). Identification of Disease-Relevant Modulators of the SHH Pathway in the Developing Brain. *Development* 148, dev199307. doi:10.1242/dev.199307

Miller, E. A., Rasmussen, S. A., Siega-Riz, A. M., Frías, J. L., and Honein, M. A .and National Birth Defects Prevention Study (2010). Risk Factors for Non-syndromic Holoprosencephaly in the National Birth Defects Prevention Study. *Am. J. Med. Genet.* 154C, 62–72. doi:10.1002/ajmg.c.30244

Monuki, E. S. (2007). The Morphogen Signaling Network in Forebrain Development and Holoprosencephaly. *J. Neuropathol. Exp. Neurol.* 66, 566–575. doi:10.1097/nen.0b013e3180986e1b

Mouden, C., de Tayrac, M., Dubourg, C., Rose, S., Carré, W., Hamdi-Rozé, H., et al. (2015). Homozygous STIL Mutation Causes Holoprosencephaly and Microcephaly in Two Siblings. *PLoS One* 10, e0117418. doi:10.1371/journal.pone.0117418

Muenke, M., and Beachy, P. A. (2001). "Holoprosencephaly," in *The Metabolic & Molecular Bases of Inherited Disease*. Editors C. R. Scriver, A. L. Beaudet, W. S. Sly, and D. Valle (New York: McGraw-Hill), 6203–6230.

Neri, G., Sammito, V., Romano, C., Sanfilippo, S., Opitz, J. M., and Reynolds, J. F. (1988). Facial Midline Defect in the Fetal Alcohol Syndrome. Embryogenetic Considerations in Two Clinical Cases. *Am. J. Med. Genet.* 29, 477–482. doi:10.1002/ajmg.1320290302

Pande, S., Radhakrishnan, P., Shetty, N. M., Shukla, A., and Girisha, K. M. (2021). Hedgehog Acyl-transferase-related Multiple Congenital Anomalies: Report of an Additional Family and Delineation of the Syndrome. *Am. J. Med. Genet.* 185, 2756–2765. doi:10.1002/ajmg.a.62186

Petrov, K., Wierbowski, B. M., and Salic, A. (2017). Sending and Receiving Hedgehog Signals. *Annu. Rev. Cel Dev. Biol.* 33, 145–168. doi:10.1146/annurev-cellbio-100616-060847

Qi, X., and Li, X. (2020). Mechanistic Insights into the Generation and Transduction of Hedgehog Signaling. *Trends Biochem. Sci.* 45, 397–410. doi:10.1016/j.tibs.2020.01.006

Radhakrishnan, A., Rohatgi, R., and Siebold, C. (2020). Cholesterol Access in Cellular Membranes Controls Hedgehog Signaling. *Nat. Chem. Biol.* 16, 1303–1313. doi:10.1038/s41589-020-00678-2

Reece, A. S., and Hulse, G. K. (2019). Cannabis Teratology Explains Current Patterns of Coloradan Congenital Defects: The Contribution of Increased Cannabinoid Exposure to Rising Teratological Trends. *Clin. Pediatr. (Phila)* 58, 1085–1123. doi:10.1177/0009922819861281

Reece, A. S., and Hulse, G. K. (2020). Contemporary Epidemiology of Rising Atrial Septal Defect Trends across USA 1991-2016: a Combined Ecological Geospatiotemporal and Causal Inferential Study. *BMC Pediatr.* 20, 539. doi:10.1186/s12887-020-02431-z

Rivera-González, K. S., Beames, T. G., and Lipinski, R. J. (2021). Examining the Developmental Toxicity of Piperonyl Butoxide as a Sonic Hedgehog Pathway Inhibitor. *Chemosphere* 264, 128414. doi:10.1016/j.chemosphere.2020.128414

Roessler, E., Belloni, E., Gaudenz, K., Jay, P., Berta, P., Scherer, S. W., et al. (1996). Mutations in the Human Sonic Hedgehog Gene Cause Holoprosencephaly. *Nat. Genet.* 14, 357–360. doi:10.1038/ng1196-357

Roessler, E., Hu, P., Marino, J., Hong, S., Hart, R., Berger, S., et al. (2018a). Common Genetic Causes of Holoprosencephaly Are Limited to a Small Set of Evolutionarily Conserved Driver Genes of Midline Development Coordinated by TGF-β, Hedgehog, and FGF Signaling. *Hum. Mutat.* 39, 1416–1427. doi:10.1002/humu.23590

Roessler, E., Hu, P., and Muenke, M. (2018b). Holoprosencephaly in the Genomics Era. *Am. J. Med. Genet.* 178, 165–174. doi:10.1002/ajmg.c.31615

Roessler, E., Vélez, J. I., Zhou, N., and Muenke, M. (2012). Utilizing Prospective Sequence Analysis of SHH, ZIC2, SIX3 and TGIF in Holoprosencephaly Probands to Describe the Parameters Limiting the Observed Frequency of Mutant Gene×gene Interactions. *Mol. Genet. Metab.* 105, 658–664. doi:10.1016/j.ymgme.2012.01.005

Sagner, A., and Briscoe, J. (2019). Establishing Neuronal Diversity in the Spinal Cord: a Time and a Place. *Development* 146, dev182154. doi:10.1242/dev.182154

Santiago-Colón, A., Rocheleau, C. M., Chen, I. C., Sanderson, W., Waters, M. A., Lawson, C. C., et al. (2020). Association between Maternal Occupational Exposure to Polycyclic Aromatic Hydrocarbons and Rare Birth Defects of the Face and central Nervous System. *Birth Defects Res.* 112, 404–417. doi:10.1002/bdr2.1643

Seppala, M., Xavier, G. M., Fan, C.-M., and Cobourne, M. T. (2014). Boc Modifies the Spectrum of Holoprosencephaly in the Absence of Gas1 Function. *Biol. Open* 3, 728–740. doi:10.1242/bio.20147989

Sharpe, H. J., Wang, W., Hannoush, R. N., and de Sauvage, F. J. (2015). Regulation of the Oncoprotein Smoothened by Small Molecules. *Nat. Chem. Biol.* 11, 246–255. doi:10.1038/nchembio.1776

Shiota, K. (2021). A Life-table Analysis of the Intrauterine Fate of Malformed Human Embryos and Fetuses. *Birth Defects Res.* 113, 623–632. doi:10.1002/bdr2.1888

Shiota, K., and Yamada, S. (2010). Early Pathogenesis of Holoprosencephaly. *Am. J. Med. Genet.* 154C, 22–28. doi:10.1002/ajmg.c.30248

Solomon, B. D., Bear, K. A., Wyllie, A., Keaton, A. A., Dubourg, C., David, V., et al. (2012). Genotypic and Phenotypic Analysis of 396 Individuals with Mutations inSonic Hedgehog. *J. Med. Genet.* 49, 473–479. doi:10.1136/jmedgenet-2012-101008

Solomon, B. D., Lacbawan, F., Mercier, S., Clegg, N. J., Delgado, M. R., Rosenbaum, K., et al. (2010). Mutations in ZIC2 in Human Holoprosencephaly: Description of a Novel ZIC2 Specific Phenotype and Comprehensive Analysis of 157 Individuals. *J. Med. Genet.* 47, 513–524. doi:10.1136/jmg.2009.073049

Stokes, B., Berger, S. I., Hall, B. A., Weiss, K., Martinez, A. F., Hadley, D. W., et al. (2018). SIX3 Deletions and Incomplete Penetrance in Families Affected by Holoprosencephaly. *Congenit. Anom.* 58, 29–32. doi:10.1111/cga.12234

Sulik, K. K., and Johnston, M. C. (1982). Embryonic Origin of Holoprosencephaly: Interrelationship of the Developing Brain and Face. *Scan Electron. Microsc.* 1, 309–322.

Sulik, K. K., Johnston, M. C., and Webb, M. A. (1981). Fetal Alcohol Syndrome: Embryogenesis in a Mouse Model. *Science* 214, 936–938. doi:10.1126/science.6795717

Summers, A. D., Reefhuis, J., Taliano, J., and Rasmussen, S. A. (2018). Nongenetic Risk Factors for Holoprosencephaly: An Updated Review of the Epidemiologic Literature. *Am. J. Med. Genet.* 178, 151–164. doi:10.1002/ajmg.c.31614

Suttie, M., Wozniak, J. R., Parnell, S. E., Wetherill, L., Mattson, S. N., Sowell, E. R., et al. (2018). Combined Face-Brain Morphology and Associated Neurocognitive Correlates in Fetal Alcohol Spectrum Disorders. *Alcohol. Clin. Exp. Res.* 42, 1769–1782. doi:10.1111/acer.13820

Tekendo-Ngongang, C., Kruszka, P., Martinez, A. F., and Muenke, M. (2019). Novel Heterozygous Variants in KMT2D Associated with Holoprosencephaly. *Clin. Genet.* 96, 266–270. doi:10.1111/cge.13598

Tekendo-Ngongang, C., Muenke, M., and Kruszka, P. (2020). "Holoprosencephaly Overview," in *GeneReviews*. Editors P. M. Adam, H. H. Ardinger, and R. A. Pagon (Seattle, WA: University of Washington).

Wang, J., Lu, J., Mook, R. A., Jr, Zhang, M., Zhao, S., Barak, L. S., et al. (2012). The Insecticide Synergist Piperonyl Butoxide Inhibits Hedgehog Signaling: Assessing Chemical Risks. *Toxicol. Sci.* 128, 517–523. doi:10.1093/toxsci/kfs165

Webster, W. S., Walsh, D. A., McEwen, S. E., and Lipson, A. H. (1983). Some Teratogenic Properties of Ethanol and Acetaldehyde in C57BL/6J Mice: Implications for the Study of the Fetal Alcohol Syndrome. *Teratology* 27, 231–243. doi:10.1002/tera.1420270211

Wilson, S. W., and Houart, C. (2004). Early Steps in the Development of the Forebrain. *Develop. Cel* 6, 167–181. doi:10.1016/s1534-5807(04)00027-9

Young, N. M., Chong, H. J., Hu, D., Hallgrímsson, B., and Marcucio, R. S. (2010). Quantitative Analyses Link Modulation of Sonic Hedgehog Signaling to Continuous Variation in Facial Growth and Shape. *Development* 137, 3405–3409. doi:10.1242/dev.052340

Zhang, W., Hong, M., Bae, G.-U., Kang, J.-S., and Krauss, R. S. (2011). Bocmodifies the Holoprosencephaly Spectrum ofCdomutant Mice. *Dis. Model. Mech.* 4, 368–380. doi:10.1242/dmm.005744

Zhang, W., Kang, J.-S., Cole, F., Yi, M.-J., and Krauss, R. S. (2006). Cdo Functions at Multiple Points in the Sonic Hedgehog Pathway, and Cdo-Deficient Mice Accurately Model Human Holoprosencephaly. *Develop. Cel* 10, 657–665. doi:10.1016/j.devcel.2006.04.005

Conflict of Interest: The authors declare that the research was conducted in the absence of any commercial or financial relationships that could be construed as a potential conflict of interest.

Publisher's Note: All claims expressed in this article are solely those of the authors and do not necessarily represent those of their affiliated organizations, or those of the publisher, the editors and the reviewers. Any product that may be evaluated in this article, or claim that may be made by its manufacturer, is not guaranteed or endorsed by the publisher.

frontiers in Cell and Developmental Biology

REVIEW
published: 17 January 2022
doi: 10.3389/fcell.2021.784700

Autosomal Recessive Primary Microcephaly: Not Just a Small Brain

Sami Zaqout[1,2]* *and Angela M. Kaindl*[3,4,5]

[1]Department of Basic Medical Sciences, College of Medicine, QU Health, Qatar University, Doha, Qatar, [2]Biomedical and Pharmaceutical Research Unit, QU Health, Qatar University, Doha, Qatar, [3]Institute of Cell and Neurobiology, Charité—Universitätsmedizin Berlin, Berlin, Germany, [4]Center for Chronically Sick Children (Sozialpädiatrisches Zentrum, SPZ), Charité—Universitätsmedizin Berlin, Berlin, Germany, [5]Department of Pediatric Neurology, Charité—Universitätsmedizin Berlin, Berlin, Germany

Microcephaly or reduced head circumference results from a multitude of abnormal developmental processes affecting brain growth and/or leading to brain atrophy. Autosomal recessive primary microcephaly (MCPH) is the prototype of isolated primary (congenital) microcephaly, affecting predominantly the cerebral cortex. For MCPH, an accelerating number of mutated genes emerge annually, and they are involved in crucial steps of neurogenesis. In this review article, we provide a deeper look into the microcephalic MCPH brain. We explore cytoarchitecture focusing on the cerebral cortex and discuss diverse processes occurring at the level of neural progenitors, early generated and mature neurons, and glial cells. We aim to thereby give an overview of current knowledge in MCPH phenotype and normal brain growth.

Keywords: MCPH genes, microcephaly, brain, intellectual disability, neuronal differentiation, animal models, brain malformation

OPEN ACCESS

Edited by:
Annette Hammes,
Max Delbrück Center for Molecular Medicine (MDC), Germany

Reviewed by:
Kara Cerveny,
Reed College, United States
Valentina Massa,
University of Milan, Italy

***Correspondence:**
Sami Zaqout
sami.zaqout@qu.edu.qa
sami.zaqout@charite.de

Specialty section:
This article was submitted to Morphogenesis and Patterning, a section of the journal Frontiers in Cell and Developmental Biology

Received: *28 September 2021*
Accepted: *01 December 2021*
Published: *17 January 2022*

Citation:
Zaqout S and Kaindl AM (2022) Autosomal Recessive Primary Microcephaly: Not Just a Small Brain. Front. Cell Dev. Biol. 9:784700. doi: 10.3389/fcell.2021.784700

INTRODUCTION

Microcephaly is clinically defined by a significant reduction of the occipito-frontal head circumference (OFC) of more than two (microcephaly) or three (severe microcephaly) SDs below the mean for a given sex, age, and ethnicity (von der Hagen et al., 2014). The prevalence of microcephaly ranges between 1.5 and 8.7 per 10,000 births in Europe and the United States, respectively (Cragan et al., 2016; Morris et al., 2016). However, 15%–20% of children with developmental delay have microcephaly (Sassaman and Zartler, 1982; Watemberg et al., 2002; Aggarwal et al., 2013). Depending on the time of appearance, microcephaly can be classified as primary/congenital or secondary/postnatal (Passemard et al., 2013; Woods and Parker, 2013; Zaqout et al., 2017). It has been suggested that the primary causes of microcephaly lead to a reduction in the number of generated neurons, while the secondary causes mainly affect the dendritic complexity and synaptic formations (Woods, 2004). Primary microcephaly is by definition present at birth, and it can be caused by environmental and/or genetic factors (Zaqout et al., 2017; Alcantara and O'Driscoll, 2014; Kaindl et al., 2010). Various environmental factors such as infections, toxins, radiation, or alcohol result in primary microcephaly. The recent identification of epidemic infections with the Zika virus as a cause for primary microcephaly has highlighted this rare condition as a key topic in neuroscience to understand normal brain development (Kleber de Oliveira et al., 2016; Subramanian et al., 2019). This condition is an addition to the genetic prototype of isolated primary microcephaly, autosomal recessive primary microcephaly (microcephaly primary hereditary (MCPH)).

MCPH is a group of rare heterogeneous neurodevelopmental disorders characterized by intellectual disability and a significant reduction in the brain volume reflected by a reduction in

the head circumference already at birth (Kaindl et al., 2010; Zaqout et al., 2017; Slezak et al., 2021). The reduction in brain volume in MCPH cases affects disproportionately the neocortex, though without obvious changes in the cortical organization (Kaindl et al., 2010; Kraemer et al., 2011; Jayaraman et al., 2018). The increasing use of whole-exome sequencing (WES) has uncovered a growing number of novel and disease-causing MCPH variants (Boycott et al., 2013). Simultaneously, further radiological and postmortem studies expand the spectrum of brain malformations reported in individuals with MCPH. The prevalence of MCPH differs from 1:10,000 in populations with a high rate of consanguineous marriage to 1:250,000 in the general population (Van Den Bosch, 1959; Cox et al., 2006). In consanguineous families, most MCPH diagnosed cases reveal homozygous variants in the disease-causing gene. However, compound heterozygous variants are increasingly discovered in MCPH patients, raising the importance of using advanced and accurate diagnosis methods for such cases (Jean et al., 2020).

Currently (December 2021), twenty-eight MCPH-related genes have been identified and tagged sequentially as MCPH1–MCPH28 (MCPH; OMIM phenotypic series: PS251200; Siskos et al., 2021) (**Table 1**). Still, more genetic loci are expected to exist given the fact that approximately 62% of western Europeans/North Americans and 25% of Indians/Pakistani families diagnosed with MCPH fail to show linkage to any of the MCPH loci (Verloes et al., 1993; Kaindl et al., 2010; Sajid Hussain et al., 2013). Most *MCPH* gene variants are nonsense, frameshift, or splice site-affecting variants leading to a production of non-functional, truncated proteins (Kaindl et al., 2010; Barbelanne and Tsang, 2014; Jean et al., 2020). Most of the MCPH genes encode centrosomal and/or pericentriolar matrix (PCM) proteins that are, in turn, ubiquitously expressed (Kaindl et al., 2010; Hussain et al., 2013; Barbelanne and Tsang, 2014). It is therefore not surprising to find that many MCPH proteins are involved in centriole biogenesis including organization, maturation, and distribution (Subramanian et al., 2019; Jean et al., 2020). Furthermore, MCPH proteins play crucial roles in microtubule dynamics, mitotic spindle formation, DNA damage responses, Wnt signaling, transcriptional regulation, and cell cycle checkpoint control (Kraemer et al., 2011; Mahmood et al., 2011; Jayaraman et al., 2018; Jean et al., 2020). Disruption of one or more of these functions during cortical neurogenesis adversely affects neuronal progenitor proliferation, differentiation, and survival leading to a severe reduction in the total number of generated neurons reflected by the microcephaly phenotype. Being highly conserved among species, ongoing research on MCPH animal models deems to be an important key for understanding the pathomechanisms behind microcephaly as well as the role of MCPH proteins during normal brain development (Gilbert et al., 2005; Woods et al., 2005; Zaqout et al., 2017). Although microcephaly found in MCPH patients simulates an evolutionary retrogression of the brain size (McHenry, 1994), human brain evolution cannot be attributed solely to the protein-coding sequences of MCPH genes (Pervaiz et al., 2021). Therefore, it has been hypothesized that complex conditional effects of human-specific coding and non-coding regulatory changes in MCPH only assist this evolution process (Pervaiz et al., 2021).

Classically, radiological investigations of patients with MCPH fail to show severe brain malformation except for simplified neocortical gyration. However, the increasing number of reported MCPH-linked mutations reveals that further deformities in brain architecture might occur (**Table 2**). The overall aim of this review is to explore the various effects of *MCPH* disease-causing genes on the cytoarchitecture of the cerebral cortex.

NORMAL CORTICOGENESIS

MCPH arises principally from a decreased production of neurons due to defects in progenitor proliferation, differentiation, and/or apoptosis during critical stages of brain development. Hence, it is important to briefly review the normal process of cortical neurogenesis before discussing the multiple facets of MCPH protein functions in maintaining a smooth running of this process.

Before the neurogenesis journey begins, the neural stem cells represented by neuroepithelial progenitors (NE) at the ventricular zone (VZ) undergo initial expansion in number through symmetrical cell divisions (Homem et al., 2015). Once the antiproliferative gene Tis21 starts to be expressed, NE cells begin to switch from proliferative division to neuronic division (Götz and Huttner, 2005). Simultaneously, NE cells transform gradually into more fate-restricted progenitors known as radial glial cells (RGCs) as an indication for their glial gene expressions (Götz and Huttner, 2005; Mori et al., 2005; Subramanian et al., 2019). RGCs possess apical processes attaching to the ventricular surface and basal processes reaching the basement membrane (future pial surface) (Homem et al., 2015). RGCs expand their number and exhibit a much higher number of asymmetrical cell divisions as compared with NE cells (Subramanian et al., 2019). During cell expansion, RGC nuclei show a characteristic interkinetic nuclear migration (INM) synchronized with the cell cycle phases during proliferation (Kosodo et al., 2011). The RGC nuclei migrate toward the basal side of the developing cortex during G1 phase and remain there during S phase before they migrate apically during G2 phase and proceed with M-phase once they reach the ventricular surface (Kosodo et al., 2011; Miyata et al., 2014). This pattern of migration during early neurogenesis requires functional microtubules and actin filaments (Götz and Huttner, 2005). It has been proposed that INM allows RGC rapid proliferation while maintaining their dense packing and determines cell fate through signaling gradients along their migration pathway (Götz and Huttner, 2005; Baye and Link, 2007; Del Bene et al., 2008). It is therefore very likely to find defects in neurogenesis involving RGC expansion and neuronal cell fate decisions when INM is disrupted (Latasa et al., 2009). Intriguingly, INM shows differences between species and might affect the total number of the generated neurons and thence the brain size (Okamoto et al., 2014).

TABLE 1 | List of microcephaly primary hereditary (MCPH) genes and related animal/organism models.

Locus	Protein	Gene	Location	OMIM	Model organisms	Generation method	Key findings	Ref
MCPH1	Microcephalin 1	*MCPH1*	8p23.1	607117	*Xenopus*	1. *Drosophila in vitro* expression cloning IVEC (DIVEC)	1. dMCPH1 is a substrate of anaphase-promoting complex (APC)	Hainline et al. (2014)
					Fly	2. Deletion of the *mcph1* gene by imprecise excision of a P-element	2. Lethal phenotype due to mitotic arrest, uncoordinated centrosome, and nuclear cycles	Brunk et al. (2007)
					Rodent	3. *Mcph1*-knockout mice (deletion of exon 4–5)	3. Premature increase in asymmetrical neural progenitor cell (NPC) divisions, uncoupled mitosis and centrosome cycle, misoriented mitotic spindle alignment	Gruber et al. (2011)
						4. *Mcph1*-knockout mice (gene trap)	4. Shorter survival rates, defected mitotic chromosome condensation	Trimborn et al. (2010)
						5. *Brit1*-knockout mice (gene targeting)	5. Hypersensitive to γ-irradiation, defective DNA repair, infertility, meiotic defects	Liang et al. (2010)
MCPH2	WD-repeat-containing protein 62	*WDR62*	19q13.12	613583	Fish	1. Morpholino-mediated knockdown of *wdr62*	1. Reduction in head and eye size, prometaphase delay, increased apoptosis	Novorol et al. (2013)
					Rodent	2. *Wdr62*-knockout mice (gene trap)	2. Abnormalities in asymmetric centrosome inheritance, neuronal migration delays, altered neuronal differentiation, prometaphase delay, infertility	Sgourdou et al. (2017)
						3. *Wdr62*-knockout mice (gene trap)	3. Mitotic arrest, cell death, reduced thickness of upper cortical neuronal layers, dwarfism	Chen et al. (2014)
						4. ShRNA knockdown of *Wdr62* in rats (*in utero* electroporation)	4. Premature differentiation of NPCs, abnormal spindle formation, and mitotic division	Xu et al. (2014)
						5. SiRNA knockdown of *Wdr62* in mice (*in utero* electroporation)	5. Spindle orientation defects, delayed mitotic progression, reduced NPC proliferation, increased cell cycle exit	Bogoyevitch et al. (2012)
						6. *Wdr62*-knockout mice ($Wdr62^{f/f}$; homologous recombination followed by germline transmission)	6. Mild microcephaly, reduced NPC number, impaired mitosis, increased apoptosis, increased cilium length	Zhang et al. (2019a)
					Human cerebral organoid	7. $WDR62^{-/-}$ cerebral organoids (mutant Human pluripotent stem cell (hPSC) lines; CRISPR-Cas9)	7. Reduced organoid size, reduced outer radial glial cell (oRGC) proliferation, impaired mitosis, increased NPC vertical division, premature differentiation, increased apoptosis, increased cilium length	
MCPH3	Cyclin-dependent kinase 5 regulatory subunit-associated protein 2	*CDK5RAP2*	9q33.2	608201	Fly	1. *Centrosomin* (*cnn*) knockout flies (chemical mutagenesis)	1. Nuclear cleavage defects, microtubule organization defects, abnormal mitotic spindle formation	Megraw et al. (1999)
							Disconnections between centrioles and PCM	Lucas and Raff, (2007)
					Rodent	2. *Hertwig's anemia* mouse (inversion of exon 4 of *Cdk5rap2*)	2a. Fewer total neurons with special reduction in upper cortical neurons, abnormal spindle formation, and mitotic division, defective mitotic spindle orientation, premature cell cycle exit, increased cell death	Lizarraga et al. (2010)
							2b. Reduced dendritic complexity of layer 2/3 pyramidal neurons, increased spine density, shifted excitation—inhibition balance toward excitation	Zaqout et al. (2019)
						3. shRNA knockdown of *Cdk5rap2* in mouse (*in utero* electroporation)	3. Premature differentiation of NPCs, reduced proliferation, increased cell cycle exit	Buchman et al. (2010)
					Human cerebral organoid	4. RNAi knockdown of *CDK5RAP2* (co-electroporating green fluorescent protein (GFP) with shRNAs) and patient-derived cerebral organoids	4. Premature neural differentiation, increased NPC oblique, and vertical divisions	Lancaster et al. (2013)
MCPH4	Kinetochore scaffold 1	*KNL1*	15q15.1	609173	Rodent	1. Conditional *Knl1* knockout in mouse brain	1. Impaired NPC proliferation, missegregated chromosomes, DNA damage and p53 activation, rapid and robust apoptosis	Shi et al. (2019)

(Continued on following page)

TABLE 1 | (*Continued*) List of microcephaly primary hereditary (MCPH) genes and related animal/organism models.

Locus	Protein	Gene	Location	OMIM	Model organisms	Generation method	Key findings	Ref
MCPH5	Abnormal spindle-like, microcephaly associated protein	*ASPM*	1q31.3	605481	Fish	2. Morpholino-mediated knockdown of *aspm*	2a. Reduction in head and eye size, prometaphase delay, increased apoptosis	Novorol et al. (2013)
							2b. Reduction in head and eye size, mitotic arrest, increased apoptosis	Kim et al. (2011a)
					Fly	3. Mutagenesis (x-irradiation)	3. High mitotic index, metaphase arrest, mitotic and meiotic non-disjunction, hemi-spindles formation	Gonzalez et al. (1990)
						4. Mutagenesis (recombinant chromosomes)	4a. Arrested mitotic cycle at metaphase, high frequency of polyploid cells, defected sex chromosome disjunction	Ripoll et al. (1985)
							4b. Disrupted microtubule-organizing centers, failure of cytokinesis	Riparbelli et al. (2002)
					Rodent	5. esiRNA knockdown of *Aspm* in Tis21–GFP knockin mice (*in utero* electroporation)	5. Centrosome detachment, altered cleavage plane orientation, increased non-NE fate, increased neuron-like fate	Fish et al. (2006)
						6. *Aspm*-knockout mice (gene trap)	6. Mild microcephaly, midbody localization defects, Major germline defects	Pulvers et al. (2010)
						7. *Aspm*-knockout mice (removal of exons 2 and 3)	7. Much thicker layer I and thinner layer VI cortical neurons, aberrant expression of Tbr1 and Satb2 in the subplate	Fujimori et al. (2014)
					Ferret	8. *Aspm* germline knockout ferret	8. Severe microcephaly, displaced and altered NPC proportions, increased number of IPCs, increased apoptosis	Johnson et al. (2018)
					Human cerebral organoid	9. RNAi knockdown of *ASPM* (co-electroporating GFP with shRNAs) and patient-derived cerebral organoids	9. Reduced organoid size, proliferation defect, reduced number of RGs and oRGs	Li et al. (2017)
MCPH6	Centromeric protein J	*CENPJ*	13q12.2	609279	Fly	1. Mutations in the *DSas-4* gene (P-element insertion)	1. Morphologically normal, no detectable centrioles or centrosomes, lack of cilia, early postnatal lethality	Basto et al. (2006)
						2. Point mutations	2. Centriole loss, reduced binding affinity of the DSas-4 and Ana2 interaction	Cottee et al. (2013)
					Rodent	3. Conditional *Cenpj* knockout in mouse brain	3. Long cilia and abnormal cilia disassembly, uncompleted cell division, reduced cell proliferation, increased apoptosis	Ding et al. (2019)
						4. *Cenpj*-knockout mice (cassette insertion between exons 4 and 5)	4. Microcephaly, dwarfism, skeletal abnormalities, increased levels of DNA damage, and apoptosis	McIntyre et al. (2012)
MCPH7	SCL/TAL1-interrupting locus protein	*STIL*	1p33	181590	Fish	1. Morpholino-mediated knockdown of *wdr62*	1. Reduction in head and eye size, prometaphase delay, increased apoptosis	Novorol et al. (2013)
						2. *Cassiopeia* (*csp*) mutant zebrafish	2. Embryonic lethality, high mitotic index, highly disorganized mitotic spindles, lack of centrosomes, increased apoptosis	Pfaff et al. (2007)
					Rodent	3. *Stil*-knockout mice (removal of exons 3–5)	3a. Embryonic lethality, defected neural folding, randomization of left-right asymmetry, impaired response to Sonic 3b. Hedgehog (SHH) signaling	Izraeli et al. (1999)
							Lack of centrioles and primary cilia	David et al. (2014)
MCPH8	Centrosomal protein 135 kD	*CEP135*	4q12	611423	Alga	1. *bld10* flagella-less mutants (insertional mutagenesis)	1. Lack of basal bodies, disorganized mitotic spindles and cytoplasmic microtubules, abnormal cell division, and slow growth	Matsuura et al. (2004)
						2. *bld10* null mutants (series of truncations)	2. Basal-body defects	Hiraki et al. (2007)
					Protozoa	3. SiRNA knockdown of *bld10* in *Paramecium*	3. Abnormal basal body assembly	Jerka-Dziadosz et al. (2010)
					Fly	4. *bld10*-knockout flies (transposon insertion)	4a. Disrupted localization of the inner and outer centriole components	Roque et al. (2012)
							4b. Short centrioles and basal bodies, immotile sperm, infertility	Mottier-Pavie and Megraw, (2009)
							4c. Lack of singlet microtubules and disassembly of central microtubule pair	Carvalho-Santos et al. (2012)

(Continued on following page)

TABLE 1 | (*Continued*) List of microcephaly primary hereditary (MCPH) genes and related animal/organism models.

Locus	Protein	Gene	Location	OMIM	Model organisms	Generation method	Key findings	Ref
						5. *plp* RNAi knockdown in *bld10* mutant flies	5. Spindle alignment and centrosome segregation defects, perturbed centrosome asymmetry, mispositioned microtubule-organizing centers (MTOCs)	Singh et al. (2014)
MCPH9	Centrosomal protein 152 kD	*CEP152*	15q21.1	613529	Fly	1. *asterless* (*asl*^{1}, *asl*^{2}, *asl*^{3}) mutant flies (P-element-mediated transformation)	1. Defect in PCM stabilization and centrosome segregation, reduced microtubule nucleation, severe defects in meiotic spindle assembly	Varmark et al. (2007)
						2. *asterless* (*asl*^{mecD}) mutant flies (P-element-mediated transformation)	2. Lack of centrioles, basal bodies, and cilia	Blachon et al. (2008)
					Fish	3. Morpholino-mediated knockdown of *cep152*	3. Curly tail (ciliary defects)	
MCPH10	Zinc finger protein 335	*ZNF335*	20q13.12	610827	Rodent	1. *Znf335*-knockout mice (gene trap) 2. Conditional *Znf335* knockout in mouse brain (flanked promoter and exon1/2) 3. shRNA knockdown of *Znf335* in mice (*in utero* electroporation)	1. Early embryonic lethality 2. Lack all cortical structure and cortical neurons, enlarged ventricles 3. Disrupted NPC proliferation, premature differentiation, abnormal cell RGs orientation, disorganized dendritic outgrowth, lack of apical dendritic process	Yang et al. (2012)
MCPH11	Polyhomeotic-like 1 protein	*PHC1*	12p13.31	602978	N/A			
MCPH12	Cyclin-dependent kinase 6	*CDK6*	7q21.2	603368	Rodent	1. *Cdk6* knockout mice (removal of 1st coding exon)	1. Develop normally, slight hematopoiesis deficit	Malumbres et al. (2004)
MCPH13	Centromeric protein E	*CENPE*	4q24	117143	Fly	1. Mutations in *cenp-meta* gene (P-element-mediated disruption)	1. Embryonic lethality, defects in metaphase chromosome alignment	Yucel et al. (2000)
					Rodent	2. Conditional and complete *Cenp-e* gene disruptions in mouse	2. Early developmental arrest, mitotic chromosome misalignment	Putkey et al. (2002)
MCPH14	SAS-6 centriolar assembly protein	*SASS6*	1p21.2	609321	Worm	1. RNAi knockdown of *sas-6* in *Caenorhabditis elegans*	1. Abnormal centrosome duplication cycle	Leidel et al. (2005)
					Fish	2. *cellular atoll* (*cea*) mutant zebrafish	2. Defects in nuclear division, mitotic spindle formation, and centrosome duplication	Yabe et al. (2007)
					Fly	3. *sas-6*-knockout flies	3. Lack of cohesion between centrioles	Rodrigues-Martins et al. (2007)
MCPH15	Major facilitator superfamily domain-containing protein 2A	*MFSD2A*	1p34.2	614397	Fish	1. Morpholino-mediated knockdown of *mfsd2a*	1. Embryonic lethality before neural maturation, disrupted blood–brain barrier (BBB) integrity	Guemez-Gamboa et al. (2015)
					Rodent	2. *Mfsd2a*-knockout mice (gene targeting)	2a. Increased plasma lysophosphatidylcholine (LPC)	
							2b. Reduced body weight and length, increased energy expenditure, increased BAT β-oxidation, increased ataxic movement	Berger et al. (2012)
							2c. Reduced levels of DHA in the brain, microcephaly, neuronal cell loss in hippocampus and cerebellum, cognitive deficits, and severe anxiety	Nguyen et al. (2014)
							2d. Specific reduction in the retinal outer rod segment length, disorganized outer rod segment discs, reduction and mislocalization of rhodopsin, activated microglia	Wong et al. (2016)
						3. *Mfsd2a*-knockout mice (gene trap)	3. Leaky BBB, dramatic increase in central nervous system (CNS) endothelial cell vesicular transcytosis	Ben-Zvi et al. (2014)
						4. Mfsd2a-endothelial-specific knockout mice	4. Reduced neuronal arborization and decreased dendrite length	Chan et al. (2018)
MCPH16		*ANKLE2*	12q24.33	616062	Worm	1. *ax475* mutant worms (missense mutation in the *lem-4L* open reading	1. Abnormal nuclear morphology	Asencio et al. (2012)

(Continued on following page)

TABLE 1 | (*Continued*) List of microcephaly primary hereditary (MCPH) genes and related animal/organism models.

Locus	Protein	Gene	Location	OMIM	Model organisms	Generation method	Key findings	Ref
	Ankyrin repeat- and lem domain-containing protein 2					frame (ORF)) and RNAi knockdown of *lem-4L* in *C. elegans* embryos		
					Fly	2. *Ankle2*^{A} knockout (ethyl methanesulfonate (EMS) chemical mutagenesis)	2. Loss of thoracic bristles, severe reduction in neuroblast, impaired cell proliferation, increased apoptosis	Yamamoto et al. (2014)
						3. *Ankle2*^{A} knockout (EMS chemical mutagenesis) and Ankle2^{CRIMIC} knockout (CRISPR-Cas9)	3. Disrupted endoplasmic reticulum and nuclear envelope morphology, spindle alignment defects, disrupted asymmetric cell division pathway	Link et al. (2019)
MCPH17	Citron rho-interacting serine/threonine kinase	*CIT*	12q24.23	605629	Fly	1. *dck*^{2} knockout (EMS chemical mutagenesis)	1. Defective in both neuroblast and spermatocyte cytokinesis, abnormal F actin and anillin rings	Naim et al. (2004)
					Rodent	2. *Flathead* (*fh*) mutant rats (spontaneous mutation, deletion within exon 1 of *Citron-K*)	2a. Reduced brain size, dysgenesis of neocortex, hippocampus, cerebellum, and retina, increased apoptosis, seizures, tremor, impaired coordination, and premature death	Roberts et al. (2000)
							2b. Reduced brain size, cytokinesis failure, binucleated cells	Sarkisian et al. (2002)
							2c. Decrease in the number of interneurons, hypertrophied soma and dendritic arbors of interneurons, increased apoptosis, cytokinesis failure, binucleated cells	Sarkisian et al. (2001)
						3. Citron-K-knockout mice (gene targeting)	3. Depletion of microneurons in the olfactory bulb, hippocampus, and cerebellum, increased apoptosis, abnormal cytokinesis, tremor and severe ataxia, reduced life span due to lethal epilepsy	Di Cunto et al. (2000)
MCPH18	WD repeat and FYVE domain-containing 3	*WDFY3*	4q21.23	617485	Fly	1. Blue cheese (*bchs*) knockout flies (P-element-mediated disruption)	1a. Extensive neurodegeneration, premature adult death, formation of protein aggregates, neuronal apoptosis	Finley et al. (2003)
							1b. Morphological abnormalities in motor neurons, increased apoptosis, reduced endolysosomal vesicles mobility	Lim and Kraut, (2009)
						2. *hALFY* mutant flies (single point mutation)	2. Reduced brain volume, very fragile and malformed brain, clusters of disorganized neurons, severe rough eye phenotype	Kadir et al. (2016)
					Rodent	3. *Disconnected* mutant mice (*Wdfy3*$^{disc/disc}$; spontaneous nonsense mutation in exon 59 of 67 of *Wdfy3*)	3. Perinatal lethality, enlarged frontal cortical aspects, tangential expansion but lateral thinning of the neocortical neuroepithelium, focal cortical dysplasia, abnormal ganglionic eminences, enlarged ventricles, reduction in the size of the olfactory bulbs	Orosco et al. (2014)
						4. *Wdfy3*-knockout mice (*Wdfy3*$^{lacZ/lacZ}$; gene targeting)	4. Perinatal lethality, more drastic thinning and lengthening of the neocortex, focal cortical dysplasias	
						5. *Wdfy3*-haploinsufficiency mice (*Wdfy3*$^{+/lacZ}$; gene targeting)	5a. Deficiencies in mitochondrial function, defective mitophagy, accumulation of defective mitochondria, compromised fatty acid β-oxidation	Napoli et al. (2018)
							5b. Decreased mitochondrial localization at synaptic terminals, decreased synaptic density, defective brain glycophagy, cerebellar hypoplasia	Napoli et al. (2021)
							5c. Macrocephaly, deficits in motor coordination and associative learning, downregulation of the Wnt signaling pathway	Le Duc et al. (2019)
MCPH19	Coatomer protein complex, subunit beta 2 (beta prime)	*COPB2*	3q23	606990	Rodent	1. *Copb2*-knockout mice *Copb2*$^{Zfn/Zfn}$; Zinc-Finger nuclease mediated deletion within exon 12) *Copb2*-knockout mice (*Copb2*$^{null/null}$; CRISPR-Cas9)	1. Early embryonic lethality before organogenesis	DiStasio et al. (2017)

(Continued on following page)

TABLE 1 | (*Continued*) List of microcephaly primary hereditary (MCPH) genes and related animal/organism models.

Locus	Protein	Gene	Location	OMIM	Model organisms	Generation method	Key findings	Ref
						2. Mice homozygous for the patient mutation (*Copb2*$^{R254C/R254C}$; CRISPR-Cas9)	2. Viable and do not have cortical malformations	
						3. Mice heterozygous for the patient mutation and a null allele (*Copb2*$^{R254C/Zfn}$; CRISPR-Cas9)	3. Perinatal lethality, reduced brain size, reduction in layer V cortical neurons, increased apoptosis	
MCPH20	Kinesin family member 14	*KIF14*	1q32.1	611279	Fish	1. *kif14* mutant zebrafish (sa24165 mutant line Kettleborough et al. (2013))	1. Microcephaly, eye defects, body curvature, cardiac edema, glomerular cysts, high mitotic index, ciliopathy-like phenotypes	Reilly et al. (2019)
					Fly	2. Mutations in the *Klp38B* gene (P-element insertion)	2. Semi-lethality, abnormal cell cycle progression, failure of cytokinesis, rough eyes, missing bristles, abnormal abdominal cuticles	Ohkura et al. (1997)
					Rodent	3. *Laggard* (*lag*) mutant mice (spontaneous mutation, disruption within exon 5 of *Kif14*) and *Kif14* knockout mice (gene targeting)	3. Small head, tremor, ataxic gait, severe hypomyelination in the CNS, disrupted cytoarchitecture in the neocortex, hippocampus, and cerebellar cortex, increased apoptosis during late neurogenesis	Fujikura et al. (2013)
MCPH21	Non-SMC condensin I complex, subunit D2	*NCAPD2*	12p13.31	615638	Rodent	1. *Ncaph2* condensin II mutant mice (*Ncaph2*$^{I15N/I15N}$; ENU chemical mutagenesis)	1. Isolated T-lymphocyte developmental defect, reduced brain size, increased anaphase DNA bridge formation in apical NPCs, impaired chromosome segregation	Gosling et al. (2007), Martin et al. (2016)
MCPH22	Non-SMC condensin II complex subunit D3	*NCAPD3*	11q25	609276				
MCPH23	Non-SMC condensin I complex subunit H	*NCAPH*	2q11.2	602332				
MCPH24	Nucleoporin 37	*NUP37*	12q23.2	609264	*Xenopus*	1. Morpholino-mediated knockdown of *nup107*, *nup85*, or *nup133*	1. Disrupted glomerulogenesis	Braun et al. (2018)
					Fish	2. *nup107* or *nup85* knockout in zebrafish (CRISPR-Cas9)	2. Developmental anomalies, early lethality	
MCPH25	Trafficking protein particle complex subunit 14	*TRAPPC14*	7q22.1	618350	Fish	1. *map11* knockout in zebrafish (CRISPR-Cas9)	1. Microcephaly, decreased neuronal proliferation	Perez et al. (2019)
						2. Morpholino-mediated knockdown of *c7orf43*	2. Curved bodies, small eyes, ciliogenesis defects	Cuenca et al. (2019)
MCPH26	Lamin B1	*LMNB1*	5q23.2	150340	Rodent	1. *Lmnb1*-knockout mice (*Lmnb1*$^{\Delta/\Delta}$; gene trap)	1a. Perinatal lethality, abnormal lung development and bone ossification, abnormal skeleton and skull shape	Vergnes et al. (2004)
							1b. Perinatal lethality, absence of the cortical layering with reduced number of neurons, absence of lamination in the hippocampus, absence of cerebellar foliation, impaired neuronal migration, reduced NPC proliferation, solitary nuclear bleb in cortical neurons	Coffinier et al. (2011)
						2. Forebrain-specific *Lmnb1*-knockout mice (*Emx1-Cre Lmnb1*$^{fl/fl}$)	2. Very small cortex, low neuronal density, lack of upper cortical layers, nuclear blebs in embryonic neurons, nuclear membrane ruptures, increased apoptosis, asymmetric distribution of Lmnb2	Coffinier et al. (2011), Chen et al. (2019)
MCPH27	Lamin B2	*LMNB2*	19p13.3	150341	Rodent	3. *Lmnb1/Lmnb2*-knockout mice (*Lmnb1*$^{-/-}$*Lmnb2*$^{-/-}$; gene targeting)	3. Defects in lungs, diaphragms, and brains, thinner cerebral cortex, disorganized cortical layers, impaired neuronal migration, altered cleavage plane orientation, increased cell cycle exit	Kim et al. (2011b)
						4. *Lmnb2*-knockout mice (*Lmnb2*$^{-/-}$; gene targeting)	4. Perinatal lethality, impaired neuronal migration, layering defects in the cerebral cortex and hippocampus, absence of cerebellar foliation, absence of a discrete Purkinje cell layer, elongated nuclei in cortical neurons	Coffinier et al. (2010), Coffinier et al. (2011)

(Continued on following page)

TABLE 1 | (*Continued*) List of microcephaly primary hereditary (MCPH) genes and related animal/organism models.

Locus	Protein	Gene	Location	OMIM	Model organisms	Generation method	Key findings	Ref
						5. Forebrain-specific *Lmnb2*-knockout mice (*Emx1-Cre Lmnb2*$^{fl/fl}$)	5. Small cortex, cortical defect more pronounced after birth, abnormal layering of cortical neurons, elongated nuclei in embryonic neurons, normal distribution of Lmnb1 at the nuclear rim	Coffinier et al. (2011)
MCPH28	Ribosomal RNA processing 7 homolog A	*RRP7A*	22q13.2	619449	Fish	1. *rrp7a* mutant zebrafish (sa11429 mutant line (Kettleborough et al., 2013))	1. Premature lethality, reduced brain size, reduced eye size, increased apoptosis	Farooq et al. (2020)

Asymmetrical division of an RGC at the ventricular surface generates a self-renewing RG daughter cell and either a postmitotic neuron or a basal progenitor (intermediate progenitor cell (IPC)) (Homem et al., 2015; Subramanian et al., 2019). It has been earlier believed that the asymmetrical division of RGCs is principally driven by a change in mitotic spindle positions leading to a shift of the cleavage plane orientation from perpendicular (vertical) to parallel (horizontal) relative to the ventricular surface (Chenn and McConnell, 1995; Zhong et al., 1996; Kosodo et al., 2004; Fietz and Huttner, 2011; Homem et al., 2015). However, further investigations revealed that the rate of asymmetrical divisions in RGCs is not necessarily altered by the orientation of the cleavage plane (Morin et al., 2007; Konno et al., 2008; Postiglione et al., 2011). The asymmetrical RGC fate might be affected by inheriting centrioles with different maturity and primary cilium (Wang et al., 2009; Goetz and Anderson, 2010; Paridaen et al., 2013). It has been also shown that alterations in RGC cycle length control the shift from self-renewing divisions to neurogenic divisions (Calegari and Huttner, 2003; Calegari et al., 2005; Pilaz et al., 2009; Arai et al., 2011). Furthermore, it has been proposed that Notch signaling triggers neurogenic cell fate either by its distinct apicobasal gradient during INM or through asymmetric inheritance of endosomes positive for Sara (Smad anchor for receptor activation) (Del Bene et al., 2008; Nerli et al., 2020). This latter is achieved by targeting signaling endosomes to the central spindle by the action of plus-end kinesin motor (Klp98A) (Derivery et al., 2015).

Unlike RGCs, IPCs lack the connection with the ventricular surface and settle mainly in the subventricular zone (SVZ) basal to the VZ (Rakic, 2009; Homem et al., 2015; Subramanian et al., 2019; Heide and Huttner, 2021). IPCs undergo some proliferative divisions and terminate by generating two cortical neurons (Noctor et al., 2004; Pontious et al., 2008; Rakic, 2009). Asymmetrical divisions of RGCs in many mammals, especially in primates, yield an additional generation of a special type of basal progenitors known as basal RGCs (outer RGCs (oRGCs)) (Homem et al., 2015). Compared with IPCs, the oRGCs show a much higher proliferative capacity, which amplifies the total number of generated neurons and contribute to the characteristic folded cerebral cortex observed in primates, especially in humans (Reillo et al., 2011; Fietz et al., 2010; Hansen et al., 2010; Betizeau et al., 2013; Heide and Huttner, 2021). The newly established 3D *in vitro* human brain organoid model exhibits a considerable number of oRGCs (Lancaster et al., 2013; Zhang et al., 2019a).

Postmitotic cortical neurons are generated from both VZ and SVZ neural progenitors in an inside-out manner by which later-born neurons (superficial layers IV–II) bypass earlier-born neurons (deep layers VI–V) (Molyneaux et al., 2007; Leone et al., 2008). This pattern of neural generation is under spatiotemporal, cell cycle, and competency precise controls of neural progenitor fates (Kohwi and Doe, 2013). Eventually, six neural layers are created in the developing cerebral cortex, and the neurons start the formation of their distinctive dendrites, axons, and functional synapses. The fully developed cortical network contains 80% glutamatergic excitatory neurons produced by VZ and SVZ neural progenitors located in the dorsal telencephalon and 20% GABAergic inhibitory neurons that originated from the medial and caudal ganglionic eminence (Marín, 2013; Costa and Müller, 2014). The terminal number of generated cortical neurons is affected not only by the original number of neural progenitors but also by their starting and ending proliferation points and their cell lineage (Homem et al., 2015).

At the final stage of neurogenesis, RGCs lose their neuronal lineage and the connection with the apical surface switching to glial cell generators (Malatesta et al., 2000; Qian et al., 2000). Cortical astrocytes are firstly detected followed by oligodendrocytes, and the number of both glial cells is hugely expanded postnatally (Qian et al., 2000). Glial cells induce the development of white matter and axonal outgrowth by producing myelin and forming astrocytic branches (Subramanian et al., 2019). Taken together, forming a normal cerebral cortex requires highly organized spatiotemporal control for the neural progenitor populations to generate different neuronal and glial subtypes. Any defect during this process can lead to a major impact on brain development.

BRAIN PHENOTYPE IN INDIVIDUALS WITH MICROCEPHALY PRIMARY HEREDITARY

The morphological changes in the brain structure of MCPH individuals have been mainly identified by radiological studies. Most MCPH cases show a reduction in brain volume associated with a simplified neocortical gyration pattern. However, the increased number of reported mutations and the ongoing neuroimaging of MCPH individuals reveal further brain malformations (**Table 2**). Some of these structural changes point toward the causative *MCPH* gene (e.g., the association between malformations of basal ganglia and mutations in gene encoding zinc finger-335 protein (*ZNF335*; *MCPH10*) (Sato et al.,

TABLE 2 | Brain malformations associated with microcephaly primary hereditary (MCPH) additional to microcephaly.

Locus	Gene	Brain malformations	Key findings	Ref
MCPH1	*MCPH1*	Corpus callosum abnormalities	Mild hypoplasia	Hosseini et al. (2012)
			Agenesis of the genu	Neitzel et al. (2002)
		Pachygyria	+	Neitzel et al. (2002), Trimborn et al. (2004)
			Thickening of fronto-parietal and temporal gyri	Hosseini et al. (2012)
		Heterotopia	Nodular neuronal heterotopia (ventricular, infratentorial, and subependymal)	Neitzel et al. (2002), Trimborn et al. (2004)
			Periventricular neuronal heterotopias	Trimborn et al. (2004)
		Frontal lobe hypoplasia	+	Neitzel et al. (2002)
		Ventricular system abnormalities	Dilatation of lateral ventricles (dorsal and temporal), dilated external liquor space	
		Myelination/white matter abnormalities	Slight retardation of myelination of cerebral medullary layer	
MCPH2	*WDR62*	Corpus callosum abnormalities	Hypoplasia	Bilgüvar et al. (2010), Yu et al. (2010), Farag et al. (2013), Memon et al. (2013), Sgourdou et al. (2017), Zombor et al. (2019), Slezak et al. (2021)
			Dysplasia	Poulton et al. (2014)
			Abnormally shaped corpus callosum, agenesis of the rostral part	Bilgüvar et al. (2010)
			Dysmorphic with a thick body and a small genu	Yu et al. (2010)
			Incomplete genu and small splenium	
			Thinning of the corpus callosum with absence of the splenium	Banerjee et al. (2016)
		Pachygyria	+	Bilgüvar et al. (2010), Bhat et al. (2011), Bacino et al. (2012), Bastaki et al. (2016), Slezak et al. (2021)
			Diffuse pachygyria	Sgourdou et al. (2017), Zombor et al. (2019)
			Severe pachygyria	Poulton et al. (2014)
		Lissencephaly/agyria	Microlissencephaly	Bilgüvar et al. (2010), Bhat et al. (2011), Bastaki et al. (2016), Slezak et al. (2021)
		Polymicrogyria	+	Bilgüvar et al. (2010), Poulton et al. (2014)
			Widespread polymicrogyria	Yu et al. (2010)
			Polymicrogyria in the right hemisphere	Slezak et al. (2021)
			Bilateral polymicrogyria	Bhat et al. (2011)
			Bilateral parietal polymicrogyria	Murdock et al. (2011)
			Extensive polymicrogyria in the left cerebral hemisphere	
			Extensive areas of polymicrogyria in the right frontal lobe	Nardello et al. (2018)
		Abnormal Sylvian fissure	Under-opercularization	Bilgüvar et al. (2010), Poulton et al. (2014)
			Widened Sylvian fissure	Farag et al. (2013)
			Open Sylvian fissures	Bacino et al. (2012)
		Schizencephaly	+	Memon et al. (2013)
			Open-lip schizencephaly	Bilgüvar et al. (2010)
			Narrow right temporoparietal open lip schizencephaly, right temporoparietal open lip schizencephaly	Yu et al. (2010)
			Suspected schizencephaly in the right parietal lobe	Banerjee et al. (2016)
			Closed schizencephaly in the right cerebral hemisphere	Slezak et al. (2021)
		Heterotopia	Subcortical heterotopia, bilateral band heterotopia in the posterior frontal and parietal lobes	Yu et al. (2010)
			Band heterotopias	Bhat et al. (2011)
			A focus of gray matter heterotopia in the right parietal region	Murdock et al. (2011)
		Hemispherical asymmetry	Asymmetric microcephalic hemispheres	Bilgüvar et al. (2010), Zombor et al. (2019)
			Volume loss worse on the left than the right cerebral hemisphere	Yu et al. (2010), Murdock et al. (2011)
			Volume loss worse on the right than the left cerebral hemisphere	Kousar et al. (2011), Rupp et al. (2014), Slezak et al. (2021)
		Frontal lobe hypoplasia	+	Farag et al. (2013)
		Hippocampal abnormalities	Dysmorphic	Bilgüvar et al. (2010)
			Simplified hippocampal gyration	Farag et al. (2013)
			Dysplasia of the temporal lobe with small hippocampus	Banerjee et al. (2016)
		Infratentorial abnormalities	Unilateral cerebellar hypoplasia, unilateral brainstem atrophy	Bilgüvar et al. (2010)
			Cerebellar hypoplasia	Farag et al. (2013)
			Slight atrophy of the brain stem and cerebellum	Banerjee et al. (2016)
		Ventricular system abnormalities	Dilated ventricles	Yu et al. (2010), Memon et al. (2013)
			Prominent extra-axial cerebrospinal	Kousar et al. (2011)
			Slight expansion of bilateral brain ventricles, obvious expansion of the fourth ventricle	Banerjee et al. (2016)
			Asymmetrical enlargement of the ventricles, dilated Virchow–Robin spaces	Zombor et al. (2019)
			Posterior horn-dominant enlargement of the lateral ventricles	Slezak et al. (2021)
		Thickened gray matter	+	Poulton et al. (2014), Zombor et al. (2019), Slezak et al. (2021)
			Diffusely thickened cortex	Bilgüvar et al. (2010)
			Mildly thickened cortex (~5 mm)	Nicholas et al. (2010)
		Blurred gray-white matter junction	Loss of gray–white junction	Bilgüvar et al. (2010)
			Ill-defined gyral and nuclei pattern	Kousar et al. (2011)
			Indistinct gray–white matter border in certain areas	Zombor et al. (2019)
			Gray–white matter blurring involving the left parietooccipital cortex	Nardello et al. (2018)

(Continued on following page)

TABLE 2 | (*Continued*) Brain malformations associated with microcephaly primary hereditary (MCPH) additional to microcephaly.

Locus	Gene	Brain malformations	Key findings	Ref
		Myelination/white matter abnormalities	Leukodystrophy, dysplasia of the white matter	Banerjee et al. (2016)
			Thin white matter	Zombor et al. (2019)
			Reduced white matter volume	Slezak et al. (2021)
MCPH3	*CDK5RAP2*	Corpus callosum abnormalities	Hypoplasia	Alfares et al. (2018)
			Agenesis/hypogenesis	Issa et al. (2013)
		Hypothalamic abnormalities	Interhypothalamic adhesion	Nasser et al. (2020)
		Thickened gray matter	+	Alfares et al. (2018)
		Myelination/white matter abnormalities	Bilateral enhancement in the white matter (white matter disorder)	
MCPH4	*KNL1*	Infratentorial abnormalities	Cerebellar vermis hypoplasia	Saadi et al. (2016)
		Ventricular system abnormalities	Wide cyst in the posterior fossa communicating with an expanded fourth ventricle	
MCPH5	*ASPM*	Corpus callosum abnormalities	Thick corpus callosum	Passemard et al. (2009), Saadi et al. (2009), Létard et al. (2018)
			Agenesis of splenium	Passemard et al. (2009)
			Agenesis of rostrum	
			Partial agenesis	Abdel-Hamid et al. (2016)
			Hypoplasia	Abdel-Hamid et al. (2016), Létard et al. (2018)
		Pachygyria	+	Létard et al. (2018), Shaheen et al. (2019)
			Temporal pachygyria	Ariani et al. (2013)
		Polymicrogyria	Extensive unilateral perisylvian polymicrogyria from the frontal pole to the occipital pole	Passemard et al. (2009)
			Extensive bilateral posterior polymicrogyria	Létard et al. (2018)
			Polymicrogyria in frontoinsular region	
		Frontal lobe hypoplasia	Severe hypoplasia of the frontal lobes	Saadi et al. (2009)
			Frontal lobes are short and hypoplastic	Desir et al. (2008)
		Infratentorial abnormalities	Mild asymmetric cerebellar hypoplasia	Passemard et al. (2009)
			Ipsilateral pons hypoplasia	
			Cerebellar vermis and/or hemispheres hypoplasia	Abdel-Hamid et al. (2016), Létard et al. (2018)
			Elongated superior cerebellar peduncles	Létard et al. (2018)
			Relatively small pons	Abdel-Hamid et al. (2016)
			Thin brain stem	Ariani et al. (2013), Létard et al. (2018)
		Ventricular system abnormalities	Occipital horns of the lateral ventricles enlarged	Passemard et al. (2009)
			Dysmorphic frontal ventricles	Passemard et al. (2009)
			Enlarged lateral ventricles and colpocephaly	Abdel-Hamid et al. (2016)
			Large porencephalic cyst communicating with lateral ventricle	
			Small midline cyst	
			Ventricular enlargement	Létard et al. (2018)
			Arachnoid cyst in the posterior fossa	
			Enlarged Virchow–Robin spaces	
			Enlarged subarachnoid spaces, mega cisterna magna	
		Myelination/white matter abnormalities	Reduced white matter	Abdel-Hamid et al. (2016)
			Myelination delay	Létard et al. (2018)
MCPH6	*CENPJ*	N/A		
MCPH7	*STIL*	Corpus callosum abnormalities	Partial agenesis of the corpus callosum	Mouden et al. (2015), Shaheen et al. (2019)
			Short dysmorphic corpus callosum	Kakar et al. (2015)
		Holoprosencephaly	Lobar holoprosencephaly	Kakar et al. (2015), Mouden et al. (2015)
		Frontal lobe hypoplasia	Disproportionately short frontal lobes, continuity of the right and left frontal lobes at the level of the basal ganglia and lateral ventricles	Kakar et al. (2015)
			Straight and atrophic frontal lobe	Cheng et al. (2020)
		Infratentorial abnormalities	Atrophy of the vermis	Mouden et al. (2015)
			Cerebellar hypovermis dysplasia	Cheng et al. (2020)
		Ventricular system abnormalities	Absence of ventricular frontal horns	Mouden et al. (2015)
			Absence of occipital lobe and a large unilateral temporal and occipital fluid cavity communicating	
			Small third ventricle, enlarged lateral ventricles posteriorly	Kakar et al. (2015)
			Large porencephalic cyst replacing most of the posterior right hemisphere	
			Dilatation of the fourth ventricle	Cheng et al. (2020)
		Blurred gray-white matter junction	+	Cheng et al. (2020)
		Myelination/white matter abnormalities	Diffuse severe reduction of the white matter volume	Kakar et al. (2015)
MCPH8	*CEP135*	Heterotopia	Bilateral nodular heterotopia in the peritrigonal regions	Bamborschke et al. (2020)
MCPH9	*CEP152*	Corpus callosum abnormalities	Severe hypogenesis	Shaheen et al. (2019)

(Continued on following page)

TABLE 2 | (*Continued*) Brain malformations associated with microcephaly primary hereditary (MCPH) additional to microcephaly.

Locus	Gene	Brain malformations	Key findings	Ref
		Polymicrogyria	+	
		Ventricular system abnormalities	Inter-hemispheric cyst at left aspect of the falx continuous with the third ventricle	
MCPH10	*ZNF335*	Corpus callosum abnormalities	Thin corpus callosum	Stouffs et al. (2018)
		Lissencephaly/agyria	Anterior agyria and a posterior simplified gyral pattern	
		Basal ganglia abnormalities	Absent basal ganglia	Stouffs et al. (2018)
			Invisible basal ganglia	Sato et al. (2016)
			Volume loss in basal ganglia (putamen atrophy)	Caglayan et al. (2021)
			Patchy areas of the altered signal in the left thalamoganglionic region	Rana et al. (2019)
		Infratentorial abnormalities	Hypoplasia of brainstem and cerebellum	Sato et al. (2016), Stouffs et al. (2018)
			Cerebellar atrophy	Rana et al., (2019), Caglayan et al. (2021)
		Ventricular system abnormalities	Enlarged ventricles	Stouffs et al. (2018)
		Myelination/white matter abnormalities	Hypomyelination	Sato et al. (2016), Stouffs et al. (2018), Caglayan et al. (2021)
MCPH11	*PHC1*	N/A		
MCPH12	*CDK6*			
MCPH13	*CENPE*	Corpus callosum abnormalities	Partial agenesis of the corpus callosum	Mirzaa et al. (2014)
		Frontal lobe hypoplasia	Low forehead	
		Infratentorial abnormalities	Cerebellar hypoplasia	
		Lissencephaly/agyria	Diffuse severely simplified gyral pattern with virtually no gyri over the frontal lobe	
		Myelination/white matter abnormalities	Immature white matter	
MCPH14	*SASS6*	Lissencephaly/agyria	No gyral or sulcal development	Zhang et al. (2019b)
		Basal ganglia abnormalities	Poorly confined basal ganglia and missing delineation of the internal capsule	Khan et al. (2014)
		Infratentorial abnormalities	Dysmorphic infratentorial region with hypoplasia of the vermis cerebella	
		Ventricular system abnormalities	No bilateral frontal horns or cavum septi pellucidi present	Zhang et al. (2019b)
			Abnormal formation of the lateral ventricles	Khan et al. (2014)
MCPH15	*MFSD2A*	Corpus callosum abnormalities	Hypoplasia	Guemez-Gamboa et al. (2015), Scala et al. (2020)
		Infratentorial abnormalities	Inferior vermian hypoplasia	Scala et al. (2020)
			Pontine hypoplasia	
			Hypoplasia of brain stem and cerebellum	Guemez-Gamboa et al. (2015)
		Ventricular system abnormalities	Enlarged ventricles	Guemez-Gamboa et al. (2015), Harel et al. (2018), Scala et al. (2020)
			Hydrocephaly	Shaheen et al. (2019)
		Myelination/white matter abnormalities	White matter reduction	Alakbarzade et al. (2015), Harel et al. (2018), Scala et al. (2020)
MCPH16	*ANKLE2*	Corpus callosum abnormalities	Agenesis	Yamamoto et al. (2014)
			Partial agenesis	Shaheen et al. (2019)
		Pachygyria	Coarsening of the gyral sulcal pattern and some thickening consistent with pachygyria	
		Polymicrogyria	Polymicrogyria-like cortical brain malformations	Yamamoto et al. (2014)
		Infratentorial abnormalities	Hypoplastic cerebellum	Shaheen et al. (2019)
		Ventricular system abnormalities	Small frontal horns of the lateral ventricles with mildly enlarged posterior horns	Yamamoto et al. (2014)
		Thickened gray matter	Mildly thickened cortex	
MCPH17	*CIT*	Corpus callosum abnormalities	Hypogenesis	Li et al. (2016a)
			Agenesis	Harding et al. (2016), Shaheen et al. (2016)
		Lissencephaly/agyria	Lissencephaly	Harding et al. (2016), Shaheen et al. (2016)
		Infratentorial abnormalities	Cerebellar and brainstem hypoplasia	Harding et al. (2016)
		Ventricular system abnormalities	Enlarged ventricles	Harding et al. (2016), Shaheen et al. (2016)
		Myelination/white matter abnormalities	Diminished white matter	Shaheen et al. (2016)
MCPH18	*WDFY3*	N/A		
MCPH19	*COPB2*	Corpus callosum abnormalities	Thin corpus callosum	DiStasio et al. (2017)
		Ventricular system abnormalities	Slight dilation of the lateral, third and fourth ventricles	
		Myelination/white matter abnormalities	Delayed myelination	
MCPH20	*KIF14*	Corpus callosum abnormalities	Agenesis	Moawia et al. (2017), Reilly et al. (2019)
			Partial agenesis	Makrythanasis et al. (2018)
		Lissencephaly/agyria	Microlissencephaly	Makrythanasis et al. (2018)
			+	Moawia et al. (2017)

(Continued on following page)

TABLE 2 | (*Continued*) Brain malformations associated with microcephaly primary hereditary (MCPH) additional to microcephaly.

Locus	Gene	Brain malformations	Key findings	Ref
		Infratentorial abnormalities	Cerebellar hypoplasia	Moawia et al. (2017), Reilly et al. (2019)
		Ventricular system abnormalities	Large basal cisterns	Makrythanasis et al. (2018)
			Interhemispheric cyst	Moawia et al. (2017)
		Thickened gray matter	Slightly thickened cortex	Moawia et al. (2017)
MCPH21 MCPH22 MCPH23	*NCAPD2* *NCAPD3* *NCAPH*	N/A		
MCPH24	*NUP37*	Infratentorial abnormalities	Cerebellar vermis hypoplasia	Braun et al. (2018)
MCPH25	*TRAPPC14*	Corpus callosum abnormalities	Hypoplasia	Perez et al. (2019)
		Myelination/white matter abnormalities	Diminished white matter	
MCPH26	*LMNB1*	Corpus callosum abnormalities	Thin corpus callosum	Cristofoli et al. (2020)
			Dysgenesis	
			+	
		Pachygyria		
		Lissencephaly/agyria		
		Ventricular system abnormalities	Enlarged ventricles	
MCPH27	*LMNB2*	Ventricular system abnormalities	Enlarged ventricles	Parry et al. (2021)
		Myelination/white matter abnormalities	Diminished white matter	
MCPH28	*RRP7A*	Corpus callosum abnormalities	Volume loss especially in the anterior half	Farooq et al. (2020)

2016; Stouffs et al., 2018; Rana et al., 2019; Caglayan et al., 2021)). The increasing number of reported brain malformations in MCPH individuals widens its pathogenesis spectrum. This indicates that the disruption of MCPH proteins not only is affecting the generation of neurons but could additionally affect neuronal differentiation, migration, dendritic and axonal outgrowth, and synaptogenesis. This is understandable given the fact that MCPH proteins are highly expressed in various neuroprogenitor organelles, especially the centrosome. In the following sections, we will discuss the consequences of *MCPH* mutations on brain development.

ACCIDENTS DURING THE BRAIN DEVELOPMENT JOURNEY IN MICROCEPHALY PRIMARY HEREDITARY

Studying the molecular mechanisms behind the pathogenesis of MCPH is very limited in humans. In fact, *MCPH* genes are highly conserved among different species (Woods et al., 2005; Gilbert et al., 2005), and this led to the discovery of several MCPH animal models mimicking the human phenotype (**Table 1**). Therefore, most of our current knowledge on the role of MCPH proteins in brain development is enriched through extensive studies on MCPH animal models. However, the pronounced difference of the human brain compared with most of the studied MCPH animal models establishes a new research direction toward 3D *in vitro* human brain organoid systems in studying the pathogenesis of microcephaly (Muzio and Consalez, 2013; Gabriel et al., 2020). The remarkable presence of oRGCs in this model opens the door for deeper insights into their role during the course of this disease in humans (Lancaster et al., 2013; Zhang et al., 2019a). As many MCPH proteins share overlapped functions, we saw to categorize them according to their major role(s) rather than discussing each one individually (**Figure 1**).

Dysfunctional Centrosome

Almost one-third of *MCPH* mutations occur in centrosomal or mitotic spindle proteins. Defective centrosomes can affect cell cycle progression and cell division, leading to abnormal chromosomal numbers, cell cycle arrest, and apoptosis (Barbelanne and Tsang, 2014). It has been proposed that alterations of the cleavage plane orientation during NE proliferation increase asymmetric cell divisions (Buchman and Tsai, 2007; Knoblich, 2008; Zhong and Chia, 2008). This, in turn, leads to an early consumption of progenitor cells at the expense of a premature generation of neurons with ultimately reduced number, thence a smaller brain (Fish et al., 2006; Buchman et al., 2010; Kaindl et al., 2010; Lizarraga et al., 2010). In this notion, several MCPH mouse models show a shift in the cleavage plan orientation of NE cells favoring neurogenic cell fate (Fish et al., 2006; Lizarraga et al., 2010; Pulvers et al., 2010; Gruber et al., 2011; Xu et al., 2014). This evidence has been also supported by human brain organoid models (Lancaster et al., 2013; Zhang et al., 2019a). Intriguingly, most of the MCPH fly models with defected centrosomal proteins exhibit normal brain size (Basto et al., 2006; Lucas and Raff, 2007; Roque et al., 2012), indicating that changes in the cleavage plane

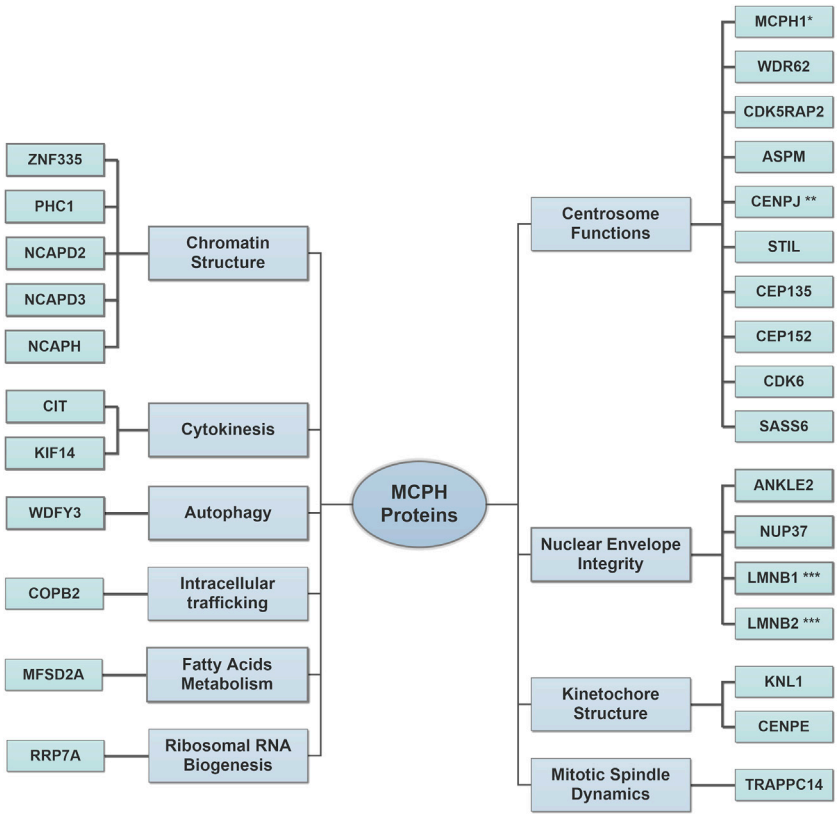

FIGURE 1 | Major roles of microcephaly primary hereditary (MCPH) proteins in brain development. The increased number of discovered MCPH proteins expands the pathomechanism spectrum to include several cellular components. Centrosome Functions: the proteins of this group regulate proper centrosomal functions to balance the transition between neural progenitor cell (NPC) proliferation and differentiation by controlling cell cycle progression and cell cycle exit fraction. Nuclear Envelope Integrity: the proteins of this group affect the proper spindle alignment and cell fate determinants during NPC proliferation and protect radial glial cell (RGC) nuclei from mechanical stress injury during INM. Kinetochore Structure: the proteins of this group assure the correct alignment of chromosomes during mitosis. Mitotic Spindle Dynamics: the proteins of this group regulate the spindle dynamics and cell division. Chromatin Structure: the proteins of this group regulate gene expression during neurogenesis and assure proper DNA damage repair. Cytokinesis: the proteins of this group regulate the terminal step in the cell cycle, which leads to a physical separation between the daughter cells. Autophagy: the proteins of this group facilitate the removal of cytosolic protein aggregates and maintain mitochondrial homeostasis. Intracellular trafficking: the proteins of this group control the cellular retrograde trafficking from the Golgi to the endoplasmic reticulum. Fatty Acid Metabolisms: the proteins of this group affect the postnatal neuronal morphogenesis, which requires a normal lipogenesis process. Ribosomal RNA Biogenesis: the proteins of this group regulate ribosomal RNA processing and affect primary cilia resorption. Please refer to (**Table 1**) for full protein names. *MCPH1 is also involved in chromatin structure. **CENPJ is also involved in kinetochore structure. ***LMNB1 and LMNB2 are also involved in mitotic spindle dynamics.

orientation might only have a minor impact on brain growth. Alternatively, flies could have compensatory mechanisms bypassing the effect of the misoriented cleavage plane (Nigg and Raff, 2009). On the other hand, further studies discovered MCPH mouse models with the microcephaly phenotype, though unaffected cleavage plane (Pulvers et al., 2010; Marjanović et al., 2015). Furthermore, depletion of some other MCPH centrosomal proteins in mice does not affect brain growth at all (Malumbres et al., 2004).

The neural progenitor cell (NPC) symmetrical proliferation speed is frequently reduced in mutated *MCPH* genes, which encode centrosomal proteins (Lizarraga et al., 2010; Gruber et al., 2011; Sgourdou et al., 2017; Ding et al., 2019). This is much obvious toward the end of neurogenesis (Lizarraga et al., 2010; Gruber et al., 2011; Sgourdou et al., 2017) when the later-born neurons (superficial layers II–IV) start to be generated. Together with the premature generation of neurons, this explains why superficial cortical neurons are the most affected in most MCPH models (Lizarraga et al., 2010; Chen et al., 2014). This is in line with postmortem histological analysis described in a case of *WD-repeat-containing protein 62 gene* (*WDR62*; *MCPH2*) mutation (Yu et al., 2010). In addition, MCPH proteins are important for the normal distribution of cells between cortical zones. Knockout of *abnormal spindle-like*, *microcephaly-associated gene* (*Aspm*) in ferret increases the number of generated oRGCs, affecting the RGC overall proliferative capacity (Johnson et al., 2018). Likewise, knockdown of the cyclin-dependent kinase five regulatory subunit-associated protein two gene *Cdk5rap2* in a mouse model alters the distribution of progenitor pool leading to more generation of basal progenitors (Buchman et al., 2010). By contrast, somatosensory cortical layer VI has been reported to be thinner in an *Aspm* knockout mouse model (Fujimori et al., 2014). Indeed, several *in vivo* and *in vitro* studies including human brain organoid

models revealed that *MCPH* centrosomal genes balance the transition between NPC proliferation and differentiation by controlling cell cycle progression and cell cycle exit fraction (Buchman et al., 2010; Lizarraga et al., 2010; Bogoyevitch et al., 2012; Lancaster et al., 2013; Hainline et al., 2014; Zhang et al., 2019a). This explains, respectively, the reduced proliferation and premature neuronal differentiation detected in the respective MCPH animal models. Furthermore, using the conditional knockout mouse model, it has been shown that centromeric protein J (Cenpj) regulates NPC cell cycle progression by regulating cilium disassembly during neurogenesis (Ding et al., 2019). Similarly, depletion of *WDR62* and centrosomal-P4.1-associated protein (*CPAP*) in human cerebral organoids impairs the cilium disassembly and cell cycle progression (Gabriel et al., 2016; Zhang et al., 2019a).

It has been reported that mutations in genes encoding MCPH centrosomal proteins alter the maturation and cellular number of centrosomes (Pfaff et al., 2007; Rodrigues-Martins et al., 2007; Yabe et al., 2007; Megraw et al., 2011; Hussain et al., 2012; McIntyre et al., 2012; Hussain et al., 2013; Arquint and Nigg, 2014). This, in turn, might affect the proper distribution of chromosomes to daughter cells leading to spindle instability and mitotic delay or arrest at metaphase checkpoint (Ripoll et al., 1985; Gonzalez et al., 1990; Megraw et al., 1999; Riparbelli et al., 2002; Matsuura et al., 2004; Pfaff et al., 2007; Lizarraga et al., 2010; Kim et al., 2011a; Vitale et al., 2011; Novorol et al., 2013; Chen et al., 2014). In most of these cases, such defect triggers the apoptotic cascade leading to cellular loss (Pfaff et al., 2007; Lizarraga et al., 2010; Vitale et al., 2011; McIntyre et al., 2012; Novorol et al., 2013; Chen et al., 2014). Remarkably, increased apoptosis of NPCs—associated with or without proliferation/differentiation defects—contributes to the microcephaly phenotype by depleting the neural stem cell pool (Izraeli et al., 1999; Pfaff et al., 2007; Lizarraga et al., 2010; Gruber et al., 2011; McIntyre et al., 2012; Sgourdou et al., 2017; Zhang et al., 2019a; Ding et al., 2019). Intriguingly, neuronal populations also seem to be vulnerable to apoptosis during later stages of development (Lizarraga et al., 2010).

Apparently, the impact of mutated MCPH centrosomal genes in brain development not only is restricted to NPC proliferation and differentiation phase but also exceeds it to affect neuronal migration, dendritic and axonal outgrowth, and synaptogenesis. The presence of gray matter heterotopia, polymicrogyria, lissencephaly, and pachygyria in several MCPH conditions points toward impaired neuronal migration (**Table 2**) (Leventer et al., 2010; Yu et al., 2010). The signs of this impairment have been reported in postmortem histopathological MCPH samples and various MCPH animal models (Yu et al., 2010; Buchman et al., 2011; Xu et al., 2014). Besides that, an interesting role of Cdk5rap2 in regulating dendritic development and synaptogenesis in superficial cortical layer II/III has been reported (Zaqout et al., 2019). The contribution of dendritic complexity deficits in the microcephaly phenotype points toward a progressive nature during the MCPH course (van Dyck and Morrow, 2017).

Defective Chromatin Structure

Chromatin structure is a golden stone for gene expression regulation during neurogenesis. Mutations in genes encoding chromatin-linked proteins expand the pathomechanism spectrum of the MCPH. *Microcephalin* (*BRCT/BRIT1*) mutated cells taken from MCPH1 individuals and mouse models displayed premature chromosome condensation (PCC) associated with a high frequency of prophase-like cells and defective DNA damage repair (Jackson et al., 2002; Neitzel et al., 2002; Liang et al., 2010; Trimborn et al., 2010). This feature has been considered as a diagnostic marker for individuals with MCPH1 gene mutations (Jackson et al., 2002). In flies, *mcph1* mutants display embryonic lethality due to mitotic arrest and uncoordinated centrosome/nuclear cycles in early syncytial cell cycles (Brunk et al., 2007). Likewise, mutations in gene encoding *polyhomeotic-like one protein* (*PHC1*; *MCPH11*) are associated with aberrant DNA damage repair (Awad et al., 2013). In addition, *PHC1* mutations disturb the expression of Nanog and the ubiquitination of histone H2A, in which the former maintains pluripotency and the latter affects the cell cycle progression by the accumulation of Geminin (Awad et al., 2013; Chen et al., 2021).

Complete ablation of *Znf335* gene in mice is embryonically lethal, but conditional knockout leads to a reduction in the cortical size affecting the forebrain much severely (Yang et al., 2012). This has been attributed to disruptions in NPC proliferation, cell fate, and neuronal differentiation (Yang et al., 2012). Consistently, postmortem histopathological studies on brain samples taken from ZNF335 patients reveal a severe reduction in the neuronal number associated with abnormalities in neuronal morphogenesis, migration, and polarity (Yang et al., 2012).

Mutations in genes encoding condensin complex proteins NCAPD2, NCAPD3, and NCAPH have been linked to MCPH21, 22, and 23, respectively (Martin et al., 2016). One of the hallmarks of hypomorphic Ncaph2 mice is the formation of a chromatin bridge in apical NPCs (Martin et al., 2016). These bridges result from failed sister chromatid disentanglement leading to chromosome segregation errors and aneuploidy (Martin et al., 2016). Subsequently, NPCs undergo a reduced cell proliferation and an increased apoptosis without obvious alterations in spindle orientations or cell fat (Martin et al., 2016).

Deformed Kinetochore Proteins

Mutations in genes encoding kinetochore scaffold one protein (KNL1, previously known as CASC5) and centromere-associated protein E (CENPE) have been linked to MCPH4 (Jamieson et al., 1999; Genin et al., 2012; Mirzaa et al., 2014; Saadi et al., 2016; Szczepanski et al., 2016; Zarate et al., 2016). Proper function of proteins associated with centromeric kinetochore assures the correct alignment of chromosomes during mitosis; else, spindle assembly checkpoint (SAC) is activated and suspends the mitotic progression (Cleveland et al., 2003; Musacchio and Salmon, 2007; Santaguida and Musacchio, 2009; Hori and Fukagawa, 2012). Conditional knockout of *Knl1* in mouse cortical NPCs results in DNA damage due to chromosomal segregation errors (Shi et al., 2019). This triggers a p53-dependent apoptotic cascade and leads to massive loss of NPCs and microcephaly (Shi et al., 2019). Similar to MCPH centrosomal proteins, the progressive loss of NPCs in *Knl1* conditional knockout mice affects mainly the later-born neurons (superficial layers II–IV) (Shi et al., 2019). CENPE facilitates the transition from metaphase to anaphase during the cell cycle (Yen et al., 1991). Disruption of Cenpe function in mice

and *Drosophila* leads to early embryonic lethality due to chromosomal instability (Yucel et al., 2000; Putkey et al., 2002).

Interruption of Fatty Acids Uptake Into the Brain

Proper brain development and function require essential omega-3 fatty acids, which need to be obtained from the circulation via specific transporters (Alakbarzade et al., 2015). Sodium-dependent lysophosphatidylcholine (LPC) transporter (MFSD2A) is exclusively expressed in the endothelium of the blood–brain barrier (BBB) and a major transport facilitator for docosahexaenoic acid (DHA) (Ben-Zvi et al., 2014; Nguyen et al., 2014; Alakbarzade et al., 2015; Guemez-Gamboa et al., 2015). Depending on the transporter residual activity, mutations in *MFSD2A* (*MCPH15*) gene is associated with either a progressive microcephaly syndrome or a much lethal phenotype (Berger et al., 2012; Alakbarzade et al., 2015; Guemez-Gamboa et al., 2015; Harel et al., 2018; Scala et al., 2020). The progressive feature associated with the milder form of this disease raises the possibility that LPC transportation is continuously required for membrane biogenesis in the brain (Alakbarzade et al., 2015; Scala et al., 2020). Endothelial-specific deletion of *Mfsd2a* in mice leads to a microcephaly phenotype accompanied by a reduction in neuronal arborization and dendritic length (Chan et al., 2018). Interestingly, neuronal loss detected in *Mfsd2a* knockout mice was restricted to cerebellar Purkinje cells and hippocampal CA1 and CA3 regions (Nguyen et al., 2014). Taken together, these data demonstrate that, unlike other MCPHs, Mfsd2a deficiency affects the postnatal neuronal morphogenesis, which requires a normal lipogenesis process (van Deijk et al., 2017; Ziegler et al., 2017; Chan et al., 2018). Notably, variable degrees of white matter reduction have been also reported in *MCPH15* individuals (Alakbarzade et al., 2015; Harel et al., 2018; Scala et al., 2020). Further studies are required to assess to which extent do white matter deficits contribute to the microcephaly phenotype (Huang and Li, 2021).

Altered Nuclear Envelope

Mutations in several genes encoding nuclear envelop components have been recently linked to MCPH conditions. Ankyrin repeat- and lem domain-containing protein 2 (Ankle2) is localized to the endoplasmic reticulum and nuclear envelope (Link et al., 2019). *Drosophila dAnkle2* mutant larvae show a reduction in the brain size due to impaired nuclear envelope integrity, which eventually affects proper spindle alignment and cell fate determinants during NPC proliferation (Link et al., 2019). Another study, however, suggests that the reduction in *Drosophila dAnkle2* mutant NPCs cells is due to defects in proliferation and massive apoptosis rather than an alteration in asymmetrical cell division (Yamamoto et al., 2014). In this line, *Caenorhabditis elegans* ANKLE2 ortholog protein (LEM-4L) plays a critical role in mitosis by facilitating nuclear envelope reassembly during mitotic exit (Asencio et al., 2012).

Individuals with mutations in genes encoding various nuclear pore complex proteins (NPC) are diagnosed with severe forms of nephrotic syndrome (Braun et al., 2018). However, mutations in NPC subunit component nucleoporin 37 (NUP37) also exhibit intellectual disability and MCPH (Braun et al., 2018). More recently and yet to be linked to a specific OMIM MCPH number, mutations in NUP85 subunit are associated with a reduction in brain volume, delayed myelination, agenesis of the corpus callosum, gray matter heterotopia, and frontal lobe cortical malformation (Ravindran et al., 2021). Fibroblasts derived from NUP85 individuals are characterized by reduced cell viability, proliferation rate, abnormal mitotic spindle apparatus, and altered cytoskeletal protein expressions (Ravindran et al., 2021). As most of the studies performed in viable animal models with NPC defects focused on the nephrotic phenotype, further investigations to understand their effects on brain growth are still warranted.

B-type lamins 1 and 2 (LMNB1/2) are intermediate filament proteins involved in nuclear envelope reassembly, in which the deficiency leads to fragile nuclei more susceptible to nuclear membrane (NM) rupture (Coffinier et al., 2011; Chen et al., 2019). In humans, mutations in LMNB1 and LMNB2 have been linked to MCPH26 and MCPH27, respectively (Cristofoli et al., 2020; Parry et al., 2021). During early neurogenesis, RGC nuclei undergo INM, which represents mechanical stress that threatens RGCs with weakened nuclear lamina (Chen et al., 2019). Therefore, lack of murine Lmnb1/2 during this critical step triggers NPC apoptosis and leads to abnormal neuronal migration reflected by disorganized cortical layering (Kim et al., 2011b; Coffinier et al., 2011; Young et al., 2012; Chen et al., 2019). This migration defect not only is confined to the cerebral cortex but also affects the hippocampal and cerebellar layering (Coffinier et al., 2010; Coffinier et al., 2011). In addition, it has been proposed that Lmnb1/2 is localized at the mitotic spindle and plays a role in INM and neuronal migration via interaction with dynein in organizing NPC spindle orientation (Tsai et al., 2006; Kim et al., 2011b). However, no abnormal metaphase spindle formation has been noticed in lymphoblastoid cells (LCLs) derived from LMNB1 individuals (Cristofoli et al., 2020).

Defective Cytokinesis

Cytokinesis is the terminal step in the cell cycle, which leads to a physical separation between the daughter cells. Defects in this process frequently result in the formation of binucleated cells, aneuploidy, chromosomal instability, cell cycle arrest, and apoptosis (Li et al., 2016a). Notably, the elevated number of binucleated cells—including pyramidal and Purkinje cells—is considered as a key feature for cytokinesis failures (Di Cunto et al., 2000; Roberts et al., 2000; Reilly et al., 2019). Citron rho-interacting kinase (CIT) midbody protein has important roles in cytokinesis, and its defect leads to MCPH17 in humans (Li et al., 2016a; Basit et al., 2016; Harding et al., 2016; Shaheen et al., 2016). Postmortem histopathological analysis of brain samples taken from *MCPH17* individuals reveals a thickened neocortex with disorganized layers and unmyelinated white matter with scattered neurons (Harding et al., 2016). In addition, the cerebellar cortex and hippocampus show dysplastic and hypoplastic features, and Purkinje cells exhibit a simplified dendritic tree where many of them are multinucleated (Harding et al., 2016). Studies conducted in *Cit* knockout rodent models reveal that NPCs undergo massive apoptosis due to interrupted cytokinesis (Di Cunto et al., 2000; Roberts et al., 2000). In these models, binucleated neurons have been detected in several brain

and spinal cord regions; however, apoptosis seems to be more pronounced in the cerebral cortex, granular layers of cerebellum, hippocampus, and olfactory bulb (Di Cunto et al., 2000; Sarkisian et al., 2002). In addition, the high rate of cell death reported at the ganglionic eminence reduces the total number of generated interneurons (Sarkisian et al., 2001; Di Cunto et al., 2000). Consistent with human brain findings, cerebellar Purkinje cells are disorganized and show underdeveloped dendritic complexity (Di Cunto et al., 2000). The presence of disorganized cortical layering and scattered neurons in the white matter should raise the possibility of an abnormal migration process even though it is yet to be confirmed by further studies.

The role of CIT in cytokinesis requires a proper function of kinesin family 14 (KIF14) microtubule motor protein (Makrythanasis et al., 2018). It is then unsurprising to realize that mutations in *KIF14* also lead to MCPH by a common mechanism as *CIT* mutations (Moawia et al., 2017; Makrythanasis et al., 2018; Reilly et al., 2019). This is supported by several studies conducted in various animal models with depleted *KIF14* homologs (Ohkura et al., 1997; Fujikura et al., 2013; Reilly et al., 2019). Mutations of *Drosophila KIF14* homolog, also known as kinesin-like protein at 38B (*KLP38B*), affect the cell cycle progression due to cytokinesis failure (Ohkura et al., 1997). In the same notion, *Laggard* mice (*lag*), an animal model for KIF14, are characterized by microcephaly, cortical dysgenesis, and severe hypomyelination as a consequence of massive apoptosis during late neurogenesis (Fujikura et al., 2013). Consequently, Cux1-positive upper cortical neurons are much reduced in number, and some of them are displaced (Fujikura et al., 2013). Similar to *Cit* knockout models, *lag* mice show scattered cerebellar Purkinje cells with simplified dendritic trees pointing toward abnormalities in neuronal migration and neurite formation (Fujikura et al., 2013).

Disturbed Autophagy and Mitochondrial Dynamics

MCPH18 is caused by mutations in gene encoding *WD repeat and FYVE domain-containing 3* (*WDFY3*), also known as *Autophagy-*

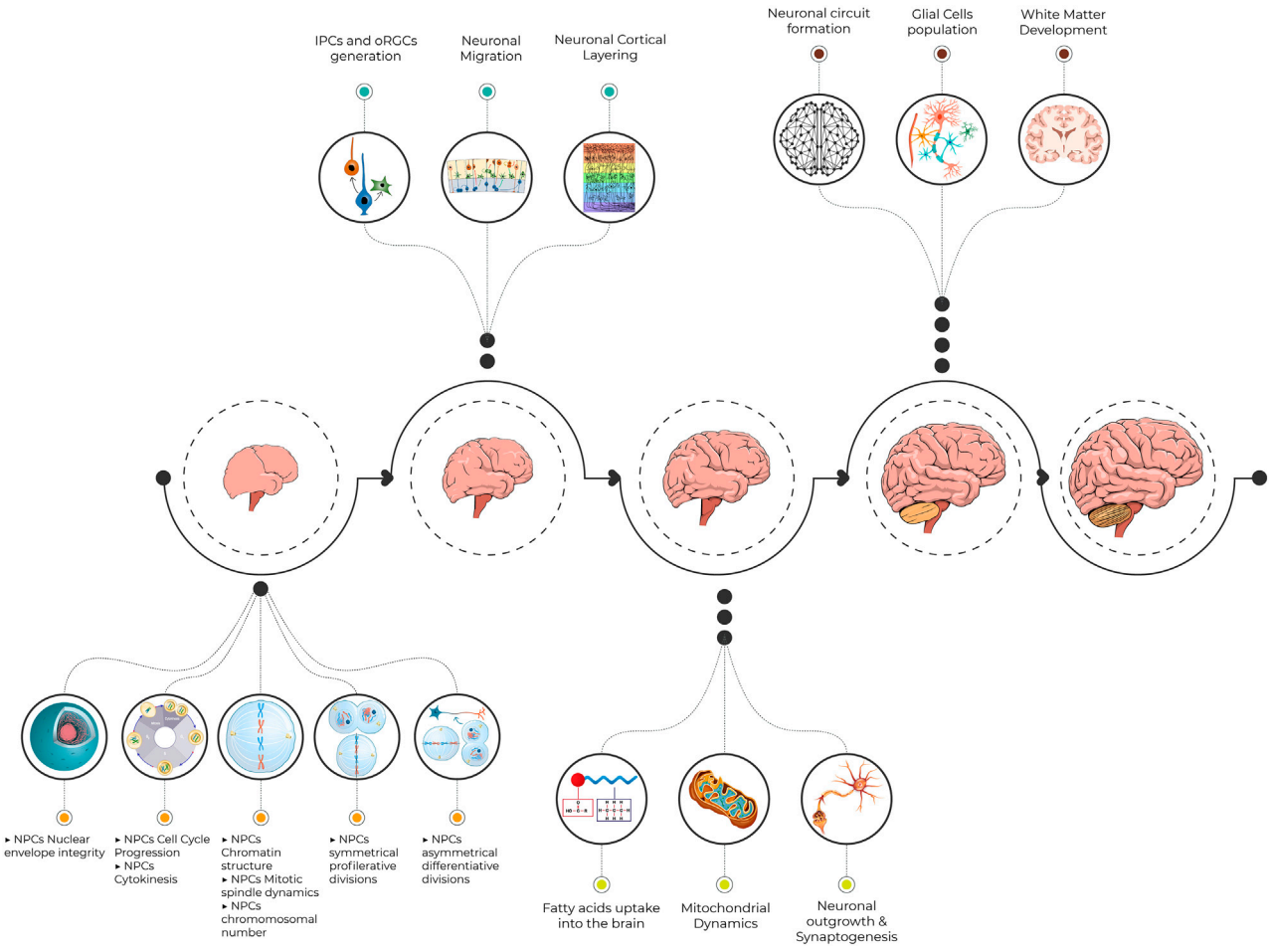

FIGURE 2 | An illustrative figure demonstrating the pathway toward normal brain development. Minor defects at crucial steps in neurogenesis result in various neurodevelopmental disorders including MCPH. NPCs, neural progenitor cells; IPCs, intermediate progenitor cells; oRGCs, outer radial glial cells; MCPH, microcephaly primary hereditary.

Linked FYVE (*ALFY*) (Kadir et al., 2016). Normally, this scaffolding protein facilitates the removal of cytosolic protein aggregates, which, in turn, maintains mitochondrial homeostasis (Kadir et al., 2016; Napoli et al., 2018; Napoli et al., 2021). Wdfy3 is highly expressed in RGCs, and its loss of function prevents the transition from symmetrical proliferative divisions to asymmetrical differentiative divisions by altering the Wnt signaling cascade (Tacchelly-Benites et al., 2013; Orosco et al., 2014; Kadir et al., 2016). The imbalance in NPCs mode of cell division leads to regional differences in neocortical thickness and opposing phenotypes of micro- and macrocephaly (Orosco et al., 2014; Le Duc et al., 2019). On the other hand, the disruption of mitochondrial dynamics in *Wdfy3* mutant mice decreases the synaptic density, alters the synaptic plasticity, and probably affects dendritic development (Napoli et al., 2018; Napoli et al., 2021). Remarkably, proteins involved in GABAergic neurotransmission are downregulated in *Wdfy3* mutant mice (Napoli et al., 2021). Furthermore, Wdfy3 plays a role in neural migration during early neurogenesis (Orosco et al., 2014).

Interrupted Intracellular Trafficking

Coatomer Protein Complex Subunit Beta 2 (COPB2) controls the cellular retrograde trafficking from the Golgi to the endoplasmic reticulum (Orci et al., 1993; Letourneur et al., 1994). Interestingly, mutations in *COPB2* interrupt brain growth and lead to MCPH19 (DiStasio et al., 2017). While the complete loss of Copb2 is incompatible with life, partial loss of Copb2 in mice interferes with the growth of the brain (DiStasio et al., 2017). This has been associated with increased cell death and a high number of proliferative cells positive for phosphorylated histone H3 (pH3) (DiStasio et al., 2017). Still, further studies are necessitated to dissect the exact role of Copb2 in controlling brain size.

Disturbed Mitotic Spindle Dynamics

Trafficking protein particle complex subunit 14 (TRAPPC14)—also known as microtubule-associated protein 11 (MAP11)—is localized to mitotic spindles and interacts with α-tubulin regulates the spindle dynamics and cell division (Perez et al., 2019). Recently, *TRAPPC14* mutations have been linked to MCPH25 in human and microcephaly phenotypes in the zebrafish model (Perez et al., 2019). This has been mainly attributed to a decreased brain cell proliferation due to altered spindle dynamics affecting the mitotic progression and probably the cytokinesis, however, without increased apoptosis (Perez et al., 2019). In addition, TRAPPC14 has been implicated in ciliogenesis and cilia stability, which, in turn, could affect brain growth (Cuenca et al., 2019).

Defective Ribosome Biogenesis

The most recently diagnosed MCPH28 cases have been linked to a mutation in *Ribosomal RNA Processing seven Homolog A* (*RRP7A*) (Farooq et al., 2020). It is known that mutations in genes involved in ribosome biogenesis are associated with neurodevelopmental defects together with other abnormalities (Hetman and Slomnicki, 2019). The encoded RRP7A protein shows high expression in RGCs and cellular localizations at the centrosome, primary cilium, and nucleolus (Farooq et al., 2020). Depletion of RRP7A alters ribosomal RNA processing and affects primary cilia resorption, causing a delay in S-phase entry and progression (Farooq et al., 2020). Mutated rrp7a zebrafish embryos display a reduction in the expression pattern of some proliferation and neural differentiation markers, while TUNEL assay analysis indicates increased apoptosis (Farooq et al., 2020). These findings might result from defective rrp7a functions at the level of centrosome and/or primary cilia. MicroRNA processing has been identified as a contributing factor in temporal fate specification (Kohwi and Doe, 2013). Thus, dysregulated ribosomal RNA processing with subsequent nucleolar stress establishes a new insight into MCPH pathomechanisms.

MICROCEPHALY PRIMARY HEREDITARY VERSUS INFECTION-INDUCED MICROCEPHALY

After describing the genetic component of microcephaly, we here shed some light on some infectious agents associated with microcephaly. Particularly *Toxoplasma gondii*, cytomegalovirus, rubella virus, and syphilis, but also the herpes simplex virus, HIV, and Zika virus, have been reported in children born with microcephaly. The severity of microcephaly depends not only on the type of the infectious agent but much importantly on the gestational age when an infection occurs (Devakumar et al., 2018). It has been shown that neural progenitors are targeted by these pathogens; however, the mechanisms by which most of these infections lead to microcephaly are not fully understood (Devakumar et al., 2018). Nevertheless, the epidemic infections with the Zika virus and its association with congenital microcephaly triggered extensive research in this field. Several studies based on various *in vitro* and *in vivo* models point toward NPC cell cycle arrest or an increase in cell death upon the infection with the Zika virus (Adams Waldorf et al., 2016; Li et al., 2016b; Cugola et al., 2016; Garcez et al., 2016; Tang et al., 2016; Wu et al., 2016). Intriguingly, several MCPH genes including *Mcph1*, *Aspm*, *Cdk5rap2*, *Stil*, and *Cep135* are downregulated in brain tissues extracted from Zika-infected mice (Li et al., 2016b; Wu et al., 2016). This raises the possibility that infection-induced microcephaly might alter brain growth via altering the expression of various MCPH genes. However, the direct impact of infectious agents on the pathogenesis of microcephaly cannot be ruled out.

CONCLUSION

The journey during brain growth and development is impeded at specific points with crucial steps (**Figure 2**). Minor defects at any of these developmental points result in various neurodevelopmental disorders including MCPH. The earlier the insult during the journey, the greater the impact on brain growth. The major obstacle is faced during the rapid NPC proliferation just before the commencing generation of neurons. Either decreased proliferation or increased NPCs apoptosis depletes the neuronal stem cell pool and ultimately leads to a smaller number of generated neurons. Obviously, most MCPHs are caused by mutations in centrosomal proteins. Hence,

dysfunctional centrosome alters NPC proliferation, cell cycle progression, and cell fate determination. In addition, the resulting aneuploidy and increased DNA damage response associated with some mutated MCPH genes trigger apoptosis. The accelerated number of discovered MCPH genes expands the pathomechanism spectrum of this disease beyond the centrosomal component. Similarly, the simultaneous generation of animal models mimicking the human MCPH phenotype provides a strong platform for future studies to dissect further molecular mechanisms behind the microcephaly phenotype. This will also expand our knowledge of normal brain growth and evolution.

AUTHOR CONTRIBUTIONS

SZ wrote the initial manuscript draft and generated the figures and tables. AK revised the manuscript. Both authors approved the final article.

ACKNOWLEDGMENTS

We acknowledge support from the Open Access Publication Fund of Charité—Universitätsmedizin Berlin. We also thank Mr. Ahmed Hany Amarah for his help in designing **Figure 2**.

REFERENCES

Abdel-Hamid, M. S., Ismail, M. F., Darwish, H. A., Effat, L. K., Zaki, M. S., and Abdel-Salam, G. M. H. (2016). Molecular and Phenotypic Spectrum ofASPM-Related Primary Microcephaly: Identification of Eight Novel Mutations. *Am. J. Med. Genet.* 170, 2133–2140. doi:10.1002/ajmg.a.37724

Adams Waldorf, K. M., Stencel-Baerenwald, J. E., Kapur, R. P., Studholme, C., Boldenow, E., Vornhagen, J., et al. (2016). Fetal Brain Lesions after Subcutaneous Inoculation of Zika Virus in a Pregnant Nonhuman Primate. *Nat. Med.* 22, 1256–1259. doi:10.1038/nm.4193

Aggarwal, A., Mittal, H., Patil, R., Debnath, S., and Rai, A. (2013). Clinical Profile of Children with Developmental Delay and Microcephaly. *J. neurosciences Rural Pract.* 04, 288–291. doi:10.4103/0976-3147.118781

Alakbarzade, V., Hameed, A., Quek, D. Q. Y., Chioza, B. A., Baple, E. L., Cazenave-Gassiot, A., et al. (2015). A Partially Inactivating Mutation in the Sodium-dependent Lysophosphatidylcholine Transporter MFSD2A Causes a Non-lethal Microcephaly Syndrome. *Nat. Genet.* 47, 814–817. doi:10.1038/ng.3313

Alcantara, D., and O'Driscoll, M. (2014). Congenital Microcephaly. *Am. J. Med. Genet.* 166, 124–139. doi:10.1002/ajmg.c.31397

Alfares, A., Alhufayti, I., Alsubaie, L., Alowain, M., Almass, R., Alfadhel, M., et al. (2018). A New Association between CDK5RAP2 Microcephaly and Congenital Cataracts. *Ann. Hum. Genet.* 82, 165–170. doi:10.1111/ahg.12232

Arai, Y., Pulvers, J. N., Haffner, C., Schilling, B., Nüsslein, I., Calegari, F., et al. (2011). Neural Stem and Progenitor Cells Shorten S-phase on Commitment to Neuron Production. *Nat. Commun.* 2, 154. doi:10.1038/ncomms1155

Ariani, F., Mari, F., Amitrano, S., Di Marco, C., Artuso, R., Scala, E., et al. (2013). Exome Sequencing Overrides Formal Genetics: ASPM Mutations in a Case Study of Apparent X-linked Microcephalic Intellectual Deficit. *Clin. Genet.* 83, 288–290. doi:10.1111/j.1399-0004.2012.01901.x

Arquint, C., and Nigg, E. A. (2014). STIL Microcephaly Mutations Interfere with APC/C-mediated Degradation and Cause Centriole Amplification. *Curr. Biol.* 24, 351–360. doi:10.1016/j.cub.2013.12.016

Asencio, C., Davidson, I. F., Santarella-Mellwig, R., Ly-Hartig, T. B. N., Mall, M., Wallenfang, M. R., et al. (2012). Coordination of Kinase and Phosphatase Activities by Lem4 Enables Nuclear Envelope Reassembly during Mitosis. *Cell* 150, 122–135. doi:10.1016/j.cell.2012.04.043

Awad, S., Al-Dosari, M. S., Al-Yacoub, N., Colak, D., Salih, M. A., Alkuraya, F. S., et al. (2013). Mutation in PHC1 Implicates Chromatin Remodeling in Primary Microcephaly Pathogenesis. *Hum. Mol. Genet.* 22, 2200–2213. doi:10.1093/hmg/ddt072

Bacino, C. A., Arriola, L. A., Wiszniewska, J., and Bonnen, P. E. (2012). WDR62 Missense Mutation in a Consanguineous Family with Primary Microcephaly. *Am. J. Med. Genet.* 158a, 622–625. doi:10.1002/ajmg.a.34417

Bamborschke, D., Daimagüler, H. S., Hahn, A., Hussain, M. S., Nürnberg, P., and Cirak, S. (2020). Mutation in CEP135 Causing Primary Microcephaly and Subcortical Heterotopia. *Am. J. Med. Genet.* 182, 2450–2453. doi:10.1002/ajmg.a.61762

Banerjee, S., Chen, H., Huang, H., Wu, J., Yang, Z., Deng, W., et al. (2016). Novel Mutations c.28G>T (p.Ala10Ser) and c.189G>T (p.Glu63Asp) in WDR62 Associated with Early Onset Acanthosis and Hyperkeratosis in a Patient with Autosomal Recessive Microcephaly Type 2. *Oncotarget* 7, 78363–78371.

Barbelanne, M., and Tsang, W. Y. (2014). Molecular and Cellular Basis of Autosomal Recessive Primary Microcephaly. *Biomed. Res. Int.* 2014, 547986. doi:10.1155/2014/547986

Basit, S., Al-Harbi, K. M., Alhijji, S. A. M., Albalawi, A. M., Alharby, E., Eldardear, A., et al. (2016). CIT, a Gene Involved in Neurogenic Cytokinesis, Is Mutated in Human Primary Microcephaly. *Hum. Genet.* 135, 1199–1207. doi:10.1007/s00439-016-1724-0

Bastaki, F., Mohamed, M., Nair, P., Saif, F., Tawfiq, N., Aithala, G., et al. (2016). Novel Splice-Site Mutation inWDR62revealed by Whole-Exome Sequencing in a Sudanese Family with Primary Microcephaly. *Congenit. Anom.* 56, 135–137. doi:10.1111/cga.12144

Basto, R., Lau, J., Vinogradova, T., Gardiol, A., Woods, C. G., Khodjakov, A., et al. (2006). Flies without Centrioles. *Cell* 125, 1375–1386. doi:10.1016/j.cell.2006.05.025

Baye, L. M., and Link, B. A. (2007). Interkinetic Nuclear Migration and the Selection of Neurogenic Cell Divisions during Vertebrate Retinogenesis. *J. Neurosci.* 27, 10143–10152. doi:10.1523/jneurosci.2754-07.2007

Ben-Zvi, A., Lacoste, B., Kur, E., Andreone, B. J., Mayshar, Y., Yan, H., et al. (2014). Mfsd2a Is Critical for the Formation and Function of the Blood-Brain Barrier. *Nature* 509, 507–511. doi:10.1038/nature13324

Berger, J. H., Charron, M. J., and Silver, D. L. (2012). Major Facilitator Superfamily Domain-Containing Protein 2a (MFSD2A) Has Roles in Body Growth, Motor Function, and Lipid Metabolism. *PLoS One* 7, e50629. doi:10.1371/journal.pone.0050629

Betizeau, M., Cortay, V., Patti, D., Pfister, S., Gautier, E., Bellemin-Ménard, A., et al. (2013). Precursor Diversity and Complexity of Lineage Relationships in the Outer Subventricular Zone of the Primate. *Neuron* 80, 442–457. doi:10.1016/j.neuron.2013.09.032

Bhat, V., Girimaji, S., Mohan, G., Arvinda, H., Singhmar, P., Duvvari, M., et al. (2011). Mutations in WDR62, Encoding a Centrosomal and Nuclear Protein, in Indian Primary Microcephaly Families with Cortical Malformations. *Clin. Genet.* 80, 532–540. doi:10.1111/j.1399-0004.2011.01686.x

Bilgüvar, K., Öztürk, A. K., Louvi, A., Kwan, K. Y., Choi, M., Tatlı, B., et al. (2010). Whole-exome Sequencing Identifies Recessive WDR62 Mutations in Severe Brain Malformations. *Nature* 467, 207–210. doi:10.1038/nature09327

Blachon, S., Gopalakrishnan, J., Omori, Y., Polyanovsky, A., Church, A., Nicastro, D., et al. (2008). Drosophila Asterless and Vertebrate Cep152 Are Orthologs Essential for Centriole Duplication. *Genetics* 180, 2081–2094. doi:10.1534/genetics.108.095141

Bogoyevitch, M. A., Yeap, Y. Y., Qu, Z., Ngoei, K. R., Yip, Y. Y., Zhao, T. T., et al. (2012). WD40-repeat Protein 62 Is a JNK-Phosphorylated Spindle Pole Protein Required for Spindle Maintenance and Timely Mitotic Progression. *J. Cel Sci* 125, 5096–5109. doi:10.1242/jcs.107326

Boycott, K. M., Vanstone, M. R., Bulman, D. E., and MacKenzie, A. E. (2013). Rare-disease Genetics in the Era of Next-Generation Sequencing: Discovery to Translation. *Nat. Rev. Genet.* 14, 681–691. doi:10.1038/nrg3555

Braun, D. A., Lovric, S., Schapiro, D., Schneider, R., Marquez, J., Asif, M., et al. (2018). Mutations in Multiple Components of the Nuclear Pore Complex Cause Nephrotic Syndrome. *J. Clin. Invest.* 128, 4313–4328. doi:10.1172/jci98688

Brunk, K., Vernay, B., Griffith, E., Reynolds, N. L., Strutt, D., Ingham, P. W., et al. (2007). Microcephalin Coordinates Mitosis in the syncytialDrosophilaembryo. *J. Cel. Sci.* 120, 3578–3588. doi:10.1242/jcs.014290

Buchman, J. J., Durak, O., and Tsai, L.-H. (2011). ASPM Regulates Wnt Signaling Pathway Activity in the Developing Brain. *Genes Dev.* 25, 1909–1914. doi:10.1101/gad.16830211

Buchman, J. J., and Tsai, L.-H. (2007). Spindle Regulation in Neural Precursors of Flies and Mammals. *Nat. Rev. Neurosci.* 8, 89–100. doi:10.1038/nrn2058

Buchman, J. J., Tseng, H.-C., Zhou, Y., Frank, C. L., Xie, Z., and Tsai, L.-H. (2010). Cdk5rap2 Interacts with Pericentrin to Maintain the Neural Progenitor Pool in the Developing Neocortex. *Neuron* 66, 386–402. doi:10.1016/j.neuron.2010.03.036

Caglayan, A. O., Yaghouti, K., Kockaya, T., Kemer, D., Cankaya, T., Ameziane, N., et al. (2021). Biallelic ZNF335 Mutations Cause Basal Ganglia Abnormality with Progressive Cerebral/cerebellar Atrophy. *J. Neurogenet.* 35, 23–28. doi:10.1080/01677063.2020.1833006

Calegari, F., Haubensak, W., Haffner, C., and Huttner, W. B. (2005). Selective Lengthening of the Cell Cycle in the Neurogenic Subpopulation of Neural Progenitor Cells during Mouse Brain Development. *J. Neurosci.* 25, 6533–6538. doi:10.1523/jneurosci.0778-05.2005

Calegari, F., and Huttner, W. B. (2003). An Inhibition of Cyclin-dependent Kinases that Lengthens, but Does Not Arrest, Neuroepithelial Cell Cycle Induces Premature Neurogenesis. *J. Cel. Sci.* 116, 4947–4955. doi:10.1242/jcs.00825

Carvalho-Santos, Z., Machado, P., Alvarez-Martins, I., Gouveia, S. M., Jana, S. C., Duarte, P., et al. (2012). BLD10/CEP135 Is a Microtubule-Associated Protein that Controls the Formation of the Flagellum central Microtubule Pair. *Developmental Cel* 23, 412–424. doi:10.1016/j.devcel.2012.06.001

Chan, J. P., Wong, B. H., Chin, C. F., Galam, D. L. A., Foo, J. C., Wong, L. C., et al. (2018). The Lysolipid Transporter Mfsd2a Regulates Lipogenesis in the Developing Brain. *Plos Biol.* 16, e2006443. doi:10.1371/journal.pbio.2006443

Chen, J.-F., Zhang, Y., Wilde, J., Hansen, K. C., Lai, F., and Niswander, L. (2014). Microcephaly Disease Gene Wdr62 Regulates Mitotic Progression of Embryonic Neural Stem Cells and Brain Size. *Nat. Commun.* 5, 3885. doi:10.1038/ncomms4885

Chen, L., Tong, Q., Chen, X., Jiang, P., Yu, H., Zhao, Q., et al. (2021). PHC1 Maintains Pluripotency by Organizing Genome-wide Chromatin Interactions of the Nanog Locus. *Nat. Commun.* 12, 2829. doi:10.1038/s41467-021-22871-0

Chen, N. Y., Yang, Y., Weston, T. A., Belling, J. N., Heizer, P., Tu, Y., et al. (2019). An Absence of Lamin B1 in Migrating Neurons Causes Nuclear Membrane Ruptures and Cell Death. *Proc. Natl. Acad. Sci. USA* 116, 25870–25879. doi:10.1073/pnas.1917225116

Cheng, C., Yang, Y., Zhu, X., Yu, X., Zhang, T., Yang, F., et al. (2020). Novel Compound Heterozygous Variants in the STIL Gene Identified in a Chinese Family with Presentation of Foetal Microcephaly. *Eur. J. Med. Genet.* 63, 104091. doi:10.1016/j.ejmg.2020.104091

Chenn, A., and McConnell, S. K. (1995). Cleavage Orientation and the Asymmetric Inheritance of Notchl Immunoreactivity in Mammalian Neurogenesis. *Cell* 82, 631–641. doi:10.1016/0092-8674(95)90035-7

Cleveland, D. W., Mao, Y., and Sullivan, K. F. (2003). Centromeres and Kinetochores. *Cell* 112, 407–421. doi:10.1016/s0092-8674(03)00115-6

Coffinier, C., Chang, S. Y., Nobumori, C., Tu, Y., Farber, E. A., Toth, J. I., et al. (2010). Abnormal Development of the Cerebral Cortex and Cerebellum in the Setting of Lamin B2 Deficiency. *Proc. Natl. Acad. Sci.* 107, 5076–5081. doi:10.1073/pnas.0908790107

Coffinier, C., Jung, H.-J., Nobumori, C., Chang, S., Tu, Y., Barnes, R. H., 2nd, et al. (2011). Deficiencies in Lamin B1 and Lamin B2 Cause Neurodevelopmental Defects and Distinct Nuclear Shape Abnormalities in Neurons. *MBoC* 22, 4683–4693. doi:10.1091/mbc.e11-06-0504

Costa, M. R., and Müller, U. (2014). Specification of Excitatory Neurons in the Developing Cerebral Cortex: Progenitor Diversity and Environmental Influences. *Front Cel Neurosci* 8, 449. doi:10.3389/fncel.2014.00449

Cottee, M. A., Muschalik, N., Wong, Y. L., Johnson, C. M., Johnson, S., Andreeva, A., et al. (2013). Crystal Structures of the CPAP/STIL Complex Reveal its Role in Centriole Assembly and Human Microcephaly. *eLife* 2, e01071. doi:10.7554/eLife.01071

Cox, J., Jackson, A. P., Bond, J., and Woods, C. G. (2006). What Primary Microcephaly Can Tell Us about Brain Growth. *Trends Mol. Med.* 12, 358–366. doi:10.1016/j.molmed.2006.06.006

Cragan, J. D., Isenburg, J. L., Parker, S. E., Alverson, C. J., Meyer, R. E., Stallings, E. B., et al. (2016). Population-based Microcephaly Surveillance in the United States, 2009 to 2013: An Analysis of Potential Sources of Variation. *Birth Defects Res. A: Clin. Mol. Teratology* 106, 972–982. doi:10.1002/bdra.23587

Cristofoli, F., Moss, T., Moore, H. W., Devriendt, K., Flanagan-Steet, H., May, M., et al. (2020). De Novo Variants in LMNB1 Cause Pronounced Syndromic Microcephaly and Disruption of Nuclear Envelope Integrity. *Am. J. Hum. Genet.* 107, 753–762. doi:10.1016/j.ajhg.2020.08.015

Cuenca, A., Insinna, C., Zhao, H., John, P., Weiss, M. A., Lu, Q., et al. (2019). The C7orf43/TRAPPC14 Component Links the TRAPPII Complex to Rabin8 for Preciliary Vesicle Tethering at the Mother Centriole during Ciliogenesis. *J. Biol. Chem.* 294, 15418–15434. doi:10.1074/jbc.ra119.008615

Cugola, F. R., Fernandes, I. R., Russo, F. B., Freitas, B. C., Dias, J. L. M., Guimarães, K. P., et al. (2016). The Brazilian Zika Virus Strain Causes Birth Defects in Experimental Models. *Nature* 534, 267–271. doi:10.1038/nature18296

David, A., Liu, F., Tibelius, A., Vulprecht, J., Wald, D., Rothermel, U., et al. (2014). Lack of Centrioles and Primary Cilia inSTIL−/−mouse Embryos. *Cell Cycle* 13, 2859–2868. doi:10.4161/15384101.2014.946830

Del Bene, F., Wehman, A. M., Link, B. A., and Baier, H. (2008). Regulation of Neurogenesis by Interkinetic Nuclear Migration through an Apical-Basal Notch Gradient. *Cell* 134, 1055–1065. doi:10.1016/j.cell.2008.07.017

Derivery, E., Seum, C., Daeden, A., Loubéry, S., Holtzer, L., Jülicher, F., et al. (2015). Polarized Endosome Dynamics by Spindle Asymmetry during Asymmetric Cell Division. *Nature* 528, 280–285. doi:10.1038/nature16443

Desir, J., Cassart, M., David, P., Van Bogaert, P., and Abramowicz, M. (2008). Primary Microcephaly with ASPM Mutation Shows Simplified Cortical Gyration with Antero-Posterior Gradient Pre- and post-natally. *Am. J. Med. Genet.* 146A, 1439–1443. doi:10.1002/ajmg.a.32312

Devakumar, D., Bamford, A., Ferreira, M. U., Broad, J., Rosch, R. E., Groce, N., et al. (2018). Infectious Causes of Microcephaly: Epidemiology, Pathogenesis, Diagnosis, and Management. *Lancet Infect. Dis.* 18, e1–e13. doi:10.1016/s1473-3099(17)30398-5

Di Cunto, F., Imarisio, S., Hirsch, E., Broccoli, V., Bulfone, A., Migheli, A., et al. (2000). Defective Neurogenesis in Citron Kinase Knockout Mice by Altered Cytokinesis and Massive Apoptosis. *Neuron* 28, 115–127. doi:10.1016/s0896-6273(00)00090-8

Ding, W., Wu, Q., Sun, L., Pan, N. C., and Wang, X. (2019). Cenpj Regulates Cilia Disassembly and Neurogenesis in the Developing Mouse Cortex. *J. Neurosci.* 39, 1994–2010. doi:10.1523/jneurosci.1849-18.2018

DiStasio, A., Driver, A., Sund, K., Donlin, M., Muraleedharan, R. M., Pooya, S., et al. (2017). Copb2 Is Essential for Embryogenesis and Hypomorphic Mutations Cause Human Microcephaly. *Hum. Mol. Genet.* 26, 4836–4848. doi:10.1093/hmg/ddx362

Farag, H. G., Froehler, S., Oexle, K., Ravindran, E., Schindler, D., Staab, T., et al. (2013). Abnormal Centrosome and Spindle Morphology in a Patient with Autosomal Recessive Primary Microcephaly Type 2 Due to Compound Heterozygous WDR62 Gene Mutation. *Orphanet J. Rare Dis.* 8, 178. doi:10.1186/1750-1172-8-178

Farooq, M., Lindbæk, L., Krogh, N., Doganli, C., Keller, C., Mönnich, M., et al. (2020). RRP7A Links Primary Microcephaly to Dysfunction of Ribosome Biogenesis, Resorption of Primary Cilia, and Neurogenesis. *Nat. Commun.* 11, 5816. doi:10.1038/s41467-020-19658-0

Fietz, S. A., and Huttner, W. B. (2011). Cortical Progenitor Expansion, Self-Renewal and Neurogenesis-A Polarized Perspective. *Curr. Opin. Neurobiol.* 21, 23–35. doi:10.1016/j.conb.2010.10.002

Fietz, S. A., Kelava, I., Vogt, J., Wilsch-Bräuninger, M., Stenzel, D., Fish, J. L., et al. (2010). OSVZ Progenitors of Human and Ferret Neocortex Are Epithelial-like and Expand by Integrin Signaling. *Nat. Neurosci.* 13, 690–699. doi:10.1038/nn.2553

Finley, K. D., Edeen, P. T., Cumming, R. C., Mardahl-Dumesnil, M. D., Taylor, B. J., Rodriguez, M. H., et al. (2003). Blue cheeseMutations Define a Novel, Conserved Gene Involved in Progressive Neural Degeneration. *J. Neurosci.* 23, 1254–1264. doi:10.1523/jneurosci.23-04-01254.2003

Fish, J. L., Kosodo, Y., Enard, W., Paabo, S., and Huttner, W. B. (2006). Aspm Specifically Maintains Symmetric Proliferative Divisions of Neuroepithelial Cells. *Proc. Natl. Acad. Sci.* 103, 10438–10443. doi:10.1073/pnas.0604066103

Fujikura, K., Setsu, T., Tanigaki, K., Abe, T., Kiyonari, H., Terashima, T., et al. (2013). Kif14 Mutation Causes Severe Brain Malformation and Hypomyelination. *PLoS One* 8, e53490. doi:10.1371/journal.pone.0053490

Fujimori, A., Itoh, K., Goto, S., Hirakawa, H., Wang, B., Kokubo, T., et al. (2014). Disruption of Aspm Causes Microcephaly with Abnormal Neuronal Differentiation. *Brain Development* 36, 661–669. doi:10.1016/j.braindev.2013.10.006

Gabriel, E., Ramani, A., Altinisik, N., and Gopalakrishnan, J. (2020). Human Brain Organoids to Decode Mechanisms of Microcephaly. *Front. Cell. Neurosci.* 14, 115. doi:10.3389/fncel.2020.00115

Gabriel, E., Wason, A., Ramani, A., Gooi, L. M., Keller, P., Pozniakovsky, A., et al. (2016). CPAP Promotes Timely Cilium Disassembly to Maintain Neural Progenitor Pool. *Embo J.* 35, 803–819. doi:10.15252/embj.201593679

Garcez, P. P., Loiola, E. C., Madeiro da Costa, R., Higa, L. M., Trindade, P., Delvecchio, R., et al. (2016). Zika Virus Impairs Growth in Human Neurospheres and Brain Organoids. *Science* 352, 816–818. doi:10.1126/science.aaf6116

Genin, A., Desir, J., Lambert, N., Biervliet, M., Van Der Aa, N., Pierquin, G., et al. (2012). Kinetochore KMN Network Gene CASC5 Mutated in Primary Microcephaly. *Hum. Mol. Genet.* 21, 5306–5317. doi:10.1093/hmg/dds386

Gilbert, S. L., Dobyns, W. B., and Lahn, B. T. (2005). Genetic Links between Brain Development and Brain Evolution. *Nat. Rev. Genet.* 6, 581–590. doi:10.1038/nrg1634

Goetz, S. C., and Anderson, K. V. (2010). The Primary Cilium: a Signalling centre during Vertebrate Development. *Nat. Rev. Genet.* 11, 331–344. doi:10.1038/nrg2774

Gonzalez, C., Saunders, R. D., Casal, J., Molina, I., Carmena, M., Ripoll, P., et al. (1990). Mutations at the Asp Locus of Drosophila lead to Multiple Free Centrosomes in Syncytial Embryos, but Restrict Centrosome Duplication in Larval Neuroblasts. *J. Cel Sci* 96 (Pt 4), 605–616. doi:10.1242/jcs.96.4.605

Gosling, K. M., Makaroff, L. E., Theodoratos, A., Kim, Y.-H., Whittle, B., Rui, L., et al. (2007). A Mutation in a Chromosome Condensin II Subunit, Kleisin Beta, Specifically Disrupts T Cell Development. *Proc. Natl. Acad. Sci.* 104, 12445–12450. doi:10.1073/pnas.0704870104

Götz, M., and Huttner, W. B. (2005). The Cell Biology of Neurogenesis. *Nat. Rev. Mol. Cel. Biol.* 6, 777–788.

Gruber, R., Zhou, Z., Sukchev, M., Joerss, T., Frappart, P.-O., and Wang, Z.-Q. (2011). MCPH1 Regulates the Neuroprogenitor Division Mode by Coupling the Centrosomal Cycle with Mitotic Entry through the Chk1-Cdc25 Pathway. *Nat. Cel Biol* 13, 1325–1334. doi:10.1038/ncb2342

Guemez-Gamboa, A., Nguyen, L. N., Yang, H., Zaki, M. S., Kara, M., Ben-Omran, T., et al. (2015). Inactivating Mutations in MFSD2A, Required for omega-3 Fatty Acid Transport in Brain, Cause a Lethal Microcephaly Syndrome. *Nat. Genet.* 47, 809–813. doi:10.1038/ng.3311

Hainline, S. G., Rickmyre, J. L., Neitzel, L. R., Lee, L. A., and Lee, E. (2014). The Drosophila MCPH1-B Isoform Is a Substrate of the APCCdh1 E3 Ubiquitin Ligase Complex. *Biol. open* 3, 669–676. doi:10.1242/bio.20148318

Hansen, D. V., Lui, J. H., Parker, P. R. L., and Kriegstein, A. R. (2010). Neurogenic Radial Glia in the Outer Subventricular Zone of Human Neocortex. *Nature* 464, 554–561. doi:10.1038/nature08845

Harding, B. N., Moccia, A., Drunat, S., Soukarieh, O., Tubeuf, H., Chitty, L. S., et al. (2016). Mutations in Citron Kinase Cause Recessive Microlissencephaly with Multinucleated Neurons. *Am. J. Hum. Genet.* 99, 511–520. doi:10.1016/j.ajhg.2016.07.003

Harel, T., Quek, D. Q. Y., Wong, B. H., Cazenave-Gassiot, A., Wenk, M. R., Fan, H., et al. (2018). Homozygous Mutation in MFSD2A, Encoding a Lysolipid Transporter for Docosahexanoic Acid, Is Associated with Microcephaly and Hypomyelination. *Neurogenetics* 19, 227–235. doi:10.1007/s10048-018-0556-6

Heide, M., and Huttner, W. B. (2021). Human-Specific Genes, Cortical Progenitor Cells, and Microcephaly. *Cells* 10, 1209. doi:10.3390/cells10051209

Hetman, M., and Slomnicki, L. P. (2019). Ribosomal Biogenesis as an Emerging Target of Neurodevelopmental Pathologies. *J. Neurochem.* 148, 325–347. doi:10.1111/jnc.14576

Hiraki, M., Nakazawa, Y., Kamiya, R., and Hirono, M. (2007). Bld10p Constitutes the Cartwheel-Spoke Tip and Stabilizes the 9-fold Symmetry of the Centriole. *Curr. Biol.* 17, 1778–1783. doi:10.1016/j.cub.2007.09.021

Homem, C. C. F., Repic, M., and Knoblich, J. A. (2015). Proliferation Control in Neural Stem and Progenitor Cells. *Nat. Rev. Neurosci.* 16, 647–659. doi:10.1038/nrn4021

Hori, T., and Fukagawa, T. (2012). Establishment of the Vertebrate Kinetochores. *Chromosome Res.* 20, 547–561. doi:10.1007/s10577-012-9289-9

Hosseini, M. M., Tonekaboni, S. H., Papari, E., Bahman, I., Behjati, F., Kahrizi, K., et al. (2012). A Novel Mutation in MCPH1 Gene in an Iranian Family with Primary Microcephaly. *J. Pak Med. Assoc.* 62, 1244–1247.

Huang, B., and Li, X. (2021). The Role of Mfsd2a in Nervous System Diseases. *Front. Neurosci.* 15, 730534. doi:10.3389/fnins.2021.730534

Hussain, M. S., Baig, S. M., Neumann, S., Nürnberg, G., Farooq, M., Ahmad, I., et al. (2012). A Truncating Mutation of CEP135 Causes Primary Microcephaly and Disturbed Centrosomal Function. *Am. J. Hum. Genet.* 90, 871–878. doi:10.1016/j.ajhg.2012.03.016

Hussain, M. S., Baig, S. M., Neumann, S., Peche, V. S., Szczepanski, S., Nürnberg, G., et al. (2013). CDK6 Associates with the Centrosome during Mitosis and Is Mutated in a Large Pakistani Family with Primary Microcephaly. *Hum. Mol. Genet.* 22, 5199–5214. doi:10.1093/hmg/ddt374

Issa, L., Mueller, K., Seufert, K., Kraemer, N., Rosenkotter, H., Ninnemann, O., et al. (2013). Clinical and Cellular Features in Patients with Primary Autosomal Recessive Microcephaly and a Novel CDK5RAP2 Mutation. *Orphanet J. Rare Dis.* 8, 59–73. doi:10.1186/1750-1172-8-59

Izraeli, S., Lowe, L. A., Bertness, V. L., Good, D. J., Dorward, D. W., Kirsch, I. R., et al. (1999). The SIL Gene Is Required for Mouse Embryonic Axial Development and Left-Right Specification. *Nature* 399, 691–694. doi:10.1038/21429

Jackson, A. P., Eastwood, H., Bell, S. M., Adu, J., Toomes, C., Carr, I. M., et al. (2002). Identification of Microcephalin, a Protein Implicated in Determining the Size of the Human Brain. *Am. J. Hum. Genet.* 71, 136–142. doi:10.1086/341283

Jamieson, C. R., Govaerts, C., and Abramowicz, M. J. (1999). Primary Autosomal Recessive Microcephaly: Homozygosity Mapping of MCPH4 to Chromosome 15. *Am. J. Hum. Genet.* 65, 1465–1469. doi:10.1086/302640

Jayaraman, D., Bae, B.-I., and Walsh, C. A. (2018). The Genetics of Primary Microcephaly. *Annu. Rev. Genom. Hum. Genet.* 19, 177–200. doi:10.1146/annurev-genom-083117-021441

Jean, F., Stuart, A., and Tarailo-Graovac, M. (2020). Dissecting the Genetic and Etiological Causes of Primary Microcephaly. *Front. Neurol.* 11, 570830. doi:10.3389/fneur.2020.570830

Jerka-Dziadosz, M., Gogendeau, D., Klotz, C., Cohen, J., Beisson, J., and Koll, F. (2010). Basal Body Duplication in Paramecium: the Key Role of Bld10 in Assembly and Stability of the Cartwheel. *Cytoskeleton (Hoboken)* 67, 161–171. doi:10.1002/cm.20433

Johnson, M. B., Sun, X., Kodani, A., Borges-Monroy, R., Girskis, K. M., Ryu, S. C., et al. (2018). Aspm Knockout Ferret Reveals an Evolutionary Mechanism Governing Cerebral Cortical Size. *Nature* 556, 370–375. doi:10.1038/s41586-018-0035-0

Kadir, R., Harel, T., Markus, B., Perez, Y., Bakhrat, A., Cohen, I., et al. (2016). ALFY-controlled DVL3 Autophagy Regulates Wnt Signaling, Determining Human Brain Size. *Plos Genet.* 12, e1005919. doi:10.1371/journal.pgen.1005919

Kaindl, A. M., Passemard, S., Kumar, P., Kraemer, N., Issa, L., Zwirner, A., et al. (2010). Many Roads lead to Primary Autosomal Recessive Microcephaly. *Prog. Neurobiol.* 90, 363–383. doi:10.1016/j.pneurobio.2009.11.002

Kakar, N., Ahmad, J., Morris-Rosendahl, D. J., Altmüller, J., Friedrich, K., Barbi, G., et al. (2015). STIL Mutation Causes Autosomal Recessive Microcephalic Lobar Holoprosencephaly. *Hum. Genet.* 134, 45–51. doi:10.1007/s00439-014-1487-4

Kettleborough, R. N. W., Busch-Nentwich, E. M., Harvey, S. A., Dooley, C. M., de Bruijn, E., van Eeden, F., et al. (2013). A Systematic Genome-wide Analysis of Zebrafish Protein-Coding Gene Function. *Nature* 496, 494–497. doi:10.1038/nature11992

Khan, M. A., Rupp, V. M., Orpinell, M., Hussain, M. S., Altmüller, J., Steinmetz, M. O., et al. (2014). A Missense Mutation in the PISA Domain of HsSAS-6 Causes Autosomal Recessive Primary Microcephaly in a Large Consanguineous Pakistani Family. *Hum. Mol. Genet.* 23, 5940–5949. doi:10.1093/hmg/ddu318

Kim, H.-T., Lee, M.-S., Choi, J.-H., Jung, J.-Y., Ahn, D.-G., Yeo, S.-Y., et al. (2011). The Microcephaly Gene Aspm Is Involved in Brain Development in Zebrafish. *Biochem. Biophysical Res. Commun.* 409, 640–644. doi:10.1016/j.bbrc.2011.05.056

Kim, Y., Sharov, A. A., McDole, K., Cheng, M., Hao, H., Fan, C.-M., et al. (2011). Mouse B-type Lamins Are Required for Proper Organogenesis but Not by Embryonic Stem Cells. *Science* 334, 1706–1710. doi:10.1126/science.1211222

Kleber de Oliveira, W., Cortez-Escalante, J., De Oliveira, W. T. G. H., do Carmo, G. M. I., Henriques, C. M. P., Coelho, G. E., et al. (2016). Increase in Reported Prevalence of Microcephaly in Infants Born to Women Living in Areas with Confirmed Zika Virus Transmission during the First Trimester of Pregnancy - Brazil, 2015. *MMWR Morb. Mortal. Wkly. Rep.* 65, 242–247. doi:10.15585/mmwr.mm6509e2

Knoblich, J. A. (2008). Mechanisms of Asymmetric Stem Cell Division. *Cell* 132, 583–597. doi:10.1016/j.cell.2008.02.007

Kohwi, M., and Doe, C. Q. (2013). Temporal Fate Specification and Neural Progenitor Competence during Development. *Nat. Rev. Neurosci.* 14, 823–838. doi:10.1038/nrn3618

Konno, D., Shioi, G., Shitamukai, A., Mori, A., Kiyonari, H., Miyata, T., et al. (2008). Neuroepithelial Progenitors Undergo LGN-dependent Planar Divisions to Maintain Self-Renewability during Mammalian Neurogenesis. *Nat. Cel Biol* 10, 93–101. doi:10.1038/ncb1673

Kosodo, Y., Röper, K., Haubensak, W., Marzesco, A.-M., Corbeil, D., and Huttner, W. B. (2004). Asymmetric Distribution of the Apical Plasma Membrane during Neurogenic Divisions of Mammalian Neuroepithelial Cells. *Embo J.* 23, 2314–2324. doi:10.1038/sj.emboj.7600223

Kosodo, Y., Suetsugu, T., Suda, M., Mimori-Kiyosue, Y., Toida, K., Baba, S. A., et al. (2011). Regulation of Interkinetic Nuclear Migration by Cell Cycle-Coupled Active and Passive Mechanisms in the Developing Brain. *EMBO J.* 30, 1690–1704. doi:10.1038/emboj.2011.81

Kousar, R., Hassan, M. J., Khan, B., Basit, S., Mahmood, S., Mir, A., et al. (2011). Mutations in WDR62 Gene in Pakistani Families with Autosomal Recessive Primary Microcephaly. *BMC Neurol.* 11, 119. doi:10.1186/1471-2377-11-119

Kraemer, N., Issa, L., Hauck, S. C. R., Mani, S., Ninnemann, O., and Kaindl, A. M. (2011). What's the Hype about CDK5RAP2? *Cell. Mol. Life Sci.* 68, 1719–1736. doi:10.1007/s00018-011-0635-4

Lancaster, M. A., Renner, M., Martin, C.-A., Wenzel, D., Bicknell, L. S., Hurles, M. E., et al. (2013). Cerebral Organoids Model Human Brain Development and Microcephaly. *Nature* 501, 373–379. doi:10.1038/nature12517

Latasa, M. J., Cisneros, E., and Frade, J. M. (2009). Cell Cycle Control of Notch Signaling and the Functional Regionalization of the Neuroepithelium during Vertebrate Neurogenesis. *Int. J. Dev. Biol.* 53, 895–908. doi:10.1387/ijdb.082721ml

Le Duc, D., Giulivi, C., Hiatt, S. M., Napoli, E., Panoutsopoulos, A., Harlan De Crescenzo, A., et al. (2019). Pathogenic WDFY3 Variants Cause Neurodevelopmental Disorders and Opposing Effects on Brain Size. *Brain.* 142, 2617–2630. doi:10.1093/brain/awz198

Leidel, S., Delattre, M., Cerutti, L., Baumer, K., and Gönczy, P. (2005). SAS-6 Defines a Protein Family Required for Centrosome Duplication in *C. elegans* and in Human Cells. *Nat. Cel Biol* 7, 115–125. doi:10.1038/ncb1220

Leone, D. P., Srinivasan, K., Chen, B., Alcamo, E., and McConnell, S. K. (2008). The Determination of Projection Neuron Identity in the Developing Cerebral Cortex. *Curr. Opin. Neurobiol.* 18, 28–35. doi:10.1016/j.conb.2008.05.006

Létard, P., Drunat, S., Vial, Y., Duerinckx, S., Ernault, A., Amram, D., et al. (2018). Autosomal Recessive Primary Microcephaly Due to ASPM Mutations: An Update. *Hum. Mutat.* 39, 319–332.

Letourneur, F., Gaynor, E. C., Hennecke, S., Démollière, C., Duden, R., Emr, S. D., et al. (1994). Coatomer Is Essential for Retrieval of Dilysine-Tagged Proteins to the Endoplasmic Reticulum. *Cell* 79, 1199–1207. doi:10.1016/0092-8674(94)90011-6

Leventer, R. J., Jansen, A., Pilz, D. T., Stoodley, N., Marini, C., Dubeau, F., et al. (2010). Clinical and Imaging Heterogeneity of Polymicrogyria: a Study of 328 Patients. *Brain.* 133, 1415–1427. doi:10.1093/brain/awq078

Li, C., Xu, D., Ye, Q., Hong, S., Jiang, Y., Liu, X., et al. (2016). Zika Virus Disrupts Neural Progenitor Development and Leads to Microcephaly in Mice. *Cell Stem Cell* 19, 120–126. doi:10.1016/j.stem.2016.04.017

Li, H., Bielas, S. L., Zaki, M. S., Ismail, S., Farfara, D., Um, K., et al. (2016). Biallelic Mutations in Citron Kinase Link Mitotic Cytokinesis to Human Primary Microcephaly. *Am. J. Hum. Genet.* 99, 501–510. doi:10.1016/j.ajhg.2016.07.004

Li, R., Sun, L., Fang, A., Li, P., Wu, Q., and Wang, X. (2017). Recapitulating Cortical Development with Organoid Culture *In Vitro* and Modeling Abnormal Spindle-like (ASPM Related Primary) Microcephaly Disease. *Protein Cell* 8, 823–833. doi:10.1007/s13238-017-0479-2

Liang, Y., Gao, H., Lin, S.-Y., Peng, G., Huang, X., Zhang, P., et al. (2010). BRIT1/MCPH1 Is Essential for Mitotic and Meiotic Recombination DNA Repair and Maintaining Genomic Stability in Mice. *Plos Genet.* 6, e1000826. doi:10.1371/journal.pgen.1000826

Lim, A., and Kraut, R. (2009). The Drosophila BEACH Family Protein, Blue Cheese, Links Lysosomal Axon Transport with Motor Neuron Degeneration. *J. Neurosci.* 29, 951–963. doi:10.1523/jneurosci.2582-08.2009

Link, N., Chung, H., Jolly, A., Withers, M., Tepe, B., Arenkiel, B. R., et al. (2019). Mutations in ANKLE2, a ZIKA Virus Target, Disrupt an Asymmetric Cell Division Pathway in Drosophila Neuroblasts to Cause Microcephaly. *Developmental Cel* 51, 713–729. e716. doi:10.1016/j.devcel.2019.10.009

Lizarraga, S. B., Margossian, S. P., Harris, M. H., Campagna, D. R., Han, A.-P., Blevins, S., et al. (2010). Cdk5rap2 Regulates Centrosome Function and Chromosome Segregation in Neuronal Progenitors. *Development* 137, 1907–1917. doi:10.1242/dev.040410

Lucas, E. P., and Raff, J. W. (2007). Maintaining the Proper Connection between the Centrioles and the Pericentriolar Matrix Requires Drosophila Centrosomin. *J. Cel Biol* 178, 725–732. doi:10.1083/jcb.200704081

Mahmood, S., Ahmad, W., and Hassan, M. J. (2011). Autosomal Recessive Primary Microcephaly (MCPH): Clinical Manifestations, Genetic Heterogeneity and Mutation Continuum. *Orphanet J. Rare Dis.* 6, 39–54. doi:10.1186/1750-1172-6-39

Makrythanasis, P., Maroofian, R., Stray-Pedersen, A., Musaev, D., Zaki, M. S., Mahmoud, I. G., et al. (2018). Biallelic Variants in KIF14 Cause Intellectual Disability with Microcephaly. *Eur. J. Hum. Genet.* 26, 330–339. doi:10.1038/s41431-017-0088-9

Malatesta, P., Hartfuss, E., and Gotz, M. (2000). Isolation of Radial Glial Cells by Fluorescent-Activated Cell Sorting Reveals a Neuronal Lineage. *Development* 127, 5253–5263. doi:10.1242/dev.127.24.5253

Malumbres, M., Sotillo, R., Santamaría, D., Galán, J., Cerezo, A., Ortega, S., et al. (2004). Mammalian Cells Cycle without the D-type Cyclin-dependent Kinases Cdk4 and Cdk6. *Cell* 118, 493–504. doi:10.1016/j.cell.2004.08.002

Marín, O. (2013). Cellular and Molecular Mechanisms Controlling the Migration of Neocortical Interneurons. *Eur. J. Neurosci.* 38, 2019–2029.

Marjanović, M., Sánchez-Huertas, C., Terré, B., Gómez, R., Scheel, J. F., Pacheco, S., et al. (2015). CEP63 Deficiency Promotes P53-dependent Microcephaly and Reveals a Role for the Centrosome in Meiotic Recombination. *Nat. Commun.* 6, 7676. doi:10.1038/ncomms8676

Martin, C.-A., Murray, J. E., Carroll, P., Leitch, A., Mackenzie, K. J., Halachev, M., et al. (2016). Mutations in Genes Encoding Condensin Complex Proteins Cause Microcephaly through Decatenation Failure at Mitosis. *Genes Dev.* 30, 2158–2172. doi:10.1101/gad.286351.116

Matsuura, K., Lefebvre, P. A., Kamiya, R., and Hirono, M. (2004). Bld10p, a Novel Protein Essential for Basal Body Assembly in Chlamydomonas. *J. Cel Biol* 165, 663–671. doi:10.1083/jcb.200402022

McHenry, H. M. (1994). Tempo and Mode in Human Evolution. *Proc. Natl. Acad. Sci.* 91, 6780–6786. doi:10.1073/pnas.91.15.6780

McIntyre, R. E., Lakshminarasimhan Chavali, P., Ismail, O., Carragher, D. M., Sanchez-Andrade, G., Forment, J. V., et al. (2012). Disruption of Mouse Cenpj, a Regulator of Centriole Biogenesis, Phenocopies Seckel Syndrome. *Plos Genet.* 8, e1003022. doi:10.1371/journal.pgen.1003022

Megraw, T. L., Li, K., Kao, L. R., and Kaufman, T. C. (1999). The Centrosomin Protein Is Required for Centrosome Assembly and Function during Cleavage in Drosophila. *Development* 126, 2829–2839. doi:10.1242/dev.126.13.2829

Megraw, T. L., Sharkey, J. T., and Nowakowski, R. S. (2011). Cdk5rap2 Exposes the Centrosomal Root of Microcephaly Syndromes. *Trends Cel Biol.* 21, 470–480. doi:10.1016/j.tcb.2011.04.007

Memon, M. M., Raza, S. I., Basit, S., Kousar, R., Ahmad, W., and Ansar, M. (2013). A Novel WDR62 Mutation Causes Primary Microcephaly in a Pakistani Family. *Mol. Biol. Rep.* 40, 591–595. doi:10.1007/s11033-012-2097-7

Mirzaa, G. M., Vitre, B., Carpenter, G., Abramowicz, I., Gleeson, J. G., Paciorkowski, A. R., et al. (2014). Mutations in CENPE Define a Novel Kinetochore-Centromeric Mechanism for Microcephalic Primordial Dwarfism. *Hum. Genet.* 133, 1023–1039. doi:10.1007/s00439-014-1443-3

Miyata, T., Okamoto, M., Shinoda, T., and Kawaguchi, A. (2014). Interkinetic Nuclear Migration Generates and Opposes Ventricular-Zone Crowding: Insight into Tissue Mechanics. *Front. Cel Neurosci* 8, 473. doi:10.3389/fncel.2014.00473

Moawia, A., Shaheen, R., Rasool, S., Waseem, S. S., Ewida, N., Budde, B., et al. (2017). Mutations of KIF14 Cause Primary Microcephaly by Impairing Cytokinesis. *Ann. Neurol.* 82, 562–577. doi:10.1002/ana.25044

Molyneaux, B. J., Arlotta, P., Menezes, J. R. L., and Macklis, J. D. (2007). Neuronal Subtype Specification in the Cerebral Cortex. *Nat. Rev. Neurosci.* 8, 427–437. doi:10.1038/nrn2151

Mori, T., Buffo, A., and Götz, M. (2005). The Novel Roles of Glial Cells Revisited: the Contribution of Radial Glia and Astrocytes to Neurogenesis. *Curr. Top. Dev. Biol.* 69, 67–99. doi:10.1016/s0070-2153(05)69004-7

Morin, X., Jaouen, F., and Durbec, P. (2007). Control of Planar Divisions by the G-Protein Regulator LGN Maintains Progenitors in the Chick Neuroepithelium. *Nat. Neurosci.* 10, 1440–1448. doi:10.1038/nn1984

Morris, J. K., Rankin, J., Garne, E., Loane, M., Greenlees, R., Addor, M.-C., et al. (2016). Prevalence of Microcephaly in Europe: Population Based Study. *Bmj* 354, i4721. doi:10.1136/bmj.i4721

Mottier-Pavie, V., and Megraw, T. L. (2009). DrosophilaBld10 Is a Centriolar Protein that Regulates Centriole, Basal Body, and Motile Cilium Assembly. *MBoC* 20, 2605–2614. doi:10.1091/mbc.e08-11-1115

Mouden, C., de Tayrac, M., Dubourg, C., Rose, S., Carré, W., Hamdi-Rozé, H., et al. (2015). Homozygous STIL Mutation Causes Holoprosencephaly and Microcephaly in Two Siblings. *PLoS One* 10, e0117418. doi:10.1371/journal.pone.0117418

Murdock, D. R., Clark, G. D., Bainbridge, M. N., Newsham, I., Wu, Y.-Q., Muzny, D. M., et al. (2011). Whole-exome Sequencing Identifies Compound Heterozygous Mutations in WDR62 in Siblings with Recurrent Polymicrogyria. *Am. J. Med. Genet.* 155, 2071–2077. doi:10.1002/ajmg.a.34165

Musacchio, A., and Salmon, E. D. (2007). The Spindle-Assembly Checkpoint in Space and Time. *Nat. Rev. Mol. Cel Biol* 8, 379–393. doi:10.1038/nrm2163

Muzio, L., and Consalez, G. G. (2013). Modeling Human Brain Development with Cerebral Organoids. *Stem Cel Res Ther* 4, 154. doi:10.1186/scrt384

Naim, V., Imarisio, S., Di Cunto, F., Gatti, M., and Bonaccorsi, S. (2004). DrosophilaCitron Kinase Is Required for the Final Steps of Cytokinesis. *MBoC* 15, 5053–5063. doi:10.1091/mbc.e04-06-0536

Napoli, E., Panoutsopoulos, A. A., Kysar, P., Satriya, N., Sterling, K., Shibata, B., et al. (2021). Wdfy3 Regulates Glycophagy, Mitophagy, and Synaptic Plasticity. *J. Cereb. Blood Flow Metab.*, 0271678X2110273. doi:10.1177/0271678x211027384

Napoli, E., Song, G., Panoutsopoulos, A., Riyadh, M. A., Kaushik, G., Halmai, J., et al. (2018). Beyond Autophagy: a Novel Role for Autism-Linked Wdfy3 in Brain Mitophagy. *Sci. Rep.* 8, 11348. doi:10.1038/s41598-018-29421-7

Nardello, R., Fontana, A., Antona, V., Beninati, A., Mangano, G. D., Stallone, M. C., et al. (2018). A Novel Mutation of WDR62 Gene Associated with Severe Phenotype Including Infantile Spasm, Microcephaly, and Intellectual Disability. *Brain Development* 40, 58–64. doi:10.1016/j.braindev.2017.07.003

Nasser, H., Vera, L., Elmaleh-Bergès, M., Steindl, K., Letard, P., Teissier, N., et al. (2020). CDK5RAP2 Primary Microcephaly Is Associated with Hypothalamic, Retinal and Cochlear Developmental Defects. *J. Med. Genet.* 57, 389–399. doi:10.1136/jmedgenet-2019-106474

Neitzel, H., Neumann, L. M., Schindler, D., Wirges, A., Tönnies, H., Trimborn, M., et al. (2002). Premature Chromosome Condensation in Humans Associated with Microcephaly and Mental Retardation: a Novel Autosomal Recessive Condition. *Am. J. Hum. Genet.* 70, 1015–1022. doi:10.1086/339518

Nerli, E., Rocha-Martins, M., and Norden, C. (2020). Asymmetric Neurogenic Commitment of Retinal Progenitors Involves Notch through the Endocytic Pathway. *eLife* 9. doi:10.7554/eLife.60462

Nguyen, L. N., Ma, D., Shui, G., Wong, P., Cazenave-Gassiot, A., Zhang, X., et al. (2014). Mfsd2a Is a Transporter for the Essential omega-3 Fatty Acid Docosahexaenoic Acid. *Nature* 509, 503–506. doi:10.1038/nature13241

Nicholas, A. K., Khurshid, M., Désir, J., Carvalho, O. P., Cox, J. J., Thornton, G., et al. (2010). WDR62 Is Associated with the Spindle Pole and Is Mutated in Human Microcephaly. *Nat. Genet.* 42, 1010–1014. doi:10.1038/ng.682

Nigg, E. A., and Raff, J. W. (2009). Centrioles, Centrosomes, and Cilia in Health and Disease. *Cell* 139, 663–678. doi:10.1016/j.cell.2009.10.036

Noctor, S. C., Martínez-Cerdeño, V., Ivic, L., and Kriegstein, A. R. (2004). Cortical Neurons Arise in Symmetric and Asymmetric Division Zones and Migrate through Specific Phases. *Nat. Neurosci.* 7, 136–144. doi:10.1038/nn1172

Novorol, C., Burkhardt, J., Wood, K. J., Iqbal, A., Roque, C., Coutts, N., et al. (2013). Microcephaly Models in the Developing Zebrafish Retinal Neuroepithelium point to an Underlying Defect in Metaphase Progression. *Open Biol.* 3, 130065. doi:10.1098/rsob.130065

Ohkura, H., Török, T., Tick, G., Hoheisel, J., Kiss, I., and Glover, D. M. (1997). Mutation of a Gene for a Drosophila Kinesin-like Protein, Klp38B, Leads to Failure of Cytokinesis. *J. Cel Sci* 110 (Pt 8) (Pt 8), 945–954. doi:10.1242/jcs.110.8.945

Okamoto, M., Shinoda, T., Kawaue, T., Nagasaka, A., and Miyata, T. (2014). Ferret-mouse Differences in Interkinetic Nuclear Migration and Cellular Densification in the Neocortical Ventricular Zone. *Neurosci. Res.* 86, 88–95. doi:10.1016/j.neures.2014.10.006

Orci, L., Palmer, D. J., Ravazzola, M., Perrelet, A., Amherdt, M., and Rothman, J. E. (1993). Budding from Golgi Membranes Requires the Coatomer Complex of Non-clathrin Coat Proteins. *Nature* 362, 648–652. doi:10.1038/362648a0

Orosco, L. A., Ross, A. P., Cates, S. L., Scott, S. E., Wu, D., Sohn, J., et al. (2014). Loss of Wdfy3 in Mice Alters Cerebral Cortical Neurogenesis Reflecting Aspects of the Autism Pathology. *Nat. Commun.* 5, 4692. doi:10.1038/ncomms5692

Paridaen, J. T. M. L., Wilsch-Bräuninger, M., and Huttner, W. B. (2013). Asymmetric Inheritance of Centrosome-Associated Primary Cilium Membrane Directs Ciliogenesis after Cell Division. *Cell* 155, 333–344. doi:10.1016/j.cell.2013.08.060

Parry, D. A., Martin, C.-A., Greene, P., Marsh, J. A., Ambrose, J. C., Arumugam, P., et al. (2021). Heterozygous Lamin B1 and Lamin B2 Variants Cause Primary Microcephaly and Define a Novel Laminopathy. *Genet. Med.* 23, 408–414. doi:10.1038/s41436-020-00980-3

Passemard, S., Kaindl, A. M., and Verloes, A. (2013). "Chapter 13 - Microcephaly," in *Handbook of Clinical Neurology*. Editors O. Dulac, M. Lassonde, and H. B. Sarnat (Elsevier), 129–141.

Passemard, S., Titomanlio, L., Elmaleh, M., Afenjar, A., Alessandri, J.-L., Andria, G., et al. (2009). Expanding the Clinical and Neuroradiologic Phenotype of Primary Microcephaly Due to ASPM Mutations. *Neurology* 73, 962–969. doi:10.1212/wnl.0b013e3181b8799a

Perez, Y., Bar-Yaacov, R., Kadir, R., Wormser, O., Shelef, I., Birk, O. S., et al. (2019). Mutations in the Microtubule-Associated Protein MAP11 (C7orf43) Cause Microcephaly in Humans and Zebrafish. *Brain.* 142, 574–585. doi:10.1093/brain/awz004

Pervaiz, N., Kang, H., Bao, Y., and Abbasi, A. A. (2021). Molecular Evolutionary Analysis of Human Primary Microcephaly Genes. *BMC Ecol. Evo* 21, 76. doi:10.1186/s12862-021-01801-0

Pfaff, K. L., Straub, C. T., Chiang, K., Bear, D. M., Zhou, Y., and Zon, L. I. (2007). The Zebra Fish Cassiopeia Mutant Reveals that SIL Is Required for Mitotic Spindle Organization. *Mol. Cel Biol* 27, 5887–5897. doi:10.1128/mcb.00175-07

Pilaz, L.-J., Patti, D., Marcy, G., Ollier, E., Pfister, S., Douglas, R. J., et al. (2009). Forced G1-phase Reduction Alters Mode of Division, Neuron Number, and Laminar Phenotype in the Cerebral Cortex. *Proc. Natl. Acad. Sci.* 106, 21924–21929. doi:10.1073/pnas.0909894106

Pontious, A., Kowalczyk, T., Englund, C., and Hevner, R. F. (2008). Role of Intermediate Progenitor Cells in Cerebral Cortex Development. *Dev. Neurosci.* 30, 24–32. doi:10.1159/000109848

Postiglione, M. P., Jüschke, C., Xie, Y., Haas, G. A., Charalambous, C., and Knoblich, J. A. (2011). Mouse Inscuteable Induces Apical-Basal Spindle Orientation to Facilitate Intermediate Progenitor Generation in the Developing Neocortex. *Neuron* 72, 269–284. doi:10.1016/j.neuron.2011.09.022

Poulton, C. J., Schot, R., Seufert, K., Lequin, M. H., Accogli, A., Annunzio, G. D., et al. (2014). Severe Presentation ofWDR62mutation: Is There a Role for Modifying Genetic Factors? *Am. J. Med. Genet.* 164, 2161–2171. doi:10.1002/ajmg.a.36611

Pulvers, J. N., Bryk, J., Fish, J. L., Wilsch-Brauninger, M., Arai, Y., Schreier, D., et al. (2010). Mutations in Mouse Aspm (Abnormal Spindle-like Microcephaly Associated) Cause Not Only Microcephaly but Also Major Defects in the Germline. *Proc. Natl. Acad. Sci.* 107, 16595–16600. doi:10.1073/pnas.1010494107

Putkey, F. R., Cramer, T., Morphew, M. K., Silk, A. D., Johnson, R. S., McIntosh, J. R., et al. (2002). Unstable Kinetochore-Microtubule Capture and Chromosomal Instability Following Deletion of CENP-E. *Developmental Cel* 3, 351–365. doi:10.1016/s1534-5807(02)00255-1

Qian, X., Shen, Q., Goderie, S. K., He, W., Capela, A., Davis, A. A., et al. (2000). Timing of CNS Cell Generation. *Neuron* 28, 69–80. doi:10.1016/s0896-6273(00)00086-6

Rakic, P. (2009). Evolution of the Neocortex: a Perspective from Developmental Biology. *Nat. Rev. Neurosci.* 10, 724–735. doi:10.1038/nrn2719

Rana, R., Gwasikoti, N., Vaswani, N. D., and Kaushik, J. S. (2019). Phenomenology of Epilepsy in a Child with a ZNF335 Encephalopathy. *Indian J. Pediatr.* 86, 967–968. doi:10.1007/s12098-019-02991-8

Ravindran, E., Jühlen, R., Vieira-Vieira, C. H., Ha, T., Salzberg, Y., Fichtman, B., et al. (2021). Expanding the Phenotype of NUP85 Mutations beyond Nephrotic Syndrome to Primary Autosomal Recessive Microcephaly and Seckel Syndrome Spectrum Disorders. *Hum. Mol. Genet.* 30, 2068–2081. doi:10.1093/hmg/ddab160

Reillo, I., de Juan Romero, C., García-Cabezas, M. Á., and Borrell, V. (2011). A Role for Intermediate Radial Glia in the Tangential Expansion of the Mammalian Cerebral Cortex. *Cereb. Cortex* 21, 1674–1694. doi:10.1093/cercor/bhq238

Reilly, M. L., Stokman, M. F., Magry, V., Jeanpierre, C., Alves, M., Paydar, M., et al. (2019). Loss-of-function Mutations inKIF14cause Severe Microcephaly and Kidney Development Defects in Humans and Zebrafish. *Hum. Mol. Genet.* 28, 778–795. doi:10.1093/hmg/ddy381

Riparbelli, M. G., Callaini, G., Glover, D. M., and Avides, M. d. C. (2002). A Requirement for the Abnormal Spindle Protein to Organise Microtubules of the central Spindle for Cytokinesis inDrosophila. *J. Cel. Sci.* 115, 913–922. doi:10.1242/jcs.115.5.913

Ripoll, P., Pimpinelli, S., Valdivia, M. M., and Avila, J. (1985). A Cell Division Mutant of Drosophila with a Functionally Abnormal Spindle. *Cell* 41, 907–912. doi:10.1016/s0092-8674(85)80071-4

Roberts, M. R., Bittman, K., Li, W.-W., French, R., Mitchell, B., LoTurco, J. J., et al. (2000). TheFlatheadMutation Causes CNS-specific Developmental Abnormalities and Apoptosis. *J. Neurosci.* 20, 2295–2306. doi:10.1523/jneurosci.20-06-02295.2000

Rodrigues-Martins, A., Bettencourt-Dias, M., Riparbelli, M., Ferreira, C., Ferreira, I., Callaini, G., et al. (2007). DSAS-6 Organizes a Tube-like Centriole Precursor, and its Absence Suggests Modularity in Centriole Assembly. *Curr. Biol.* 17, 1465–1472. doi:10.1016/j.cub.2007.07.034

Roque, H., Wainman, A., Richens, J., Kozyrska, K., Franz, A., and Raff, J. W. (2012). Drosophila Cep135/Bld10 Maintains Proper Centriole Structure but Is Dispensable for Cartwheel Formation. *J. Cel. Sci.* 125, 5881–5886. doi:10.1242/jcs.113506

Rupp, V., Rauf, S., Naveed, I., Windpassinger, C., and Mir, A. (2014). A Novel Single Base Pair Duplication in WDR62 Causes Primary Microcephaly. *BMC Med. Genet.* 15, 107. doi:10.1186/s12881-014-0107-4

Saadi, A., Borck, G., Boddaert, N., Chekkour, M. C., Imessaoudene, B., Munnich, A., et al. (2009). Compound Heterozygous ASPM Mutations Associated with Microcephaly and Simplified Cortical Gyration in a Consanguineous Algerian Family. *Eur. J. Med. Genet.* 52, 180–184. doi:10.1016/j.ejmg.2009.03.013

Saadi, A., Verny, F., Siquier-Pernet, K., Bole-Feysot, C., Nitschke, P., Munnich, A., et al. (2016). Refining the Phenotype Associated with CASC5 Mutation. *Neurogenetics* 17, 71–78. doi:10.1007/s10048-015-0468-7

Sajid Hussain, M., Marriam Bakhtiar, S., Farooq, M., Anjum, I., Janzen, E., Reza Toliat, M., et al. (2013). Genetic Heterogeneity in Pakistani Microcephaly Families. *Clin. Genet.* 83, 446–451. doi:10.1111/j.1399-0004.2012.01932.x

Santaguida, S., and Musacchio, A. (2009). The Life and Miracles of Kinetochores. *Embo J.* 28, 2511–2531. doi:10.1038/emboj.2009.173

Sarkisian, M. R., Frenkel, M., Li, W., Oborski, J. A., and LoTurco, J. J. (2001). Altered Interneuron Development in the Cerebral Cortex of the Flathead Mutant. *Cereb. Cortex* 11, 734–743. doi:10.1093/cercor/11.8.734

Sarkisian, M. R., Li, W., Di Cunto, F., D'Mello, S. R., and LoTurco, J. J. (2002). Citron-kinase, a Protein Essential to Cytokinesis in Neuronal Progenitors, Is Deleted in the Flathead Mutant Rat. *J. Neurosci.* 22, Rc217. doi:10.1523/JNEUROSCI.22-08-j0001.2002

Sassaman, E. A., and Zartler, A. S. (1982). Mental Retardation and Head Growth Abnormalities. *J. Pediatr. Psychol.* 7, 149–156. doi:10.1093/jpepsy/7.2.149

Sato, R., Takanashi, J., Tsuyusaki, Y., Kato, M., Saitsu, H., Matsumoto, N., et al. (2016). Association between Invisible Basal Ganglia and ZNF335 Mutations: A Case Report. *Pediatrics* 138, 138. doi:10.1542/peds.2016-0897

Scala, M., Chua, G. L., Chin, C. F., Alsaif, H. S., Borovikov, A., Riazuddin, S., et al. (2020). Biallelic MFSD2A Variants Associated with Congenital Microcephaly, Developmental Delay, and Recognizable Neuroimaging Features. *Eur. J. Hum. Genet.* 28, 1509–1519. doi:10.1038/s41431-020-0669-x

Sgourdou, P., Mishra-Gorur, K., Saotome, I., Henagariu, O., Tuysuz, B., Campos, C., et al. (2017). Disruptions in Asymmetric Centrosome Inheritance and WDR62-Aurora Kinase B Interactions in Primary Microcephaly. *Sci. Rep.* 7, 43708. doi:10.1038/srep43708

Shaheen, R., Hashem, A., Abdel-Salam, G. M. H., Al-Fadhli, F., Ewida, N., and Alkuraya, F. S. (2016). Mutations in CIT, Encoding Citron Rho-Interacting Serine/threonine Kinase, Cause Severe Primary Microcephaly in Humans. *Hum. Genet.* 135, 1191–1197. doi:10.1007/s00439-016-1722-2

Shaheen, R., Maddirevula, S., Ewida, N., Alsahli, S., Abdel-Salam, G. M. H., Zaki, M. S., et al. (2019). Genomic and Phenotypic Delineation of Congenital Microcephaly. *Genet. Med.* 21, 545–552. doi:10.1038/s41436-018-0140-3

Shi, L., Qalieh, A., Lam, M. M., Keil, J. M., and Kwan, K. Y. (2019). Robust Elimination of Genome-Damaged Cells Safeguards against Brain Somatic Aneuploidy Following Knl1 Deletion. *Nat. Commun.* 10, 2588. doi:10.1038/s41467-019-10411-w

Singh, P., Ramdas Nair, A., and Cabernard, C. (2014). The Centriolar Protein Bld10/Cep135 Is Required to Establish Centrosome Asymmetry in Drosophila Neuroblasts. *Curr. Biol.* 24, 1548–1555. doi:10.1016/j.cub.2014.05.050

Siskos, N., Stylianopoulou, E., Skavdis, G., and Grigoriou, M. E. (2021). Molecular Genetics of Microcephaly Primary Hereditary: An Overview. *Brain Sci.* 11. doi:10.3390/brainsci11050581

Slezak, R., Smigiel, R., Obersztyn, E., Pollak, A., Dawidziuk, M., Wiszniewski, W., et al. (2021). Further Delineation of Phenotype and Genotype of Primary Microcephaly Syndrome with Cortical Malformations Associated with Mutations in the WDR62 Gene. *Genes* 12, 594. doi:10.3390/genes12040594

Stouffs, K., Stergachis, A. B., Vanderhasselt, T., Dica, A., Janssens, S., Vandervore, L., et al. (2018). Expanding the Clinical Spectrum of Biallelic ZNF335 Variants. *Clin. Genet.* 94, 246–251. doi:10.1111/cge.13260

Subramanian, L., Calcagnotto, M. E., and Paredes, M. F. (2019). Cortical Malformations: Lessons in Human Brain Development. *Front. Cel Neurosci* 13, 576. doi:10.3389/fncel.2019.00576

Szczepanski, S., Hussain, M. S., Sur, I., Altmüller, J., Thiele, H., Abdullah, U., et al. (2016). A Novel Homozygous Splicing Mutation of CASC5 Causes Primary Microcephaly in a Large Pakistani Family. *Hum. Genet.* 135, 157–170. doi:10.1007/s00439-015-1619-5

Tacchelly-Benites, O., Wang, Z., Yang, E., Lee, E., and Ahmed, Y. (2013). Toggling a Conformational Switch in Wnt/β-Catenin Signaling: Regulation of Axin Phosphorylation. *BioEssays* 35, 1063–1070. doi:10.1002/bies.201300101

Tang, H., Hammack, C., Ogden, S. C., Wen, Z., Qian, X., Li, Y., et al. (2016). Zika Virus Infects Human Cortical Neural Progenitors and Attenuates Their Growth. *Cell Stem Cell* 18, 587–590. doi:10.1016/j.stem.2016.02.016

Trimborn, M., Bell, S. M., Felix, C., Rashid, Y., Jafri, H., Griffiths, P. D., et al. (2004). Mutations in Microcephalin Cause Aberrant Regulation of Chromosome Condensation. *Am. J. Hum. Genet.* 75, 261–266. doi:10.1086/422855

Trimborn, M., Ghani, M., Walther, D. J., Dopatka, M., Dutrannoy, V., Busche, A., et al. (2010). Establishment of a Mouse Model with Misregulated Chromosome Condensation Due to Defective Mcph1 Function. *PLoS One* 5, e9242. doi:10.1371/journal.pone.0009242

Tsai, M.-Y., Wang, S., Heidinger, J. M., Shumaker, D. K., Adam, S. A., Goldman, R. D., et al. (2006). A Mitotic Lamin B Matrix Induced by RanGTP Required for Spindle Assembly. *Science* 311, 1887–1893. doi:10.1126/science.1122771

van Deijk, A.-L. F., Camargo, N., Timmerman, J., Heistek, T., Brouwers, J. F., Mogavero, F., et al. (2017). Astrocyte Lipid Metabolism Is Critical for Synapse Development and Function *In Vivo*. *Glia* 65, 670–682. doi:10.1002/glia.23120

Van Den Bosch, J. (1959). Microcephaly in the Netherlands: a Clinical and Genetical Study. *Ann. Hum. Genet.* 23, 91–116. doi:10.1111/j.1469-1809.1958.tb01455.x

van Dyck, L. I., and Morrow, E. M. (2017). Genetic Control of Postnatal Human Brain Growth. *Curr. Opin. Neurol.* 30, 114–124. doi:10.1097/wco.0000000000000405

Varmark, H., Llamazares, S., Rebollo, E., Lange, B., Reina, J., Schwarz, H., et al. (2007). Asterless Is a Centriolar Protein Required for Centrosome Function and Embryo Development in Drosophila. *Curr. Biol.* 17, 1735–1745. doi:10.1016/j.cub.2007.09.031

Vergnes, L., Peterfy, M., Bergo, M. O., Young, S. G., and Reue, K. (2004). Lamin B1 Is Required for Mouse Development and Nuclear Integrity. *Proc. Natl. Acad. Sci.* 101, 10428–10433. doi:10.1073/pnas.0401424101

Verloes, A., Drunat, S., Gressens, P., and Passemard, S. (1993). "Primary Autosomal Recessive Microcephalies and Seckel Syndrome Spectrum Disorders," in *GeneReviews(R)*. Editors R. A. Pagon, M. P. Adam, H. H. Ardinger, S. E. Wallace, A. Amemiya, L. J. H. Bean, et al. (Seattle (WA).

Vitale, I., Galluzzi, L., Castedo, M., and Kroemer, G. (2011). Mitotic Catastrophe: a Mechanism for Avoiding Genomic Instability. *Nat. Rev. Mol. Cel Biol* 12, 385–392. doi:10.1038/nrm3115

von der Hagen, M., Pivarcsi, M., Liebe, J., von Bernuth, H., Didonato, N., Hennermann, J. B., et al. (2014). Diagnostic Approach to Microcephaly in Childhood: a Two-center Study and Review of the Literature. *Dev. Med. Child. Neurol.* 56, 732–741. doi:10.1111/dmcn.12425

Wang, X., Tsai, J.-W., Imai, J. H., Lian, W.-N., Vallee, R. B., and Shi, S.-H. (2009). Asymmetric Centrosome Inheritance Maintains Neural Progenitors in the Neocortex. *Nature* 461, 947–955. doi:10.1038/nature08435

Watemberg, N., Silver, S., Harel, S., and Lerman-Sagie, T. (2002). Significance of Microcephaly Among Children with Developmental Disabilities. *J. Child. Neurol.* 17, 117–122. doi:10.1177/088307380201700205

Wong, B. H., Chan, J. P., Cazenave-Gassiot, A., Poh, R. W., Foo, J. C., Galam, D. L. A., et al. (2016). Mfsd2a Is a Transporter for the Essential ω-3 Fatty Acid Docosahexaenoic Acid (DHA) in Eye and Is Important for Photoreceptor Cell Development. *J. Biol. Chem.* 291, 10501–10514. doi:10.1074/jbc.m116.721340

Woods, C. G., Bond, J., and Enard, W. (2005). Autosomal Recessive Primary Microcephaly (MCPH): A Review of Clinical, Molecular, and Evolutionary Findings. *Am. J. Hum. Genet.* 76, 717–728. doi:10.1086/429930

Woods, C. G. (2004). Human Microcephaly. *Curr. Opin. Neurobiol.* 14, 112–117. doi:10.1016/j.conb.2004.01.003

Woods, C. G., and Parker, A. (2013). Investigating Microcephaly. *Arch. Dis. Child.* 98, 707–713. doi:10.1136/archdischild-2012-302882

Wu, K.-Y., Zuo, G.-L., Li, X.-F., Ye, Q., Deng, Y.-Q., Huang, X.-Y., et al. (2016). Vertical Transmission of Zika Virus Targeting the Radial Glial Cells Affects Cortex Development of Offspring Mice. *Cell Res* 26, 645–654. doi:10.1038/cr.2016.58

Xu, D., Zhang, F., Wang, Y., Sun, Y., and Xu, Z. (2014). Microcephaly-associated Protein WDR62 Regulates Neurogenesis through JNK1 in the Developing Neocortex. *Cel Rep.* 6, 104–116. doi:10.1016/j.celrep.2013.12.016

Yabe, T., Ge, X., and Pelegri, F. (2007). The Zebrafish Maternal-Effect Gene Cellular Atoll Encodes the Centriolar Component Sas-6 and Defects in its Paternal Function Promote Whole Genome Duplication. *Developmental Biol.* 312, 44–60. doi:10.1016/j.ydbio.2007.08.054

Yamamoto, S., Jaiswal, M., Charng, W.-L., Gambin, T., Karaca, E., Mirzaa, G., et al. (2014). A drosophila Genetic Resource of Mutants to Study Mechanisms Underlying Human Genetic Diseases. *Cell* 159, 200–214. doi:10.1016/j.cell.2014.09.002

Yang, Y. J., Baltus, A. E., Mathew, R. S., Murphy, E. A., Evrony, G. D., Gonzalez, D. M., et al. (2012). Microcephaly Gene Links Trithorax and REST/NRSF to Control Neural Stem Cell Proliferation and Differentiation. *Cell* 151, 1097–1112. doi:10.1016/j.cell.2012.10.043

Yen, T. J., Compton, D. A., Wise, D., Zinkowski, R. P., Brinkley, B. R., Earnshaw, W. C., et al. (1991). CENP-E, a Novel Human Centromere-Associated Protein Required for Progression from Metaphase to Anaphase. *EMBO J.* 10, 1245–1254. doi:10.1002/j.1460-2075.1991.tb08066.x

Young, S. G., Jung, H.-J., Coffinier, C., and Fong, L. G. (2012). Understanding the Roles of Nuclear A- and B-type Lamins in Brain Development. *J. Biol. Chem.* 287, 16103–16110. doi:10.1074/jbc.r112.354407

Yu, T. W., Mochida, G. H., Tischfield, D. J., Sgaier, S. K., Flores-Sarnat, L., Sergi, C. M., et al. (2010). Mutations in WDR62, Encoding a Centrosome-Associated Protein, Cause Microcephaly with Simplified Gyri and Abnormal Cortical Architecture. *Nat. Genet.* 42, 1015–1020. doi:10.1038/ng.683

Yucel, J. K., Marszalek, J. D., McIntosh, J. R., Goldstein, L. S. B., Cleveland, D. W., and Philp, A. V. (2000). CENP-meta, an Essential Kinetochore Kinesin Required for the Maintenance of Metaphase Chromosome Alignment in Drosophila. *J. Cel Biol* 150, 1–12. doi:10.1083/jcb.150.1.1a

Zaqout, S., Morris-Rosendahl, D., and Kaindl, A. M. (2017). Autosomal Recessive Primary Microcephaly (MCPH): An Update. *Neuropediatrics* 48, 135–142. doi:10.1055/s-0037-1601448

Zaqout, S., Blaesius, K., Wu, Y.-J., Ott, S., Kraemer, N., Becker, L.-L., et al. (2019). Altered Inhibition and Excitation in Neocortical Circuits in Congenital Microcephaly. *Neurobiol. Dis.* 129, 130–143. doi:10.1016/j.nbd.2019.05.008

Zarate, Y. A., Kaylor, J. A., Bosanko, K., Lau, S., Vargas, J., and Gao, H. (2016). First Clinical Report of an Infant with Microcephaly andCASC5mutations. *Am. J. Med. Genet.* 170, 2215–2218. doi:10.1002/ajmg.a.37726

Zhang, W., Yang, S.-L., Yang, M., Herrlinger, S., Shao, Q., Collar, J. L., et al. (2019). Modeling Microcephaly with Cerebral Organoids Reveals a WDR62-Cep170-KIF2A Pathway Promoting Cilium Disassembly in Neural Progenitors. *Nat. Commun.* 10, 2612. doi:10.1038/s41467-019-10497-2

Zhang, Y., Li, H., Pang, J., Peng, Y., Shu, L., and Wang, H. (2019). Novel SASS6 Compound Heterozygous Mutations in a Chinese Family with Primary Autosomal Recessive Microcephaly. *Clinica Chim. Acta* 491, 15–18. doi:10.1016/j.cca.2019.01.007

Zhong, W., and Chia, W. (2008). Neurogenesis and Asymmetric Cell Division. *Curr. Opin. Neurobiol.* 18, 4–11. doi:10.1016/j.conb.2008.05.002

Zhong, W., Feder, J. N., Jiang, M.-M., Jan, L. Y., and Jan, Y. N. (1996). Asymmetric Localization of a Mammalian Numb Homolog during Mouse Cortical Neurogenesis. *Neuron* 17, 43–53. doi:10.1016/s0896-6273(00)80279-2

Ziegler, A. B., Thiele, C., Tenedini, F., Richard, M., Leyendecker, P., Hoermann, A., et al. (2017). Cell-Autonomous Control of Neuronal Dendrite Expansion via the Fatty Acid Synthesis Regulator SREBP. *Cel Rep.* 21, 3346–3353. doi:10.1016/j.celrep.2017.11.069

Zombor, M., Kalmár, T., Nagy, N., Berényi, M., Telcs, B., Maróti, Z., et al. (2019). A Novel WDR62 Missense Mutation in Microcephaly with Abnormal Cortical Architecture and Review of the Literature. *J. Appl. Genet.* 60, 151–162. doi:10.1007/s13353-019-00486-y

Conflict of Interest: The authors declare that the research was conducted in the absence of any commercial or financial relationships that could be construed as a potential conflict of interest.

Publisher's Note: All claims expressed in this article are solely those of the authors and do not necessarily represent those of their affiliated organizations, or those of the publisher, the editors, and the reviewers. Any product that may be evaluated in this article, or claim that may be made by its manufacturer, is not guaranteed or endorsed by the publisher.

frontiers in Cell and Developmental Biology

ORIGINAL RESEARCH
published: 21 January 2022
doi: 10.3389/fcell.2022.777887

Alx1 Deficient Mice Recapitulate Craniofacial Phenotype and Reveal Developmental Basis of *ALX1*-Related Frontonasal Dysplasia

Paul P. R. Iyyanar[1†], *Zhaoming Wu*[1†], *Yu Lan*[1,2,3], *Yueh-Chiang Hu*[1,3] *and Rulang Jiang*[1,2,3*]

[1]Division of Developmental Biology, Cincinnati Children's Hospital Medical Center, Cincinnati, OH, United States, [2]Division of Plastic Surgery, Cincinnati Children's Hospital Medical Center, Cincinnati, OH, United States, [3]Departments of Pediatrics and Surgery, University of Cincinnati College of Medicine, Cincinnati, OH, United States

Loss of ALX1 function causes the frontonasal dysplasia syndrome FND3, characterized by severe facial clefting and microphthalmia. Whereas the laboratory mouse has been the preeminent animal model for studying developmental mechanisms of human craniofacial birth defects, the roles of ALX1 in mouse frontonasal development have not been well characterized because the only previously reported *Alx1* mutant mouse line exhibited acrania due to a genetic background-dependent failure of cranial neural tube closure. Using CRISPR/Cas9-mediated genome editing, we have generated an *Alx1-deletion* mouse model that recapitulates the FND craniofacial malformations, including median orofacial clefting and disruption of development of the eyes and alae nasi. *In situ* hybridization analysis showed that *Alx1* is strongly expressed in frontonasal neural crest cells that give rise to periocular and frontonasal mesenchyme. $Alx1^{del/del}$ embryos exhibited increased apoptosis of periocular mesenchyme and decreased expression of ocular developmental regulators *Pitx2* and *Lmxb1* in the periocular mesenchyme, followed by defective optic stalk morphogenesis. Moreover, $Alx1^{del/del}$ embryos exhibited disruption of frontonasal mesenchyme identity, with loss of expression of *Pax7* and concomitant ectopic expression of the jaw mesenchyme regulators *Lhx6* and *Lhx8* in the developing lateral nasal processes. The function of ALX1 in patterning the frontonasal mesenchyme is partly complemented by ALX4, a paralogous ALX family transcription factor whose loss-of-function causes a milder and distinctive FND. Together, these data uncover previously unknown roles of ALX1 in periocular mesenchyme development and frontonasal mesenchyme patterning, providing novel insights into the pathogenic mechanisms of *ALX1*-related FND.

Keywords: cleft palate, craniofacial development, frontonasal dysplasia, microphthalmia, neural crest, orofacial cleft, periocular mesenchyme, alx1

OPEN ACCESS

Edited by:
Dalit Sela-Donenfeld, The Hebrew University of Jerusalem, Israel

Reviewed by:
Amnon Sharir, Hebrew University of Jerusalem, Israel
Sylvie Schneider-Maunoury, Institut National de la Santé et de la Recherche Médicale (INSERM), France

***Correspondence:**
Rulang Jiang
Rulang.Jiang@cchmc.org

†These authors have contributed equally to this work and share first authorship

Specialty section:
This article was submitted to Morphogenesis and Patterning, a section of the journal Frontiers in Cell and Developmental Biology

Received: *16 September 2021*
Accepted: *04 January 2022*
Published: *21 January 2022*

Citation:
Iyyanar PPR, Wu Z, Lan Y, Hu Y-C and Jiang R (2022) Alx1 *Deficient Mice Recapitulate Craniofacial Phenotype and Reveal Developmental Basis of* ALX1*-Related Frontonasal Dysplasia. Front. Cell Dev. Biol. 10:777887. doi: 10.3389/fcell.2022.777887*

INTRODUCTION

Frontonasal dysplasia (FND), also known as median cleft face syndrome, is a group of congenital craniofacial disorders characterized by ocular hypertelorism, midline facial cleft affecting the nose and/or upper lip and palate, broad and flattened nasal bridge, notching or clefting of the nasal alae, and is sometimes associated with anterior cranium bifidum and other malformations (Wu et al., 2007; Kayserili et al., 2009; Twigg et al., 2009; Farlie et al., 2016). Most of the bones, cartilages, and

other connective tissues in the face are derived from a transient embryonic cell population called the cranial neural crest cells (CNCCs), which arise at the anterior neural plate border in human embryos in the third week of gestation, corresponding to about embryonic day (E) 8.0 in mice (Jiang et al., 2000; O'Rahilly and Müller, 2007; Yoshida et al., 2008; Zalc et al., 2021). The first group of CNCCs delaminate from the region lateral to the prospective forebrain and anterior midbrain, migrate ventrally to surround the ventral forebrain and interact with both neural and surface ectoderm to form the embryonic frontonasal prominence (FNP) by mid-fourth week of human gestation, corresponding to about E9.0 in mice (Jiang et al., 2006). The second group of CNCCs delaminate at the posterior midbrain and anterior hindbrain level and migrate ventrally to interact with the surface ectoderm to form the maxillary and mandibular processes. Thus, the initial facial primordia, observed in four-week-old human embryos and E9.5 mouse embryos, consist of the single FNP located rostrally to the primitive mouth, a pair of maxillary processes (MxP) flanking and a pair of mandibular processes at the caudal boundary of the primitive mouth (Jiang et al., 2006). As facial development continues, the FNP gives rise to paired medial nasal processes (MNP) and lateral nasal processes (LNP) flanking each of the nasal pits. Formation of the intact upper lip involves extensive directional growth and subsequent fusion of the MNP, LNP, and MxP as well as merging of the nasal processes to fill the facial midline (Jiang et al., 2006). Thus, the causes of FND are complex and could result from genetic and/or environmental perturbations of CNCC migration, proliferation, survival, differentiation, or the lip fusion processes.

Whilst most FND cases occur sporadically with unknown etiology, homozygous loss-of-function mutations in *ALX1*, *ALX3*, or *ALX4*, have been associated with distinct recessive FNDs. Disruption of *ALX1* causes severe facial clefting and microphthalmia in FND3 patients, whereas loss of function mutations in *ALX3* and *ALX4* underlie the milder FND1 and FND2 syndromes, respectively (Kayserili et al., 2009; Twigg et al., 2009; Uz et al., 2010; Pini et al., 2020). A mutation altering the splice acceptor of the fourth exon of *ALX1* has been associated with a milder form of FND3, with patients displaying ptosis (droopy upper eyelid), broad nasal root, short and wide nasal bridge, bifid or depressed nasal tip and anteverted nares (Ullah et al., 2017). The *Alx* genes encode homeodomain-containing transcription factors that are expressed in partly overlapping patterns during craniofacial development (Beverdam and Meijlink, 2001; McGonnell et al., 2011; Dee et al., 2013). Gene knockout studies of each of the *Alx* genes in mice had been reported prior to the discovery of *ALX* gene mutations in human FND patients. An *Alx1* gene-knockout mouse line, in which the first three exons of the *Alx1* gene were replaced with a *neomycin* expression cassette ($Alx1^{tm1Crm}$ is the official name of that *Alx1* gene-knockout allele), exhibited aberrant apoptosis of the embryonic forebrain mesenchyme and failure of cranial neural tube closure in homozygous mutant mice (Zhao et al., 1996). Mice lacking *Alx3* function did not have an obvious defect in craniofacial development, whereas mice lacking *Alx4* function exhibited multiple developmental defects, including limb malformations and ventral body wall defects but only mild frontonasal defect with variable open eyelid at birth (Qu et al., 1997; Beverdam et al., 2001). In addition, a severe midline nasal clefting phenotype has been reported in mice carrying three to four disrupted alleles of *Alx3* and *Alx4* together or the $Alx1^{tm1Crm/+}Alx4^{-/-}$ genotype (Qu et al., 1999; Beverdam et al., 2001). Although Zhao et al. (1996) indicated that the penetrance of neural tube defect in $Alx1^{tm1Crm/tm1Crm}$ mouse embryos was genetic background dependent, with about 65% of the $Alx1^{tm1Crm/tm1Crm}$ embryos in the B6/129 hybrid background displayed neural tube defect compared to 100% penetrance in the 129/SvEv inbred background (Zhao et al., 1996), no specific analysis of frontonasal development in the $Alx1^{tm1Crm/tm1Crm}$ mice, with or without neural tube defect, has been reported. Several laboratories have studied ALX1 function in craniofacial development using zebrafish models. Dee et al. (2013) reported that morpholino knockdown of *alx1* function in zebrafish embryos resulted in defective frontonasal neural crest cell migration and catastrophic failure of facial cartilage formation (Dee et al., 2013). However, Pini et al. (2020) showed that genetic loss of *alx1* function did not affect the development and viability of the majority of homozygous zebrafish mutants, with only a subtle deformity in facial cartilages detected in about 5% of the homozygous *alx1* mutant fish (Pini et al., 2020). Mitchell et al. (2021) independently generated and analyzed *alx1* loss-of-function mutant zebrafish lines and confirmed that ALX1 function is not essential for craniofacial development in zebrafish (Mitchell et al., 2021). Altogether, although there have been several genetic studies of ALX1 function in mice and zebrafish, the cellular and molecular mechanisms mediating ALX1 function in frontonasal development remain unresolved.

In this study, we generated *Alx1*-deficient mice using CRISPR/Cas9-mediated genome editing in the C57BL/6N inbred strain and found that *Alx1* mutant mice recapitulated craniofacial defects found in *ALX*-related FND patients, including frontonasal malformations, notching of the upper lip, cleft palate, and eye morphogenesis defects (Farlie et al., 2016). In contrast to the defective CNCC migration reported in zebrafish *alx1* morphants (Dee et al., 2013), CNCC migration to the FNP and pharyngeal arches occurred normally in the *Alx1* mutant mouse embryos. Further analyses identified novel roles of ALX1 in patterning the frontonasal and periocular mesenchyme, revealing a crucial role for ALX1 in determining the identity of the frontonasal neural crest-derived LNP mesenchyme and in patterning the midface.

RESULTS

Mice Lacking *Alx1* Function Recapitulate Craniofacial and Ocular Defects in ALX-Related FND Patients

To investigate the mechanism involving ALX1 in frontonasal development, we generated a new mutant mouse line carrying a deletion of exon-2 of the *Alx1* gene ($Alx1^{del}$) using

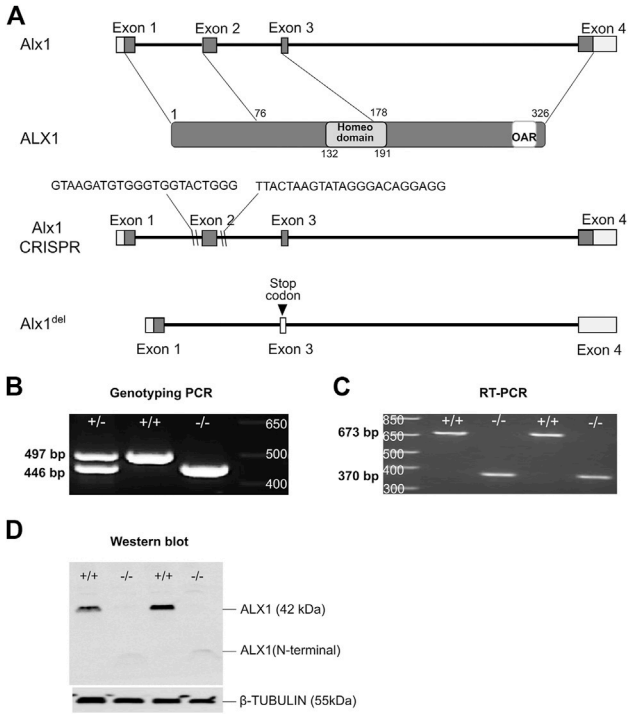

FIGURE 1 | Generation of *Alx1*-deletion mice using CRISPR/Cas9-mediated genome editing. **(A)** Schematics of the strategy for generating $Alx1^{del/+}$ mice using the CRISPR/Cas9 technology. The top row shows the genomic organization of the mouse *Alx1* locus. Exons 1–4 are boxed with coding regions filled in grey color and the domains of ALX1 protein represented in the second row. Lines point to the exons of the *Alx1* gene with the corresponding region in the ALX1 protein. The DNA-binding Homeodomain and the OAR domain, a conserved domain in the C-terminal region of several paired-like homedomain proteins including *Drosophila* Orthopedia and Aristaless and vertebrate Rax, are marked. The locations of sgRNA target sequences are indicated in intron-1 and intron-2 regions, respectively, in the schematic in the third row, whereas the fourth row depicts the $Alx1^{del}$ allele that lacks exon-2 and flanking sequences in between the two sgRNA target sites. The exon-2 deletion results in a frameshift and premature translational STOP codon in the exon-3 sequence. **(B)** PCR genotyping of the embryos from the intercross of heterozygous $Alx1^{del/+}$ mice. The amplicons from wildtype and $Alx1^{del}$ alleles are 497 bp and 446 bp, respectively. **(C)** RT-PCR analysis using primers from exon1 to exon4, respectively, reveals a wildtype amplicon of 673 bp and an $Alx1^{del}$ allele-specific product of 370 bp. **(D)** Western blot analysis using a polyclonal anti-ALX1 antibody raised against the full-length ALX1 protein reveals a lack of the full-length ALX1 protein in the $Alx1^{del/del}$ embryos. $Alx1^{del/del}$ embryos produced a truncated N-terminal product of around 10.5 kDa +/-, $Alx1^{del/+}$; +/+, wildtype; –/–, $Alx1^{del/del}$.

CRISPR/Cas9-mediated genome editing in the C57BL/6N inbred mice (**Figures 1A–C**). Sequencing of RT-PCR products from $Alx1^{del/+}$ and $Alx1^{del/del}$ embryos confirmed that the $Alx1^{del}$ allele produced mutant mRNAs from splicing exon-1 to exon-3, which led to a frame-shift and is predicted to produce a truncated protein product containing only the N-terminal region of the ALX1 protein lacking the homeodomain and the C-terminal Aristaless domain (Brouwer et al., 2003). Indeed, western blot analysis confirmed that the $Alx1^{del/del}$ embryos lacked full-length ALX1 protein and only produced a truncated product that was expressed at low levels but still detectable using the polyclonal anti-ALX1 antibody (**Figure 1D**).

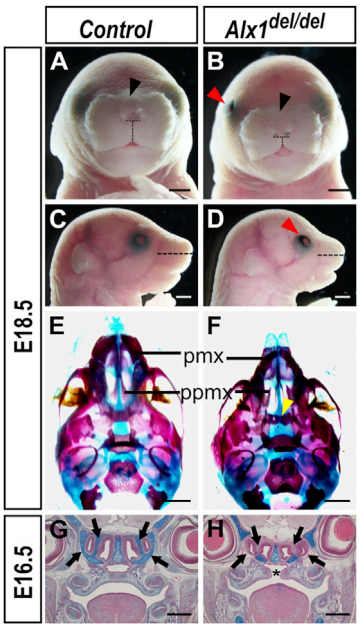

FIGURE 2 | Craniofacial defects in the $Alx1^{del/del}$ embryos. **(A–D)** Whole mount frontal **(A, B)** and lateral **(C, D)** views of control **(A, C)** and $Alx1^{del/del}$ **(B, D)** embryos at E18.5. $Alx1^{del/del}$ embryos exhibit open eyelid [red arrowhead in **(B, D)**], shorter snout [compare horizontal dashed lines in **(C, D)**], wider nasal bridge [black arrowhead in **(B)**] and notching of the upper lip. Dashed horizontal lines in A and B mark the inter-nostril distance, whereas vertical dashed lines mark the length of the philtrum for measurements in **Supplementary Figure S1**. **(E, F)** Palatal view of the head skeleton preparations of E18.5 control **(E)** and $Alx1^{del/del}$ **(F)** embryos. $Alx1^{del/del}$ embryos exhibit hypoplastic premaxilla, malformed palatal processes, and hypoplastic presphenoid bone [yellow arrowhead in **(F)**]. **(G, H)** Frontal sections of control **(G)** and $Alx1^{del/del}$ **(H)** embryo heads at E16.5. Asterisk in H marks the cleft palate. Black arrows point to the lateral nasal cartilages in the wildtype control **(G)** and the defective nasal cartilages in the $Alx1^{del/del}$ embryos **(H)**. Scale bars in **(A–F)** and **(G, H)** are 500 μm and 1 mm, respectively. pmx, premaxilla; ppmx, palatal process of the maxillary bone.

$Alx1^{del/+}$ mice appeared indistinguishable from wildtype littermates. Examination of pups and fetuses from $Alx1^{del/+}$ mice intercrosses revealed that $Alx1^{del/del}$ pups exhibited shortened snout, flattened nasal bridge with increased distance between the nostrils, short philtrum, and midline notching of the upper lip (**Figures 2A–D**, n = 6 for each genotype; and **Supplementary Figure S1**). $Alx1^{del/del}$ pups were born alive but died soon after, most likely due to the cleft palate defect (n = 4 for each genotype examined by serial frontal sections at E16.5). In addition, 35 out of 50 E18.5 or newborn $Alx1^{del/del}$ pups examined showed open eyelid unilaterally (**Figures 2B,D**). Analysis of skeletal preparations revealed that $Alx1^{del/del}$ embryos had hypoplastic premaxilla and presphenoid bone, and malformed palatal processes (**Figures 2E,F**) (n = 5 for each genotype). Histological analyses of E16.5 $Alx1^{del/del}$ embryos and control littermates showed that, in addition to cleft palate defect, the $Alx1^{del/del}$ embryos had disruptions of nasal cartilages (**Figures 2G,H**) (n = 4 for each genotype). No neural tube defect has been detected in over 200 $Alx1^{del/del}$ embryos analyzed in the C57BL/6N background.

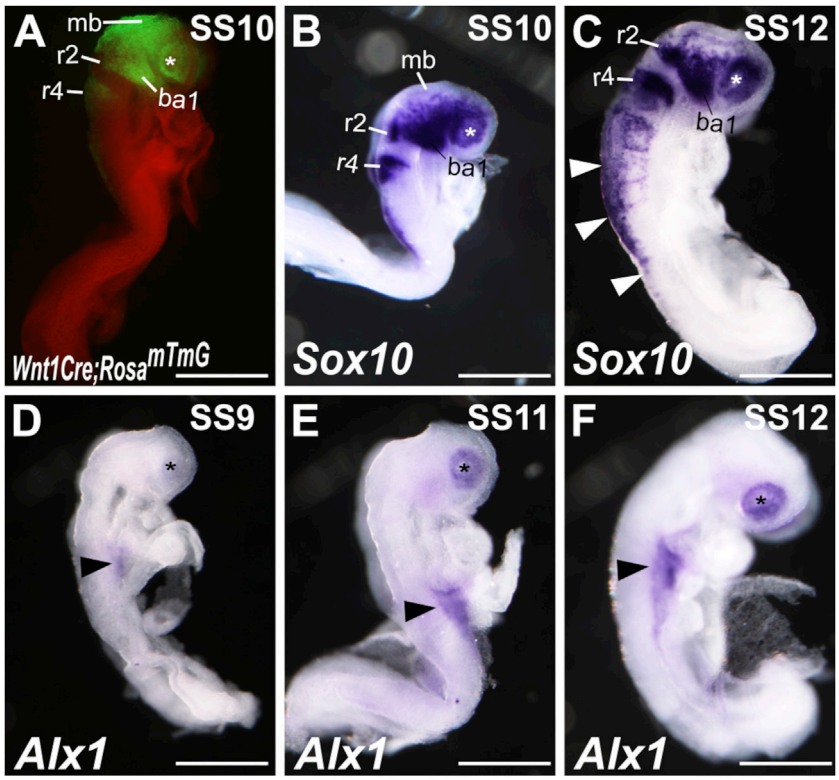

FIGURE 3 | *Alx1* expression during early craniofacial development. **(A)** Lateral view of a *Wnt1-Cre;Rosa26*^{mTmG} embryo at somite stage (SS)10 showing GFP (green) labeled dorsal midbrain neuroepithelium and cranial neural crest cells. **(B, C)** Lateral views of wildtype SS10 **(B)** and SS12 **(C)** embryos showing the patterns of *Sox10* mRNA expression detected by whole mount *in situ* hybridization (blue/purple color). White arrowheads in **(C)** point to the *Sox10* expression in the trunk neural crest cells. **(D–F)** Lateral views of wildtype SS9 **(D)**, SS11 **(E)**, and SS12 **(F)** embryos showing the patterns of *Alx1* mRNA expression detected by whole mount *in situ* hybridization (blue/purple color). The asterisk in A-F mark the location of the optic placode. Arrowheads in **(D–F)** point to the *Alx1* expression in the lateral plate mesoderm. Scale bar, 500 μm. ba1, branchial arch 1; mb, midbrain; r2, rhombomere 2; r4, rhombomere 4.

We outcrossed the $Alx1^{del/+}$ mice to 129/S6 inbred mice, a subline derived from the original 129/SvEv inbred strain (Simpson et al., 1997) that was used to analyze the $Alx1^{tm1Crm}$ allele (Zhao et al., 1996), for two generations and then intercrossed the N2 $Alx1^{del/+}$ male and female mice to analyze $Alx1^{del/del}$ pups in the 129 X C57BL/6 hybrid background. Only 5 of 48 (~10%) $Alx1^{del/del}$ embryos harvested from E16.5 to E18.5 in this hybrid background displayed an exencephaly phenotype (**Supplementary Figures S2A–C**). While the frequency of $Alx1^{del/del}$ embryos exhibiting anterior neural tube defect in this study is low, these results confirm that loss of *Alx1* function causes a genetic background-dependent defect in anterior neural tube closure in mice. The $Alx1^{del/del}$ embryos with exencephaly showed more severe ocular defect but fused secondary palate (n = 5), whereas cleft palate was observed in all E16.5 or older $Alx1^{del/del}$ embryos that did not have exencephaly and subjected to examination of palate morphology (n = 16) (**Supplementary Figures S2E,F**). All $Alx1^{del/del}$ pups in the 129 X C57BL/6 hybrid background exhibited similar frontonasal defects as in the C57BL/6N inbred background, including flattened nasal bridge, midline notching of the upper lip, and disruption of nasal cartilages (**Supplementary Figures S2A–F**). These midfacial defects in $Alx1^{del/del}$ mice closely recapitulate the midfacial developmental defects in *ALX*-related patients.

Alx1 is Expressed in the CNCC-Derived Mesenchyme of the LNP and MNP as Well as in the Periocular Mesenchyme

To understand the cellular mechanism of ALX1 function in frontonasal and ocular development, we analyzed the patterns of *Alx1* mRNA expression during early CNCC development. Previous lineage tracing and single-cell RNA sequencing (scRNA-seq) studies have shown that CNCCs first initiate delamination from the anterior neural plate border at about 4-somite stage (SS4) in mouse embryos and migrate to the facial prominences by SS8–SS10 (Yoshida et al., 2008; Zalc et al., 2021). At SS10, the *Wnt1-Cre;Rosa26*$^{mTmG/+}$ mouse embryos, in which all CNCCs as well as Wnt1-expressing dorsal mid- and hindbrain neuroepithelial cells were genetically labeled by the expression of green fluorescent protein (GFP), clearly showed CNCCs populating the periocular region and the first branchial arches (**Figure 3A**). *In situ* hybridization analysis also showed strong expression of the *Sox10* mRNAs, a marker of pluripotent

neural crest cells, in the CNCCs populating the periocular region and first branchial arches in SS10 wildtype mouse embryos (**Figure 3B**). By SS12, in addition to expression in the CNCCs, *Sox10* mRNAs were detected in the trunk neural crest cells migrating ventrally from the dorsal neural tube region (**Figure 3C**). In contrast to the patterns of robust *Sox10* mRNA expression in migrating neural crest cells, the earliest *Alx1* mRNA expression in the cranial region of the mouse embryos was detected in the periocular region from SS9 to SS11 (**Figures 3D,E**). *Alx1* mRNA expression was not detected in migrating CNCCs lateral to the mid- and hindbrain tissues at these stages, in contrast to the GFP expression pattern in the *Wnt1-Cre;Rosa26*$^{mTmG/+}$ embryos and *Sox10* mRNA expression pattern in the wildtype embryos (compare **Figures 3D,E** with **Figures 3A,B**). At SS12, *Alx1* mRNA expression in neural crest cells was still restricted to the periocular region and was not detected in *Sox10*-expressing migrating neural crest cells in either the cranial or trunk regions by *in situ* hybridization analysis (Figure 3F, compared with **Figure 3C**).

To further clarify the patterns of *Alx1* expression during early CNCC development, we analyzed the scRNA-seq data of early CNCCs harvested from SS4 - SS10 mouse embryos that were recently reported by Zalc et al. (2021). This dataset provides an extremely deep whole transcriptome sequencing of the individual CNCCs around the time of active delamination from the anterior neural plate border and migration towards the early facial primordia, with the median number of over 6,500 detected genes per cell (Zalc et al., 2021). As shown in **Supplementary Figure S3A**, unsupervised clustering of this early CNCC scRNA-seq dataset clearly clustered the cells into six major groups, identified as the neuroepithelial and pre-delamination CNCC "precursors," the "migrating CNCCs," the "post-migratory CNCCs," cranial "placode" cells, "cranial mesoderm" cells, and "endothelial cells," respectively, according to their marker gene expression profiles (**Supplementary Figures S3A–L**; **Supplementary Table S1**). Whereas high levels of *Sox10* mRNA expression was detected in all migrating and post-migratory CNCCs, while *Foxd3* was highly expressed in the migrating CNCCs but down-regulated in post-migratory CNCCs in these samples (**Supplementary Figures S3D,E**), *Alx1* mRNA expression was mainly detected in post-migratory CNCCs harvested from SS8 and SS10 embryos, with low level of *Alx1* mRNAs detected in a subset of migrating CNCCs harvested from SS6 embryos (**Supplementary Figure S3G**). We also analyzed expression of *Alx3* and *Alx4* in this scRNA-seq dataset and found that expression of both *Alx3* and *Alx4* mRNAs was detected in a subset of post-migratory CNCCs harvested from SS10 embryos (**Supplementary Figures S3H,I**), indicating that expression of both *Alx3* and *Alx4* in the CNCC lineage was activated later than that of *Alx1*. Altogether, while the high sensitivity of the scRNA-seq analysis detected *Alx1* mRNA expression in a subset of migrating CNCCs that was not detected in our *in situ* hybridization analysis, these data consistently demonstrate that *Alx1* expression was activated after the onset of CNCC migration and that *Alx1* exhibited a more restricted pattern of expression than that of *Sox10* in CNCCs during early craniofacial development.

We next analyzed *Alx1* expression during frontonasal development from E8.75 to E10.5 (**Figures 4A–D**). Frontal views of the embryos showed that *Alx1* mRNAs were concentrated in the lateral regions of the FNP but absent from the anterior midline region overlying the developing forebrain at this developmental stage (**Figures 4B,D**). At E10.5, strong *Alx1* mRNA expression was detected in the MNP and LNP, with moderate levels of expression also detected in the distal region of the MxP directly adjacent to the LNP (**Figures 4E,F**). Immunofluorescent staining of serial sections from the E10.5 embryos showed that ALX1 protein was strongly expressed in the CNCC-derived periocular mesenchyme as well as in the mesenchyme of the LNP and MNP, but no ALX1 expression was detected in any of the epithelial tissues, such as the neural epithelium of the brain, optic cup, optic stalk, and the facial and nasal epithelium (**Figures 4G,H**). These data indicate that ALX1 primarily acts in the CNCCs to regulate frontonasal development.

Loss of *Alx1* function did not Affect CNCC Migration to the Facial Primordia but Disrupted Optic Stalk Morphogenesis

We next examined whether ALX1 is required for CNCC migration to the facial primordia by using the *Wnt1-Cre:Rosa26*^{mTmG} mediated genetic lineage tracing (Danielian et al., 1998; Muzumdar et al., 2007). As shown in **Figure 5**, similar patterns of GFP-labeled CNCCs in the frontonasal and periocular regions as well as in the branchial arches were observed in the control and *Alx1*$^{del/del}$ embryos at E9.5 and E10.5 (**Figures 5A–D**). For embryos examined at E10.5, lateral views of the head consistently detected smaller eyes in the *Alx1*$^{del/del}$ embryos but the contribution of GFP-labeled CNCCs in the nasal, maxillary, and mandibular processes appeared similar in the *Alx1*$^{del/del}$ embryo and control littermates (**Figures 5C,D**). To further verify that the frontonasal neural crest cells migrated normally to the FNP in the *Alx1*$^{del/del}$ embryos, we analyzed the expression of known frontonasal mesenchyme markers, *Alx3* and *Alx4,* and found that both were similarly expressed in the frontonasal prominence in the control and *Alx1*$^{del/del}$ littermates at E9.5 (**Figures 5E–H**). These results indicate that early migration of cranial neural crest cells to the FNP was not overtly affected in the *Alx1*$^{del/del}$ mouse embryos, which is consistent with our finding that *Alx1* expression was absent in early migrating CNCCs and was highly expressed in post-migratory periocular CNCCs and the frontonasal mesenchyme.

Since FND3 patients exhibited extreme microphthalmia and other ocular defects including eyelid coloboma and asymmetric optic nerves (Uz et al., 2010; Pini et al., 2020), we analyzed the ocular developmental defects in *Alx1*$^{del/del}$ embryos. In addition to open eyelids, we found that the *Alx1*$^{del/del}$ pups consistently exhibited smaller eyeballs but the inter-eye distance was not significantly different from wildtype littermates (**Supplementary Figures S1D,E**). Histological analysis of E16.5 embryos showed that the *Alx1*$^{del/del}$ mutants had deformed optic cup and optic stalk (**Figures 6A,B**) (n = 4 for each genotype).

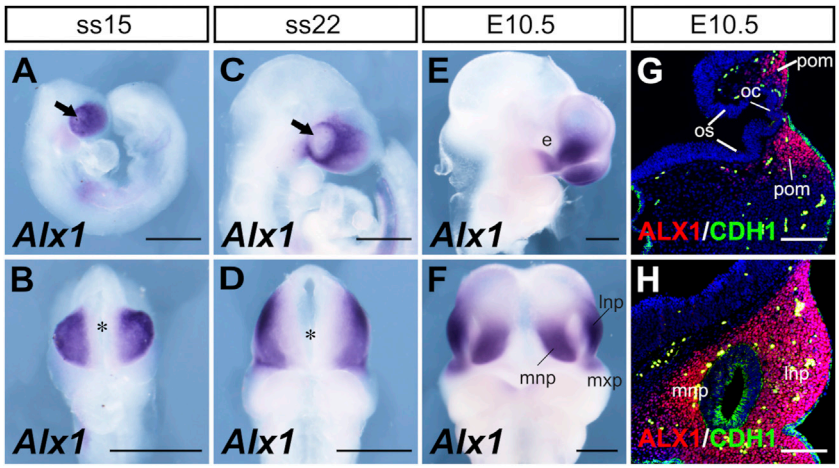

FIGURE 4 | Patterns of expression of *Alx1* during frontonasal development. Whole mount lateral **(A, C, E)** and frontal **(B, D, F)** views of the *Alx1* mRNA expression (blue/purple color) pattern in wildtype embryos at SS15 **(A, B)**, SS22 **(C, D)** and E10.5 **(E, F)**. Arrows in **(A, C)** point to the optic placode. Asterisk in **(B, D)** marks the position of the anterior neural ridge. **(G, H)** Representative frontal sections of E10.5 wildtype embryos showing immunofluorescent staining of ALX1 (red) and CDH1 (E-cadherin) (green) proteins, respectively, in the periocular **(G)** and frontonasal **(H)** tissues. DAPI counterstaining is shown in blue. Scale bars in **(A–F)** and **(G, H)** are 500 and 200 μm, respectively. e, eye; lnp, lateral nasal process; mnp, medial nasal process; mxp, maxillary process; oc, optic cup; os, optic stalk; pom, periocular mesenchyme.

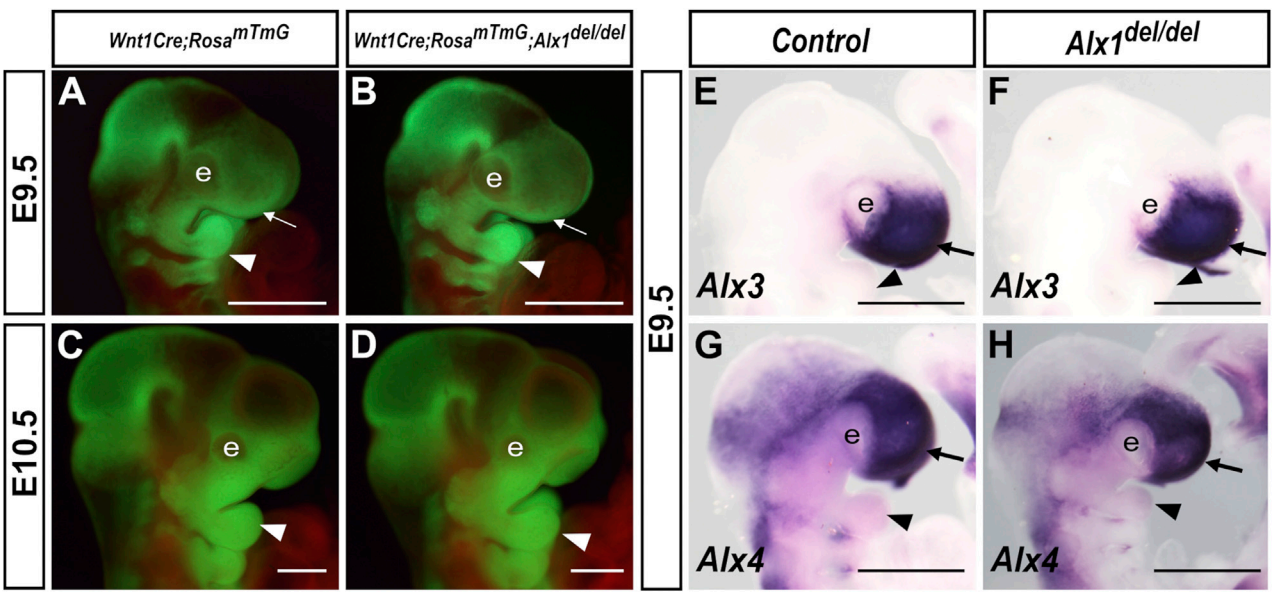

FIGURE 5 | Cranial neural crest migration to the facial primordia and expression of frontonasal neural crest marker genes appeared normal in *Alx1*$^{del/del}$ embryos. **(A–D)** Representative lateral views of whole mount embryo heads showing GFP (green) labeled neural crest cells in the developing facial primordia from *Wnt1-Cre;Rosa26*$^{mTmG/+}$ **(A, C)** and *Wnt1-Cre;Rosa26*$^{mTmG/+}$;*Alx1*$^{del/del}$ **(B, D)** embryos at E9.5 **(A, B)**, and E10.5 **(C, D)**. White arrow in A and B points to the frontonasal prominence, whereas the white arrowhead in **(A–D)** points to the mandibular arch. **(E–H)** Lateral views of whole mount embryo heads showing expression (blue/purple color) of *Alx3* **(E, F)** and *Alx4* **(G, H)** mRNAs in control **(E, G)** and *Alx1*$^{del/del}$ embryos **(F, H)** at E9.5. Arrow in E-H points to the frontonasal prominence, whereas the arrowhead points to the mandibular arch. e, eye. Scale bars, 500 μm.

During early eye development, invagination of the optic vesicle results in the formation of asymmetric optic cup with a ventral groove, called the optic fissure, at the ventral side of the optic cup and optic stalk (Tao and Zhang, 2014). From E10.5 to E12.5 in mouse embryogenesis, as the distance between the ventral diencephalon and optic cup increases, the optic stalk epithelium extends along both the medial-lateral and dorsal-ventral axes and changes from an initially 10–12-cell thick neuroblastic epithelial layer to a 1-2-cell thick bilayered epithelial structure around the proximally projected retinal

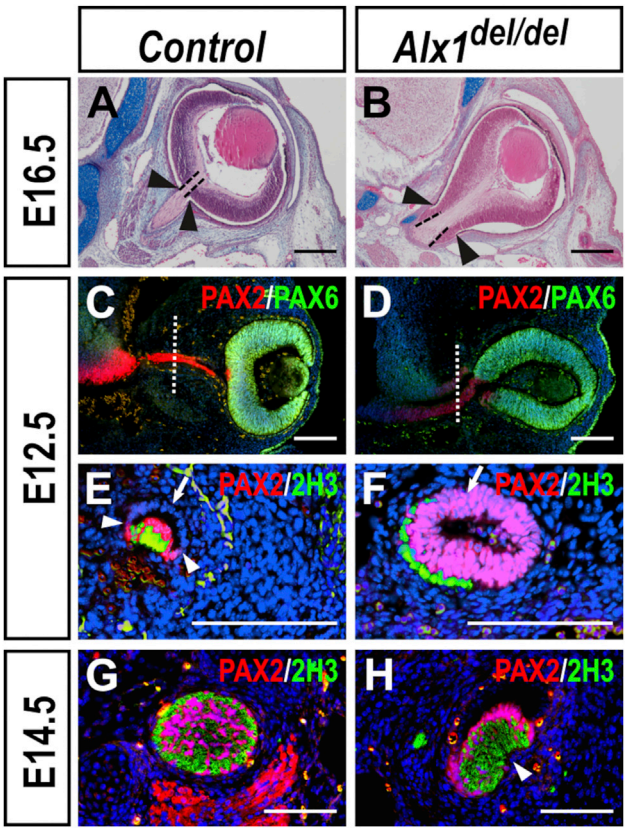

FIGURE 6 | Ocular developmental defects in *Alx1*$^{del/del}$ embryos. **(A, B)** Frontal sections of control **(A)** and *Alx1*$^{del/del}$ **(B)** embryo heads at E16.5. Dashed lines in **(A, B)** mark the exit of the optic nerve from the optic cup, whereas arrowheads point to the proximal boundary of the retinal pigment epithelium. **(C, D)** Immunofluorescent detection of PAX2 (red) and PAX6 (green) in frontal sections of control **(C)** and *Alx1*$^{del/del}$ **(D)** embryo heads at E12.5. White dotted lines in **(C, D)** indicate the corresponding plane of sagittal sections shown in Panels **(E, F)**, respectively. **(E–H)** Immunofluorescent detection of PAX2 (red) and neurofilament in the retinal ganglion axons recognized by the 2H3 monoclonal antibody (green) in sagittal sections through the middle of optic stalk in control **(E, G)** and *Alx1*$^{del/del}$ **(F, H)** embryos at E12.5 **(E, F)** and E14.5 **(G, H)**. White arrowheads in **(E)** point to the boundary of PAX2 expression in the ventral region of the optic stalk epithelium in the control embryo whereas the white arrows in **(E, F)** point to the dorsal region of the optic stalk epithelium. Note that both the PAX2-positive ventral region and the PAX2-negative dorsal/outer layer of the optic epithelium in the E12.5 control embryo **(E)** is 1-2 cell thick and the bilayered optic stalk epithelium wraps around the retinal ganglion axons (green), with the ventral optic fissure still open. In contrast, the optic stalk epithelium in the E12.5 *Alx1*$^{del/del}$ embryo **(F)** is 4-6-cell thick and failed to wrap around the retinal ganglion axons (green). White arrowhead in **(H)** points failure of optic fissure closure in the E14.5 *Alx1*$^{del/del}$ embryo. Scale bars in **(A, B)** and **(C–H)** are 400 and 200 μm, respectively.

ganglion axons in the optic groove (Evans and Gage, 2005). To better understand the ocular developmental defects in the *Alx1*$^{del/del}$ embryos, we analyzed the patterns of molecular marker expression for the optic cup, optic stalk, and axonal neurofilament in serial sections through the developing optic stalk. At E12.5, while the optic cup and optic stalk neuroepithelia were marked by expression of PAX6 and PAX2, respectively, in

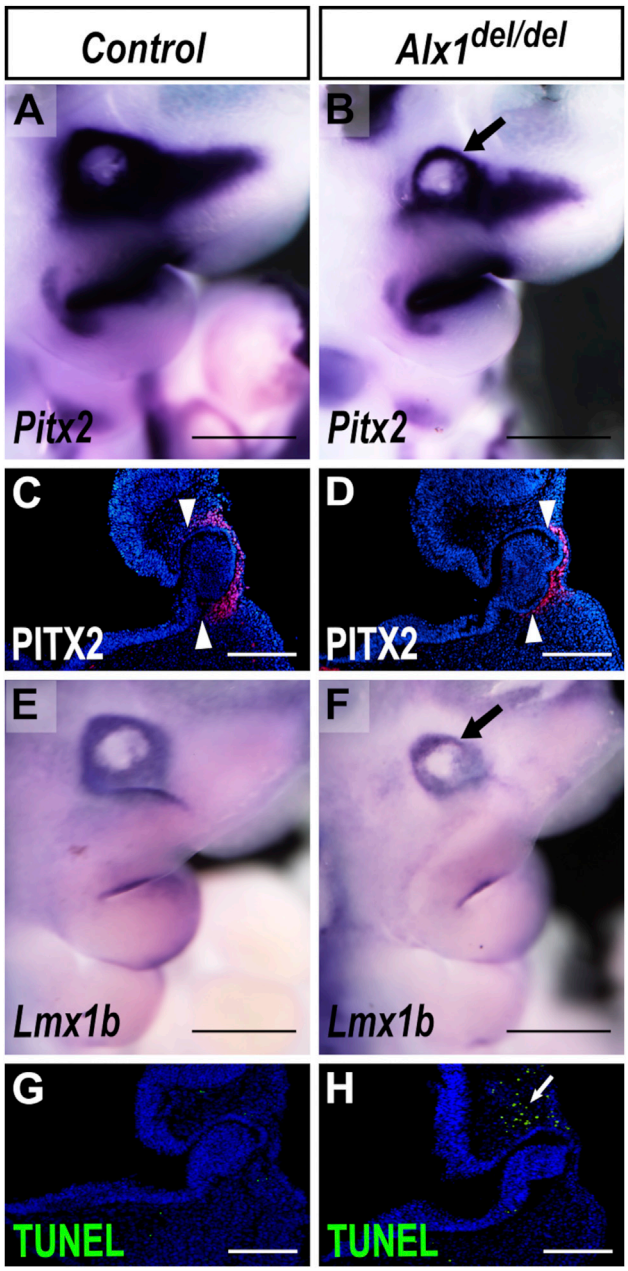

FIGURE 7 | Altered patterns of gene expression and increased apoptosis of the periocular mesenchyme in *Alx1*$^{del/del}$ embryos. **(A, B)** Lateral views of whole mount embryo heads showing *Pitx2* mRNA expression (blue/purple color) in control **(A)** and *Alx1*$^{del/del}$ **(B)** embryos at E10.5. Arrow in **(B)** points to the reduction in the domain of *Pitx2* expression in the periocular region in *Alx1*$^{del/del}$ embryos. **(C, D)** Representative frontal sections of E10.5 embryo heads showing immunofluorescent staining of PITX2 protein (red) in the periocular mesenchyme in wildtype **(C)** and *Alx1*$^{del/del}$ **(D)** embryos. White arrowheads in **(C, D)** point to the restricted domain of PITX2 expression in control and *Alx1*$^{del/del}$ embryos, respectively. **(E, F)** Lateral views of whole mount embryo heads showing *Lmx1b* expression (blue/purple color) in control **(E)** and *Alx1*$^{del/del}$ **(F)** embryos at E10.5. Arrow in **(F)** points to the reduction in the domain of *Lmx1b* expression in the *Alx1*$^{del/del}$ embryo. **(G, H)** Representative frontal sections of E10.5 embryo heads showing TUNEL staining (green) in the periocular mesenchyme in wildtype **(G)** and *Alx1*$^{del/del}$

(*Continued*)

FIGURE 7 | (H) embryos. White arrow in **(H)** points to the domain of cell death detected by TUNEL assay in the *Alx1*$^{del/del}$ embryo. Scale bars in **(A, B, E, F)** are 500 μm. Scale bars in **(C, D, G, H)** are 200 μm.

both the control and *Alx1*$^{del/del}$ littermates, the optic cup was abnormally extended along the medial-lateral axis in the *Alx1*$^{del/del}$ embryos compared with the control embryos (**Figures 6C,D**) (n = 6 for each genotype). In addition, while the optic stalk epithelium in the E12.5 control embryos had thinned out to a 1–2-cell thick bilayered epithelial structure around the retinal ganglion axons (positive for 2H3 immunostaining) in the optic groove, with only the ventral/inner layer of the optic stalk epithelium expressing PAX2 (**Figure 6E**) (n = 3), the optic stalk epithelium in the *Alx1*$^{del/del}$ littermates remained as an epithelial tube, with a central lumen surrounded by a 4-6-cell thick PAX2+ epithelium, connecting the ventral diencephalon to the optic cup (**Figures 6D,F**), and with the retinal ganglion axons lying outside of the optic stalk (**Figure 6F**) (n = 3). By E14.5, the PAX2+ cells of the optic stalk had delaminated and integrated with the retinal ganglion axons, forming the organized optic nerve bundle in the control embryos (**Figure 6G**) (n = 3). In the E14.5 *Alx1*$^{del/del}$ embryos, however, the PAX2+ optic stalk cells and the retinal ganglion axons remained largely segregated, with the PAX2+ epithelium partly wrapping around the nerve fibers (**Figure 6H**) (n = 3). These results indicate that ALX1 function is required for optic stalk and optic nerve morphogenesis in mice.

The defect in optic stalk morphogenesis in the *Alx1*$^{del/del}$ mutants appeared remarkably similar to the optic stalk morphogenesis defect previously reported in mice with neural crest lineage-specific inactivation of *Pitx2* (Evans and Gage, 2005). While *Pitx2* mRNAs were expressed in the periocular mesenchyme surrounding the developing eye in the wildtype embryos at E10.5, expression of *Pitx2* mRNAs in the periocular mesenchyme was apparently reduced in the E10.5 *Alx1*$^{del/del}$ embryos (**Figures 7A,B**). Immunodetection of PITX2 protein revealed a domain-specific loss of PITX2 protein expression in the periocular mesenchyme surrounding the optic cup (**Figures 7C,D**). Furthermore, we found that expression of *Lmx1b*, another key ocular developmental regulator (Pressman et al., 2000), was also reduced in the periocular mesenchyme in the E10.5 *Alx1*$^{del/del}$ embryos in comparison with control littermates (**Figures 7E,F**). Since *Alx1* is expressed in the periocular neural crest cells but not in the optic stalk or optic cup epithelium (**Figures 4G,H**), these data suggest that ALX1 acts upstream of *Pitx2* and *Lmx1b* in the periocular neural crest cells to regulate eye development. In addition, we found that the *Alx1*$^{del/del}$ embryos consistently exhibited increased apoptosis of the periocular mesenchyme cells located dorsally to the optic cup at E10.5, compared with control littermates (**Figures 7G,H**) (n = 4 for each genotype). This regional loss of periocular mesenchyme during early eye development likely also contributed to the ocular defects in *Alx1*$^{del/del}$ mice.

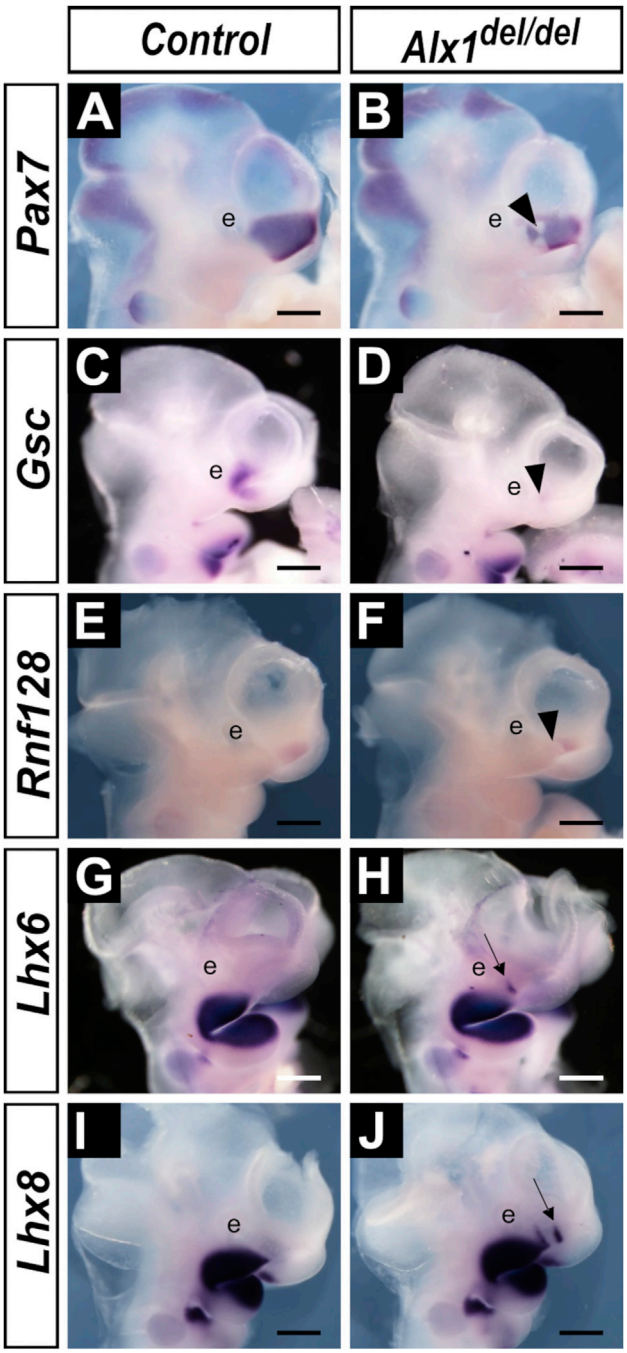

FIGURE 8 | *Alx1*$^{del/del}$ embryos exhibit altered patterns of gene expression in the developing lateral nasal processes. **(A–J)** Lateral views of whole mount embryo heads showing patterns of expression of *Pax7* **(A, B)**, *Gsc* **(C, D)**, *Rnf128* **(E, F)**, *Lhx6* **(G, H)**, and *Lhx8* **(I, J)** mRNAs in the control **(A, C, E, G, I)** and *Alx1*$^{del/del}$ **(B, D, F, H, J)** embryos at E10.5. Arrowhead in **(B, D, F)** points to the domain showing reduction and disruption of the *Pax7, Gsc,* and *Rnf128* expression, respectively, in the *Alx1*$^{del/del}$ embryos. Arrow in **(H, J)** points to the domain of ectopic *Lhx6* and *Lhx8* expression, respectively, in the lateral nasal processes in the *Alx1*$^{del/del}$ embryos. e, eye. Scale bars, 500 μm.

ALX1 Regulates Regional Patterning of the Frontonasal Mesenchyme

To characterize the developmental mechanism underlying the frontonasal defects in *Alx1*$^{del/del}$ embryos, we compared patterns of expression of several marker genes for distinct regions of the CNCC-derived frontonasal and jaw mesenchyme, respectively. First, we analyzed the expression of *Pax7*, which is critical for nasal cartilage formation (Mansouri et al., 1996). *Pax7* is specifically expressed in the lateral nasal mesenchyme at E10.5 in wildtype embryos (**Figure 8A**). In the *Alx1*$^{del/del}$ embryos, the *Pax7* expression domain is reduced and is disrupted at the caudal third of the lateral nasal process adjacent to the maxillary process (**Figure 8B**). Disruption or loss of caudal lateral nasal mesenchyme gene expression was further validated by comparing the patterns of expression of *Gsc* and *Rnf128* in the wildtype and *Alx1*$^{del/del}$ littermates (**Figures 8C–F**). Next, we analyzed whether the loss of LNP marker gene expression in the *Alx1*$^{del/del}$ embryos reflected a defect in patterning of the facial mesenchyme by comparing the expression of marker genes of the maxillary and mandibular mesenchyme in the *Alx1*$^{del/del}$ embryos and their littermates. Whereas *Lhx6* and *Lhx8* were strongly expressed in the maxillary and mandibular mesenchyme but absent in the lateral nasal mesenchyme in E10.5 wildtype embryos (**Figures 8G,I**), both *Lhx6* and *Lhx8* mRNAs were found ectopically expressed in the caudal region of the lateral nasal processes in the *Alx1*$^{del/del}$ embryos (**Figures 8H,J**). These data indicate that ALX1 plays a crucial role in patterning the lateral nasal mesenchyme.

ALX1 Function in Patterning the Frontonasal Mesenchyme is Partly Complemented by ALX4

Whereas the *Alx1*$^{del/del}$ embryos exhibited evident frontonasal defects including shortened snout, flattened nasal bridge, upper lip notching and premaxillary hypoplasia, *Alx4*$^{-/-}$ mouse embryos showed failure of eyelid closure but relatively normal frontonasal development (**Supplementary Figures S4A,D**), as previously reported (Qu et al., 1997; Curtain et al., 2015). The *Alx4*$^{-}$ allele (official allele name *Alx4*$^{lst-2J}$) used in this study originally arose in the C57BL/6J inbred background and carries a spontaneous 33.4 kb deletion of the 5′ and exon1 region of the *Alx4* gene (Curtain et al., 2015). In our mouse colony the *Alx4*$^{+/-}$ mice had been previously outcrossed to the wildtype CD1 mice. During this study of *Alx1*/*Alx4* compound mutants, we examined over 30 *Alx1*$^{del/del}$ embryos generated from *Alx1*$^{del/+}$;*Alx4*$^{+/-}$ intercrosses and did not detect any phenotypic difference from the *Alx1*$^{del/del}$ embryos analyzed in the C56BL/6 inbred background. However, deleting one allele of *Alx4* in the *Alx1*$^{del/del}$ embryos exacerbated the midfacial phenotype with widened and depressed nasal bridge, shortened philtrum, and further malformed premaxilla in the *Alx1*$^{del/del}$*Alx4*$^{+/-}$ embryos (**Supplementary Figures S4B,E**). Furthermore, *Alx1*$^{del/del}$*Alx4*$^{-/-}$ double homozygous mutants exhibited a wide-open midline facial cleft (**Supplementary Figures S4C,F**). These data indicate that, while ALX1 function is essential for frontonasal development, ALX4 partly complements ALX1 function in frontonasal morphogenesis.

We next investigated whether ALX4 plays a complementary role to ALX1 in the patterning of the LNP mesenchyme. Compared with the patchy reduction of *Pax7* expression in the caudal region of the LNP in the E10.5 *Alx1*$^{del/del}$ embryos (**Figures 8A,B**), E10.5 *Alx1*$^{del/del}$*Alx4*$^{+/-}$ embryos exhibited a clear loss of *Pax7* expression from the caudal region of the LNP and *Alx1*$^{del/del}$*Alx4*$^{-/-}$ embryos exhibited a much-reduced domain of *Pax7* expression in the LNP (**Figures 9A–F**). In a mirror image pattern to the loss of *Pax7* mRNA expression in the caudal region of the LNP, both *Lhx6* and *Lhx8* exhibited enhanced ectopic expression in the caudal region of the LNP in the E10.5 *Alx1*$^{del/del}$*Alx4*$^{+/-}$ embryos and further expanded domain of ectopic expression in the LNP in the *Alx1*$^{del/del}$*Alx4*$^{-/-}$ embryos (**Figures 9G–R**) compared with the patterns of expression in the control and *Alx1*$^{del/del}$ embryos (**Figures 8G–J**). Furthermore, the *Alx1*$^{del/del}$*Alx4*$^{-/-}$ embryos exhibited ectopic activation of *Lhx6* and *Lhx8* expression in the MNP as well (**Figures 9L,R**). These data indicate that ALX1 plays a critical, predominant role in patterning the lateral nasal mesenchyme with ALX4 partly complementing its function for determining the frontonasal mesenchyme identity.

DISCUSSION

Although a decade has passed since pathogenic mutations in each of the *ALX* family genes *ALX1*, *ALX3*, and *ALX4*, were first reported in FND3, FND1, and FND2 patients, respectively (Kayserili et al., 2009; Twigg et al., 2009; Uz et al., 2010), the cellular and molecular mechanisms involving the ALX transcription factors in frontonasal development remain largely unresolved. FND3 patients exhibited severe frontonasal hypoplasia, microphthalmia, and cleft lip and palate (Uz et al., 2010; Pini et al., 2020), whereas FND1 and FND2 patients displayed milder but distinctive midfacial defects including hypertelorism with ptosis or blepharophimosis, depressed nasal bridge with absent or bifid nasal tip, cleft nasal alae, midline notching of the upper lip, and cranium bifidum (Kayserili et al., 2009; Twigg et al., 2009; Farlie et al., 2016). In this study, we generated mice carrying a deletion of exon-2 of the *Alx1* gene and demonstrated that the *Alx1*$^{del/del}$ mice recapitulate many of the craniofacial defects reported in *ALX*-related FND patients, including eye defects, midfacial hypoplasia with disruption of the nasal cartilages, notching of the upper lip, and cleft palate. Our analyses of the *Alx1*$^{del/del}$ mouse embryos revealed previously unknown roles of ALX1 in regulating regional specification of the CNCC-derived frontonasal mesenchyme. In addition to generating an excellent animal model for understanding the pathogenic mechanisms underlying *ALX1*-related FNDs, these studies provide novel insights into the mechanisms underlying frontonasal patterning during embryonic development of the craniofacial region.

One of the characteristic features of FND is ocular hypertelorism (Sedano et al., 1970; Twigg et al., 2009), also known as orbital hypertelorism, with both terms used to

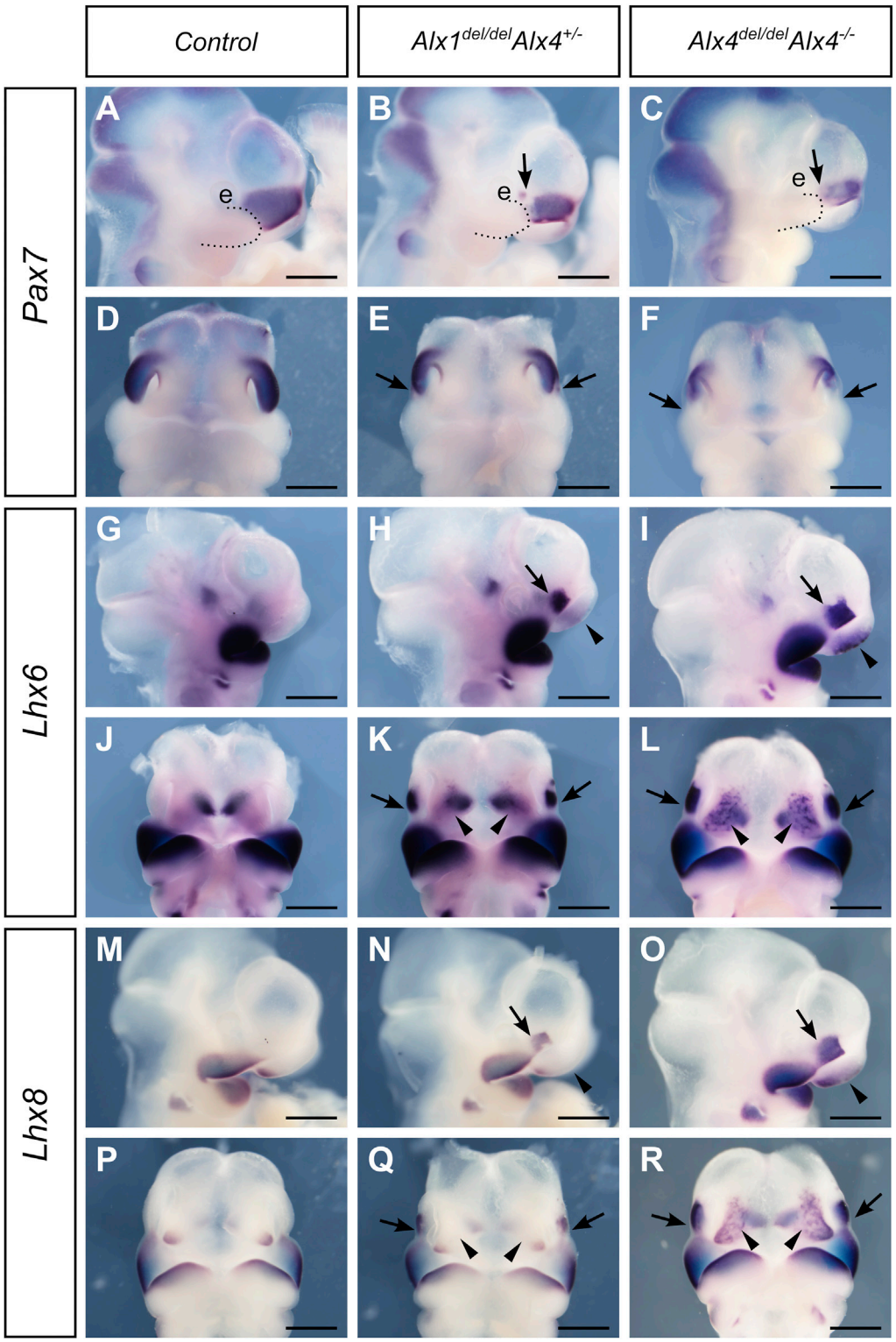

FIGURE 9 | ALX4 partly complements ALX1 function in regulating frontonasal development. Lateral **(A–C)** and frontal **(D–F)** views of whole mount embryo heads showing patterns of *Pax7* mRNA expression in the control **(A, D)**, *Alx1*$^{del/del}$*Alx4*$^{+/-}$ **(B, E)**, and *Alx1*$^{del/del}$*Alx4*$^{-/-}$ **(C, F)** embryos at E10.5. Arrow points to the domain of reduced *Pax7* expression in the lateral nasal process of the *Alx1*$^{del/del}$*Alx4*$^{+/-}$ **(B, E)** and *Alx1*$^{del/del}$*Alx4*$^{-/-}$ **(C, F)** embryos, respectively. **(G–L)** Lateral **(G–I)** and frontal **(J–L)** views of whole mount embryo heads showing patterns of *Lhx6* mRNA expression in the control **(G, J)**, *Alx1*$^{del/del}$*Alx4*$^{+/-}$ **(H, K)**, and *Alx1*$^{del/del}$*Alx4*$^{-/-}$ **(I, L)** embryos at E10.5. Arrows and arrowheads point to the domain of ectopic *Lhx6* expression in the lateral and medial nasal processes, respectively, in the in the *Alx1*$^{del/del}$*Alx4*$^{+/-}$ **(H,** (*Continued*)

FIGURE 9 | K) and *Alx1*$^{del/del}$*Alx4*$^{-/-}$ **(I, L)** embryos. **(M–R)** Lateral **(M–O)** and frontal **(P–R)** views of whole mount embryo heads showing patterns of *Lhx8* mRNA expression in the control **(M, P)**, *Alx1*$^{del/del}$*Alx4*$^{+/-}$ **(N, Q)**, and *Alx1*$^{del/del}$*Alx4*$^{-/-}$ **(O, R)** embryos at E10.5. Arrows and arrowheads point to the domain of ectopic *Lhx8* expression in the lateral and medial nasal processes, respectively, in the *Alx1*$^{del/del}$*Alx4*$^{+/-}$ **(N, Q)** and *Alx1*$^{del/del}$*Alx4*$^{-/-}$ **(O, R)** embryos. e, eye. Scale bars, 500 μm.

describe widely spaced eyes (Babbs et al., 2011; Sharma, 2014). Ocular hypertelorism is not a disease in and of itself, but rather a physical finding in many craniofacial syndromes, including FNDs and several craniosynostotsis syndromes (Cohen et al., 1995). During prenatal development, the relative position of the eyes changes dramatically, from formation of the optic cup at the lateral sides of the embryonic human head at about 180° from each other in the fifth week of gestation to the frontally located eyes with about a 70° angle between the bilateral optic nerves at the optic chiasm at birth, primarily due to the dramatic growth and expansion of the brain and neurocranium (Cohen et al., 1995). During early postnatal years, although the distance between the orbits increases as the head growth continues, the optic angle further decreases to 68° in adults (Cohen et al., 1995). Compared to humans, the animal models commonly used for craniofacial development studies, including chick and mouse, would be considered naturally extremely hyperteloric as their eyes are laterally positioned. The exact pathogenic mechanisms underlying ocular hypertelorism remain unclear. Several theories of pathogenesis have been suggested, including disruption of nasal capsule formation resulting in the primitive brain vesicle filling the facial midline space and preventing medial migration of the orbits, median facial cleft that disrupts medial integration and causes morphokinetic arrest, early ossification of the lesser wings of the sphenoid bone that fixes the orbits in fetal positions, and premature closure of cranial sutures preventing orbital migration and development (Cohen et al., 1995; Sharma, 2014). The *Alx1*$^{del/del}$ mice exhibited flat and widened nasal bridge, disruption of nasal cartilage formation, notching of the upper lip and cleft palate, but the inter-eye distance was not significantly different from control littermates. The lack of a true ocular hypertelorism phenotype in the *Alx1*$^{del/del}$ mice primarily reflects the differences in the medializing morphogenetic movement of the orbits during mouse and human craniofacial development and does not diminish the value of the *Alx1*$^{del/del}$ mice as an animal model for understanding the molecular and developmental mechanisms underlying FND.

FND3 patients exhibited varying ocular defects including anophthalmia, extreme microphthalmia, and asymmetric optic nerves (Uz et al., 2010; Pini et al., 2020). We found that *Alx1* is expressed in the periocular neural crest cells and not in the optic cup or optic stalk epithelium, but *Alx1*$^{del/del}$ embryos exhibited disruption of optic stalk morphogenesis. The morphological and cellular defects in optic stalk morphogenesis in the *Alx1*$^{del/del}$ embryos were remarkably similar to the optic stalk defects in mouse embryos with neural crest-specific deletion of *Pitx2* (Evans and Gage, 2005). We found that *Pitx2* expression was reduced in the periocular neural crest cells in the *Alx1*$^{del/del}$ embryos at E10.5. Expression of *Lmx1b* was also reduced in the periocular neural crest cells in the *Alx1*$^{del/del}$ embryos, suggesting that *Alx1* is involved in the maintenance or activation of periocular neural crest differentiation program and that the optic stalk defect resulted from a cell non-autonomous function of ALX1 in the periocular neural crest cells.

A previous study of *alx1* morpholino-treated zebrafish embryos showed that *alx1* knockdown inhibited frontonasal CNCC migration and caused catastrophic disruption of facial cartilage formation, which led to the conclusion that ALX1-related FND results from defective CNCC migration (Dee et al., 2013). However, recent reports showed that most *alx1*-null zebrafish mutants developed into adults with no obvious developmental defects (Pini et al., 2020; Mitchell et al., 2021). It has been shown that neural crest migration and survival in zebrafish embryos are susceptible to morpholino-induced artifacts (Boer et al., 2016). Thus, whether ALX1 plays a critical role in CNCC migration requires further validation. Dee et al. (2013) reported that *alx1* expression was activated in the rostral CNCC precursor cells in SS5 zebrafish embryos whereas CNCC migration did not begin until after SS10 (Dee et al., 2013). However, analysis of a recently reported scRNA-seq dataset for early CNCCs from SS4 to SS10 mouse embryos (Zalc et al., 2021) indicates that *Alx1* expression was initially activated in a subset of migrating CNCCs after their onset of migration to the facial primordia. Our analysis of the genetically labeled CNCCs in the *Alx1*$^{del/del}$ and control embryos did not detect any overt changes in CNCC distribution in the early facial primordia at E9.5. However, our results have not ruled out the possibility that loss of function of *Alx1* might have subtle effects on CNCC migration in the periocular or frontonasal regions that requires more sensitive detection methods to uncover. On the other hand, our analyses of the *Alx1*$^{del/del}$ embryos identified a previously unknown role of ALX1 in regulating the regional patterning of the neural crest-derived frontonasal mesenchyme. Whereas *Pax7* and *Rnf128* were specifically expressed in the LNP mesenchyme and *Lhx6* and *Lhx8* were specifically expressed in the maxillary and mandibular mesenchyme in wildtype mouse embryos at E10.5, *Alx1*$^{del/del}$ embryos exhibited a loss of *Pax7* expression and concomitant ectopic expression of *Lhx6* and *Lhx8* in the LNP domain adjacent to the maxillary processes. *Pax7* deficient mice exhibited nasal cartilage and capsule defects (Mansouri et al., 1996). Thus, the loss of *Pax7* expression could account for the defect of nasal cartilage differentiation in the *Alx1*$^{del/del}$ embryos at later stages. Lhx6 and Lhx8 are critical regulators of maxillary, palate, and tooth development (Zhao et al., 1999; Denaxa et al., 2009; Cesario et al., 2015). The ectopic activation of *Lhx6* and *Lhx8* expression in the embryonic LNP likely also contributes to the frontonasal defects in the *Alx1*$^{del/del}$ embryos at later stages.

Previous studies have uncovered molecular mechanisms patterning the CNCCs populating the pharyngeal arches (PA), but very little is known about how the most anterior CNCCs that populate the frontonasal region are patterned. After the neural

crest cells arrive at their destined locations, they respond to intrinsic and external signals to adopt their regional identities directed by the expression of combinations of transcription factors (Depew et al., 2002). PA1 and PA2 are defined by a HOX-code, wherein loss of *Hoxa2* function resulted in the loss of PA2 skeletal elements and mirror duplication of PA1 elements (Gendron-Maguire et al., 1993; Rijli et al., 1993). Within PA1, the maxillary-mandibular identity is defined by a DLX-code, wherein loss of *Dlx5/6* function resulted in a homeotic transformation of the mandible into the maxilla (Depew et al., 2002). Here, we show for the first time that ALX1/4 regulates the regional identity of the CNCC-derived frontonasal mesenchyme. Whereas DLX5/6 controls mandibular identity through activation of *Hand2* gene expression (Charité et al., 2001; Sato et al., 2008), our finding that the $Alx1^{del/del}Alx4^{-/-}$ embryos exhibited dramatically reduced *Pax7* expression in the LNP and concomitant ectopic *Lhx6* and *Lhx8* expression in both the LNP and MNP suggests that the ALX1/4 transcription factors act to regulate frontonasal mesenchyme identity by repressing expression of the jaw developmental regulators including LHX6 and LHX8. Further studies elucidating whether ALX1 directly represses expression of *Lhx6* and *Lhx8* expression and how ectopic *Lhx6/Lhx8* expression contributes to the frontonasal developmental defects in the $Alx1^{del/del}$ embryos will lead to clearer understanding of the molecular mechanisms regulating frontonasal development and patterning.

MATERIALS AND METHODS

Generation of $Alx1^{del}$ Mice

The sgRNA target sites were selected according to the on- and off-target scores from the CRISPR design web tool (http://CRISPOR.org) (Haeussler et al., 2016). The selected sgRNAs, targeting specific sequences in intron-1 (GTAAGATGTGGGTGGTAC T) and intron 2 (TTACTAAGTATAGGGACAGG) regions, respectively of the *Alx1* gene, were transcribed *in vitro* using the MEGAshorscript T7 kit (ThermoFisher), purified by using the MEGAclear Kit (ThermoFisher) and stored at −80°C. Individual sgRNA was incubated with CAS9 protein (ThermoFisher) at 37°C for 5 min to form the ribonucleoprotein complex and validated in a small batch of mouse zygotes following electroporation, *in vitro* culture to the blastocyst stage, and genotyping. The mixture of sgRNAs (50 ng/μL each) and CAS9 protein (150 ng/μL) was injected into the cytoplasm of fertilized eggs of the C57BL/6N inbred mice using a piezo-driven microinjection technique (Scott and Hu, 2019). Injected eggs were transferred on the same day into the oviductal ampulla of pseudopregnant CD-1 female mice at approximately 25 eggs per recipient. Pups were born and genotyped by PCR to identify founder mice and Sanger sequencing to verify the deletion of exon-2 and flanking sequences of the *Alx1* locus.

All animal work procedures were performed following the recommendations in the Guide for Care and Use of Laboratory Animals by the National Institutes of Health and approved by Institutional Animal Care and Use Committee (IACUC) at Cincinnati Children's Hospital Medical Center.

Mouse Breeding and Genotyping PCR

Heterozygous $Alx1^{del/+}$ mice were maintained in the C57BL/6N background. Embryos from the $Alx1^{del/+}$ intercrosses were collected at respective stages with the noon of the vaginal plug observed as E0.5. $Alx1^{del/+}$ intercross embryos were genotyped using the following primers, *Alx1* WT3F: GAAGCATTCTCA GCTAAGACTTG, *Alx1* WT3R: GCAGTATTACGTGCTGAA GTGGT, *Alx1* 3F: GGATTCATACCTCATTGCAGTC. For analysis in the 129 x C57BL/6 hybrid background, $Alx1^{del/+}$ male mice were bred with 129/S6 inbred females and the female progeny were back-crossed with 129/S6 males to generate N2 males and females, which were intercrossed and embryos were analyzed for skeletal preparations at E18.5 and histology at E16.5.

The $Alx4^{lst-2J/+}$ (referred here as $Alx4^{+/-}$; Jax Stock #000221) (Curtain et al., 2015) mice were obtained from the Jackson Laboratory. $Alx4^{+/-}$ mice had been outcrossed to wildtype CD1 mice in the past and had been maintained by crossing to C57BL/6N mice. For the generation and analysis of *Alx1*/*Alx4* compound mutants, $Alx1^{del/+}Alx4^{+/-}$ mice were intercrossed, and the embryos dissected at predetermined developmental stages for skeletal preparations or *in situ* hybridization analyses.

RT-PCR Analysis

PCR primers, forward 5′-GGAGACGCTGGACAATGAGT-3′ and reverse 5′-AGGCGAGTGAGAGTAAGGTG-3′, were used to amplify a 673 bp fragment from exon1 to exon4 of *Alx1* (NM_172553.4). RT-PCR products were gel-purified and sequence-verified at the DNA Core Facility in Cincinnati Children's Hospital Medical Center.

Western Blot Analyses

Western blot analyses were carried out as reported previously (Iyyanar and Nazarali, 2017; Okello et al., 2017). In brief, frontonasal and periocular tissues of E11.5 wild-type and $Alx1^{del/del}$ embryos, respectively, were lysed in RIPA buffer containing protease inhibitor cocktail. Proteins were quantified using a BCA assay kit (ThermoFisher) and 20 μg proteins were separated on a 4–20% mini-PROTEAN gradient gel (Bio-Rad) and blotted onto a PVDF membrane. Primary antibodies used were anti-ALX1 rabbit polyclonal (1:2000; Proteintech 16372-1-AP) and anti-β-tubulin mouse monoclonal (1:1000; DSHB E7).

Histology and Skeletal Preparations

For histological analyses, embryos were dissected at desired stages from timed pregnant mice, fixed in 4% paraformaldehyde, dehydrated through an ethanol series, embedded in paraffin, sectioned at 7 μm thickness, and stained with Alcian blue followed by hematoxylin and eosin. Skeletal preparations of E18.5 embryos were processed and stained with Alizarin red and Alcian blue as previously described (Ovchinnikov, 2009).

Quantitative Measurement of the Midfacial Defects in $Alx1^{del/del}$ Embryos

Snout length, philtrum length, diameter of the eyeballs, internostril and inter-eye distances were measured using ImageJ software and lateral or frontal view pictures of three pairs of

E16.5 control and *Alx1*$^{del/del}$ littermates. Data are represented as mean ± SEM. Statistical analysis was performed by unpaired t-test using the GraphPad Prism software. $p < 0.05$ was considered as statistically significant difference.

Immunofluorescent Staining and TUNEL Assay

Immunofluorescent staining was performed as previously described (Xu et al., 2016). The following primary antibodies were used: rabbit polyclonal anti-ALX1 (1:200; Proteintech 16372-1-AP), mouse monoclonal anti E-cadherin (BD Biosciences; 610,182), rabbit monoclonal anti-PAX2 (1:400; Abcam Ab79389), mouse monoclonal anti-PAX6 (1:25; DSHB AB_528,427), rabbit monoclonal anti-PITX2 (1:200; Abcam Ab221142), and mouse 2H3 monoclonal anti-neurofilament antibody (1:600; Developmental Studies Hybridoma Bank). Cell death was determined using a TUNEL assay kit in paraffin sections as per manufacturer's protocol (Promega).

Whole Mount *in situ* Hybridization

Whole mount *in situ* hybridization was carried out as previously described (Baek et al., 2011). Embryos were staged by counting somite numbers. For each probe analyzed, a minimum of three embryos of each genotype were analyzed and only probes that detected consistent patterns of expression in all samples were considered as valid results. The plasmid templates of the *Alx1*, *Gsc*, and *Rnf128* probes were amplified by PCR and cloned into pBSKII vector using the following primers, *Alx1* F: TATACG GGGTTTTCGAACCA, *Alx1* R: CACTCTGTTGCAGCCTCA AG; *Gsc* F: CTGTCCGAGTCCAAATCGCT, *Gsc* R: AGCATC GACAACATCCTGG; *Pax7* F: GGGTAGGGGGCACAGAGG CA, *Pax7* R: CCGGGCCAGCAGGTGGTTTC; *Pitx2* F: ACA TACTCATAGATGAGATG, *Pitx2* R: GAAATCAAAAAGGTC GAGTT; *Rnf128* F: CAACAGGACTGCCAATCAGG, *Rnf128* R: TGCACCGTAACCAGTTACCAA; *Sox10* F: CGAAGCTTC CATCTCACGACCCCAGTTT, *Sox10* R: CCGGATCCAGGC GAGAAGAAGGCTAGGT. The *Lhx6* and *Lhx8* (Grigoriou et al., 1998), and *Lmx1b* (Liu and Johnson, 2010) probes were received from published sources.

Analysis of CNCC scRNA-Seq Data

The scRNA-seq data for the SS4 - SS10 mouse embryonic CNCCs (Zalc et al., 2021) were obtained from the NCBI GEO database (accession number GSE162035). Data analysis was performed using the Seurat package (version 4.0.4, R version 4.0.3) (Hao et al., 2021). Data normalization was performed using the function SCTransform and the heterogeneity associated with ribosomal content and ERCC spike-in content were regressed out. Principal component analysis (PCA) was performed using the function RunPCA. Non-linear dimension reduction was carried out using the function RunUMAP utilizing the first 30 principal components (PCs). The function FindNeighbors was used to construct the Shared Nearest Neighbor (SNN) graph using the first 30 PCs and cell clustering was performed using the function FindClusters with resolution set to 0.2. The cell identities were determined based on their marker genes, which were identified using the FindAllMarkers function.

DATA AVAILABILITY STATEMENT

The raw data supporting the conclusion of this article will be made available by the authors, without undue reservation.

ETHICS STATEMENT

The animal study was reviewed and approved by Institutional Animal Care and Use Committee (IACUC) at Cincinnati Children's Hospital Medical Center.

AUTHOR CONTRIBUTIONS

YL and RJ designed research; PI, ZW, YL, and Y-CH performed research; PI, ZW, YL, and RJ analyzed data; PI and RJ wrote the manuscript; PI, ZW, YL, Y-CH, and RJ revised the paper.

FUNDING

This work was supported by the National Institutes of Health/ National Institute of Dental and Craniofacial Research (NIH/ NIDCR) (grant numbers R01DE027046 and R01DE029417).

ACKNOWLEDGMENTS

We thank the CCHMC Transgenic Animal and Genome Editing Core Facility for help with the generation of the *Alx1*^{del} mice. We thank Xiaochen Xue for assisting with the initial analysis of *Alx1/ Alx4* compound mutant mice.

SUPPLEMENTARY MATERIAL

The Supplementary Material for this article can be found online at: https://www.frontiersin.org/articles/10.3389/fcell.2022.777887/full#supplementary-material

REFERENCES

Babbs, C., Stewart, H. S., Williams, L. J., Connell, L., Goriely, A., Twigg, S. R. F., et al. (2011). Duplication of the EFNB1 Gene in Familial Hypertelorism: Imbalance in ephrin-B1 Expression and Abnormal Phenotypes in Humans and Mice. *Hum. Mutat.* 32 (8), 930–938. doi:10.1002/humu.21521

Baek, J.-A., Lan, Y., Liu, H., Maltby, K. M., Mishina, Y., and Jiang, R. (2011). Bmpr1a Signaling Plays Critical Roles in Palatal Shelf Growth and Palatal Bone Formation. *Dev. Biol.* 350 (2), 520–531. doi:10.1016/j.ydbio.2010.12.028

Beverdam, A., and Meijlink, F. (2001). Expression Patterns of Group-I Aristaless-Related Genes during Craniofacial and Limb Development. *Mech. Dev.* 107 (1-2), 163–167. doi:10.1016/s0925-4773(01)00450-6

Beverdam, A., Brouwer, A., Reijnen, M., Korving, J., and Meijlink, F. (2001). Severe Nasal Clefting and Abnormal Embryonic Apoptosis in Alx3/Alx4 Double Mutant Mice. *Development* 128 (20), 3975–3986. doi:10.1242/dev.128.20.3975

Boer, E. F., Jette, C. A., and Stewart, R. A. (2016). Neural Crest Migration and Survival Are Susceptible to Morpholino-Induced Artifacts. *PLoS One* 11 (12), e0167278. doi:10.1371/journal.pone.0167278

Brouwer, A., ten Berge, D., Wiegerinck, R., and Meijlink, F. (2003). The OAR/aristaless Domain of the Homeodomain Protein Cart1 Has an Attenuating Role *In Vivo*. *Mech. Dev.* 120 (2), 241–252. doi:10.1016/s0925-4773(02)00416-1

Cesario, J. M., Landin Malt, A., Deacon, L. J., Sandberg, M., Vogt, D., Tang, Z., et al. (2015). Lhx6andLhx8promote Palate Development through Negative Regulation of a Cell Cycle Inhibitor gene,p57Kip2. *Hum. Mol. Genet.* 24 (17), 5024–5039. doi:10.1093/hmg/ddv223

Charité, J., McFadden, D. G., Merlo, G., Levi, G., Clouthier, D. E., Yanagisawa, M., et al. (2001). Role of Dlx6 in Regulation of an Endothelin-1-dependent, dHAND Branchial Arch Enhancer. *Genes Dev.* 15 (22), 3039–3049. doi:10.1101/gad.931701

Cohen, M. M., Jr., Richieri-Costa, A., Guion-Almeida, M. L., and Saavedra, D. (1995). Hypertelorism: Interorbital Growth, Measurements, and Pathogenetic Considerations. *Int. J. Oral Maxillofac. Surg.* 24 (6), 387–395. doi:10.1016/s0901-5027(05)80465-5

Curtain, M., Heffner, C. S., Maddox, D. M., Gudis, P., Donahue, L. R., and Murray, S. A. (2015). A Novel Allele of Alx4 Results in Reduced Fgf10 Expression and Failure of Eyelid Fusion in Mice. *Mamm. Genome* 26 (3-4), 173–180. doi:10.1007/s00335-015-9557-z

Danielian, P. S., Muccino, D., Rowitch, D. H., Michael, S. K., and McMahon, A. P. (1998). Modification of Gene Activity in Mouse Embryos In Utero by a Tamoxifen-Inducible Form of Cre Recombinase. *Curr. Biol.* 8 (24), 1323–S2. doi:10.1016/s0960-9822(07)00562-3

Dee, C. T., Szymoniuk, C. R., Mills, P. E. D., and Takahashi, T. (2013). Defective Neural Crest Migration Revealed by a Zebrafish Model of Alx1-Related Frontonasal Dysplasia. *Hum. Mol. Genet.* 22 (2), 239–251. doi:10.1093/hmg/dds423

Denaxa, M., Sharpe, P. T., and Pachnis, V. (2009). The LIM Homeodomain Transcription Factors Lhx6 and Lhx7 Are Key Regulators of Mammalian Dentition. *Dev. Biol.* 333 (2), 324–336. doi:10.1016/j.ydbio.2009.07.001

Depew, M. J., Lufkin, T., and Rubenstein, J. L. R. (2002). Specification of Jaw Subdivisions by Dlx Genes. *Science* 298 (5592), 381–385. doi:10.1126/science.1075703

Evans, A. L., and Gage, P. J. (2005). Expression of the Homeobox Gene Pitx2 in Neural Crest Is Required for Optic Stalk and Ocular Anterior Segment Development. *Hum. Mol. Genet.* 14 (22), 3347–3359. doi:10.1093/hmg/ddi365

Farlie, P. G., Baker, N. L., Yap, P., and Tan, T. Y. (2016). Frontonasal Dysplasia: Towards an Understanding of Molecular and Developmental Aetiology. *Mol. Syndromol* 7 (6), 312–321. doi:10.1159/000450533

Gendron-Maguire, M., Mallo, M., Zhang, M., and Gridley, T. (1993). Hoxa-2 Mutant Mice Exhibit Homeotic Transformation of Skeletal Elements Derived from Cranial Neural Crest. *Cell* 75 (7), 1317–1331. doi:10.1016/0092-8674(93)90619-2

Grigoriou, M., Tucker, A. S., Sharpe, P. T., and Pachnis, V. (1998). Expression and Regulation of Lhx6 and Lhx7, a Novel Subfamily of LIM Homeodomain Encoding Genes, Suggests a Role in Mammalian Head Development. *Development* 125 (11), 2063–2074. doi:10.1242/dev.125.11.2063

Haeussler, M., Schönig, K., Eckert, H., Eschstruth, A., Mianné, J., Renaud, J.-B., et al. (2016). Evaluation of Off-Target and On-Target Scoring Algorithms and Integration into the Guide RNA Selection Tool CRISPOR. *Genome Biol.* 17 (1), 148. doi:10.1186/s13059-016-1012-2

Hao, Y., Hao, S., Andersen-Nissen, E., Mauck, W. M., 3rd, Zheng, S., Butler, A., et al. (2021). Integrated Analysis of Multimodal Single-Cell Data. *Cell* 184 (13), 3573–3587. doi:10.1016/j.cell.2021.04.048

Iyyanar, P. P. R., and Nazarali, A. J. (2017). Hoxa2 Inhibits Bone Morphogenetic Protein Signaling during Osteogenic Differentiation of the Palatal Mesenchyme. *Front. Physiol.* 8, 929. doi:10.3389/fphys.2017.00929

Jiang, R., Bush, J. O., and Lidral, A. C. (2006). Development of the Upper Lip: Morphogenetic and Molecular Mechanisms. *Dev. Dyn.* 235 (5), 1152–1166. doi:10.1002/dvdy.20646

Jiang, X., Rowitch, D. H., Soriano, P., McMahon, A. P., and Sucov, H. M. (2000). Fate of the Mammalian Cardiac Neural Crest. *Development* 127 (8), 1607–1616. doi:10.1242/dev.127.8.1607

Kayserili, H., Uz, E., Niessen, C., Vargel, I., Alanay, Y., Tuncbilek, G., et al. (2009). ALX4 Dysfunction Disrupts Craniofacial and Epidermal Development. *Hum. Mol. Genet.* 18 (22), 4357–4366. doi:10.1093/hmg/ddp391

Liu, P., and Johnson, R. L. (2010). Lmx1b Is Required for Murine Trabecular Meshwork Formation and for Maintenance of Corneal Transparency. *Dev. Dyn.* 239 (8), 2161–2171. doi:10.1002/dvdy.22347

Mansouri, A., Stoykova, A., Torres, M., and Gruss, P. (1996). Dysgenesis of Cephalic Neural Crest Derivatives in Pax7−/− Mutant Mice. *Development* 122 (3), 831–838. doi:10.1242/dev.122.3.831

McGonnell, I. M., Graham, A., Richardson, J., Fish, J. L., Depew, M. J., Dee, C. T., et al. (2011). Evolution of the Alx Homeobox Gene Family: Parallel Retention and Independent Loss of the Vertebrate Alx3 Gene. *Evol. Dev.* 13 (4), 343–351. doi:10.1111/j.1525-142X.2011.00489.x

Mitchell, J. M., Sucharov, J., Pulvino, A. T., Brooks, E. P., Gillen, A. E., and Nichols, J. T. (2021). The Alx3 Gene Shapes the Zebrafish Neurocranium by Regulating Frontonasal Neural Crest Cell Differentiation Timing. *Development* 148 (7), dev197483. doi:10.1242/dev.197483

Muzumdar, M. D., Tasic, B., Miyamichi, K., Li, L., and Luo, L. (2007). A Global Double-Fluorescent Cre Reporter Mouse. *Genesis* 45 (9), 593–605. doi:10.1002/dvg.20335

Okello, D. O., Iyyanar, P. P. R., Kulyk, W. M., Smith, T. M., Lozanoff, S., Ji, S., et al. (2017). Six2 Plays an Intrinsic Role in Regulating Proliferation of Mesenchymal Cells in the Developing Palate. *Front. Physiol.* 8, 955. doi:10.3389/fphys.2017.00955

O'Rahilly, R., and Müller, F. (2007). The Development of the Neural Crest in the Human. *J. Anat.* 211 (3), 335–351. doi:10.1111/j.1469-7580.2007.00773.x

Ovchinnikov, D. (2009). Alcian Blue/Alizarin Red Staining of Cartilage and Bone in Mouse: Figure 1. *Cold Spring Harb Protoc.* 2009 (3), pdb.prot5170. doi:10.1101/pdb.prot5170

Pini, J., Kueper, J., Hu, Y. D., Kawasaki, K., Yeung, P., Tsimbal, C., et al. (2020). ALX 1- Related Frontonasal Dysplasia Results from Defective Neural Crest Cell Development and Migration. *EMBO Mol. Med.* 12 (10), e12013. doi:10.15252/emmm.202012013

Pressman, C. L., Chen, H., and Johnson, R. L. (2000). LMX1B, a LIM Homeodomain Class Transcription Factor, Is Necessary for normal Development of Multiple Tissues in the Anterior Segment of the Murine Eye. *Genesis* 26 (1), 15–25. doi:10.1002/(sici)1526-968x(200001)26:1<15:aid-gene5>3.0.co;2-v

Qu, S., Niswender, K. D., Ji, Q., van der Meer, R., Keeney, D., Magnuson, M. A., et al. (1997). Polydactyly and Ectopic ZPA Formation in Alx-4 Mutant Mice. *Development* 124 (20), 3999–4008. doi:10.1242/dev.124.20.3999

Qu, S., Tucker, S. C., Zhao, Q., deCrombrugghe, B., and Wisdom, R. (1999). Physical and Genetic Interactions between Alx4 and Cart1. *Development* 126 (2), 359–369. doi:10.1242/dev.126.2.359

Rijli, F. M., Mark, M., Lakkaraju, S., Dierich, A., Dollé, P., and Chambon, P. (1993). A Homeotic Transformation Is Generated in the Rostral Branchial Region of the Head by Disruption of Hoxa-2, Which Acts as a Selector Gene. *Cell* 75 (7), 1333–1349. doi:10.1016/0092-8674(93)90620-6

Salazar-Ciudad, I., Garcia-fernández, J., and Solé, R. V. (2000). Gene Networks Capable of Pattern Formation: from Induction to Reaction-Diffusion. *J. Theor. Biol.* 205 (4), 587–603. doi:10.1006/jtbi.2000.2092

Sato, T., Kurihara, Y., Asai, R., Kawamura, Y., Tonami, K., Uchijima, Y., et al. (2008). An Endothelin-1 Switch Specifies Maxillomandibular Identity. *Proc. Natl. Acad. Sci.* 105 (48), 18806–18811. doi:10.1073/pnas.0807345105

Scott, M. A., and Hu, Y.-C. (2019). Generation of CRISPR-Edited Rodents Using a Piezo-Driven Zygote Injection Technique. *Methods Mol. Biol.* 1874, 169–178. doi:10.1007/978-1-4939-8831-0_9

Sedano, H. O., Michael Cohen, M., Jirasek, J., and Gorlin, R. J. (1970). Frontonasal Dysplasia. *J. Pediatr.* 76 (6), 906–913. doi:10.1016/s0022-3476(70)80374-2

Sharma, R. K. (2014). Hypertelorism. *Indian J. Plast. Surg.* 47 (3), 284–292. doi:10.4103/0970-0358.146572

Simpson, E. M., Linder, C. C., Sargent, E. E., Davisson, M. T., Mobraaten, L. E., and Sharp, J. J. (1997). Genetic Variation Among 129 Substrains and its Importance for Targeted Mutagenesis in Mice. *Nat. Genet.* 16 (1), 19–27. doi:10.1038/ng0597-19

Tao, C., and Zhang, X. (2014). Development of Astrocytes in the Vertebrate Eye. *Dev. Dyn.* 243 (12), 1501–1510. doi:10.1002/dvdy.24190

Twigg, S. R. F., Versnel, S. L., Nürnberg, G., Lees, M. M., Bhat, M., Hammond, P., et al. (2009). Frontorhiny, a Distinctive Presentation of Frontonasal Dysplasia Caused by Recessive Mutations in the ALX3 Homeobox Gene. *Am. J. Hum. Genet.* 84 (5), 698–705. doi:10.1016/j.ajhg.2009.04.009

Ullah, A., Kalsoom, U. E., Umair, M., John, P., Ansar, M., Basit, S., et al. (2017). Exome Sequencing Revealed a Novel Splice Site Variant in the ALX1 Gene Underlying Frontonasal Dysplasia. *Clin. Genet.* 91 (3), 494–498. doi:10.1111/cge.12822

Uz, E., Alanay, Y., Aktas, D., Vargel, I., Gucer, S., Tuncbilek, G., et al. (2010). Disruption of ALX1 Causes Extreme Microphthalmia and Severe Facial Clefting: Expanding the Spectrum of Autosomal-Recessive ALX-Related Frontonasal Dysplasia. *Am. J. Hum. Genet.* 86 (5), 789–796. doi:10.1016/j.ajhg.2010.04.002

Wu, E., Vargevik, K., and Slavotinek, A. M. (2007). Subtypes of Frontonasal Dysplasia Are Useful in Determining Clinical Prognosis. *Am. J. Med. Genet.* 143A (24), 3069–3078. doi:10.1002/ajmg.a.31963

Xu, J., Liu, H., Lan, Y., Aronow, B. J., Kalinichenko, V. V., and Jiang, R. (2016). A Shh-Foxf-Fgf18-Shh Molecular Circuit Regulating Palate Development. *Plos Genet.* 12 (1), e1005769. doi:10.1371/journal.pgen.1005769

Yoshida, T., Vivatbutsiri, P., Morriss-Kay, G., Saga, Y., and Iseki, S. (2008). Cell Lineage in Mammalian Craniofacial Mesenchyme. *Mech. Dev.* 125 (9-10), 797–808. doi:10.1016/j.mod.2008.06.007

Zalc, A., Sinha, R., Gulati, G. S., Wesche, D. J., Daszczuk, P., Swigut, T., et al. (2021). Reactivation of the Pluripotency Program Precedes Formation of the Cranial Neural Crest. *Science* 371 (6529), eabb4776. doi:10.1126/science.abb4776

Zhao, Q., Behringer, R. R., and de Crombrugghe, B. (1996). Prenatal Folic Acid Treatment Suppresses Acrania and Meroanencephaly in Mice Mutant for the Cart1 Homeobox Gene. *Nat. Genet.* 13 (3), 275–283. doi:10.1038/ng0796-275

Zhao, Y., Guo, Y.-J., Tomac, A. C., Taylor, N. R., Grinberg, A., Lee, E. J., et al. (1999). Isolated Cleft Palate in Mice with a Targeted Mutation of the LIM Homeobox Gene Lhx8. *Proc. Natl. Acad. Sci.* 96 (26), 15002–15006. doi:10.1073/pnas.96.26.15002

Conflict of Interest: The authors declare that the research was conducted in the absence of any commercial or financial relationships that could be construed as a potential conflict of interest.

Publisher's Note: All claims expressed in this article are solely those of the authors and do not necessarily represent those of their affiliated organizations, or those of the publisher, the editors, and the reviewers. Any product that may be evaluated in this article, or claim that may be made by its manufacturer, is not guaranteed or endorsed by the publisher.

frontiers in Cell and Developmental Biology

ORIGINAL RESEARCH
published: 01 February 2022
doi: 10.3389/fcell.2021.777652

Loss of *Foxd4* Impacts Neurulation and Cranial Neural Crest Specification During Early Head Development

Riley McMahon[1,2]*, *Tennille Sibbritt*[1], *Nadar Aryamanesh*[1], *V. Pragathi Masamsetti*[1,2] and *Patrick P. L. Tam*[1,2]*

[1]Embryology Research Unit, Children's Medical Research Institute, Sydney, NSW, Australia, [2]School of Medical Sciences, Faculty of Medicine and Health, The University of Sydney, Darlington, NSW, Australia

The specification of anterior head tissue in the late gastrulation mouse embryo relies on signaling cues from the visceral endoderm and anterior mesendoderm (AME). Genetic loss-of-function studies have pinpointed a critical requirement of LIM homeobox 1 (LHX1) transcription factor in these tissues for the formation of the embryonic head. Transcriptome analysis of embryos with gain-of-function LHX1 activity identified the forkhead box gene, *Foxd4,* as one downstream target of LHX1 in late-gastrulation E7.75 embryos. Our analysis of single-cell RNA-seq data show *Foxd4* is co-expressed with *Lhx1* and *Foxa2* in the anterior midline tissue of E7.75 mouse embryos, and in the anterior neuroectoderm (ANE) at E8.25 alongside head organizer genes *Otx2* and *Hesx1*. To study the role of *Foxd4* during early development we used CRISPR-Cas9 gene editing in mouse embryonic stem cells (mESCs) to generate bi-allelic frameshift mutations in the coding sequence of *Foxd4*. In an *in vitro* model of the anterior neural tissues derived from *Foxd4*-loss of function (LOF) mESCs and extraembryonic endoderm cells, expression of head organizer genes as well as *Zic1* and *Zic2* was reduced, pointing to a need for FOXD4 in regulating early neuroectoderm development. Mid-gestation mouse chimeras harbouring *Foxd4*-LOF mESCs displayed craniofacial malformations and neural tube closure defects. Furthermore, our *in vitro* data showed a loss of FOXD4 impacts the expression of cranial neural crest markers *Twist1* and *Sox9*. Our findings have demonstrated that FOXD4 is essential in the AME and later in the ANE for rostral neural tube closure and neural crest specification during head development.

Keywords: Foxd4, head development, anterior neuroectoderm, neural tube defects, cranial neural crest

OPEN ACCESS

Edited by:
Kerstin Feistel,
University of Hohenheim, Germany

Reviewed by:
Gabriel L. Galea,
University College London,
United Kingdom
Heather C. Etchevers,
INSERM U1251 Centre de Génétique Médicale de Marseille (MMG), France

***Correspondence:**
Riley McMahon
rmcmahon@cmri.org.au
Patrick P. L. Tam
ptam@cmri.org.au

Specialty section:
This article was submitted to Morphogenesis and Patterning, a section of the journal Frontiers in Cell and Developmental Biology

Received: *15 September 2021*
Accepted: *30 December 2021*
Published: *01 February 2022*

Citation:
McMahon R, Sibbritt T, Aryamanesh N, Masamsetti VP and Tam PPL (2022) Loss of Foxd4 *Impacts Neurulation and Cranial Neural Crest Specification During Early Head Development. Front. Cell Dev. Biol. 9:777652. doi: 10.3389/fcell.2021.777652*

INTRODUCTION

The head is the first major body part to form immediately following gastrulation in vertebrate embryos, arising from the anterior germ layer tissues. In mice, the anterior-posterior axis is polarized by the visceral endoderm cells that are relocated from the distal tip of the epiblast to become the anterior visceral endoderm (AVE) Perea-Gómez et al. (1999). The AVE is involved in inducing anterior neuroectoderm (ANE) identity in the anterior epiblast prior to the anterior mesendoderm (AME) tissue re-enforcing the identity (Thomas and Beddington, 1996; Kimura et al., 2000). The role of the AME tissue at late gastrulation is to antagonize the posteriorizing

signaling activity such as WNT and BMP (Arkell and Tam, 2012). Knock-out mouse models for key transcription factors *Lhx1* and *Foxa2,* expressed in both the AVE and AME, result in severe truncation of the embryonic head (Ang and Rossant, 1994; Shawlot and Behringer, 1995). The lack of *Lhx1* and *Foxa2* activity disrupts the formation of AME and notochord tissues, resulting in the loss of head precursor tissues (Kinder et al., 2003). Earlier work has identified many of the downstream targets of LHX1 in the AME are involved in the suppression of WNT signaling including *Gsc*, *Dkk1* and *Cer1* (Fossat et al., 2015; McMahon et al., 2019). To further study the potential target of LHX1 in the E7.75 mouse embryos, a conditional *Lhx1*-LOF model was used to identify the genes that are down-regulated with *Lhx1*-LOF (Sibbritt et al., 2018). Genes identified as potential targets of LHX1 include head organizer transcription factors *Hesx1* and *Otx2*, as well as *Foxd4*. *Hesx1* and *Otx2* are both expressed in the AME and ANE of early-head-fold stage (E7.75) embryos, *Hesx1* expression is then up-regulated in the forebrain, whilst *Otx2* is expressed in the midbrain of neurulation stage embryos (Simeone et al., 1993; Hermesz et al., 1996). Knockout of either genes resulted in a truncated head at early-organogenesis stage (Matsuo et al., 1995; Martinez-Barbera et al., 2000).

Foxd4 is a member of the forkhead/winged helix-box transcription factors that is expressed in the notochord, AME and ANE of mouse embryos (Kaestner et al., 1995). *Foxd4* has been previously identified as a downstream target of *Foxa2* and *Otx2*. In E7.75 embryos lacking *Foxa2* activity, *Foxd4* was only expressed in the anterior neurectoderm, and missing in the AME (Tamplin et al., 2008). Conversely, in E7.75 *Otx2*$^{-/-}$ embryos, the expression of *Foxd4* was restricted to the distal AME and absent from the ANE (Rhinn et al., 1998). *Foxd4* is highly conserved between vertebrate species including humans, mice, frogs and zebrafish (Odenthal and Nüsslein-Volhard, 1998; Neilson et al., 2012). It contains an N-terminal acidic blob (AB) domain, a 100-amino acid forkhead domain and a C-terminal Engrailed homology (Eh1) domain. In *Xenopus* the AB domain was shown to activate neural precursor genes *Gem* and *Zic2*, whilst the Eh1 domain acted as a transcriptional repressor of genes responsible for neural differentiation (*Sox1, Irx*) (Neilson et al., 2012). FOXD4 is required in the transition of the mouse embryonic stem cell (mESCs) from pluripotency to neuroectoderm precursor cells (Sherman et al., 2017), though the function of FOXD4 *in vivo* has not been elucidated.

Our study explored the role FOXD4 plays in the anterior midline tissue and the ANE of the mouse embryo. We showed that *Foxd4* is co-expressed with head organizer genes *Lhx1* and *Foxa2* in the AME and notochord of late-gastrulation embryo, it is also co-expressed with *Otx2* and *Hesx1* in the ANE of the early somite stage embryo. Using *in vitro* and *in vivo* models generated using CRISPR-Cas9 gene edited mESCs, we showed that the loss of FOXD4 function resulted in a reduction in head organizer activity and the disruption of cranial neural crest (CNC) development. Furthermore, *Foxd4*-LOF chimeric embryos displayed dysmorphology of craniofacial structures and neural tube closure defects.

MATERIALS AND METHODS

Cell Culture

R1 mESCs were grown on mouse embryonic fibroblasts (MEFs) and maintained in DMEM (Thermo Fisher Scientific), 12.5% heat inactivated fetal calf serum (Fisher Biotec), 10 mM β-mercaptoethanol, 1x non-essential amino acids (Thermo Fisher Scientific), 1X nucleosides (Merck) and 1X leukemia inhibitory factor (LIF). Cells were passaged at 70% confluency, 2–3 days after seeding onto pre-plated MEFs. For chimera generation, mESCs were maintained in 2i/LIF media (Ying et al., 2008) for at least 2 passages before use.

For *Lhx1* overexpression in chimeric embryos, two doxycycline inducible A2. loxCre mESC lines were used that either express a FLAG tagged wild-type *Lhx1* or tagged truncated *Lhx1* coding region lacking the functional LIM domains and homeodomain (Sibbritt et al., 2018).

Extraembryonic endoderm (XEN) cells were generated from blastocyst stage embryos as previously described (Niakan et al., 2013). ARC/s and *DsRed.T3* mice (from the Australian Animal Resources Centre) were maintained as homozygous breeding pairs. ARC/s females were crossed with *DsRed.T3* males, blastocyst stage embryos were collected and plated onto MEFs in TS cell medium; RPMI 1640 (Gibco), 20% fetal calf serum (Fisher Biotec), 2 mM L-glutamine (Gibco), β-mercaptoethanol, 1 mM sodium pyruvate (Gibco), 1% penicillin-streptomycin plus 24 ng/ml FGF4 (Sigma-Aldrich, cat. no. F8424) and 1 µg/ml heparin (Sigma-Aldrich, cat. no. H3393) for 20 days. The *dsRed* expressing XEN cells were then expanded on gelatin and maintained without FGF4 and heparin.

CRISPR Editing

Foxd4 edited mESCs were generated as described previously (Sibbritt et al., 2019). Guide RNAs targeting the N-terminal region of *Foxd4* were designed using (Benchling [Biology Software], 2021) (gRNA 1: 5′-CAGTCCTCTAAGTTCCGACC, gRNA 2: 5′-GGAGCGATCCCTGCAGAGGC) and ligated into pSpCas9(BB)-2A-Puro (PX459) V2.0 (a gift from Feng Zhang (Ran et al., 2013)). To induce editing, 5×10^6 R1 mESCs were electroporated with 2.5 µg of plasmid DNA and plated onto mouse embryonic fibroblasts (MEFs) for 24 h before puromycin selection for 48 h. Individual clones were expanded on MEF coated plates and genotyped for correct edits in the *Foxd4* coding region.

The genotyping PCR products were gel purified and sub-cloned into the pGEM-T Easy Vector System (Promega) as per manufacturer's protocol. At least 10 plasmids from each cell line were Sanger sequenced to identify mutations in each allele.

Neuruloid Differentiation

Assemblies of mESCs and XEN cells (neuruloids) were generated as described previously (Bérenger-Currias et al., 2020) with some modifications. Approximately 2.5×10^6 mESCs and 0.5×10^6 XEN cells were mixed and placed in each well of a 24-well plate on 400 µm Aggrewells (Stem Cell Technologies) with 2 ml of N2B27 media, and then spun at 400 g for 3 minutes. The cells were cultured in Aggrewells for 48 h, and next transferred to low

adhesion plates on a shaking platform with a 24-h pulse of 3 μm CHIR99021. CHIR99021 was then removed, and neuruloids were collected after a further 24 h of culture for RNA preparation and whole mount immunofluorescence microscopy.

Neural Precursor Differentiation

Neural precursor differentiation of mESCs was initiated using embryoid bodies (EBs) as previously described (Varshney et al., 2017; Fan et al., 2021). After 4 days of differentiation, EBs were collected and plated on laminin (5 μg/ml) coated tissue culture plates in N2B27 media for a further 4 days of culture, then collected for RNA preparation or fixed in 4% paraformaldehyde for immunofluorescence imaging.

Chimera Production

Chimeras were generated as previously described (Sibbritt et al., 2019; Fan et al., 2021). Briefly, ARC/s females were crossed with *Ds. RedT3* stud males, at E2.5 the uteri and oviducts were flushed to collect 8-cell stage embryo collection. 13–15 mESCs were injected per 8-cell *DsRed.T3* embryo, which were incubated overnight. 10 to 12 injected blastocyst-stage embryos were transferred to each E2.5 pseudo-pregnant ARC/s female recipient. E8.0—E11.5 embryos were collected 5–8 days after embryo transfer and imaged immediately on the Zeiss SteREO Lumar. V12 stereomicroscope to determine relative contribution of *dsRed* host cells versus injected mESCs. Relative intensity of dsRed.T3 fluorescence of each chimeric embryo was measured using ImageJ. The mean fluorescence of the dsRed.T3 channel was collated for each embryo and the background signal was subtracted. The mean fluorescence value was then displayed relative to embryo without ESC contribution at each stage. Animal experimentations were performed in compliance with animal ethics and welfare guidelines stipulated by the Children's Medical Research Institute/Children's Hospital at Westmead Animal Ethics Committee under protocol number C346.

Immunofluorescence Imaging

Whole-mount immunostaining of chimeric embryos was performed as described in Fan et al. (2021), while immunostaining of neuruloids was performed as described in Dekkers et al. (2019). A list of antibodies and concentrations used are outlined in **Supplementary Table S2**. Embryos and neuruloids were imaged using Zeiss Cell Observer Spinning Disk Confocal Microscope. Three-dimensional images of the samples were produced using optical slices and tiling. Zeiss Zen microscopy analysis software was used to collapse the confocal stacks and stitch together tiles to generate maximum intensity projection (MIP) images.

Immunofluorescence imaging of neural precursor cells on glass cover slips was performed as described in Sibbritt et al. (2018) and imaged using the Zeiss Axio Imager M1 microscope.

RT-qPCR

RNA was extracted using the RNeasy Mini Kit (Qiagen) for cells and Rneasy Micro Kit (Qiagen) for embryos, according to manufacturer's protocol. cDNA was synthesised from 1 μg of RNA (or 0.3 μg for E8.0 embryos) using the SuperScript III First-Stand Synthesis System (Invitrogen, Cat. No. 18080-051) as per the manufacturer's protocol, using random hexamers to prime the single-stranded RNA. Unless otherwise stated, quantitative PCR (qPCR) primers were designed using Primer-BLAST to span exon junctions of the functional mRNA transcript (all qPCR primers are listed in **Supplementary Table S1**). PowerUp SYBR Green PCR Master Mix (Thermo Fisher Scientific) and 0.4 μM of both forward and reverse primers were made to a total volume of 10uL PCR reaction. Samples were loaded into a 384 well plate (Thermo Fisher Scientific) and run on the QuantStudio 6 Flex Real-Time PCR System (Applied Biosystems). All reactions were performed in technical triplicates, relative gene expression was calculated using the comparative CT method, normalised to the housekeeping genes, *Actb* or *Ubc*.

Statistical significance was determined using an unpaired, two-tailed Student's t-test, assuming unequal variances for single comparisons. p values were obtained relative to wild-type cells/chimeras if not indicated otherwise. Differences were considered significant if the $^{*}p < 0.05$, $^{**}p < 0.01$, $^{***}p < 0.001$, $^{****}p < 0.0001$.

Bioinformatics Analysis of Single-Cell RNA-Seq Data

The processed read counts and metadata from Pijuan-Sala et al. (2019) were downloaded from https://github.com/MarioniLab/EmbryoTimecourse 2018. Reads were converted to a *Seurat* object and quality control of scRNA-seq data was performed with the *Seurat* package version 4.0.0 (Stuart et al., 2019) in *R* version 4.0.3. The data consisted of 29,452 genes with 139,331 single cells. The *scater/Bioconductor* package (McCarthy et al., 2017) was used to create QC metrics for the genes of interest. The *dittoSeq* package/Bioconductor (Bunis et al., 2020) was used for visualization of reduced dimension plots. Hierarchical cluster analysis was performed on a subset of cells expressing *Foxd4* for each stage using *hclust* (Müllner, 2013) with parameters "complete" method and "Euclidean" distance.

RESULTS

Lhx1, *Foxa2* and *Otx2* Are Co-expressed With *Foxd4* in Early Mouse Embryo

A previous study has shown that conditional ablation of *Lhx1* in the epiblast reduced the expression of *Foxd4* in the anterior tissues of embryos (Sibbritt et al., 2018). Based on this finding, we hypothesise that the LHX1/FOXA2/OTX2 transcription factor complex drives the expression of *Foxd4* in the AME at E7.75 and in the ANE at E8.25. We validated our hypothesis that LHX1 can affect transcription of *Foxd4* using an *Lhx1*-overexpressing embryo model. Doxycycline inducible FLAG-*Lhx1* and FLAG-*Lhx1*-Δ (lacking functional domains) mESC lines were used to generate mouse chimeras (**Figure 1A**). Chimeras with high mESC contribution were collected at E7.75 following 24h of doxycycline treatment. Expression of wild-type *Lhx1* mRNA was 60-fold higher in FLAG-*Lhx1* vs

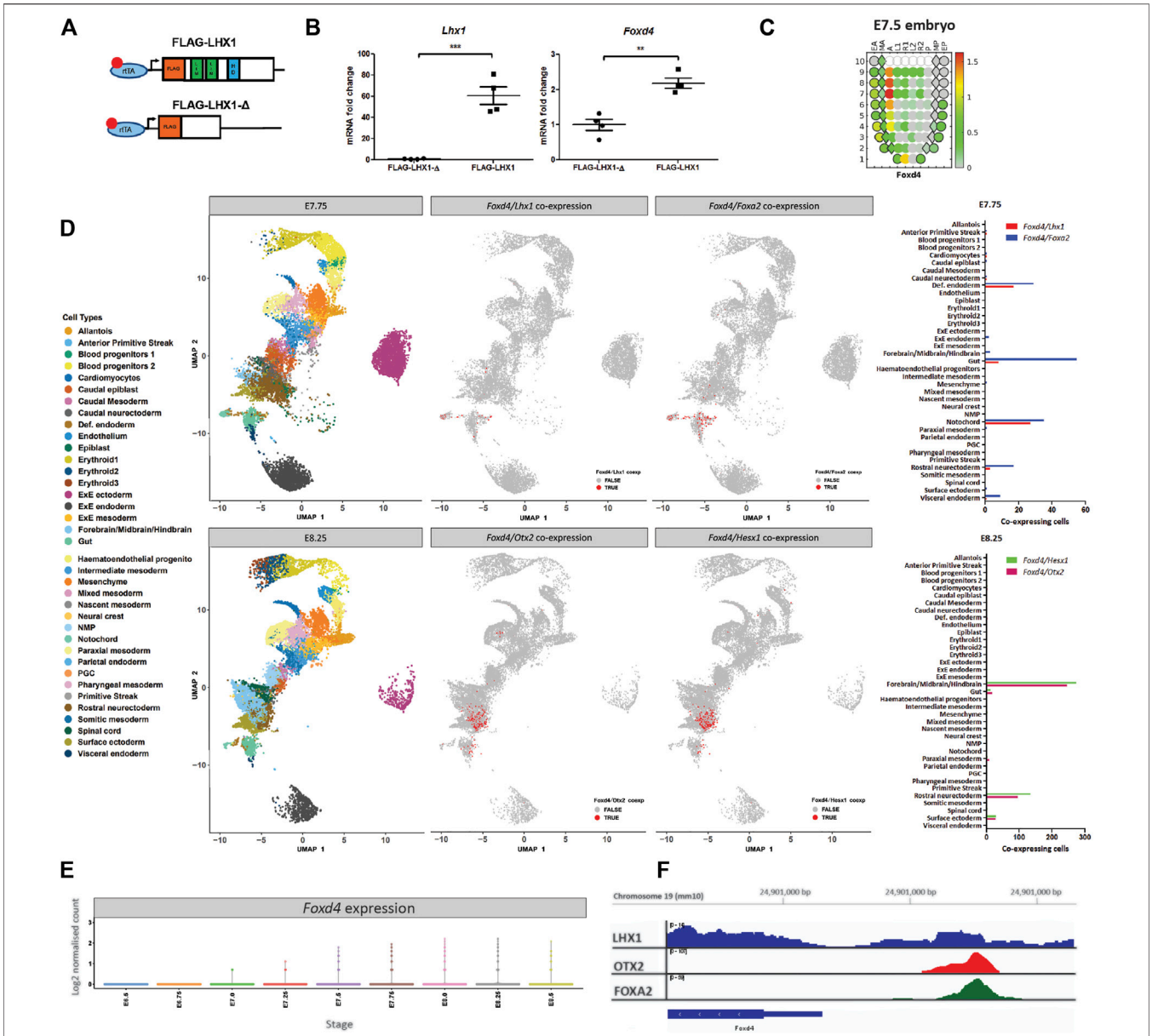

FIGURE 1 | *Foxd4* is upregulated in an *Lhx1*-overexpressing embryo system and shows co-expression with *Lhx1*, *Foxa2* and *Otx2* in the late-to post-gastrulation mouse embryo. **(A)** Schematic representation of the *Hprt* locus of the A2lox.cre mouse ESCs (Iacovino et al., 2011) containing a tetracycline response element (TRE) followed by either FLAG-*Lhx1* wild-type coding sequence or FLAG-*Lhx1*-Δ mutant sequence lacking LIM domains and homeodomain. **(B)** RT-qPCR analysis of the expression of wild-type *Lhx1* and *Foxd4* (relative to *Actb*) in FLAG-*Lhx1*-Δ and FLAG-*Lhx1* E7.75 chimeras, respectively, with 24h of doxycycline treatment. Graphs are presented as mean ± SEM of four independent treatments (**$p < 0.01$, ***$p < 0.001$ by Student's t test). **(C)** Corn plot shows the expression pattern of *Foxd4* in wild-type E7.5 embryos (Peng et al., 2019). High expression is seen in the anterior midline tissue and neurectoderm. The relative expression level is indicated by the color bar and the maximum relative expression in fragments per kilobase of transcript per million mapped reads (FPKM) is shown. **(D)** Uniform Manifold Approximation and Projection for Dimension Reduction (UMAP) for individual cells at E7.75 and at E8.25 (data from Pijuan-Sala et al., 2019). Colours represent the relevant cell types expressing the genes of interest. Co-expression of *Foxd4*/*Lhx1* and *Foxd4*/*Foxa2* are found in the notochord and definitive endoderm cell types in E7.75 embryo. Co-expression of *Foxd4* and *Otx2* as well as *Foxd4* and *Hesx1* in E8.25 embryos in the forebrain/midbrain/hindbrain and rostral neurectoderm cell types. **(E)** Expression of *Foxd4* in whole mouse embryos at E6.5 to E8.5. Log2 normalised count is presented. **(F)** University of California at Santa Cruz (UCSC) track view of ChIP-seq wiggle plot overlays showing enrichment of LHX1 (blue), OTX2 (red) and FOXA2 (green) at an upstream regulatory region of *Foxd4* on chromosome 19: 24,902,170–24,902,900 (mm10 genome).

FLAG-*Lhx1*-Δ (**Figure 1B**). A significant increase in *Foxd4* transcripts (**Figure 1C**) indicates that enhanced LHX1 activity affected the expression of *Foxd4*.

Using the publicly available eGastrulation spatial transcriptome dataset (Peng et al., 2019), we are able to investigate the location and relative level of *Foxd4* expression

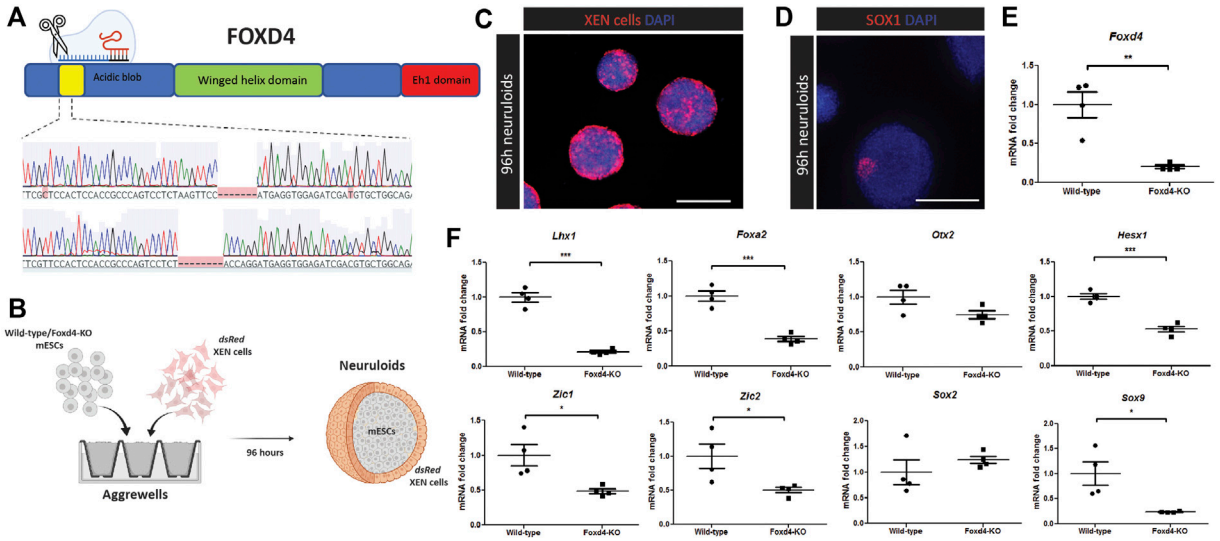

FIGURE 2 | CRISPR-Cas9 editing of *Foxd4* coding region in mESCs results in reduced expression of anterior head and neural markers *in vitro*. **(A)** Schematic representation of CRISPR-Cas9 editing on *Foxd4*. The protein domains of FOXD4 encompasses the N-terminal DNA binding acidic blob domain, the winged helix domain and the C-terminal Eh1 domain. CRISPR-Cas9 gRNAs targeted the DNA sequence corresponding to the N-terminal acidic blob domain of *Foxd4,* resulting in two alleles with 7bp and 8bp deletions, respectively. **(B)** Schematic representation of an *in vitro* model of anterior late gastrulation mouse embryos (Bérenger-Currias et al., 2020). Wild-type or $Foxd4^{\Delta7/\Delta8}$ mESCs and *dsRed* XEN cells are co-cultured in aggrewells in N2B27 media. After 48 h, 3D organoids were moved to shaking culture with 3 μM of CHIR-99021 added for 24 h. The organoids were then collected after 96h of differentiation. **(C)** Neuruloids containing XEN cells expressing *dsRed* colonizing the outside of the neuruloids, and ESCs colonizing the core. Single z-stack. N = 4. Scale bar = 300 μm. **(D)** 96 h differentiated wild-type neuruloids show expression of early neural marker SOX1. Maximum intensity z projection. N = 4 replicate experiments. Scale bar = 300 μm. **(E)** RT-qPCR analysis of the expression of *Foxd4* (relative to *Ubc*) in Wild-type and $Foxd4^{\Delta7/\Delta8}$ neuruloids. **(F)** RNA expression of anterior tissue markers *Foxa2, Lhx1, Otx2* and *Hesx1*, neural precursor markers *Zic1, Zic2, Sox2* and neural crest marker *Sox9* (relative to *Ubc*). Data are presented as mean ± SEM of four independent experiments (*$p < 0.05$, **$p < 0.01$, ***$p < 0.001$ by Student's t test).

in the late gastrulation stage mouse embryo. The highest level of *Foxd4* expression can be seen in the anterior midline cell population and the neurectoderm (**Figure 1C**), consistent with previous *in situ* hybridization data (Tamplin et al., 2008). The spatial expression of *Foxd4* in late gastrulation mouse embryos overlaps with the known locations of genes that have been shown to be critical for embryonic head development such as *Lhx1*, *Foxa2*, *Otx2* and *Hesx1*.

To investigate the expression of these transcription factors at higher resolution, we used previously published single-cell RNA-seq data of wild-type mouse embryos (Pijuan-Sala et al., 2019). At E7.75 *Foxd4* is highly expressed in the notochord cell lineage (**Supplementary Figure 1A**), which gives rise to the midline mesendoderm tissues (Yamanaka et al., 2007). At this stage *Lhx1* and *Foxa2* share similar expression profiles (**Supplementary Figure 1A**) and our analysis identified co-expression of *Foxd4* with either *Lhx1* or *Foxa2* expressing cells in the notochord and definitive endoderm populations (**Figure 1D**). At E8.25 *Foxd4* is highly expressed in rostral neurectoderm and forebrain/midbrain/hindbrain cell populations. Similarly, the head organizer genes *Otx2* and *Hesx1* are expressed in these cell populations (**Supplementary Figure 1A**). Our analysis highlighted several groups of cells that share co-expression of *Foxd4, Otx2* and *Hesx1* at E8.25 (**Figure 1D**). *Foxd4* expression in the whole embryo is increasing at E7.5 and peaks at E8.0 (**Figure 1E**).

To elucidate if these transcription factors bind to the regulatory region of the *Foxd4* locus in mouse cells we retrieved the binding data from publicly available ChIP-seq dataset. LHX1 ChIP-seq data in differentiated P19 carcinoma cells shows a low confidence peak ~1k bp upstream of the *Foxd4* transcriptional start site (TSS) (**Figure 1F**) (Costello et al., 2015). ChIP-seq data of OTX2 in epiblast like-cells (Buecker et al., 2014) and FOXA2 in mesendoderm cells (Cernilogar et al., 2019) show high confidence peaks in the same locus on chromosome 19: 24,902,170–24,902,900 (mm10 genome). These data suggest the binding of a LHX1/OTX2/FOXA2 transcription factor complex upstream of the *Foxd4* TSS.

CRISPR-Cas9 Editing of *Foxd4* Coding Region Disrupts the Transcriptional Program of Anterior Epiblast *in vitro*

In *Foxd4/5*, the *Foxd4* paralog in *Xenopus,* the AB domain has been shown to be a transcriptional activator of neural transcription factors (Neilson et al., 2012). We targeted this AB domain region in mESCs with CRISPR-Cas9 mediated genome editing (**Figure 2A**). Following screening, we chose clones with a bi-allelic frameshift mutation in the N-terminal region of *Foxd4,* at the beginning of the AB domain (Foxd4 $^{\Delta7/\Delta8}$, $Foxd4^{\Delta2/\Delta2}$ (**Figure 2A**, **Supplementary Figure 2A**). We also used a different gRNA targeting the region between the AB and forkhead domain of *Foxd4,* to exclude off-target effects of

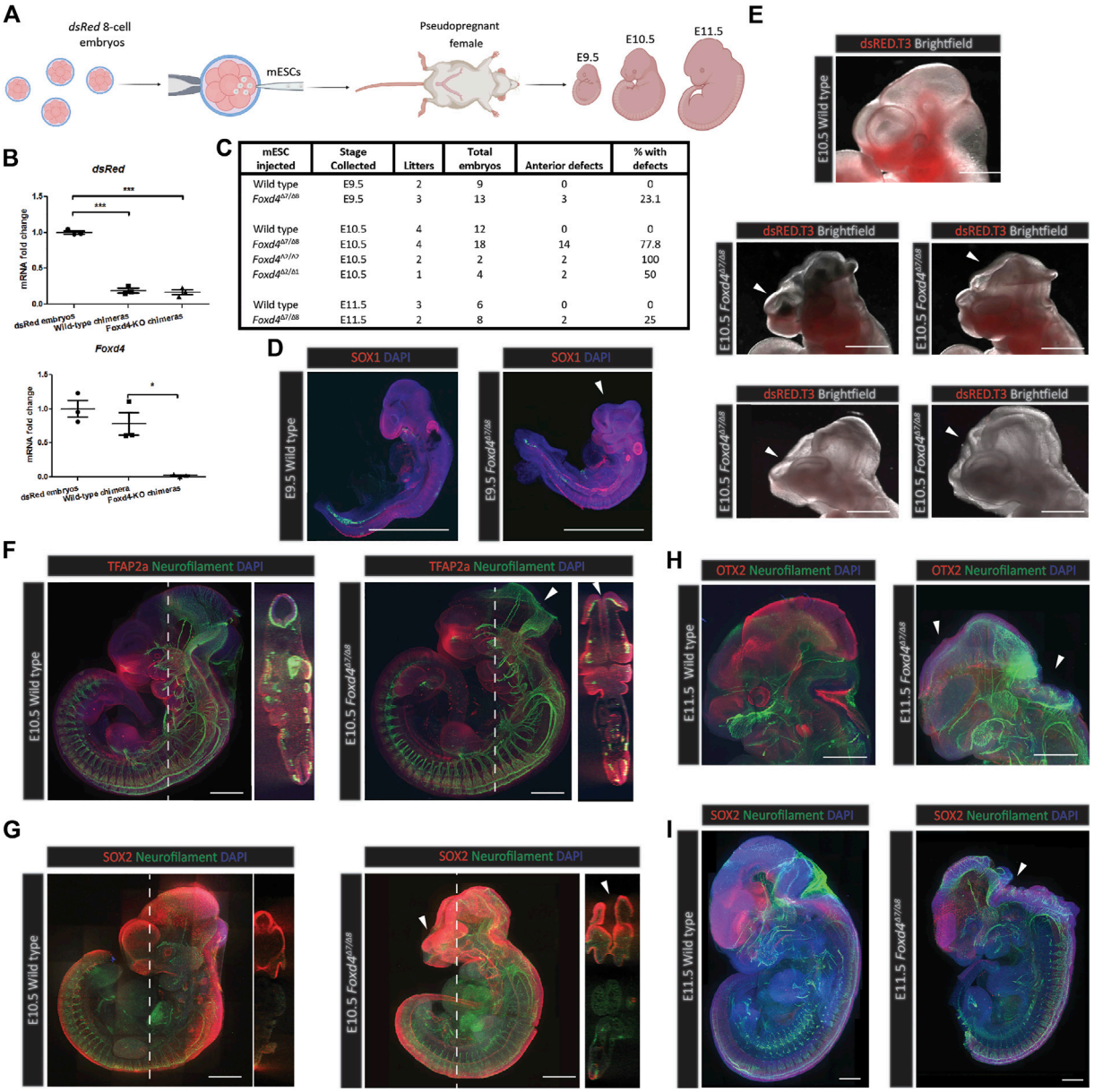

FIGURE 3 | *Foxd4*-LOF mESC derived chimeras display neural tube closure defect and craniofacial dysmorphology. **(A)** Schematic representation of the generation of chimera mouse embryos. Chimeras were generated using wild-type or *Foxd4*$^{\Delta 7/\Delta 8}$ mESCs injected into 8-cell mouse embryo expressing *dsRed*. Following *in vitro* culture, the blastocyst stage embryos were transferred to the uteri of pseudo-pregnant female mice and were collected at various post-implantation time points up to E11.5. **(B)** Wildtype and *Foxd4*$^{\Delta 7/\Delta 8}$ mESC derived chimeras show similar contribution of mESCs through RT-qPCR analysis of *dsRed* mRNA compared to un-injected *dsRed* embryos (relative to *Ubc*) at E8.0. Expression of *Foxd4* (relative to *Ubc*) shows a significant reduction in *Foxd4*$^{\Delta 7/\Delta 8}$ chimeras vs wild-type chimeras. Data are presented as mean ± SEM of three independent embryos (***$p < 0.001$, *$p < 0$ 0.05 by Student's t test). **(C)** Wild-type and *Foxd4*-LOF chimeras collected at E9.5, E10.5 and E11.5 with percentage of specimens showing anterior defects. **(D)** *Foxd4*$^{\Delta 7/\Delta 8}$ E9.5 chimera displays truncated head, stained for SOX1 (red) and DAPI (blue), Maximum intensity z projection (Full panels for immunofluorescence imaging of chimeras are in **Supplementary Figure 3**). **(E)** The range of head phenotypes in *Foxd4*$^{\Delta 7/\Delta 8}$ E10.5 chimeras showing neural tube closure defects and craniofacial deformities. Brightfield imaging and dsRed merged image. **(F)** Neural tube closure defect of a representative *Foxd4*$^{\Delta 7/\Delta 8}$ derived E10.5 chimera, stained for neurofilament (green), TFAP2a (red) and DAPI (blue). Left: Maximum intensity z projection, right: coronal plane through z stacks. **(G)** Craniofacial defect of a representative *Foxd4*$^{\Delta 7/\Delta 8}$ E10.5 chimera stained for neurofilament (green), SOX2 (red) and DAPI (blue). Left: Maximum intensity z projection, right: coronal plane through z stacks. **(H)** OTX2 expression in the mid-brain and eye is reduced in representative *Foxd4*$^{\Delta 7/\Delta 8}$ E11.5 chimera embryo (red), Neurofilament staining (green) reveals exencephaly in mutant chimera. Maximum intensity z projection. **(I)** Open neural tube in a representative *Foxd4*$^{\Delta 7/\Delta 8}$ E11.5 chimera embryo, stained for neurofilament (green), SOX2 (red) and DAPI (blue). Maximum intensity z projection. All scale bars = 500 μm.

CRISPR-Cas9 genome editing. Using the second gRNA we obtained a clone with a 2 bp deletion and a 1 bp insertion in respective alleles (Foxd4$^{\Delta 2/\Delta 1}$, **Supplementary Figure 2D**). Despite trying numerous antibodies from different manufacturers, we were unable to get a reliable signal to assay the expression of the predicted truncated FOXD4 protein in our knockout mESC line (data not shown).

To study the downstream genetic targets of FOXD4 during development, we used an *in vitro* model of the anterior epiblast (neuruloid) generated through the co-culture of mESCs and extraembryonic endoderm (XEN) (**Figure 2B**) (Bérenger-Currias et al., 2020). The XEN cells express genes that are highly expressed in the extraembryonic endoderm including *Foxa2*, *Sox17* and *Gata4*, but do not express pluripotency markers, *Oct4* and *Sox2* (**Supplementary Figure 3A, B**). The *dsRed* expressing XEN cells colonized the exterior portion of the neuruloid (**Figure 2C**, **Supplementary Figure 3C**), where they may act in a similar way to the anterior visceral endoderm population in the embryo. In contrast to embryoid bodies differentiated for the same period, we showed significantly higher expression of anterior markers *Otx2, Lhx1*, *Hesx1* as well as *Foxd4* (**Supplementary Figure 3D**). Wild-type neuruloids expressed early neurectoderm marker SOX1 in distinct regions of the neuruloids (**Figure 2D**, **Supplementary Figure 3E**).

Compared with neuruloids generated using wild-type mESCs, *Foxd4*$^{\Delta 7/\Delta 8}$ neuruloids had significantly reduced expression of *Foxd4* transcripts (**Figure 2E**). *Lhx1*, *Hesx1* and *Foxa2* transcripts were also significantly reduced (**Figure 2F**). This result indicates that FOXD4 is crucial for the appropriate specification of the precursor tissues to the embryonic head and notochord. Comparable to results seen in *Xenopus* (Neilson et al., 2012), knock-out of *Foxd4* caused the reduction in expression of neural ectodermal genes *Zic1* and *Zic2* (**Figure 2F**). Expression of the neural progenitor gene *Sox2* was not changed in *Foxd4*$^{\Delta 7/\Delta 8}$ neuruloids, whereas the transcripts of early neural crest cell (NCC) marker *Sox9* was significantly reduced, indicating a role for *Foxd4* in the establishment of the NCC population. Our analysis of scRNA-seq data from Pijuan-Sala et al. (2019) showed *Foxd4* is co-expressed with *Zic2* and *Sox9* but not *Zic1* at E7.75 and E8.25 in the ANE tissues (**Supplementary Figure 1B**).

Mouse Chimeric Embryos Derived From *Foxd4-LOF* mESCs Display Neural Tube and Craniofacial Defects

To analyze the function of FOXD4 during mouse development, wild-type or *Foxd4*-LOF mESCs were injected into 8-cell host embryos ubiquitously expressing *dsRed* (**Figure 3A**). Host embryos were injected with either wild-type or *Foxd4*$^{\Delta 7/\Delta 8}$ mESCs (15 embryos each), chimeric embryos were collected at E8.0 and the relative contribution of mESCs was quantified using fluorescence microscopy. Three chimeras of each genotype with high (>60%) contribution were kept for RNA assay (**Supplementary Figure 4A**). E8.0 chimeras that showed high contribution of mESCs in fluorescence imaging had significantly lower *dsRed* expression compared to un-injected embryos (**Figure 3B**). Chimeras with high contribution of *Foxd4* $^{\Delta 7/\Delta 8}$ mESCs showed significantly reduced *Foxd4* expression compared to wild-type mESC injected chimeras (**Figure 3B**).

Foxd4-LOF chimeric embryos had visible neural tube closure defects and truncated forebrain tissue at E9.5, E10.5 and E11.5, whilst none of the wild-type mESC derived chimeras that were collected displayed an abnormal head phenotype (**Figure 3C**). At E9.5, 3/13 *Foxd4*$^{\Delta 7/\Delta 8}$ chimeras displayed anterior defects, compared to 0/9 for wild-type chimeras (**Supplementary Figures 5A,B** and **6A,B**). No anterior defects were evident in E10.5 wild-type chimeras (0/12) (**Supplementary Figure 7A,B**). 14/18 *Foxd4*$^{\Delta 7/\Delta 8}$, 2/2 *Foxd4*$^{\Delta 2/\Delta 2}$, and 2/4 *Foxd4*$^{\Delta 2/\Delta 1}$ chimeras collected at E10.5 displayed anterior developmental defects (**Supplementary Figures 2C,F** and **8A,B**). Finally, 0/6 wild-type E11.5 chimeras and 2/8 E11.5 *Foxd4*$^{\Delta 7/\Delta 8}$ chimeras showed anterior defects (**Supplementary Figure 9A,B**).

Foxd4$^{\Delta 7/\Delta 8}$ chimeras collected at E9.5 with high contribution had comparable expression of neuroectoderm marker SOX1, though displayed severe truncation of the head tissue compared to wild-type control (**Figure 3D**, **Supplementary Figure 4B**). At E10.5 a range of head defect phenotypes were evident in *Foxd4*$^{\Delta 7/\Delta 8}$, *Foxd4*$^{\Delta 2/\Delta 2}$ and *Foxd4*$^{\Delta 2/\Delta 1}$ chimeras (**Figure 3E**, **Supplementary Figure 2C,F**). NEFM (neurofilament) staining shows exencephaly in the midbrain and hindbrain, though there were no defects in the caudal neural tube in any *Foxd4*-LOF chimeras (**Figure 3F**). Craniofacial defects were also common among *Foxd4*-LOF chimeras including truncated facial tissue and abnormal forebrain patterning (**Figures 3E,G**, **Supplementary Figure 4D**).

In *Foxd4*$^{\Delta 7/\Delta 8}$ chimeras collected at E11.5, exencephaly was evident in the rostral neural tube (**Figures 3H,I**, **Supplementary Figures 4E,F**). The protein OTX2 that is normally expressed in the midbrain and eyes of E11.5 wild-type embryo, was not detected in *Foxd4*$^{\Delta 7/\Delta 8}$ chimeras (**Figure 3H**). All the defects seen were in anterior head and neural tube tissues, indicating the specific role of FOXD4 in the anterior neural and midline tissue in late gastrulation/early organogenesis.

FOXD4 Is Required for Anterior Neurectoderm and Neural Crest Specification

We adapted a protocol from Varshney et al. (2017) for the differentiation of mESCs to neural precursor cells (NPC) (**Figure 4A**), revealed by high levels of *Foxd4* expression in wild-type NPCs at Day 8 of culture (**Figure 4B**). NCC markers *Twist1* and *Sox9* were also highly expressed in the NPCs compared to undifferentiated mESCs (**Figure 4B**). Both wild-type and *Foxd4*$^{\Delta 7/\Delta 8}$ mESCs expressed a high level of neural ectoderm marker SOX1 and neuron specific Class III β-tubulin (TUBB3) (**Figure 4C**). *Foxd4*$^{\Delta 7/\Delta 8}$ day 8 NPCs had significantly reduced *Foxd4* mRNA expression compared to the wild-type (**Figure 4D**). mRNA expression of neurectoderm markers *Pax4* and *Nestin (Nes)* were not significantly different in *Foxd4*$^{\Delta 7/\Delta 8}$ NPCs (**Figure 4D**). In contrast, the head organizer genes *Otx2, Lhx1* and *Foxa2* were significantly reduced (**Figures 4E,F**). The loss of *Otx2* expression is consistent with the reduction in OTX2

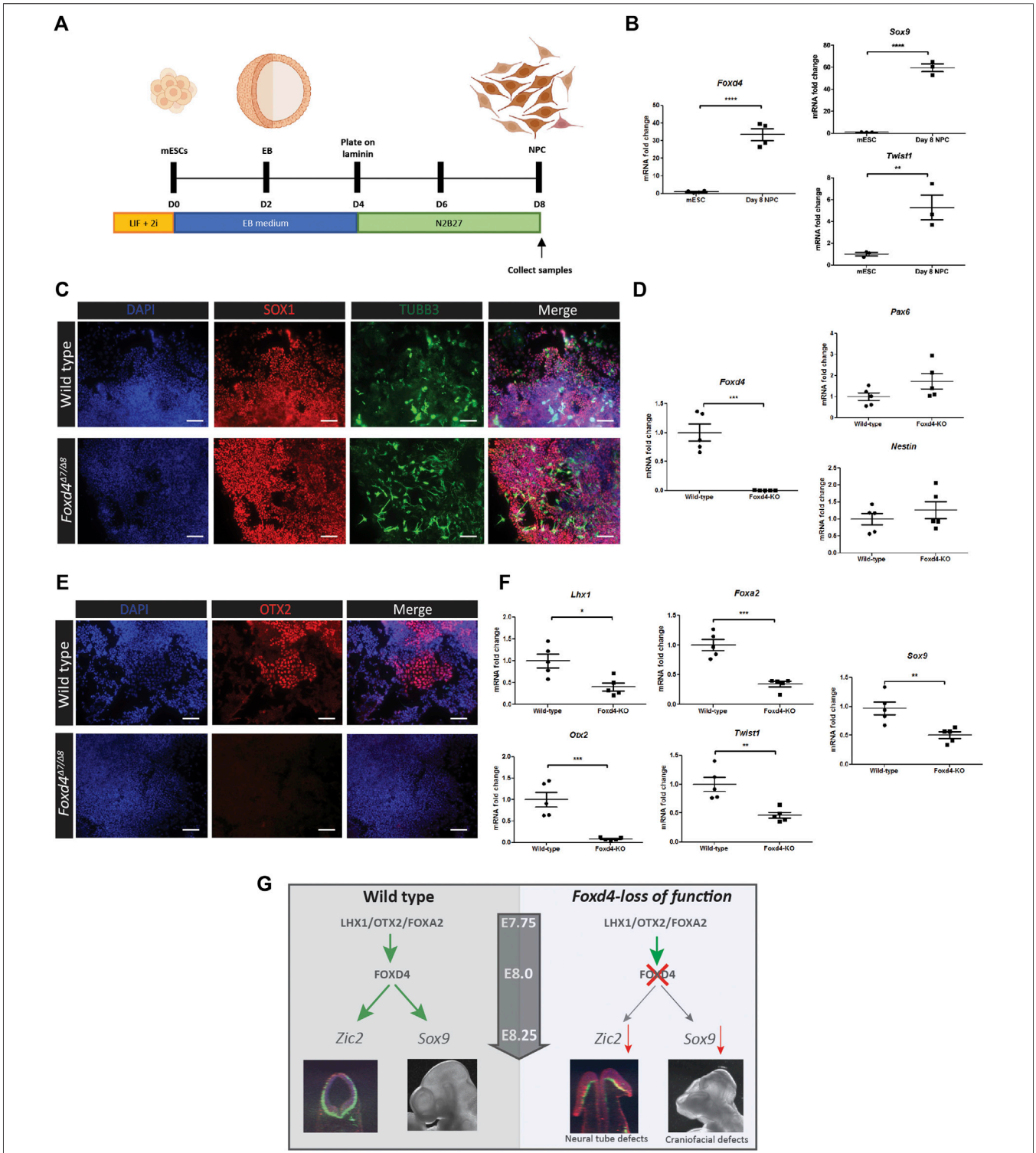

FIGURE 4 | Genes associated with anterior tissues and neural crest cells are downregulated in *Foxd4*-LOF mESCs during neural differentiation. **(A)** Schematics of neural precursor cell differentiation protocol. mESCs were cultured in 2i/Lif media without feeder cells. mESCs are cultured in aggrewells in EB media for 48 h before being placed on shaker plates for a further 48 h. The EBs were then moved onto laminin coated dishes and cultured in N2B27 media for 4 days **(B)** RT-qPCR analysis shows 30-fold increase in expression of *Foxd4* (relative to *Ubc*) neural precursor cells (NPCs) compared to mESCs. *Sox9* and *Twist1* are also highly expressed compared to undifferentiated mESCs (N = . **(C)** Wildtype and *Foxd4*$^{\Delta 7/\Delta 8}$ NPCs both show strong expression of SOX1 (red) and Tubulin-βIII (green) after 8 days of differentiation. N = 4. Scale bar = 100 μm. **(D)** RT-qPCR analysis shows significantly reduced *Foxd4* expression, though comparable level of expression of *Pax6* and *Nes* (relative to *Ubc*) in *Foxd4*$^{\Delta 7/\Delta 8}$ NPCs compared to wild-type NPCs. **(E)** *Foxd4*$^{\Delta 7/\Delta 8}$ NPCs do not express OTX2 (*Continued*)

FIGURE 4 | (red) after 8 days of differentiation. N = 4. Scale bar = 100 μm. **(F)** RT-qPCR analysis shows reduced expression of *Foxd4*, *Lhx1*, *Otx2, Foxa2*, *Twist1 and Sox9* (relative to *Ubc*) in wild-type vs $Foxd4^{\Delta 7/\Delta 8}$ Day 8 NPCs. Data are presented as mean ± SEM of four independent treatments (*$p < 0$ 0.05, **$p <$ 0 0.01, ***$p < 0$ 0.001 by Student's t test). **(G)** Schematic: In the anterior tissue of the E7.75 mouse embryo, *Foxd4* expression is controlled by the LHX1/OTX2/FOXA2 TF complex. FOXD4 is then required for regulating the expression of *Zic2* in the ANE for neurulation. The loss of FOXD4 function in the neuroectoderm leads deficiency of cranial neural crest cells, revealed by the reduced expression of *Sox9* and craniofacial defects in *Foxd4*-LOF chimeric embryos.

expression seen in the *in vivo* model (**Figure 3H**). NCC markers *Twist1* and *Sox9* were also downregulated in $Foxd4^{\Delta 7/\Delta 8}$ NPCs (**Figure 4F**) compared to wild-type, though our scRNA-seq analysis did not show significant co-expression of *Foxd4* and *Twist1* at E7.75 or E8.25 (**Figure 1B**).

DISCUSSION

Our study has revealed a novel role of FOXD4 in the development of the embryonic head and neural tube in mouse embryos. Single cell transcriptomic analysis confirms published spatial RNA expression pattern in E7.5-E7.75 embryos showing *Foxd4* expression in the anterior midline and anterior neurectoderm tissues (Kaestner et al., 1995). The anterior midline cell population at E7.75 marked by *Lhx1* and *Foxa2* are the precursors of the anterior mesendoderm underlying neuroectoderm of the head folds (Kinder et al., 2003). Co-expression of *Foxd4* with *Lhx1* and *Foxa2* in the anterior midline (notochord) and definitive endoderm populations at E7.75 imply a shared mechanism of these transcription factors in these tissues. Reduced *Foxa2* or *Lhx1* expression in the anterior embryo has been shown to ablate *Foxd4* expression in the same region (Tamplin et al., 2008; Sibbritt et al., 2018). Furthermore, ChIP-seq data show LHX1 and FOXA2 binding sites upstream of *Foxd4*. Our *in vitro* results show that a loss of FOXD4 activity also reduces the expression of *Lhx1* and *Foxa2*. This shared relationship may indicate that all three transcription factors act together to define the anterior midline tissue of the late gastrulation stage mouse embryo.

For neural induction of the anterior epiblast, firstly the anterior visceral endoderm (AVE) establishes the adjacent neurectoderm, then the AME acts to maintain the neurogenic differentiation (reviewed in Martinez-Barbera and Beddington, 2003). *Foxd4* is not expressed highly in the AVE; its expression peaks at E8.0-E8.25 in anterior neurectoderm where it is co-expressed with two other anterior neurectoderm marker genes *Otx2* and *Hesx1* (**Figure 1D**). *Hesx1* and *Otx2* are expressed in the forebrain and midbrain of the developing mouse embryos and mutations in each of these transcription factors result in truncated or deficient head tissues (Matsuo et al., 1995; Martinez-Barbera et al., 2000). In $Foxd4^{\Delta 7/\Delta 8}$ neuruloids, *Hesx1* expression is significantly reduced and similarly there is no OTX2 protein expression in $Foxd4^{\Delta 7/\Delta 8}$ neural precursor cells. These findings indicate that FOXD4 is essential in the anterior neurectoderm tissues of the late gastrula stage mouse embryo. An evident phenotype of *Foxd4*-LOF mESC derived chimeras is the reduced head size and forebrain defect. This phenotype coupled with reduced expression of OTX2 in E11.5 $Foxd4^{\Delta 7/\Delta 8}$ chimeras show that FOXD4 is required for the development of anterior neurectoderm in mouse embryos.

In *Xenopus* embryos, the homolog of *Foxd4* (*Foxd4/5*) is crucial for the induction and maintenance of neurectoderm cells at gastrula and neural plate stage of development (Yan et al., 2009; Neilson et al., 2012). The AB domain in the N-terminal FOXD4/5 protein was shown to upregulate the immature neural precursor marker *Zic2,* and the mouse, FOXD4 has homologous activity when expressed in *Xenopus* embryos (Sherman et al., 2017). In an *in vitro Foxd4*-LOF neuruloid model, the expression of *Zic2* is also significantly down-regulated, consistent with literature showing that a loss *Zic2* function in the embryo leads to neural tube defects (Warr et al., 2008). Despite a reduction in *Zic2* expression, closure defects were only found in the rostral neural tube *Foxd4*-LOF mESC derived chimeras. The expression of *Zic2* in the caudal neural tube may therefore be influenced by other factors such as PAX3 or CDX2 (Zhao et al., 2014). It is likely that a primary function of FOXD4 is to regulate *Zic2* activity in the anterior neurectoderm to enable proper neural tube closure (**Figure 4G**). Contrary to a previous study in mESCs (Sherman et al., 2017), we found FOXD4 is not needed to generate neural precursor cells *in vitro*. $Foxd4^{\Delta 7/\Delta 8}$ neural precursor cells (NPCs) express neural precursor markers SOX1, TUBB3, *Pax6* and *Nes* at levels equivalent to wild-type NPCs. Likewise, in *Foxd4*-LOF chimeras, neurofilament is expressed at levels similar to wild type, although the pattern of innervation is disrupted.

A closely related protein to FOXD4; FOXD3, also contains acidic, forkhead and Eh1 domains (Wijchers et al., 2006) and has been demonstrated to be essential for NCC specification and maintenance of neural crest progenitor cells (Dottori et al., 2001; Teng et al., 2008). Our *in vitro* models also indicate that FOXD4 is driving early NCC specification. The NCCs are a migratory population of cells that arise firstly at border of neural plate and non-neural ectoderm cells (Wang et al., 2011). After gastrulation, cranial neural crest (CNC) cells delaminate from the dorsal neural tube and begin to express CNC specific markers including *Sox9* and *Twist1* (Mori-Akiyama et al., 2003; Soldatov et al., 2019). In the $Foxd4^{\Delta 7/\Delta 8}$ neuruloids and NPCs, *Sox9* transcripts are significantly downregulated compared to wild-type controls. Similarly, RNA expression of neural crest-related gene, *Twist1*, was reduced in $Foxd4^{\Delta 7/\Delta 8}$ NPCs. Our scRNA-seq analysis also shows co-expression of *Foxd4* and *Sox9* in CNC precursor populations of the rostral neurectoderm. We therefore propose that FOXD4 is regulating the expression of *Sox9* in the CNC progenitor population and has a shared function alongside FOXD3 to specify CNC cells. A loss of FOXD4 activity may be affecting the allocation of the CNC precursor population and further impacts on the pattern of cranial nerve innervation of the head tissues (**Figure 4G**). These data indicate that FOXD4 is not required for the specification of neuronal cell lineages but is

required for the differentiation of the head tissues and specification of CNC tissue.

CONCLUSION

Our study has revealed that FOXD4 acts in conjunction with LHX1, FOXA2, OTX2, and HESX1 to regulate the activity of key genes associated with neural tube morphogenesis and CNC specification in the anterior midline tissue and the anterior neurectoderm tissues. Further study of the transcriptional targets of FOXD4 in the neuroectoderm and neural crest cells will shed more light on the pleiotropic role of this transcription factor in craniofacial development.

DATA AVAILABILITY STATEMENT

All the code for data analysis is publicly available at https://github.com/naryamanesh/Pijuan_Foxd4. All the mESC and XEN cell lines generated for this article are freely available to the scientific community upon request.

ETHICS STATEMENT

The animal study was reviewed and approved by the Children's Medical Research Institute / Children's Hospital at Westmead Animal Ethics Committee.

AUTHOR CONTRIBUTIONS

RM designed experiments, carried out most of the experiments presented in the manuscript, analysed the data, and wrote the manuscript. TS conceived and designed experiments, generated the CRISPR-edited cell line and some of the chimera embryos. NA developed the code to analyse the single-cell bioinformatics data and generated figures. VM designed experiments, helped with the immunofluorescence imaging, supervised the research, and edited the manuscript. PT conceived, designed, and supervised the research and edited the manuscript.

FUNDING

Our work was supported by the Australian Research Council (DP 160100933), Mr James Fairfax (Bridgestar Pty Ltd) and the Luminesce Alliance—Innovation for Children's Health, a joint venture between the Sydney Children's Hospitals Network, the Children's Medical Research Institute (CMRI), and the Children's Cancer Institute, established with the support of the NSW Government. RM was supported by University of Sydney Research Training Program Scholarship and CMRI Scholarship. PPLT was supported by the National Health and Medical Research Council Research Fellowship (Grant 1110751).

SUPPLEMENTARY MATERIAL

The Supplementary Material for this article can be found online at: https://www.frontiersin.org/articles/10.3389/fcell.2021.777652/full#supplementary-material

Supplementary Figure S1 | (A) Uniform Manifold Approximation and Projection for Dimension Reduction (UMAP) for individual cells at E7.75 and E8.25 (data from Pijuan-Sala et al, 2019). Colours represent the relevant cell types expressing the genes of interest: *Foxd4*, *Lhx1* and *Foxa2* at E7.75 and *Foxd4, Otx2* and *Hesx1* at E8.25. *Foxd4* at E7.75 shows highest expression in notochord, neurectoderm and definitive endoderm. *Foxd4* at E8.25 shows highest expression in definitive endoderm, notochord, forebrain/midbrain/hindbrain and rostral neurectoderm. **(B)** UMAP for individual cells at E7.75 and E8.25 (data from Pijuan-Sala et al. (2019). Colours represent the relevant cell types expressing the genes of interest. Co-expression data of *Foxd4* with *Zic1*, *Zic2*, *Twist1* or *Sox9* are shown in red. Co-expression of *Foxd4*/*Zic2* and *Foxd4*/*Sox9* are mainly in the rostral neurectoderm at E7.75 and forebrain/midbrain/hindbrain in E8.25 embryos.

Supplementary Figure S2 | (A) Schematic representation of CRISPR-Cas9 editing on *Foxd4* for clone $Foxd4^{\Delta 2/\Delta 2}$. CRISPR-Cas9 gRNA 1 targeted the DNA sequence corresponding to the N-terminal AB domain of *Foxd4,* resulting in 2bp deletions in each allele. **(B)** Relative fluorescence intensity of host derived tissue (dsRed.T3) over area for each $Foxd4^{\Delta 2/\Delta 2}$ chimera collected at E10.5 (compared to un-injected E10.5 embryos). **(C)** Brightfield and dsRed.T3 imaging of E10.5 $Foxd4^{\Delta 2/\Delta 2}$ chimeras ranked from least mESC contribution to most. Arrows indicate anterior defect. **(D)** Schematic representation of CRISPR-Cas9 editing on *Foxd4* for clone $Foxd4^{\Delta 2/\Delta 1}$. CRISPR-Cas9 gRNA 2 targeted the DNA sequence corresponding to the region between the AB and forehead domains of *Foxd4,* resulting in a 2bp deletion and 1bp insertion in each allele. **(E)** Relative fluorescence intensity of host derived tissue (dsRed.T3) over area for each $Foxd4^{\Delta 2/\Delta 1}$ chimera collected at E10.5 (compared to un-injected E10.5 embryos). **(F)** Brightfield and dsRed.T3 imaging of E10.5 $Foxd4^{\Delta 2/\Delta 1}$ chimeras ranked from least mESC contribution to most. Arrows indicate anterior defect. All scale bars = 500μm

Supplementary Figure S3 | (A) Immunofluorescence imaging of extraembryonic endoderm (XEN) cells derived from *dsRed*-expressing E3.5 mouse blastocysts. XEN cells show expression of endoderm markers FOXA2 and SOX17 but not pluripotency factor OCT4. N=4. Scale bar = 50 μm. **(B)** RT-qPCR analysis shows expression of endoderm genes, *Foxa2* and *Sox17*, extraembryonic endoderm gene *Gata6* and pluripotency factor, *Sox2* (relative to *Actb*) in dsRed-positive XEN cells compared to R1 mESCs. N=1. **(C)** Neuruloids showing dsRed-expressing XEN cells localized on the outside of the neuruloids, while the ESCs colonized the core. Wild-type neuruloids show SOX1 expression. Single z-stack. N=4. Scale bar = 300 μm. **(D)** RT-qPCR analysis shows increased expression of anterior tissue genes, *Lhx1, Otx2, Foxd4* and *Hesx1* (relative to *Actb*) in Day 4 neuruloids compared to conventional Day 4 embryoid bodies (EBs). N=1. **(E)** 96 hour differentiated wild-type neuruloids show expression of early neural marker SOX1. Maximum intensity z projection. N= 4. Scale bar = 300 μm.

Supplementary Figure S4 | (A) Brightfield and dsRed imaging of E8.0 dsRed.T3 embryos and E8.0 chimeras with either wild-type or $Foxd4^{\Delta 7/\Delta 8}$ mESCs. **(B)** Wild-type and $Foxd4^{\Delta 7/\Delta 8}$ E9.5 chimeras stained for SOX1 (red). $Foxd4^{\Delta 7/\Delta 8}$ chimera displays truncated head. Maximum intensity z projection. **(C)** Neural tube defect of representative $Foxd4^{\Delta 7/\Delta 8}$ E10.5 chimera embryo stained for neurofilament (green), TFAP2a (red) and DAPI (blue). Maximum intensity z projection. **(D)** Craniofacial defect of representative $Foxd4^{\Delta 7/\Delta 8}$ E10.5 chimera embryo stained for neurofilament (green), SOX2 (red) and DAPI (blue). Maximum intensity z projection. **(E)** Mid-brain/eye marker OTX2 expression is reduced in representative $Foxd4^{\Delta 7/\Delta 8}$ derived E11.5 chimera embryo (red), neurofilament staining (green) reveals exencephaly in mutant chimera. Maximum intensity z projection. **(F)** Exencephaly shown in representative $Foxd4^{\Delta 7/\Delta 8}$ derived E11.5 chimera embryo, stained for neurofilament (green), SOX2 (red) and DAPI (blue). Maximum intensity z projection. Scale bar = 500 μm

Supplementary Figure S5 | (A) Relative fluorescence intensity of host derived tissue (dsRed.T3) over area for each wild-type chimera collected at E9.5 (compared to un-injected E9.5 embryos). **(B)** Brightfield and dsRed.T3 imaging of E9.5 wild-type chimeras ranked from low mESC contribution to high. All scale bars = 500μm

Supplementary Figure S6 | (A) Relative fluorescence intensity of host derived tissue (dsRed.T3) over area for each *Foxd4*$^{\Delta 7/\Delta 8}$ chimera collected at E9.5 (compared to un-injected E9.5 embryos). **(B)** Brightfield and dsRed.T3 imaging of E9.5 *Foxd4*$^{\Delta 7/\Delta 8}$ chimeras ranked from low mESC contribution to high. Arrows indicate anterior defect. All scale bars = 500 μm

Supplementary Figure S7 | (A) Relative fluorescence intensity of host derived tissue (dsRed.T3) over area for each wild-type chimera collected at E10.5 (compared to un-injected E10.5 embryos). **(B)** Brightfield and dsRed.T3 imaging of E10.5 wild-type chimeras ranked from low mESC contribution to high. All scale bars = 500 μM

Supplementary Figure S8 | (A) Relative fluorescence intensity of host derived tissue (dsRed.T3) over area for each *Foxd4*$^{\Delta 7/\Delta 8}$ chimera collected at E10.5 (compared to un-injected E10.5 embryos). **(B)** Brightfield and dsRed.T3 imaging of E10.5 *Foxd4*$^{\Delta 7/\Delta 8}$ chimeras ranked from low mESC contribution to high. Arrows indicate anterior defect. All scale bars = 500 μM

Supplementary Figure S9 | (A) Relative fluorescence intensity of host derived tissue (dsRed.T3) over area for each wild-type chimera collected at E11.5 (compared to un-injected E11.5 embryos). **(B)** Relative fluorescence intensity of host derived tissue (dsRed.T3) over area for each *Foxd4*$^{\Delta 7/\Delta 8}$ chimera collected at E11.5 (compared to un-injected E11.5 embryos). **(C)** Brightfield and dsRed.T3 imaging of E11.5 wild-type chimeras ranked from low mESC contribution to high. **(D)** Brightfield and dsRed.T3 imaging of E11.5 *Foxd4*$^{\Delta 7/\Delta 8}$ chimeras ranked from low mESC contribution to high. Arrows indicate anterior defect. All scale bars = 500μM

REFERENCES

Ang, S.-L., and Rossant, J. (1994). HNF-3β Is Essential for Node and Notochord Formation in Mouse Development. *Cell* 78 (4), 561–574. doi:10.1016/0092-8674(94)90522-3

Arkell, R. M., and Tam, P. P. L. (2012). Initiating Head Development in Mouse Embryos: Integrating Signalling and Transcriptional Activity. *Open Biol.* 2 (3), 120030. doi:10.1098/rsob.120030

Benchling [Biology Software] (2021). Retrieved from https://benchling.com. (Accessed June 19, 2019).

Bérenger-Currias, N. M., Mircea, M., Adegeest, E., van den Berg, P. R., Feliksik, M., Hochane, M., et al. (2020). Early Neurulation Recapitulated in Assemblies of Embryonic and Extraembryonic Cells. *BioRxiv*. doi:10.1101/2020.02.13.947655

Buecker, C., Srinivasan, R., Wu, Z., Calo, E., Acampora, D., Faial, T., et al. (2014). Reorganization of Enhancer Patterns in Transition from Naive to Primed Pluripotency. *Cell stem cell* 14 (6), 838–853. doi:10.1016/j.stem.2014.04.003

Bunis, D. G., Andrews, J., Fragiadakis, G. K., Burt, T. D., and Sirota, M. (2020). dittoSeq: Universal User-Friendly Single-Cell and Bulk RNA Sequencing Visualization Toolkit. *Bioinformatics* 36 (22-23), 5535–5536. doi:10.1093/bioinformatics/btaa1011

Cernilogar, F. M., Hasenöder, S., Wang, Z., Scheibner, K., Burtscher, I., Sterr, M., et al. (2019). Pre-Marked Chromatin and Transcription Factor Co-Binding Shape the Pioneering Activity of Foxa2. *Nucleic Acids Res.* 47 (17), 9069–9086. doi:10.1093/nar/gkz627

Costello, I., Nowotschin, S., Sun, X., Mould, A. W., Hadjantonakis, A.-K., Bikoff, E. K., et al. (2015). Lhx1 Functions Together with Otx2, Foxa2, and Ldb1 to Govern Anterior Mesendoderm, Node, and Midline Development. *Genes Dev.* 29 (20), 2108–2122. doi:10.1101/gad.268979.115

Dekkers, J. F., Alieva, M., Wellens, L. M., Ariese, H. C. R., Jamieson, P. R., Vonk, A. M., et al. (2019). High-Resolution 3D Imaging of Fixed and Cleared Organoids. *Nat. Protoc.* 14 (6), 1756–1771. doi:10.1038/s41596-019-0160-8

Dottori, M., Gross, M. K., Labosky, P., and Goulding, M. (2001). The Winged-Helix Transcription Factor Foxd3 Suppresses Interneuron Differentiation and Promotes Neural Crest Cell Fate. *Development* 128 (21), 4127–4138. doi:10.1242/dev.128.21.4127

Fan, X., Masamsetti, V. P., Sun, J. Q., Engholm-Keller, K., Osteil, P., Studdert, J., et al. (2021). TWIST1 and Chromatin Regulatory Proteins Interact to Guide Neural Crest Cell Differentiation. *Elife* 10, e62873. doi:10.7554/elife.62873

Fossat, N., Ip, C. K., Jones, V. J., Studdert, J. B., Khoo, P.-L., Lewis, S. L., et al. (2015). Context-Specific Function of the LIM Homeobox 1 Transcription Factor in Head Formation of the Mouse Embryo. *Development* 142 (11), 2069–2079. doi:10.1242/dev.120907

Hermesz, E., Mackem, S., and Mahon, K. A. (1996). Rpx: A Novel Anterior-Restricted Homeobox Gene Progressively Activated in the Prechordal Plate, Anterior Neural Plate and Rathke's Pouch of the Mouse Embryo. *Development* 122 (1), 41–52. doi:10.1242/dev.122.1.41

Iacovino, M., Bosnakovski, D., Fey, H., Rux, D., Bajwa, G., Mahen, E., et al. (2011). Inducible Cassette Exchange: A Rapid and Efficient System Enabling Conditional Gene Expression in Embryonic Stem and Primary Cells. *Stem Cells* 29 (10), 1580–1588. doi:10.1002/stem.715

Kaestner, K. H., Monaghan, A. P., Kern, H., Ang, S.-L., Weitz, S., Lichter, P., et al. (1995). The Mouse Fkh-2 Gene. *J. Biol. Chem.* 270 (50), 30029–30035. doi:10.1074/jbc.270.50.30029

Kimura, C., Yoshinaga, K., Tian, E., Suzuki, M., Aizawa, S., and Matsuo, I. (2000). Visceral Endoderm Mediates Forebrain Development by Suppressing Posteriorizing Signals. *Develop. Biol.* 225 (2), 304–321. doi:10.1006/dbio.2000.9835

Kinder, S. J., Tsang, T. E., Ang, S. L., Behringer, R. R., and Tam, P. P. (2003). Defects of the Body Plan of Mutant Embryos Lacking Lim1, Otx2 or Hnf3beta Activity. *Int. J. Dev. Biol.* 45 (1), 347–355. doi:10.1387/IJDB.11291865

Martinez-Barbera, J. P., and Beddington, R. S. (2003). Getting Your Head Around Hex and Hesx1: Forebrain Formation in Mouse. *Int. J. Dev. Biol.* 45 (1), 327–336. doi:10.1387/IJDB.11291863

Martinez-Barbera, J. P., Rodriguez, T. A., and Beddington, R. S. P. (2000). The Homeobox Gene Hesx1 Is Required in the Anterior Neural Ectoderm for Normal Forebrain Formation. *Develop. Biol.* 223 (2), 422–430. doi:10.1006/dbio.2000.9757

Matsuo, I., Kuratani, S., Kimura, C., Takeda, N., and Aizawa, S. (1995). Mouse Otx2 Functions in the Formation and Patterning of Rostral Head. *Genes Dev.* 9 (21), 2646–2658. doi:10.1101/gad.9.21.2646

McCarthy, D. J., Campbell, K. R., Lun, A. T., and Wills, Q. F. (2017). Scater: Pre-Processing, Quality Control, Normalization and Visualization of Single-Cell RNA-Seq Data in R. *Bioinformatics* 33 (8), 1179–1186. doi:10.1093/bioinformatics/btw777

McMahon, R., Sibbritt, T., Salehin, N., Osteil, P., and Tam, P. P. L. (2019). Mechanistic Insights from the LHX1-Driven Molecular Network in Building the Embryonic Head. *Develop. Growth Differ.* 61 (5), 327–336. doi:10.1111/dgd.12609

Mori-Akiyama, Y., Akiyama, H., Rowitch, D. H., and de Crombrugghe, B. (2003). Sox9 Is Required for Determination of the Chondrogenic Cell Lineage in the Cranial Neural Crest. *Proc. Natl. Acad. Sci.* 100 (16), 9360–9365. doi:10.1073/pnas.1631288100

Müllner, D. (2013). Fastcluster: Fast Hierarchical, Agglomerative Clustering Routines for R and Python. *J. Stat. Softw.* 53 (1), 1–18. doi:10.18637/jss.v053.i09

Neilson, K. M., Klein, S. L., Mhaske, P., Mood, K., Daar, I. O., and Moody, S. A. (2012). Specific Domains of FoxD4/5 Activate and Repress Neural Transcription Factor Genes to Control the Progression of Immature Neural Ectoderm to Differentiating Neural Plate. *Develop. Biol.* 365 (2), 363–375. doi:10.1016/j.ydbio.2012.03.004

Niakan, K. K., Schrode, N., Cho, L. T. Y., and Hadjantonakis, A.-K. (2013). Derivation of Extraembryonic Endoderm Stem (XEN) Cells from Mouse Embryos and Embryonic Stem Cells. *Nat. Protoc.* 8 (6), 1028–1041. doi:10.1038/nprot.2013.049

Odenthal, J., and Nüsslein-Volhard, C. (1998). Fork Head Domain Genes in Zebrafish. *Develop. Genes Evol.* 208 (5), 245–258. doi:10.1007/s004270050179

Peng, G., Suo, S., Cui, G., Yu, F., Wang, R., Chen, J., et al. (2019). Molecular Architecture of Lineage Allocation and Tissue Organization in Early Mouse Embryo. *Nature* 572 (7770), 528–532. doi:10.1038/s41586-019-1469-8

Perea-Gómez, A., Shawlot, W., Sasaki, H., Behringer, R. R., and Ang, S. (1999). HNF3beta and Lim1 Interact in the Visceral Endoderm to Regulate Primitive Streak Formation and Anterior-Posterior Polarity in the Mouse Embryo. *Development* 126 (20), 4499–4511. doi:10.1242/dev.126.20.4499

Pijuan-Sala, B., Griffiths, J. A., Guibentif, C., Hiscock, T. W., Jawaid, W., Calero-Nieto, F. J., et al. (2019). A Single-Cell Molecular Map of Mouse Gastrulation and Early Organogenesis. *Nature* 566 (7745), 490–495. doi:10.1038/s41586-019-0933-9

Ran, F. A., Hsu, P. D., Wright, J., Agarwala, V., Scott, D. A., and Zhang, F. (2013). Genome Engineering Using the CRISPR-Cas9 System. *Nat. Protoc.* 8 (11), 2281–2308. doi:10.1038/nprot.2013.143

Rhinn, M., Dierich, A., Shawlot, W., Behringer, R. R., Le Meur, M., and Ang, S. L. (1998). Sequential Roles for Otx2 in Visceral Endoderm and Neuroectoderm for Forebrain and Midbrain Induction and Specification. *Development* 125 (5), 845–856. doi:10.1242/dev.125.5.845

Shawlot, W., and Behringer, R. R. (1995). Requirement for Liml in Head-Organizer Function. *Nature* 374 (6521), 425–430. doi:10.1038/374425a0

Sherman, J. H., Karpinski, B. A., Fralish, M. S., Cappuzzo, J. M., Dhindsa, D. S., Thal, A. G., et al. (2017). Foxd4 Is Essential for Establishing Neural Cell Fate and for Neuronal Differentiation. *Genesis* 55 (6), e23031. doi:10.1002/dvg.23031

Sibbritt, T., Ip, C. K., Khoo, P. L., Wilkie, E., Jones, V., Sun, J. Q. J., et al. (2018). A Gene Regulatory Network Anchored by LIM Homeobox 1 for Embryonic Head Development. *Genesis* 56 (9), e23246. doi:10.1002/dvg.23246

Sibbritt, T., Osteil, P., Fan, X., Sun, J., Salehin, N., Knowles, H., et al. (2019). "Gene Editing of Mouse Embryonic and Epiblast Stem Cells," in *Mouse Cell Culture*. Editor I Bertoncello (New York, NY: Springer), 77–95. doi:10.1007/978-1-4939-9086-3_6

Simeone, A., Acampora, D., Mallamaci, A., Stornaiuolo, A., D'Apice, M. R., Nigro, V., et al. (1993). A Vertebrate Gene Related to Orthodenticle Contains a Homeodomain of the Bicoid Class and Demarcates Anterior Neuroectoderm in the Gastrulating Mouse Embryo. *EMBO J.* 12 (7), 2735–2747. doi:10.1002/j.1460-2075.1993.tb05935.x

Soldatov, R., Kaucka, M., Kastriti, M. E., Petersen, J., Chontorotzea, T., Englmaier, L., et al. (2019). Spatiotemporal Structure of Cell Fate Decisions in Murine Neural Crest. *Science* 364 (6444), eaas9536. doi:10.1126/science.aas9536

Stuart, T., Butler, A., Hoffman, P., Hafemeister, C., Papalexi, E., Mauck, W. M., III, et al. (2019). Comprehensive Integration of Single-Cell Data. *Cell* 177 (7), 1888–1902. doi:10.1016/j.cell.2019.05.031

Tamplin, O. J., Kinzel, D., Cox, B. J., Bell, C. E., Rossant, J., and Lickert, H. (2008). Microarray Analysis of Foxa2 Mutant Mouse Embryos Reveals Novel Gene Expression and Inductive Roles for the Gastrula Organizer and its Derivatives. *BMC genomics* 9 (1), 511–519. doi:10.1186/1471-2164-9-511

Teng, L., Mundell, N. A., Frist, A. Y., Wang, Q., and Labosky, P. A. (2008). Requirement for Foxd3 in the Maintenance of Neural Crest Progenitors. *Development* 135 (9), 1615–1624. doi:10.1242/dev.012179

Thomas, P., and Beddington, R. (1996). Anterior Primitive Endoderm May Be Responsible for Patterning the Anterior Neural Plate in the Mouse Embryo. *Curr. Biol.* 6 (11), 1487–1496. doi:10.1016/s0960-9822(96)00753-1

Varshney, M. K., Inzunza, J., Lupu, D., Ganapathy, V., Antonson, P., Rüegg, J., et al. (2017). Role of Estrogen Receptor Beta in Neural Differentiation of Mouse Embryonic Stem Cells. *Proc. Natl. Acad. Sci. USA* 114 (48), E10428–E10437. doi:10.1073/pnas.1714094114

Wang, W.-D., Melville, D. B., Montero-Balaguer, M., Hatzopoulos, A. K., and Knapik, E. W. (2011). Tfap2a and Foxd3 Regulate Early Steps in the Development of the Neural Crest Progenitor Population. *Develop. Biol.* 360 (1), 173–185. doi:10.1016/j.ydbio.2011.09.019

Warr, N., Powles-Glover, N., Chappell, A., Robson, J., Norris, D., and Arkell, R. M. (2008). Zic2 -Associated Holoprosencephaly Is Caused by a Transient Defect in the Organizer Region during Gastrulation. *Hum. Mol. Genet.* 17 (19), 2986–2996. doi:10.1093/hmg/ddn197

Wijchers, P. J. E. C., Burbach, J. P. H., and Smidt, M. P. (2006). In Control of Biology: Of Mice, Men and Foxes. *Biochem. J.* 397 (2), 233–246. doi:10.1042/bj20060387

Yamanaka, Y., Tamplin, O. J., Beckers, A., Gossler, A., and Rossant, J. (2007). Live Imaging and Genetic Analysis of Mouse Notochord Formation Reveals Regional Morphogenetic Mechanisms. *Develop. Cel* 13 (6), 884–896. doi:10.1016/j.devcel.2007.10.016

Yan, B., Neilson, K. M., and Moody, S. A. (2009). foxD5 Plays a Critical Upstream Role in Regulating Neural Ectodermal Fate and the Onset of Neural Differentiation. *Develop. Biol.* 329 (1), 80–95. doi:10.1016/j.ydbio.2009.02.019

Ying, Q.-L., Wray, J., Nichols, J., Batlle-Morera, L., Doble, B., Woodgett, J., et al. (2008). The Ground State of Embryonic Stem Cell Self-Renewal. *Nature* 453 (7194), 519–523. doi:10.1038/nature06968

Zhao, T., Gan, Q., Stokes, A., Lassiter, R. N. T., Wang, Y., Chan, J., et al. (2014). β-Catenin Regulates Pax3 and Cdx2 for Caudal Neural Tube Closure and Elongation. *Development* 141 (1), 148–157. doi:10.1242/dev.101550

Conflict of Interest: The authors declare that the research was conducted in the absence of any commercial or financial relationships that could be construed as a potential conflict of interest.

Publisher's Note: All claims expressed in this article are solely those of the authors and do not necessarily represent those of their affiliated organizations, or those of the publisher, the editors and the reviewers. Any product that may be evaluated in this article, or claim that may be made by its manufacturer, is not guaranteed or endorsed by the publisher.

frontiers in Cell and Developmental Biology

ORIGINAL RESEARCH
published: 07 February 2022
doi: 10.3389/fcell.2022.786052

Repressive Interactions Between Transcription Factors Separate Different Embryonic Ectodermal Domains

Steven L. Klein[1†], *Andre L. P. Tavares*[1†], *Meredith Peterson*[2], *Charles H. Sullivan*[3] and *Sally A. Moody*[1*]

[1]Department of Anatomy and Cell Biology, The George Washington University School of Medicine and Health Sciences, Washington, D.C., DC, United States, [2]Department of Biology, State College, Penn State University, University Park, PA, United States, [3]Department of Biology, Grinnell College, Grinnell, IA, United States

The embryonic ectoderm is composed of four domains: neural plate, neural crest, pre-placodal region (PPR) and epidermis. Their formation is initiated during early gastrulation by dorsal-ventral and anterior-posterior gradients of signaling factors that first divide the embryonic ectoderm into neural and non-neural domains. Next, the neural crest and PPR domains arise, either *via* differential competence of the neural and non-neural ectoderm (binary competence model) or *via* interactions between the neural and non-neural ectoderm tissues to produce an intermediate neural border zone (NB) (border state model) that subsequently separates into neural crest and PPR. Many previous gain- and loss-of-function experiments demonstrate that numerous TFs are expressed in initially overlapping zones that gradually resolve into patterns that by late neurula stages are characteristic of each of the four domains. Several of these studies suggested that this is accomplished by a combination of repressive TF interactions and competence to respond to local signals. In this study, we ectopically expressed TFs that at neural plate stages are characteristic of one domain in a different domain to test whether they act cell autonomously as repressors. We found that almost all tested TFs caused reduced expression of the other TFs. At gastrulation these effects were strictly within the lineage-labeled cells, indicating that the effects were cell autonomous, i.e., due to TF interactions within individual cells. Analysis of previously published single cell RNAseq datasets showed that at the end of gastrulation, and continuing to neural tube closure stages, many ectodermal cells express TFs characteristic of more than one neural plate stage domain, indicating that different TFs have the opportunity to interact within the same cell. At neurula stages repression was observed both in the lineage-labeled cells and in adjacent cells not bearing detectable lineage label, suggesting that cell-to-cell signaling has begun to contribute to the separation of the domains. Together, these observations directly demonstrate previous suggestions in the literature that the segregation of embryonic ectodermal domains initially involves cell autonomous, repressive TF interactions within an individual cell followed by the subsequent advent of non-cell autonomous signaling to neighbors.

Keywords: neural plate, neural border zone, neural crest, placode, epidermis, foxd4

OPEN ACCESS

Edited by:
Kerstin Feistel,
University of Hohenheim, Germany

Reviewed by:
Jean-Pierre Saint-Jeannet,
New York University, United States
Fabienne Lescroart,
INSERM U1251 Centre de Génétique Médicale de Marseille (MMG), France

****Correspondence:***
Sally A. Moody
samoody@gwu.edu

†These authors share first authorship

Specialty section:
This article was submitted to Morphogenesis and Patterning, a section of the journal Frontiers in Cell and Developmental Biology

Received: *29 September 2021*
Accepted: *10 January 2022*
Published: *07 February 2022*

Citation:
Klein SL, Tavares ALP, Peterson M, Sullivan CH and Moody SA (2022) Repressive Interactions Between Transcription Factors Separate Different Embryonic Ectodermal Domains. Front. Cell Dev. Biol. 10:786052. doi: 10.3389/fcell.2022.786052

1 INTRODUCTION

Shortly after gastrulation is completed, the vertebrate embryonic ectoderm is composed of four distinct domains with different fates. The neural plate (NP) will become the brain and spinal cord, the neural crest (NC) will give rise to most of the peripheral nervous system as well as some non-neural tissues, the pre-placodal region (PPR) will contribute to the cranial sensory organs and sensory ganglia, and the epidermis (Epi) will become the skin and its appendages. The process by which these domains arise is believed to involve two main steps: at gastrula stages the embryonic ectoderm is separated into neural and non-neural domains by ventral-to-dorsal (or lateral-to-medial, depending on the animal) gradients of Wnt and BMP signaling, and subsequently the NC and PPR arise at the border between them (reviewed in Stuhlmiller and Garcia-Castro, 2012; Saint-Jeannet and Moody, 2014; Schlosser, 2014; Schlosser et al., 2014; Moody and LaMantia, 2015; Streit, 2018; Seal and Monsoro-Burq, 2020; Thawani and Groves, 2020; Schlosser, 2021). By late neural plate stages, each of the four domains is characterized by a distinct suite of transcription factors (TFs) that are thought to impose domain-specific identity (reviewed in Grocott et al., 2012; Milet and Monsoro-Burq, 2012; Moody and LaMantia, 2015; Streit, 2018; Seal and Monsoro-Burq, 2020; Thawani and Groves, 2020).

Two models have been proposed for how the NC and PPR domains segregate. The "binary competence" model posits that due to the expression of different combinations of TFs and region-specific signals, the lateral border of the neural ectoderm becomes competent to give rise to NC and the medial border of the non-neural ectoderm becomes competent to give rise to the PPR (Ahrens and Schlosser, 2005; Schlosser, 2008; Pieper et al., 2012; Schlosser, 2021). The "border state" model posits that interactions between the neural and non-neural ectoderm produce an intermediate neural border zone (NB) that contains common precursors of both NC and PPR, and their domains subsequently separate *via* differential responses to signals from the underlying tissues and the expression of TFs that are enriched in either the NC or PPR by late neural plate stages (reviewed in Moody and LaMantia, 2015; Seal and Monsoro-Burq, 2020; Thawani and Groves, 2020; Schlosser 2021). This idea is supported by transcriptomic analyses of dissected pieces of ectoderm in frog and chick that showed that at first TFs characteristic of dorsal/midline ectoderm broadly overlap with TFs characteristic of ventral/lateral ectoderm, which by the end of gastrulation resolves into regionally-distinct transcriptional signatures (Hintze et al., 2017; Plouhinec et al., 2017; Trevers et al., 2018). By late neural plate/neurula stages these signatures become more distinct with the expression of TFs that are thought to specify a particular domain. Thus, the acquisition of distinct NP, NC, PPR and Epi fates appears to be a gradual process that involves, at least in part, TF interactions that eventually segregate domains.

Consistent with these transcriptomic analyses, lipophilic dye tracing of small groups of cells (Streit, 2002; Ezin et al., 2009; Pieper et al., 2011) suggested that the NB is comprised of a mixture of cells that initially are competent to give rise to cells typical of all four neural plate stage domains. Supporting this idea, analysis of TF protein expression at the single cell level found that a subset of cells in the NB expressed TFs characteristic of more than one neural plate stage domain (Roellig et al., 2017). By experimentally manipulating the levels of Sox2 (used as a marker of NP) and Pax7 (used as a marker of NC), these authors suggested the possibility that within a single cell there is competition between TFs that is repressive in nature and ultimately determines the cell's domain-specific fate. Building upon this work, we asked whether TFs that are enriched in a particular domain at neural plate stages, so-called "landmark" genes (Plouhinec et al., 2017), repress TFs that are enriched in a different domain by taking advantage of the *Xenopus* 16-cell stage fate map (Moody, 1987) to ectopically express the TFs (**Figure 1**). In nearly every case we found that ectopic expression of TFs enriched in a specific domain at neural plate stages reduced the expression of TFs characteristic of the other three domains.

To assess whether these effects were cell autonomous, we lineage traced the cells that ectopically expressed the exogenous TF. We found that at gastrula stages only the cells carrying the lineage tracer showed reduced TF expression, whereas at neural plate stages reduced TF expression often was additionally observed in cells adjacent to the labeled clone, suggesting that cell-to-cell signaling likely had begun to contribute to segregating the domains. The consistent pattern of mutually reduced expression regardless of the domain or the TF requires that TFs characteristic of more than one domain be expressed in a single cell, as indicated by the protein expression data of Roellig et al. (2017). Since all previous transcriptomic studies were accomplished on bulk RNA preparations of

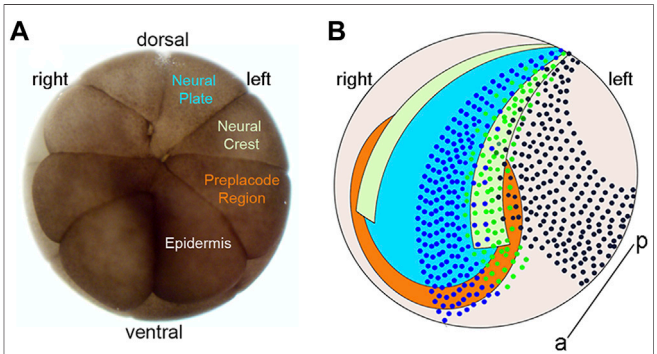

FIGURE 1 | Blastomere fate map and location of clones at neural plate stages. **(A)** Animal view of a 16-cell *Xenopus laevis* embryo indicating the major precursors of the neural plate (blue), neural crest (light green), pre-placode region (PPR; orange) and epidermis (light brown) on the embryo's left side. **(B)** Cartoon of the ectodermal domains at the neural plate stage with dorsal to the top, anterior to the front, and the anterior-posterior axis (a–p) indicated by a line. Dark blue dots indicate a clone of cells derived from a left blastomere injection that occupies the left neural plate (blue) and left anterior PPR (orange). Green dots indicate a clone of cells derived from a left blastomere injection that occupies the left neural plate border including the left neural crest (light green) and left posterior PPR (orange). Dark brown dots indicate a clone of cells derived from a left blastomere injection that occupies the left dorso-lateral epidermis (light brown).

microdissected ectodermal pieces or explants, instead we analyzed a published single-cell RNAseq dataset at the end of gastrulation and at neural tube closure (Briggs et al., 2018). At both stages we detected numerous cells that expressed TFs characteristic of more than one neural plate stage domain. Together, these data support the idea that the segregation of the four ectodermal domains involves mutual repression between TFs characteristic of more than one neural plate stage domain at the single cell level, and later likely includes signaling between cells.

2 MATERIALS AND METHODS

2.1 Obtaining Embryos and Microinjections

Fertilized *Xenopus laevis* eggs were obtained by gonadotropin-induced natural mating of wild type, outbred adult frogs as previously described (Moody, 2018a). Embryos were selected at the 2-cell stage if the first cleavage furrow bisected the lightly pigmented region of the animal hemisphere to accurately identify the dorsal-ventral axis (Klein, 1987; Miyata et al., 1987). When these selected embryos reached the 16-cell stage, one animal blastomere that is the major precursor of one of the ectodermal domains (**Figure 1**; Moody, 1987) was microinjected with 1 nL of a solution containing 100 pg of TF mRNA and 100 pg of lineage tracer mRNA, according to standard methods (Moody, 2018b). This amount of TF mRNA injected was the lowest of the levels reported in previous studies (cited in **Section 2.2**) that characterized these TFs to alter gene expression.

2.2 *In vitro* Synthesis of mRNAs and Antisense RNA Probes

5′capped and polyadenylated mRNAs encoding TFs expressed by cells in the neural plate (*foxd4l1.1*; Sullivan et al., 2001), neural crest (*foxd3*, Sasai et al., 2001; *msx1*, Suzuki et al., 1997; Tribulo et al., 2003; Monsoro-Burq et al., 2005; *zic1*, *zic2*, and *zic3*, Nakata et al., 1997, Nakata et al., 1998), PPR (*six1;* Brugmann et al., 2004), or epidermis (*dlx5*, Papalopulu and Kintner, 1993; Luo et al., 2001), as well as a nucleus-localized *β-galactosidase* (*nβgal*) as a lineage tracer, were synthesized *in vitro* (mMessage mMachine kit, ThermoFisher). Antisense RNA probes for *in situ* hybridization (ISH) were synthesized *in vitro* (MEGAscript kit; ThermoFisher) as previously described (Yan et al., 2009).

2.3 Fixation, Histochemistry and *in situ* Hybridization

Embryos were cultured to gastrula (st 11.5–13) or neurula (st 16–18) stages (Nieuwkoop and Faber, 1994), fixed in 4% paraformaldehyde (in 0.1 M MOPS, 2 mM EGTA Magnesium, 1 mM $MgSO_4$, pH 7.4), stained for βGal histochemistry to reveal the cells that received the exogenous mRNA, and processed for *in situ* hybridization (ISH) as previously described (Yan et al., 2009). Each experiment was repeated in 2–5 independent trials with different sets of parents to ensure genetic diversity in the samples. Embryos were scored for gene expression changes, comparing the injected (β-Gal-positive) versus the uninjected side of the same embryo, independently by at least two of the authors, and the values reported are means of their independent scores. For **Figures 2–5**, only embryos in which the β-Gal-positive cells were within the domain of the assessed gene were included in the analysis. For **Figure 6**, only embryos in which βGal-positive cells were not within the domain of the assessed gene were included in the numbers presented in **Tables 1**, **2**. As injection controls, only *nβgal* mRNA was injected into a blastomere, and the expression of at least 2 TFs enriched in each domain were analyzed by ISH. In nearly every case, the expression domain on the injected side was the same as that on the uninjected side of the same embryo [NP: *foxd4* (100%, $n = 11$), *sox2* (100%; $n = 18$), *irx1* (100%, $n = 22$); NC: *foxd3* (94.7%, $n = 19$), *sox9* (95.5%, $n = 22$); PPE: *six1* (100%, $n = 25$), *irx1* (100%, $n = 22$), *sox9* (100%, $n = 22$); Epi: *dlx5* (100%, $n = 22$), *foxi* (100%, $n = 31$)]. These controls verify that the observed expression changes reported below were due to the TF mRNAs not the lineage tracer.

2.4 Analysis of Single Cell RNAseq Dataset

We utilized the single cell RNAseq dataset generated by Briggs et al. (2018), which is available online at https://kleintools.hms.harvard.edu/tools/currentDatasetsList_xenopus_v2.html. We extracted data from reference SPRING plots for Stage 13 and Stage 18 embryos. These plots contain K-nearest-neighbor (knn) graphs that are used for visualization of data clusters. In these graphs, each cell is represented as a node that extends edges to other nodes/cells that have a similar expression of genes (Weinreb et al., 2018). The Stage 13 plot contains 8,931 raw cells and the Stage 18 plot contains 12,432 raw cells.

Analyses were performed using a two-step process for cell selection. First, aiming to only analyze cells related to neural plate, neural crest, PPR, and epidermis, cells located in "celltype" clusters, designated based on similar transcriptomic signatures, representing these domains were selected. At stage 13, the selected "celltype"clusters were: "anterior neural plate", "chordal neural plate", "ionocyte", "neural crest", "non-neural ectoderm", and "placodal area". At stage 18, the selected "celltype"clusters were: "adenohypophyseal placode", "anterior neural tube - fezf1", "anterior neural tube - nkx2-1/nkx2-4", "anterior placodal area", "chordal neural crest", "chordal neural plate border", "cranial neural crest", "epibranchial and lateral line placodes", "epidermal - aqp3", "epidermal progenitor - tp63/ctbs", "epidermal progenitor - tp63/tll2", "ionocyte", "olfactory placode", "otic placode", "placodal neuron - eya2/neurog1/neurod1", "posterior neural tube", "posterior placodal area", and "trigeminal and profundal placodes". Next, at each stage all cells within the composite of selected clusters that expressed either foxd4l1.1 | FOXD4L1.1, sox2 | SOX2, msx1 | LOC100125666, foxd3 | FOXD3, zic2 | ZIC2-A, six1 | SIX1, dlx5 | DLL3, or foxi1 | FOXI1E were selected and their expression profiles downloaded using the "SPRING data for selection" tool. Eight transcription factor dataset files per stage containing all genes expressed in the selected cells were generated: *foxd4* (stage 13: 44 cells; stage 18: 200 cells), *sox2* (stage 13: 1,192 cells; stage 18:

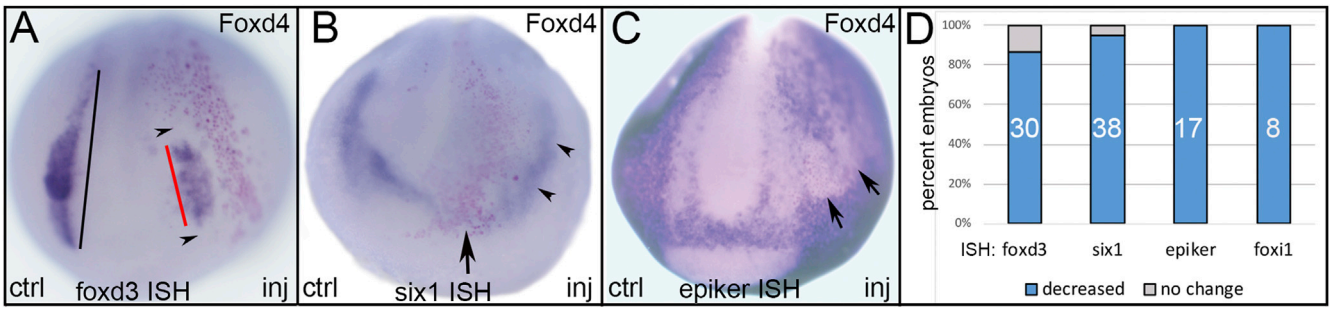

FIGURE 2 | The effects of expressing an NP-enriched transcription factor, Foxd4, in ectopic domains. **(A)** Ectopic expression of Foxd4 (NP TF) in a neural crest precursor blastomere showed reduced size of the *foxd3* neural crest domain (red bar) on the injected side of the embryo. Compare to the length of the *foxd3* expression domain on the control side (black bar). Note that *foxd3* is reduced both in areas occupied by lineage-labeled cells (red dots) as well as areas adjacent to these cells (black arrowheads). ctrl, control side; inj, injected side, anterior view with dorsal to the top. **(B)** Ectopic expression of Foxd4 (NP TF) at the anterior dorsal midline (red dots) eliminated *six1* expression in the anterior PPR (arrow), and reduced expression in the posterior PPR (black arrowheads) adjacent to the lineage-labeled cells. Anterior view with dorsal to the top. **(C)** Ectopic expression of Foxd4 (NP TF) in a lateral position (red dots) eliminated the expression of *epidermis-specific keratin* (*epiker*) in the lateral epidermis (arrows). Anterior view with dorsal to the top. **(D)** The percentage of embryos in which ectopic Foxd4 reduced expression of neural crest (*foxd3*), PPR (*six1*) or epidermis (*epiker*, *foxi1*) genes. Numbers within the bars denote sample size.

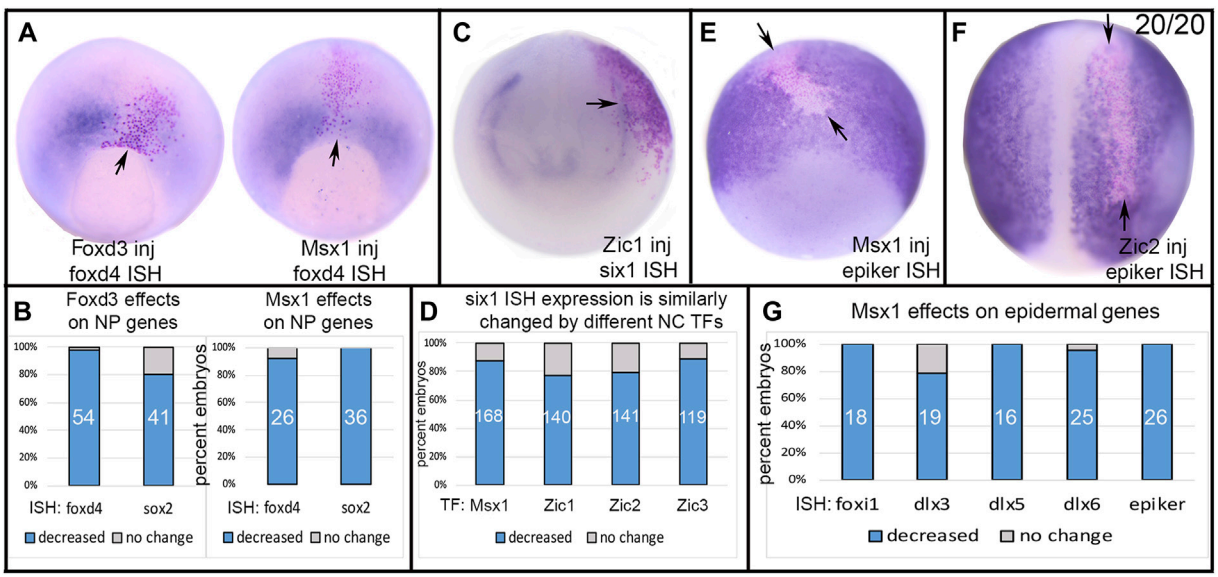

FIGURE 3 | The effects of expressing NC-enriched transcription factors in ectopic domains. **(A)** Ectopic expression of Foxd3 or Msx1(NC TFs) in a neural plate precursor blastomere resulted in reduced expression of *foxd4* (NP TF) only in the region of the lineage-labeled cells (red dots, arrow). Vegetal views at midgastrula (st 11.5) with dorsal to the top. **(B)** The percentage of embryos in which the neural plate expression of *foxd4* or *sox2* were reduced by ectopic expression of either Foxd3 or Msx1. Numbers within the bars denote sample size. **(C)** Ectopic expression of Zic1 (NC TF) in a placode precursor blastomere reduced the PPR expression of *six1* (arrow) in cells expressing Zic1 (red dots). Anterior view with dorsal to the top. **(D)** The percentage of embryos in which the PPR expression of *six1* was reduced by ectopic expression of four different NC TFs. Numbers within the bars denote sample size. **(E)** Ectopic expression of Msx1 (NC TF) in an epidermis precursor blastomere reduced the Epi expression of *epiker* (between arrows) only in cells ectopically expressing Msx1 (red dots). Ventral view of gastrula stage with dorsal to the top. **(F)** Ectopic expression of Zic2 (NC TF) in an epidermis precursor blastomere reduced the Epi expression of *epiker* (between arrows) only in cells ectopically expressing Zic2 (red dots). Dorsal view of neurula stage with anterior to the top. **(G)** The percentage of embryos in which the expression of several Epi genes was reduced by ectopic expression of Msx1. Numbers within the bars denote sample size.

1,079 cells), *msx1* (stage 13: 284 cells; stage 18: 529 cells), *foxd3* (stage 13: 4 cells; stage 18: 32 cells), *zic2* (stage 13: 128 cells; stage 18: 437 cells), *six1* (stage 13: 111 cells; stage 18: 188 cells), *dlx5* (stage 13: 233 cells; stage 18: 148 cells), foxi1 (stage 13: 191 cells; stage 18: 121 cells). We then determined the number of single cells expressing at least two (**Tables 3**, **5**) or more (**Tables 4**, **6**, **7**) transcription factors. In each table, the number of cells that expressed both the selected transcription factor (each column) and one of the other eight analyzed genes (each row) was tabulated. The bottom row of **Tables 3**, **5** denotes the number

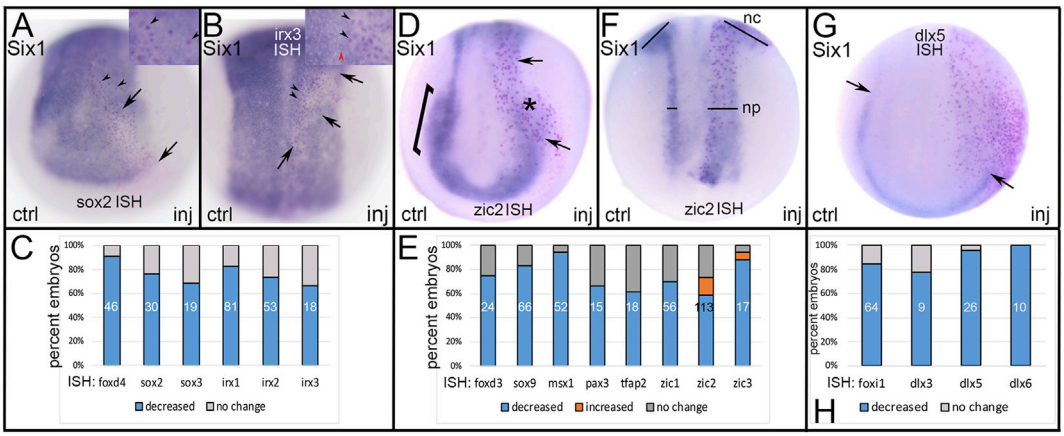

FIGURE 4 | The effects of expressing a PPR-enriched transcription factor, Six1, in ectopic domains. **(A)** Ectopic expression of Six1 (PPR TF) in a neural plate precursor blastomere (red dots between arrows) showed reduced expression of *sox2* (NP TF). Arrowheads in low magnification image and inset indicate Six1-expressing cells containing a red lineage-tagged nucleus surrounded by clear cytoplasm denoting reduced *sox2* expression. In this case, the effect was cell autonomous. ctrl, control side; inj, injected side, anterior view with dorsal to the top. **(B)** Ectopic expression of Six1 (PPR TF) in a neural plate precursor blastomere (red dots between arrows) showed reduced expression of *irx3* (NP TF). Black arrowheads in low magnification image and inset indicate Six1-expressing cells containing a red lineage-tagged nucleus surrounded by clear cytoplasm denoting reduced *irx3* expression. In this case, the effect was cell autonomous. Red arrowhead in inset indicates a cell that does not ectopically express Six1 (clear nucleus) and expresses normal levels of *irx3* (dark blue), for comparison. Dorsal view with anterior to the top. **(C)** The percentage of embryos in which the expression of several NP-enriched genes were reduced by ectopic expression of Six1. Numbers within the bars denote sample size. **(D)** Ectopic expression of Six1 (PPR TF) in a neural crest precursor blastomere (red dots between arrows) showed reduced expression of *zic2* in both the neural plate (arrows) and neural crest (*) domains. The NC domain of *zic2* on the control side is indicated by a bracket. Anterior view with dorsal to the top. **(E)** The percentage of embryos in which the expression of several NC-enriched genes was reduced (blue) or expanded (orange) by ectopic expression of Six1. Numbers within the bars denote sample size. **(F)** In a small number of embryos, ectopically expressed Six1 (PPR TF) expanded the neural plate (np) and neural crest (nc) expression domains of *zic2*. Bars compare the widths between control (ctrl) and injected (inj) sides. Dorsal view with anterior to the top. **(G)** Ectopic expression of Six1 (PPR TF) in a lateral precursor blastomere (red dots) reduced expression of *dlx5* (Epi TF) in the epidermis along the border zone. Arrows indicate the posterior limit of the *dlx5* domain on control (ctrl) and injected (inj) sides. Anterior view with dorsal to the top. **(H)** The percentage of embryos in which the expression of several Epi-enriched genes was reduced by ectopic expression of Six1. Numbers within the bars denote sample size.

of cells across all selected "celltype" clusters that expressed the selected transcription factor (each column), in other words the pool of all cells in the dataset in the selected "celltype" cluster that expressed that gene. This number did not equal the sum of cells in each column because a single cell can express more than two transcription factors.

3 RESULTS

Many previous studies showed that as the embryonic ectoderm gradually resolves into four distinct domains, numerous TFs are expressed in overlapping patterns that eventually segregate during neurulation into NP, NC, PPR and Epi, each of which characteristically expresses a subset of these TFs (reviewed in Moody and LaMantia, 2015; Seal and Monsoro-Burq, 2020; Thawani and Groves, 2020; Schlosser 2021). It is commonly posed that the overlapping expression domains are sharpened into distinct domains by repressive interactions between these TFs, similar to the interactions between *gap* genes during segmentation in *Drosophila* (reviewed in Jaeger, 2011). To test this possibility, we ectopically expressed TFs that are thought to specify one domain by neural plate stages in a clone of cells that populates a different domain by targeted microinjections of mRNAs into 16-cell blastomere precursors of each domain (**Figure 1**). Using whole mount ISH, we then assessed the resulting expression patterns of a domain-enriched gene compared to the control, uninjected side of the same embryo. While previous studies focused on *sox2* and *sox3* as NP specifiers, we uniquely focused on the forkhead transcription factor Foxd4l1.1, henceforth referred to as Foxd4, because of its three advantages. It is one of the earliest expressed NP genes (Sullivan et al., 2001; Sherman et al., 2017); it is required for the expression of many other NP genes, including *sox2-3* and *irx1-3*; and none of these TFs feedback to regulate it (Yan et al., 2009; Klein and Moody, 2015; Gaur et al., 2016). As in other studies, we ectopically expressed the NC specifier, Foxd3, but additionally ectopically expressed several other TFs that are acknowledged NC specifiers (Msx1, Zic1; Plouhinec et al., 2014; Plouhinec et al., 2017). We also tested other Zic family members (Zic2, Zic3) that are understudied but likewise enriched in the NC domain at neural plate stages and are thought to be functionally redundant with Zic1 (Nakata et al., 1997; Nakata et al., 1998; Sasai et al., 2001; Grocott et al., 2012). We ectopically expressed Six1 to test the effect of an acknowledged PPR specifier that is required for the expression of other PPE genes, including *eya1*, *sox11* and *irx1* (Brugmann et al., 2004; Yan et al., 2015; Riddiford and Schlosser, 2016; Hintze et al., 2017; Sullivan et al., 2019). We ectopically expressed Dlx5 to test the effect of a TF that specifies the dorso-lateral epidermis in *Xenopus* (Luo et al., 2001).

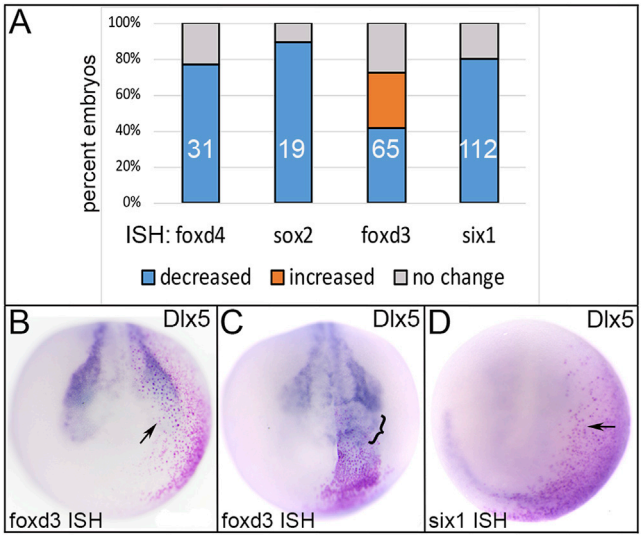

FIGURE 5 | The effects of expressing an Epi-enriched transcription factor, Dlx5, in ectopic domains. **(A)** The percentage of embryos in which ectopically expressed Dlx5 reduced (blue) or expanded (orange) expression of neural plate (*foxd4, sox2*), neural crest (*foxd3*) or PPR (*six1*) genes. Numbers within the bars denote sample size. **(B)** Ectopic expression of Dlx5 (Epi TF) in a neural crest precursor blastomere (red dots) reduced expression of *foxd3* (NC TF; arrow). Anterior view with dorsal to the top. **(C)** Ectopic expression of Dlx5 (Epi TF) in a neural plate blastomere (red dots) broadened the expression of *foxd3* (NC TF; bracket). Anterior view with dorsal to the top. **(D)** Ectopic expression of Dlx5 (Epi TF) in a placode precursor blastomere (red dots) reduced the expression of *six1* (PPR TF; arrow). Anterior view with dorsal to the top.

3.1 Ectopic Expression of Domain-Enriched TFs Repress TFs Characteristic of Each of the Other Domains

Ectopic expression of Foxd4, a TF that is highly expressed in the early neural ectoderm, acts upstream of several NP genes and can induce their ectopic expression, including *gmnn*, *sox2, sox3, and sox11* (Sullivan et al., 2001; Yan et al., 2009; Gaur et al., 2016), reduced at high frequencies the expression of TFs that at neural plate stages are enriched in either NC, PPR or Epi (**Figure 2**). We found that ectopic expression of Foxd4 in the dorso-lateral region reduced the NC domain of *foxd3* (**Figures 2A,D**) and the PPR domain of *six1* (**Figures 2B,D**). Ectopic expression of Foxd4 in the more ventral ectoderm eliminated expression of an epidermis-specific keratin (*krt12.4*, herein named *epiker*; **Figures 2C,D**), confirming previous reports (Yan et al., 2009; Gaur et al., 2016), as well as *foxi1* (**Figure 2D**), which is enriched in the epidermis at late gastrula and neural plate stages (Plouhinec et al., 2017). In no case did ectopic Foxd4 up-regulate the expression of any of the tested NC, PPR or Epi genes.

Foxd3, a key neural crest specifier (Plouhinec et al., 2017; Lukoseviciute et al., 2018), induced the expression of several other neural crest markers in *Xenopus* (Sasai et al., 2001). Msx1 also upregulates *foxd3*, *slug* and *twist* (Tribulo et al., 2003; Monsoro-Burq et al., 2005), and Zic1-3 upregulate *slug* and *twist* (Nakata et al., 1997; Nakata et al., 1998). Herein, we found that Zic2 and Zic3 also increased *foxd3* (54%, n = 56 and 67%, n = 53, respectively). Ectopic expression of Foxd3 reduced at high frequencies the expression of TFs that at neural plate stages are enriched in either NP, PPR or Epi (**Figure 3**). Ectopic expression of Foxd3 in the dorsal midline reduced the early NP expression of *foxd4* and *sox2* (**Figures 3A,B**). Msx1, another NC specifier, had very similar effects on *foxd4* and

TABLE 1 | The number of cases in which cells distant from the lineage label showed reduced expression at gastrula stages.

mRNA injected	*foxd4* ISH	*sox2* ISH	*msx1* ISH	*foxi1* ISH
	st11-13	st11-13	st11-13	st11-13
foxd3	0/3	0/2	No cases	No cases
msx1	0/15	0/6	No cases	0/6
six1	0/11	No cases	0/5	0/11
dlx5	0/3	0/4	No cases	No cases

"No cases" means that the dataset did not contain any embryos with distant, lineage-labeled clones.

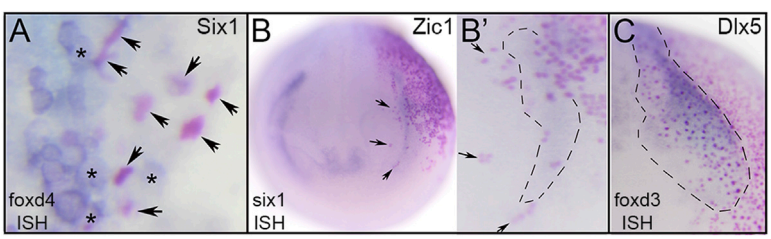

FIGURE 6 | TF effects are cell-autonomous at gastrula stages but likely include signaling to neighbors at neurula stages. **(A)** Dorsal midline of gastrula showing Six1-expressing cells that have lineage-labeled nuclei (arrows, red dots). Each of the lineage-labeled cells showed reduced *foxd4* expression (clear cytoplasm). In contrast, uninjected neighbors (asterisks, clear nuclei) showed high levels of *foxd4* expression (blue cytoplasm). **(B)** Ectopic expression of Zic1 (NC TF) in a placode precursor blastomere (red dots) showing Zic1-expressing cells on right side of neurula stage embryo (red nuclei) overlapping with the reduced *six1* PPR expression domain (blue). Anterior view with dorsal to the top. B′ shows a higher magnification of the *six1* PPR domain on the injected side. For orientation, arrows point to the same cells as in B. Each of the lineage-labeled cells showed reduced *six1* PPR expression, but within the region surrounded by the dashed line, uninjected neighbors also had reduced expression. **(C)** Ectopic expression of Dlx5 (Epi TF) in a neural crest precursor blastomere (red dots) showing Dlx5-expressing cells (red nuclei) within the *foxd3* neural crest expression domain outlined by dashes of a neurula stage embryo. Within that domain, lineage-labeled cells showed reduced *foxd3* neural crest expression, but it also was reduced in adjacent uninjected neighbors. Anterior view with medial to the left and dorsal to top.

TABLE 2 | The number of cases in which cells distant from the lineage label showed reduced expression at neurula stages.

mRNA injected	*foxd3* ISH	*six1* ISH	*dlx3* ISH	*dlx5* ISH	*dlx6* ISH	*foxi1* ISH
	st16-18	st16-18	st16-18	st16-18	st16-18	st16-18
foxd4	27/27 (100%)	14/19 (73.7%)	2/5 (40%)	No cases	3/5 (60%)	6/9 (66.7%)
msx1	11/15 (73.3%)	5/18 (27.8%)	0/1	1/11 (9.1%)	2/6 (33.3%)	4/6 (66.7%)
six1	No cases	Not done	0/3	0/3	0/6	0/4
dlx5	2/9 (22.2%)	7/14 (50%)	Not done	Not done	Not done	Not done

"No cases" means that that the dataset did not contain any embryos with distant, lineage-labeled clones. "Not done" means that we did not perform this experimental combination.

TABLE 3 | The number of single cells co-expressing at least two domain-enriched transcription factors at stage 13.

	foxd4[a]	*sox2*[a]	*msx1*[a]	*foxd3*[a]	*zic2*[a]	*six1*[a]	*dlx5*[a]	*foxi1*[a]
foxd4[c]	-	23	1	0	0	0	0	0
sox2[c]	31	—	67	1	40	37	68	5
msx1[c]	1	36	—	0	6	6	7	2
foxd3[c]	0	0	0	—	0	0	0	0
zic2[c]	9	373	44	0	—	4	12	1
six1[c]	0	11	6	0	1	—	21	1
dlx5[c]	1	44	25	0	8	28	—	15
foxi1[c]	0	2	4	0	0	0	1	—
Total # of cells[a]	44	1192	284	4	128	111	233	191

[a]*Transcription factor dataset that was queried. Single cells were selected based on the expression of the transcription factor at the top of each column in all selected "celltype" clusters defined in* ***Section 2.4****.*

[b]*The total number of cells across all selected "celltype" clusters that co-expressed the transcription factor at the top of each column. This number did not equal the sum of cells in each column because a single cell can express more than two transcription factors.*

[c]*The transcription factor that was co-expressed with the factor at the top of each column.*

sox2 (**Figures 3A,B**). A previous study also showed that Msx1 repressed the NP expression of *sox3* (Maharana and Schlosser, 2018). We previously demonstrated that ectopically expressing Foxd3 in the PPR reduced the expression domain of *six1* (Brugmann et al., 2004). We expanded this observation by testing whether other TFs enriched in the NC domain at neural plate stages had a similar effect. Indeed, we found that injecting *msx1*, *zic1*, *zic2* or *zic3* mRNAs into blastomeres that contribute to the PPR reduced *six1* expression in the majority of embryos (**Figures 3C,D**). Previous work demonstrated that Foxd3 represses the expression of *epiker* (Sasai et al., 2001). We expanded this observation and found that ectopic Msx1 and Zic2 also repressed several TFs enriched in the Epi domain at neural plate stages (*foxi1*, *dlx3*, *dlx5*, *dlx6*, *epiker*) (**Figures 3E–G**). In no case did TFs enriched in the NC at neural plate stages up-regulate the expression of any of the tested NP, PPR or Epi genes.

Six1 is a PPR specifier (Brugmann et al., 2004; Hintze et al., 2017) that upregulates the expression of other PPR genes, including *eya1*, *sox11* and *irx1* (Brugmann et al., 2004; Yan et al., 2015; Riddiford and Schlosser, 2016; Sullivan et al., 2019), but herein we found that it does not alter the PPR expression of other members of the Six family (*six2*, $n = 48$; *six4.1*, $n = 53$). Ectopic expression of Six1 frequently reduced the expression of TFs that at neural plate stages are enriched in either NP, NC or Epi (**Figure 4**). Ectopic expression of Six1 in the dorsal midline decreased the expression of several genes expressed in the early NP including *foxd4*, *sox2*, *sox3*, *irx1*, *irx2* and *irx3* (**Figures 4A–C**). Previous work indicated that Six1 promotes PPR fates by upregulating other PPR genes and downregulating the NC specifier *foxd3* (Brugmann et al., 2004). In concordance with those findings, we observed that ectopic expression of Six1 in NC progenitors reduced the expression of many TFs enriched in the NC domain at neural plate stages - *foxd3*, *sox9*, *msx1*, *pax3*, *tfap2* and *zic1-3* - in the majority of embryos (**Figures 4D,E**). Interestingly, a small percentage of embryos showed expansion of *zic2* and *zic3* expression in their NC and NP domains (**Figures 4E,F**). Ectopic expression of Six1 in the ventral ectoderm reduced expression of several TFs enriched in the Epi domain at neural plate stages (*foxi1, dlx3, dlx5, dlx6*; **Figures 4G,H**).

Dlx5 is a specifier of the dorso-lateral epidermis in *Xenopus* (Luo et al., 2001), and upregulates the epidermal genes *Gata3* and *foxi1* in chick, fish and frog (McLarren et al., 2003; Matsuo-Takasaki et al., 2005; Kwon et al., 2010; Pieper et al., 2012). Ectopic expression of Dlx5 frequently reduced the expression of TFs that at neural plate stages are enriched in either NP, NC or PPR (**Figure 5**). Dlx5 misexpression in the dorsal ectoderm reduced early NP expression of *foxd4* and *sox2* (**Figure 5A**); the latter result is consistent with a similar experiment in chick (McLarren et al., 2003). Dlx5 misexpression in the dorso-lateral region resulted in both reduced and expanded *foxd3* (**Figures 5A–C**), but only reduced *six1* (**Figures 5A,D**) expression. The latter result was surprising since previous work indicated that Dlx5 directly upregulates *Six1* in mouse (Sato et al., 2010) and is required for *six1* expression (Woda et al., 2003; reviewed in Grocott et al., 2012).

TABLE 4 | The number of single cells co-expressing three or four domain-enriched transcription factors at stage 13.

	*foxd4**	*sox2**	*msx1**	*zic2**	*six1**	*dlx5**	*foxi1**
sox2+six1$^+$	-	-	1	-	-	10	-
sox2+msx1$^+$	-	-	-	1	1	-	-
sox2+zic2$^+$	7	-	26	-	-	8	-
sox2+dlx5$^+$	1	-	-	5	11	-	-
msx1+zic2$^+$	-	21	-	-	-	-	-
zic2+dlx5$^+$	-	8	-	-	-	-	1
foxd4+zic2$^+$	-	5	-	-	-	-	-
six1+dlx5$^+$	-	1	1	-	-	-	-
msx1+six1$^+$	-	1	-	-	-	-	-
msx1+dlx5$^+$	-	-	-	-	1	-	-
sox2+zic2+dlx5$^+$	-	-	1	-	-	-	-
sox2+six1+dlx5$^+$	-	-	1	-	-	-	-
sox2+msx1+dlx5$^+$	-	-	-	-	1	-	-

Cells labeled with the same color co-expressed the same combination of three or four domain-enriched transcription factors.
**Transcription factor dataset that was queried.*
+ The transcription factor that was co-expressed with the factor at the top of each column.

3.2 Reduced Expression at Gastrula Stages is Cell Autonomous Whereas at Neurula Stages it is Both Cell Autonomous and Non-autonomous

In analyzing the specimens presented above, we noticed that in some cases the reduction in gene expression was always cell autonomous, i.e., reduction was only observed in cells that also were marked by the lineage tracer (e.g., **Figures 3A,E**), whereas for others the target TF was reduced in both the cells carrying the lineage tracer (cell-autonomous) and in adjacent cells not labeled by the lineage tracer (e.g., **Figures 2A,B**). This suggested that for some genes the effects were strictly within the single cell that inherited the injected mRNA (βGal-positive), whereas for others signaling from that cell to nearby neighbors likely also was involved. For the frequency analyses presented in **Figures 2–5**, we only scored embryos in which the lineage tracer overlapped with the domain being analyzed. However, in most experimental batches there usually were a few embryos in which the lineage tracer did not overlap but was in proximity to the domain of interest, likely due to mistargeted injections at cleavage stages. When we screened these cases, we found that for genes that were analyzed at late gastrula stages (*foxd4*, *sox2*, *msx1*, *dlx5*), there were no cases, regardless of the injected mRNA, of non-autonomous reduction of expression; reduction was only observed in βGal-positive cells (**Figure 6A**; **Table 1**). In contrast, for genes that were analyzed at neurula stages (*foxd3*, *six1*, *dlx3*, *dlx5*, *dlx6*, *foxi1*), there often were cases of reduced expression distant from the lineage labeled cells (**Figures 2A**,**B**, **6B**,C; **Table 2**); this occurred most frequently when *foxd4* or *msx1* mRNA was injected. These results suggest that as development progresses, signaling from cells ectopically expressing the neural plate stage domain-enriched TFs likely contributes to the segregation of these domains.

3.3 Single Cell RNAseq Analysis

These analyses demonstrate that TFs enriched in the four domains at neural plate stages reduce the expression of TFs

TABLE 5 | The number of single cells co-expressing at least two domain-enriched transcription factors at stage 18.

	foxd4[a]	***sox2***[a]	***msx1***[a]	***foxd3***[a]	***zic2***[a]	***six1***[a]	***dlx5***[a]	***foxi1***[a]
foxd4$^+$	-	46	10	6	11	6	3	1
sox2$^+$	87	-	153	3	358	103	11	13
msx1$^+$	15	107	-	11	95	15	36	10
foxd3$^+$	1	4	2	-	3	2	1	0
zic2$^+$	35	307	97	8	-	7	4	4
six1$^+$	12	42	8	3	2	-	3	3
dlx5$^+$	11	79	92	4	12	48	-	20
foxi1$^+$	11	18	15	3	3	4	1	-
Total # of cells[b]	200	1079	529	32	437	188	148	121

[a]*Transcription factor dataset that was queried. Single cells were selected based on the expression of the transcription factor at the top of each column in all selected "celltype" clusters defined in* ***Section 2.4****.*
[b]*The total number of cells across all selected "celltype" clusters that co-expressed the transcription factor at the top of each column. This number did not equal the sum of cells in each column because a single cell can express more than two transcription factors.*
[c]*The transcription factor that was co-expressed with the factor at the top of each column.*

characteristic of each of the other domains. For these effects to be direct, the different TFs need to be expressed in the same cell. In fact, transcriptomic screens indicate that the early ectodermal regions express overlapping sets of TFs (Plouhinec et al., 2014; Hintze et al., 2017; Plouhinec et al., 2017; Trevers et al., 2018) and antibody staining demonstrated that single cells in these regions co-express more than 1 TF characteristic of a neural plate stage domain (Roellig et al., 2017). To assess whether the TFs we analyzed would be able to directly repress each other within a single cell, we mined the available *Xenopus* single cell RNAseq dataset (Briggs et al., 2018) and evaluated the co-expression pattern of TFs to determine whether they would have the opportunity to interact within single cells.

From the stage 13 dataset, a stage at the end of gastrulation that exclusively showed cell autonomous effects in our ISH assays, we captured cells expressing a particular TF within tissues annotated by Briggs et al. (2018) as "celltype" clusters that correspond to neural plate, neural crest, placode or non-neural ectoderm domains by their overall transcriptome signature. For each TF captured from these combined domains we assessed the number of cells that co-expressed at least one other domain-enriched gene. Most cells within a TF dataset, except for the *foxd4* dataset, expressed only that TF (i.e., were single labeled for the selected TF), but a large number expressed two different TFs (**Table 3**). Of the *foxd4*-expressing cells, many also expressed *sox2* and several also expressed *zic2*. We detected only 1 *foxd4*-expressing cell that also expressed *msx1* or *dlx5* and none that also expressed *foxd3*, *six1* or *foxi1*. Thus, almost all *foxd4*-expressing cells only co-expressed TFs that also are enriched in the NP. Of the *sox2*-expressing cells, a large number also expressed *zic2*, and only a few also expressed *foxd4*, *msx1*, *six1*, *dlx5* or *foxi1*; none co-expressed *foxd3*. Thus, *sox2*-expressing cells mostly co-expressed TFs that also are enriched in NP and/or NC. Of the *msx1*-expressing cells, many also expressed *sox2* or *zic2*, and a small number also expressed *foxd4*, *six1*, *dlx5* or *foxi1*. Thus, *msx1*-expressing cells mostly co-expressed TFs characteristic of the NB (i.e., NC + PPR). At stage 13, only four cells in the neural crest cluster expressed *foxd3* and one of those also expressed *sox2;* we know from other studies that *foxd3* is only just beginning to be expressed, so this small number of *foxd3*-positive cells is not unexpected. Of the *zic2*-expressing cells, many also expressed *sox2* and a small number also expressed *msx1*, *six1* or *dlx5*; none co-expressed *foxd4, foxd3* or *foxi1*. This confirms that *zic2*-expressing cells mostly co-expressed TFs enriched in NP and/or NC. Of the *six1*-expressing cells, many also expressed *sox2* or *dlx5*, and a small number also expressed *msx1* or *zic2*; none co-expressed *foxd4, foxd3* or *foxi1*. Thus, *six1*-expressing cells mostly co-expressed TFs characteristic of the NB. Of the *dlx5*-expressing cells, many also expressed *sox2* or s*ix1,* and a small number also expressed *msx1*, *zic2* or *foxi1*; none co-expressed *foxd4* or *foxd3*. Thus, *dlx5*-expressing cells also mostly co-expressed TFs characteristic of the NB. Of the *foxi1*-expressing cells, a small number also expressed *sox2*, *msx1*, *zic2*, *six1* or *dlx5*; none co-expressed *foxd4* or *foxd3*. Thus, some *foxi1*-expressing cells mostly co-expressed NB genes. These data demonstrate that by the end of gastrulation, many of the cells identified as belonging to a particular ectodermal domain or "celltype" cluster by their overall transcriptomic signature (Briggs et al., 2018), co-express more than one domain-enriched TF. Thus, there is ample opportunity for repressive interactions between TFs within single cells at the end of gastrulation.

This analysis was repeated for stage 13 cells that expressed more than two of the selected domain-enriched TFs. We found that only a small number expressed three different TFs and rare cells expressed four different TFs (**Table 4**). For cells expressing three different TFs, we found that, independent of the TF dataset analyzed, particular combinations of 3 TFs predominated (color coded in **Table 4**): *sox2+zic2+foxd4* (orange, n = 12 cells), *sox2+msx1+zic2* (yellow, n = 48), *sox2+zic2+dlx5* (blue, n = 21), *sox2+six1+dlx5* (green, n = 22), *sox2+msx1+six1* (red, n = 3), and *msx1+six1+dlx5* (grey, n = 2). Overall, *sox2*-positive cells were most frequently co-expressed with other TFs. These data demonstrate that at the end of gastrulation, many cells express more than one domain-enriched TF and triple- and quadruple-labeled cells were present but not abundant. These single cell transcriptomic analyses confirm the bulk RNAseq study that reported that different pieces of ectoderm dissected at the end of gastrulation express TFs characteristic of more than one neural plate stage domain (Plouhinec et al., 2017). Our observation that by the end of gastrulation single cells rarely carry the transcriptional signature of all four domains is consistent with their report that the dissected domains have distinct transcriptional signatures by this stage. However, the combinations suggest a preferred domain combination: *sox2+zic2+foxd4* likely represents NP; *sox2+msx1+zic2* and *sox2+zic2+dlx5* likely represent the neural crest portion of the NB; *sox2+six1+dlx5*, *sox2+msx1+six1* and *msx1+six1+dlx5* likely represent the PPR portion of the NB. The quadruple labeled cell signatures were each consistent with an NB signature.

Since numerous cells in chick co-express TFs characteristic of more than one domain even as late as neural tube closure (Roellig et al., 2017), we asked if the same occurs in *Xenopus* by performing the single cell RNAseq analysis on the stage 18 (neural tube closure) dataset from Briggs et al. (2018). It should be noted that the complexity of the several selected "celltype" clusters within the SPRING plot for this stage made it difficult to eliminate the possibility of that some non-domain cells were included in the analysis. Nonetheless, for the most part the patterns of TF co-expression were similar to those observed at stage 13. Of the *foxd4*-expressing cells, many also expressed *sox2* or *zic2* and only a small number also expressed *msx1, foxd3*, *six1*, *dlx5,* or *foxi1*. This pattern was very similar to that of the stage 13 dataset in which most *foxd4*-expressing cells only co-expressed TFs that also are enriched in the NP. Of the *sox2*-expressing cells, many also expressed *zic2* or *msx1*, and a smaller number also expressed *foxd4*, *msx1*, *foxd3*, *six1*, *dlx5* or *foxi1*. Of the *msx1*-expressing cells, many also expressed *sox2*, *zic2* or *dlx5*, and a small number also expressed *foxd4*, *foxd3*, *six1* or *foxi1*. Of the *foxd3*-expressing cells, several also expressed *msx1* or *zic2*, a few also expressed *foxd4*, and a small number also expressed *sox2*, *six1*, *dlx5* or *foxi1*. Of the *zic2*-expressing cells, many also expressed *sox2* or *msx1,* and a small number also expressed *foxd4*, *foxd3*, *six1*, *dlx5*, or *foxi1*. Of the *six1*-expressing cells, many also expressed *sox2* or *dlx5*, and a small number also

TABLE 6 | Number of single cells co-expressing three domain-enriched transcription factors at stage 18.

	*foxd4**	*sox2**	*msx1**	*foxd3**	*zic2**	*six1**	*dlx5**	*foxi1**
sox2+foxd3$^+$	-	-	-	-	1	1	-	-
sox2+foxd4$^+$	-		-	-	9	-	-	-
sox2+dlx5$^+$	-	-	6	-	9	23	-	2
sox2+foxi1$^+$	-	-	1	-	1	1	-	-
sox2+zic2$^+$	19	-	66	-	-	3	-	2
sox2+msx1$^+$	1	-	-	-	60	2	1	1
sox2+six1$^+$	-	-	1	1	1	-	2	1
dlx5+msx1$^+$	1	2	-	-	-	3	-	5
dlx5+foxd4$^+$	-	2	1	-	-	1	-	-
dlx5+six1$^+$	1	17	1	-	-	-	-	1
dlx5+zic2$^+$	-	9	3	1	-	-	-	-
dlx5+foxi1$^+$	-	1	7	-	-	1	-	-
dlx5+foxd3$^+$	-	1	-	-	-	-	-	-
foxd4+msx1$^+$	-	-	-	1	1	-	2	-
zic2+six1$^+$	2	-		-	-	-	-	-
zic2+msx1$^+$	1	50	-	2	-	-	2	-
zic2+foxd4$^+$	-	9	1		-	-	-	-
zic2+foxi1$^+$	-	2	-	-	-	-	-	-
zic2+foxd3$^+$	-	1	-	-	-	-	-	-

Cells labeled with the same color co-expressed the same combination of three domain-enriched transcription factors.

**Transcription factor dataset that was queried.*

$^+$The transcription factors that were co-expressed with the factor at the top of each column.

expressed *foxd4, msx1*, *foxd3*, *zic2* or *foxi1*. In each of these cases, the patterns of TF co-expression were similar to those observed at stage 13. However, the co-expression patterns of TFs that are Epi-enriched at neural plate stages were moderately different from stage 13. Of the *dlx5*-expressing cells, some also expressed *msx1* and a small number also expressed *foxd4, sox2*, *foxd3, zic2*, *six1* or *foxi1*; this is different from the stage 13 co-expression that was predominantly *sox2* or *six1*. Of the *foxi1*-expressing cells, most co-expressed *dlx5*, several co-expressed *sox2* or *msx1*, and a small number co-expressed *foxd4*, *zic2*, or *six1*; none co-expressed *foxd3*. This was a shift towards dlx5 co-expression compared to stage 13. When this analysis was extended to cells co-expressing three or more TFs, we found that many cells co-expressed three of the selected domain-enriched TFs (**Table 6**). The pattern of expression was more complex compared to stage 13, perhaps because there were many more cells and more complex "celltype" clusters in the dataset. However, like stage 13, particular combinations predominated, as color coded in **Table 6**: *foxd4*-expressing cells mostly co-expressed other NP-enriched genes; *sox2*-, *zic2*- and *msx1*-expressing cells predominantly co-expressed each other; *six1*-expressing cells mostly co-expressed *dlx5;* and very few *dlx5*- or *foxi1*-expressing cells co-expressed three or more TFs (**Tables 5**, **6**). It also was rare for cells in these clusters to co-express 4 or 5 TFs (**Table 7**). Overall, these data indicate that even as late as neural tube closure, many of the cells identified as belonging to the four ectodermal domains by their overall transcriptomic signature (Briggs et al., 2018) co-express more than one domain-enriched

TABLE 7 | Number of single cells co-expressing four or more domain-enriched transcription factors at stage 18.

	*foxd4**	*sox2**	*msx1**	*foxd3**	*zic2**	*six1**	*dlx5**	*foxi1**
sox2+zic2+foxi1$^+$	2	-	1	-	-	-	-	-
sox2+zic2+msx1$^+$	1	-	-	-	-	-	-	-
sox2+zic2+foxd4$^+$	-	-	2	-	-	-	-	-
sox2+zic2+dlx5+	-	-	1	-	-	2	-	-
sox2+six1+dlx5$^+$	1	-	1	-	-	-	-	-
sox2+six1+msx1$^+$	-	-	-	1	1	-	-	-
sox2+dlx5+foxi1$^+$	1	-	-	-	-	2	-	-
sox2+dlx5+foxd4$^+$	-	-	-	-	-	2	-	-
sox2+ msx1+dlx5$^+$	-	-	-	-	3	5	-	-
sox2+msx1+foxi1$^+$	-	-	-	-	2	-	-	-
sox2+msx1+foxd4$^+$	-	-	-	-	1	-	-	-
sox2+foxd3+msx1$^+$	-	-	-	-	1	-	-	-
zic2+msx1+foxi1$^+$	-	1	-	1	-	-	-	-
zic2+msx1+foxd4$^+$	-	1	-	-	-	-	1	-
zic2+six1+dlx5$^+$	-	3	-	-	-	-	-	-
dlx5+six1+msx1	-	3	-	-	-	-	-	-
dlx5+six1+foxd4	-	2	-	-	-	-	-	-
dlx5+six1+foxi1	-	3	-	-	-	-	-	-
dlx5+foxd4+foxi1$^+$	-	1	-	-	-	-	-	-
dlx5+foxd4+msx1$^+$	-	-	-	1	-	-	-	-
foxd4+msx1+foxd3$^+$	-	1	-	-	-	-	-	-
sox2+zic2+msx1+ foxi1$^+$	1	-	-	-	-	-	-	-
foxd4+zic2+msx1+ foxi1$^+$	-	1	-	-	-	-	-	-
dlx5+foxd4+zic2+ six1$^+$	-	-	1	-	-	-	-	-
sox2+foxd4+six1+ msx1+dlx5$^+$	-	-	-	1	-	-	-	-

Cells labeled with the same color co-expressed the same combination of four or more domain-enriched transcription factors.

**Transcription factor dataset that was queried.*

$^+$The transcription factors that were co-expressed with the factor at the top of each column.

TF, providing an opportunity for continued repressive interactions between TFs within single cells.

4 DISCUSSION

It is well appreciated that the embryonic ectoderm becomes separated into neural and non-neural domains in response to signaling gradients of various growth factors, in particular BMP, Wnt and FGF (reviewed in Stuhlmiller and Garcia-Castro, 2012; Saint-Jeannet and Moody, 2014; Pla and Monsoro-Burq, 2018; Streit, 2018; Schlosser, 2021). By the time that the neural tube closes four domains - NP, NC, PPR and Epi—can be distinguished by a distinct suite of TFs that are thought to impose domain-specific identity (reviewed in Milet and Monsoro-Burq, 2012; Moody and LaMantia, 2015; Streit, 2018; Seal and Monsoro-Burq, 2020; Thawani and Groves, 2020). However, a number of studies have shown that the TFs that we used in our study as landmarks of these four domains are not exclusively expressed. Even as early as gastrulation, expression domains overlap and regions are broadly competent to give rise to other domains when transplanted (Schlosser and Ahrens, 2004; Pieper et al., 2012; reviewed in; Grocott et al., 2012; Schlosser, 2021). For example, Plouhinec et al. (2014), Plouhinec et al. (2017) reported that although dissected regions of gastrula ectoderm could be recognized by their overall transcriptomic signatures, genes considered highly specific for one region could be detected at lower levels of expression in adjacent regions. In addition, many TFs that are considered "domain-specific" at neurula stages are required at early stages for the formation of more than one domain, and at later stages participate in specifying the fate of a single domain. For example, using both loss- and gain-of function approaches, Maharana and Schlosser (2018) demonstrated that Zic1, Pax3, Hairy2b, TFap2, Msx1, Vent2 and Foxi1 each are required for the normal expression of an NC specifier (*foxd3*) and a PPR specifier (*six1*). Likewise, at early stages *msx1* is required in the NB for the expression of both NC and PPR genes, but at later stages promotes NC and represses PPR fates (Tribulo et al., 2003; Monsoro-Burq et al., 2005; Phillips et al., 2006).

In the present study, we examined whether the ectopic expression of a TF considered a specifier of one neural plate stage domain would alter the expression of TFs enriched in the other domains. We found that the expression of nearly every TF was reduced by the introduction of every other domain-enriched TF. One exception was the occasional expansion of *zic2* and *zic3* NC domains by Six1. This result is consistent with previous work. Maharana and Schlosser (2018) showed by knockdown experiments that Six1 is required for the NC expression of a related gene, *zic1*, and that Six1 overexpression expands *zic1*. Likewise, Brugmann et al. (2004) showed by knockdown that Six1 is required for *zic2* expression and in some cases over-expression expands the *zic2* domain. The other exception was the observed expansion of *foxd3* by Dlx5 in about a third of the cases. In *Xenopus*, Dlx5 is considered a specifier of dorso-lateral epidermis (Luo et al., 2001), but at early stages its expression domain overlaps the NB which contains NC progenitors. In chick, Dlx5 tends to downregulate *msx1* (McLarren et al., 2003; Stuhlmiller and Garcia-Castro, 2012) and in fish and frog Dlx family members upregulate *foxi1* (Matsuo-Takasaki et al., 2005; Kwon et al., 2010; Pieper et al., 2012). While some gene regulatory networks depict members of the Dlx family as promoting PPR fate and repressing NC fate (e.g., Grocott et al., 2012), others indicate that at early gastrula stages Dlx factors promote both PPR and NC genes (McLarren et al., 2003; Maharana and Schlosser, 2018). These exceptions point out that it will be important to experimentally discriminate between the early and later effects of each of these TFs in future experiments. Nonetheless, the overwhelmingly consistent observation that TFs enriched in one neural plate stage domain reduced the expression of TFs enriched in a different domain supports previous proposals (Schlosser, 2006; Grocott et al., 2012; Moody and LaMantia, 2015; Roellig et al., 2017) that mutual transcriptional repression between TFs contributes to the segregation of the four ectodermal domains.

4.1 Domain-Specifying Transcription Factors Act in a Mutually Repressive Manner

In order for one TF to reduce the expression of another TF they either are both expressed in the same cell and regulate each other's expression in a cell autonomous manner, or they regulate downstream signaling pathways that affect gene expression in adjacent cells. In our analysis of lineage-labeled clones we found that at gastrula stages the effect of an ectopically expressed TF was exclusively cell autonomous, indicating that the mis-expressed TF repressed the target TF by acting within the same cell. It also suggests that individual cells normally express factors that are characteristic of more than one domain that interact transcriptionally to eventually result in a domain-specific fate. By analyzing a single cell RNAseq dataset of ectodermal clusters at the end of gastrulation, we indeed identified many cells that expressed TFs typical of more than one domain. These findings support the conclusions of several previous studies. Microarray analysis of precisely dissected ectodermal domains from chick showed that PPR gene clusters expressed many NP-enriched and NC-enriched genes (Hintze et al., 2017). RNAseq analysis of similarly dissected *Xenopus* domains showed that while transcriptomic signatures could be discerned for the various domains as early as late gastrula, the neural border tissue expressed TFs characteristic of more than one domain (Plouhinec et al., 2017). At the single cell level using antibody staining for TF proteins, Roellig et al. (2017) reported that about 50% of NB cells co-expressed two different "domain-specific" TFs and about 7% expressed three markers. These authors also found that Sox2, designated an NP TF, and Pax7, designated an NC TF, were mutually repressive within single cells. Interestingly, other studies noted that the Roellig et al. (2017) data showed a preference among the NB progenitors for expressing primarily NP + NC markers, suggestive of the binary competence model (Maharana and Schlosser, 2018; Pla and Monsoro-Burq, 2018). Our analysis of the single cell RNAseq data of Briggs et al. (2018) showed a similar preference among both stage 13 and stage 18

clusters to express NP + NC markers (**Tables 3–7**). In accord with the results from Roellig et al. (2017), we also find single cells at neural tube closure stages that continue to express multiple domain-enriched TFs. Together, these results support the proposed model in which individual ectodermal cells are initially multipotent (Grocott et al., 2012; Hintze et al., 2017; Roellig et al., 2017; Trevers et al., 2018); individual cells express TFs that over time repress each other to subsequently determine a cell's domain-specific fate by restricting their transcriptomic signature.

4.2 Cell-to-Cell Signaling Contributes to Domain Separation by Neurula Stages

In the embryo as well as in organoids, boundaries form between different progenitor fields as cells acquire different regional, tissue and functional fates. Boundary formation is documented to involve interactions between adjacent fields that include differential transcriptional programs, position within a morphogen gradient, local cell-cell interactions and highly regulated cell rearrangements (Irvine and Rauskolb, 2001; Dahmann et al., 2011; Jaeger, 2011; Martyn and Gartner, 2021). Many studies have demonstrated that progenitor cells and gene expression territories characteristic of the four ectodermal domains initially overlap and gradually segregate in response to local interactions assumed to be at the boundaries (reviewed in Moody and Saint-Jeannet, 2014; Saint-Jeannet and Moody, 2014; Pla and Monsoro-Burq, 2018; Schlosser, 2021). In concordance, we observed that TFs enriched in one neural plate stage domain reduced the expression of TFs enriched in the adjacent domains. For example, NC-enriched TFs reduced the expression of both NP-enriched genes and PPR-enriched genes, and PPR-enriched TFs reduced the expression of both NC-enriched genes and Epi-enriched genes. However, we also observed this effect after ectopic expression of a TF in a non-adjacent domain, for example, an NP-enriched gene mis-expressed in the PPR or Epi. By methodically expressing a domain-enriched TF in each of the major precursors of each of the other domains, we found that in every case TFs of both adjacent and non-adjacent domains caused mutual repression. This indicates that the interactions that segregate NP, NC, PPR and Epi domains are not confined to local interactions at boundaries.

There are several comprehensive reviews of the multiple studies that demonstrate both local and distant signaling that regulate the formation of the four ectodermal domains (Grocott et al., 2012; Milet and Monsoro-Burq, 2012; Stuhlmiller and Garcia-Castro, 2012; Saint-Jeannet and Moody, 2014; Schlosser, 2014; Pla and Monsoro-Burq, 2018; Streit, 2018; Schlosser, 2021). Inductive signals can be transmitted through the plane of the ectoderm and from underlying mesoderm and pharyngeal endoderm (Papalopulu and Kintner, 1993; Woda et al., 2003; Ahrens and Schlosser, 2005; Litsiou et al., 2005; Pieper et al., 2012; Watanabe et al., 2015; Hintze et al., 2017; Trevers et al., 2017). Our ISH analyses indicate that at gastrulation stages cell-cell signaling plays little role in transcriptional repression within an ectodermal domain; changes in gene expression were limited exclusively to cells carrying the lineage label. However, while clones expressing ectopic TFs at neurula stages also exhibited a predominance of cell autonomous reduced expression, we also observed repression in cells adjacent to, but not overlapping with, the lineage-labeled cells. This observation suggests that the mis-expressed TF also repressed the target TF indirectly *via* cell-to-cell signaling. While there are several examples of cell-cell signaling being important in placode and neural crest induction (Begbie et al., 1999; Brugmann et al., 2004; Ahrens and Schlosser, 2005; Litsiou et al., 2005; Monsoro-Burq et al., 2005; Watanabe et al., 2015; Hintze et al., 2017; Plouhinec et al., 2017; reviewed in; Milet and Monsoro-Burq, 2012; Stuhlmiller and Garcia-Castro, 2012; Saint-Jeannet and Moody, 2014; Pla and Monsoro-Burq, 2018; Streit, 2018; Schlosser, 2021), there also is evidence for indirect signaling. For example, Dlx5 indirectly induces epidermal and PPR genes (McLarren et al., 2003) and Zic1 affects PPR gene expression at a distance by regulating retinoic acid signaling (Jaurena et al., 2015; Dubey et al., 2021). Since an alternate explanation is that the *nβgal* mRNA was selectively diluted in part of the clone, it will be important to confirm our lineage tracing data by grafting TF-expressing cells into an ectopic domain and observing reduced expression in the adjacent host tissue, as has been elegantly shown for *dlx5* and *six1* in *Xenopus* (Woda et al., 2003; Ahrens and Schlosser, 2005). If such future experiments support the involvement of cell-cell signaling initiated by the TFs studied in this work, it will be important to determine whether the signals originate within the plane of the ectoderm or from underlying tissues.

4.3 Domain Separation is Gradual

Many different experimental approaches indicate that the separation of the four ectodermal domains is a gradual process. For example, a microarray analysis of a large number of genes expressed by PPR explants proposed that head mesoderm induces a "pre-neural" state that expresses a few TFs that then induce a "PPR-primed state" that expresses genes that next induce PPR specifier genes (Hintze et al., 2017). A transcriptomic study of the developmental timing of gene expression in the chick epiblast indicated that at pre-primitive streak stages this tissue is already specified to a neural plate border state (Trevers et al., 2018). A comprehensive gain- and loss-of-function analysis showed that dorsal ectoderm TFs (*zic1-5*, *sox3*) and ventral ectoderm TFs (*dlx3/5*, *gata2/3*, *vent1/2*, *foxi1/3*, *msx1*) broadly overlap in an intermediate zone, and this overlap deceases over development until boundaries are formed. Principal component analysis of the transcriptomes of dissected *Xenopus* ectodermal regions revealed distinct domains at gastrula stages that resolved as development proceeded (Plouhinec et al., 2017). Our data also indicate that transcriptional interactions that specify the fate of a domain begin as early as gastrulation stages; by mid-gastrula NC, PPR and Epi factors reduced the expression of NP factors (*foxd4*, *sox2*) and NC and PPR factors reduced Epi factors (*dlx5*, *foxi1*, *epiker*). Roellig et al. (2017) analyzed protein rather than transcript levels and also found single cells expressing more than one domain-typical TF protein as early as gastrula and as late as neural fold closure. Although they did not provide the spatial distribution of these cells, the authors noted that double- and triple-labeled Six1-

positive cells predominated in the lateral side of the border zone, which is where the PPR will form. They also quantitatively mapped the protein expression domains of four domain-enriched TFs, albeit not at the single cell level, and also found evidence of some regionalization of expression. The NP domain highly expressed Sox2 protein but not the other TFs; the border zone adjacent to the NP expressed moderate levels of Sox2, Pax7 and Tfap2a; the middle region of the border zone expressed high levels of Pax7 and Tfap2a and lower levels of Sox2; the lateral region of the border zone expressed low levels of Sox2 and Pax7 and moderate levels of Tfap2a and Six1; and only Tfap2a and Six1 were expressed in the most lateral region analyzed. It would be most interesting, when specific antibodies for the TFs analyzed in our study are available in *Xenopus*, to use a similar approach to determine whether there is any spatial restriction of cells expressing single or multiple TFs as predicted by the scRNAseq data.

4.4 Conclusion

Together, several previous studies and the data presented herein provide overwhelming evidence that the segregation of the four embryonic ectodermal domains begins during gastrulation. We found that at this stage it is mediated primarily by direct repressive interactions between TFs expressed within individual cells, but by late neural plate stages indirect interactions with adjacent cells assists in establishing boundaries and driving ultimate domain-specific fate decisions. Several future experiments are needed to more fully understand the molecular regulation of these processes, such as identifying: 1) stage- and domain-specific enhancers; 2) the TFs bound to them; and 3) the identity of and tissue source of the non-autonomous signals initiated by these TFs. With this information a more complete gene regulatory network can be constructed and utilized to predict dysmorphologies that may arise due to subtle changes in gene expression and interactions.

DATA AVAILABILITY STATEMENT

The datasets presented in this study can be found in the paper and in Briggs et al. (2018).

ETHICS STATEMENT

The animal study was reviewed and approved by GWU IACUC.

AUTHOR CONTRIBUTIONS

Data generation and analysis: SK, AT, MP, CS, and SM. Writing manuscript: SK, AT, and SM. Reviewing and revising manuscript: SK, AT, MP, CS, and SM.

FUNDING

This work was supported by grants from the National Science Foundation (IOS-0817902) and National Institutes of Health (DE022065 and DE026434). We acknowledge additional funding from the George Washington University and Grinnell College.

ACKNOWLEDGMENTS

We thank Jenni Xu (George Washington University) for performing some of the microinjections of mRNAs. We thank Himani Datta Majumdar for performing the ISH. This work was made possible with the support of Xenbase (http://www.xenbase.org/, RRID: SCR_003280) and the National *Xenopus* Resource (http://mbl.edu/xenopus/, RRID:SCR_013731).

REFERENCES

Ahrens, K., and Schlosser, G. (2005). Tissues and Signals Involved in the Induction of Placodal Six1 Expression in *Xenopus Laevis*. *Develop. Biol.* 288, 40–59. doi:10.1016/j.ydbio.2005.07.022

Begbie, J., Brunet, J. F., Rubenstein, J. L., and Graham, A. (1999). Induction of the Epibranchial Placodes. *Development* 126, 895–902. doi:10.1242/dev.126.5.895

Briggs, J. A., Weinreb, C., Wagner, D. E., Megason, S., Peshkin, L., Kirschner, M. W., et al. (2018). The Dynamics of Gene Expression in Vertebrate Embryogenesis at Single-Cell Resolution. *Science* 360, eaar5780. doi:10.1126/science.aar5780

Brugmann, S. A., Pandur, P. D., Kenyon, K. L., Pignoni, F., and Moody, S. A. (2004). Six1 Promotes a Placodal Fate within the Lateral Neurogenic Ectoderm by Functioning as Both a Transcriptional Activator and Repressor. *Development* 131, 5871–5881. doi:10.1242/dev.01516

Dahmann, C., Oates, A. C., and Brand, M. (2011). Boundary Formation and Maintenance in Tissue Development. *Nat. Rev. Genet.* 12, 43–55. doi:10.1038/nrg2902

Dubey, A., Yu, J., Liu, T., Kane, M. A., and Saint-Jeannet, J. P. (2021). Retinoic Acid Production, Regulation and Containment through Zic1, Pitx2c and Cyp26c1 Control Cranial Placode Specification. *Development* 148, dev193227. doi:10.1242/dev.193227

Ezin, A. M., Fraser, S. E., and Bronner-Fraser, M. (2009). Fate Map and Morphogenesis of Presumptive Neural Crest and Dorsal Neural Tube. *Develop. Biol.* 330, 221–236. doi:10.1016/j.ydbio.2009.03.018

Gaur, S., Mandelbaum, M., Herold, M., Majumdar, H. D., Neilson, K. M., Maynard, T. M., et al. (2016). Neural Transcription Factors Bias Cleavage Stage Blastomeres to Give Rise to Neural Ectoderm. *Genesis* 54, 334–349. doi:10.1002/dvg.22943

Grocott, T., Tambalo, M., and Streit, A. (2012). The Peripheral Sensory Nervous System in the Vertebrate Head: A Gene Regulatory Perspective. *Develop. Biol.* 370, 3–23. doi:10.1016/j.ydbio.2012.06.028

Hintze, M., Prajapati, R. S., Tambalo, M., Christophorou, N. A. D., Anwar, M., Grocott, T., et al. (2017). Cell Interactions, Signals and Transcriptional Hierarchy Governing Placode Progenitor Induction. *Development* 144, 2810–2823. doi:10.1242/dev.147942

Irvine, K. D., and Rauskolb, C. (2001). Boundaries in Development: Formation and Function. *Annu. Rev. Cel Dev. Biol.* 17, 189–214. doi:10.1146/annurev.cellbio.17.1.189

Jaeger, J. (2011). The Gap Gene Network. *Cell. Mol. Life Sci.* 68, 243–274. doi:10.1007/s00018-010-0536-y

Jaurena, M. B., Juraver-Geslin, H., Devotta, A., and Saint-Jeannet, J.-P. (2015). Zic1 Controls Placode Progenitor Formation Non-Cell Autonomously by Regulating Retinoic Acid Production and Transport. *Nat. Commun.* 6, 7476. doi:10.1038/ncomms8476

Klein, S. L., and Moody, S. A. (2015). Early Neural Ectodermal Genes Are Activated by Siamois and Twin during Blastula Stages. *Genesis* 53, 308–320. doi:10.1002/dvg.22854

Klein, S. L. (1987). The First Cleavage Furrow Demarcates the Dorsal-Ventral Axis in Xenopus Embryos. *Develop. Biol.* 120, 299–304. doi:10.1016/0012-1606(87)90127-8

Kwon, H.-J., Bhat, N., Sweet, E. M., Cornell, R. A., and Riley, B. B. (2010). Identification of Early Requirements for Preplacodal Ectoderm and Sensory Organ Development. *Plos Genet.* 6, e1001133. doi:10.1371/journal.pgen.1001133

Litsiou, A., Hanson, S., and Streit, A. (2005). A Balance of FGF, BMP and WNT Signalling Positions the Future Placode Territory in the Head. *Development* 132, 4051–4062. doi:10.1242/dev.01964

Lukoseviciute, M., Gavriouchkina, D., Williams, R. M., Hochgreb-Hagele, T., Senanayake, U., Chong-Morrison, V., et al. (2018). From pioneer to Repressor: Bimodal Foxd3 Activity Dynamically Remodels Neural Crest Regulatory Landscape *In Vivo*. *Develop. Cel* 47, 608–628. doi:10.1016/j.devcel.2018.11.009

Luo, T., Matsuo-Takasaki, M., and Sargent, T. D. (2001). Distinct Roles for Distal-Less GenesDlx3 andDlx5 in Regulating Ectodermal Development inXenopus. *Mol. Reprod. Dev.* 60, 331–337. doi:10.1002/mrd.1095

Maharana, S. K., and Schlosser, G. (2018). A Gene Regulatory Network Underlying the Formation of Pre-Placodal Ectoderm in *Xenopus Laevis*. *BMC Biol.* 16, 79. doi:10.1186/s12915-018-0540-5

Martyn, I., and Gartner, Z. J. (2021). Expanding the Boundaries of Synthetic Development. *Develop. Biol.* 474, 62–70. doi:10.1016/j.ydbio.2021.01.017

Matsuo-Takasaki, M., Matsumura, M., and Sasai, Y. (2005). An Essential Role of Xenopus Foxi1a for Ventral Specification of the Cephalic Ectoderm during Gastrulation. *Development* 132, 3885–3894. doi:10.1242/dev.01959

McLarren, K. W., Litsiou, A., and Streit, A. (2003). Dlx5 Positions the Neural Crest and Preplacode Region at the Border of the Neural Plate. *Develop. Biol.* 259, 34–47. doi:10.1016/s0012-1606(03)00177-5

Milet, C., and Monsoro-Burq, A. H. (2012). Neural Crest Induction at the Neural Plate Border in Vertebrates. *Develop. Biol.* 366, 22–33. doi:10.1016/j.ydbio.2012.01.013

Miyata, S., Kageura, H., and Kihara, H. K. (1987). Regional Differences of Proteins in Isolated Cells of Early Embryos of *Xenopus Laevis*. *Cel Differ.* 21, 47–52. doi:10.1016/0045-6039(87)90447-7

Monsoro-Burq, A.-H., Wang, E., and Harland, R. (2005). Msx1 and Pax3 Cooperate to Mediate FGF8 and WNT Signals during Xenopus Neural Crest Induction. *Develop. Cel* 8, 167–178. doi:10.1016/j.devcel.2004.12.017

Moody, S. A. (1987). Fates of the Blastomeres of the 16-Cell Stage *Xenopus* Embryo. *Develop. Biol.* 119, 560–578. doi:10.1016/0012-1606(87)90059-5

Moody, S. A., and LaMantia, A.-S. (2015). Transcriptional Regulation of Cranial Sensory Placode Development. *Curr. Top. Dev. Biol.* 111, 301–350. doi:10.1016/bs.ctdb.2014.11.009

Moody, S. A. (2018a). Lineage Tracing and Fate Mapping in Xenopus Embryos. *Cold Spring Harb Protoc.* 2018 (12), pdb.prot097253. doi:10.1101/pdb.prot097253

Moody, S. A. (2018b). Microinjection of mRNAs and Oligonucleotides. *Cold Spring Harb Protoc.* 2018 (12), pdb.prot097261. doi:10.1101/pdb.prot097261

Moody, S. A., and Saint-Jeannet, J. P. (2014). "Determination of Pre-placodal Ectoderm and Sensory Placodes," in *Principles of Developmental Genetics*. Second edition (NY: Elsevier), 331–356.

Nakata, K., Nagai, T., Aruga, J., and Mikoshiba, K. (1998). Xenopus Zic family and its role in neural and neural crest development1During submission of this paper, Mizuseki et al., reported the Xenopus Zic-related-1 gene which was highly homologous to mouse Zic1 gene (Mizuseki et al., 1998). Accession No. Zic1, AB009564; Zic2, AB009565.1. *Mech. Develop.* 75, 43–51. doi:10.1016/s0925-4773(98)00073-2

Nakata, K., Nagai, T., Aruga, J., and Mikoshiba, K. (1997). *Xenopus* Zic3, a Primary Regulator Both in Neural and Neural Crest Development. *Proc. Natl. Acad. Sci.* 94, 11980–11985. doi:10.1073/pnas.94.22.11980

Nieuwkoop, P. D., and Faber, J. (1994). *Normal Table of* Xenopus laevis *(Daudin)*. New York: Garland Science.

Papalopulu, N., and Kintner, C. (1993). *Xenopus* Distal-Less Related Homeobox Genes Are Expressed in the Developing Forebrain and Are Induced by Planar Signals. *Development* 117, 961–975. doi:10.1242/dev.117.3.961

Phillips, B. T., Kwon, H.-J., Melton, C., Houghtaling, P., Fritz, A., and Riley, B. B. (2006). Zebrafish msxB, msxC and msxE Function Together to Refine the Neural-Nonneural Border and Regulate Cranial Placodes and Neural Crest Development. *Develop. Biol.* 294, 376–390. doi:10.1016/j.ydbio.2006.03.001

Pieper, M., Ahrens, K., Rink, E., Peter, A., and Schlosser, G. (2012). Differential Distribution of Competence for Panplacodal and Neural Crest Induction to Non-Neural and Neural Ectoderm. *Development* 139, 1175–1187. doi:10.1242/dev.074468

Pieper, M., Eagleson, G. W., Wosniok, W., and Schlosser, G. (2011). Origin and Segregation of Cranial Placodes in *Xenopus Laevis*. *Develop. Biol.* 360, 257–275. doi:10.1016/j.ydbio.2011.09.024

Pla, P., and Monsoro-Burq, A. H. (2018). The Neural Border: Induction, Specification and Maturation of the Territory that Generates Neural Crest Cells. *Develop. Biol.* 444 (Suppl. 1), S36–S46. doi:10.1016/j.ydbio.2018.05.018

Plouhinec, J.-L., Medina-Ruiz, S., Borday, C., Bernard, E., Vert, J.-P., Eisen, M. B., et al. (2017). A Molecular Atlas of the Developing Ectoderm Defines Neural, Neural Crest, Placode, and Nonneural Progenitor Identity in Vertebrates. *Plos Biol.* 15, e2004045. doi:10.1371/journal.pbio.2004045

Plouhinec, J.-L., Roche, D. D., Pegoraro, C., Figueiredo, A. L., Maczkowiak, F., Brunet, L. J., et al. (2014). Pax3 and Zic1 Trigger the Early Neural Crest Gene Regulatory Network by the Direct Activation of Multiple Key Neural Crest Specifiers. *Develop. Biol.* 386, 461–472. doi:10.1016/j.ydbio.2013.12.010

Riddiford, N., and Schlosser, G. (2016). Dissecting the Pre-Placodal Transcriptome to Reveal Presumptive Direct Targets of Six1 and Eya1 in Cranial Placodes. *eLife* 5, e17666. doi:10.7554/eLife.17666

Roellig, D., Tan-Cabugao, J., Esaian, S., and Bronner, M. E. (2017). Dynamic Transcriptional Signature and Cell Fate Analysis Reveals Plasticity of Individual Neural Plate Border Cells. *eLife* 6, e21620. doi:10.7554/eLife.21620

Saint-Jeannet, J.-P., and Moody, S. A. (2014). Establishing the Pre-Placodal Region and Breaking it into Placodes with Distinct Identities. *Develop. Biol.* 389, 13–27. doi:10.1016/j.ydbio.2014.02.011

Sasai, N., Mizuseki, K., and Sasai, Y. (2001). Requirement ofFoxD3-Class Signaling for Neural Crest Determination in Xenopus. *Development* 128, 2525–2536. doi:10.1242/dev.128.13.2525

Sato, S., Ikeda, K., Shioi, G., Ochi, H., Ogino, H., and Kawakami, H. K. (2010). Conserved Expression of Mouse *Six1* in the Pre-Placodal Region (PPR) and Identification of an Enhancer for the Rostral PPR. *Develop. Biol.* 344, 158–171. doi:10.1016/j.ydbio.2010.04.029

Schlosser, G., and Ahrens, K. (2004). Molecular Anatomy of Placode Development in *Xenopus Laevis*. *Develop. Biol.* 271, 439–466. doi:10.1016/j.ydbio.2004.04.013

Schlosser, G. (2008). Do vertebrate Neural Crest and Cranial Placodes Have a Common Evolutionary Origin? *BioEssays* 30, 659–672. doi:10.1002/bies.20775

Schlosser, G. (2014). Early Embryonic Specification of Vertebrate Cranial Placodes. *Wires Dev. Biol.* 3, 349–363. doi:10.1002/wdev.142

Schlosser, G. (2006). Induction and Specification of Cranial Placodes. *Develop. Biol.* 294, 303–351. doi:10.1016/j.ydbio.2006.03.009

Schlosser, G. (2021). "Origin of Cranial Placodes from a Common Primordium," in *Development of Sensory and Neurosecretory Cell Types: Vertebrate Cranial Placodes, Volume 1* (Boca Raton, FL: CRC Press), 43–70. doi:10.1201/9781315162317-3

Schlosser, G., Patthey, C., and Shimeld, S. M. (2014). The Evolutionary History of Vertebrate Cranial Placodes II. Evolution of Ectodermal Patterning. *Develop. Biol.* 389, 98–119. doi:10.1016/j.ydbio.2014.01.019

Seal, S., and Monsoro-Burq, A. H. (2020). Insights into the Early Gene Regulatory Network Controlling Neural Crest and Placode Fate Choices at the Neural Border. *Front. Physiol.* 11, 608812. doi:10.3389/fphys.2020.608812

Sherman, J. H., Karpinski, B. A., Fralish, M. S., Cappuzzo, J. M., Dhindsa, D. S., Thal, A. G., et al. (2017). Foxd4 Is Essential for Establishing Neural Cell Fate and for Neuronal Differentiation. *Genesis* 55 (6). doi:10.1002/dvg.23031

Streit, A. (2002). Extensive Cell Movements Accompany Formation of the Otic Placode. *Develop. Biol.* 249, 237–254. doi:10.1006/dbio.2002.0739

Streit, A. (2018). Specification of Sensory Placode Progenitors: Signals and Transcription Factor Networks. *Int. J. Dev. Biol.* 62, 195–205. doi:10.1387/ijdb.170298as

Stuhlmiller, T. J., and García-Castro, M. I. (2012). Current Perspectives of the Signaling Pathways Directing Neural Crest Induction. *Cel. Mol. Life Sci.* 69, 3715–3737. doi:10.1007/s00018-012-0991-8

Sullivan, C. H., Majumdar, H. D., Neilson, K. M., and Moody, S. A. (2019). Six1 and Irx1 Have Reciprocal Interactions during Cranial Placode and Otic Vesicle Formation. *Develop. Biol.* 446, 68–79. doi:10.1016/j.ydbio.2018.12.003

Sullivan, S. A., Akers, L., and Moody, S. A. (2001). foxD5a, a Xenopus Winged Helix Gene, Maintains an Immature Neural Ectoderm via Transcriptional Repression that Is Dependent on the C-Terminal Domain. *Develop. Biol.* 232, 439–457. doi:10.1006/dbio.2001.0191

Suzuki, A., Ueno, N., and Hemmati-Brivanlou, A. (1997). *Xenopus Msx1* Mediates Epidermal Induction and Neural Inhibition by BMP4. *Development* 124, 3037–3044. doi:10.1242/dev.124.16.3037

Thawani, A., and Groves, A. K. (2020). Building the Border: Development of the Chordate Neural Plate Border Region and its Derivatives. *Front. Physiol.* 11, 608880. doi:10.3389/fphys.2020.608880

Trevers, K. E., Prajapati, R. S., Hintze, M., Stower, M. J., Strobl, A. C., Tambalo, M., et al. (2018). Neural Induction by the Node and Placode Induction by Head Mesoderm Share an Initial State Resembling Neural Plate Border and ES Cells. *Proc. Natl. Acad. Sci. USA* 115, 355–360. doi:10.1073/pnas.1719674115

Tribulo, C., Aybar, M. J., Nguyen, V. H., Mullins, M. C., and Mayor, R. (2003). Regulation of Msx Genes by a Bmp Gradient Is Essential for Neural Crest Specification. *Development* 130, 6441–6452. doi:10.1242/dev.00878

Watanabe, T., Kanai, Y., Matsukawa, S., and Michiue, T. (2015). Specific Induction of Cranial Placode Cells fromXenopusectoderm by Modulating the Levels of BMP, Wnt, and FGF Signaling. *Genesis* 53, 652–659. doi:10.1002/dvg.22881

Weinreb, C., Wolock, S., and Klein, A. M. (2018). SPRING: A Kinetic Interface for Visualizing High Dimensional Single-Cell Expression Data. *Bioinformatics* 34, 1246–1248. doi:10.1093/bioinformatics/btx792

Woda, J. M., Pastagia, J., Mercola, M., and Artinger, K. B. (2003). Dlx Proteins Position the Neural Plate Border and Determine Adjacent Cell Fates. *Development* 130, 331–342. doi:10.1242/dev.00212

Yan, B., Neilson, K. M., and Moody, S. A. (2009). foxD5 Plays a Critical Upstream Role in Regulating Neural Ectodermal Fate and the Onset of Neural Differentiation. *Develop. Biol.* 329, 80–95. doi:10.1016/j.ydbio.2009.02.019

Yan, B., Neilson, K. M., Ranganathan, R., Maynard, T., and Moody, A. S. A. (2015). Microarray Identification of Novel Genes Downstream of Six1, a Critical Factor in Cranial Placode, Somite, and Kidney Development. *Dev. Dyn.* 244, 181–210. doi:10.1002/dvdy.24229

Conflict of Interest: The authors declare that the research was conducted in the absence of any commercial or financial relationships that could be construed as a potential conflict of interest.

Publisher's Note: All claims expressed in this article are solely those of the authors and do not necessarily represent those of their affiliated organizations, or those of the publisher, the editors, and the reviewers. Any product that may be evaluated in this article, or claim that may be made by its manufacturer, is not guaranteed or endorsed by the publisher.

frontiers in Cell and Developmental Biology

ORIGINAL RESEARCH
published: 22 February 2022
doi: 10.3389/fcell.2022.777121

The Ribosomal Protein L5 Functions During *Xenopus* Anterior Development Through Apoptotic Pathways

Corinna Schreiner[1,2†], *Bianka Kernl*[1,2†], *Petra Dietmann*[1], *Ricarda J. Riegger*[1], *Michael Kühl*[1] *and Susanne J. Kühl*[1*]

[1]*Institute of Biochemistry and Molecular Biology, Ulm University, Ulm, Germany,* [2]*International Graduate School in Molecular Medicine Ulm, Ulm, Germany*

Ribosomal biogenesis is a fundamental process necessary for cell growth and division. Ribosomal protein L5 (Rpl5) is part of the large ribosomal subunit. Mutations in this protein have been associated with the congenital disease Diamond Blackfan anemia (DBA), a so called ribosomopathy. Despite of the ubiquitous need of ribosomes, clinical manifestations of DBA include tissue-specific symptoms, e.g., craniofacial malformations, eye abnormalities, skin pigmentation failure, cardiac defects or liver cirrhosis. Here, we made use of the vertebrate model organism *Xenopus laevis* and showed a specific expression of *rpl5* in the developing anterior tissue correlating with tissues affected in ribosomopathies. Upon Rpl5 knockdown using an antisense-based morpholino oligonucleotide approach, we showed different phenotypes affecting anterior tissue, i.e., defective cranial cartilage, malformed eyes, and microcephaly. Hence, the observed phenotypes in *Xenopus laevis* resemble the clinical manifestations of DBA. Analyses of the underlying molecular basis revealed that the expression of several marker genes of neural crest, eye, and brain are decreased during induction and differentiation of the respective tissue. Furthermore, Rpl5 knockdown led to decreased cell proliferation and increased cell apoptosis during early embryogenesis. Investigating the molecular mechanisms underlying Rpl5 function revealed a more than additive effect between either loss of function of Rpl5 and loss of function of c-Myc or loss of function of Rpl5 and gain of function of Tp53, suggesting a common signaling pathway of these proteins. The co-injection of the apoptosis blocking molecule Bcl2 resulted in a partial rescue of the eye phenotype, supporting the hypothesis that apoptosis is one main reason for the phenotypes occurring upon Rpl5 knockdown. With this study, we are able to shed more light on the still poorly understood molecular background of ribosomopathies.

Keywords: RPL5, *Xenopus laevis*, ribosomal biogenesis, ribosomopathy, c-myc, tp53

OPEN ACCESS

Edited by:
Annette Hammes, Max Delbrück Center for Molecular Medicine (MDC), Germany

Reviewed by:
Tim Ott, University of Hohenheim, Germany
Sylvie Schneider-Maunoury, Institut National de la Santé et de la Recherche Médicale (INSERM), France

***Correspondence:**
Susanne J. Kühl
susanne.kuehl@uni-ulm.de

†These authors have contributed equally to this work and share first authorship

Specialty section:
This article was submitted to Morphogenesis and Patterning, a section of the journal Frontiers in Cell and Developmental Biology

Received: *14 September 2021*
Accepted: *08 February 2022*
Published: *22 February 2022*

Citation:
Schreiner C, Kernl B, Dietmann P, Riegger RJ, Kühl M and Kühl SJ (2022) The Ribosomal Protein L5 Functions During Xenopus Anterior Development Through Apoptotic Pathways. Front. Cell Dev. Biol. 10:777121. doi: 10.3389/fcell.2022.777121

Abbreviations: c-myc, MYC proto-oncogene; DBA, Diamond Blackfan anemia; DEPC, diethyl pyro carbonate; hBCL2, human B cell lymphoma 2; MDM2, mouse double minute 2 homolog; MO, morpholino oligonucleotide; NCC, neural crest cell; Pes1, Pescadillo homologue 1; pH3, phospho histone 3; Ppan, Peter pan; RISC, RNA-induced silencing complex; RNP, ribonucleoprotein; RPE, retinal pigmented epithelium; Rpl5, ribosomal protein L5; Rpl11, ribosomal protein L11; RT, reverse transcriptase; Tp53, tumor protein p53; TUNEL, terminal deoxynucleotidyl transferase dUTP-biotin nick end labeling; WMISH, whole mount *in situ* hybridization.

INTRODUCTION

Cell growth and division are fundamental for the development of any multicellular organism. These processes are highly regulated and hence, during embryogenesis, each dividing cell requires an adequate number of ribosomes to cope with the demand for translation. This demand is ensured by ribosome biogenesis, which mainly takes place in the nucleolus and nucleus. It requires around 200 factors and the three RNA polymerases, Pol I, Pol II, and Pol III, for pre-rRNA transcription, pre-rRNA processing, and ribosome assembly (Melnikov et al., 2012; Baßler and Hurt, 2019; Pecoraro et al., 2021).

Defects in ribosome biogenesis can lead to congenital diseases called ribosomopathies (Narla and Ebert, 2010; Farley-Barnes et al., 2019; Kang et al., 2021). Ribosomopathies such as the Diamond Blackfan anemia (DBA) or the Shwachman Diamond syndrome include various clinical manifestations. Regardless of the ubiquitous need of ribosomes in every cell of every organism, symptoms are often tissue-specific and include defects in craniofacial morphology, cardiac defects, skin pigmentation failure, bone marrow failure, and neurological impairments (Shwachman et al., 1964; Narla and Ebert, 2010; Brooks et al., 2014; Myers et al., 2014; Ross and Zarbalis, 2014; Jenkinson et al., 2016; Kostjukovits et al., 2017; Vlachos et al., 2018; Aspesi and Ellis, 2019; Farley-Barnes et al., 2019). Additionally, almost all ribosomopathies have a predisposition to develop tumors and eventually cancer (De Keersmaecker et al., 2015). Several genes have been identified whose mutations lead to impaired pre-rRNA transcription, pre-rRNA processing, or ribosome assembly (Valdez et al., 2004; Weaver et al., 2015; Jenkinson et al., 2016; Kostjukovits et al., 2017; Warren, 2018).

The ribosomal protein L5 (Rpl5) is one of those genes identified. Together with the ribosomal protein L11 (Rpl11) and the 5S rRNA, Rpl5 forms the 5S-ribonucleoprotein (RNP) complex, which is part of the 60S ribosomal subunit (Zhang and Lu, 2009; Leidig et al., 2014). Mutations in *rpl5* and the loss of Rpl5 function give rise to DBA in human (Gazda et al., 2008; Cmejla et al., 2009; Quarello et al., 2010).

As a consequence of disturbed ribosomal biogenesis, nucleolar stress and the subsequent increased number of free ribosomal proteins, the molecule MYC proto-oncogene (c-Myc) is affected. c-Myc enhances the transcriptional performance of all three RNA polymerases I-III crucial for ribosomal biogenesis and hence intensively contributes to this biological process (Gomez-Roman et al., 2003; Arabi et al., 2005; van Riggelen et al., 2010). It was shown in human cells, that upon cellular stress induced by defective ribosomal biogenesis, free ribosomal proteins Rpl5 and Rpl11 accumulate and can bind to *c-myc* RNA and induce *c-myc* RNA degradation by transporting it to the RNA-induced silencing complex (RISC). Consequently, *c-myc* RNA levels are reduced upon *rpl5* overexpression and increased upon Rpl5 knockdown (Liao et al., 2014). As a regulator of the neural crest, c-Myc reduction has been shown to lead to malformed cranial cartilages in *Xenopus* embryos (Bellmeyer et al., 2003).

A second molecule regulated by free ribosomal proteins is Tumor protein p53 (Tp53). In several human cell lines, free ribosomal proteins induce an activation of Tp53. This occurs by binding of 5S-RNP or free Rpl5 or/Rpl11 to and inactivation of the key regulator mouse double minute 2 homolog (MDM2). As a result, Tp53, that is not degraded by MDM2, accumulates and activates the pro-apoptotic pathway thereby contributing to the pathology of ribosomopathies (Dai and Lu, 2004; Zhang and Lu, 2009; Fumagalli et al., 2012; Sulima et al., 2019). Several studies in mice, zebrafish, and frogs have shown that craniofacial phenotypes, typical phenotypes for a ribosomopathy, can be rescued upon reducing Tp53 levels (Jones et al., 2008; Zhao et al., 2014; Griffin et al., 2015; Calo et al., 2018).

During early development, *Xenopus laevis* embryos contain a maternal store of mRNAs, proteins, and ribosomes (Wallace, 1960; Brown, 1964). This allows the embryo to be independent of *de novo* ribosomal biogenesis until stage 26 which has been shown by anucleolated mutants, that are not able to synthesize ribosomes, but can survive until swimming tadpole stage (Brown, 1964; Pierandrei-Amaldi and Amaldi, 1994). Although, *Xenopus laevis* seems to be independent of ribosomal biogenesis, RNA for ribosomal proteins, e.g., *rpl5* RNA, is detected throughout the early embryonic development (Pierandrei-Amaldi and Amaldi, 1994; Session et al., 2016; Briggs et al., 2018). Hence, the embryo contains *rpl5* RNA at developmental stages, during which it does not require *de novo* ribosomal biogenesis. This raises the question of whether Rpl5 has a function starting earlier than the start of *de novo* ribosomal biogenesis.

The aim of the following study was to investigate a potential function of Rpl5 during early anterior development of *Xenopus laevis* and to analyze whether we can recapitulate any phenotypes of ribosomopathies in this model organism. Therefore, expression analysis of *rpl5* as well as tissue-specific knockdown approaches *via* antisense-based morpholino oligonucleotides (MO) were performed. The molecular basis underlying the Rpl5 knockdown-induced phenotype was investigated by analyzing tissue-specific marker genes of the eye, the brain, and the neural crest, and proliferation as well as apoptosis. Additionally, the molecular mechanism was investigated by exploring the effects of Rpl5 knockdown on the two molecules Tp53 and c-Myc.

MATERIALS AND METHODS

Xenopus laevis

Xenopus leavis embryos were generated, cultured and staged according to standard protocols (Nieuwkoop and Faber, 1954; Sive et al., 2000). All procedures were performed according to the German animal use and care law and approved by the German state administration Baden-Württemberg (Regierungspräsidium Tübingen). Embryos were cultivated in 0.1 × Modified Barth´s saline with HEPES buffer (MBSH) and fixed with MEMFA(T) [0.1 M MOPS (pH 7.4), 2 mM EGTA, 1 mM $MgSO_4$, 4% formaldehyde, (0.1% Tween20)].

Synteny Analysis and Protein Alignment of *Ribosomal Protein L5*

Synteny analysis and protein alignment of Rpl5 were performed using NCBI Gene Bank for *Homo sapiens* (NP_000960; Gene ID: 6125); *Mus musculus* (NP_058676; Gene ID: 100503670); *Gallus gallus* (NP_989912; Gene ID: 395269); *Danio rerio* (NP_956050; Gene ID: 326961); and the Xenbase platform (xenbase.org) for *Xenopus laevis* [NP_001079377; Gene ID: XB-GENE-6251827 (rpl5.S); NP_001079437; Gene ID: XB-GENE-983917 (rpl5.L)] and for *Xenopus tropicalis* (NP_988881; Gene ID: XB-GENE-983912). For protein alignments, the online tool NCBI protein blast was used.

Morpholino Oligonucleotides, Cloning, and Microinjections

An Rpl5 morpholino oligonucleotide (MO) with the sequence 5′-CAT TTT GCT CTA TTT TGT CCC GTC G -3′ was designed, targeting the 5′UTR of *Xenopus laevis rpl5*. MOs for c-Myc and Tp53 were used as previously described (Bellmeyer et al., 2003; Cordenonsi et al., 2003). The gene-specific MOs and a standard Control MO were obtained from Gene Tools (Philomath, OR, United States). The MOs were diluted in diethyl pyro carbonate (DEPC) treated water.

To proof the binding specificity of Rpl5 MO, the MO binding sites were cloned in frame with and in front of the *GFP* (*green fluorescent protein*) gene as previously described (Gessert et al., 2007) using the following sequences:

Rpl5_MO_bs_GFP_l: 5′-GAT CCC GAC GGG ACA AAA TAG AGC AAA ATG GGG-3′,

Rpl5_MO_bs_GFP_r: 5′-AAT TCC CCA TTT TGC TCT ATT TTG TCC CGT CGG-3′,

Δ5′Rpl5_MO_bs_GFP_l: 5′-GAT CCA CTT GTT CTT TTT GCA GGA TCC ATG GGG-3′,

Δ5′Rpl5_MO_bs_GFP_r: 5′-AAT TCC CCA TGG ATC CTG CAA AAA GAA CAA GTG-3′,

1 ng of the respective MO-GFP RNA fusion construct was injected bilaterally together with 10 ng of Rpl5 MO, or Control MO into embryos at the two-cell stage and GFP expression was checked with an Olympus MVX10 fluorescence microscope.

If not indicated otherwise, 15–20 ng Rpl5 MO, 5 ng c-Myc MO, 2.5–5 ng Tp53 MO, or 15–20 ng Control MO were injected into one animal-dorsal blastomere of eight-cell embryos targeting anterior neural tissue (Moody and Kline, 1990). 0.5 ng *GFP* RNA was co-injected and served as injection control. The un-injected side served as internal control. To adjust the amount of RNA or MO per injection, *GFP* RNA and Control MO were used, respectively.

For rescue attempts, an *rpl5* construct was cloned with the following primers: rpl5_Bam_l: 5′-GGA TCC ATG GGG TTC GTA AAG GTC GTC AAG-3′ and rpl5_Bam_r: 5′-GGA TCC TTA GCT GTC TGC CTT CTC CTG AG-3′. This rescue construct is not targeted by the Rpl5 MO due to an altered sequence in the 5′UTR region. Rescue experiments were performed by co-injecting Rpl5 MO with 0.5 ng *rpl5* RNA. *c-myc* RNA, *tp53* RNA, and *human B cell lymphoma 2 (hBCL2)* RNA for injection were used as previously described (Bugner et al., 2011; Hampp et al., 2016).

Experiments which tested effects of low doses were carried out by injecting 5 ng Rpl5 MO and 0.5 ng *tp53* RNA unilaterally alone or in combination; furthermore, by injecting 5 ng Rpl5 MO and 5 ng c-Myc MO unilaterally alone or in combination.

Whole Mount *In Situ* Hybridization

WMISHs were performed according to established protocols (Hemmati-Brivanlou et al., 1990; Lufkin, 2007). Digoxygenin-labeled antisense RNA probes were generated against different mRNAs by using T7, T3, or SP6 RNA polymerase (Roche). We cloned the open reading frame of *Xenopus laevis rpl5* into the pSC-B vector (Stratagene) with the cloning primers rpl5_l: 5′-CGT TTG GGC TGT GAC TAT CCG GTC-3′ and rpl5_r: 5′-TTA GCT GTC TGC CTT CTC CTG AGC-3′. *In vitro* transcription with T3 RNA polymerases (Roche) resulted in digoxygenin-labelled antisense RNA probes. Furthermore, we cloned the open reading frame of *Xenopus laevis tp53* into the pCS2+ vector (Rupp and Weintraub) with the cloning primers tp53_l: 5′-GGG ATC CAT GCT GAG A-3′ and tp53_r: 5′-AAG GCC TCA TGG CTG T-3′. *In vitro* transcription with T7 RNA polymerase (Roche) resulted in digoxygenin-labelled antisense RNA probes. We used the following RNA anti-sense probes as described previously: *hba3 (hemoglobin alpha 3 subunit)* (cDNA clone MGC:64476 IMAGE:6881400), *actc1 (actin, alpha, cardiac muscle 1)* (cDNA clone MGC:52636 IMAGE:4681379), *c-myc* (Bugner et al., 2011), *celf1 (CUGBP Elav-like family, member 1)* (Day and Beck, 2011), *cryba1 (crystallin beta A1)* (Day and Beck, 2011), *egr2 (early growth response 2)* (Cizelsky et al., 2013), *foxc1 (forkhead box C1)* (Köster et al., 1998), *gata2 (gata binding protein 2)* (cDNA clone MGC:131004 IMAGE:7978680), *otx2 (orthodenticle homeobox 2)* (Lamb et al., 1993), *pax6 (paired box 6t)* (Hitchcock et al., 1996; Hollemann et al., 1998), *pou4f1* (POU class 4 homeobox 1) (Liu et al., 2000), prox1 *(prospero homeobox 1)* (Dyer et al., 2003), *rax (retina and anterior neural fold homeobox)* (Furukawa et al., 1997), *rho (rhodopsin)* (Chang and Harris, 1998), *snai2 (snail family zinc finger 2)* (clone ID: pMX363), *sox3 (sex determining region Y-box 3)* (Maurus et al., 2005), *twist1 (twist family bHLH transcription factor 1)* (Gessert et al., 2007), and *vsx1 (visual system homeobox 1)* (Hayashi et al., 2000).

Histology

Wildtype embryos as well as MO-injected embryos were embedded into gelatine and glutaraldehyde. Sections were performed with a thickness of 25 µm using a vibratome (Vibratome 1500 Classic, The Vibratome Company).

Cartilage Staining by Alcian Blue Staining

In order to investigate the craniofacial cartilage, wildtype embryos and embryos injected with 20 ng Rpl5 MO were fixed at stage 45 and stained with Alcian blue as previously described (Gessert et al., 2007). Afterwards, the cranial cartilage was dissected and photographed.

Phospho Histone 3 Staining and Terminal Deoxynucleotidyl Transferase dUTP Nick End Labeling Assay

Proliferative cells were stained for phospho histone 3 (pH3). Apoptotic cells were stained with the terminal deoxynucleotidyl transferase dUTP-biotin nick end labeling (TUNEL) assay. Both assays were performed at stage 13 and 23 according to established protocols (Gessert et al., 2007; Cizelsky et al., 2013).

Quantitative Tissue Measurements

All quantitative measurements were performed using pictures of unilaterally Control MO, Rpl5 MO, Rpl5 MO + *rpl5* RNA, Rpl5 MO + *c-myc* RNA, Rpl5 MO + Tp53 MO, Rpl5 MO + *hBCL2* RNA -injected embryos of one representative experiment. The area of the eye, the apex angle of coloboma, and the head width were measured using the software ImageJ (Wayne Rasband). For brain size analyses, brains of fixed stage 42 embryos were dissected and photographed. ImageJ was used to measure the area of the brain.

To analyze the area of *tp53* and *c-myc* expression, Rpl5 MO and Control MO-injected embryos were photographed after WMISH. By using ImageJ, area of expression was selected and measured (**Figures 6G,H**, **7G,H**, red area).

RT-PCR

Total RNA was isolated from *Xenopus* embryos using the peqGOLD RNAPure Kit (PEQLAB) following the manufacturer´s protocol. cDNA synthesis was carried out using random primers and the Superscript II reverse transcriptase (Invitrogen). For semi-quantitative RT-PCR the following primers were used: *gapdh_RT_forward*: 5′-GCC GTG TAT GTG GTG GAA TCT-3′, *gapdh_RT_reverse*: 5′-AAG TTG TCG TTG ATG ACC TTT GC-3′, *rpl5_RT_forward*: 5′-GGT GCC TTC ACA TGC TAC CT-3′, and *rpl5_RT_reverse*: 5′-GCA CTG GAT TCT CCC GAA TA-3′.

Imaging

For imaging whole *Xenopus* embryos, an Olympus MVX10 (fluorescence) or Olympus SZX12 microscope and an Olympus UC50 camera were used. Vibratome sections were imaged with an Olympus BX60 microscope and an Olympus DP70 or an Olympus DP28 camera. Images were processed with ImageJ and Affinity Designer 1.10.4.

Statistics

Data was analyzed with the software GraphPad Prism 9. Only experiments with a higher survival rate than 50% and an absolute survival number of at least 20 individuals per group were considered for statistic evaluation. Only experiments with more than three independent experiments were evaluated statistically. To determine statistical differences the nonparametric Mann-Whitney rank sum test was used. Statistical significances are indicated as: $*p \leq 0.05$; $**p \leq 0.01$, $***p \leq 0.001$, $****p \leq 0.0001$.

RESULTS

Genomic Analysis of *rpl5*

To compare the genomic region of *rpl5* between different species, an *in silico* synteny analysis was carried out. The genomes of *Homo sapiens*, *Mus musculus*, *Gallus gallus*, *Xenopus laevis* (both pseudoallels), *Xenopus tropicalis*, and *Danio rerio* were considered (**Supplementary Figure S1A**). The synteny analysis revealed a highly conserved genomic region of *rpl5*. Additionally, a protein alignment was performed, which showed high homology between the different species (**Supplementary Figure S1B**).

Ribosomal Protein L5 is Specifically Expressed in the Developing *Xenopus laevis*

Earlier, *rpl5* expression was shown in whole embryos at stages 27 and 32 during *Xenopus* development (Scholnick et al., 1997; Wischnewski et al., 2000). Session et al. provided RNA-sequencing data showing *rpl5* expression throughout the entire embryonic development (Session et al., 2016). To provide a more detailed expression study, we here investigated *rpl5* expression by RT-PCR and WMISH during many different embryonic developmental stages. RT-PCR showed *rpl5* to be expressed maternally and zygotically throughout stages 1–40 (**Figure 1A**). WMISH with an *rpl5*-specific antisense probe was performed at various developmental stages starting after gastrulation throughout late tailbud stages to investigate the spatiotemporal expression of *rpl5* (**Figures 1B–J**). During stage 13 *rpl5* expression was mainly found in the anterior neural plate where *rax* is expressed as well (**Figures 1B,F**). At neural stages, *rpl5* is mainly expressed in the neural folds (white arrowhead), which was confirmed by *snai2* expression in whole mount embryos as well as sections (**Figures 1B,G**). At stage 23, *rpl5* expression was found in the migrating anterior neural crest cells (NCCs) (white arrow), the developing eye (red arrow), the neural tube, and the somites (orange arrowhead) as shown in comparison to the expression of somite-specific marker gene *actc1* (**Figure 1B**, **Supplementary Figure S2A**). At stage 28, *rpl5* expression is enriched in the ventral blood islands, where *gata2* and *hba3* are expressed as well (**Supplementary Figure S2B**). Late tailbud stages 30 and 35 show enriched *rpl5* expression in the developing eye (red arrow), the brain (blue arrow), the anterior NCCs (white arrow), the somites (orange arrowhead), and the ventral blood islands (blue arrowhead) (**Figures 1C,D**). Transversal sections of the midbrain at stage 30 and 35 revealed a stronger *rpl5* expression in the dorsal midbrain compared to the ventral part (**Figures 1E,H**); *otx2* and *pax6* were used as marker genes of the brain. Analyzing *rpl5* expression in the eye area at stage 35 showed strong expression in the lens and the ciliary marginal zone (CMZ) (**Figures 1E,I**). *rax* served as marker gene for the CMZ, *cryba1* and *celf1* as marker genes for the lens (**Figures 1E,I**). Furthermore, *rpl5* transcripts are enriched in the NCC-derived periocular mesenchyme as shown in comparison to *foxc1* expression (**Figures 1E,I**). In longitudinal sections of stage 35 embryos, *rpl5* expression is

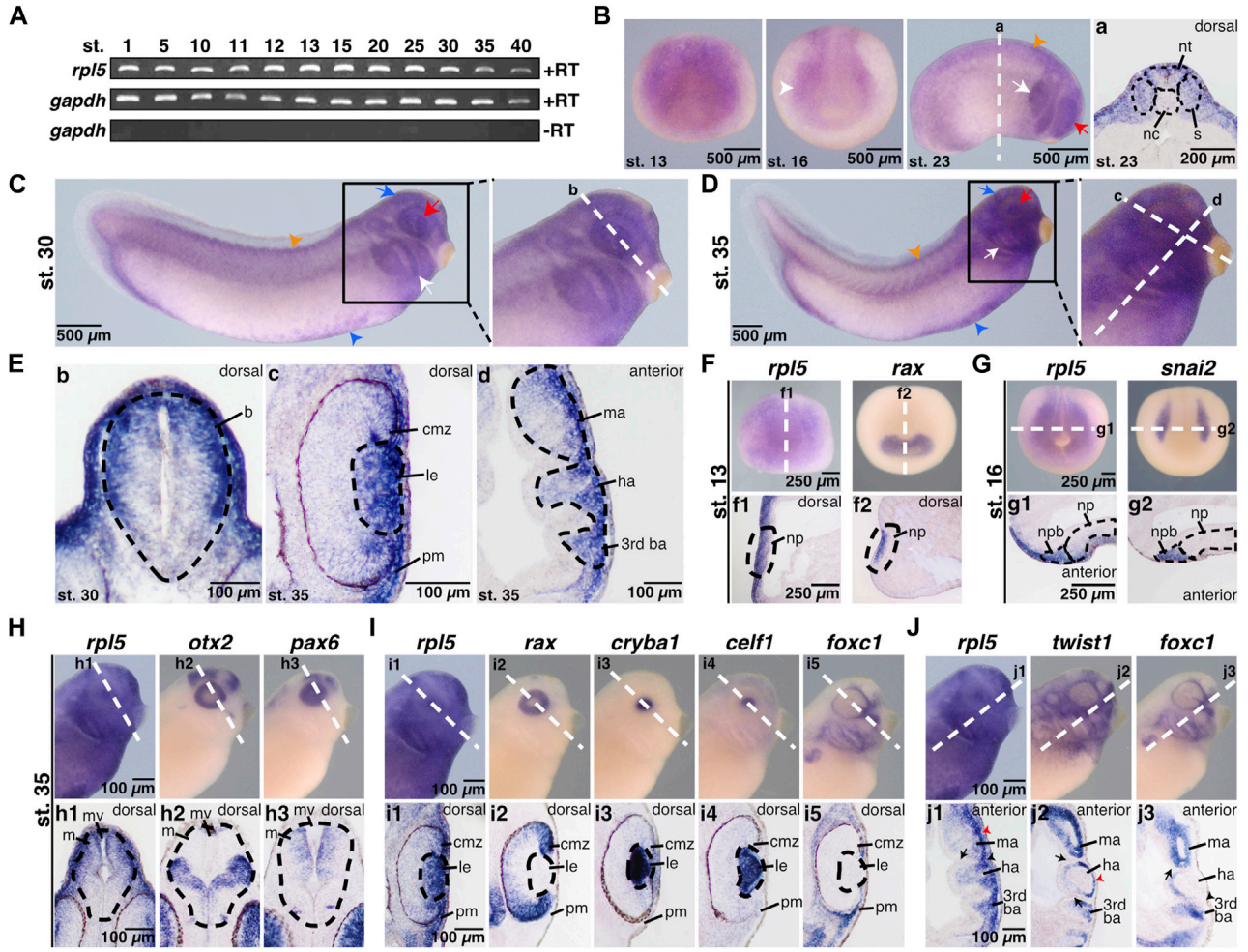

FIGURE 1 | Spatial and temporal expression of *rpl5* in *Xenopus* laevis. **(A)** By reverse transcriptase PCR *rpl5* expression was analyzed in entire embryos throughout different developmental embryonic stages (stages 1–40). *rpl5* was found to be maternally (stages 1 and 5) and zygotically (stages 10–40) expressed during the entire embryonic development. *gapdh* served as loading control, *gapdh* minus reverse transcriptase as negative control. **(B–J)** *rpl5* expression and expression of different marker genes were visualized by whole mount *in situ* hybridization in *Xenopus laevis* at indicated stages. Section orientation is indicated in each figure by "dorsal" or "anterior" for dorsal-vegetal or anterior-posterior orientation, respectively. White dotted lines represent level of sections shown in lowercase letters **(a-j3)**. **(B)** Anterior views are shown for stage 13 and 16. During neurulation at stages 13 and 16, *rpl5* was mainly detected in the anterior neural plate (white arrowhead). At stage 23 (lateral view), *rpl5* was expressed in the branchial arches (white arrow), somites (orange arrowhead), and the developing eye (red arrow). **(a)** Transversal sections show *rpl5* expression in the neural tube and somites (indicated by black dotted lines), and the lateral mesoderm. **(C,D)** Lateral views. During late tailbud stages 30 and 35, *rpl5* expression was mainly detected in the developing eye (red arrow), the branchial arches (white arrow), the brain (blue arrow), the somites (orange arrowhead), and the ventral blood islands (blue arrowhead). **(E) (b)** Transversal section reveals *rpl5* expression in the brain (outlined by black dotted line), in which *rpl5* is enriched in the dorsal-lateral part of the mesencephalon. **(c)** Transversal section at stage 35, *rpl5* transcripts are found in the lens (outlined by black dotted line), the ciliary marginal zone and the periocular mesenchyme. **(d)** Longitudinal section is given. *rpl5* was expressed in the mandibular, hyoid and third branchial arch (outlined by black dotted line). **(F)** *rpl5* expression in comparison to the marker gene *rax* at stage 13. Anterior view of embryos is shown. Sagittal sections shown in **(f1)** and **(f2)** reveal expression of both genes in the neural plate (outlined by black dotted lines). **(G)** Expression of *rpl5* and *snai2* (marker gene for NCCs) at stage 16. Anterior views are given. During NCC induction, *rpl5* transcripts are enriched in the neural plate border (outlined by black dotted lines). **(g1)** and **(g2)** transversal sections are shown. **(H)** Expression of *rpl5* and the two brain marker genes *otx2* and *pax6* at stage 35. Lateral views are given. *rpl5* expression is mainly enriched in the dorsal part of the mesencephalon as shown in comparison to *otx2* and *pax6* expression. Brains are indicated by black dotted lines. **(h1–h3)** show transversal sections. **(I)** Expression of *rpl5* and the four marker genes *rax*, *cryba1*, *celf1*, and *foxc1*. Lateral views are shown. Transversal sections are given in **(i1–i5)**. *rpl5* expression is found in the ciliary marginal zone, where *rax* is expressed as well **(i1,2)**. *rpl5* transcripts are enriched in the lens (indicated by black dotted lines) as seen in comparison to the lens-specific marker genes *cryba* and *celf1* (i1,3,4), and in the NCC-derived periocular mesenchyme like *foxc1* **(i1,5)**. **(J)** Expression of *rpl5* and the two NCC marker genes *twist1* and *foxc1*. Lateral views are shown. **(j1–j3)** represent longitudinal sections. *rpl5* is expressed in all three branchial arches (mandibular arch, hyoid arch, and third branchial arch), where *twist1* and *foxc1* expression is located as well. Cranial placodes and ganglia are indicated by black arrowheads; red arrowheads indicate migrating NCCs and black arrows indicate the endodermal part of the pharyngeal pouches. Abbreviations: b, brain; ba, branchial arch; cmz, ciliary marginal zone; ha, hyoid arch; le, lens; m, mesencephalon; ma, mandibular arch; mv, mesencephalic ventricle; nc, notochord; np, neural plate; npb, neural plate border; nt, neural tube; pm, periocular mesenchyme; RT, reverse transcriptase; s, somites.

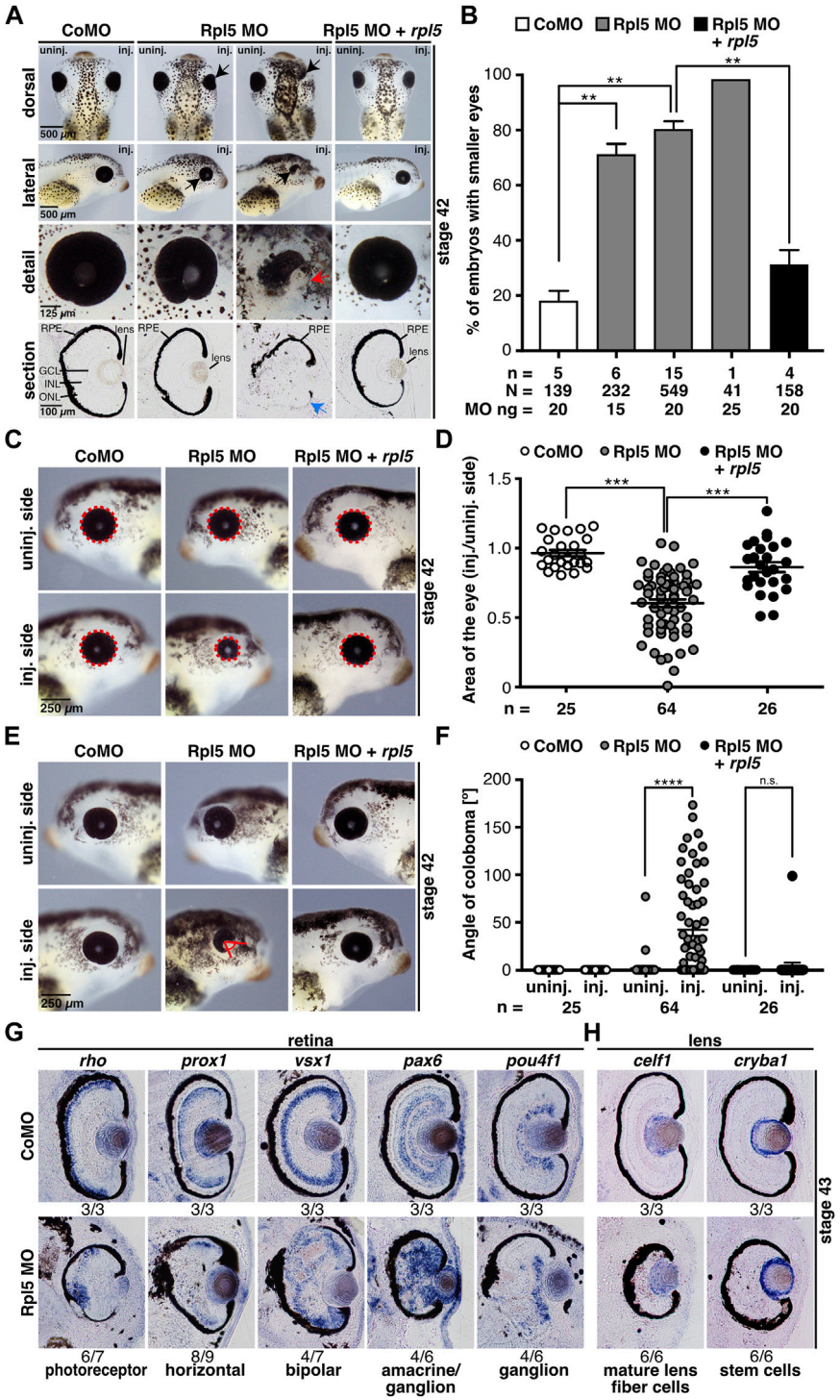

FIGURE 2 | Rpl5 MO injection leads to a severe eye phenotype. **(A)** *Xenopus* embryos injected with Control MO, Rpl5 MO and Rpl5 MO + *rpl5* and evaluated at stage 42. The injected side was compared to the uninjected side. Dorsal, lateral, and detail views, as well as sections are shown. Rpl5 MO-injected embryos developed smaller and malformed eyes (black arrows) in a MO dose-dependent manner. Detailed view of deformed eyes is depicted (red arrow). Section view shows disrupted retinal pigmented epithelium (blue arrow, section orientation is dorsal (upper part) to ventral (lower part)). **(B)** Statistical analysis of data given in **(A)**. The eye phenotype was rescued by co-injecting 0.5 ng *rpl5* RNA. **(C)** The area of the eye (red dotted line) on the injected side was compared to uninjected side of Control MO, Rpl5 MO, and Rpl5 MO + *rpl5*-injected embryos at stage 42. **(D)** Statistical evaluation of data given in **(C)**. Embryos showed significantly smaller eyes upon Rpl5 depletion. This phenotype was rescued upon co-injection of *rpl5* RNA. **(E)** The angle of eye fissure (red lines) of stage 42 embryos was measured and the injected side compared to the uninjected side. **(F)** Statistical analysis of data given in **(E)**. Rpl5 morphants showed a coloboma phenotype in a large number of individuals. This

(*Continued*)

FIGURE 2 | phenotype was rescued upon co-injecting *rpl5* RNA. **(G)** At stage 43, different cell layers of the retinal lamination were analyzed by whole mount *in situ* hybridization using well-known marker genes as described in the main text. Transversal sections of Control MO and Rpl5 MO-injected embryos are depicted. Upon Rpl5 knockdown all depicted cell types were delocalized and cell layers are disrupted. Number below the columns indicate the number of embryos showing the depicted phenotype per number of embryos analyzed. Section orientation is dorsal (upper part) to ventral (lower part). **(H)** *celf1*, a marker gene for mature lens fiber cells and *cryba1*, a marker gene for lens stem cells, were analyzed at stage 43 embryos injected with either Rpl5 MO or Control MO. Both lens-specific marker genes were not affected upon Rpl5 MO injection. Number below the columns indicate the number of embryos showing the depicted phenotype per number of embryos analyzed. Section orientation is dorsal (upper part) to ventral (lower part). Abbreviations: CoMO, Control morpholino oligonucleotide; GCL, ganglion cell layer; INL, inner nuclear cell layer, inj., injected; n, number of independent experiments; N, number of injected embryos and analyzed; n.s., non-significant; ONL, outer nuclear cell layer; RPE, retinal pigmented epithelium; Rpl5 MO, ribosomal protein L5 morpholino oligonucleotide; uninj., uninjected. Error bars indicate standard error of the means; $^{**}p \leq 0.01$, $^{***}p \leq 0.001$, $^{****}p \leq 0.0001$.

located in the mandibular arch, the hyoid arch and the third branchial arch, where *twist1* and *foxc1* are expressed as well (**Figures 1E,J**).

Knockdown of Ribosomal Protein L5 Affects Proper *Xenopus* Eye Development

As Rpl5 was found to be highly expressed in anterior neural tissue, the impact of Rpl5 knockdown on anterior neural development of *Xenopus laevis* was investigated using an antisense-based MO approach. Therefore, an Rpl5 MO targeting the 5′UTR of *rpl5* was designed (**Supplementary Figure S3A**). Its binding affinity was checked with an MO binding affinity assay (**Supplementary Figure S3B**).

To reduce Rpl5 translation, the MO was injected into one animal-dorsal blastomere of eight-cell stage embryos to directly target anterior neural tissue (Moody and Kline, 1990). The uninjected site served as internal control and co-injection of 0.5 ng *GFP* RNA was used to track the correct injection site. Control MO injections served as injection control. Injection of Rpl5 MO led to deformed and smaller eyes in a MO dose-dependent manner whereas Control MO injection led to normally developed eyes (**Figures 2A,B**). Additionally, vibratome sections showed a disturbed retinal pigmented epithelium (RPE) (**Figure 2A**). To describe the observed eye defects in more detail, we quantitatively measured the area of the eye on the injected and uninjected side, respectively. The injection of Rpl5 MO led to a reduction of the eye area of around 40% compared to the uninjected side and to Control MO injected embryos (**Figures 2C,D**). Furthermore, we investigated the formation of colobomas by measuring the apex angle. The injection of Rpl5 MO resulted in a coloboma phenotype (**Figures 2E,F**). All above-described eye phenotypes were rescued upon co-injection of Rpl5 MO together with an *rpl5* RNA, which is not targeted by the Rpl5 MO, implicating the specificity of the Rpl5 MO-induced eye phenotype (**Figures 2A–F**).

To further analyze the disturbed RPE upon Rpl5 MO injection, WMISH experiments were performed using well-known retina cell type marker genes (Cizelsky et al., 2013): *rho* for photoreceptor cells, *prox1* for horizontal cells, *vsx1* for bipolar cells, *pax6* for amacrine and ganglion cells, and *pou4f1* for ganglion cells. Vibratome sections showed a severe disorganization of all different retinal layers whereas the uninjected side and Control MO-injected embryos showed proper retinal organization (**Figure 2G** and **Supplementary Figure S4**). As Rpl5 was found to be strongly expressed in the lens (**Figure 1E**), we analyzed two lens-specific marker genes, *celf1* for mature lens fiber cells and *cryba1* for lens stem cells (Day and Beck, 2011). Neither the injection of Rpl5 MO nor Control MO affected the lens-specific marker genes (**Figure 2H**).

Additionally, the expression of eye-specific marker genes was analyzed *via* WMISH upon Rpl5 reduction to investigate the molecular basis of the described eye phenotype (**Figures 3A–D**). During eye field induction at stage 13, the expression of the eye-specific marker genes *rax* and *pax6* were significantly reduced upon Rpl5 MO injection, whereas the Control MO injection had no effect on both marker genes. The pan-neural marker gene *sox3* was not affected upon Rpl5 as well as Control MO injection (**Figures 3A,B**). At stage 23, when eye cells differentiate, the expression of *rax*, *pax6*, and *otx2* was reduced in around 70% of the Rpl5 morphants, whereas Control MO-injected embryos showed normally expressed marker genes (**Figures 3C,D**).

Since the expression of eye-specific marker genes was affected in Rpl5 morphants, we further analyzed the eye tissue in sections of Rpl5 MO and Control MO-injected embryos. Rpl5 depletion led to a disturbed evagination of the eye vesicle on the injected side. Control MO injection had no effect on eye vesicle development (**Figure 3E**).

Affected Brain Development Upon Knockdown of Ribosomal Protein L5

The impact of Rpl5 depletion was further investigated in the brain (**Figure 4**). Therefore, brains from Rpl5 MO- as well as Control MO-injected embryos fixed at stage 42 were isolated. Area measurements of both hemispheres showed a significant reduction of the brain upon Rpl5 knockdown. The uninjected side, as well as Control MO-injected embryos showed no reduction. Furthermore, this phenotype was rescued upon co-injecting *rpl5* RNA (**Figures 4A,B**).

In order to gain further insights into the molecular basis, we performed WMISH experiments using well-established brain marker genes: *pax6* for the forebrain, *otx2* for the forebrain

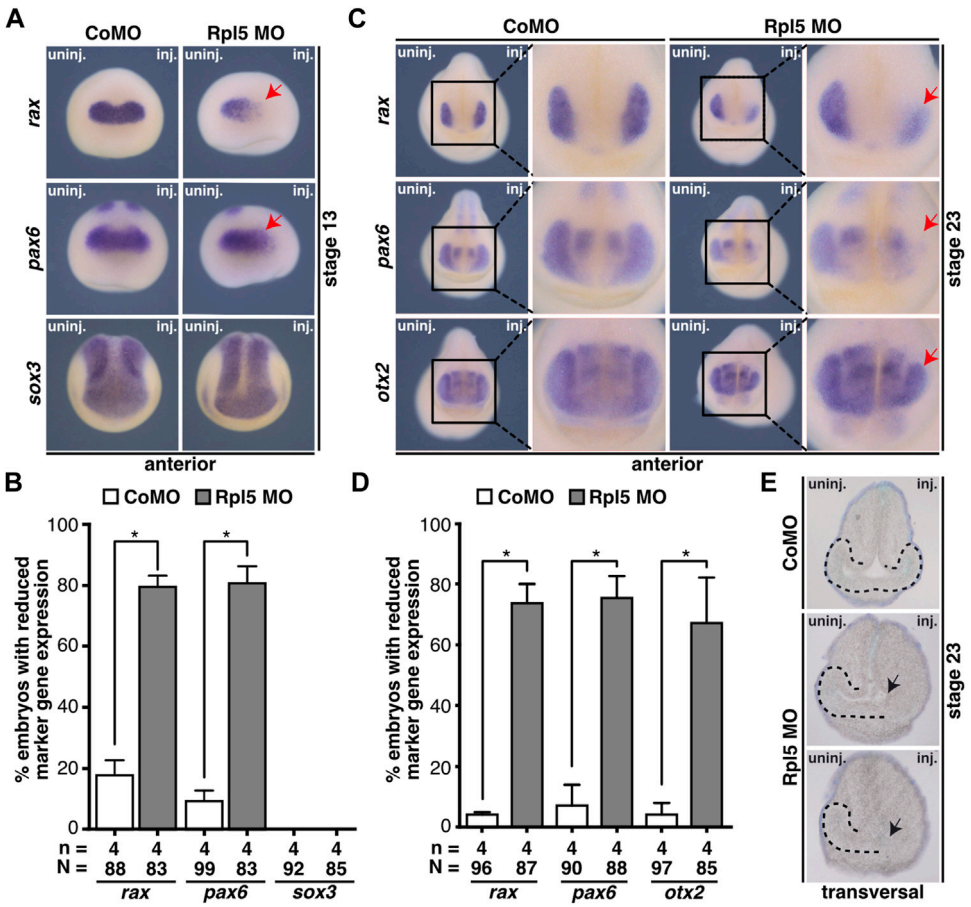

FIGURE 3 | Rpl5 knockdown interferes with eye-specific marker expression and eye vesicle evagination. **(A)** Anterior views of stage 13 embryos are given. By whole mount *in situ* hybridization the expression of the eye-specific marker genes *rax* and *pax6* and the pan-neural marker gene *sox3* was investigated in embryos injected with Control MO or Rpl5 MO. The expression of *rax* as well as *pax6* was reduced upon Rpl5 depletion (red arrows), whereas Control MO injection did not alter the expression. Expression of *sox3* was not altered, neither in Control MO nor in Rpl5 MO injected embryos. **(B)** Statistical analysis of data shown in **(A)**. **(C)** Anterior views are depicted. At stage 23, Control MO and Rpl5 MO-injected embryos were analyzed regarding the expression of eye-specific marker genes *rax*, *pax6*, and *otx2* by whole mount *in situ* hybridization. All three marker genes showed reduced expression in the eye field (red arrows) upon Rpl5 knockdown. Control MO injection did not result in altered gene expression. **(D)** Statistical analysis showed a significantly reduced expression in all three marker genes. **(E)** Transversal sections of stage 23 embryos injected with either Control MO or Rpl5 MO are shown. Section orientation is dorsal (upper part) to ventral (lower part). Eye vesicles in embryos injected with Rpl5 MO do not evaginate (indicated by black arrows). Control MO injection do not affect eye vesicle evagination. Eye vesicle is indicated by black dotted line. Abbreviations: CoMO, Control morpholino oligonucleotide; inj., injected; n, number of independent experiments; N, number of injected embryos and analyzed; Rpl5 MO, ribosomal protein L5 morpholino oligonucleotide; uninj., uninjected. Error bars indicate standard error of the means; $^*p \leq 0.05$.

and midbrain, and *egr2* for the hindbrain. At stage 13, embryos injected with Rpl5 MO showed a drastic decrease in *pax6* expression in the neural plate (**Figures 4C,D**). The expression of all three marker genes, *pax6, otx2,* and *egr2,* was reduced during brain cell differentiation at stage 23 at the Rpl5 MO-injected side (**Figures 4E,F**). Brain marker gene expression was not affected at the uninjected side as well as in Control MO-injected morphants.

Ribosomal Protein L5 Interferes With Cranial Cartilage Development in *Xenopus*

As shown in **Figure 1**, *rpl5* is highly expressed in the anterior NCCs which contribute to the formation of the cranial cartilage (Jacobson, 1991). Therefore, head development including cranial cartilage structures was investigated upon Rpl5 knockdown. Head width measurements showed a significantly narrower head on the Rpl5-MO-injected side, whereas Control MO injection resulted in normally developed heads (**Figures 5A,B**). This phenotype was rescued by co-injecting *rpl5* RNA. Furthermore, cranial cartilages of MO-injected embryos were stained by Alcian blue and dissected at stage 45 to accurately describe the observed phenotype. Structures of the cranial cartilage such as the Meckel's cartilage, the tectum anterius, and the branchial arches were reduced and disrupted upon Rpl5 depletion (**Figure 5C**). The wildtype control as well as the uninjected side showed normally developed cranial cartilages.

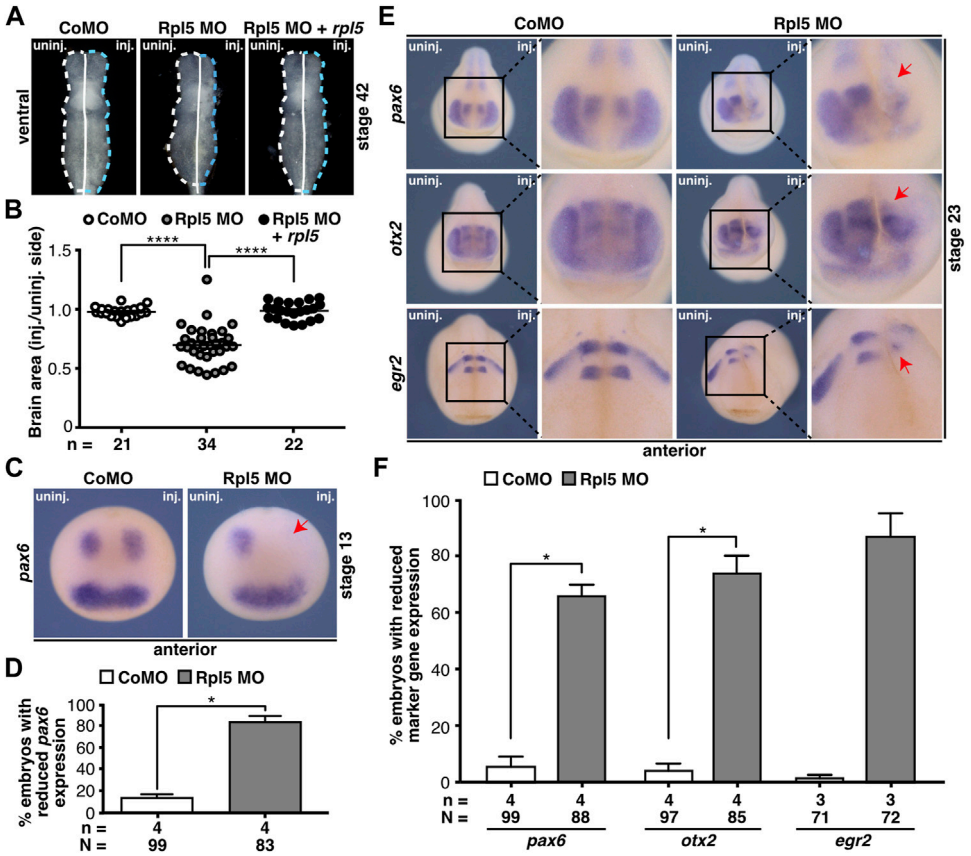

FIGURE 4 | Rpl5 depletion affects proper brain development. **(A)** Brains of Control MO, Rpl5 MO, and Rpl5 MO + *rpl5* RNA-injected embryos were dissected, the area of the brains was measured, and injected side was compared to uninjected side. Dotted lines indicate measured area. Ventral views of brains are given. **(B)** The area of the Rpl5 MO-injected side was significantly smaller compared to the uninjected side. Control MO-injection did not affect the area of the brain. This phenotype was rescued upon co-injecting *rpl5* RNA. **(C)** Anterior views of embryos are depicted. The marker gene *pax6* was analyzed in the anterior neural tube of embryos injected either with Control MO or Rpl5 MO. Rpl5 morphants showed a drastic reduction in expression (red arrow) on the injected side in 80% of the embryos, whereas Control MO injected embryos showed no reduction in *pax6* expression. **(D)** Statistical analysis of data shown in **(C)**. **(E)** Anterior views of embryos are given. At stage 23, the brain-specific marker genes *pax6*, *otx2*, and *egr2* were investigated by whole mount *in situ* hybridization in embryos injected with Control MO or Rpl5 MO. In the developing brain, all three investigated marker genes showed reduced expression (red arrows) upon Rpl5 MO injection but not upon Control MO injection. **(F)** Statistical analysis of data shown in **(E)**. Abbreviations: CoMO, Control morpholino oligonucleotide; inj., injected; n, number of independent experiments; N, number of injected embryos and analyzed; Rpl5 MO, ribosomal protein L5 morpholino oligonucleotide; uninj., uninjected. Error bars indicate standard error of the means; $^{*}p \leq 0.05$, $^{****}p \leq 0.0001$.

To analyze the molecular basis of the described phenotype, the NCC-specific marker genes *snai2* and *twist1* were investigated by WMISH experiments at stages 15 and 20. During NCC induction (stage 15), both marker genes showed a decrease in expression in around 80% of the Rpl5 MO-injected embryos. During NCC migration (stage 20) *snai2* as well as *twist1* expression was reduced and shortened in 80–90% of the Rpl5 MO- compared to Control MO-injected embryos (**Figures 5D–G**).

Loss of Ribosomal Protein L5 Affects *Xenopus* Blood Development

Rpl5 was also found to be expressed in the blood islands (**Figure 1**, **Supplementary Figure S2B**). To investigate Rpl5 depletion in this disease-relevant tissue, we analyzed two hematopoiesis specific marker genes, *gata2* and *hba3*. *gata2* is a hematopoietic transcription factor and serves as marker gene for hematopoietic stem and progenitor cells (Katsumura et al., 2017), whereas *hba3* is part of hemoglobin and therefore located in mature erythrocytes. *gata2* expression was not affected upon Rpl5 depletion (**Supplementary Figures S5A,B**). However, the expression of *hba3* was reduced on the Rpl5 MO-injected side (**Supplementary Figures S5C,D**). Control MO injection did not alter expression of either of the marker genes.

Taken together, Rpl5 is crucial for a proper development of the eye, the brain, the NCC-derived cranial cartilage, and the blood during *Xenopus* embryogenesis. The observed phenotypes in *Xenopus laevis* mirror the clinical manifestations seen in patients suffering from ribosomopathies, which makes

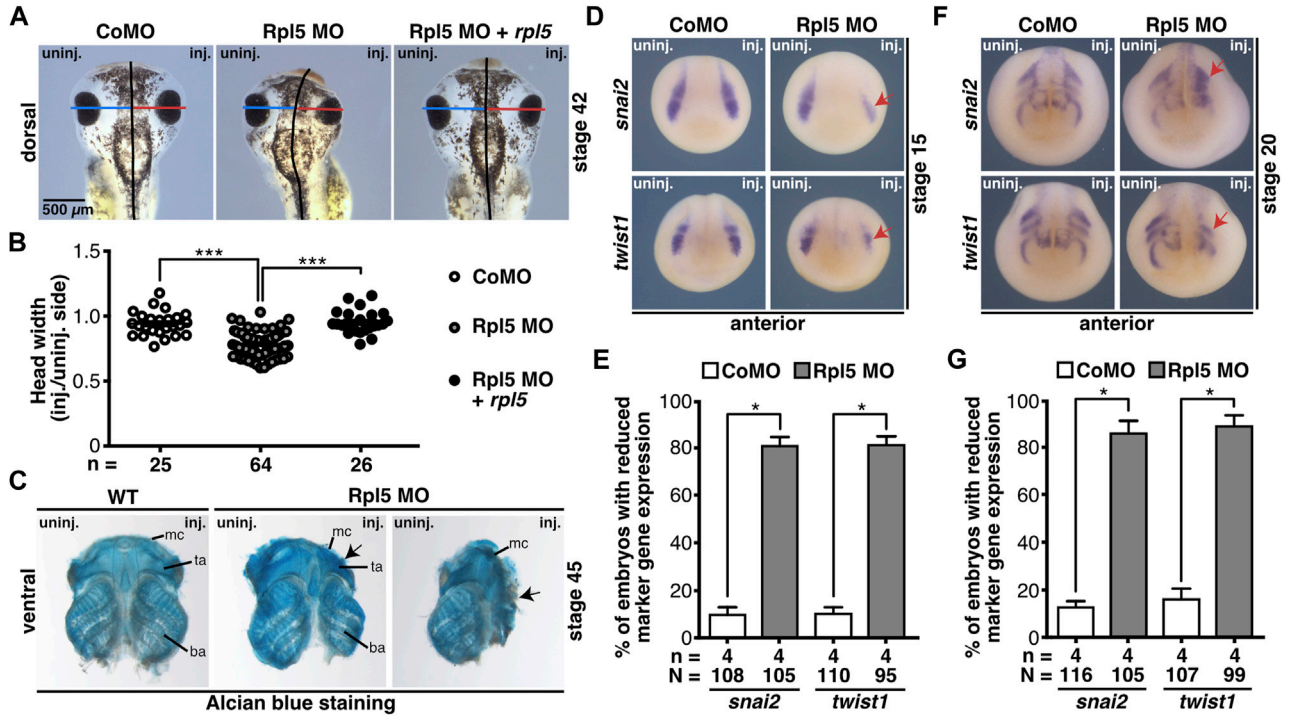

FIGURE 5 | Rpl5 MO injection hinders proper development of the cranial cartilage. **(A)** The head width was measured and the Control MO, Rpl5 MO, or Rpl5 MO + *rpl5* RNA-injected side compared to the uninjected side of stage 42 embryos. Blue and red lines indicate measured width; black line represents the embryo midline. **(B)** Rpl5 depletion led to significantly narrower heads, which was rescued upon *rpl5* RNA co-injecting. **(C)** Cranial cartilage was dissected from stage 45 wildtype embryos and Rpl5 morphants. Rpl5 knockdown resulted in deformed cartilages structures (black arrows) like the Meckel's cartilage, the tectum anterius, and the branchial arch. Ventral views of cranial cartilages are shown. **(D)** Anterior views of embryos are depicted. *snai2* and *twist1* were investigated as marker genes of the neural crest in stage 15 embryos. Reduced marker gene expression is indicated with red arrows. **(E)** Upon Rpl5 depletion both marker genes were significantly reduced in 80% of the embryos. **(F)** Anterior views of embryos are given. Expression of *snai2* and *twist1* were analyzed at stage 20 during NCC migration. Red arrows indicate reduced marker gene expression. **(G)** Both marker genes showed a significant reduction in expression in around 85% of the Rpl5 MO-injected embryos. Abbreviations: ba, branchial arch; CoMO, Control morpholino oligonucleotide; inj., injected; mc, Meckel's cartilage; n, number of independent experiments; N, number of injected embryos and analyzed; Rpl5 MO, ribosomal protein L5 morpholino oligonucleotide; ta, tectum anterius; uninj., uninjected; WT, wildtype. Error bars indicate standard error of the means; $*p \leq 0.05$, $***p \leq 0.001$.

Xenopus a valuable model organism to investigate the disease in detail.

Rpl5 Depletion Affects Proliferative Pathways

To investigate whether the reduced anterior neural structures are a result of a disturbed cell proliferation, stage 13 and 23 embryos were analyzed *via* pH3 staining. At stage 13 the number of proliferative cells did not alter upon Rpl5 MO injection (**Figures 6A,B**). However, at stage 23 Rpl5 depletion resulted in a significantly decreased number of proliferative cells (**Figures 6C,D**). Control MO injection did not lead to altered proliferation (**Figures 6A–D**).

c-Myc is a crucial regulator for proliferative processes in the cell (Gomez-Roman et al., 2003; Arabi et al., 2005). Since the number of proliferative cells decreased in Rpl5-depleted embryos, we investigated c-Myc in the following experiments. Furthermore, *c-myc* RNA has been shown to be degraded by free Rpl5 and Rpl11 upon cellular stress, e.g., induced by ribosomal biogenesis defects as they occur during ribosomopathies (Liao et al., 2014). Additionally, the knockdown of c-Myc has been found to lead to a cranial cartilage phenotype in *Xenopus* embryos as well as mice (Bellmeyer et al., 2003; Wei et al., 2007) similar as observed here for Rpl5 depletion. Hence, *c-myc* expression was analyzed in stage 15 embryos injected with Rpl5 MO. The embryos showed a reduced *c-myc* expression on the injected side, whereas Control MO injection had no effect on *c-myc* expression (**Figures 6E,F**). A quantitative analysis confirmed this result (**Figures 6G,H**). Furthermore, we co-injected Rpl5 MO and *c-myc* RNA to analyze a possible rescue mechanism. The area of the eyes was quantitatively measured and injected side was compared to uninjected side. Upon co-injecting Rpl5 MO together with 0.25 ng *c-myc* RNA, the area of the injected eye significantly increased in comparison to Rpl5 MO injection (**Figures 6I,J**). To further investigate a common pathway of Rpl5 and c-Myc, low doses of Rpl5 MO and c-Myc MO were injected alone and in combination. Low doses of Rpl5 MO and c-Myc MO resulted in a mild eye or head phenotype in few embryos. The injection of both MOs together led to a more than additive eye or head phenotype in a high

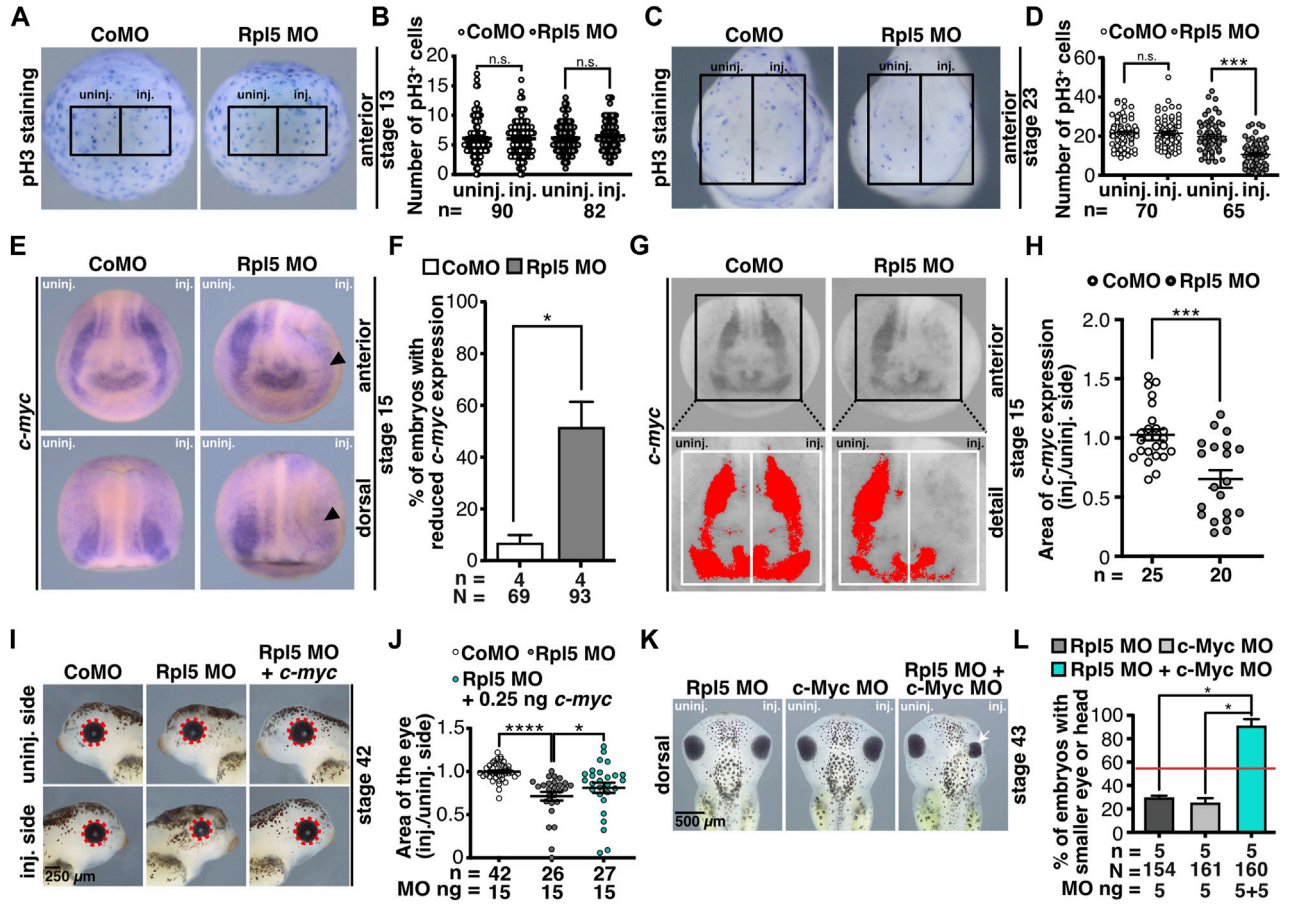

FIGURE 6 | Rpl5 depletion interferes with pathway of proliferation. **(A)** Proliferative cells of embryos injected with Control MO or Rpl5 MO were stained *via* a pH3 antibody at stage 13. Anterior views are shown. Number of proliferative cells were compared in the area of the anterior neural plate of the injected side and the uninjected side (black boxes indicate the area where proliferative cells were counted). **(B)** In Rpl5 morphants and control embryos the number of pH3 positive cells did not alter between injected and uninjected side. **(C)** At stage 23 proliferative cells were stained *via* pH3 staining in Rpl5 and Control MO injected embryos. Anterior view of embryos is shown. The number of proliferative cells was compared between injected and uninjected side (black boxes indicate the area where cells were counted). **(D)** Rpl5 morphants had a reduced number of pH3 positive cells on the injected side, whereas the uninjected side and Control MO-injected embryos were not affected. **(E)** Embryos injected with either Control MO or Rpl5 MO were fixed at stage 15 and *c-myc* expression was analyzed by WMISH. Reduced *c-myc* expression is indicated by black arrowhead. **(F)** *c-myc* expression was significantly reduced on the Rpl5 MO-injected side, whereas Control MO injection did not alter *c-myc* expression. **(G)** Area of *c-myc* expression (red area) was measured in stage 15 embryos injected with either Control MO or Rpl5 MO. The injected side was compared to the uninjected side (white boxes). **(H)** Upon Rpl5 depletion, the area of *c-myc* expression was significantly reduced in Rpl5 morphants compared to control embryos. **(I)** Embryos were injected with Control MO, Rpl5 MO, or Rpl5 MO + 0.25 ng *c-myc* RNA, fixed at stage 42 and photographed. The area of the eye (red dotted line) was measured and the injected side was compared to the uninjected side. **(J)** 15 ng Rpl5 MO injection resulted in significantly smaller eyes. Injection of 15 ng Rpl5 MO together with 0.25 ng *c-myc* RNA significantly increased the eye area compared to Rpl5 MO injection alone. Control MO injection did not affect the eye area. **(K)** Eight-cell stage embryos were injected with 10 ng Control MO, 5 ng Rpl5 MO and 5 ng c-Myc MO alone or in combination. Embryos were fixed and analyzed regarding a smaller head or eye (white arrow) at stage 43. **(L)** Embryos injected with Control MO did not develop malformed eyes or heads. Rpl5 MO and c-Myc MO injection alone resulted in smaller eyes or narrower heads in around 30% of the embryos. The simultaneous injection of Rpl5 MO and c-Myc MO led to smaller eyes or heads in 90% of the embryos. Red line indicates sum of embryos showing an eye or head phenotype injected with 5 ng Rpl5 MO and 5 ng c-Myc MO. Abbreviations: *c-myc*, *Myc proto-oncogene*; CoMO, Control morpholino oligonucleotide; inj., injected; n, number of independent experiments; N, number of injected embryos and analyzed; n.s., non-significant; pH3, phospho histone 3; Rpl5 MO, ribosomal protein L5 morpholino oligonucleotide; uninj., uninjected. Error bars indicate standard error of the means; $*p \leq 0.05$, $***p \leq 0.001$, $****p \leq 0.0001$.

number of embryos (**Figures 6K,L**). This effect was not extended to the number of proliferative cells at stage 23. This was analyzed by pH3 staining in embryos injected with low doses of Rpl5 MO and c-Myc MO alone and in combination (**Supplementary Figures S6A,B**).

In conclusion, this data suggests that Rpl5 depletion affects proliferation during organogenesis. c-Myc and Rpl5 share a common pathway and rescue experiments indicate that c-Myc is downstream of Rpl5.

Rpl5 Depletion Affects Apoptotic Pathways

To investigate whether cell apoptosis contributes to the observed anterior phenotypes, we analyzed stage 13 and stage 23 embryos *via* TUNEL staining upon Rpl5 depletion. At both developmental

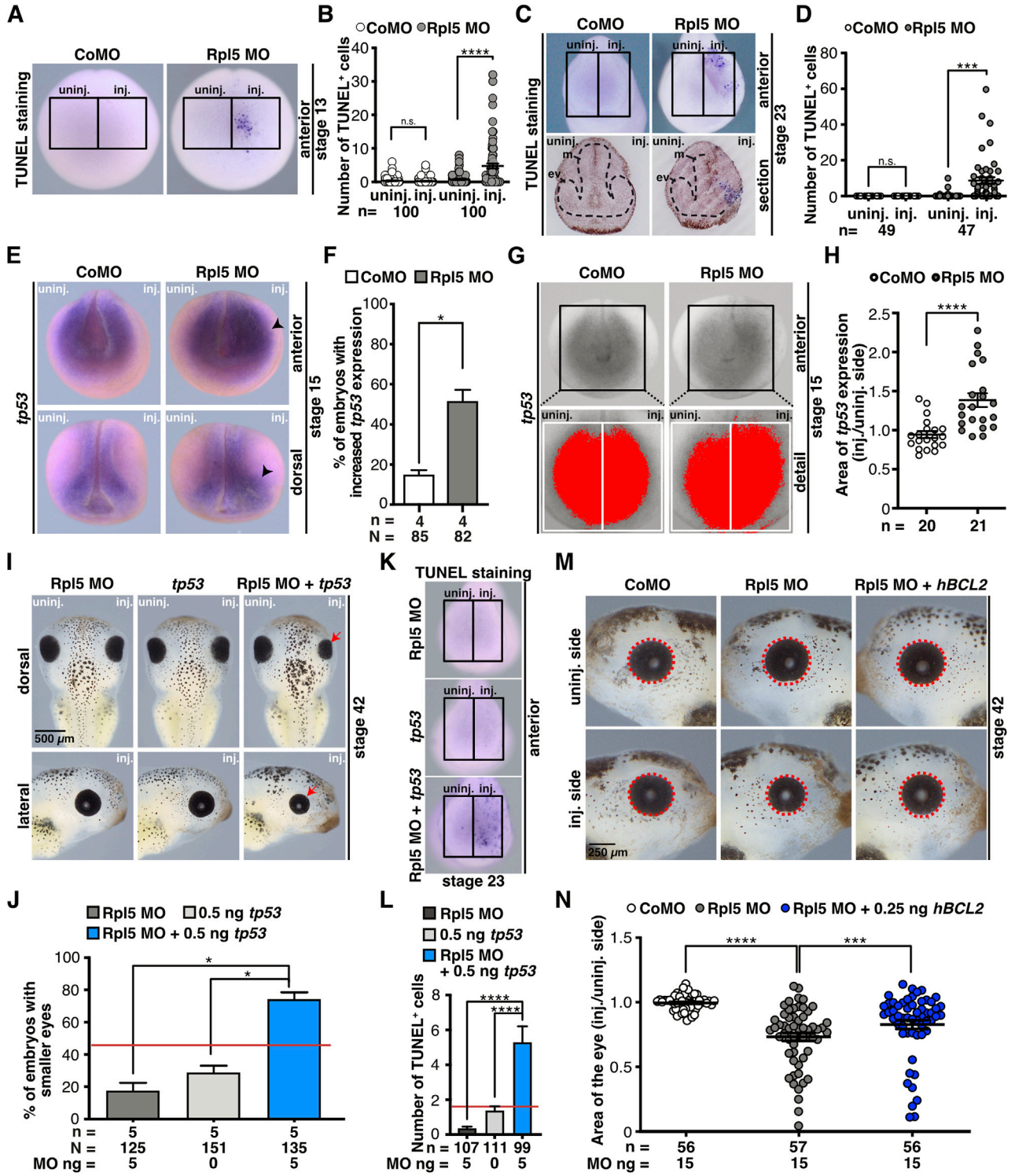

FIGURE 7 | Rpl5 depletion affects apoptotic pathways. **(A)** Late apoptotic cells were stained in stage 13 embryos injected with Control and Rpl5 MO *via* TUNEL staining. Anterior views are shown. Number of apoptotic cells was counted in the area of the anterior neural plate (black boxes indicate the area where apoptotic cells were counted) and the injected side was compared to the uninjected side. **(B)** Control MO injection did not increase the number of apoptotic cells. Rpl5 MO injection led to a significantly increased number of apoptotic cells. **(C)** Anterior views are shown in the upper row. Lower row shows transversal sections of embryos heads [dorsal (upper part) to ventral (lower part) oriented section]. Black dotted line indicates eye vesicle and mesencephalon. Apoptotic cells were detected *via* TUNEL staining at stage 23 and counted in the anterior part of whole embryos (indicated by black boxes). The injected side was compared to the uninjected side. **(D)** Upon Rpl5

(*Continued*)

FIGURE 7 | depletion, embryos depicted an increased number of apoptotic cells in the anterior neural tissue. **(E)** At stage 15, embryos injected with Control MO or Rpl5 MO were fixed and *tp53* expression was analyzed by WMISH. Anterior and dorsal views are given. Increased *tp53* expression is indicated by black arrowheads. **(F)** More than 50% of the embryos showed an increase in *tp53* expression upon Rpl5 knockdown. **(G)** The area of *tp53* expression (red area) on the injected side was compared to the uninjected side (white boxes) in stage 15 embryos. **(H)** Compared to the control group, the area of *tp53* increased significantly upon Rpl5 MO injection. **(I)** 5 ng Rpl5 MO and 0.5 ng *tp53* RNA were injected alone and in combination into eight-cell stage embryos. At stage 42, embryos were analyzed regarding a smaller eye phenotype (red arrows). Injection of Rpl5 MO or *tp53* RNA alone resulted in smaller eyes in a small number of embryos (18 and 30%). Injection of both resulted in smaller eyes in more than 70% of the embryos. **(J)** Statistical analysis of data given in **(I)**. Red line indicates sum of embryos showing an eye phenotype injected with 5 ng Rpl5 MO and 0.5 ng *tp53* RNA. **(K)** Embryos were injected with 5 ng Rpl5 MO or 0.5 ng *tp53* RNA alone or in combination, fixed at stage 23 and apoptotic cells were stained *via* TUNEL staining. Anterior view of embryos is given. The number of apoptotic cells was counted in the anterior region (indicated by black boxes). **(L)** Rpl5 MO and *tp53* RNA injection resulted in a low number of TUNEL positive cells. Combined injection shows a high number of TUNEL positive cells. Red line indicates sum of TUNEL positive cells in embryos injected with 5 ng Rpl5 MO and 0.5 ng *tp53* RNA. Data of TUNEL staining is depicted after background noise reduction, performed for each injection condition separately. This was achieved by subtracting the average number of TUNEL positive cells of the uninjected side of the nominal number of TUNEL positive cells of the injected side. If this resulted in a negative value, it is reported as zero. **(M)** At eight-cell stage, embryos were injected with Control MO, Rpl5 MO, or Rpl5 MO together with 0.25 ng *hBCL2* RNA and fixed at stage 42. Eye area (red dotted line) was quantitatively measured and injected side was compared to the uninjected side. **(N)** Control MO injection did not affect the area of the eye, whereas Rpl5 MO injection led to smaller eyes. The combined injection of Rpl5 MO and 0.25 ng *hBCL2* significantly increased the area of the eye compared to Rpl5 MO injection alone. Abbreviations: CoMO, Control morpholino oligonucleotide; ev, eye vesicle; *hBCL2*, *human B cell lymphoma 2*; inj., injected; m, mesencephalon; n, number of independent experiments; N, number of injected embryos and analyzed; n.s., non-significant; Rpl5 MO, ribosomal protein L5 morpholino oligonucleotide; *tp53*, *tumor protein p53*; TUNEL, Terminal deoxynucleotidyl transferase dUTP-biotin nick end labeling; uninj., uninjected. Error bars indicate standard error of the means; $^{*}p \leq 0.05$, $^{***}p \leq 0.001$, $^{****}p \leq 0.0001$.

stages, the anterior tissue showed a significantly increased number of apoptotic cells on the injected side (**Figures 7A–D**). At stage 23, transversal sections of the head showed TUNEL-positive cells in the developing eye tissue (**Figure 7C**). Control MO injection did not increase the number of apoptotic cells at stage 13 or 23.

Previous studies described that upon defective ribosomal biogenesis—e.g., induced by Rpl5 knockdown—free Rpl5 or Rpl11 or the 5S-RNP complex can lead to Tp53 pathway activation by binding MDM2 and hence an apoptotic signalling cascade is activated (Dai and Lu, 2004; Sulima et al., 2019). Furthermore, it was shown in several animal models that the knockout of *tp53* rescued craniofacial phenotypes occurring during ribosomopathies (Jones et al., 2008; Zhao et al., 2014; Griffin et al., 2015; Calo et al., 2018). Therefore, we investigated whether the simultaneous knockdown of Rpl5, which itself might induce defective ribosomal biogenesis, and Tp53 can rescue the Rpl5 MO-induced phenotype. However, the phenotype was not rescued (**Supplementary Figures S6C,D**). To exclude also a subtle rescue, the eye area was analyzed quantitatively; which also showed no rescue (**Supplementary Figures S6E–H**). At stage 15, however, *tp53* expression was significantly increased on the Rpl5 MO-injected side, whereas the un-injected side or the Control MO injection did not alter *tp53* expression (**Figures 7E,F**). A quantitative analysis confirmed the *tp53* increase upon Rpl5 depletion (**Figures 7G,H**). To further characterize a possible common pathway between Rpl5 and Tp53, we investigated whether the gain of Tp53 function worsens the Rpl5 MO-induced phenotype by injecting Rpl5 MO and *tp53* RNA alone and in combination using low doses into one animal-dorsal blastomere of eight-cell stage embryos. The injection of either 5 ng Rpl5 MO or 0.5 ng *tp53* RNA resulted in a small number of embryos with smaller eyes (30 and 17% respectively). In contrast, the combined injection of both in low doses resulted in smaller eyes in around 75% of the injected embryos (**Figures 7I,J**). Furthermore, low doses of either Rpl5 MO or *tp53* RNA were injected alone or in combination into the animal-dorsal blastomere of eight-cell stage embryos and the number of apoptotic cells was analyzed at stage 23 *via* TUNEL staining. The injection of either Rpl5 MO or *tp53* RNA resulted in a small number of apoptotic cells on the injected side. However, the simultaneous injection of both low doses increased the number of apoptotic cells drastically (**Figures 7K,L**). This more than additive effect of Rpl5 and Tp53 on the late phenotype as well as the number of apoptotic cells at stage 23 suggests a common pathway of the two molecules.

To further investigate whether apoptosis contributes to the observed phenotypes, Rpl5 MO was injected in combination with the apoptosis blocker *hBCL2* RNA. BCL2 blocks the intrinsic apoptotic pathway by several mechanisms (Siddiqui et al., 2015). Rpl5 MO was injected alone and together with 0.25 ng *hBCL2* RNA unilaterally into one animal-dorsal blastomere of eight-cell stage embryos. At stage 42, the area of the eye was measured and the injected side was compared to the uninjected side. The co-injection of *hBCL2* RNA partially rescued the eye phenotype in Rpl5 morphants (**Figures 7M,N**).

DISCUSSION

In this study, the ribosomal protein Rpl5 has been shown to be required for proper development of anterior organs and tissues such as the eyes, the brain, and the cranial cartilage in *Xenopus laevis*. Furthermore, the Rpl5 knockdown led to increased apoptosis and decreased proliferation. These findings were in line with decreased *c-myc* expression and increased *tp53* expression. Additionally, common pathways were elucidated between Rpl5 and Tp53 and c-Myc, respectively. The co-injection of apoptosis blocker *BCL2* led to a partial rescue of the Rpl5 MO-induced eye phenotype. We found that Rpl5 depletion results in early phenotypes occurring before organogenesis—even though in previous studies early *Xenopus* development has been shown to be independent of ribosomal biogenesis (Brown, 1964; Pierandrei-Amaldi and Amaldi, 1994). This suggests that Rpl5 might have additional functions beyond its role in ribosome formation.

The extensive expression analysis of *rpl5* throughout the embryonic development of *Xenopus laevis* showed a detailed

expression in the neural tissue, such as the developing eye and brain, as well as the NCCs. These findings are consistent with previously published expression patterns of *rpl5* in *Xenopus laevis* (Scholnick et al., 1997; Wischnewski et al., 2000; Session et al., 2016). Furthermore, *rpl5* expression is located in tissues which are mainly affected in patients suffering from ribosomopathies (Narla and Ebert, 2010; Farley-Barnes et al., 2019).

Here, we showed that the knockdown of Rpl5 results in a severe eye and brain phenotype. As shown in **Figure 3E**, the evagination of the eye vesicle is hindered upon Rpl5 depletion. This early disruption of the eye development most likely contributes later to a disturbed eye cup invagination and therefore contributes to a malformed eye. We found a disturbed retinal lamination. Interestingly, all cell types were present. Previous studies revealed that cell adhesion defects appearing as increased intercellular spaces cause this phenotype (Seigfried et al., 2017). As shown in **Figure 3**, *pax6* expression is reduced in Rpl5 morphants, which might contribute to these developmental defects in the retina, since it has been shown that several cell adhesion molecules are direct targets of Pax6 (Rungger-Brändle et al., 2010). Furthermore, Rax, which we found to be reduced in Rpl5 morphants, might affect proper retinal lamination since 1) Rax has been shown to impact retinal lamination in mice embryos (Rodgers et al., 2018) and 2) Rax-dependent genes have been shown to be necessary for proper retina lamination in *Xenopus* (Pan et al., 2018). Marker genes for the lens were not affected upon Rpl5 depletion suggesting that a disturbed development of the lens placodes does not contribute to the disorganized retinal lamination.

Ribosomal proteins other than Rpl5 also affect proper eye as well as brain development as Pescadillo homologue 1 (Pes1) and Peter Pan (Ppan) lead to malformed eyes, including coloboma, as well as microcephaly in developing *Xenopus laevis* (Gessert et al., 2007; Bugner et al., 2011). Watkins-Chow and others have shown that Rps7-mutated mice develop uveal coloboma and microphthalmia (Watkins-Chow et al., 2013). Mutations in human ribosomal proteins are also linked to defects in eye development (Kuze et al., 2009). Brain defects have been found in patients carrying a mutated Rpl10 or Rps23, as they show an increased incidence in microcephaly, seizures, aphasia, ataxia, and intellectual disability (Brooks et al., 2014; Bourque et al., 2018). In summary, these findings highlight the importance of Rpl5 in proper brain and eye development.

In order to gain insight into the observed defects on a molecular basis, marker gene expression was investigated at stages 13 and 23. Reduced expression of eye-specific marker genes *rax* and *pax6* implicate defects in early eye field induction as well as in eye cell differentiation in Rpl5-deficient embryos. Moreover, expression of the brain-specific marker genes *pax6*, *otx2*, and *egr2* was reduced upon Rpl5 depletion. The pan-neural maker gene *sox3*, however, was not affected, indicating that neural induction is not disturbed in general. In earlier studies we showed, that the depletion of Pes1 and Ppan also lead to reduced *pax6*, *rax*, and *otx2* expression in *Xenopus* (Gessert et al., 2007; Bugner et al., 2011). In mice, Pax6 depletion results in absent eyes (Georgala et al., 2011). In human, mutations in the *PAX6* gene are linked to a variety of eye defects such as aniridia, corneal opacification or cataract, as well as autism spectrum disorder (Maekawa et al., 2009; Cvekl and Callaerts, 2017). Not only *PAX6*, but also *OTX2*, *RAX*, and *EGR2* have been associated with eye and brain defects in humans (Gonzalez-Rodriguez et al., 2010; Nakayama et al., 2015; Sevilla et al., 2015; Deml et al., 2016). Taken together, these data indicate that the disturbed expression of these marker genes, as a result of Rpl5 knockdown, contribute to the eye and brain phenotype occurring in *Xenopus laevis* and that the induction as well as cell differentiation is perturbed. It would be highly interesting to analyze these genes in patients with a mutated *RPL5* gene and patients suffering from other ribosomopathies.

Following the induction of NCCs during neural tube closure, these cells migrate towards the ventral part of the body and build the cranial cartilage as one derivative (Jacobson, 1991). The reduced expression of NCC-specific marker genes, *twist1* and *snai2* at stages 15 and 20, shows that the induction as well as the migration of NCCs is impaired upon Rpl5 knockdown. These defects become apparent in the destructed cranial cartilage observed in Rpl5-deficient embryos at stage 45. Griffin et al. demonstrated in *Xenopus* embryos that knockdown of Nol11, another factor for ribosomal biogenesis, results in a reduced expression of several marker genes for cranial NCCs such as *twist1* (Griffin et al., 2015). Additionally, we showed a reduced expression of *snai2* and *twist1* during Ppan knockdown (Bugner et al., 2011).

In human, mutations in ribosomal proteins, like Rpl5, found in DBA patients have also been linked to craniofacial defects (Lipton et al., 2006). Furthermore, our observations are in line with Rps7 knockdown mice, showing skeletal defects, resulting in reduced body length (Watkins-Chow et al., 2013) as well as Rps19 and Rps20-mutated mice with pigmentation and skin defects (McGowan et al., 2008). In *Xenopus* embryos, previous studies moreover showed that knockdown of the ribosomal factors Pes1, Ppan, as well as Nol11 results in malformed cranial cartilages (Gessert et al., 2007; Bugner et al., 2011; Griffin et al., 2015).

Earlier studies revealed that the knockdown of ribosomal biogenesis factors, such as Ppan, results in early phenotypes—occurring as reduced marker gene expression—which are independent of ribosomal biogenesis in *Xenopus* (Bugner et al., 2011). Hence, *Xenopus laevis* is a suitable model organism to study ribosomal biogenesis factors and proteins in a ribosomal independent way. Since we here also observed a very early phenotype, we investigated the molecular mechanism underlying Rpl5 loss of function during *Xenopus*.

In this study, Rpl5 depletion led to a decreased number of proliferative cells. Since c-Myc is a major regulator of proliferative processes and ribosomal biogenesis, we analyzed the molecule c-Myc and showed a decrease in *c-myc* expression in the cranial NCCs, a partial rescue of the eye phenotype was achieved by co-injecting *c-myc* RNA, and a more than additive effect was found between loss of Rpl5 function and loss of c-Myc function. In line, Bellmeyer and others showed that the depletion of c-Myc results in deformed cranial cartilages in *Xenopus* embryos (Bellmeyer et al., 2003). According to Liao et al., free Rpl5 and Rpl11 proteins are capable of reducing *c-myc* RNA levels by directly binding *c-myc* RNA and transporting it to RISC eventually degrading

c-myc RNA. The authors showed in a culture cell line that the knockdown of Rpl5 induces *c-myc* expression, whereas *rpl5* overexpression leads to *c-myc* degradation (Liao et al., 2014). Our findings are not in line with these results suggesting a different mechanism. Possibly, the depletion of Rpl5 might induce ribosomal stress, which eventually leads to a reduced *c-myc* expression by, e.g., free Rpl11 (Challagundla et al., 2011). Furthermore, Rpl5 may fulfill a role independent of ribosome biogenesis and affect c-Myc in a free-ribosomal way. Other mechanisms might be involved. However, based on our results that 1) *c-myc* expression is reduced upon Rpl5 depletion, 2) simultaneous loss of Rpl5 function and loss of c-Myc function leads to a more than additive effect, and 3) the Rpl5 MO-induced eye phenotype is partially rescued upon *c-myc* co-injection, we hypothesize a common signaling pathway of these two molecules, with c-Myc being downstream of Rpl5.

Furthermore, Rpl5 depletion was found to increase the number of apoptotic cells. To further analyze the mechanism underlying increased apoptosis, we investigated Tp53, a molecule which has been found to be accumulated and activated during disturbed ribosomal biogenesis by different ribosomal proteins (Dai and Lu, 2004); and which can initiate apoptosis as a transcription factor for genes necessary for apoptosis and by transcriptional-independent mechanisms, e.g., by directly targeting mitochondria inducing permeabilization of the mitochondrial membrane, which eventually leads to apoptosis (Kiraz et al., 2016). As mentioned above, several studies have shown that craniofacial abnormalities, which occurred during ribosomopathies, were rescued by knocking out *tp53* (Jones et al., 2008; Zhao et al., 2014; Griffin et al., 2015; Calo et al., 2018). In our study, however, we were not able to rescue the anterior neural phenotype by co-injecting Tp53 MO suggesting that the observed phenotype is not solely due to Tp53 activation as a consequence of disturbed ribosome biogenesis, e.g., through other free ribosomal proteins. This observation would be in line with the well accepted idea that early *Xenopus* embryos can rely on maternal ribosomes and do not require *de novo* synthesis of ribosomes. We observed, however, *tp53* expression to be increased on RNA level upon Rpl5 knockdown. In addition, the more than additive effect between Rpl5 knockdown and Tp53 overexpression suggests a common signaling pathway between those two molecules. Furthermore, by co-injecting *hBCL2* RNA we were able to partially rescue the Rpl5 MO-induced eye phenotype. The proto-oncogene *BCL2* is a blocker of apoptosis and mutations in the *BCL2* gene lead to cancer (Reed, 2008). In line with our results, it has been shown that Tp53 directly or indirectly blocks antiapoptotic BCL2 contributing to further cell death (Hemann and Lowe, 2006). Hence, the possible Bcl2 inhibition by Tp53, which is induced by Rpl5 depletion, can be counteracted by co-injection of *hBCL2* RNA in rescue experiments. This suggests that increased apoptosis is to a great extent contributor to the here observed phenotypes in *Xenopus laevis*.

Based on our results that *tp53* expression is increased in the anterior tissue during early embryonic development and *hBCL2* co-injection rescued the Rpl5 MO-induced phenotype, it is conceivable that continuous cell death induced by Tp53 pathway activation may lead to the different morphogenesis phenotypes.

Although it is widely accepted that early *Xenopus* embryos can rely on maternal ribosomes and thus do not require ribosome biogenesis during early stages of development, another explanation of the observed phenotypes might also be possible. In line with the different morphogenesis phenotypes are also the so-called ribosome concentration theory and the "specialized" ribosomes hypothesis. In the first case one could assume that maternal ribosomes are not equally distributed to all cells of the embryo resulting in cells that require *de novo* ribosome synthesis earlier than others. According to this theory, the translation of specific mRNAs may also depend on ribosome concentration and therefore again translational landscape might be altered (Lodish, 1974; Mills and Green, 2017; Cheng et al., 2019; Farley-Barnes et al., 2019). "Specialized" ribosomes are one hypothesis, in which already naturally existing heterogeneous ribosomes further acquire diverse abilities in distinct tissues due to changes in ribosomal assembly and composition (Mills and Green, 2017; Genuth and Barna, 2018; Ferretti and Karbstein, 2019; Norris et al., 2021). Both theories might contribute to the different morphogenesis phenotypes but are not yet investigated in *Xenopus* embryos.

Taken together, our findings indicate a role of Rpl5 for early *Xenopus* neural development and should foster additional experiments to examine the potential underlying mechanisms.

DATA AVAILABILITY STATEMENT

The original contributions presented in the study are included in the article/**Supplementary Material**, further inquiries can be directed to the corresponding author.

ETHICS STATEMENT

The animal study was reviewed and approved by German state administration Baden-Württemberg (Regierungspräsidium Tübingen).

AUTHOR CONTRIBUTIONS

SK, MK, and CS conceived and designed the experiments. CS, BK, PD, and RR performed the experiments. CS, BK, SK, and MK wrote the manuscript. All authors analyzed and discussed the data and commented on the manuscript.

ACKNOWLEDGMENTS

We thank Paul Krieg for providing plasmids.

SUPPLEMENTARY MATERIAL

The Supplementary Material for this article can be found online at: https://www.frontiersin.org/articles/10.3389/fcell.2022.777121/full#supplementary-material

Supplementary Figure S1 | Rpl5 synteny analysis and protein comparison between different species. **(A)** Synteny analysis of *rpl5* in *Homo sapiens*, *Mus musculus*, *Gallus gallus*, *Xenopus laevis L*, *Xenopus laevis S*, *Xenopus tropicalis*, and *Danio rerio*. Comparing the genomic region next to *rpl5* showed a conservation across the different species. **(B)** Protein alignment of Rpl5 of the different species *Homo sapiens*, *Mus musculus*, *Gallus gallus*, *Xenopus laevis L*, *Xenopus laevis S*, *Xenopus tropicalis*, *Danio rerio*. Protein homology is given in % compared to *Homo sapiens*. Abbreviations: aa, amino acid; Rpl5, ribosomal protein L5.

Supplementary Figure S2 | Spatial and temporal expression of *rpl5* in *Xenopus laevis* (extended). **(A)** *rpl5* expression was analyzed in wildtype stage 23 embryos *via* WMISH. Lateral views and sections are shown. *rpl5* transcripts are enriched in migrating NCCs (white arrow), the developing eye (red arrow), and somites (orange arrowhead). White dotted line represents level of transversal sections in **(a1,2)**, where *rpl5* expression was found in the neural tube and somites (indicated by black dotted lines). *actc1* was used as marker gene for somites. Section orientation is dorsal (upper part) to ventral (lower part). **(B)** Ventral view of the embryos is given. At stage 28, embryos show *rpl5* expression in the ventral blood islands (blue arrowhead), where *gata2* and *hba3* are expressed as well. Abbreviations: nc, notochord; nt, neural tube; s, somites.

Supplementary Figure S3 | Morpholino oligonucleotide binding affinity assay. **(A)** Binding sites (bs) of Rpl5 MO and the *Δ5′UTR rpl5* construct on *Xenopus rpl5*. Blue letters indicate the start codon. Grey letters indicate differences between Rpl5 MO binding site and the Δ5′UTR rpl5 construct. **(B)** Binding specificity test of Rpl5 MO. Co-injection of 1 ng *rpl5 MO bs-GFP* together with 10 ng Control MO led to GFP expression. 1 ng *rpl5 MO bs-GFP* injected with 10 ng Rpl5 MO efficiently blocked GFP translation. Co-injection of *Δ5′UTR rpl5 MO bs-GFP* along with 10 ng Rpl5 MO, however, led to GFP expression. Abbreviations: bs, binding site; CoMO, Control morpholino oligonucleotide; GFP, green fluorescent protein; n, number of independent experiments; N, number of injected embryos and analyzed; Rpl5 MO, ribosomal protein L5 morpholino oligonucleotide; UTR, untranslated region.

Supplementary Figure S4 | Retinal lamination upon Rpl5 knock down in detail. Analysis of retinal lamination specific marker genes, *rho*, *prox1*, *vsx1*, *pax6*, and *pou4f1* in Control MO and Rpl5 MO-injected embryos at stage 43. The entire eye of the uninjected and injected side are shown as well as a detailed view (indicated by black boxes) of the respective cell layer. Control MO injection did not alter the retinal lamination. Rpl5 depletion led to mild and severe phenotypes with disturbed retinal layer and malformed eyes. Number below the columns indicate the number of embryos showing the depicted phenotype per number of embryos analyzed. Abbreviations: CoMO, Control morpholino oligonucleotide; inj., injected; Rpl5 MO, ribosomal protein L5 morpholino oligonucleotide; uninj., uninjected.

Supplementary Figure S5 | Rpl5 depletion affects erythropoiesis. **(A)** 15 ng Control MO or Rpl5 MO were injected into one ventral blastomere of eight-cell stage embryos to target blood islands. Ventral view of embryos is given. Embryos were fixed at stage 28 and *gata2* expression was analyzed *via* WMISH. **(B)** *gata2* expression was not affected by either Rpl5 MO or Control MO injection. **(C)** Embryos were injected with 15 ng Control MO or Rpl5 MO into one ventral blastomere at eight-cell stage. Morphants were fixed at stage 28 and *hba3* expression was analyzed by WMISH. Ventral view of embryos is shown. Embryos injected with Rpl5 MO show a reduced *hba3* expression on the injected side (indicated by black arrowhead), whereas Control MO injection did not reduce *hba3* expression. **(D)** Statistical analysis of data shown in **(C)**. Abbreviations: CoMO, Control morpholino oligonucleotide; inj., injected; n, number of independent experiments; N, number of injected embryos and analyzed; n.s., non-significant; Rpl5 MO, ribosomal protein L5 morpholino oligonucleotide; uninj., uninjected. Error bars indicate standard error of the means; $^{*}p \leq 0.05$.

Supplementary Figure S6 | Combined injection of Rpl5 MO and c-Myc MO did not alter proliferation and simultaneous injection of Rpl5 MO and Tp53 MO did not rescue the Rpl5 MO-induced phenotype. **(A)** Embryos were injected with 5 ng Rpl5 MO, 5 ng c-Myc MO or 5 ng Rpl5 MO together with 5 ng c-Myc MO into one animal-dorsal blastomere at eight-cell stage. Embryos were fixed at stage 23 and proliferative cells were stained with a pH3 antibody. Anterior views are shown. Number of proliferative cells was counted (black boxes indicate area where pH3 positive cells were counted) and pH3 positive cells on the injected sides were compared between the three different conditions. **(B)** The number of proliferative cells did not alter between Control MO, Rpl5 MO, and Rpl5 MO together with c-Myc MO injection. **(C)** Control MO (17.5 ng or 20 ng), Rpl5 MO (15 ng), and Rpl5 MO (15 ng) + Tp53 MO (2.5 ng or 5 ng) were injected into eight-cell stage embryos to directly target anterior neural tissue. Embryos were fixed at stage 43 and analyzed regarding smaller eyes or heads (white arrows). **(D)** Statistical analysis showed that Rpl5 MO alone as well as in combination with Tp53 MO resulted in a severe eye and head phenotype. The here tested Tp53 MO amount did not rescue the Rpl5 MO-induced phenotype. **(E)** 17.5 ng Control MO, 15 ng Rpl5 MO, or 15 ng Rpl5 MO together with 2.5 ng Tp53 MO were injected at eight-cell stage. Embryos were fixed at stage 43 and subsequently photographed. Area of the eye (red dotted line) was measured and the injected side was compared to the uninjected side. **(F)** Rpl5 MO injection alone and in combination with Tp53 MO resulted in significantly smaller eyes on the injected side. Control MO injection did not reduce eye size. **(G)** 20 ng Control MO, 15 ng Rpl5 MO, or 15 ng Rpl5 MO together with 5 ng Tp53 MO were injected at eight-cell stage. Embryos were fixed at stage 43 and subsequently photographed. Area of the eye (red dotted line) was measured and the injected side compared to the uninjected side. **(H)** Control MO injection did not reduce the eye area. Rpl5 MO injection alone as well as together with Tp53 MO results in smaller eye areas. Tp53 depletion did not rescue the Rpl5 MO-induced phenotype in the here tested conditions. Abbreviations: c-Myc MO, Myc proto-oncogene morpholino oligonucleotide; CoMO, Control morpholino oligonucleotide; inj., injected; n, number of independent experiments; N, number of injected embryos and analyzed; n.s., non-significant; pH3, phospho histone 3; Rpl5 MO, ribosomal protein L5 morpholino oligonucleotide; Tp53 MO, Tumor protein p53 morpholino oligonucleotide; uninj., uninjected. Error bars indicate standard error of the means; $^{*}p \leq 0.05$; $^{****}p \leq 0.0001$.

REFERENCES

Arabi, A., Wu, S., Ridderstråle, K., Bierhoff, H., Shiue, C., Fatyol, K., et al. (2005). c-Myc Associates with Ribosomal DNA and Activates RNA Polymerase I Transcription. *Nat. Cel Biol* 7, 303–310. doi:10.1038/ncb1225

Aspesi, A., and Ellis, S. R. (2019). Rare Ribosomopathies: Insights into Mechanisms of Cancer. *Nat. Rev. Cancer* 19, 228–238. doi:10.1038/s41568-019-0105-0

Baßler, J., and Hurt, E. (2019). Eukaryotic Ribosome Assembly. *Annu. Rev. Biochem.* 88, 281–306. doi:10.1146/annurev-biochem-013118-110817

Bellmeyer, A., Krase, J., Lindgren, J., and LaBonne, C. (2003). The Protooncogene C-Myc Is an Essential Regulator of Neural Crest Formation in xenopus. *Developmental Cel* 4, 827–839. doi:10.1016/s1534-5807(03)00160-6

Bourque, D. K., Hartley, T., Nikkel, S. M., Pohl, D., Tétreault, M., Kernohan, K. D., et al. (2018). A De Novo Mutation in RPL10 Causes a Rare X-Linked Ribosomopathy Characterized by Syndromic Intellectual Disability and Epilepsy: A New Case and Review of the Literature. *Eur. J. Med. Genet.* 61, 89–93. doi:10.1016/j.ejmg.2017.10.011

Briggs, J. A., Weinreb, C., Wagner, D. E., Megason, S., Peshkin, L., Kirschner, M. W., et al. (2018). The Dynamics of Gene Expression in Vertebrate Embryogenesis at Single-Cell Resolution. *Science* 360, eaar5780. doi:10.1126/science.aar5780

Brooks, S. S., Wall, A. L., Golzio, C., Reid, D. W., Kondyles, A., Willer, J. R., et al. (2014). A Novel Ribosomopathy Caused by Dysfunction of RPL10 Disrupts Neurodevelopment and Causes X-Linked Microcephaly in Humans. *Genetics* 198, 723–733. doi:10.1534/genetics.114.168211

Brown, D. D. (1964). RNA Synthesis during Amphibian Development. *J. Exp. Zool.* 157, 101–113. doi:10.1002/jez.1401570115

Bugner, V., Tecza, A., Gessert, S., and Kühl, M. (2011). Peter Pan Functions Independently of its Role in Ribosome Biogenesis during Early Eye and Craniofacial Cartilage Development in *Xenopus laevis*. *Development* 138, 2369–2378. doi:10.1242/dev.060160

Calo, E., Gu, B., Bowen, M. E., Aryan, F., Zalc, A., Liang, J., et al. (2018). Tissue-selective Effects of Nucleolar Stress and rDNA Damage in Developmental Disorders. *Nature* 554, 112–117. doi:10.1038/nature25449

Challagundla, K. B., Sun, X.-X., Zhang, X., DeVine, T., Zhang, Q., Sears, R. C., et al. (2011). Ribosomal Protein L11 Recruits miR-24/miRISC to Repress C-Myc Expression in Response to Ribosomal Stress. *Mol. Cell Biol.* 31, 4007–4021. doi:10.1128/MCB.05810-11

Chang, W. S., and Harris, W. A. (1998). Sequential Genesis and Determination of Cone and Rod Photoreceptors inXenopus. *J. Neurobiol.* 35, 227–244. doi:10.1002/(sici)1097-4695(19980605)35:3<227::aid-neu1>3.0.co;2-0

Cheng, Z., Mugler, C. F., Keskin, A., Hodapp, S., Chan, L. Y.-L., Weis, K., et al. (2019). Small and Large Ribosomal Subunit Deficiencies Lead to Distinct Gene

Expression Signatures that Reflect Cellular Growth Rate. *Mol. Cel* 73, 36–47. e10. doi:10.1016/j.molcel.2018.10.032

Cizelsky, W., Hempel, A., Metzig, M., Tao, S., Hollemann, T., Kühl, M., et al. (2013). sox4 and Sox11 Function during *Xenopus laevis* Eye Development. *PLoS ONE* 8, e69372. doi:10.1371/journal.pone.0069372

Cmejla, R., Cmejlova, J., Handrkova, H., Petrak, J., Petrtylova, K., Mihal, V., et al. (2009). Identification of Mutations in the Ribosomal Protein L5 (RPL5) and Ribosomal Protein L11 (RPL11) Genes in Czech Patients with Diamond-Blackfan Anemia. *Hum. Mutat.* 30, 321–327. doi:10.1002/humu.20874

Cordenonsi, M., Dupont, S., Maretto, S., Insinga, A., Imbriano, C., and Piccolo, S. (2003). Links between Tumor Suppressors. *Cell* 113, 301–314. doi:10.1016/s0092-8674(03)00308-8

Cvekl, A., and Callaerts, P. (2017). PAX6: 25th Anniversary and More to Learn. *Exp. Eye Res.* 156, 10–21. doi:10.1016/j.exer.2016.04.017

Dai, M.-S., and Lu, H. (2004). Inhibition of MDM2-Mediated P53 Ubiquitination and Degradation by Ribosomal Protein L5. *J. Biol. Chem.* 279, 44475–44482. doi:10.1074/jbc.M403722200

Day, R. C., and Beck, C. W. (2011). Transdifferentiation from Cornea to Lens in *Xenopus laevis* Depends on BMP Signalling and Involves Upregulation of Wnt Signalling. *BMC Developmental Biol.* 11, 54. doi:10.1186/1471-213X-11-54

De Keersmaecker, K., Sulima, S. O., and Dinman, J. D. (2015). Ribosomopathies and the Paradox of Cellular Hypo- to Hyperproliferation. *Blood* 125, 1377–1382. doi:10.1182/blood-2014-10-569616

Deml, B., Reis, L. M., Lemyre, E., Clark, R. D., Kariminejad, A., and Semina, E. V. (2016). Novel Mutations in PAX6, OTX2 and NDP in Anophthalmia, Microphthalmia and Coloboma. *Eur. J. Hum. Genet.* 24, 535–541. doi:10.1038/ejhg.2015.155

Dyer, M. A., Livesey, F. J., Cepko, C. L., and Oliver, G. (2003). Prox1 Function Controls Progenitor Cell Proliferation and Horizontal Cell Genesis in the Mammalian Retina. *Nat. Genet.* 34, 53–58. doi:10.1038/ng1144

Farley-Barnes, K. I., Ogawa, L. M., and Baserga, S. J. (2019). Ribosomopathies: Old Concepts, New Controversies. *Trends Genet.* 35, 754–767. doi:10.1016/j.tig.2019.07.004

Ferretti, M. B., and Karbstein, K. (2019). Does Functional Specialization of Ribosomes Really Exist? *RNA* 25, 521–538. doi:10.1261/rna.069823.118

Fumagalli, S., Ivanenkov, V. V., Teng, T., and Thomas, G. (2012). Suprainduction of P53 by Disruption of 40S and 60S Ribosome Biogenesis Leads to the Activation of a Novel G2/M Checkpoint. *Genes Dev.* 26, 1028–1040. doi:10.1101/gad.189951.112

Furukawa, T., Kozak, C. A., and Cepko, C. L. (1997). Rax, a Novel Paired-type Homeobox Gene, Shows Expression in the Anterior Neural Fold and Developing Retina. *Proc. Natl. Acad. Sci.* 94, 3088–3093. doi:10.1073/pnas.94.7.3088

Gazda, H. T., Sheen, M. R., Vlachos, A., Choesmel, V., O'Donohue, M.-F., Schneider, H., et al. (2008). Ribosomal Protein L5 and L11 Mutations Are Associated with Cleft Palate and Abnormal Thumbs in Diamond-Blackfan Anemia Patients. *Am. J. Hum. Genet.* 83, 769–780. doi:10.1016/j.ajhg.2008.11.004

Genuth, N. R., and Barna, M. (2018). The Discovery of Ribosome Heterogeneity and its Implications for Gene Regulation and Organismal Life. *Mol. Cel* 71, 364–374. doi:10.1016/j.molcel.2018.07.018

Georgala, P. A., Carr, C. B., and Price, D. J. (2011). The Role of Pax6 in Forebrain Development. *Devel Neurobio* 71, 690–709. doi:10.1002/dneu.20895

Gessert, S., Maurus, D., Rössner, A., and Kühl, M. (2007). Pescadillo Is Required for *Xenopus laevis* Eye Development and Neural Crest Migration. *Developmental Biol.* 310, 99–112. doi:10.1016/j.ydbio.2007.07.037

Gomez-Roman, N., Grandori, C., Eisenman, R. N., and White, R. J. (2003). Direct Activation of RNA Polymerase III Transcription by C-Myc. *Nature* 421, 290–294. doi:10.1038/nature01327

Gonzalez-Rodriguez, J., Pelcastre, E. L., Tovilla-Canales, J. L., Garcia-Ortiz, J. E., Amato-Almanza, M., Villanueva-Mendoza, C., et al. (2010). Mutational Screening of CHX10, GDF6, OTX2, RAX and SOX2 Genes in 50 Unrelated Microphthalmia-Anophthalmia-Coloboma (MAC) Spectrum Cases. *Br. J. Ophthalmol.* 94, 1100–1104. doi:10.1136/bjo.2009.173500

Griffin, J. N., Sondalle, S. B., del Viso, F., Baserga, S. J., and Khokha, M. K. (2015). The Ribosome Biogenesis Factor Nol11 Is Required for Optimal rDNA Transcription and Craniofacial Development in Xenopus. *Plos Genet.* 11, e1005018. doi:10.1371/journal.pgen.1005018

Hampp, S., Kiessling, T., Buechle, K., Mansilla, S. F., Thomale, J., Rall, M., et al. (2016). DNA Damage Tolerance Pathway Involving DNA Polymerase ι and the Tumor Suppressor P53 Regulates DNA Replication fork Progression. *Proc. Natl. Acad. Sci. USA* 113, E4311–E4319. doi:10.1073/pnas.1605828113

Hayashi, T., Huang, J., and Deeb, S. S. (2000). RINX(VSX1), a Novel Homeobox Gene Expressed in the Inner Nuclear Layer of the Adult Retina. *Genomics* 67, 128–139. doi:10.1006/geno.2000.6248

Hemann, M. T., and Lowe, S. W. (2006). The P53-Bcl-2 Connection. *Cell Death Differ* 13, 1256–1259. doi:10.1038/sj.cdd.4401962

Hemmati-Brivanlou, A., Frank, D., Bolce, M. E., Brown, B. D., Sive, H. L., and Harland, R. M. (1990). Localization of Specific mRNAs in Xenopus Embryos by Whole-Mount *In Situ* Hybridization. *Development* 110, 325–330. doi:10.1242/dev.110.2.325

Hitchcock, P. F., Macdonald, R. E., VanDeRyt, J. T., and Wilson, S. W. (1996). Antibodies against Pax6 Immunostain Amacrine and Ganglion Cells and Neuronal Progenitors, but Not Rod Precursors, in the normal and Regenerating Retina of the Goldfish. *J. Neurobiol.* 29, 399–413. doi:10.1002/(sici)1097-4695(199603)29:3<399::aid-neu10>3.0.co;2-4

Hollemann, T., Bellefroid, E., and Pieler, T. (1998). The Xenopus Homologue of the Drosophila Gene Tailless Has a Function in Early Eye Development. *Development* 125, 2425–2432. doi:10.1242/dev.125.13.2425

Jacobson, M. (1991). *Developmental Neurobiology*. Boston, MA: Springer US. doi:10.1007/978-1-4757-4954-0

Jenkinson, E. M., Rodero, M. P., Kasher, P. R., Uggenti, C., Oojageer, A., Goosey, L. C., et al. (2016). Mutations in SNORD118 Cause the Cerebral Microangiopathy Leukoencephalopathy with Calcifications and Cysts. *Nat. Genet.* 48, 1185–1192. doi:10.1038/ng.3661

Jones, N. C., Lynn, M. L., Gaudenz, K., Sakai, D., Aoto, K., Rey, J.-P., et al. (2008). Prevention of the Neurocristopathy Treacher Collins Syndrome through Inhibition of P53 Function. *Nat. Med.* 14, 125–133. doi:10.1038/nm1725

Kang, J., Brajanovski, N., Chan, K. T., Xuan, J., Pearson, R. B., and Sanij, E. (2021). Ribosomal Proteins and Human Diseases: Molecular Mechanisms and Targeted Therapy. *Sig Transduct Target. Ther.* 6, 323. doi:10.1038/s41392-021-00728-8

Katsumura, K. R., Bresnick, E. H., and Gata (2017). Factor Mechanisms GroupThe GATA Factor Revolution in Hematology. *Blood* 129, 2092–2102. doi:10.1182/blood-2016-09-687871

Kiraz, Y., Adan, A., Kartal Yandim, M., and Baran, Y. (2016). Major Apoptotic Mechanisms and Genes Involved in Apoptosis. *Tumor Biol.* 37, 8471–8486. doi:10.1007/s13277-016-5035-9

Köster, M., Dillinger, K., and Knöchel, W. (1998). Expression Pattern of the Winged helix Factor XFD-11 during Xenopus Embryogenesis. *Mech. Development* 76, 169–173. doi:10.1016/s0925-4773(98)00123-3

Kostjukovits, S., Klemetti, P., Valta, H., Martelius, T., Notarangelo, L. D., Seppänen, M., et al. (2017). Analysis of Clinical and Immunologic Phenotype in a Large Cohort of Children and Adults with Cartilage-Hair Hypoplasia. *J. Allergy Clin. Immunol.* 140, 612–614. e5. doi:10.1016/j.jaci.2017.02.016

Kuze, M., Matsubara, H., and Uji, Y. (2009). Ocular Hypertelorism and Exotropia as Presenting Signs in Diamond-Blackfan Anemia. *Jpn. J. Ophthalmol.* 53, 67–68. doi:10.1007/s10384-008-0610-2

Lamb, T. M., Knecht, A. K., Smith, W. C., Stachel, S. E., Economides, A. N., Stahl, N., et al. (1993). Neural Induction by the Secreted Polypeptide Noggin. *Science* 262, 713–718. doi:10.1126/science.8235591

Leidig, C., Thoms, M., Holdermann, I., Bradatsch, B., Berninghausen, O., Bange, G., et al. (2014). 60S Ribosome Biogenesis Requires Rotation of the 5S Ribonucleoprotein Particle. *Nat. Commun.* 5, 3491. doi:10.1038/ncomms4491

Liao, J.-M., Zhou, X., Gatignol, A., and Lu, H. (2014). Ribosomal Proteins L5 and L11 Co-operatively Inactivate C-Myc via RNA-Induced Silencing Complex. *Oncogene* 33, 4916–4923. doi:10.1038/onc.2013.430

Lipton, J. M., Atsidaftos, E., Zyskind, I., and Vlachos, A. (2006). Improving Clinical Care and Elucidating the Pathophysiology of Diamond Blackfan Anemia: an Update from the Diamond Blackfan Anemia Registry. *Pediatr. Blood Cancer* 46, 558–564. doi:10.1002/pbc.20642

Liu, W., Khare, S. L., Liang, X., Peters, M. A., Liu, X., Cepko, C. L., et al. (2000). All Brn3 Genes Can Promote Retinal Ganglion Cell Differentiation in the Chick. *Development* 127, 3237–3247. doi:10.1242/dev.127.15.3237

Lodish, H. F. (1974). Model for the Regulation of mRNA Translation Applied to Haemoglobin Synthesis. *Nature* 251, 385–388. doi:10.1038/251385a0

Lufkin, T. (2007). *In Situ* Hybridization of Whole-Mount Mouse Embryos with RNA Probes: Hybridization, Washes, and Histochemistry. *Cold Spring Harb Protoc.* 2007, pdb.prot4823. doi:10.1101/pdb.prot4823

Maekawa, M., Iwayama, Y., Nakamura, K., Sato, M., Toyota, T., Ohnishi, T., et al. (2009). A Novel Missense Mutation (Leu46Val) of PAX6 Found in an Autistic Patient. *Neurosci. Lett.* 462, 267–271. doi:10.1016/j.neulet.2009.07.021

Maurus, D., Héligon, C., Bürger-Schwärzler, A., Brändli, A. W., and Kühl, M. (2005). Noncanonical Wnt-4 Signaling and EAF2 Are Required for Eye Development in *Xenopus laevis*. *EMBO J.* 24, 1181–1191. doi:10.1038/sj.emboj.7600603

McGowan, K. A., Li, J. Z., Park, C. Y., Beaudry, V., Tabor, H. K., Sabnis, A. J., et al. (2008). Ribosomal Mutations Cause P53-Mediated Dark Skin and Pleiotropic Effects. *Nat. Genet.* 40, 963–970. doi:10.1038/ng.188

Melnikov, S., Ben-Shem, A., Garreau de Loubresse, N., Jenner, L., Yusupova, G., and Yusupov, M. (2012). One Core, Two Shells: Bacterial and Eukaryotic Ribosomes. *Nat. Struct. Mol. Biol.* 19, 560–567. doi:10.1038/nsmb.2313

Mills, E. W., and Green, R. (2017). Ribosomopathies: There's Strength in Numbers. *Science* 358, eaan2755. doi:10.1126/science.aan2755

Moody, S. A., and Kline, M. J. (1990). Segregation of Fate during Cleavage of Frog (*Xenopus laevis*) Blastomeres. *Anat. Embryol.* 182, 347–362. doi:10.1007/BF02433495

Myers, K. C., Bolyard, A. A., Otto, B., Wong, T. E., Jones, A. T., Harris, R. E., et al. (2014). Variable Clinical Presentation of Shwachman-Diamond Syndrome: Update from the North American Shwachman-Diamond Syndrome Registry. *J. Pediatr.* 164, 866–870. doi:10.1016/j.jpeds.2013.11.039

Nakayama, T., Fisher, M., Nakajima, K., Odeleye, A. O., Zimmerman, K. B., Fish, M. B., et al. (2015). Xenopus Pax6 Mutants Affect Eye Development and Other Organ Systems, and Have Phenotypic Similarities to Human Aniridia Patients. *Developmental Biol.* 408, 328–344. doi:10.1016/j.ydbio.2015.02.012

Narla, A., and Ebert, B. L. (2010). Ribosomopathies: Human Disorders of Ribosome Dysfunction. *Blood* 115, 3196–3205. doi:10.1182/blood-2009-10-178129

Norris, K., Hopes, T., and Aspden, J. L. (2021). Ribosome Heterogeneity and Specialization in Development. *WIREs RNA* 12, e1644. doi:10.1002/wrna.1644

Pan, Y., Kelly, L. E., and El-Hodiri, H. M. (2018). Identification of Retinal Homeobox (Rax) Gene -dependent Genes by a Microarray Approach: The DNA Endoglycosylase Neil3 Is a Major Downstream Component of the Rax Genetic Pathway. *Dev. Dyn.* 247, 1199–1210. doi:10.1002/dvdy.24679

P. D. Nieuwkoop and J. Faber (Editors) (1954). *Normal Table of* Xenopus laevis *(Daudin): A Systematical and Chronological Survey of the Development from the Fertilized Egg till the End of Metamorphosis*. Amsterdam: North-Hollund Pub. Co.

Pecoraro, A., Pagano, M., Russo, G., and Russo, A. (2021). Ribosome Biogenesis and Cancer: Overview on Ribosomal Proteins. *IJMS* 22, 5496. doi:10.3390/ijms22115496

Pierandrei-Amaldi, P., and Amaldi, F. (1994). Aspects of Regulation of Ribosomal Protein Synthesis inXenopus Laevis. *Genetica* 94, 181–193. doi:10.1007/BF01443432

Quarello, P., Garelli, E., Carando, A., Brusco, A., Calabrese, R., Dufour, C., et al. (2010). Diamond-blackfan Anemia: Genotype-Phenotype Correlations in Italian Patients with RPL5 and RPL11 Mutations. *Haematologica* 95, 206–213. doi:10.3324/haematol.2009.011783

Reed, J. C. (2008). Bcl-2-family Proteins and Hematologic Malignancies: History and Future Prospects. *Blood* 111, 3322–3330. doi:10.1182/blood-2007-09-078162

Rodgers, H. M., Huffman, V. J., Voronina, V. A., Lewandoski, M., and Mathers, P. H. (2018). The Role of the Rx Homeobox Gene in Retinal Progenitor Proliferation and Cell Fate Specification. *Mech. Development* 151, 18–29. doi:10.1016/j.mod.2018.04.003

Ross, A. P., and Zarbalis, K. S. (2014). The Emerging Roles of Ribosome Biogenesis in Craniofacial Development. *Front. Physiol.* 5. doi:10.3389/fphys.2014.00026

Rungger-Brändle, E., Ripperger, J. A., Steiner, K., Conti, A., Stieger, A., Soltanieh, S., et al. (2010). Retinal Patterning by Pax6-dependent Cell Adhesion Molecules. *Devel Neurobio* 70, 764–780. doi:10.1002/dneu.20816

Scholnick, J., Sinor, C., Oakes, J., Outten, W., and Saha, M. (1997). Differential Expression of Xenopus Ribosomal Protein Gene XlrpS1c. *Biochim. Biophys. Acta (Bba) - Gene Struct. Expr.* 1354, 72–82. doi:10.1016/s0167-4781(97)00101-2

Seigfried, F. A., Cizelsky, W., Pfister, A. S., Dietmann, P., Walther, P., Kühl, M., et al. (2017). Frizzled 3 Acts Upstream of Alcam during Embryonic Eye Development. *Developmental Biol.* 426, 69–83. doi:10.1016/j.ydbio.2017.04.004

Session, A. M., Uno, Y., Kwon, T., Chapman, J. A., Toyoda, A., Takahashi, S., et al. (2016). Genome Evolution in the Allotetraploid Frog *Xenopus laevis*. *Nature* 538, 336–343. doi:10.1038/nature19840

Sevilla, T., Sivera, R., Martínez-Rubio, D., Lupo, V., Chumillas, M. J., Calpena, E., et al. (2015). TheEGR2gene Is Involved in Axonal Charcot–Marie–Tooth Disease. *Eur. J. Neurol.* 22, 1548–1555. doi:10.1111/ene.12782

Shwachman, H., Diamond, L. K., Oski, F. A., and Khaw, K.-T. (1964). The Syndrome of Pancreatic Insufficiency and Bone Marrow Dysfunction. *J. Pediatr.* 65, 645–663. doi:10.1016/s0022-3476(64)80150-5

Siddiqui, W. A., Ahad, A., and Ahsan, H. (2015). The Mystery of BCL2 Family: Bcl-2 Proteins and Apoptosis: an Update. *Arch. Toxicol.* 89, 289–317. doi:10.1007/s00204-014-1448-7

Sive, H. L., Grainger, R. M., and Harland, R. M. (2000). *Early Development of* Xenopus laevis*: A Laboratory Manual*. New York N.Y. Cold Spring Harbor Laboratory Press.

Sulima, S., Kampen, K., and De Keersmaecker, K. (2019). Cancer Biogenesis in Ribosomopathies. *Cells* 8, 229. doi:10.3390/cells8030229

Valdez, B. C., Henning, D., So, R. B., Dixon, J., and Dixon, M. J. (2004). The Treacher Collins Syndrome (TCOF1) Gene Product Is Involved in Ribosomal DNA Gene Transcription by Interacting with Upstream Binding Factor. *Proc. Natl. Acad. Sci.* 101, 10709–10714. doi:10.1073/pnas.0402492101

van Riggelen, J., Yetil, A., and Felsher, D. W. (2010). MYC as a Regulator of Ribosome Biogenesis and Protein Synthesis. *Nat. Rev. Cancer* 10, 301–309. doi:10.1038/nrc2819

Vlachos, A., Osorio, D. S., Atsidaftos, E., Kang, J., Lababidi, M. L., Seiden, H. S., et al. (2018). Increased Prevalence of Congenital Heart Disease in Children with Diamond Blackfan Anemia Suggests Unrecognized Diamond Blackfan Anemia as a Cause of Congenital Heart Disease in the General Population. *Circ. Genom Precis Med.* 11. doi:10.1161/CIRCGENETICS.117.002044

Wallace, H. (1960). The Development of Anucleolate Embryos of *Xenopus laevis*. *J. Embryol. Exp. Morphol.* 8, 405–413. doi:10.1242/dev.8.4.405

Warren, A. J. (2018). Molecular Basis of the Human Ribosomopathy Shwachman-Diamond Syndrome. *Adv. Biol. Regul.* 67, 109–127. doi:10.1016/j.jbior.2017.09.002

Watkins-Chow, D. E., Cooke, J., Pidsley, R., Edwards, A., Slotkin, R., Leeds, K. E., et al. (2013). Mutation of the diamond-blackfan Anemia Gene Rps7 in Mouse Results in Morphological and Neuroanatomical Phenotypes. *Plos Genet.* 9, e1003094. doi:10.1371/journal.pgen.1003094

Weaver, K. N., Watt, K. E. N., Hufnagel, R. B., Navajas Acedo, J., Linscott, L. L., Sund, K. L., et al. (2015). Acrofacial Dysostosis, Cincinnati Type, a Mandibulofacial Dysostosis Syndrome with Limb Anomalies, Is Caused by POLR1A Dysfunction. *Am. J. Hum. Genet.* 96, 765–774. doi:10.1016/j.ajhg.2015.03.011

Wei, K., Chen, J., Akrami, K., Galbraith, G. C., Lopez, I. A., and Chen, F. (2007). Neural Crest Cell Deficiency Ofc-Myc Causes Skull and Hearing Defects. *Genesis* 45, 382–390. doi:10.1002/dvg.20304

Wischnewski, J., Sölter, M., Chen, Y., Hollemann, T., and Pieler, T. (2000). Structure and Expression of Xenopus Karyopherin-B3: Definition of a Novel Synexpression Group Related to Ribosome Biogenesis. *Mech. Development* 95, 245–248. doi:10.1016/s0925-4773(00)00337-3

Zhang, Y., and Lu, H. (2009). Signaling to P53: Ribosomal Proteins Find Their Way. *Cancer Cell* 16, 369–377. doi:10.1016/j.ccr.2009.09.024

Zhao, C., Andreeva, V., Gibert, Y., LaBonty, M., Lattanzi, V., Prabhudesai, S., et al. (2014). Tissue Specific Roles for the Ribosome Biogenesis Factor Wdr43 in Zebrafish Development. *Plos Genet.* 10, e1004074. doi:10.1371/journal.pgen.1004074

Conflict of Interest: The authors declare that the research was conducted in the absence of any commercial or financial relationships that could be construed as a potential conflict of interest.

Publisher's Note: All claims expressed in this article are solely those of the authors and do not necessarily represent those of their affiliated organizations, or those of the publisher, the editors and the reviewers. Any product that may be evaluated in this article, or claim that may be made by its manufacturer, is not guaranteed or endorsed by the publisher.

Advantages of publishing in Frontiers

OPEN ACCESS
Articles are free to read for greatest visibility and readership

FAST PUBLICATION
Around 90 days from submission to decision

HIGH QUALITY PEER-REVIEW
Rigorous, collaborative, and constructive peer-review

TRANSPARENT PEER-REVIEW
Editors and reviewers acknowledged by name on published articles

Frontiers
Avenue du Tribunal-Fédéral 34
1005 Lausanne | Switzerland

Visit us: www.frontiersin.org
Contact us: frontiersin.org/about/contact

REPRODUCIBILITY OF RESEARCH
Support open data and methods to enhance research reproducibility

DIGITAL PUBLISHING
Articles designed for optimal readership across devices

FOLLOW US
@frontiersin

IMPACT METRICS
Advanced article metrics track visibility across digital media

EXTENSIVE PROMOTION
Marketing and promotion of impactful research

LOOP RESEARCH NETWORK
Our network increases your article's readership